Immunological and Structural Evaluation of Synthetic GPI (Glycosylphosphatidylinositol) and GPI-Anchored Protein

Inaugural-Dissertation
to obtain the academic degree
Doctor rerum naturalium (Dr. rer. nat.)

submitted to the Department of Biology, Chemistry and Pharmacy
of Freie Universität Berlin

by

Ankita Malik

from Haryana, India

October 2018

This work was performed between August 2014 and September 2018 under the supervision of Dr. Daniel Varón Silva in the Department of Biomolecular Systems, Max Planck Institute of Colloids and Interfaces Potsdam, and the Institute of Chemistry and Biochemistry, Freie Universität Berlin.

1st Reviewer: Dr. Daniel Varón Silva

2nd Reviewer: Prof. Dr. Mathias Christmann

Date of defense: 16.04.2019

Declaration

This is to certify that the entire work in this thesis has been carried out by Ms. Ankita Malik, if not stated otherwise. The assistance and help received during the course of investigation have been fully acknowledged.

---------- ----------

(Date, Place) (Signature)

Acknowledgements

I express my deepest gratitude to Dr. Daniel Varon Silva for his excellent support, scientific guidance and supervision throughout the last years. I also want to thank Prof. Dr. Peter Seeberger for giving me the opportunity to perform my dissertation in the biomolecular systems department at Max Planck Institute of Colloids and Interfaces.

I am thankful to Prof. Dr. Mathias Christmann for kindly agreeing to review this thesis.

I especially want to thank current and former members of the GPI group for motivational working environment and support in lab: Antonella, Maria, Renee, Hyunil, Dana, Bo-young, Monika and Sandra.

A special thanks to my esteemed colleagues and friends Silvia, Priya, Pietro, Bopanna, Martina, Bart, Mara, Mauro, Alonso, Monica, Jamal, Oren, Madhu, Marilda, Fei-Fei, Kathir, Andreia, Zhou, Deborah, Vittorio, Mike, Matt, Stella, Jiawei, CD, Cristian and Sebastian not only for their invaluable help and making science fun, but also for making this unique period of my life memorable.

In addition, I want to thank Prof. Gerald Brezesinski, Prof. Bernd Lepenies, Fridolin, Claney, Benjamin, Sharu and Jonnel for their extensive efforts and fruitful collaboration.

I thank Dorothee Böhme, Eva Settels, Olaf Niemeyer and Felix Hentschel for outstanding technical and organizational support

Finally, I would like to thank my family for unconditional support and encouragement.

List of Publications

Parts of this work have been or will be published.

Scientific Publications

- **Malik A**.; Varon Silva, D. "Advances in the Chemical Synthesis of Glycans and Glycoconjugates." *Advances in Glycobiotechnology*, Under Revision.

- Lama, S.; Schmidt, J.; **Malik, A**.; Walczak, R.; Varon Silva, D.; Völkel, A.; Oschatz, M. "Modification of Salt-templated carbon surface chemistry for efficient oxidation of glucose with supported gold catalysts." *ChemCatChem* **2018**, 10, 2458 – 2465.

- Grube, M.; Bo-Young, L.; Garg, M.; Michel, D.; **Malik, A**.; Vilotijevic, I.; Seeberger, P. H.; Varon Silva, D."Synthesis of Galactosylated Glycosylphosphatylinositols Derivatives from Trypanosoma brucei." *Chemistry – A European Journal* **2018**, 24, 3271 – 3282.

Scientific Conference and Symposia

- Sept. 2018, "Synthesis and Structural Study of Glycosylphosphatidylinositol Fragments on Monolayers", *Radboud-MPIKG Young Scientist Workshop*, Potsdam, Germany

- July 2018, "Synthesis and Structural Study of Glycosylphosphatidylinositol Fragments on Monolayers", *International Carbohydrate Symposium 2018*, Lisbon, Portugal.

- July 2018, "Synthesis of Glycosylphosphatidylinositol-Anchored Protein", Mini-Symposium at Technische Universität Braunschweig, Braunschweig, Germany

- Sept. 2017, "Synthesis of Bioactive Glycosylphosphatidylinositol Anchors from *P. falciparum*", *Ringberg Meeting of Max Planck Society*, Rottach-Egern, Germany

- April 2017, "Synthesis of Bioactive Glycosylphosphatidylinositol Anchors from *P. falciparum*", 6^{th} *RIKEN-Max Planck Symposium*, Okinawa, Japan.

- July 2016, "Synthesis of Bioactive Glycosylphosphatidylinositol Anchors from *P. falciparum*", *International Carbohydrate Symposium*, New Orleans, USA.

- April 2016, “General Strategy for the Synthesis of Bioactive Glycosylphosphatidylinositol bearing Unsaturated Lipids", *5th RIKEN-Max Planck Symposium*, Berlin, Germany.

Contents

List of Abbreviations

$(NH_4)_2CO_3$	Ammonium carbonate
$[Ir(Cod)(PPh_2Me)_2]PF_6$	(1,5-Cyclooctadiene)bis(methyldiphenylphosphine)iridium(I) Hexafluorophosphate
AAG	1-alkyl-2-acylglycerol
Ac	Acetyl
Ac_2O	Acetic anhydride
AcCl	Acylchloride
AcOH	Acetic acid
AgOTf	Silver triflate
AllylBr	Allyl Bromide
Asn	Asparagine
$BF_3.Et_2O$	Boron trifluoride diethyl etherate
Bn	Benzyl
BnBr	Benzylbromide
Boc	*tert*-Butoxycarbonyl
Bu_2SnO	Dibutyltinoxide
Bz	Benzoyl
CAN	Ceric ammonium nitrate
CCl_3CN	Trichloroacetonitrile
$CHCl_3$	Chloroform
CSA	Camphor sulfonic acid
DAG	Diacylglycerol
DAF	Decay accelerating factor
DBDIPPA	Dibenzyl diisopropyl phosphoramidite
DBU	1,8-diazabicycloundec-7-ene
DCC	*N,N'*-Dicyclohexylcarbodiimide
DCM	Dichloromethane

DDQ	2,3-Dichloro-5,6-dicyano-1,4-benzoquinone
DIPEA	N,N-Diisopropylethyl amine
DMAP	4-Dimethylaminopyridine
DMC	2-chloro-1,3-dimethylinidazolinium chloride
DMF	Dimethylformamide
DMSO	Dimethyl Sulfoxide
ER	Endoplasmic Reticulum
Et_2O	Diethyl ether
Et_3N	Triethylamine
EtNP	Phosphoethanolamine
EtOH	Ethanol
FI	Fluorescence Intensity
Fmoc	9-Fluorenylmethoxycarbonyl
FRET	Fluorescence resonance energy transfer
GAG	Glycosaminoglycan
GIPL	Glycoinositol phospholipids
GlcNAc	N-acetylglucosamine
GPI-APs	Glycosylphosphatidylinositols Anchored Proteins
GPIs	Glycosylphosphatidylinositols
GSL	Glycosphingolipids
GTP	Guanosine-5'-triphosphate
HCOOH	Formic acid
HF-Pyridine	Hydrogen fluoride in pyridine
$Hg(OAc)_2$	Mercury(II) acetate
I_2	Iodine
IL	Interleukin
Ino	Inositol
K_2CO_3	Potassium Carbonate
KLH	keyhole limpet hemocyanin
Lev	Levulinoyl
LPGs	Lipophosphoglycans
Man	Mannose
MeCN/ACN	Acetonitrile

MeOH	Methanol
MFI	Mean Fluorescence Intensity
Na	Sodium
NaH	Sodium hydride
NaOAc	Sodium Acetate
NaOMe	Sodium Methoxide
NaN_3	Sodium Azide
NapBr	2-Naphthylmethyl bromide
NCAM	Neural Cell adhesion molecules
NIS	N-iodosuccinimide
NMR	Nuclear Magnetic Resonance
NOE	Nuclear Overhauser Effect
PBS	Phosphate Buffer Saline
$Pd(OH)_2/C$	Palladium hydroxide on activated charcoal
Pd/C	Palladium on activated charcoal
$PdCl_2$	Palladium(II) Chloride
PGAP	Post GPI attachment to protein
Ph_3P	Triphenylphosphine
$PhCH(OMe)_2$	Benzaldehyde dimethyl acetal
PhMe	Toluene
PhSH	Thiophenol
PI	Phosphatidylinositol
PIG	Phosphatidylinositol Glycan
PIMs	Phosphatidylinositol mannosides
PI-PLC	Phosphoinositide phospholipase C
PivCl	Pivaloyl chloride
PNH	Paroxysmal Nocturnal Hemoglobinuria
Py	Pyridine
$Sc(OTf)_3$	Scandium(III) triflate
Ser	Serine
TBSOTf	*tert*-Butyldimethylsilyltrifluoromethanesulfonate
TCA	Trichloroacetonitrile
Tf_2O	Trfluoromethansulfonic acid anhydride, Triflic anhydride

TFA	Trifluoroacetic acid
THF	Tetrahydrofuran
Thr	Threonine
TLC	Thin Layer Chromatography
TLRs	Toll like receptors
TMSOTf	Trimethylsilyltrifluoromethanesulfonate
TNF-α	Tumor necrosis factor-alpha
VSGs	Variant Surface Glycoproteins
Zn	Zinc

Summary

Glycosylphosphatidylinositols (GPIs) are a family of complex glycolipids that are ubiquitous in eukaryotic cells. GPIs are added as a post-translational modification at the C-terminus of proteins or can be found as free glycolipids displayed on the outer leaflet of the cell membrane. GPI contains a conserved *pseudo*-pentasaccharide glycan core and a phospholipid, (Manα(1→2)Manα(1→6)Manα(1→4)GlcNα(1→6)-*myo*-Inositol-1-PO_4-lipid). GPIs and GPI-anchored proteins participate in diverse biological and pathological events and activate the host immune system during parasitic infections. These glycolipids are difficult to isolate in pure and homogeneous form, therefore, to date, chemical synthesis has remained the best way to obtain them for performing biological studies.

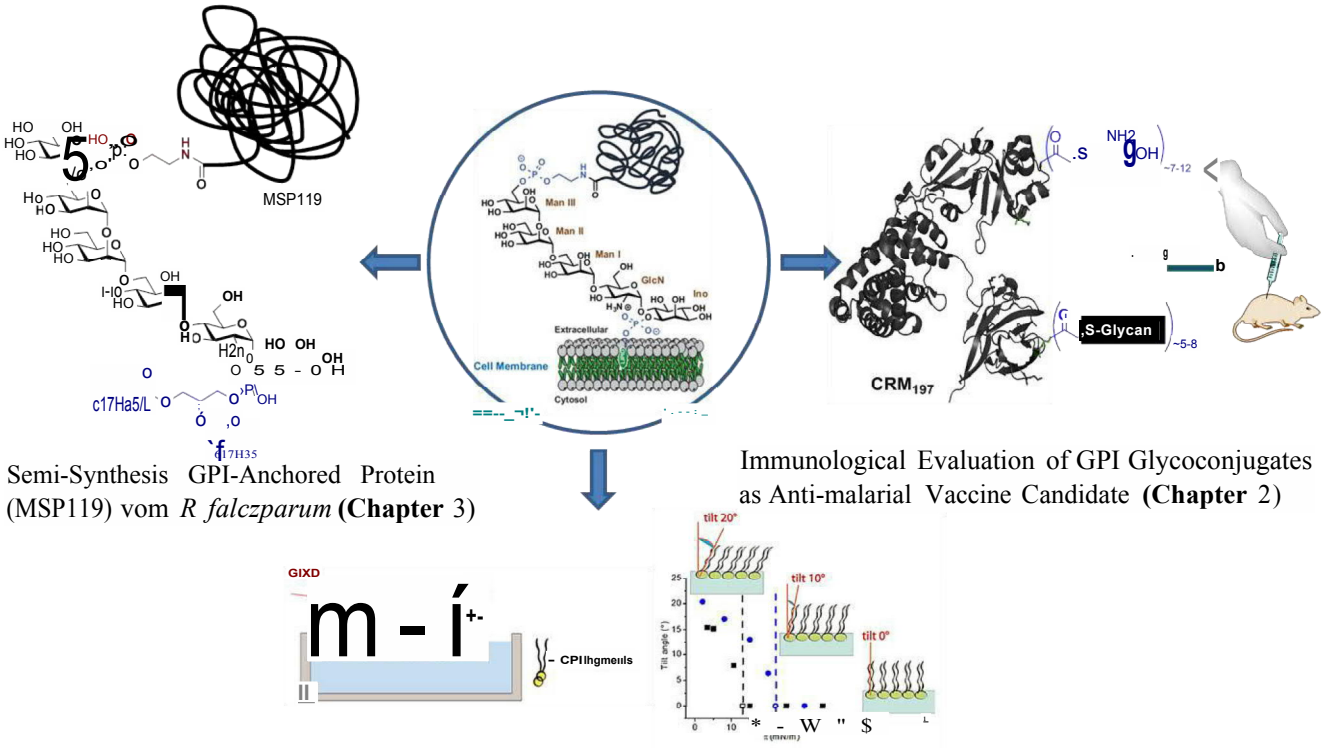

Semi-Synthesis GPI-Anchored Protein (MSP119) vom *R falczparum* **(Chapter** 3)

Immunological Evaluation of GPI Glycoconjugates as Anti-malarial Vaccine Candidate **(Chapter** 2)

Biophysical Evaluation of GPI Fıagments in Monolayers **(Chapter** 4)

Figure 1: Summary of the thesis describing the investigation of the role of GPIs in biological and biophysical aspects.

In malaria, GPIs act as a toxin during the progress of the disease and may be responsible for the strong symptoms of the infection. Therefore, the development of an antitoxic GPI-

glycoconjugate vaccine represents a promising approach to preventing malaria pathogenesis. In this work, chemical synthesis was applied to obtain GPIs and GPI-derivatives from the GPI of *Plasmodium spp.* to investigate the role of GPIs in three aspects; the design and evaluation of CRM_{197}-GPI glycoconjugates as antimalarial vaccine candidates, the semi-synthesis of GPI-anchored proteins to understand the role of GPIs on the protein function and structure, and for the evaluation of the biophysical properties of GPI fragments in monolayers as model membranes (**figure 1**).

Starting with the use of GPI as an anti-toxin vaccine, Chapter 2 comprises the design, synthesis and immunological evaluation of six structurally distinct GPI fragments from the GPI of *P. falciparum*. These fragments were designed to cover different components of the glycan moiety of the *P. falciparum* GPI structure. The GPI fragments were synthesized using a convergent synthetic strategy bearing a thiol linker that was used for their conjugation to the carrier protein without compromising the amine functionality of the glucosamine and phosphoethanolamine units. Benzyl ethers were used as a permanent protecting group and acetyl ester, TIPS and allyl ethers were used as orthogonal temporary protecting groups. Birch reduction was used for global deprotection and products were obtained as a mixture of thiol and disulfide oligosaccharides which were reduced and purified using size exclusion chromatography. The synthesised glycans were conjugated to the CRM_{197} carrier protein using *N*-succinimidyl-3-(bromoacetamido)propionate (SBAP) activation of protein followed by reaction with the thiol-glycans.

The CRM_{197}-GPI glycocojugates were tested for immunogenicity and efficacy as antimalarial vaccine candidates using C57BL/6JRj as experimental cerebral malaria (ECM) model. A structure–activity relationship of different synthetic GPIs with respect to immunogenicity by glycan array analysis was established. All the glycoconjugate immunized mice showed an increased survival compared to the control group. Cross-reactivity revealed that the length of the mannose backbone is an important epitope for immune recognition. The phosphoethanolamine present on the ManIII residue and *myo*-inositol also represent important immunogenic epitopes. This study added to current evidence that a GPI-antitoxic vaccine offers protection against *Plasmodium* GPI-induced ECM. The protection is dependent on both the antibody and cellular immune response. Furthermore, this study demonstrated that GPI composition and presentation on the carrier protein plays an important role in immune response induction.

The participation and role of GPIs of parasitic GPI-anchored proteins involved in protein–protein interactions mediating the attachment of *Plasmodium* parasites to the host cells and further infection of erythrocytes is unknown. To evaluate the biological function of GPIs and its effect on proteins involved in the infection process during malaria infection, chapter 3 describes the synthesis of a lipidated GPI containing a cysteine residue for ligation reactions with proteins. The synthesis of this GPI was successfully achieved using a [3+1+2] glycosylation strategy with trichloroacetimidate glycosyl donors to obtain the glycan moiety and late-stage phosphorylations. The challenging removal of the protecting groups was completed using a palladium catalysed hydrogenolysis followed by acid treatment in the presence of mercury salts.

The synthetic GPI glycolipid and Cys-Biotin were ligated to the 19 kDa fragment of the MSP1 protein, which is considered to be essential for the infection by the parasite. This process was carried out by using intein *trans*-splicing reactions to deliver pure **MSP1$_{19}$-GPI** and **MSP1$_{19}$-Biotin**. The protein structure of the ligation products **MSP1$_{19}$-GPI** and **MSP1$_{19}$-Biotin** were evaluated using analysis by circular dichroism (CD). CD spectra for both modified proteins, with and without GPI, were similar showing that these C-terminal modifications do not affect the overall structure of the MSP1$_{19}$ protein in solution.

Evaluation of the biological activity of **MSP1$_{19}$-GPI** and **MSP1$_{19}$-Biotin** for the activation of antigen presenting cells was completed by stimulating dendritic cells *in vitro*. This dendritic cell stimulation assay showed that both **MSP1$_{19}$-Biotin** and **MSP1$_{19}$-GPI** are able to activate the T-cells and induce the release of the cytokines TNF-α and IL-12. However, very high level of both cytokines, TNF-α and IL-12, were only observed using the **MSP1$_{19}$-GPI** conjugate. This study is the first immunological and structural evaluation of a homogeneous synthetic **MSP1$_{19}$-GPI** and showed that the GPI anchor is an important and dominant immunogenic factor in the immune response against GPI-anchored proteins from *Plasmodium*. Furthermore, this study shows the **MSP1$_{19}$-GPI** is a potential target for vaccine development.

The lipid chains present on GPIs are highly variable and contribute to the heterogeneity of GPIs. These chains interact through van der Waals forces with other lipids chains of the bilayer and participate in the formation of membrane microdomains. The presence of the large hydrophilic oligosaccharide head group in GPI distinguishes these glycolipids from other phospholipids by providing flexibility and additional hydrogen bonding that can dominate the lipid interactions. Studies of the structural arrangement of GPIs in a model membrane can provide insight into the relationship between the glycolipid composition of and its behavior in

model membranes. To evaluate the correlation between the GPI lipid components and the structural arrangement of GPI in model membranes that could explain their biological function, chapter 4 presents the synthesis of GPI fragments bearing linear, branched and unsaturated lipid chains and the results of their affinity towards the formation of substructures in monolayers at the water/air interface.

Four GPI fragments were synthesized containing the *pseudo*-disaccharide glycan and a diacylglycerol bearing either saturated, unsaturated or branched fatty acids chains. Monolayers of the glycolipids were generated and their structural parameters were determined by using IR and GIXD measurements to obtain the tilt angle of the alkyl chains and determine the change in the packing mode and lattice. GIXD patterns and contour plots of the monolayers depicted different substructures that depend on the lipid composition and the polar head group. The monolayer structures showed a correlation between an increase in zwitterionic character of the glycolipid and a reduction in the flexibility of the head group of the GPI fragment. GPI fragments containing an acetylated glucosamine were more flexible and demonstrated a reduced packing compared to the non-acetylated glycolipid. This confirmed the importance of this amine in the hydrogen bonding and electrostatic interaction for the formation of ordered structures in the membrane. These results can be directly correlated to GPI biosynthesis with the deacetylation of the glucosamine as a crucial step. The presence of branching and unsaturation at the lipid induces a similar effect and are responsible for the fluidity of the membrane. These findings suggest that the lipids play a crucial role in the organization of the GPIs in the membrane and are responsible for many cellular functions.

Altogether, this work was able to demonstrate the applicability of chemical synthesis to obtain better insight into the structural and immunological properties of GPIs and GPI-anchored protein from *Plasmodium*. Furthermore, the results of this thesis show the importance of GPIs in parasitic infection and why these glycolipids should be considered as an important component of anti-malaria vaccine development.

Zusammenfassung

Glykosylphosphatidylinositole (GPIs) sind eine Familie von komplexen Glykolipiden, die in eukaryotischen Zellen ubiquitär vorkommen. GPIs werden als posttranslationale Modifikation am C-Terminus von Proteinen hinzugefügt oder sind als freie Glykolipide auf der äußeren Oberfläche der Zellmembran zu finden. GPIs enthalten einen konservierten *Pseudo*-Pentasaccharid-Glykankern und ein Phospholipid, (Manα(1→2)Manα(1→6)Manα(1→4) GlcN-*myo*-Inositol-1-PO_4-lipid). GPIs und GPI-verankerte Proteine sind an verschiedenen biologischen und pathologischen Ereignissen beteiligt und wirken unter Anderen für die Aktivierung des Immunsystems des Wirtes bei parasitären Infektionen. GPI Glykolipide sind schwer in reiner und homogener Form aus natürlichen Quellen zu isolieren und die chemische Synthese ist der effizienteste Weg, sie für biologische Studien zu erhalten.

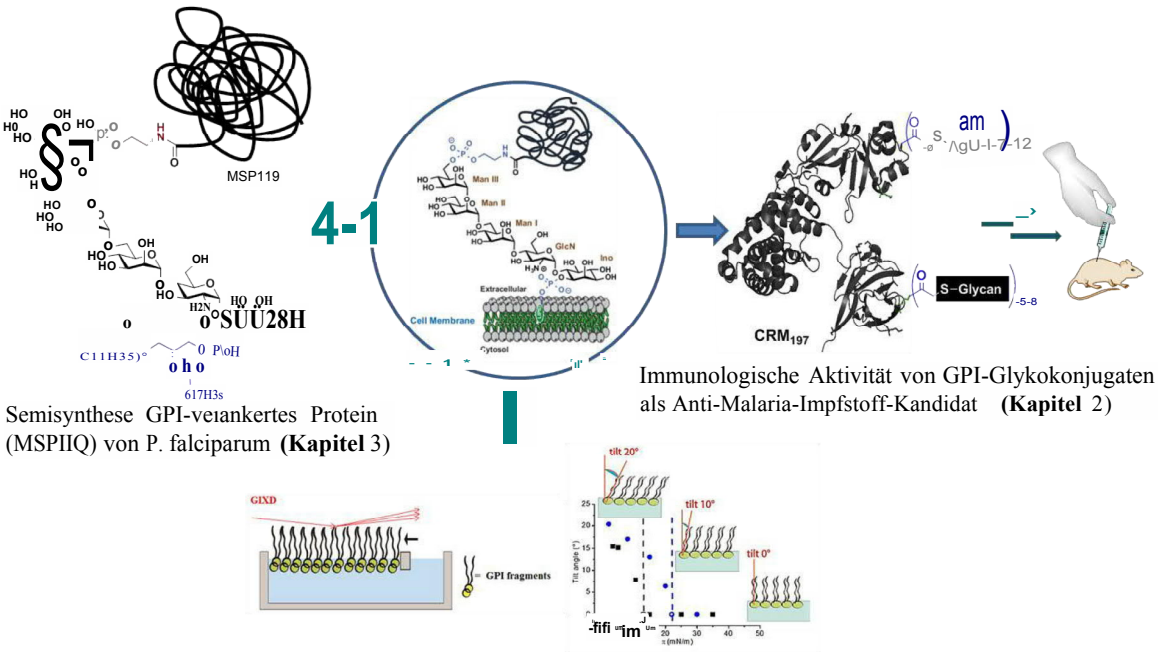

Semisynthese GPI-veıankertes Protein (MSPIIQ) von P. falciparum **(Kapitel** 3)

Immunologische Aktivität von GPI-Glykokonjugaten als Anti-Malaria-Impfstoff-Kandidat **(Kapitel** 2)

Biophysikalische Analyse von GPI-Fragmenten in Monoschichten **(Kapitel 4)**

Abbildung 1: Zusammenfassung der Arbeit, die die Untersuchung der Funktion von GPIs in biologischen und biophysikalischen Studien beschreibt.

In Malaria wirken die parasitäre GPIs während des Krankheitsverlaufs als Toxine und können für die schweren Symptome der Infektion verantwortlich sein. Daher stellt die Entwicklung

eines antitoxischen GPI-Glykokonjugat-Impfstoffs einen vielversprechenden Ansatz zur Verhinderung der Malariapathogenese dar. In dieser Arbeit wurde die chemische Synthese benutzt, um GPIs und GPI-Derivate aus dem GPI von *Plasmodium spp*. zu erhalten und die Rolle von GPIs in drei funktionelle Studien zu untersuchen: die Aktivität von CRM_{197}-GPI-Glykokonjugaten als Antimalaria-Impfstoffkandidaten, als Bausteine für die Semisynthese von GPI-verankerten Proteinen zur Untersuchung des Effekts von GPIs in die Funktion und Struktur des Protein, und für die Analyse der biophysikalischen Eigenschaften von GPI-Fragmenten in Monoschichten als Modellmembranen (**Abbildung 1**).

Beginnend mit der Verwendung von GPI als Anti-Toxin-Impfstoff umfasst Kapitel 2 das Design, die Synthese und die immunologische Untersuchung von sechs strukturell unterschiedlichen GPI-Fragmenten aus dem GPI von *P. falciparum*. Diese Fragmente wurden entwickelt, um verschiedene Komponenten des Glykanteils der *P. falciparum* GPI-Struktur abzudecken. Die GPI-Fragmente wurden mit einer konvergenten synthetischen Strategie synthetisiert und tragen einen Thiol-Linker für ihre Konjugation mit dem Trägerprotein ohne die Aminogruppen von Glucosamin und den Phosphoethanolamineinheiten zu beeinträchtigen. Benzylether wurden als permanente Schutzgruppe benutzt und Acetylester, TIPS Ether und Allylether wurden als orthogonale temporäre Schutzgruppen verwendet. Die globale Entschützung wurde durch eine Birch-Reduktion durchgeführt und die Produkte wurden als Mischung aus Thiol- und Disulfidoverbindungen erhalten, die mittels TCEP reduziert wurden und durch Größenausschlusschromatographie gereinigt wurden. Die synthetisierten Glykane wurden mit dem CRM_{197}-Trägerprotein unter Verwendung der N-Succinimidyl-3-(bromoacetamido)propionat (SBAP)-Aktivierung des Proteins konjugiert, gefolgt von der Reaktion mit den Thiol-Glykanen.

Die CRM_{197}-GPI-Glykokojugate wurden auf Immunogenität und Wirksamkeit als Antimalaria-Impfstoffkandidaten getestet, wobei C57BL/6JRj als ECM-Modell (Experimental Cerebral Malaria) verwendet wurde. Eine Struktur-Aktivitäts-Beziehung verschiedener synthetischer GPIs in Bezug auf die Immunogenität durch Glykan-Array-Analyse wurde etabliert. Alle mit Glykokonjugaten immunisierten Mäuse zeigten ein erhöhtes Überleben im Vergleich zur Kontrollgruppe. Die Kreuzreaktivität ergab, dass die Länge des Mannose-Rückgrats ein wichtiges Epitop für die Immunerkennung ist. Das am ManIII-Rest vorhandene Phosphoethanolamin und das *Myo*-Inositol stellen ebenfalls wichtige immunogene Epitope dar. Diese Studie fügte den aktuellen Erkenntnissen hinzu, dass ein GPI-antitoxischer Impfstoff Schutz vor *Plasmodium* GPI-induzierter ECM bietet. Der Schutz

ist sowohl vom Antikörper als auch von der zellulären Immunantwort abhängig. Darüber hinaus zeigte diese Studie, dass die GPI-Zusammensetzung und Präsentation auf dem Trägerprotein eine wichtige Rolle bei der Auslösung einer Immunantwort spielt.

Die Beteiligung und Rolle von GPIs in der Aktivität parasitärer GPI-verankerter Proteine, die an Protein-Protein-Wechselwirkungen beteiligt sind und die Bindung von *Plasmodium*-Parasiten an die Wirtszellen sowie die weitere Infektion von Erythrozyten vermitteln, ist unbekannt. Um die biologische Funktion von GPIs und ihre Wirkung auf Proteine zu bewerten, die während einer Malaria-Infektion und am Infektionsprozess beteiligt sind, beschreibt Kapitel 3 die Synthese eines lipidierten GPIs, das mit einem Cysteinrest für Ligationsreaktionen mit Proteinen ausgestattet war. Die Synthese des GPIs wurde erfolgreich mit einer [3+1+2] Glykosylierungsstrategie mit Verwendung von Trichloracetimidat-Glykosyl-Donatoren, um den Glykananteil zu erhalten, und folgenden Phosphorylierungen mit H-Phosphonate durchgeführt. Die anspruchsvolle Entschützung der Schutzgruppen wurde mit einer palladiumkatalysierten Hydrogenolyse und anschließender Säurebehandlung in Gegenwart von Quecksilbersalzen abgeschlossen.

Das synthetische GPI-Glykolipid und Cys-Biotin wurden an das 19 kDa-Fragment des MSP1-Proteins gebunden, das während der Infektion durch den Parasiten als wesentlich angesehen wird. Dieser Prozess wurde unter Verwendung von Intein-Transspleißreaktionen durchgeführt, um reines **$MSP1_{19}$-GPI** und **$MSP1_{19}$-Biotin** zu liefern. Die Proteinstruktur der Ligationsprodukte **$MSP1_{19}$-GPI** und **$MSP1_{19}$-Biotin** wurde durch eine Analyse mittels Zirkulardichroismus (CD) bewertet. CD-Spektren für beide modifizierten Proteine, mit und ohne GPI, zeigten einheitlich, dass diese C-terminalen Modifikationen die Gesamtstruktur des $MSP1_{19}$-Proteins in Lösung nicht beeinflussen.

Eine Untersuchung der biologischen Aktivität von **$MSP1_{19}$-GPI** und **$MSP1_{19}$-Biotin** zur Aktivierung von antigenpräsentierenden Zellen wurde *in vitro* abgeschlossen und es wurde gezeigt, dass dendritische Zellen stimuliert werden. Dieser dendritische Zellstimulationsassay zeigte, dass sowohl **$MSP1_{19}$-Biotin** als auch **$MSP1_{19}$-GPI** in der Lage sind, die Dendritische-Zellen zu aktivieren und die Freisetzung der Zytokine TNF-α und IL-12 einzuleiten. Allerdings wurden sehr hohe Konzentrationen beider Zytokine, TNF-α und IL-12, nur mit dem **$MSP1_{19}$-GPI** beobachtet. Diese Studie ist die erste immunologische und strukturelle Analyse eines homogenen synthetischen **$MSP1_{19}$-GPI** und zeigte, dass der GPI-Anker ein wichtiger und dominanter immunogener Faktor in der Immunantwort gegen GPI-verankerte

Proteine aus *Plasmodium* ist. Darüber hinaus zeigt diese Studie das **MSP1$_{19}$-GPI** als potenzielles Ziel für die Impfstoffentwicklung.

Die auf GPIs vorhandenen Lipidketten sind sehr variabel und tragen zur Heterogenität von GPIs bei. Diese Ketten interagieren durch van der Waals Kräfte mit anderen Lipidketten der Doppelschicht, die an der Bildung von Membran-Mikrodomänen beteiligt sind. Der großen hydrophilen Oligosaccharid-Kopfgruppe in GPIs unterscheidet diese Glykolipide von anderen Phospholipiden, indem sie Flexibilität und zusätzliche Wasserstoffbindung bieten, die die Lipidwechselwirkungen dominieren können. Studien über die strukturelle Anordnung von GPIs in einer Modellmembran können Erkenntnisse über den Zusammenhang zwischen der Glykolipidzusammensetzung und ihrem Verhalten in Modellmembranen liefern.

Um die Korrelation zwischen GPI-Lipidkomponenten und der strukturellen Anordnung von GPIs in Modellmembranen zu bewerten, die ihre biologische Funktion erklären könnten, stellt Kapitel 4 die Synthese von GPI-Fragmenten mit linearen, verzweigten und ungesättigten Lipidketten und die Ergebnisse ihrer Affinität zur Bildung von Substrukturen in Monoschichten an der Wasser-Luft-Grenzfläche vor.

Vier GPI-Fragmente wurden synthetisiert, die das *Pseudo*-Disaccharid Glykan und ein Diacylglycerin mit gesättigten, ungesättigten oder verzweigten Fettsäureketten enthalten. Monoschichten der Glykolipide wurden erzeugt und ihre Strukturparameter wurden mit Hilfe von IR- und GIXD-Messungen bestimmt, um den Neigungswinkel der Alkylketten zu erhalten und die Änderung im Dichtungsmodus und im Gitter zu bestimmen. GIXD-Muster und Konturdiagramme der Monoschichten zeigten verschiedene Unterstrukturen, die von der Lipidzusammensetzung und von der polaren Kopfgruppe abhängen. Die Monoschichtstruktur zeigte eine Korrelation zwischen einer Erhöhung der zwitterionischen Eigenschaften des Glykolipids und einer Verringerung der Flexibilität in der Kopfgruppe des GPI-Fragments. GPI-Fragmente, die ein acetyliertes Glucosamin enthalten, waren flexibler und präsentierten eine reduzierte Packung im Vergleich zum nicht-acetylierten Glykolipid, was die Bedeutung dieses Amins in der Wasserstoffbindung und der elektrostatischen Interaktion für die Bildung geordneter Strukturen in der Membran bestätigt. Diese Ergebnisse können direkt mit der GPI-Biosynthese korreliert werden, wobei die Deacetylierung des Glucosamins ein entscheidender Schritt ist. DIe Anwesenheit von Verzweigungen und Unsättigungen am Lipid führt zu einer ähnlichen Wirkung und ist für die Fluidität der Membran verantwortlich. Diese Ergebnisse

deuten darauf hin, dass die Lipide eine entscheidende Rolle bei der Organisation der GPIs in der Membran spielen und für viele Zellfunktionen verantwortlich sind.

Insgesamt konnte diese Arbeit die Anwendbarkeit der chemischen Synthese demonstrieren, um bessere Einblicke in die strukturellen und immunologischen Eigenschaften von GPIs und GPI verankertem Protein aus *Plasmodium spp.* zu erhalten. Darüber hinaus zeigen die Ergebnisse dieser Arbeit die Bedeutung von GPIs bei parasitären Infektionen und warum diese Glykolipide als wichtiger Bestandteil der Entwicklung von Anti-Malaria-Impfstoffen angesehen werden sollten.

1 Introduction

1.1 Carbohydrates Occurrence and Importance

Carbohydrates are the most abundant group of naturally occurring biomolecules and major constituents of plants, animals and microorganisms. They are the first product of photosynthesis, a main source of energy and play important role in the assembly of complex multicellular organs and organisms. Carbohydrates are naturally found as monosaccharides, oligosaccharides and polysaccharides with distinctive properties and complexity. They are involved in wide range of biological processes such as cell-cell recognition, proliferation of cells, fertilization, neuronal development, hormonal activities and activation of immune system.[1]

The surface of all cells is covered with a dense layer of carbohydrates, the so-called glycocalyx.[2] They are also found covalently linked to other bio-molecules, such as proteins (glycoprotein), peptides (glycopeptide) and lipids (glycolipid) in the form of glycoconjugates (**figure 1.1**).[3]

Glycoproteins carry one or more glycans covalently attached to the amino acid side chain of the protein, mostly *via* *N*- or *O*- linkage.[4-6] An *N*-glycoprotein carries a glycan chain covalently linked to an asparagine residue of a polypeptide chain (commonly involving GlcNAc residue).[7] Whereas, an *O*-glycoprotein has glycan linked to the polypeptide *via* a hydroxyl group of a serine or threonine residue.[8]

A glycolipid consists of a mono- or oligosaccharide attached to the terminal primary hydroxyl group of the lipid moiety. Glycolipids can be neutral or anionic and depending on the nature of lipid moiety it can be classified as glyceroglycolipids or sphingolipids. Glyceroglycolipid is the class of glycolipid characterized by glycerol with at least one fatty acid as the lipid moiety. Glycosphingolipids have sphingolipid as lipid moiety and can be sub classified as

gangliosides and cerebrosides. A ganglioside is an anionic glycolipid containing one or more residues of sialic acid.[9, 10] Sialylation is characteristic of mammalian glycans and is important for immune response.[4] A cereboside is a glycolipid with polysaccharide backbone and ceramide as lipid moiety. In protein–glycan interactions, particular glycans and branching is recognized. This indicates that branching plays a role in recognition processes.[5, 11, 12]

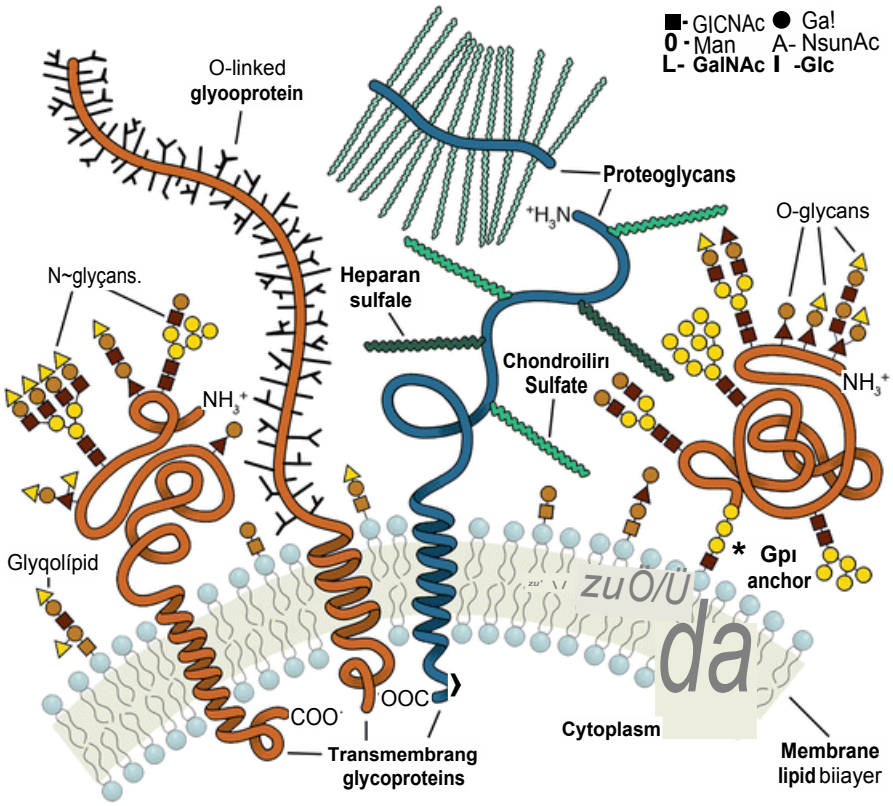

Figure 1.1: Different classes of glycans and glycocojugates found on the surface of cell.[13]

1.1.1 Biosynthesis of Carbohydrates

The structure and composition of carbohydrates present on any glycoconjugates is not genetically defined and depends on the differential expression and activity of the enzymes that are involved in their biosynthesis. The biosynthesis occurs mainly at the lumen of the endoplasmic reticulum (ER) and Golgi apparatus (**figure 1.2**). *N*-Glycans are initially synthesized in the ER as a dolichol diphosphate-linked high-mannose-type oligosaccharide containing three terminal glucose, eight mannose, and two internal GlcNAc residues. This

oligosaccharide is transferred to the Asn residues of Asn-X-Ser/Thr motifs of polypeptide chains.[14-16] The processing of oligosaccharides starts in the ER but it is mostly carried out in the Golgi apparatus.[17, 18] *O*-Glycans and glycosaminoglycans are synthesized in the Golgi by the sequential addition of sugars after the first unit is added to the Ser/Thr residues of proteins.[19] The glycosyltransferases determines the type of glycosidic linkage formed and controls the formation of a particular glycan. The glycosyltransferases involved in *N*-and *O*-glycan biosynthesis are membrane-bound enzymes and are specific for the assembly of a defined structure.[20]

Proteoglycans are glycoconjugates of proteins covalently attached to the Glycoaminoglycans (GAGS) *via* *O*-glycosidic Xyl-β-Ser motif. GAGs are anionic polysaccharide consisting of GlcNAc or *N*-sulfated glucosamine along with uronic acid. Commonly found GAGs are hyaluronic acid, heparan sulfate, heparin, and keratan sulfate. The biosynthesis of GAGs starts with the release of the precursor protein into the rough endoplasmic reticulum frequently found with *N*-linked oligosaccharides. Major posttranslational modifications occur in the Golgi complex which includes addition of the either glycosaminoglycan chains or *O*-linked oligosaccharides onto serine and threonine residues.[21-24]

Glycophosphotidylinositols (GPI) are complex glycolipids found as posttranslational modification at the C-terminus of the protein. The biosynthesis of GPI anchor occurs exclusively in the ER but some modifications to the glycan and remodeling of the lipid takes place in the Golgi apparatus.[25] The biosynthesis of GPI is discussed in detail in **section 1.2.2**.

Glycosphingolipids (GSLs) are a class of glycolipids that are conjugates to glycans and bear ceramide containing lipids.[26, 27] The ceramide is synthesized on the cytoplasmic side of the rough ER which is subsequently transferred to the luminal face and traffics to the Golgi apparatus.An important example of GSL is GlcCer that is synthesized on the cytoplasmic face of Golgi apparatus and flips into the Golgi lumen. GlcCer can be elongated by a series of glycosyltransferases in Golgi apparatus. Similar to *N*- and *O*-glycans, GSLs are involved in many physiological functions including cell–cell interactions, activation of immune responses and cell signaling.[27]

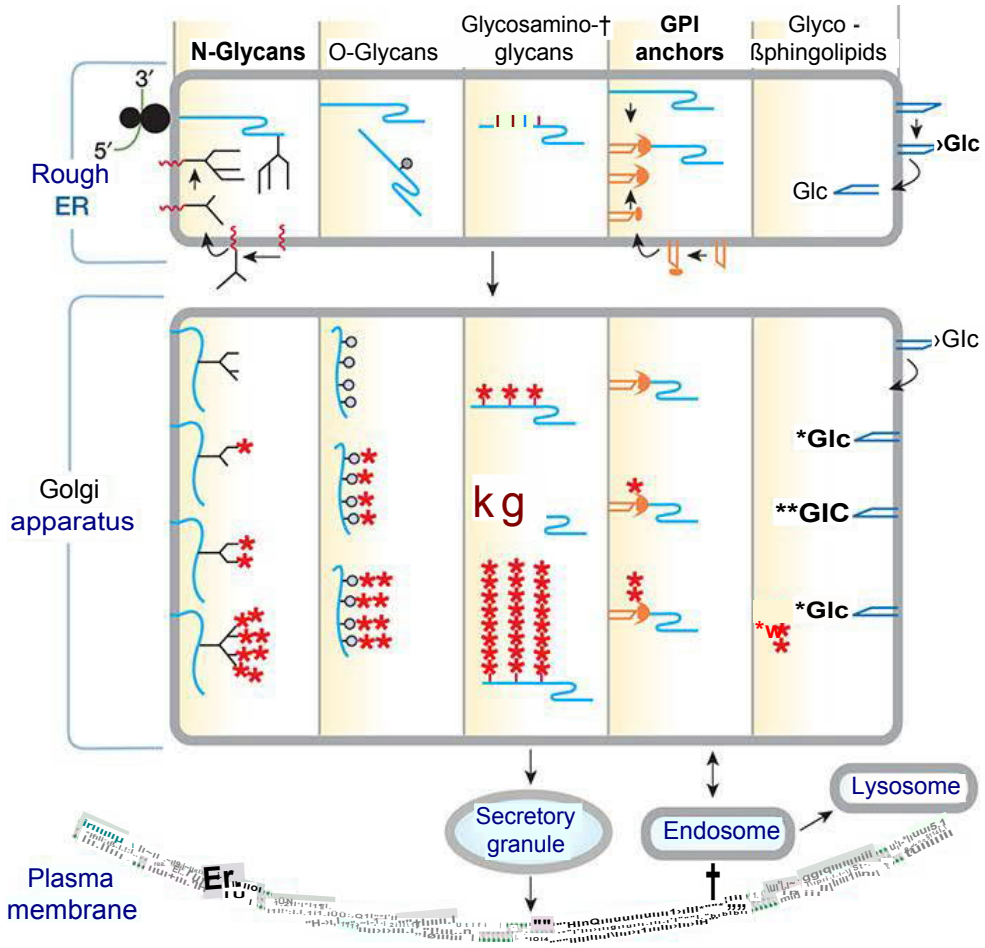

Figure 1.2: Simplified representation of biosynthesis of different types of eukaryotic glycoconjugates present in a cell. *Asterisks* represent the addition of outer sugars to glycans in the Golgi apparatus.[28]

1.2 Complexity to obtain Carbohydrates

The chemical synthesis of linear oligomers from amino acids and nucleic acids require the formation of only one type of linkage (amide bond or phosphodiester bond), which can be obtained by standardized protocols. However, the synthesis of oligosaccharides is more challenging due to the presence of multiples functional groups and their possible assembly into both linear and branch structures (**figure 1.3**). To obtain oligosaccharides chemically a high level of stereo- and regio- selectivity is required during the process.

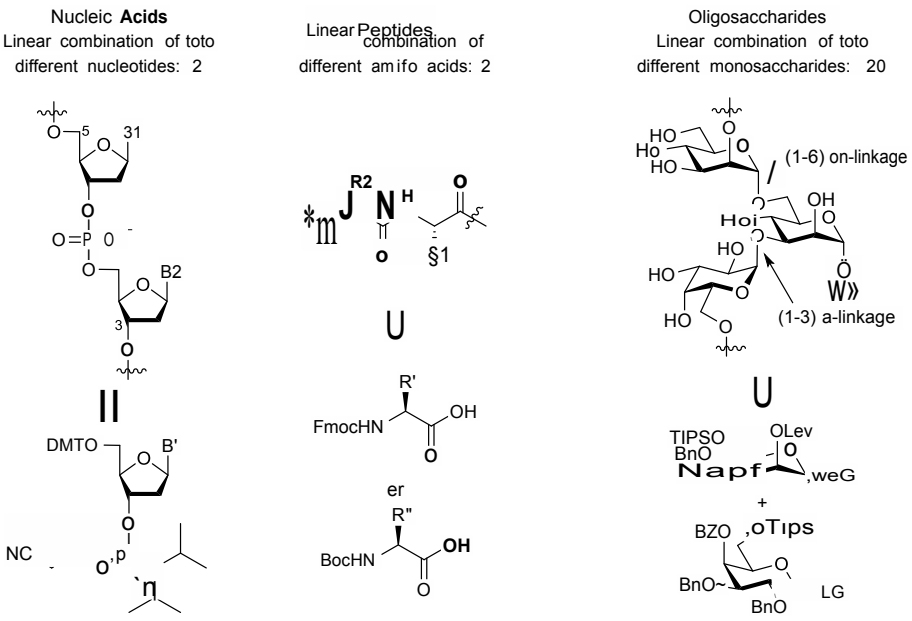

Figure 1.3: Linkages and combinational complexity found in the three major biopolymers. A) Nucleic acids, B) Proteins, C) Oligo and Polysaccharides

The lack of genetic control leads to the biosynthesis of glycoconjugates as heterogeneous mixture of glycans. The difficulty in separateion of single glycoconjugate hinders the investigations to determine the role of a defined carbohydrate structure in the biological function of these molecules. Therefore, the most convenient strategies to obtain complex glycans in homogeneous form and good quantities are chemical,[29] chemo-enzymatic[30, 31] or enzymatic synthesis.[32] These strategies provide substructures, regio-isomers or unnatural mimetics that can be aimed to get insights about role of carbohydrates in biological processes and for their application in biomedicine. Furthermore, these strategies facilitate the development of high affinity ligands,[33] mapping of immunogenic carbohydrate epitopes in polysaccharides,[34] and to introduce labelling or incorporation of linkers to simplify their use in the preparation of glycoconjugates.[35]

1.3 Organic Synthesis for Oligosaccharides

Despite remarkable progress during last years, there are no standard protocols and conditions that can be used for the synthesis of homogeneous natural and unnatural oligosaccharides.

There are two fundamental challenges in the chemical synthesis of oligosaccharides, the selective modification of specific hydroxyl groups in a carbohydrate unit and the control of the stereochemical outcome during glycosylation reactions. To overcome these problems, a large set of protecting groups, leaving groups, reaction conditions and glycosylation promoters have been established to obtain glycans having the desired structures and modifications.

The control of regioselectivity has been carried out through the use of protecting groups that are installed during the preparation of protected monosaccharides building blocks. In addition to their masking role, these groups can also participate in the steric and electronic stabilization of intermediates during the glycosylation reactions and contribute in the stereoselectivity of the reactions and thereof in the configuration of the new connection between two carbohydrate units. The selection of a particular combination of protecting groups plays a significant role in obtaining complicated glycan structures in a simplified manner.

1.3.1 Stereoselectivity in Glycosylation Reactions

The main challenge in glycosylation reactions is the control of the stereoselectivity to obtain a defined product having a 1,2-*trans*- or a 1,2-*cis*-linkage. In uncontrolled glycosylations, both linkages are almost equally formed. Therefore, to favor the formation of one product, different parameters influencing the selectivity of glycosylation need to be established and optimized. The most common methods are changing the reaction temperature, solvent, promotor, type of leaving groups used and the size and type of protecting groups (**figure 1.4b**).

A control of the reaction temperature can be used to favor the formation of more stable products through a thermodynamically controlled process at high temperatures, or to favor the formation of kinetically controlled products at low temperature. However, depending of the reactivity of the glycosylation agents, the structural features and of the protecting groups installed in both, the glycosyl donor and the glycosyl acceptor, a mixture of stereoisomers can be obtained independently of the reaction temperature used.

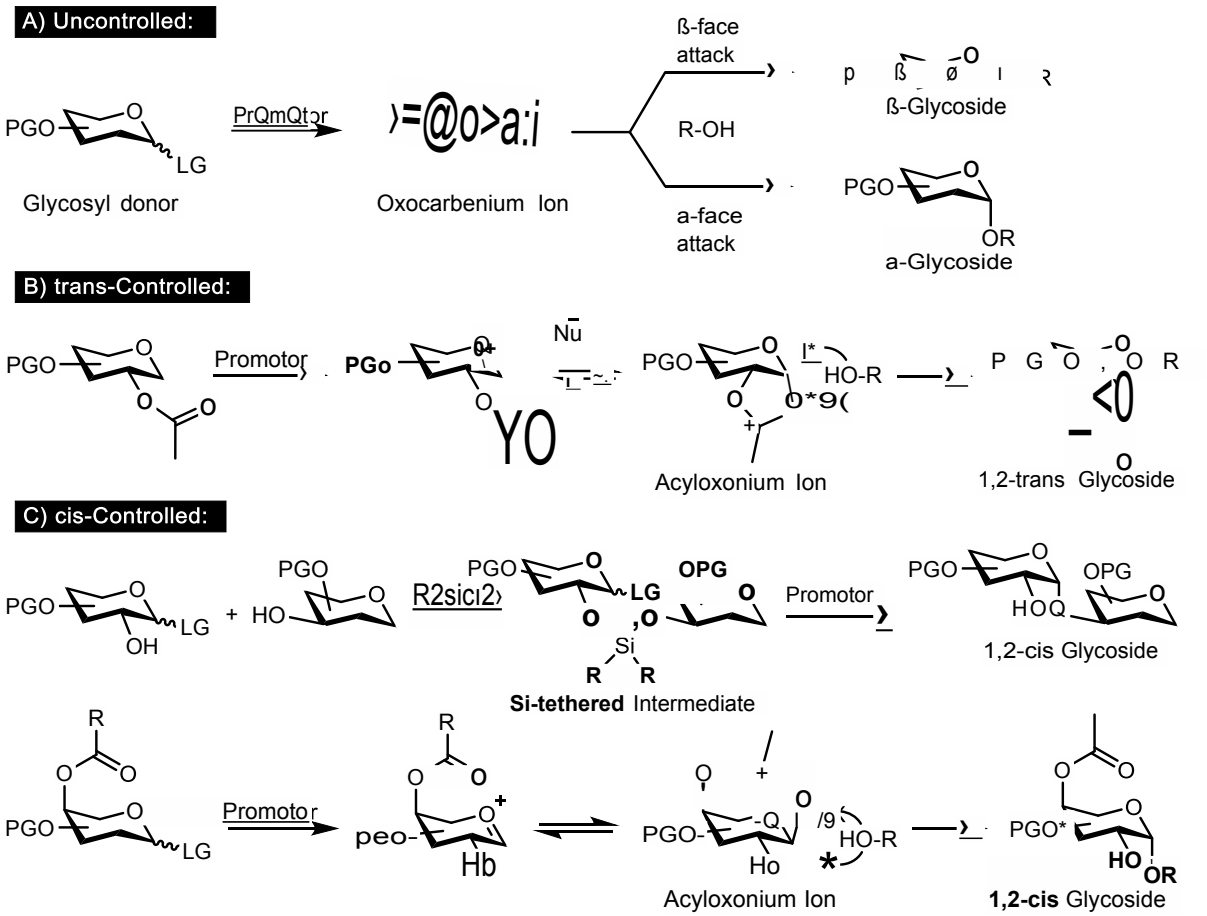

Figure 1.4: Strategies for controlling the outcome in glycosylation reactions.

In a glycosylation reaction, the leaving group at the anomeric position of the glycosyl donor is activated by the promotor in the first step of the process. These promoters are generally salts, Lewis acids and salts or esters of trifluoromethansulfonic acid (Triflates).[36] Some of the most common promoters include: $AgCO_3$, $AgClO_4$ and Ag_2O, NIS/TfOH, Tf_2O, BF_3-Et_2O, $SnCl_4$, AgOTf, TfOH and its derivatives (TMSOTf, TBSOTf and MeOTf), and more recently the use of metal salts such as AgCl, $AuCl_3$ and $CuCl_2$.[37] After the activation, the leaving group is released and an oxocarbenium ion is formed. This ion can be stabilized by adjacent protecting groups and can react with nucleophiles, i.e the hydroxyl group of the acceptor, that approach from either the top or the bottom face giving an α- or β-configured glycosylation product, or a mixture of them.

The selection of the protecting groups; especially of groups able to give neighboring participation is of exceptional importance to induce selectivity during glycosylations. An

ester, amide or carbonate function at the C-2 position of the glycosyl donor can interact with the oxocarbenium ion forming an active intermediate through the formation of a cyclic acyloxonium ion that hinders the attack of the nucleophile from the face that this group is localized (**figure 1.4b**). As a consequence, the attack from the nucleophile (glycosyl acceptor) can take place only from the opposite face forming 1,2-*trans*-products dominantly.[38]

The formation of 1,2-*cis*-linkages such as β-mannopyranosides and α-glucopyranosides is more challenging and require of additional considerations during the glycosylation reactions.[39] Some strategies to increase the selectivity to 1,2-*cis* products are the intramolecular aglycon delivery (IAD),[40] and the use of fluorides and bromides as leaving groups to favor the progress of the glycosylation via a S_N2-type mechanism.[41] Furthermore, the use of remote group participation involving a protecting group at the C-3, C-4 or C-6 position of the glycosyl donor have also been developed over the past years and are nowadays efficiently applied to ensure the synthesis of complex saccharides having 1,2-*cis* linkages (**figure 1.4c**). [42]

Other reaction conditions such as temperature and the presence of certain solvents can favor the formation of an α- or a β-product. Whereas ethers and toluene can interact with the oxocarbenium anion favoring S_N1-type conditions by a so-called inversion of the anomeric effect and support the formation of the thermodynamically stable α-linkages, acetonitrile has been described to induce the formation of an α-nitrilium-nitrile-conjugate with strong activated donors that favors the formation of equatorial β-products.[43]

1.4 Glycophosphatidylinositol (GPI)

Glycophosphotidylinositols (GPI) are complex glycolipids which are attached to the C-terminus of the protein as a posttranslational modification in eukaryotes. The surface of the cell contains many GPI and GPI like molecules such as lipophosphoglycans (LPG) or Glycoinositolphospholipids (GIPL).[44-46] GPIs exist in free form or can be found anchored to proteins. GPIs have a conserved glycan core structure bearing a phosphoethanolamine unit connecting the C-terminus of the protein to the glycan and a lipid attached to the glycan core *via* phoshodiester bond at *myo*-inositol. The GPI anchoring a protein was first identified in 1976 when a novel phospholipase, termed phosphatidylinositol phospholipase C (PI-PLC),

was found to release alkaline phosphatase from tissues. Over the next several years, PI-PLCs purified from other types of bacteria contained similar enzymatic activity and various other proteins could be released from tissues when treated with PI-PLC. This evidence suggested that these proteins are covalently attached to the cell membrane *via* a site on the protein and a phosphatidylinositol moiety embedded in the cell membrane.[47]

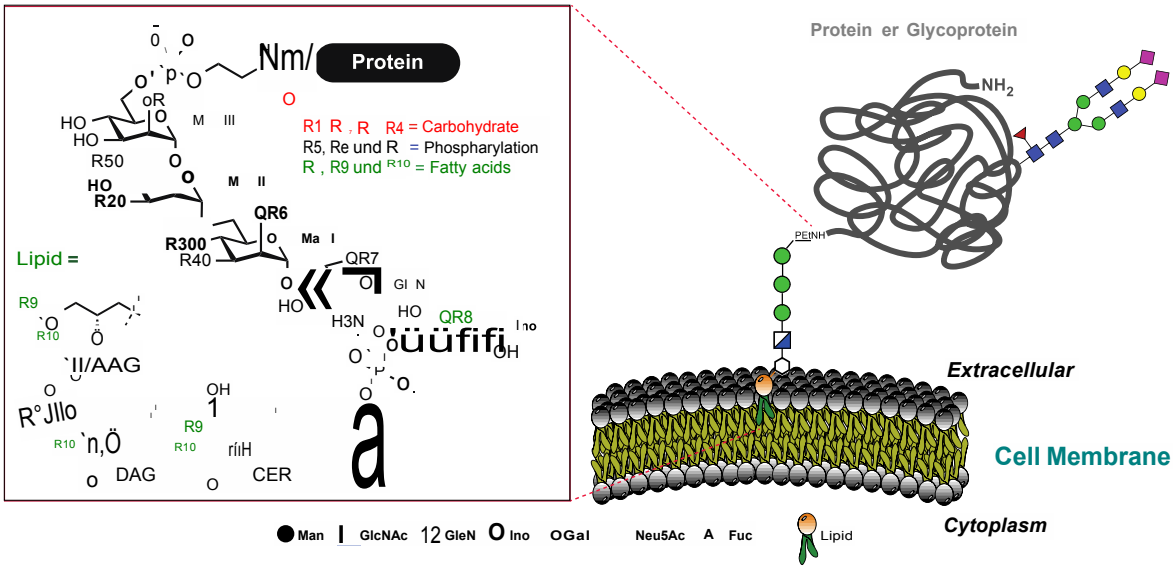

Figure 1.5: Structure and possible modifications found in Glycophosphatidylinositols anchored protein.

The first full structure of a GPI was revealed in 1988 when the GPI anchor of the variant surface proteins (VSGs) of the protozoa *Trypanosoma brucei*was described.[48, 49] Following this report, the GPI structure of the Thy-1 glycoprotein from rat brain[49] and subsequently of various free GPIs and GPI anchored proteins have been isolated from eukaryotes. Approximately 150 proteins are modified with GPI and they play an important role in the embryonic development, immune response and neurogenesis in mammals.[50]

Table 1.1: Structural diversity found in some GPI-anchors

Origin	R^1	R^2	R^3	R^4	R^5	R^6	R^7	R^8	Lipid
L. major PSP[51]	H	H	H	H	H	H	H	H	AAG
P. falciparum[52-54]	±Manα	H	H	H	H	H	H	Acyl	DAG
T. cruzi NETNES[55]	Manα	H	H	H	H	H	AEP	H	AAG
P. communis AGP[56]	H	H	±Galβ	H	H	H	H	H	CER
T. brucei VSG 117[49]	H	H	H	$Gal_{2\text{-}4}\alpha$	H	H	H	H	DAG
T. brucei VSG 121[57]	H	Galβ	H	$Gal_{2\text{-}4}\alpha$	H	H	H	H	DAG
T. gondii[58]	H	H	±Glc-GalNAcβ	H	H	H	H	H	DAG
T. congolense VSG[59]	H	H	Gal-GlcNAcβ	H	H	H	H	H	DAG
Rat brain Thy-1[60]	±Manα	H	GalNAcβ	H	H	PEtN	H	H	n.d.
Hamster brain PrP^{Sc}[61]	±Manα	H	±Sia-±Gal-GalNAcβ	H	H	PEtN	H	H	n.d.
Human CD52[62]	±Manα	H	H	H	H	PEtN	H	±pal.	DAG
Human sperm CD52[63]	H	H	H	H	H	PEtN	H	pal.	AG
Human erythrocyte CD59[64]	H	H	±GalNAcβ	H	PEtN	PEtN	H	pal.	AAG

The positions of the residues R^1 to R^8 correspond to GPI modifications described in **Figure1.5**. AAG = 1-Alkyl-2-acylglycerol; AEP = Aminoethyl phosphonate; AG = 1-Alkyl-2-*lyso*glycerol; DAG = Diacylglycerol; Gal = Galactose; GalNAc = *N*-Acetylgalactosamine; Glc = Glucose; Man = Mannose; n.d. = not determined; Sia = Sialic acid; PEtN: Phosphatidyl ethanolamine.

The GPI glycan core consists of the pseudopentasaccharide α-Man-(1→2)-α-Man-(1→6)- α-Man-(1→4) -α-GlcN-(1→6)-*myo*-Inositol (**figure 1.5**)[47] and is conserved across all species. Diverse site specific modifications and branched structures have been reported for the GPI core. The modifications can be in the form of additional acylations, phosphoethanolamine and additional saccharide units. The most common saccharide modifications include, α-mannosylation of C2 position of ManIII (found in *P. falciparum*), a β-galactose residue at the C3 of ManII and oligosaccharide branching at the C4 and C3 position of ManI. The presence of phospholipid at the C1 position of the inositol is common in all the GPIs (**table 1.1**). A late stage lipid remodeling during the GPI biosynthesis, provides GPIs with a diverse variety of lipids. This diversity includes a diacylglycerol, an alkylacylglycerol, lyso-alkylglycerols and ceramides with alkyl chains of different length and degree of unsaturation.[65] Occasionally, a fatty acid ester is present at C2 position of inositol in addition to the phospholipid (palmitoyl at C2 position of inositol in Malaria GPI). The phosphoethanolamine at C6 position of the ManIII is present in all the GPIs and is involvedin the attachment of the GPIs to the C-terminus of the protein. An additional phosphoethanolamine at the C2 position of ManI is conserved in all mammalian GPIs and at C6 position of ManII in human erythrocyte (CD59).

An aminoethylphosphonate at C6 position of GlcN is found in GPI from *Trypanosoma cruzi*.[66]

1.4.1 Function of GPI-Anchored Proteins

GPI-anchored proteins have been identified in all major cell type and tissues. GPI-anchored proteins vary in size, from the 12 amino acid glycopeptide CD52 to the 175 kDa protein CDw109.[67] GPI-anchored proteins display diverse biological functions. Many of these proteins have hydrolytic and other enzymatic activity, such as alkaline phosphatase, renal dipeptidase and erythrocyte acetylcholinesterase. Certain GPI-anchored proteins are involved in cell-cell interaction and adhesion, such as neural cell adhesion molecule (NCAM) and CD58. CD55 and CD59 are regulatory proteins of the complement system. Immunogenically important GPI-anchored proteins include CD24, CD52 and Thy-1. Folate-binding protein, CD14 and CD16b are the GPI anchored receptors.[45, 68] There are some GPI-anchored proteins that do not yet have an assigned function like the Prion protein.[69] Mutations in GPI-anchored proteins called glypicans can cause defects in cell division and tissue morphogenesis.[70]

GPI-anchored proteins are also essential for the development of roots, pollen germination and synthesis of the cell wall in plants.[71] Arabidopsis has about 250 GP1-anchored proteins that participate in cell wall deposition, defense responses, and cell signaling. Arabinogalactan proteins, a class of heavily glycosylated cell wall proteins are modified by the addition of a GPI anchor as well.[72] The yeast *Saccharomyces cerevisiae* encodes around 50 GPI-anchored proteins out of 6000 proteins, which are essential for cell wall synthesis and growth.[73, 74]

A large numbers of GPI-Anchored proteins are found on the cell surface of protozoa parasites. Examples include the variant surface glycoprotein (VSG) of *Trypanosoma brucei*, gp63 of *Leishmania* spp., circumsporozoite protein (CSP) and merozoite surface protein (MSP) of *Plasmodium* spp., and Ssp-4 of *Trypanosoma cruzi* among others. Some studies have shown that the presence GPI anchors is critical for the survival of these protozoans.[75, 76]

Malfunction in the GPI biosynthesis can lead to some disorder in humans. Paroxysmal nocturnal hemoglobinemia (PNH) is a rare hematopoietic stem cell disorder that arises from a somatic mutation of the phosphatidylinositol glycan-class A (PIG-A) gene.[77-79] Erythrocytes generating from the mutation are particularly vulnerable to lysis mediated by complement system. The gene is essential for the biosynthesis of GPI that serves as an anchor for the

membrane proteins, CD55 (decay accelerating factor) and CD59 (membrane inhibitor of reactive lysis) which are involved in the regulation of the complement system.[80, 81] The PNH cells are characterized by a total or partial lack of the GPI-anchored membrane proteins.[82] Complete deficiency of GPI-anchored proteins is embryonic lethal in mice due to malformation of brain.[83]

1.5 Biosynthesis of GPI-Anchored Protein

More than 150 different human proteins are GPI anchored and more than 40 enzymes are involved in the GPI biosynthesis. GPI-APs are involved in different biological processes and can contain protein- and cell-specific structure. GPI-APs on human erythrocytes have a different lipid structure having three lipid chains, which can be responsible for a more stable association of the plasma membrane and the long life of erythrocytes in the blood.[64, 84] **Figure 1.6** depicts the biosynthetic pathway for GPI-anchored proteins from mammals, *T. brucei*, *P. falciparum* and *T. gondii*.

1.5.1 Biosynthesis of GPI Anchor Precursor

The GPI anchor precursor is synthesized in the endoplasmic reticulum (ER) from phosphatidylinositol (PI) involving at least nine sequential reaction and 18 gene products.[85, 86] The biosynthetic pathway of GPI begins on the cytoplasmic side of ER by the transfer of GlcNAc to PI from UDP-GlcNAc mediated by GPI-GlcNAc transferase to obtain GlcNAc-PI. GPI-GlcNAc is a complex transferase consisting of 6 different PIG proteins and DPM2. PIGA has a catalytic subunit; however the function of the other proteins is not yet clear. The next step is the de-acetylation of GlcNAc-PI to obtain GlcN-PI. This process is mediated by PIG-L, an enzyme with deacetylase activity. Then, the GlcN-PI is flipped to the luminal side of ER by an unknown mechanism and it is probably mediated by a flippase, which has not been identified.[87] In the next step, an acyl chain is added to the inositol from acyl-CoA to obtain GlcN-(acyl)PI mediated by PIG-W with acyltransferase activity.[88, 89] It is followed by the sequential transfer of ManI and ManII from dolichol-phosphate-mannose (Dol-P-Man) to obtain Man-Man-GlcN-(acyl)PI mediated by 1-4mannosyltransferase (PIG-M, PIG-X) and 1-6mannosyltransferase (PIG-V) respectively.[90]

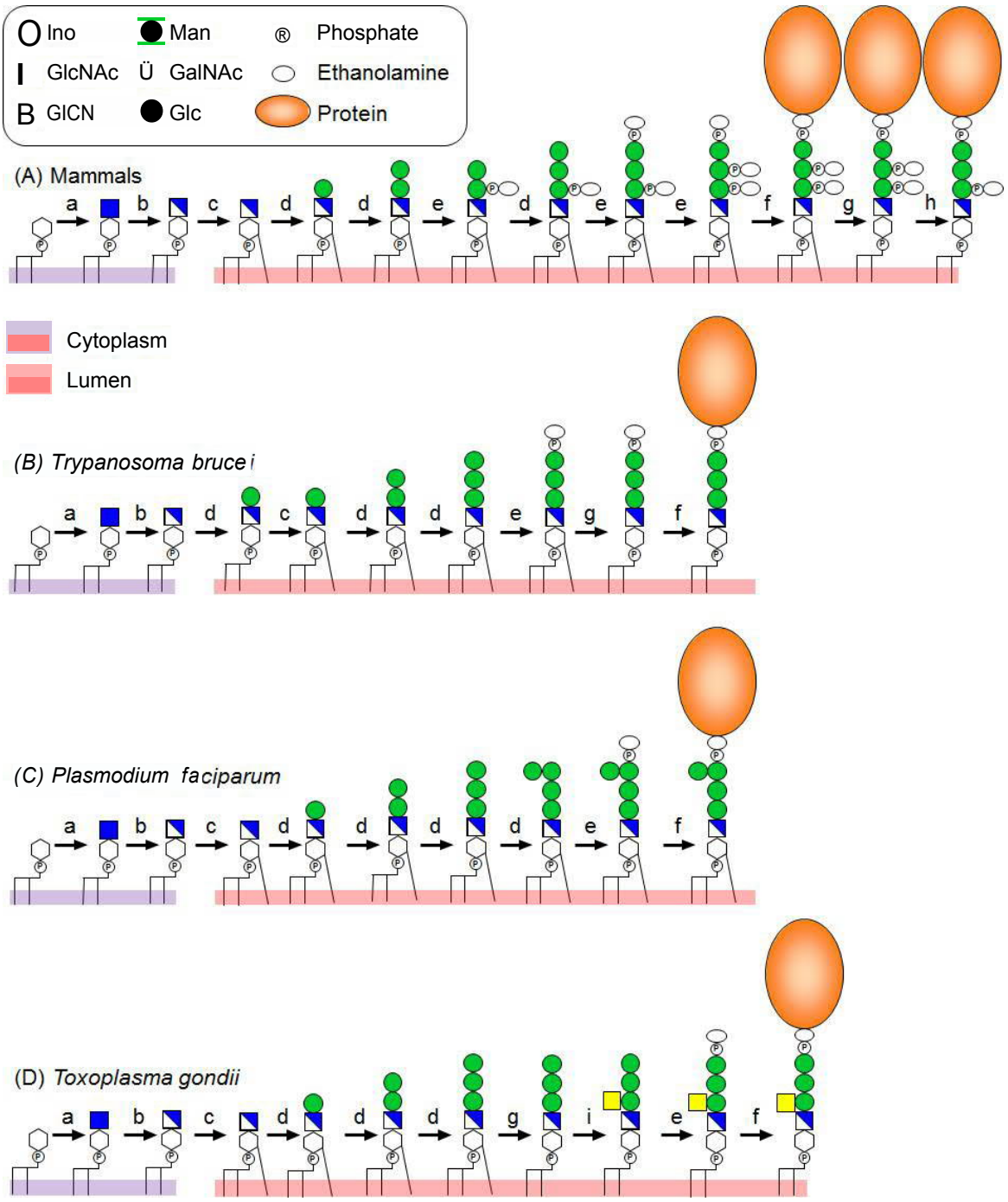

Figure 1.6: Biosynthesis of GPI-anchored protein on ER membrane from (A) mammals, (B) *T. brucei*, (C) *P. falciparum* and (D) *T. gondii*. Enzymes involved in different steps: a) GlcNAc transferase, b) deacetylase, c) acyltransferase, d) mannosyltransferase, e) ethanolamine phosphate transferase, f) transamidase, g) deacylase, h) phosphodiesterase and i) GalNAc transferase.

In next step, the phosphatidylethanolamine (EtNP) side branch is added to the second position of ManI from phosphatidylethanolamine (PE) to obtain Man-(EtNP)Man-GlcN-(acyl)PI and is mediated by GPI-ethanolamine phosphate transferase I (GPI-ETI, PIG-N). This step is only present in mammalian GPI biosynthesis. Next step is the transfer of ManIII from Dol-P-Man to obtain Man-Man-(EtNP)Man-GlcN-(acyl)PI via 1-2mannosyltransferase (PIG-B). Another EtNP is added to ManII via GPI-ETII, (consisting of PIG-G and PIG-F) as a side branch is found in mammalian GPI to obtain the GPI precursor. Finally, the EtPN responsible for making the amide bond between the GPI and the protein is added to ManIII is mediated by GPI-ethanolamine phosphate transferase III (GPI-ETIII, complex of PIG-O and PIG-F)[91](**figure 1.6A**). The addition of ManIV is found in *Plasmodium* GPI biosynthesis to generate GPI-anchor precursor (**figure 1.6C**). In case of *T. gondii, N*-acetylgalactosamine (GalNAc) is attached to the ManI via a β1-4 linkage mediated by GalNAc transferases (**figure 1.6D**).[92]

1.5.2 Posttranslational Attachment of GPI Anchor to Protein

The GPI-anchor precursors are posttranslationally attached to the C-terminus of the protein by the action of GPI transmidase. Proteins to be glypiated N-terminal signal sequence for ER translocation and a C-terminal signal sequence for GPI attachment. Translocation of preproprotein to ER takes place via translocon and is followed by N-terminal signal peptide removal and attachment to GPI. The GPI attachment is catalyzed by transamidase consisting of five proteins (PIG-K, PIG-S, PIG-T, PIG-U and GPAA1).[93]

1.5.3 Lipid Remodeling

Lipid moieties of GPI are remodeled at the ER and Golgi apparatus. After the attachment of GPI to the protein and before the exit from ER, the inositol acyl chain is cleaved by deacylase PGAP1 in most of the cells except from erythrocytic cells and some parasites.[94] The GPI-APs are then transported to the Golgi by secretory vesicles. In the Golgi, GPI-APs undergo lipid remodeling. The unsaturated fatty acid at *sn*-2 position is cleaved and replaced by the saturated fatty acid mediated by GPI specific phospholipase A2 (PGAP3) and reacylation by PGAP2. The fully remodeled GPI-AP are transported and expressed on the cell surface.[94, 95]

In yeast, the lipids of many GPI-anchored proteins are further changed from diacylglycerol to ceramide. It is possible that ceramide remodelase is required for recognizing the EtNP side chain on the GPI as a substrate. Very recently, it has been reported that CWH43 is the enzyme involved for the replacement of diacylglycerol with ceramide in GPI lipid moiety.[96, 97]

1.6 Importance of GPI Anchor

GPI anchoring is the only stable mechanism for the high affinity attachment of the protein to the cell membrane in eukaryotes. Attachment of the protein to the surface of the cell, using a single lipid chain would result in weak interactions and an easy loss of protein in extracellular matrix compared to the GPI anchor with its lipid moiety bearing a ceramide, diacyl or its alkyl, acyl moiety. Hydrophobic interactions between the lipid and the bilayer determine the binding affinity of the GPI anchor and are responsible for the lipid raft formation of the cell membrane.

1.6.1 Lipid Raft Formation

The cell membrane can organize into specialized microdomains, so-called lipid rafts.[98] They are enriched in glycosphingolipids, cholesterol, and certain types of lipidated proteins and serve diverse cellular functions. Owing to the hydrophobic nature of the lipids present in GPI, GPI-anchored proteins have been associated with lipid raft formation. Lipid rafts are formed by the self-association of lipids present in GPI, favored by their long and mostly saturated hydrocarbons that allow them to pack tightly in a bilayer having cholesterol molecules fill the voids between the associating lipids. Due to the tight packing, lipid rafts are less fluid than the surrounding phospholipid bilayer which provides unique physical properties (for details refer to chapter 4).[99, 100]

1.6.2 GPI-AP Degradation

GPI specific phospholipases C and D are responsible for GPI degradation and cleavage. The removal of the GPI anchored protein from the cell surface is a useful immunological or

developmental process that requires adhesive cell contact and can provide terminating signal for GPI anchored protein. GPI-PLD might be responsible for the restriction and regulation of GPI-anchor and can degrade the excess GPI intracellularly which are not used for anchoring to proteins.[101]

1.6.3 Signal Transduction

The GPI anchor can act as mediator between the exterior of a cell and internal signaling molecules. Antibody cross-linking of some GPI-anchored proteins can affect the transduction of cellular activation or inhibition signals, resulting in Ca^{2+} fluxes, protein tyrosine phosphorylation, or cytokine secretion.[102] These signaling are generally not observed with proteins where the GPI anchor has been replaced with a transmembrane domain, indicating that the GPI anchor is crucial for these signaling events. Although the GPI anchor does not completely cross the cell membrane, the transduction of cellular signals could occur through the physical association of the GPI anchor with other transmembrane proteins involved in intracellular signaling. [103, 104]

1.6.4 Prion Disease

Prion disease is characterized by the formation of insoluble protein plaques (PrP^{Sc}) due to the posttranslational misfolding of the GPI anchored Prion protein (PrP^{C}). Although the normal function of PrP^{C} is still unknown, it has been suggested to be a signaling molecule.[69] PrP^{C}, like many GPI-anchored proteins, is able to migrate from one cell membrane to another. This transfer requires direct cell-cell contact, an intact GPI anchor and activation of the protein kinase C. This process permits PrP^{Sc} to infect healthy PrP^{C}-containing cells. At the same time, intercellular transfer of PrP^{C} may allow PrP^{Sc} infected cells to recruit PrP^{C} from healthy cells, providing the infected cells for propagation.[105]

1.7 Chemical Synthesis of GPI

Strategies for the chemical synthesis of GPIs focus in the assembly of glycan core although the core structure for the GPI remains conserved. Different modifications can be found attached to this core structure providing structural diversity to the GPI anchor. The syntheses of natural GPIs have faced several problems, such as the stereoselective construction of the glycan part and the regioselective introduction of different modifications. The chemical challenges, coupled with increasing biological importance of this class of glycoconjugates constituted the main driving force for developing new synthetic strategies toward efficient syntheses of GPI molecules. Various GPIs have been synthesized using different glycosylation and protecting group strategies in either linear or convergent means.[106, 107] In a linear approach, the oligosaccharide is built from individual monosaccharides in a stepwise manner **(figure 1.7A)**. The convergent approach constructs the oligosaccharide from smaller building blocks, which may result in a fewer number of protecting group manipulations within the oligosaccharide chain **(figure 1.7B)**. Generally, all syntheses began with assembly of the glycan, followed by installation of the phosphate groups and a final deprotection. Nevertheless, a general unifying route that enable efficient access to a wide range of GPI anchors has not yet been developed.

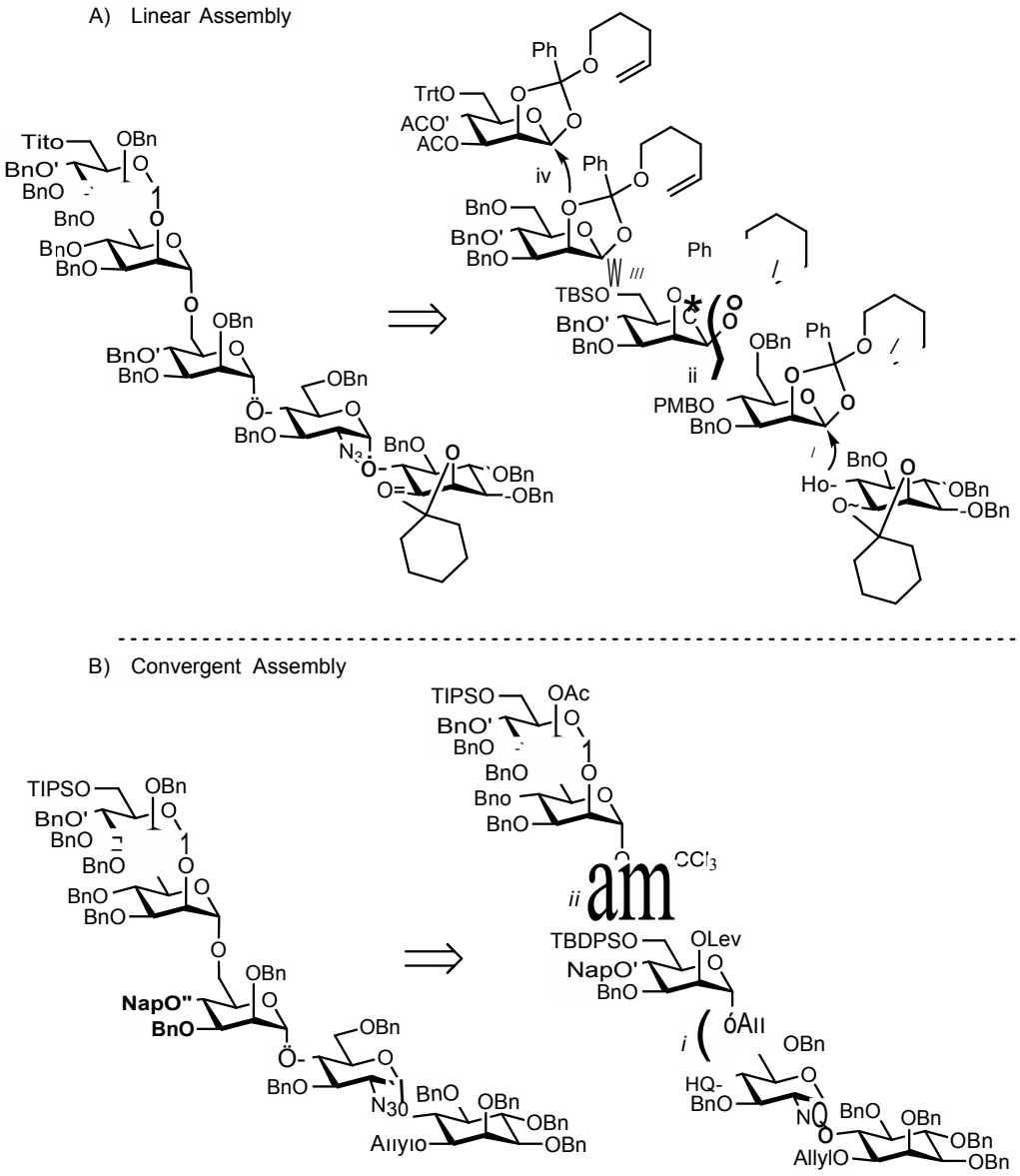

Figure 1.7: Linear and a convergent synthetic strategy of the core from glycosylphosphatidylinositol anchors. a) linear assembly;[106] b) convergent assembly.[107]

1.8 Synthesis of Glycoconjugates

In addition to oligosaccharides and polysaccharides, carbohydrates can also be found forming part of natural glycoconjugates such as glycoproteins, glycopeptides and glycolipids. Therefore, in addition to the synthesis of oligosaccharides, the synthesis of glycoconjugates plays an important role in the elucidation of the biological function of carbohydrates.

Extensive efforts have been made to establish protocols to obtain natural glycoconjugates such as glycoproteins.[108]

Natural glycoproteins exist generally a mixture of molecules having the same peptide sequence displaying diverse oligosaccharide structures at the glycosylation positions. These so-called glycoforms can have different physical and biochemical properties.[109, 110] The carbohydrates are often covalently linked to proteins via a nitrogen or an oxygen atom present in asparagine, serine or threonine residues forming *N*-linked and *O*-linked glycoproteins. *S*-linked, *P*-linked, or *C*-linked glycoproteins also exist but are less abundant.[111] Efforts to develop an appropriate method for the preparation of homogeneous glycoproteins have included molecular biology, chemical synthesis or the combination of both methods.[112]

A plethora of strategies have been investigated during the last years to obtain naturally glycosylated proteins as single glycoforms. However, there is still lack of a suitable and generalized method to obtain these molecules. Some protocols to synthesize natural *O*- and *N*-glycoproteins are fully synthetic strategies that combine carbohydrate and peptide synthesis, or semi-synthetic strategies that required of synthetic peptides and glycopeptides, and of expressed proteins that are connected by chemoselective ligation reactions. But these strategies have been limited to the synthesis of small glycoproteins (generally below 20 KDa).[113-116]

Chemical glycosylation methods and chemoselective reactions are not restricted to the synthesis of natural glycoproteins, they can also be used for generating neoglycoproteins, which are glycoproteins containing unnatural linkages between protein and oligosaccharides. Neoglycoproteins are often selected as the best alternative to investigate the function of carbohydrates because their synthesis is easier to perform and only involve a conjugation reaction of an activated glycan with the lateral chains of amino acids present on a carrier protein.

1.8.1 Synthesis of Neoglycoconjugates

Huge efforts and developments have been made during the last decades to establish strategies for the incorporation of glycans into proteins. Depending on the functional groups present on the glycans and the amino acids involved in the process, in neoglycoprotein diverse types of linkages can be formed between the carbohydrate and the protein (**figure 1.8**).

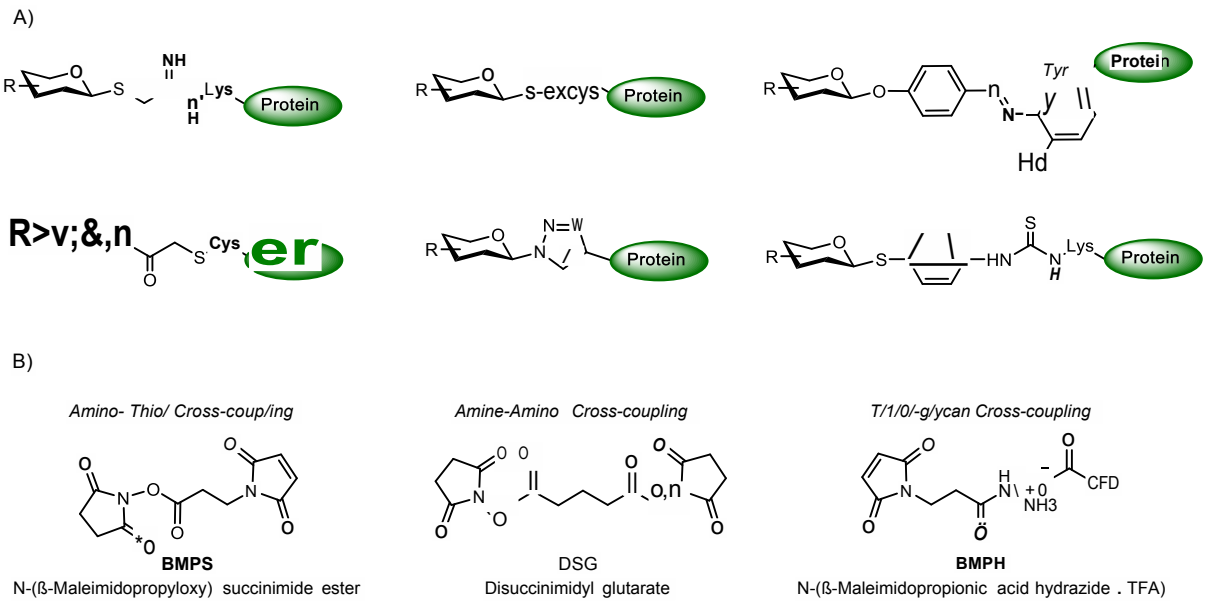

Figure 1.8: Example of linkages used for the synthesis of neoglycoconjugates. a) some typical linkages obtained in neo-glycoconjugates, b examples of linkers using for conjugation of glycans to proteins.

Carbohydrate-proteins linkages have been mostly synthesized by using the inherent reactivity of the amino group of lysine and the thiol of the cysteine side chains to achieve chemoselective reactions (**figure 1.8**).[116, 117] The resulting linkages are usually very different from the linkage in natural glycoproteins and include a spacer, but they are generally stable to biological conditions allowing the biological evaluation of neoglycoconjugates. This strategy has been the favorite strategy applied to use glycoproteins as novel protein based therapeutics, carbohydrate antigen derivatives and immunogens.[118]

Characteristic carbohydrates structures used for the preparation of neoglycoconjugates are glycans present on the surface on many pathogens. During infections, the immune system is activated by these structures inducing a response that can be detected in the form of anti-glycan antibodies. Small, pure oligosaccharides are poor immunogens inducing a low immune response that can be enhanced via the conjugation of glycans to proteins. For the attachment of glycans to proteins, active groups present at the glycan, or introduced as part of a linker at the reducing end, can be used. Commonly, these active groups are used in conjugation processes involving a chemoselective reaction with the natural functional groups present on

the protein or with functional groups introduced by site-specific modifications and mutations of the protein.[119]

For the application of neo-glycocojugates as immunogens, the presentation of multiple copies of the carbohydrate structure is also required to facilitate the interaction of the glycans with the immune system. In the development of carbohydrate vaccines, protein glycoconjugates are formed using immunogenic active carrier proteins such tetanus toxoid or to its nontoxic variant CRM197 to increase and facilitate the presentation of the glycans to the immune system inducing a specific response to the glycan (**figure 1.9**). Using these strategies diverse carbohydrates-based vaccines have been designed and are under development.[120, 121]

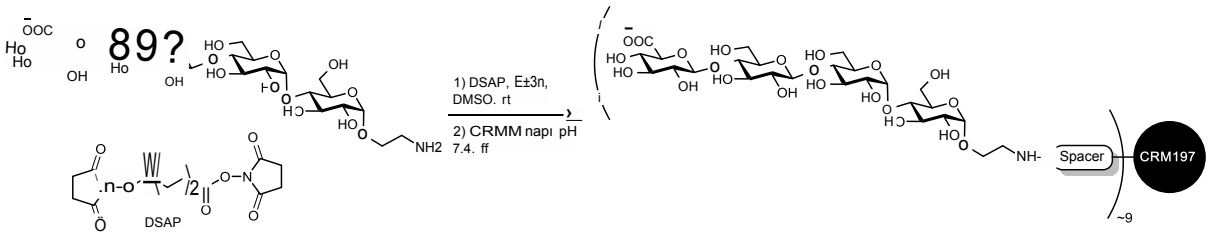

Figure 1.9: Synthetic glycoconjugates vaccine for *S. pneumonia* (ST8)[120]

Similar to natural glycoproteins, the main limitation and in general of the protein neo-glycoconjugates is the formation of heterogeneous mixtures of products, in this case having a protein modified with a variable number of glycans at different positions (amino acids) on the sequence. This heterogeneous modification of activated proteins results from the distinctive accessibility of the active groups on the protein surface for the reaction with the synthetic glycans. The lack of homogeneity hinders the determination of thermodynamic and kinetic parameters of binding events between glycoconjugates and proteins by SPR, ITC or any other method.[122] A requirement that certainly has to be fulfilled to conduct the aforementioned experiments is access to pure and defined glycoconjugates and their corresponding derivatives.

1.8.2 Synthesis of Natural Glycoconjugates

The synthesis of glycoconjugates having natural bonds and site-specific modifications is demanding and has required the development of multiple strategies. These strategies are specific for the formation of the linkage between glycan and protein for delivering O- and N-glycoproteins and to the lipids by forming glycolipids. Whereas, in O-glycoproteins glycans are attached to serine or threonine residues, in N-glycoproteins the glycans are attached to asparagine residues in the consensus sequence Asn-Xxx-Ser/Thr, Xxx being any amino acid other than proline.

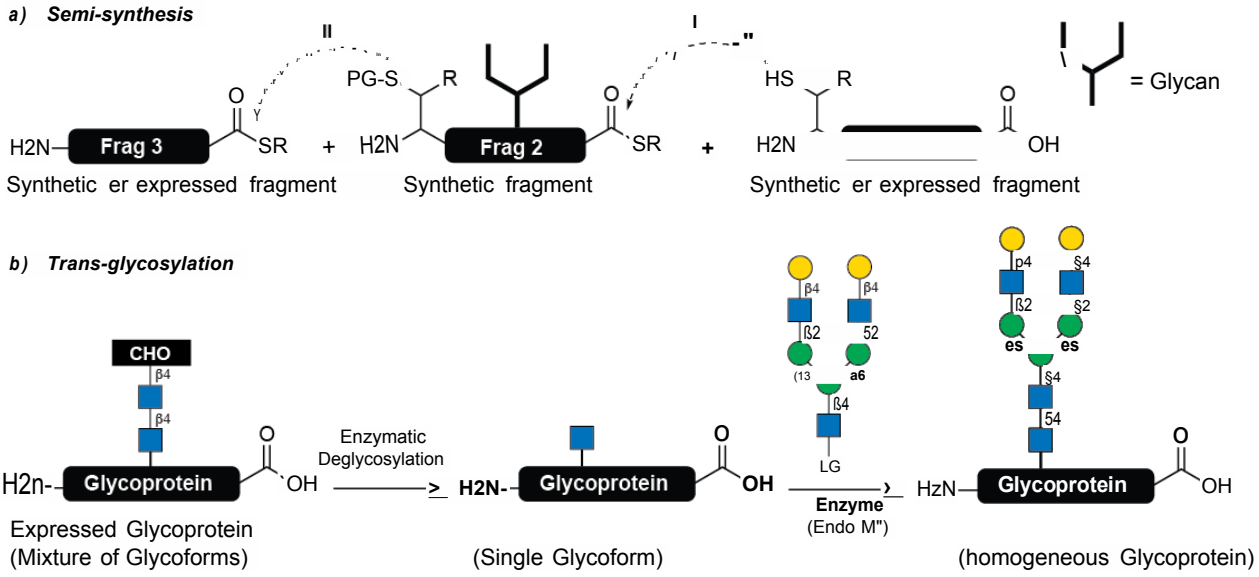

Figure 1.10: Strategies for the semi-synthesis of homogeneous glycoproteins. CHO: mixtures of structures.

N-glycoproteins are accessible via expression systems in cells lines such as Chinese Hamster Ovary cells (CHO), Human Embryonic Kidney (HEK) cells or other human cell lines. However, due the difficult control of the cell glycosylation machinery, which is out of genetic control, the expressed proteins are generally isolated as a mixture of glycoforms. Therefore, investigations aimed to investigate the role of single glycan structure on proteins, require of additional strategies.[108] Proteins synthesis and semi-synthesis have emerged as suitable strategies to obtain well-defined glycoproteins.[108] In these strategies, synthetic peptides or expressed protein fragments are ligated with synthetic glycopeptides having a defined glycan structure.[123, 124]

Chemical Synthesis of glycoproteins has been accomplished using active peptide and glycopeptide fragments, which are sequentially connected to a full sequence glycoprotein using ligation reactions.[108] Among the different ligation reactions, the native chemical ligation has been the preferred method.[125] In this strategy, the peptide are obtained as peptide thioester, or as peptide thioester precursors. These peptide thioesters can undergo a two-step chemoselective reaction with peptides having an *N*-terminal cysteine residue, which end with the formation of a native peptide bond between the *C*-terminal amino acid and the cysteine. If the synthesis of the glycoprotein requires more than two peptides, which is generally the case, peptides or glycopeptides can be obtained having a protected cysteine at the *N*-terminus that is deprotected after the first ligation is completed (**figure 1.10a**). Recently, a strategy involving the use of thioester precursors that are activated after a completed ligation has been established.[126]

In addition to glycoprotein semi-synthesis, the use of enzymes for glycan remodeling and for transferring glycans to a protein having a monosaccharide precursor, trans-glycosylation, are becoming useful methods (**figure 1.10b**).[127] The glycoproteins are generally expressed on cell lines and are treated with an endoglycosidase that cut the glycans leaving only a glucosamine unit attached to the protein. This glucosamine is used as an acceptor for the transfer of an oxazoline activated synthetic glycan having in the next step.[128] Noteworthy here is the use of glycan endoglycosidase that has been mutated to act as a glycosyltransferase.[129]

1.9 Aim of the Thesis

Glycophosphatidylinositols (GPIs) are an important class of glycolipids present at the surface of all eukaryotic cells, especially of protozoa parasites. They play an important role in the activation of the immune system during parasitic infections and have been considered as potential vaccine candidates against malaria infection. There is still a need to understand the role of different components of the glycolipid glycan core and its modifications in the activity of these molecules and on the effect of glypiation to protein structure and function.

The main objective of this thesis is to apply chemical synthesis to obtain GPIs and GPI-derivatives to investigate the role of GPIs, with and without attachment to a protein, on the activation of the immune system during malaria. To gain insight into the importance of GPIs

as an antimalarial vaccine candidate, a strategy will be designed to synthesize a library of GPI fragments to generate glycoconjugate vaccine candidates. This library may provide specific immunogenic epitopes present in the structure of GPI from *Plasmodium*. The synthesised glycans will be conjugated to the CRM_{197} carrier protein and tested for immunogenicity and efficacy as antimalarial vaccine candidates in an experimental cerebral malaria (ECM) model using C57BL/6JRj mice.

To investigate the role of protein glypiation in malaria, chemical synthesis will be also used to synthesize a GPI anchored protein from *P. falciparum* in a homogenous form. Two fragments are necessary to complete this semi-synthesis, an expressed active proteins and a GPI anchor containing a cysteine residue. The synthesis of the glycolipid will be completed using an established strategy involving a phosphorylation with cysteine-containing unit. After the ligation of the protein and the GPI, this glypiated protein will be use to obtain information about the biological functions and structure-activity relationship of the GPI-anchored proteins and the GPI structure. In vitro assays will be used to obtain information about the role of the glycolipid in the activity of the GPI-anchored protein and thereby improve the understanding of GPI anchor on the activity of proteins from *Plasmodium*.

Since GPIs are also involved in the formation of microdomains on the cell membrane which are responsible for cell signaling. Lipidated, synthetic GPI derivatives are also good tools to investigate the correlation between GPI composition and structural arrangement of GPI in model membranes. In this work, a set of structures having different glycans and lipids composition will be synthesized and used in biophysical studies towards the formation of substructures in monolayers at the water/air interface using GIXD. The monolayer structure parameters will be determined by using GIXD measurements using the tilt angle of the alkyl chains to determine the change in the packing and organization of the glycolipids.

2 Synthesis and Immunological Evaluation of Glycoconjugates from the GPI of *P. falciparum*

2.1 Introduction

Malaria is a serious and often a fatal disease caused by a protozoan parasite of the genus *Plasmodium*. It is a vector borne disease that affects humans and is a major health threat to developing countries. According to a 2016 WHO report, nearly half of the world's population is at risk of malaria infection, especially children and pregnant women in sub-Saharan Africa.[130] In 2016, 216 million cases of malaria and 445 000 deaths were reported and is thus becoming a major contributor to the global burden of infectious diseases.[131] The disease is transmitted to humans by the bite of an *anopheles* mosquito infected with one or more of the four species of *Plasmodium: P. falciparum*, *P. vivax*, *P. ovale* or *P. malariae*.

Malarial infections can be classified as either complicated or uncomplicated and are generally accompanied by symptoms that include fever, headache, weakness, muscle ache, vomiting cough and abdominal pain. While, uncomplicated malaria can be treated with the anti-malarial drugs such as artemether, dihydroartemisinin and quinine, humans affected by complicated malaria require strong drug cocktails for the treatment which usually consist of a combination of antimalarial drugs, but the patients are at a higher risk of renal failure, respiratory disease, pulmonary edema and siezures.[132] Furthermore, young children, the elderly and immunosuppressed people are at higher risk of severe malaria. The most severe form of malaria, cerebral malaria, is caused by *P. falciparum* which can lead to death.

The treatment of *P. falciparum* is becoming more complicated due the emergence of drug resistant parasite strains. Thus, there is an urgent need for new therapeutics and the development of a vaccine.[133]

2.1.1 Life Cycle of *Plasmodium*

The *Plasmodium* parasites develop in both, human and mosquito. The life cycle of the parasite comprises of two stages: a sexual stage that takes place in the mosquito and an asexual stage that takes place in the host (**figure 2.1**). The life cycle starts with the bite of an infected mosquito, injecting *Plasmodium* parasites in the form of sporozoites into the host bloodstream. These sporozoites move to the liver and invade hepatocytes. This is called the pre-erythrocytic stage and lasts about two weeks. During this time sporozoites multiply asexually in the liver without inducing any symptoms of malaria.

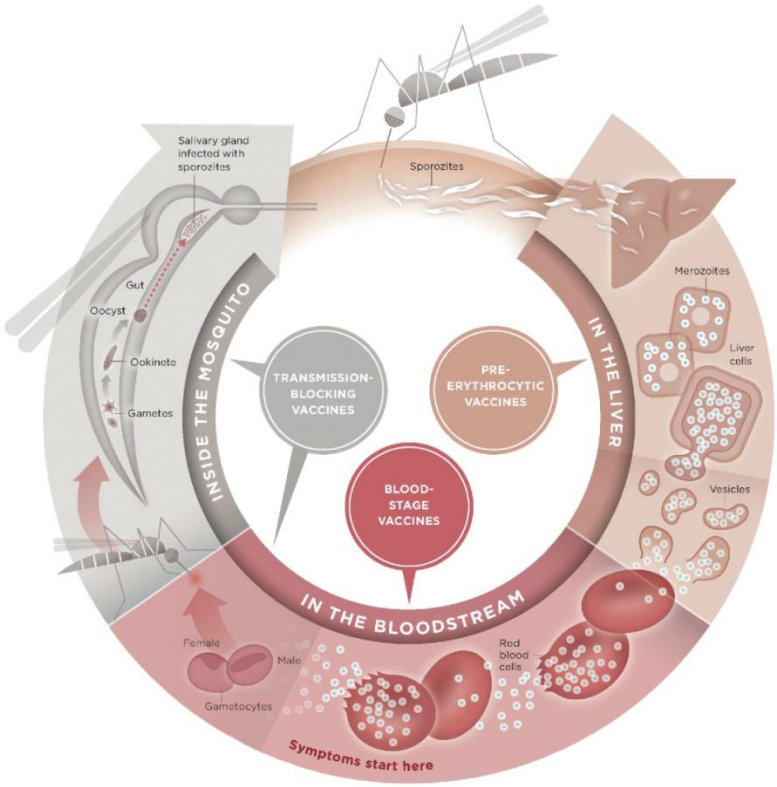

Figure 2.1: The life cycle of a *Plasmodium* parasite divided into the liver, bloodstream and mosquito stages.[134] Copyright (2009), with permission from Oxford University Press.

The erythrocytic stage begins with the release of parasites from the liver into the bloodstream in the form of merozoites. These merozoites invade red blood cells, multiply exponentially, and then burst from cells to invade other erythrocytes thus causing the symptoms of malaria.

Some of the infected red blood cells leave the cycle of asexual multiplication and these merozoites are either already setup or develop into male and female gametocytes that circulate in the blood stream. These gametocytes are taken up by mosquitoes during the bite. After a female *Anopheles* mosquito has ingested the blood from an infected person, the gametocytes develop into mature gametes. The fertilized female gametes develop into mobile ookinetes and burrow through the midgut to form oocyts in the lining of the gut. The oocysts eventually burst and release sporozoites that enter the salivary glands, which can be transferred to the host starting the cycle of infection again.[135]

The parasite is exposed to the immune system for a short time and only in the blood stage of infection. The symptoms of infection also begin during this stage of the parasite's life cycle. Therefore, efforts have been focused on developing a vaccine against this stage of the infection. This would limit the parasite growth and hence minimize the disease.[136]

2.1.2 Current Vaccine Candidates

A lot of protective measures have been taken to control malaria by reducing the number of yearly infections, but readication may only be achieved by a vaccine. Thus, a global interest in developing a vaccine for malaria has drastically increased over the past decade. Most of the tested vaccine candidates contain attenuated microbes, killed microbes or protein subunits which target either the pre-erythrocytic stage, blood stage or the transmission stage of infection.[137] The progress towards different malaria vaccines is shown in **table 2.1**.

The most effective and advanced vaccine against malaria is the RTS,S, a pre-erythrocytic vaccine that targets the circumsporozoite protein (CSP) of *P. falciparum*. This vaccine was developed by GlaxoSmithKline Biologicals and the Walter Reed Army Institute of Research.[138] The RTS,S vaccine is composed of the repeated (R) and carboxy-terminal (T) segments of the *P. falciparum* circumsporozoite (CS) protein fused to the hepatitis B surface (S) antigen. By expression of the CS fragments and the hepatitis B surface (S) antigen in yeast, these two proteins assemble into particulate structures RTS,S.[138] The RTS,S antigen was first formulated in combination with adjuvant AS02A, which is composed of an oil-in-

water emulsion and the immunostimulants, mono-phosphoryl lipid A and QS21.[139] During a series of trials, RTS,S/AS02A showed efficacy of up to 66% protection against infection.[140]

Table 2.1: **Current malaria vaccine candidates in clinical or preclinical trials** classified on the basis of infection stage.[141]

Parasite stage	Vaccine	Classification	Status
Pre-erythrocytic	PfSPZ	Whole organism (radiation attenuation)	Phase II
Pre-erythrocytic	GAP	Whole organism (genetic attenuation)	Phase I
Pre-erythrocytic	RTS,S	Subunit	Phase IV
Pre-erythrocytic	CVac	Whole organism (chemical attenuation)	Phase I
Erythrocytic	AMA1-RON2	Subunit	Preclinical
Erythrocytic	PfRH5	Subunit	Phase I
Transmission	Pfs25	Subunit	Phase I
Transmission	Pfs230	Subunit	Phase I
Transmission	Pfs47	Subunit	Preclinical

In 2009, Sacarlal et al. reported a follow up study on the immunization of African children between 1–4 years of ages with RTS,S/AS02A. In the first six months after immunization, the vaccine showed efficacy of 30% against clinical malaria, 45% against infection and 58% against severe malaria. After 45 months of immunization, the people that received the vaccine showed a lower level of parasitemia compared to control groups indicating significant vaccine efficacy.[142]

In order to improve the efficacy of the adjuvant, a new formulation was carried out having AS01B adjuvant with liposomes instead of the AS02A. Kester et al. compared the vaccine with both the adjuvants (RTS,S/AS02A and RTS,S/AS01B) in terms of immunogenicity and short- and long-term efficacy in healthy and malaria-naïve adults. Using these adjuvants the RTS,S/AS01B vaccine showed an increase in efficacy of up to 50%, however, this is not significantly different from 32% efficacy obtained with RTS,S/AS02A.

The RTS,S/AS01B vaccine also showed greater antibody response against circumsporozoite protein (CSP) as compared to the other adjuvant, providing better understanding of the mechanism of the observed protection. This is an encouraging result, but this vaccine has only

been used in combination with other drugs to fight infection. Thus, a vaccine with higher efficacy that can be used alone is still required to control malaria and to combat infection.

2.1.3 Malaria and GPI

An antitoxin vaccine represents an alternative approach to target malarial pathogenesis in the host.[143] Glycophosphatidylinositol (GPI), a glycolipid present on the surface of the parasite, has been identified as a prominent toxin in malaria that is highly conserved across the different species of *Plasmodium*. These GPIs are found both in free form as well as anchored to the C-terminus of proteins and constitute up to 90% of the protein glycosylation on the membrane of the parasites.[144, 145] *P. falciparum* synthesizes GPIs in all stages of its life cycle and this GPI biosynthesis is important for the development and survival of the parasite.[146]

The structure of the GPI of *P. falciparum* consists of a conserved *pseudo*-pentasaccharide core structure and an additional mannose attached to the terminal mannose at the non-reducing end. Additionally, wide heterogeneity is present on the lipid component attached to the inositol. *P. falciparum* GPIs are additionally acylated with palmitate (90% of the time) in most cases but occasionally with myristate (10% of the time) at the C-2 position of the inositol (**figure 2.2**).

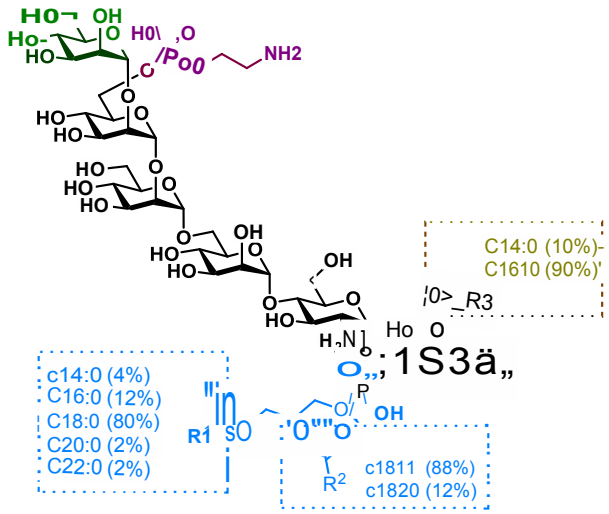

Figure 2.2: **Structure and possible modifications of the GPI from *P. falciparum***. The heterogeneity in the lipid moeity is expressed in percentage.

The phospholipid attached to the inositol is a diacylglycerol having alkyl chains of different length and degree of unsaturation depicted in **figure 2.2**. The GPI structure is highly conserved across the different *Plasmodium* species.[54]

GPIs have been shown to activate and induce the production of inflammatory cytokines in macrophages during malarial infection. Schofield et al. used parasite fractions enriched with GPIs to induce the production of TNF-α and IL-1 in macrophages from mice.[147] Furthermore, diverse studies have shown the presence of anti-GPI antibodies in the sera of patients from malaria endemic regions[148, 149]and the toxic activity of GPIs that are released into the blood stream during infection. The toxicity of these GPIs can be blocked by using GPI mediated signaling and monoclonal antibodies.[150] Thus, there is a growing interest in understanding the role of the immune response against GPIs in protection against malaria.

2.2 Synthetic GPI as Potential Anti-malarial Vaccine

Earlier studies showed that isolated GPI can induce an immune response in both rodents and humans suggesting the use of GPIs as a candidate for the development of anti-malarial vaccines.

2.2.1 Evaluation of GPI Conjugates as a Malaria Vaccine Candidate

In an initial report, Schofield et al. described the generation of a non-toxic *P. falciparum* GPI glycan derived from chemical and enzymatic hydrolysis of native GPI.[151, 152] The chemical structure of this molecule was characterized by the protein of a cyclic phosphate at the inositol residue as a product of phospholipase C action (**figure 2.3A**).[153] This semi-synthetic GPI was treated with 2-aminothiolane to obtain a thiol modification that was conjugated to a maleimide-activated carrier protein, keyhole limpet hemocyanin (KLH). This glycoconjugate was directly used to immunize mice (**figure 2.3B**).

This glycoconjugate was immunogenic and the mice were substantially protected against severe malaria with a survival rate of around 75 %, after two weeks of the parasitic challenge. Interestingly, the parasitemia did not change during the infection, indicating that the generated anti-GPI antibodies neutralized the toxin without killing the parasite (**figure 2.3C and D**).

This vaccine is still under development for clinical use,[154] however, these results provided strong evidence of the role of GPI as a dominant toxin during *P. falciparum* infection.

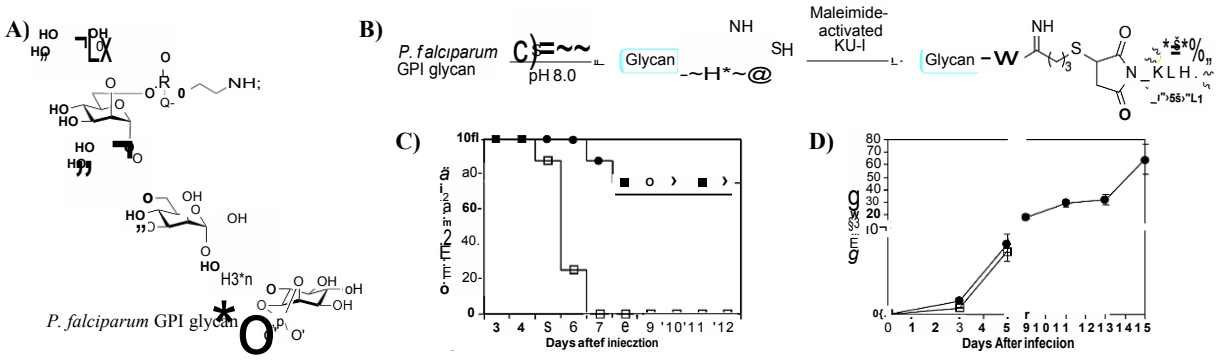

Figure 2.3: **Immunization with the synthetic GPI protects against murine cerebral malaria**. **(A)** Synthetic *P. falciparum* GPI glycan used as immunogen; **(B)** synthesis of *P. falciparum* GPI glycan-KLH conjugate; **(C)** Kaplan-Meier survival plot and **(D)** mice parasitemias post infection of KLH-glycan immunized (closed circles) and sham-immunized (open squares) mice.[153]

2.2.2 Study of the Anti-GPI Antibody Response using Microarrays

Several studies have used isolated GPIs to study the anti-GPI antibody response in malaria.[149, 155-157] The results obtained from this research were contradictory, some studies showed significant association of anti-GPI IgG response with infection[158, 159] and others did not show any relationship.[148] On the other hand some reports described the GPI glycan as the dominant epitope of the glycolipid; whereas others described the lipid part as the dominant epitope in GPI activity. The discrepancies in these results can be attributed to the difference in the composition and purity of the isolated GPIs.

In order to address this problem, a library of GPI glycan fragments of different lengths was synthesized and printed on glass slides (**figure 2.4**).[160] The obtained glycan array was used to evaluate the presence of anti-GPI antibodies by recognizing the synthesized glycans. This experiment helped to determine the epitope that was responsible for inducing the immune response and the production of specific anti-GPI antibodies in malaria. The results showed the pentasaccharide as the minimum epitope recognized by anti-GPI antibodies in sera. A comparison between the fragments with and without Man_4 identified the fourth mannose as a key recognition element for the binding of anti-GPI antibodies. The phosphoethanolamine

unit at Man_3 did not show any significant effect on the binding. Although this study did not provide any information about the role of the lipid part, it was able to provide better insight into the role of the glycan moiety in antibody development during malaria infection.

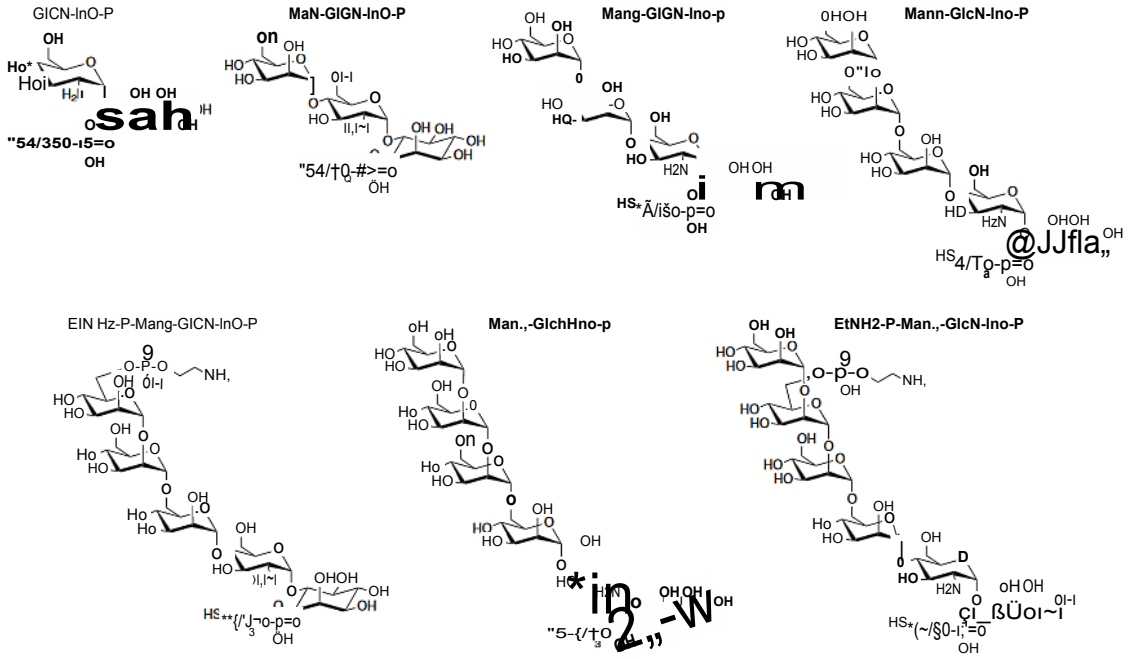

Figure 2.4: **Synthetic *P. falciparum* GPI glycan fragments** used for studying anti-GPI antibody response on microarrays.[160]

2.3 Design of Epitopes

Based on the structural information of the *P. falciparum* GPI and results from previous studies on the microarray, a new library of GPI-fragments was designed to expand the investigations on the role of the GPI glycan in malaria. This new library was designed to study other fragments of GPI and to understand the importance of the *myo*-inositol and phosphoethanol amine unit on the immunogenicity of GPIs and in the anti-GPI antibody response observed during the parasite infection. This library would also provide better insight into the role of the GPI modification as immunogenic epitopes.

Six synthetic GPI fragments with different frameshifts were designed having a terminal thiol group for conjugation with a carrier protein for immunization experiments. The fragments **GPI 1–4** were designed without the *myo*-inositol moiety whereas **GPI 1** and **GPI 3** were designed without the phosphoethanolamine unit. **GPI 6**, containing the core structure and the terminal thiol at the phosphodiester linker at the inositol part of the structure was used as a reference. The thiol linker was used to retain the amine intact during the conjugation and was installed at the reducing end of the glycans to keep the natural orientation and presentation of the GPI glycan structure on the cell membrane.

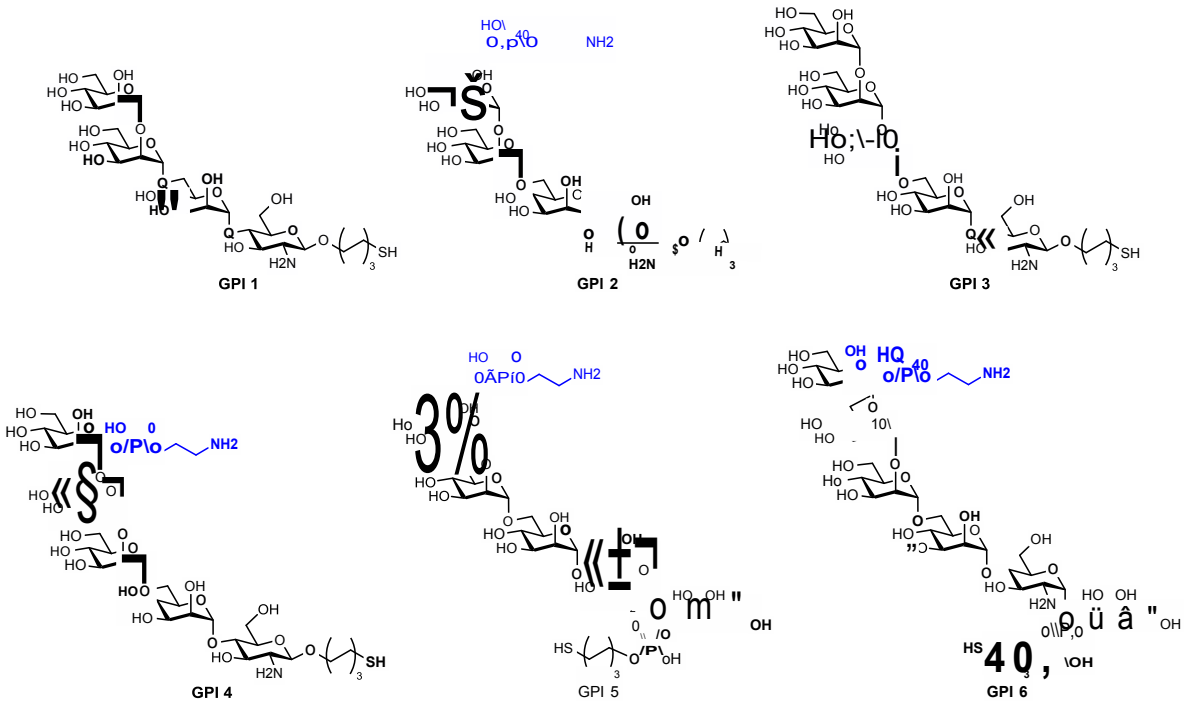

Figure 2.5: **Designed *P. falciparum* GPI fragments** for the conjugation to CRM_{197} carrier protein and for immunization studies.[†]

GPI conjugates in previous studies used KLH as carrier protein and Freund's adjuvant to enhance the immunogenicity of the glycoconjugates. However, Freund's adjuvant is not feasible for use in humans due to its high toxicity; however, the combination of CRM_{197} and alum adjuvant is approved and widely used in the development of vaccines. CRM_{197}, a non-toxic variant of the tetanus toxoid, was selected as the carrier protein for the synthesis of the

[†] Fragment **GPI 5** and **GPI 6** were synthesized by Dr. Ivan Vilotijevic and Dr. Daniel Varon Silva.

glycoconjugates with all GPI fragments. Alum was selected as adjuvant for the immunization experiments in the murine model against cerebral malaria.

2.4 Retrosynthetic Analysis

The synthesis of **GPI 1**–**4** was designed using a strategy that required common building blocks (**2-6**, **2-7** and **2-8**) for the assembly of the glycans and installation of phosphoethanolamine at the last stage of the synthesis. The phosphorylation step would be omitted in the synthesis of **GPI 1** and **GPI 3** so they would not contain phosphoethanolamine residue. A common synthetic approach can be used to synthesize all the fragments. **Figure 2.6** shows the synthetic pathway designed for all the fragments using **GPI 4** as example.

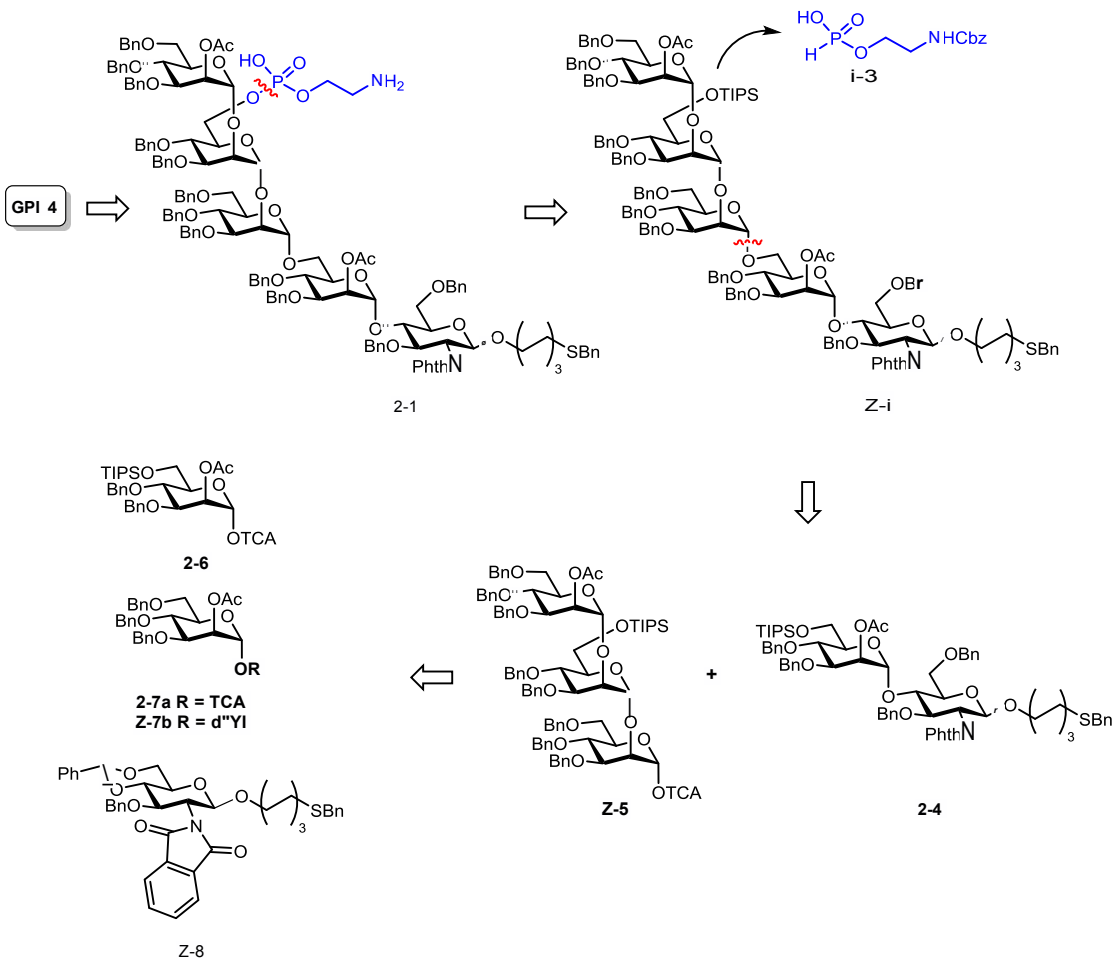

Figure 2.6: **Retrosynthetic analyses for GPI 4 employing [3+2] glycosylation strategy.**

The assembly of fragment **GPI 4** was considered with a terminal stage phosphorylation using *H*-phosphonate **2-3**. The TIPS group was considered as an orthogonal protecting group to introduce the phosphate; acetyl and phthalimide were employed at C-2 to obtain stereoselectivity during the glycosylation reactions. To obtain **GPI 5**, a [3+2] glycosylation strategy with building blocks **2-4** and **2-5** was considered. All the fragments could be obtained by using two mannose building blocks (**2-6** and **2-7**) and a glucosamine building block (**2-8**).

2.5 Results and Discussion

The mannose building blocks (**2-6** and **2-7**) were synthesized according to established protocols previously reported by our group.[161] The synthesis of the other fragments was divided into the synthesis of disaccharide and trisaccharide fragments, which were then used for glycosylation to obtain the desired GPI fragment for the immunological study. The use of the more traditional amine-functionalized linker for conjugation was avoided because of the presence of amine functionality on the GPI fragments, hence requiring additional protection steps prior to conjugation of the fragments. A thiol group can be chemoselectively coupled to carrier proteins in the presence of an amine.[162-164] Thus, the fragments were synthesized having a thiol linker at the reducing end of the glycans.

2.5.1 Synthesis of Glucosamine Building Block

The synthesis of fragments **GPI 1** to **GPI 4** started with the production of the protected glucosamine building block from commercially available glucosamine hydrochloride **2-9** as shown in **scheme 2.1**. Glucosamine **2-9** was treated with sodium methoxide and phthalic anhydride to protect the amine as a phthalimide and at the same time introduce a participating group at the C-2 position to facilitate high stereoselectivity at the anomeric position during glycosylation. The following acetylation with acetic anhydride and pyridine provided the peracetylated intermediate that was converted into thioglycoside **2-10**, stereoselectively as solely the β isomer, using 2-methyl-5-*tert*-butyl-thiophenol and BF_3-Et_2O as the Lewis acid activator. The obtained thioglycoside was deacetylated using freshly prepared sodium methoxide and the 4-*O* and 6-*O* positions of the resulting triol were blocked by the formation of 4,6-*O*-benzylidene acetal **2-11** using benzaldehyde dimethyl acetal and CSA. The free 3-*O*

position of **2-11** was benzylated using NaH and BnBr to obtain **2-12** in 63% yield. Due to the presence of thiol ether in the linker, the thioglycoside could not be used directly for glycosylation as it could interfere in the glycosylation reaction. Therefore, the thioglycoside was converted into imidate donor **2-13** by hydrolysis with NIS and H_2O followed by conversion of the hemiacetal into imidate **2-13** using trichloroacetonitrile and DBU. The obtained imidate donor **2-13** was used to glycosylate the thiol linker (6-(benzylthio)hexan-1-ol) using TMSOTf as activator to obtain the β-isomer of glucosamine building block **2-8** in 87% yield.

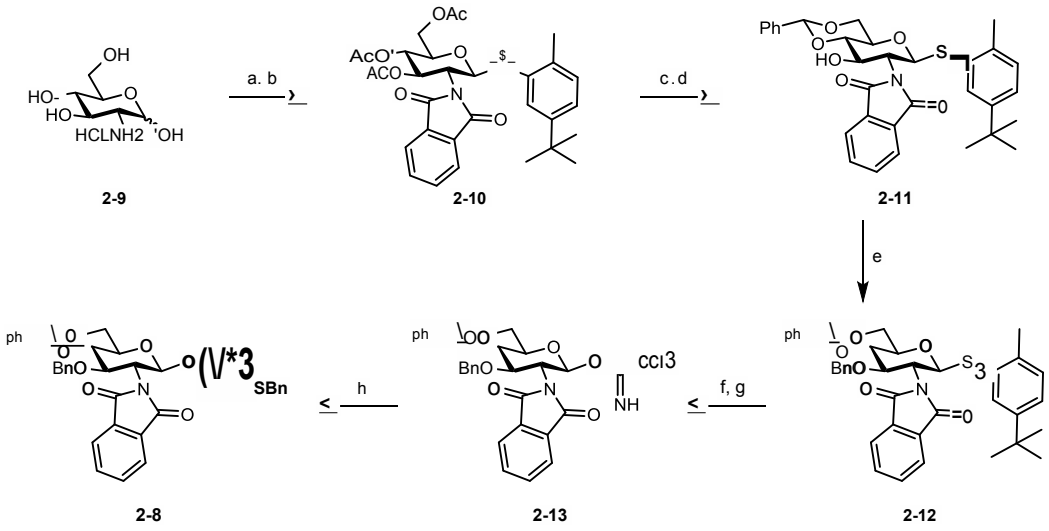

Scheme 2.1: Synthesis of glucosamine building block 2-8. a) i. NaOMe, phthalic anhydride, MeOH, rt, 16 h; Ac_2O, pyridine, rt, 12 h, 64%; b) 2-Methyl-5-*tert*-butyl-thiophenol, BF_3–Et_2O, CH_2Cl_2, rt, 12 h, 77%; c) NaOMe, MeOH, rt, 1 h, quant.; d) $PhCH(OMe)_2$, CSA, CH_3CN, rt, 3 h, 59%; e) NaH, BnBr, DMF, rt, 12 h, 63%; f) NIS, acetone-H_2O (9:1), rt, 2 h, 93%; g) CCl_3CN, DBU, CH_2Cl_2, 0 °C, 1 h, 65%; h) 6-(benzylthio)hexan-1-ol , TMSOTf, CH_2Cl_2, -40 °C to -20 °C, 1 h, 87%.

2.5.2 Synthesis of Disaccharides

The mannose α–(1→4) glucosamine disaccharide **2-15**, present in all the fragments, was used as a common building block to obtain all the fragments *via* a convergent approach involving a [2+2] or a [2+3] glycosylation. Hence, the benzylidene acetal **2-8** was selectively opened in 80% yield to the 6-*O* benzyl analog to obtain glucosamine acceptor **2-14** having a free hydroxyl at the 4-*O* position.[165] The glucosamine acceptor **2-14** was glycosylated with the mannose imidate donor **2-6** using TMSOTf in DCM to obtain the disaccharide **2-4** in 88%

yield. Then, the TIPS protecting group at the 6-*O* position of mannose was removed using HF–pyridine complex to obtain the disaccharide acceptor **2-15** in 83% yield (**scheme 2.2**).

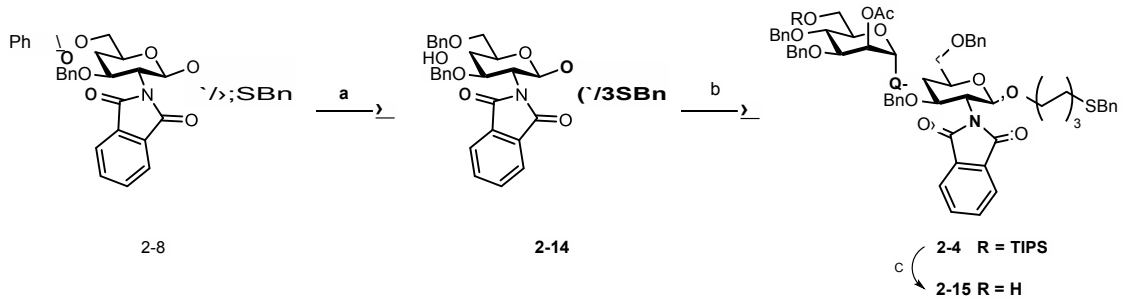

Scheme 2.2: **Synthesis of disaccharide 2-15**. a) TFAA, TFA, TES, CH_2Cl_2, 0 °C, 5 h, 80%; b) **2-6**, TMSOTf, CH_2Cl_2, -40 °C to -20 °C, 1 h, 88%; c) HF–py, THF, rt, 48 h, 83%.

The second building block corresponding to the α–(1→2)-dimannose **2-17** was obtained by deactylation of mannose building block **2-7b** using freshly prepared sodium methoxide. The following glycosylation of obtained acceptor **2-16** with the imidate donor **2-6** using TMSOTf activator in CH_2Cl_2 gave mannose dissacharide **2-17** in 80% yield. **(scheme 2.3)**

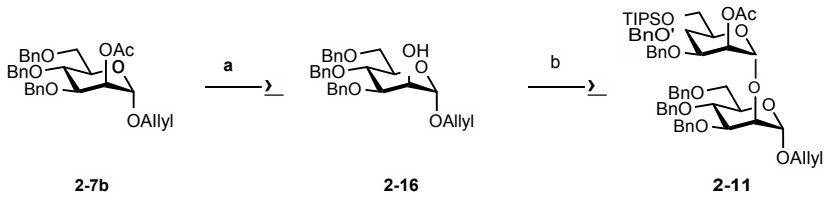

Scheme 2.3: **Synthesis of disaccharide 2-17**. a) NaOMe, MeOH/CH_2Cl_2, rt, 1 h, quant; b) **2-6**, TMSOTf, CH_2Cl_2, -40 °C to -20 °C, 1 h, 80%.

2.5.3 Assembly of the Fragments GPI 1 and 2

With the disaccharide fragments in hand, **GPI 1** and **GPI 2** were synthesized using a [2+2] glycosylation strategy. The mannose disaccharide **2-17** was deallylated using a two-step process involving Ir-catalyzed isomerization of the double bond followed by hydrolysis of the

vinyl ether with mercuric oxide, mercuric chloride and water to provide the desired hemiacetal. The obtained hemiacetal was transformed into the corresponding imidate donor **2-18** using trichloroacetonitrile and DBU. The glycosylation of disaccharide acceptor **2-15** with the disaccharide imidate donor **2-18** using TBSOTf as an acid activator gave the desired terasaccharide **2-19** as α/β mixture of 5/1 in 70% yield. The reaction was performed with diethyl ether as solvent to favor the formation of the α stereoisomer, which was isolated using flash column chromatography with silica gel as the stationary phase. The TIPS group was removed using scandium triflate in CH_3CN and water to obtain the desired tetrasaccharide alcohol **2-20**, which was used to obtain the two GPI fragments (**GPI 1** and **GPI 2**). To obtain **GPI 1**, the tetrasaccharide **2-20** was fully deprotected using a two-step protocol involving the removal of the phthalimide using ethylenediamine in butanol at 90 °C,[166, 167] and followed by Birch reduction using sodium and liquid ammonia. The fully deprotected tetrasachharide fragment **GPI 1** was obtained as a mixture of the reduced and oxidized forms of the thiol. The product **GPI 1** was purified using size exclusion column chromatography on sephadex G-15 to remove the excess salts (**scheme 2.4**).

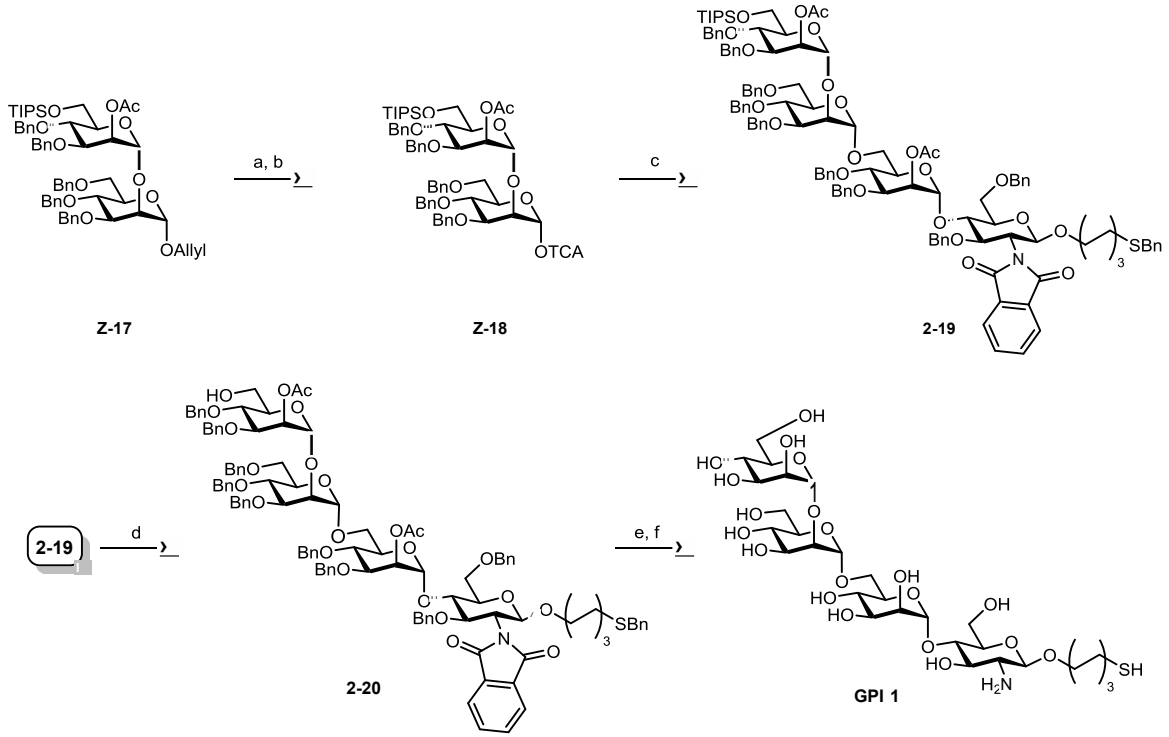

Scheme 2.4: **Synthesis of fragment GPI 1.** a) i. H_2, $[Ir(COD)(PMePh_2)_2]PF_6$, THF, rt, 12 h; ii. HgO, $HgCl_2$, acetone–H_2O (5:1), rt, 2 h, 81% ; b) CCl_3CN, DBU, CH_2Cl_2, 0 °C, 2 h, 86%; c) **2-15**, TBSOTf, Et_2O, 0 °C, 2 h, 55% (α-isomer); d) $Sc(OTf)_3$, H_2O, CH_3CN, 50 °C, 12 h, 71%; e) $(CH_2NH_2)_2$, H_2O, *n*-BuOH, 90°C, 4 h; f) i. Na, liq. NH_3, THF, -78 °C, 1 h; ii. MeOH, rt, 1 h, 57% (over two steps).

Tetrasaccharide alcohol **2-20** was phosphitylated with *H*-phosphonate **2-3** using pivolyl chloride as activator and oxidized using iodine and water to obtain the tetrasaccharide phosphate **2-21** in 66% yield. The tetrasaccharide **2-21** was fully deprotected using a two-step protocol which involved deprotection of the phthalimide using ethylenediamine in butanol at 90 °C and Birch reduction using sodium and liquid ammonia. The fully deprotected tetrasaccharide fragment **GPI 2** was obtained as a mixture of thiol and disulfide in 75% yield. The final product **GPI 2** was purified using size exclusion column chromatography on sephadex G-15 to remove the excess salts (**Scheme 2.5**).

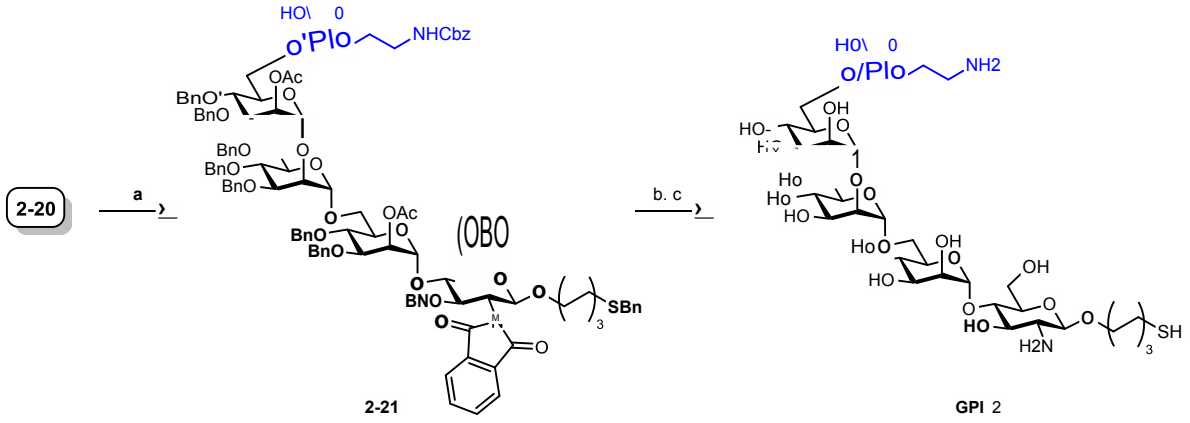

Scheme 2.5: **Synthesis of fragment GPI 2**. a) i. **2-3**, PivCl, py, rt, 16 h; ii. I_2, H_2O, py, rt, 1 h, 66% ; b) $(CH_2NH_2)_2$, H_2O, *n*-BuOH, 90 °C, 4 h; c) i. Na, liq. NH_3, THF, -78 °C, 1 h; ii. MeOH, rt, 1 h, 75% (over two steps).

2.5.4 Synthesis of the Fragments GPI 3 and 4

For the synthesis of fragments **GPI 3** and **GPI 4**, mannose disaccharide **2-17** was deacylated using freshly prepared sodium methoxide to obtain the disaccharide acceptor **2-22**. Due to the steric hindrance caused by the TIPS group on the disaccharide acceptor, the synthesis of trimannose using TMSOTf in CH_2Cl_2 as the reagent for the key glycosyation step failed. Thus, the glycosylation of disaccharide acceptor **2-22** and imidate donor **2-7a** was achieved by using TBSOTf as activator in diethyl ether to obtain the desired trimannose **2-23**. The trisaccharide **2-23** was subsequently deallylated using an iridium complex for the isomerization of the double bond followed by hydrolysis with mercuric oxide and mercuric chloride. The obtained hemiacetal was transformed into the corresponding imidate donor **2-5**

using trichloroacetonitrile and DBU. The obtained trisaccharide imidate donor **2-5** was used to glycosylate the disaccharide acceptor **2-15** using TBSOTf as activator in diethyl ether to favor the formation of the α isomer of pentasaccharide **2-2**. The TIPS group of pentasaccharide **2-2** was cleaved using scandium triflate in CH_3CN and water to obtain the pentasaccharide alcohol **2-24**. Pentasaccharide **2-24** was fully deprotected using a two-step protocol, involving the removal of the phthalimide using ethylenediamine in butanol at 90 °C followed by the Birch reduction. The fully deprotected pentasaccharide fragment **GPI 3** was obtained as a mixture of thiol and disulfide. The final product **GPI 3** was purified using size exclusion column chromatography on sephadex G-15 to remove the excess salts (**scheme 2.6**).

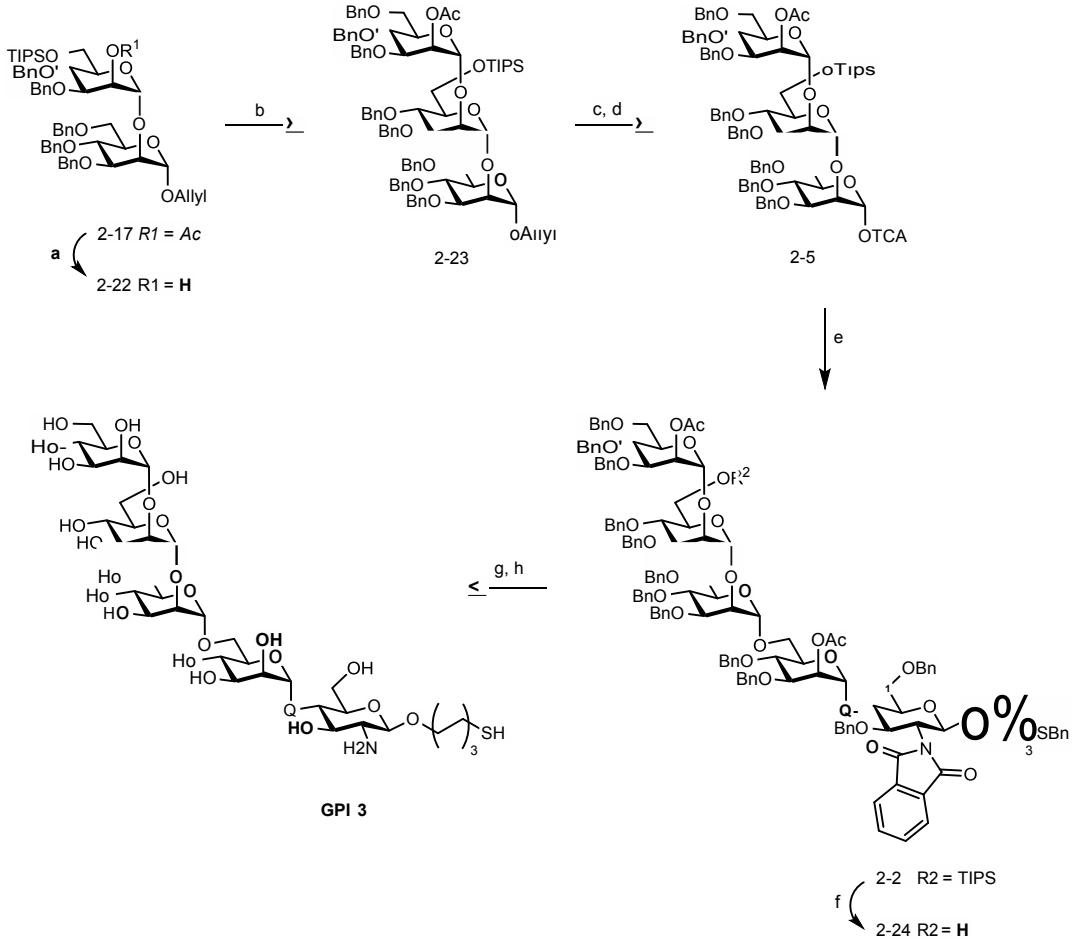

Scheme 2.6: Synthesis of fragment GPI 3. a) NaOMe, MeOH/CH_2Cl_2, rt, 12 h, quant; b) TBSOTf, Et_2O, 0 °C, 2 h, 68%; c) i. H_2, $[Ir(COD)(PMePh_2)_2]PF_6$, THF, rt, 12 h; ii. HgO, $HgCl_2$, acetone-H_2O (5:1), rt, 2 h, 64% ; d) CCl_3CN, DBU, CH_2Cl_2, 0 °C, 2 h, 80%; e) TBSOTf, Et_2O, 0 °C, 2 h, 65% (α–isomer); f) $Sc(OTf)_3$, H_2O, CH_3CN, 50 °C, 12 h, 72%; g) $(CH_2NH_2)_2$, H_2O, *n*-BuOH, 90 °C, 4 h; h) i. Na, liq. NH_3, THF, -78 °C, 1 h; ii. MeOH, rt, 1 h, 74% (over two steps).

Pentasaccharide **2-24** was phosphitylated with *H*-phosphonate **2-3** using pivolyl chloride as activator and oxidized using iodine and water to obtain tetrasaccharide phosphate **2-1** in 86% yield. Pentasaccharide **2-1** was fully deprotected using a two-step protocol, involving deprotection of the phthalamide using ethylenediamine in butanol at 90 °C followed by the Birch reduction using sodium and liquid ammonia to cleave the benzyl ethers. The fully deprotected tetrasachharide fragment **GPI 4** was obtained as a mixture of thiol and disulfide. The final product **GPI 4** was purified using size exclusion column chromatography on sephadex G-15 to remove the excess salts (**scheme 2.7**).

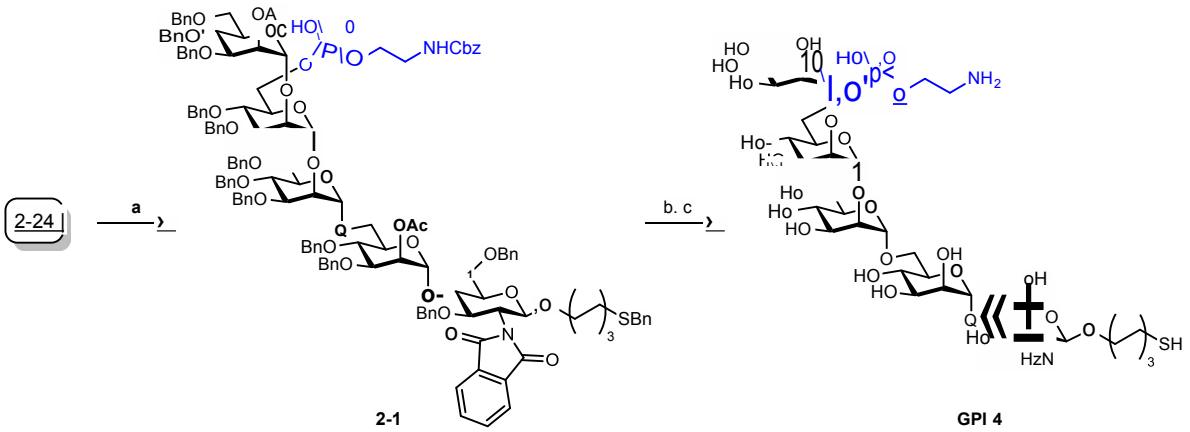

Scheme 2.7: **Synthesis of fragment GPI 4**. a) i. **2-3**, PivCl, py, rt, 16 h; ii. I_2, H_2O, pyr, rt, 1 h, 86% b) $(CH_2NH_2)_2$, H_2O, *n*-BuOH, 90 °C, 4 h; c) i. Na, liq. NH_3, THF, -78 °C, 1 h; ii. MeOH, rt, 1 h, 60% (over two steps).

The fractions containing the glycans were lyophilized and directly conjugated to the non-toxic variant of the diphtheria toxin carrier protein, CRM_{197}, which can enable a T-cell dependent immune response.[168]

2.5.5 Synthesis of Glycoconjugates

In order to obtain the glycoconjugates for immunological studies, the disulfide of **GPI 1–6** was first reduced to a thiol using polymer supported tris(2-carboxyethyl)phosphine (TCEP) resin and immediately used for the conjugation to the immunogenic carrier protein CRM_{197}. It is important to reduce the disulfide glycans before the conjugation reaction. Thiol can exist as

a free thiol as well as a disulfide, but only free thiols are nucleophilic enough to react with the activated protein during the conjugation reaction.[162-164]

The carrier protein CRM_{197} was activated by the modification of the lysine residue with 2-bromoacetates using bifunctional spacer *N*-succinimidyl-3-(bromoacetamido)propionate (SBAP). This reaction converts the free ε-amine groups into the reactive bromide. Following, a reaction of the bromide with the freshly reduced thiol of the glycan gave the desired glyco-conjugates with loading of between 5−8 glycans per molecule of carrier protein. Loading is expressed as number of glycan residues per CRM_{197} molecule. The unreacted bromides were quenched with cysteine. **Figure 2.7** depicts the conjugation process for **GPI 6** as an example. All the other conjugations followed the same protocol unless specified to generate 6 mg of the CRM_{197} glycoconjugates running two batches of 3 mg each.

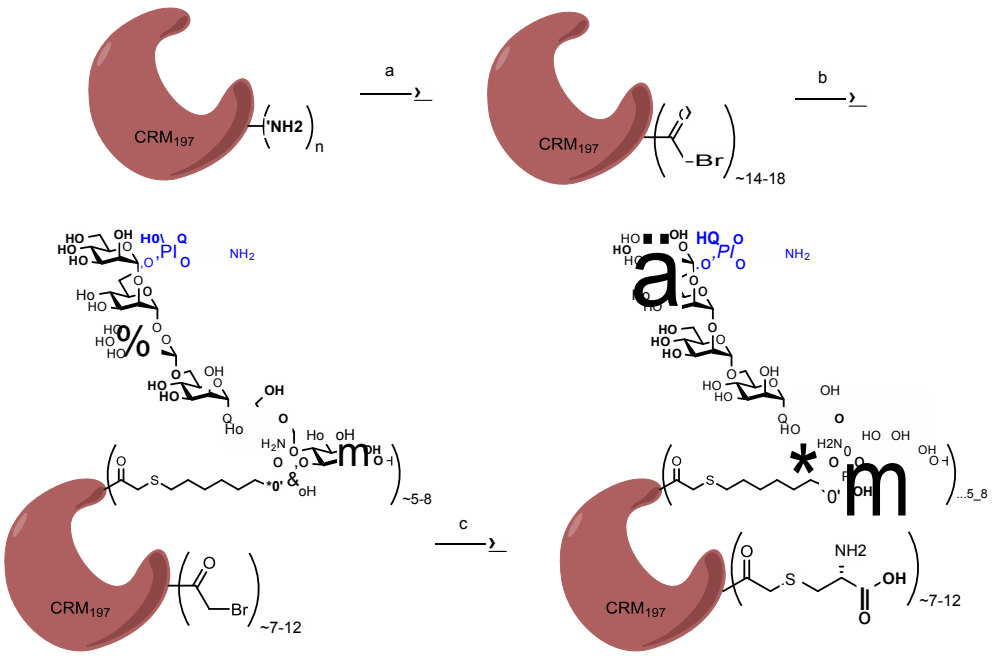

Figure 2.7: **Schematic representation of a CRM_{197}–GPI 6 glycoconjugate**. a) SBAP,0.1 M NaPi pH 7.4, rt; b) GPI 6, 0.1 M NaPi pH 8, 1mM EDTA, rt; c) L-cysteine, 0.1 M NaPi pH 8, 1mM EDTA, rt.

The conjugates were characterized using different methods (**figure 2.8)**. MALDI-TOF mass spectrometry analysis of the activated CRM_{197} shows that approximately sixteen bromides were introduced on average per molecule of CRM_{197} protein. The activated CRM_{197} protein

reacted with **GPI 6** in the second step to give the glycoconjugate with an average loading of 6.4 glycans per molecule of CRM_{197}, corresponding to about 12% of glycan by weight on average.

The other five glycoconjugates were synthesized in a similar manner and were characterized using MALDI-TOF mass spectroscopy and SDS-PAGE. Since a small variation was observed in the two different batches of the conjugates, an averaged loading was used for the calculation of the conjugates for the mice immunization study (**figure 2.9**). All the synthesized conjugates were stored in PBS buffer as 0.1 μg/μL at 4 °C.

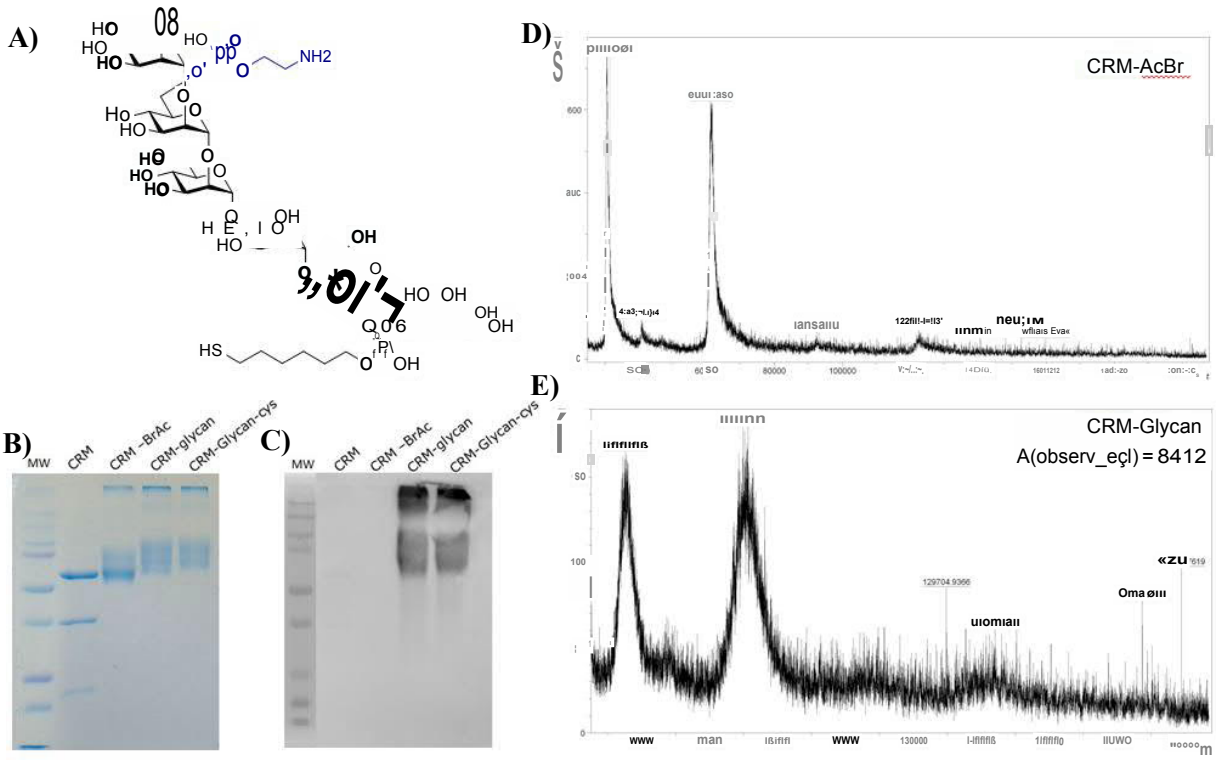

Figure 2.8: **Charaterization of CRM_{197}–GPI 6 glycoconjugate. (A)** chemical structure of **GPI 6**; **(B)** gel electrophoresis (SDS-PAGE) for different steps of the conjugation: activated CRM_{197} (CRM-BrAc) and **CRM_{197}–GPI** glycoconjugates (CRM-glycan) and quenched **CRM_{197}–GPI** (CRM-glycan-cys) stained with Coomassie Brilliant Blue; **(C)** Western blot for glycans detected by biotinylated Concavalin A; **(D)** MALDI-TOF characterization for the activated carrier protein CRM_{197} (CRM-BrAc); **(E)** MALDI-TOF characterization for glycoconjugate CRM-glycan.

A CRM_{197} conjugate of galactose (**CRM_{197}–Gal**) was also synthesized as a negative control for the immunization experiment to account for possible conformational changes of the glycan loaded carrier protein. Apart from **CRM_{197}–Gal**, only **CRM_{197}** and PBS buffer were used as control for this study.

GPI-CRVI	Batch	A m/z	**GPI molecular weight**	**Loading: GPUCRW (% of nass)**
GPI1	1	3835	781.82	4.92 (6.500 glycan)
	2	4778		6.12 (7.20 o glycan)
GPI2	1	6972	904.87	7.4 (10.2°o glycan)
	2	4329		5 (70 o glycan)
GPI3	1	5668	943.96	5.7 (8.1°o glycan)
	2	9299		9.8 (1300 glycan)
GPI4	1	9865	1067.01	9.3 (1400 glycan)
	2	9792		9.2 (13.7% glycan)
GPI5	1	5889	1146.99	5.2 (8.900 glycan)
	2	10240		8.9 (14.30<› glycan)
GPI6	1	9322	1309.13	7.12 (1300 glycan)
	2	8412		6.47 (12°<› glycan)

Figure 2.9: **Glycan loading of the CRM_{197} glycoconjugates determined by MALDI-TOF mass spectrometry.** Glycan loading was determined by MALDI and expressed as GPI molecules per CRM and as a percentage of weight for each **CRM_{197}–GPI** glycoconjugate, Δ m/z represents the difference in mass of the CRM-glycan and the activated CRM_{197}.

2.6 Immunological Results

All the immunization studies and results were obtained from Dr. Fridolin Steinbeis. The immunogenicity and the activity as anti-malarial toxin vaccine of the glycoconjugates were studied using a murine model for cerebral malaria. Five-week old female mice were divided into seven groups each consisting of 15 animals. The mice were vaccinated three times on days 0, 14 and 28 with the glycoconjugate formulated with alum adjuvant (1:2). The study groups were immunized with **CRM_{197}–GPI 1–6** glycoconjugates and control mice were immunized with **CRM_{197}–Gal**. Serum was taken at 14-day intervals on day 0, 14 and 28 for anti-GPI antibody analysis before infection and after infection on day 42. All mice were challenged on day 42 with *P. berghei* ANKA-infected erythrocytes. On day 6 post infection, five mice per group were sacrificed for immunological characterization (spleen cell composition, brain T-cell sequestration, vaccine-specific T-cell re-stimulation). The remaining ten mice per group were used for survival studies to test vaccine efficacy (**figure 2.10**).

The role of lymphoid cells ($CD8^+$ and $CD4^+$ T-cells, NK and NKT-cells) and myeloid cells (monocytes, dendritic cells, neutrophils) as well as proinflammatory cytokines (IL-1β, IL6, IL-8, IL-10, IL-4, IL-12p70, TNF-α, INF-γ) were also studied during this experiment.

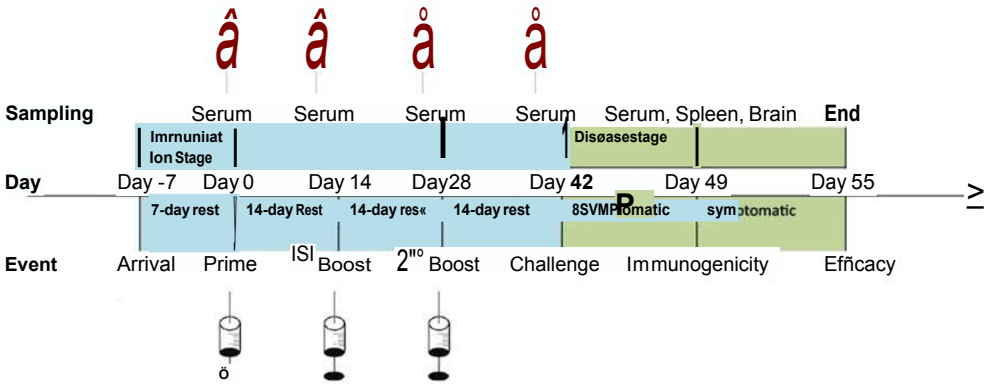

Figure 2.10: Study design for testing immunogenicity of **CRM_{197}–GPI 1–6** against **CRM_{197}–Gal** in the murine model of cerebral malaria. All the immunization studies and results were obtained from Dr. Fridolin Steinbeis.

2.6.1 Efficacy, Parasitemia and Clinical Score

Mice were immunized with glycoconjugates **CRM_{197}-GPI 1-6**, **CRM_{197}-Gal**, **CRM_{197}** and PBS as control. Control mice succumbed to experimental cerebral malaria in 100% of the cases by day 9, whereas all **CRM_{197}-GPI** immunized mice displayed improved survival compared to the control groups (10–40%). Mice that recieved **CRM_{197}-GPI 5** showed the highest survival of 40% compared to PBS, **CRM_{197}-Gal**, **CRM_{197}** control groups. However, mice immunized with **CRM_{197}-GPI 1–4** and **CRM_{197}-GPI 6** glycoconjugates showed a survival rate between 11% and 30% compared to the control group which was not significant (**figure 2.11)**.

The parasitemia was determined on days 5, 7, 9 post-infection. As shown in **figure 2.12**, the level of parasitemia was not affected by **CRM_{197}-GPI** immunization compared to the control group. The high level of errors displayed on day 12 for the individual groups were the result of low numbers of surviving mice in each group.

The appearance of experimental cerebral malaria symptoms were monitored daily from day 7 post-infection. Clinical scoring of challenged mice was found to be the highest for **CRM_{197}-Gal** control mice and lowest for **CRM_{197}-GPI 5** immunized mice at day 12 post-infection, suggesting the protective potential of the glycoconjugate used in this group of mice. Survival data are based on 9–10 mice per group and the mice that did not develop parasitemia were excluded from the study (one mouse each in **CRM_{197}-GPI 3** and **CRM_{197}-GPI 4** immunized groups) (**figure 2.13**).

As the survival study was only based on five mice, the survival rates ranging between 10–40% were unlikely to yield significant results. Thus, higher number of mice would provide better insight into the immunological evaluation for these glycoconjugates.

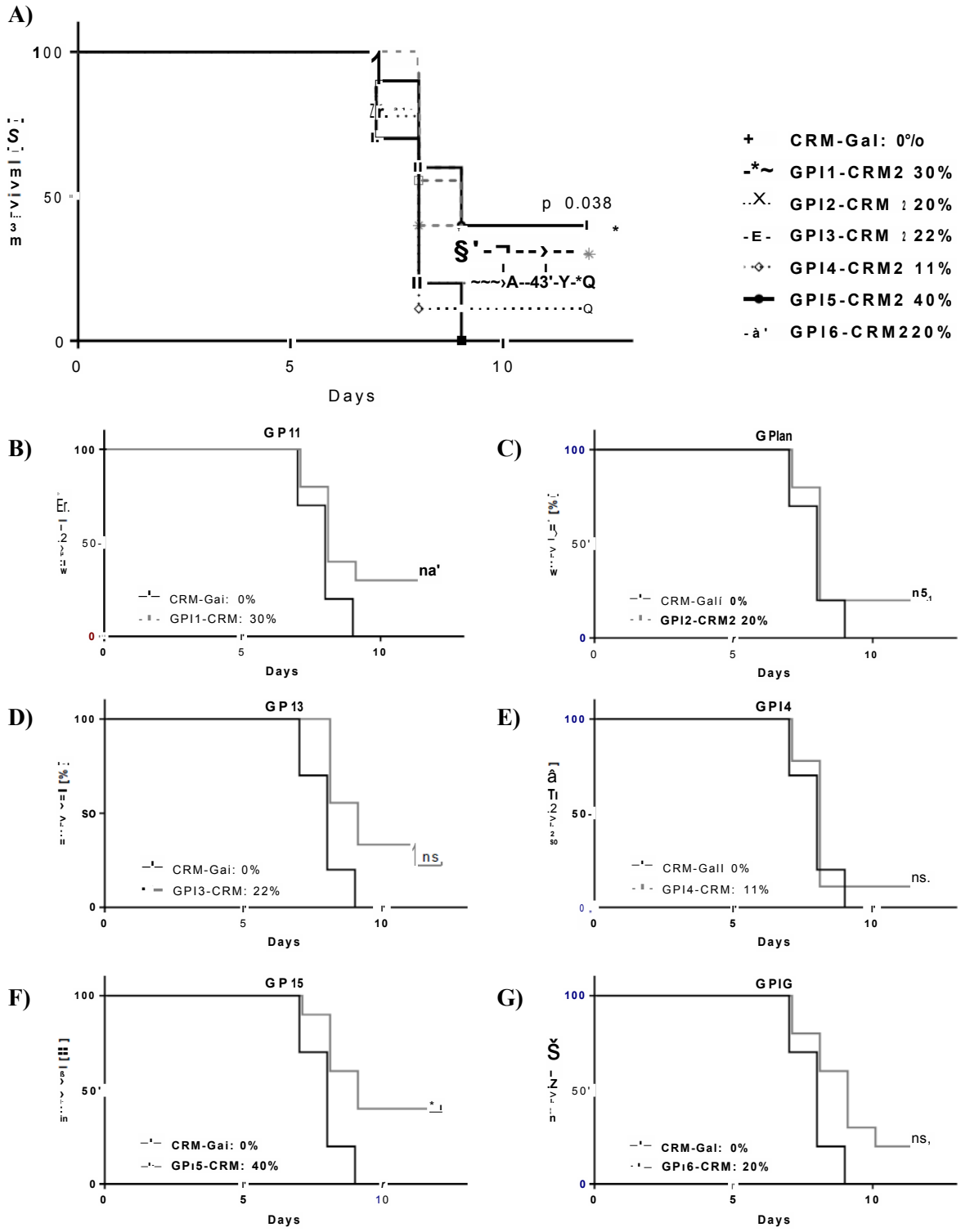

Figure 2.11: Protection against Experimental Cerebral Malaria (ECM). (A) Mice immunized with GPI conjugates displayed increased survival compared to control mice immunized with **CRM_{197}-Gal**. **(B-G)** Survival of **CRM_{197}-GPI 1–6** immunized mice against control mice. Statistical significance shown by asterisks *($p < 0.05$)

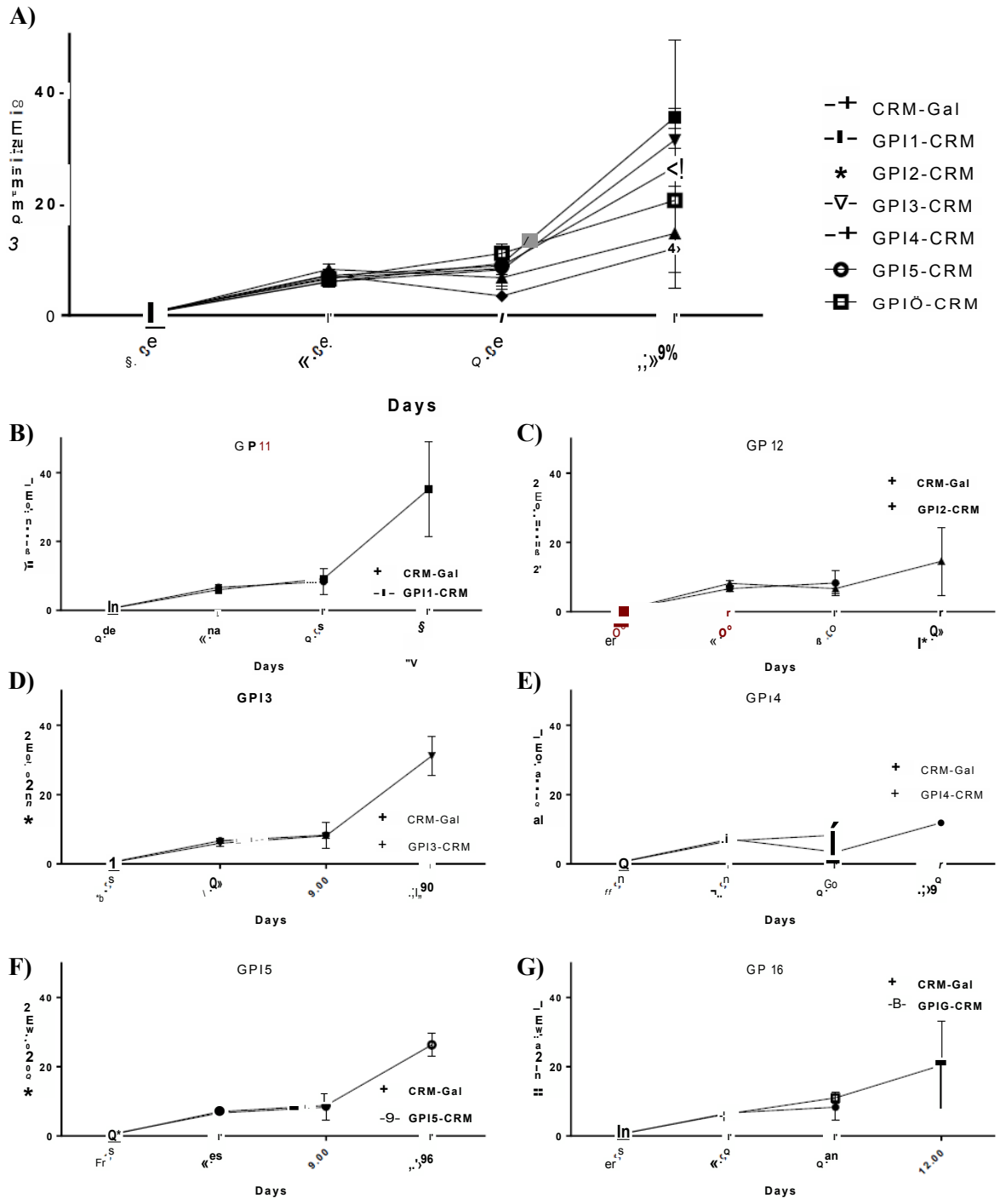

Figure 2.12: Parasitemia post infection on days 5, 7, 9 and 12 for mice infected with *P. berghei* ANKA infected erythrocytes. (A) Percentage of infected RBC for the conjugates. **(B-G)** Parasitemia of **CRM_{197}-GPI 1–6** immunized mice against control group.

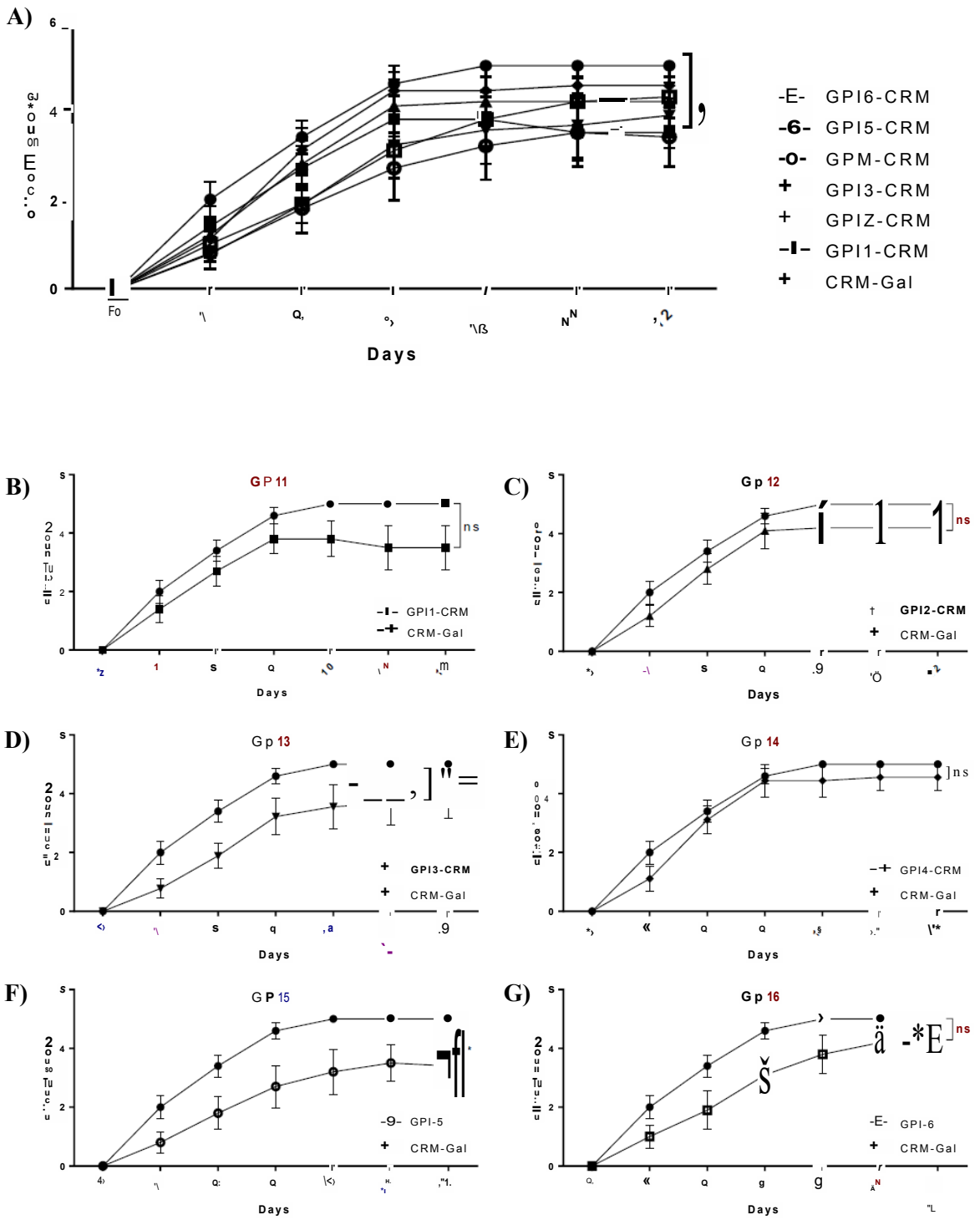

Figure 2.13: Clinical score post infection on day 5, 7, 9 and 12 for mice infected with *P. berghei* ANKA infected erythrocytes. (A) All mice were monitored for clinical symptoms. Successive points for respective symptoms of infected mice: healthy (0), ruffled fur (1), hunching (2), wobbly gait (3), limb paralysis (4), convulsions (5) and coma (6). Mice scoring ≥ 3 were euthanized, and dead mice were designated a scoring of 5. (**B-G**) Clinical score of **CRM_{197}-GPI 1–6-**immunized mice against control group. Statistical significance shown by asterisks *($p < 0.05$).

2.6.2 Anti-GPI Antibody Response and Cross-reactivity

The level of antibodies in mice against the GPI structures was determined by glycan array analysis. After the first immunization boost (day 28), all GPI fragments with a phosphoethanolamine group (**GPI 2,** and **4–6**) developed a significantly higher level of anti-GPI antibodies (**figure 2.14**). Mice immunized with **CRM_{197}-GPI 1** and **CRM_{197}-GPI 3** did not develop a significant level of antibody compared to control mice. **CRM_{197}-GPI 2** and **CRM_{197}-GPI 5** showed a drastic increase in anti-GPI antibodies immediately after day 1, whereas mice immunized with **CRM_{197}-GPI 4** and **CRM_{197}-GPI 6** showed anti-GPI antibody levels only after day 28. The highest level of anti-GPI antibodies was observed in mice from the **CRM_{197}-GPI 5** group. The antibody levels dropped for all the conjugates after infection except for **CRM_{197}-GPI 6** immunized mice.

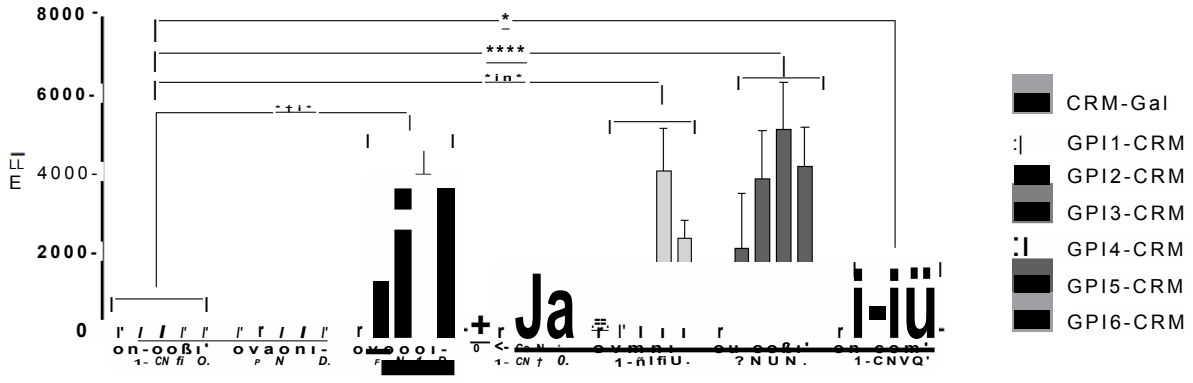

Figure 2.14: Anti-GPI antibody responses for mice immunized with CRM_{197}-GPI 1–6. Statistical significance was determined using two-way ANOVA to compare anti-GPI antibody levels between groups. Significance shown by asterisks *(p <0.05) and ****(p <0.0001). MFI = mean fluorescence intensity; PI = *post* infection.

IgG antibodies from mice immunized with **CRM_{197}-GPI 2** and **CRM_{197}-GPI 4-6** showed a high level of cross reactivity between these fragments(**figure 2.15** and **2.16**). As expected, control mice immunized with **CRM_{197}-Gal** did not develop cross-reacting antibodies against GPI epitopes, but generated antibodies against itself. The antibodies against the **CRM_{197}-GPI 1** and **CRM_{197}-GPI 3** glycoconjugates, without inositol and phosphoethanolamine, showed cross-reactivity to **GPI 2-4**, whereas no reactivity was detected against inositol containing **GPI 5** and **GPI 6** (**figure 2.16 A**). Mice immunized with **CRM_{197}-GPI 2** and **CRM_{197}-GPI 4** glycoconjugates bearing a phosphoethanolamine moiety but lacking an inositol showed high

level of cross-reacting antibodies against phosphoethanolamine containing GPIs, but almost insignificant reactivity against the inositol-containing **GPI 5** and **GPI 6** (**figure 2.16 B**). **CRM_{197}-GPI 5** and **CRM_{197}-GPI 6** induced cross-reacting antibodies with high binding affinity to **GPI 5** and **GPI 6** itself and, moderate binding to phosphoethanolamine containing **GPI 2** and **GPI 4** and undetectable binding to **GPI 1** and **GPI 3** (**figure 2.16 C**). From these results, it can be concluded that inositol and phosphoethanolamine play a very important role in the immunogenicity of glycoconjugate vaccine candidates.

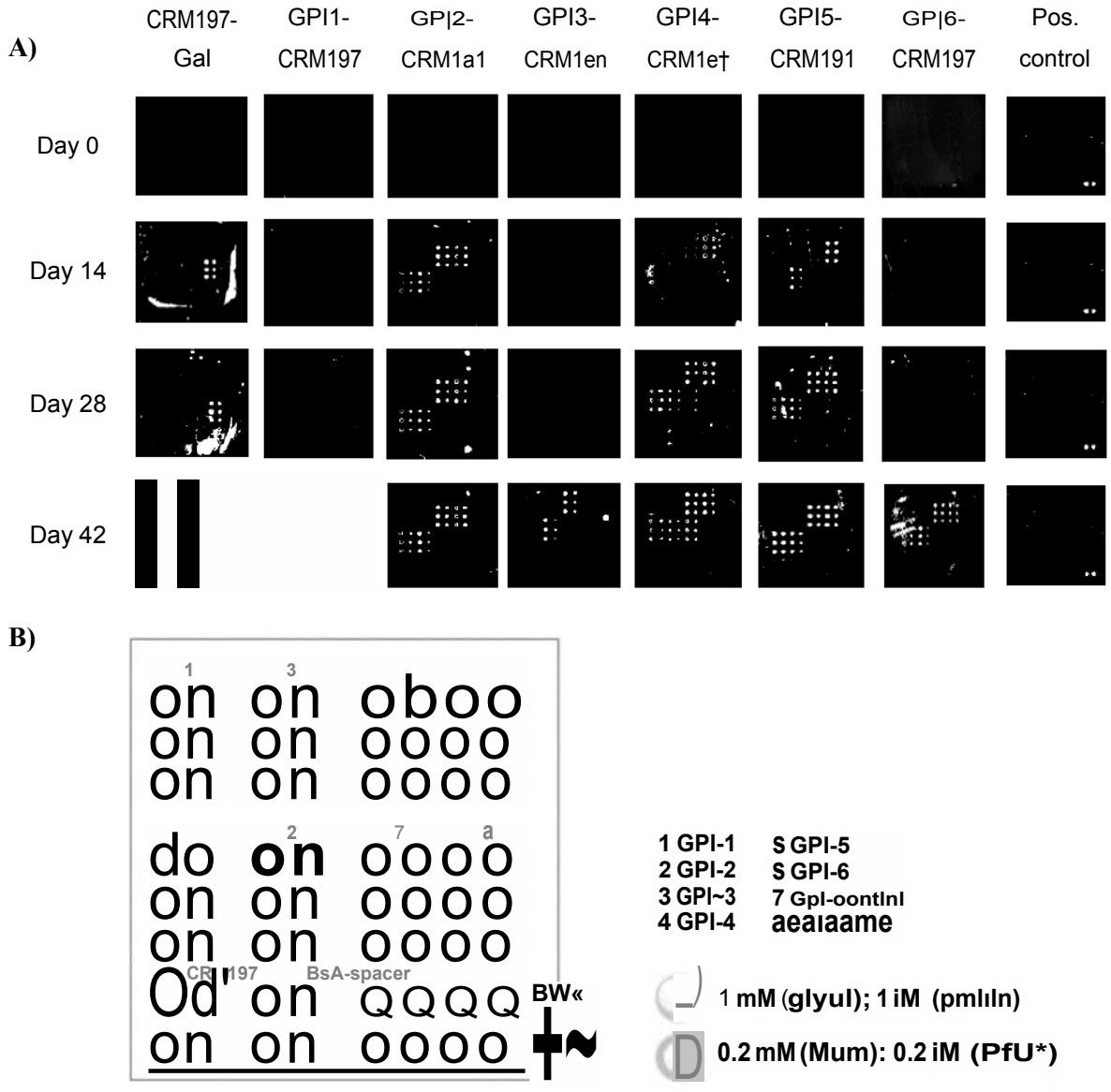

Figure 2.15: Glycan microarray for glycoconjugates at two concentrations for anti-GPI antibody level at days 0, 14, 28 and 42. **(A)** Representative microarray wells results from serum of mice immunized with **CRM_{197}-GPI 1–6** (day 0–42) and rabbit anti-*S. pneumoniae* antibodies as positive control. **(B)** Microarray printing pattern of maleimide treated glass slides (PolyAn, Berlin, Germany).

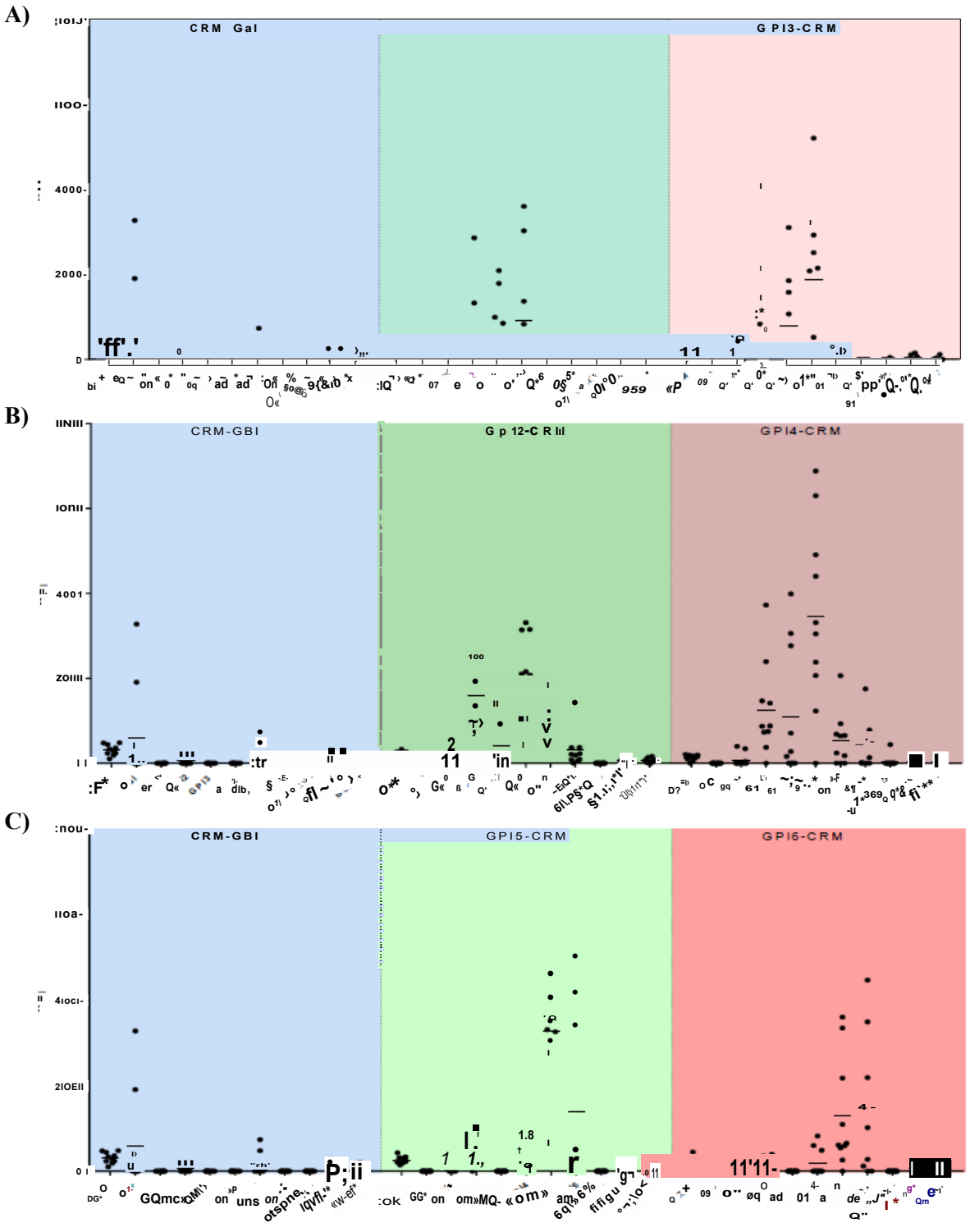

Figure 2.16: Cross-reactivity of anti-GPI antibodies after day 42. (A) Cross-reactivity of serum from **CRM_{197}-Gal, CRM_{197}-GPI 1** and **CRM_{197}-GPI 3** immunized mice against synthetic GPIs **(B)** Cross-reactivity of serum from **CRM_{197}-Gal, CRM_{197}-GPI 2** and **CRM_{197}-GPI 4** immunized mice against synthetic GPIs **(C)** Cross-reactivity of serum from **CRM_{197}-Gal, CRM_{197}-GPI 5** and **CRM_{197}-GPI 6** immunized mice against synthetic GPIs.

2.6.3 T-Cell Response

ELIspot analysis was used to determine the production of IFN-γ by the **CRM_{197}-GPI** glycoconjugates and CRM_{197} specific T-cells response upon re-stimulation of spleen cells. Increased T-cell activation was observed for CRM_{197}-GPI compared to CRM_{197} alone. **(figure 2.17A)**. No significant difference was observed in the number of glycoconjugate-specific IFN-γ producing T-cells between PBS-control and GPI immunized mice for **GPI 1**, **3** and **5**. The decreased level of INF-γ production can explain the high survival rate in those groups. Also, higher INF- γ response for glycoconjugates can be attributed to their better uptake by the cells compared to CRM_{197} alone, making them better vaccine candidates.

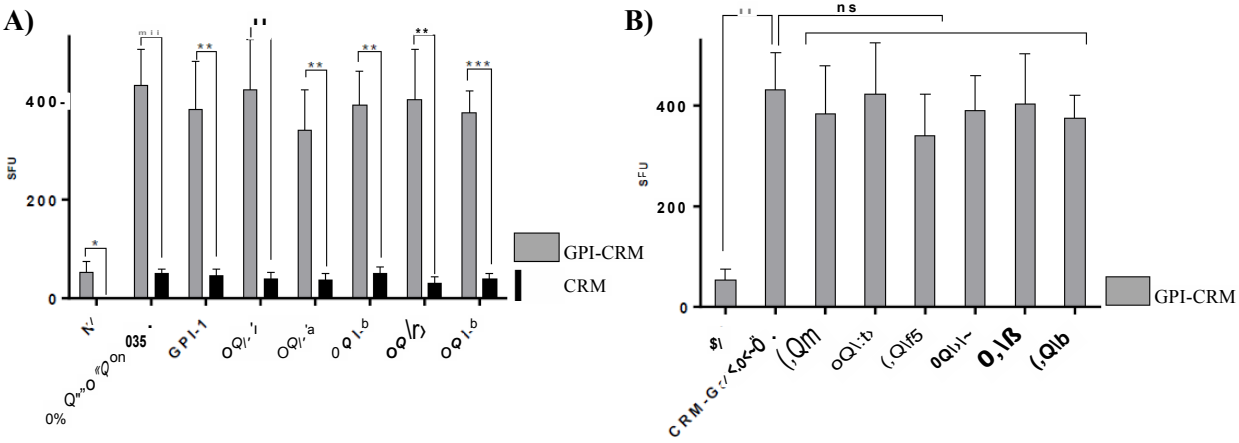

Figure 2.17: T-cell response in immunized mice. (A) IFN-γ production by T-cells upon re-stimulation of spleen cells by their immunized CRM_{197}-GPI conjugate or CRM_{197} alone. **(B)** Comparison between T-cell response for re-stimulation with glycoconjugates treated animals to non-treated animals. Statistical significance was determined using the unpaired Student's t-test, significance shown by asterisks *($p < 0.05$), **($p < 0.01$) , ***($p < 0.001$); not significant results labeled ns ($p > 0.05$). SFU = spot forming unit.

Regulatory T-cells play an important role in experimental cerebral malaria.[169] The proportion of regulatory T-cells was measured by intracellular staining of the transcription factor Forkhead-Box-Protein P3 (FoxP3) of spleen cells. An increase in regulatory T-cells was observed for all the immunized mice compared to control mice. No difference was observed in the T-cell frequency for **CRM_{197}-Gal** and **CRM_{197}-GPI** suggesting that GPI toxin does not affect regulatory T-cells (**figure 2.18**).

Downstream pro-inflammatory effects of macrophages and dendritic cells have been associated with experimental cerebral pathology and human cerebral malaria pathogenesis (**figure 2.19**). To test the impact of **CRM_{197}-GPI** conjugates on macrophage and dendritic cell composition of the spleen, flow cytometry was used. No significant changes in population size were detected regarding myeloid cell populations in spleens of immunized versus control mice. Cellular activation (measured by activation marker CD80) was significantly increased in both macrophages and dendritic cells compared to non-infected controls upon *P. berghei* ANKA challenge. Only marginal differences in cellular activation were observed between mice immunized with glycoconjugate vaccine candidates **CRM_{197}-GPI** and control **CRM_{197}-Gal** mice. The analysis shows that **CRM_{197}-GPI** did not induce an unspecific inflammatory response.

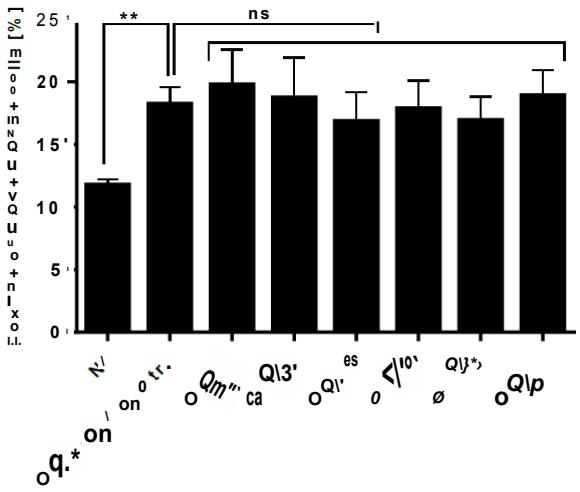

Figure 2.18: Regulatory T cell activation. On day 6 post infection, regulatory T-cells in all challenged groups were compared to the non-infected control group. Statistical significance was determined using the unpaired Student's t-test, significance shown by asterisks **($p<0.01$); not significant results labeled ns ($p>0.05$)

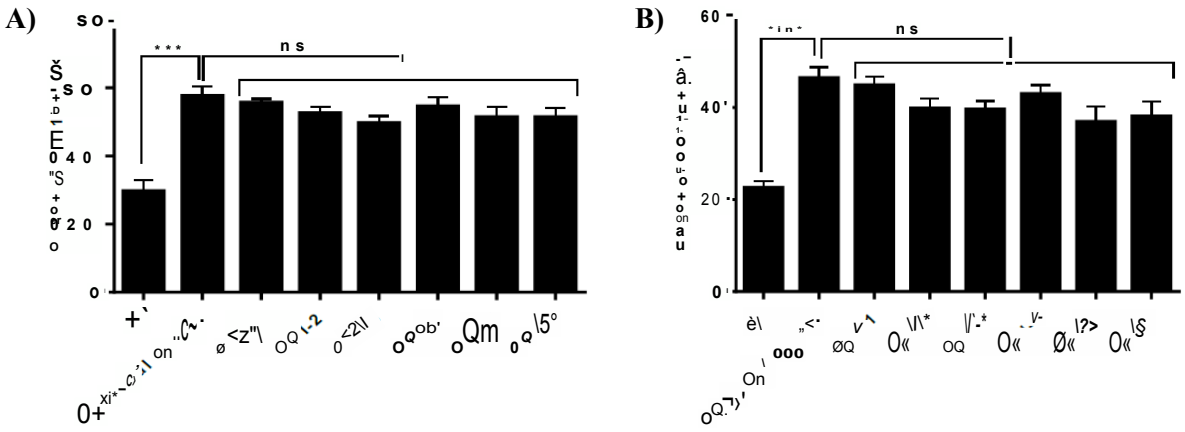

Figure 2.19: Proportion of activated (A) macrophages and (B) dendritic cells measured per $1x10^4$ spleen cells of **CRM_{197}-GPI** immunized and control mice on day 6 post infection. Significance is shown by asterisks *($p < 0.05$); not significant results labeled ns ($p > 0.05$)

In order to understand the specificity of the immune response, serum levels of pro- and anti-inflammatory cytokines (IL-6, TNF-α, IFN-γ) were measured by cytometric bead array before and after infection (days 42 and 48) of five mice per group. Low levels of IFN-γ, TNF-α, IL-6 were observed for **CRM_{197}-GPI 1-6** immunized and as well as control mice (**Figure 2.20 A, C, E**) after a second boost-vaccination, indicating that **CRM_{197}-GPI-**glycoconjugates did not induce an unspecific immune response. To investigate whether **CRM_{197}-GPI** immunization modified the humoral immune responses towards infection, serum cytokines of mice were further measured on day 48. Infected groups showed significantly increased levels of IFN-γ, TNF-α and IL-6 compared to the non-infected mice (**Figure 2.20 A, C, E**). TNF-α was not significantly increased in **CRM_{197}-GPI 1** and **CRM_{197}-GPI 5** immunized mice, and was at a comparable level to **CRM_{197}-GPI 3** and **CRM_{197}-GPI 4** (**figure 2.20 C**). The level of pro-inflammatory cytokines post infection varied between **CRM_{197}-GPI** vaccinated mice (**Figure 2.20, B, D, F**). The mice immunized with **CRM_{197}-GPI 6** showed increased levels of IFN-γ, TNF-α and IL-6, whereas levels of IFN-γ, TNF-α and IL-6 were considerably reduced for mice immunized with **CRM_{197}-GPI 5**. No significant difference in cytokine levels was observed in **CRM_{197}-GPI** glycoconjugate vaccinated versus **CRM_{197}-Gal** control mice (**figure 2.20, B, D, F**).

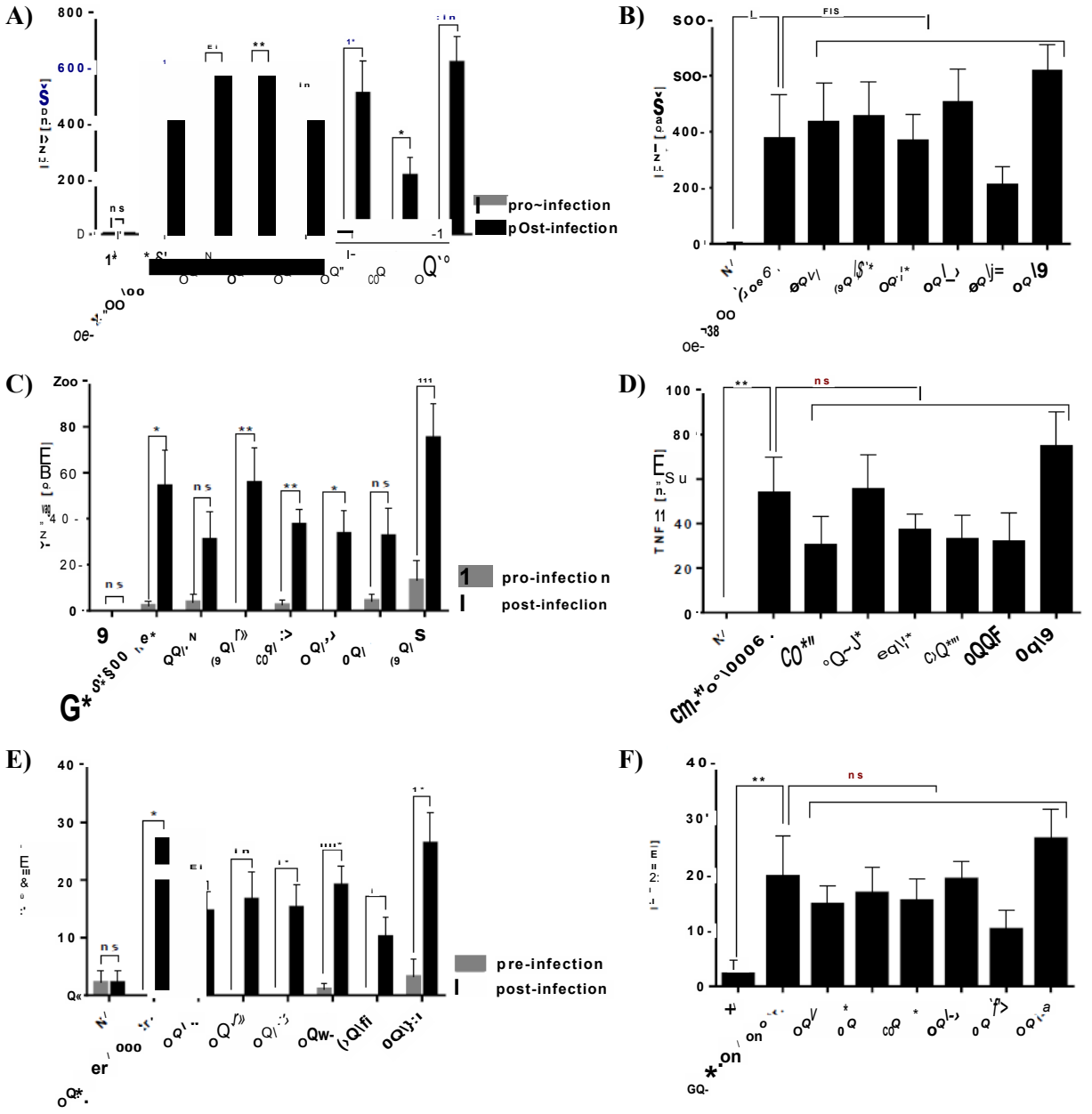

Figure 2.20: Pro-inflammatory cytokine levels of infected mice. (**A, C, E**) comparison in the level of IFN-γ, TNF-α and IL-6 for **CRM_{197}-GPI 1–6** immunized and control mice before and after infection. (**B, D, F**) Comparison in the serum levels of pro-inflammatory cytokines between non-infected mice and **CRM_{197}-GPI** vaccinated mice. Statistical significance was determined using the unpaired Student's t-test, significance shown by asterisks *(p <0.05), **(p <0.01) , ***(p <0.001); not significant results labeled ns (p >0.05)

2.7 Conclusion and Outlook

A new library of GPI fragments was designed and synthesized to improve understanding of the structure–activity relationship in regard to the immunogenicity of **CRM_{197}-GPI** glycoconjugates. The molecules were designed to cover different components of *P. falciparum* GPI structure. The structures were designed in order to understand the importance of phosphoethanolamine, inositol and the terminal mannose (ManIV) in immunological response and to deepen understanding about the structure–activity relationship. Six different structures were designed and synthesized using a convergent approach. An amino–containing linker, which is commonly used to conjugate the oligosaccharides to carrier proteins, could not be used due to the presence of the amine group at the phosphoethanolamine moiety and glucosamine residue of the GPI structure. Thus, the GPI fragments were synthesized bearing a thiol linker that can be orthogonally conjugated to the carrier protein in presence of free amines. Benzyl ethers were used as the permanent protecting group and acetyl, TIPS and allyl were used as orthogonal temporary protecting groups. Birch reduction was used for global deprotection and products were obtained as a mixture of thiol and disulfide oligosaccharide. GPI fragments were synthesized with the thiol linker either at the reducing end or at the inositol to maintain the natural presentation of the GPI on the cell membrane.

Unlike the previous study, where KLH was used as carrier protein, CRM_{197} was chosen as a carrier protein for the synthesis of glycoconjugates and alum as adjuvant to improve the immunogenicity of the vaccine candidate. They are both clinically approved and already used in many glycoconjugate vaccines. A mouse model was used for the challenge study of cerebral malaria. Mice were immunized with **CRM_{197}-GPI 1-6** glycoconjugate vaccine candidates or **CRM_{197}-Gal** as control. Ten mice from each group were used to study the efficacy of the glycoconjugates and five mice per group were used for the immunological characterization.

As expected, the conjugates varied in the induction of protection against experimental cerebral malaria. All the **CRM_{197}-GPI** immunized mice showed an increased survival compared to the control group. **CRM_{197}-GPI 5** showed the highest protection against cerebral malaria with a survival rate of 40%. Mice immunized with **CRM_{197}-GPI 2** and **CRM_{197}-GPI 4-6** displayed increased levels of anti-GPI antibodies compared to the control group. **CRM_{197}-GPI 5–**immunized mice displayed a lower level of serum IFN-γ and did not develop a

significant increase in TNF-α post infection which was not seen in the mice immunized with other GPI glycoconjugates. This can explain the increased survival of the mice immunized with **CRM_{197}-GPI 5.**

Cross-reactivity revealed that the length of the mannose backbone is important for immune recognition. **CRM_{197}-GPI 1** was slightly immunogenic and was not detected by antibodies; **CRM_{197}-GPI 3** was more immunogenic compared to **CRM_{197}-GPI 1** and also detected by cross-reacting antibodies from **CRM_{197}-GPI 1–**immunized mice. This is consistent with previous findings on human anti-GPI antibody binding that did not recognize glycan fragments containing less than five carbohydrate units (**section 2.2.2**). Phosphoethanolamine was detected as an important immunogenic epitope in mice, unlike in human anti-GPI antibody binding, where only a slight difference in antibody response was observed.[160] As described in the literature, inositol was the immunodominant epitope present in **GPI 5** and **6**.[54]

Despite the initial evidence that GPI–attached lipid moieties are important for GPI antibody recognition, synthetic GPIs lacking lipid moieties are also recognized by human antibodies. Naik et al., showed that anti-GPI antibodies are mainly directed towards the conserved glycan structure of purified *Plasmodium* GPIs in humans.[155, 160] This study was able to establish a structure–activity relationship profile between the GPI compositions in a murine model.

Plasmodium expresses both ManIV-GPI and ManIII-GPIs on the surface of the parasite. Naturally, ManIV-GPI exists as GPI anchored to the protein (MSP-1 and MSP-2) whereas ManIII-GPI exists as free GPI and ManIII-GPI is five times more abundant than GPI anchored to the protein.[144, 152] All the conjugates were synthesized with protein either at the reducing end of the oligosaccharide or at the inositol residue. The higher survival and efficacy of the glycoconjugate ManIII GPI (**GPI 5**) over ManIV GPI (**GPI 6**) can be explained by the higher abundance and natural presentation of ManIII-GPIs on the surface of the parasite which is similar to the **CRM_{197}-GPI 5**.

In the previous study, GPI-KLH glycoconjugate was synthesized with a KHL carrier protein at the phosphoethanolamine residue of the GPI where the natural presentation is similar to ManIV-GPI anchored to the protein.[54, 153] The immunized mice in this case were protected from cerebral pathology in ~80% of cases. However, a structurally related GPI conjugated to the protein from the phosphoinositol residue in this study, showed 20% protection against

cerebral malaria. This provides the evidence that the site of conjugation and the structural representation of GPI in a vaccine plays an important role in vaccine efficacy.

It can be concluded that GPI is a toxin and hence an anti-toxin GPI vaccine can decrease the severity of the disease. The protection is dependent on both the antibody and cellular immune response. GPI composition and presentation on the carrier protein plays an important role in inducing an immune response.

It was difficult to compare the survival rate for different glycoconjugates because of the small number of mice used for the challenge study. Thus, a detailed study with a larger set of mice is necessary to improve the understanding of GPI-based glycoconjugate vaccines. Immunization in a different animal model could further provide a better understanding of the mechanism of a GPI anti-toxin vaccine. Further optimization to improve the vaccine efficacy should include dose dependent responses, different carrier proteins and adjuvant systems.

A detailed immunological characterization with optimized vaccine formulation is necessary to increase vaccine efficacy and to make GPI glycoconjugates a potential antimalarial vaccine.

2.8 Experimental

2.8.1 Methods of Synthetic Chemistry

All purchased chemicals were of reagent grade and all anhydrous solvents were of high-purity grade and used as supplied except where noted otherwise. Reactions were performed in oven-dried glassware under an inert argon atmosphere unless noted otherwise. Reagent grade thiophene was dried over activated molecular sieves prior to use. Pyridine was distilled over CaH_2 prior to use. Sodium hydride suspension was washed with hexane and THF and stored in an anhydrous environment. Benzyl bromide was passed through activated basic aluminum oxide prior to use. Metal sodium was washed with hexane and stored in hexane. Analytical thin layer chromatography (TLC) was performed on Merck silica gel 60 F_{254} plates (0.25mm). Compounds were visualized by UV irradiation or heating the plate after dipping in staining solution. The staining solutions were cerium sulfate-ammonium molybdate (CAM) solution, basic potassium permanganate solution, acidic ninhydrin-acetone solution, or a 3-methoxyphenol-sulfuric acid solution (Sugar Stain). Flash column chromatography was carried out using a forced flow of the indicated solvent on Sigma Aldrich silica gel high purity

grade 60 Å (230-400 mesh particle size, for preparative column chromatography). Solvents were removed under reduced pressure using rotary evaporator and high vacuum (<1 mbar). Freeze drying of the aqueous solutions was performed using Alpha 2-4 LD Lyophilizer (Christ, Osterode am Harz, Germany)

^{1}H, ^{13}C and ^{31}P-NMR as well as all 2D-spectra (^{1}H-^{1}H COSY, ^{1}H-^{1}H TOCSY, ^{1}H-^{13}C HSQC, ^{1}H-^{13}C HMBC) were recorded on a Varian 400 (400 MHz), a Varian 600 (600 MHz), a Bruker 400 (400 MHz) and a Bruker Ascend 400 (400 MHz) spectrometer in $CDCl_3$ (7.26 ppm ^{1}H, 77.1 ppm ^{13}C), D_2O (4.79 ppm ^{1}H), MeOD (4.87 ppm and 3.31 ppm ^{1}H, 49.00 ppm ^{13}C), Acetone-d_6 (2.05 ppm and 2.84 ppm ^{1}H, 206.26 ppm and 29.84 ppm ^{13}C) unless otherwise stated. The coupling constants (*J*) are reported in Hertz (Hz). Splitting patterns are indicated as s, singlet; d, doublet; t, triplet; q, quartet; br, broad singlet; dd, doublet of doublets; m, multiplet; dt, doublet of triplets; h, hextet for ^{1}H NMR data. Signals were assigned by means of ^{1}H-^{1}H COSY, ^{1}H-^{1}H TOCSY, ^{1}H-^{13}C HSQC, ^{1}H-^{13}C HMBC spectra and version thereof. ESI mass analyses were performed by Waters Xevo G2-XS Q-TOF with an Acquity H-class UPLC and a Bruker Autoflex-speed MALDI-TOF spectrometer.

2-Methyl-5-tert-butylphenyl-3,4,6-Tetra-*O*-acetyl-2-deoxy-2-*N*-phthalimido-1-thio-β-D-glucopyranoside (2-10)

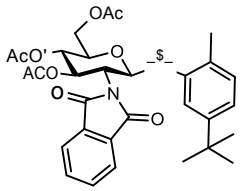

A solution of glucosamine **2-9** (10 g, 46.4 mmol) in 1 M NaOMe (60 mL) was stirred vigorously for 1 h at room temperature to obtain a milky liquid. After 1 h, the reaction mixture was filtered and washed with MeOH (50 mL). To the obtained solution, was added phthalic anhydride (10.3 g, 69.6 mmol) and Et_3N (7.12 mL, 51mmol) and reaction mixture was stirred overnight at room temperature. The reaction mixture was concentrated and crude product was dissolved in pyridine (50 mL). Then, Ac_2O (26.2 mL, 278 mmol) was added to the solution and the resulting solution was stirred overnight. The reaction mixture was diluted with aq. $NaHCO_3$, extracted with CH_2Cl_2, washed with brine, dried over Na_2SO_4 and concentrated to obtain desired peracetylated intermediate (14.06 g, 29.5mmol, 64%).

To the stirred solution of peracetylated intermediate and 2-methyl-5-*tert*butyl- thiophenol (13.55 mL, 73.6 mmol) in anhydrous CH_2Cl_2 (50mL) was added borontrifluoride etherate (7.27 mL, 58.9 mmol) dropwise and was stirred overnight at room temperature. The reaction mixture was quenched with aq. $NaHCO_3$, extracted with CH_2Cl_2, washed with brine and dried over Na_2SO_4. The solvents were removed under reduced pressure and the crude product was purified by flash column chromatography to obtain thioglycoside **2-10** (13.5 g, 22.59 mmol, 77%) as yellow oil. R_f = 0.35 (EtOAc/hexane = 1:1) ^{1}H NMR (400 MHz, $CDCl_3$) δ 7.86 (d, *J* = 7.2 Hz, 2H), 7.80 – 7.71 (m, 2H), 7.46 (d, *J* = 2.1 Hz, 1H), 7.21 (dd, *J* = 8.0, 2.1 Hz, 1H), 7.06 (d, *J* = 8.0 Hz, 1H), 5.81 (dd, *J* = 10.2, 9.2 Hz, 1H), 5.63 (d, *J* = 10.6 Hz, 1H), 5.19 (dd, *J* = 10.0, 9.3 Hz, 1H), 4.42 (t, *J* = 10.4 Hz, 1H), 4.33 (dd, *J* = 12.4, 4.7 Hz, 1H), 4.16 (dd, *J* = 12.3, 2.2 Hz, 1H), 3.86 (ddd, *J* = 10.2, 4.7, 2.2 Hz, 1H), 2.16 (s, 3H), 2.10 (s, 3H), 2.02 (s, 3H), 1.85 (s, 3H), 1.27 (s, 9H). ^{13}C NMR (101 MHz, $CDCl_3$) δ 170.74, 170.13, 169.43, 149.57(2C), 137.65, 134.44, 134.32, 131.07(2C), 130.50, 130.02(2C), 125.77(2C), 123.71, 123.62, 84.37, 75.87, 71.61, 68.64, 62.27, 53.80, 34.37, 31.23(3C), 20.80, 20.63, 20.45, 20.28.

2-Methyl-5-tert-butylphenyl-4,6-*O*-benzylidene-2-deoxy-2-*N*-phthalimido-1-thio-β-D-glucopyranoside (2-11)

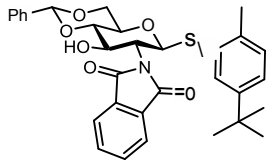

To a stirred solution of thioglycoside **2-10** (5.86 g, 9.8 mmol) in MeOH (20mL) was added freshly prepared 1 M solution of NaOMe. After 1 h, the reaction was neutralized with Amberlite IR 120 H^+ resin, filtered and concentrated. To the solution of crude product in CH_3CN (35 mL) were added benzaldehyde dimethyl acetal (2.94 mL, 19.56 mmol) and CSA (0.682 g, 2.93 mmol). The reaction mixture was stirred for 3 h at room temperature. The reaction was quenched with aq.$NaHCO_3$, extracted with CH_2Cl_2, washed with brine and dried over Na_2SO_4. The solvents were removed under reduced pressure and the crude product was purified by flash column chromatography to obtain compound **2-11** (3.23 g, 5.77 mmol, 59% over two steps). R_f = 0.4 (EtOAc/hexane = 1:1) ^{1}H NMR (400 MHz, $CDCl_3$) δ 7.91 (d, *J* = 4.8 Hz, 1H), 7.84 (d, *J* = 4.6 Hz, 1H), 7.78 – 7.71 (m, 2H), 7.53 – 7.44 (m, 4H), 7.37 (dd, *J* = 5.0, 1.7 Hz, 4H), 7.19 (dd, *J* = 8.0, 2.0 Hz, 1H), 7.05 (d, *J* = 8.0 Hz, 1H), 5.64 – 5.56 (m, 2H),

4.72 – 4.62 (m, 1H), 4.45 – 4.33 (m, 2H), 3.91 – 3.81 (m, 1H), 3.74 – 3.61 (m, 3H), 2.15 (s, 3H), 1.27 (s, 9H). ^{13}C NMR (101 MHz, $CDCl_3$) δ 149.53(2C), 136.92, 136.85, 134.24, 131.28, 130.22, 129.97, 129.39, 128.40(2C), 126.28(2C), 125.37, 123.88, 123.29, 101.99, 85.05, 82.00, 70.18, 69.72, 68.62, 55.63, 34.66, 34.40, 31.23(3C), 26.91, 20.21.

2-Methyl-5-tert-butylphenyl-3-*O*-benzyl-4,6-*O*-benzylidene-2-deoxy-2-*N*-phthalimido-1-thio-β-D-glucopyranoside (2-12)

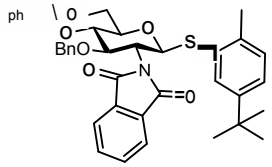

To a stirred solution of **2-11** (3 g, 5.36 mmol) in anhydrous DMF (20 mL) was added NaH (0.25 g, 10.72 mmol) at 0 °C. After 20 min, BnBr (0.96 mL, 8.04 mmol) was added and the reaction was stirred overnight at room temperature. The reaction was quenched with MeOH and concentrated. The crude product was purified by flash chromatography to obtain **2-12** (2.2 g, 3.39 mmol, 63%). R_f = 0.4 (EtOAc/hexane = 2:3) ^{1}H NMR (400 MHz, $CDCl_3$) δ 7.88 (d, *J* = 7.0 Hz, 1H), 7.73 (dt, *J* = 15.4, 6.8 Hz, 3H), 7.63 (d, *J* = 7.0 Hz, 1H), 7.53 (dd, *J* = 7.7, 1.7 Hz, 3H), 7.46 – 7.35 (m, 5H), 7.17 (dd, *J* = 8.0, 2.0 Hz, 1H), 7.06 – 6.96 (m, 3H), 6.94 – 6.82 (m, 3H), 5.65 (s, 1H), 5.54 (d, *J* = 10.6 Hz, 1H), 4.80 (d, *J* = 12.3 Hz, 1H), 4.55 – 4.42 (m, 2H), 4.44 – 4.31 (m, 2H), 3.88 (q, *J* = 9.5, 8.9 Hz, 2H), 3.70 (td, *J* = 9.8, 5.0 Hz, 1H), 2.11 (s, 3H), 1.25 (s, 9H). ^{13}C NMR (101 MHz, $CDCl_3$) δ 149.47(2C), 137.72, 137.24, 136.75, 134.02, 133.84, 131.54, 131.32, 129.96, 129.92, 129.04, 128.30(2C), 128.15(2C), 128.03(2C), 127.42, 126.03(2C), 125.21, 123.27, 101.33, 84.80, 82.88, 75.44, 74.20, 70.26, 68.71, 54.84, 34.38, 31.21(3C), 20.17.

3-*O*-benzyl-4,6-*O*-benzylidene-2-deoxy-2-*N*-phthalimido-β-D-glucopyranosyl trichloroacetimidate (2-13)

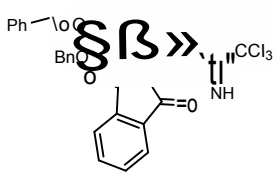

To a solution of thioglycoside **2-12** (1 g, 1.54 mmol) in a acetone-water (9:1) mixture was added NBS (0.82 g, 4.62 mmol). After 30 min., the reaction mixture was concentrated, extracted with EtOAc and washed with aq. $NaHCO_3$, water and brine. The organic layer was dried over $Na_2SO_4$and concentrated. The residue was purified by flash chromatography to obtain hemiacetal intermediate (0.7 g, 1.436 mmol, 93%). R_f = 0.3 (EtOAc/hexane = 1:1) ^{1}H NMR (400 MHz, $CDCl_3$) δ 7.73 – 7.64 (m, 4H), 7.52 – 7.45 (m, 3H), 7.41 – 7.30 (m, 2H), 7.26 (s, 0H), 7.01 – 6.80 (m, 5H), 5.60 (d, *J* = 6.6 Hz, 1H), 5.35 (d, *J* = 8.5 Hz, 1H), 4.75 (d, *J* = 12.3 Hz, 1H), 4.51 – 4.31 (m, 3H), 4.08 (dd, *J* = 10.4, 8.5 Hz, 1H), 3.79 (dt, *J* = 11.7, 9.7 Hz, 3H), 3.64 (td, *J* = 9.8, 4.9 Hz, 1H). ^{13}C NMR (101 MHz. $CDCl_3$) δ 137.74, 137.22, 133.94, 131.48, 129.01, 128.25, 128.03, 128.01, 127.42, 126.00, 123.32, 101.28, 93.22, 83.09, 74.47, 74.07, 68.73, 66.11, 57.45, 49.51, 49.30, 49.08.

To a stirred solution of hemiacetal (0.6 g, 1.23 mmol) in CH_2Cl_2 (10 mL) at 0 °C were added CCl_3CN (0.62 mL, 6.15 mmol) and DBU (0.019 mL, 0.123 mmol). The reaction mixture was stirred for 1 h at 0 °C. The resulting mixture was concentrated and purified by flash column chromatography to obtain imidate donor **2-13** (0.5 g, 0.79 mmol, 65%) as clear oil. R_f = 0.45 (EtOAc/hexane = 2:3) ^{1}H NMR (400 MHz, $CDCl_3$) δ 8.57 (s, 1H), 7.71 (s, 3H), 7.54 (dd, *J* = 7.6, 1.8 Hz, 3H), 7.46 – 7.34 (m, 3H), 7.02 (d, *J* = 6.6 Hz, 2H), 6.98 – 6.84 (m, 3H), 6.49 (d, *J* = 8.4 Hz, 1H), 5.65 (s, 1H), 5.30 (s, 2H), 4.82 (d, *J* = 12.4 Hz, 1H), 4.57 – 4.50 (m, 3H), 3.94 – 3.87 (m, 2H). ^{13}C NMR (101 MHz, $CDCl_3$) δ 160.79, 137.73, 137.11, 133.98, 131.36, 129.11, 128.32, 128.06, 127.47, 126.07, 123.41, 101.46, 94.31, 82.61, 74.31, 74.21, 68.53, 66.89, 54.70, 53.44.

1-*O*-(6-thiobenzyl)hexyl-3-*O*-benzyl-4,6-*O*-benzylidene-2-deoxy-2-*N*-phthalimido-β-D-glucopyranoside (2-8)

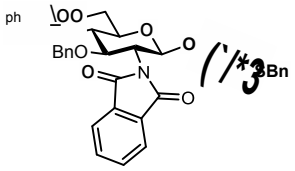

The imidate donor **2-13** (0.43 g, 0.68 mmol) and 6-(benzylthio)hexan-1-ol (0.117 g, 0.523 mmol) were co-evaporated with anhydrous toluene (3x5 mL) and dried under high vacuum for 1 h. The mixture was dissolved in anhydrous CH_2Cl_2 and activated molecular sieves were added. The solution was stirred for 10 min at room temperature and cooled to -40 °C. The

mixture was treated with TMSOTf (19 µL, 0.105 mmol) and slowly warmed to -20 °C over a period of 1 h. The reaction was diluted with CH_2Cl_2, quenched with Et_3N and concentrated. The crude product was purified by flash column chromatography to obtain **2-8** (0.32 g, 0.454 mmol, 87%). R_f = 0.4 (EtOAc/hexane = 2:3) ^{1}H NMR (400 MHz, $CDCl_3$) δ 7.68 (s, 2H), 7.57 – 7.50 (m, 3H), 7.45 – 7.19 (m, 9H), 7.04 – 6.93 (m, 3H), 6.93 – 6.84 (m, 4H), 5.63 (s, 1H), 5.19 (dd, *J* = 8.5, 3.3 Hz, 1H), 4.80 (d, *J* = 12.3 Hz, 1H), 4.51 (d, *J* = 12.4 Hz, 1H), 4.46 – 4.36 (m, 3H), 4.20 (dd, *J* = 10.4, 8.5 Hz, 1H), 3.91 – 3.71 (m, 3H), 3.63 (d, *J* = 7.5 Hz, 3H), 3.43 – 3.24 (m, 2H), 2.18 (t, *J* = 7.3 Hz, 2H), 1.38 (ddd, *J* = 23.9, 12.1, 5.5 Hz, 2H), 1.19 (dd, *J* = 10.2, 7.4 Hz, 2H), 1.13 – 0.98 (m, 4H). ^{13}C NMR (101 MHz, $CDCl_3$) δ 137.92, 137.32, 133.89, 131.53, 129.01, 128.77, 128.42, 128.29, 128.04, 127.36, 126.86, 126.04, 101.30, 98.91, 83.12, 74.57, 74.07, 69.84, 68.81, 66.09, 55.83, 36.22, 31.09, 29.11, 28.90, 28.35, 25.34.

1-*O*-(6-thiobenzyl)hexyl-3,6-*O*-benzyl-2-deoxy-2-*N*-phthalimido-β-D-glucopyranoside (2-14)

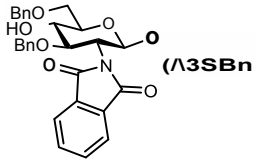

To a stirred solution of **2-8** (0.5 g, 0.72 mmol) in CH_2Cl_2 (8 mL) were added trifluoroacetic anhydride (0.31 mL, 2.16 mmol) and triethylsilane (0.58 mL, 3.6 mmol) were added at 0 °C followed by trifluoroacetic acid (0.28 mL, 3.6 mmol) drop wise. The reaction mixture was stirred at 0 °C. After 5 h, the reaction mixture was quenched with Et_3N and concentrated to give yellow oil that was purified by flash column chromatography to obtain glucoasamine acceptor **2-14** (0.4 g, 0.57 mmol, 80 %) as a colorless oil. R_f = 0.33 (Hexanes/EtOAc = 3:1) ^{1}H NMR (400 MHz, $CDCl_3$) δ 7.83 – 7.62 (m, 3H), 7.40 – 7.16 (m, 9H), 7.04 (dd, *J* = 7.3, 2.0 Hz, 2H), 6.99 – 6.87 (m, 4H), 5.28 (s, 2H), 5.10 (dd, *J* = 8.3, 3.0 Hz, 1H), 4.73 (d, *J* = 12.2 Hz, 1H), 4.63 (d, *J* = 11.9 Hz, 1H), 4.54 (dd, *J* = 20.4, 12.1 Hz, 2H), 4.26 – 4.16 (m, 1H), 4.12 (ddd, *J* = 10.7, 8.3, 1.8 Hz, 1H), 3.86 – 3.68 (m, 4H), 3.68 – 3.57 (m, 2H), 3.39 – 3.22 (m, 2H), 2.16 (t, *J* = 7.3 Hz, 1H), 1.40 – 1.30 (m, 2H), 1.20 – 1.11 (m, 2H), 1.09 – 0.94 (m, 4H). ^{13}C NMR (101 MHz, $CDCl_3$) δ 138.17, 137.55, 133.88, 128.77, 128.51, 128.42, 128.14, 127.91, 127.88, 127.81, 127.40, 126.85, 98.30, 78.64, 77.33, 77.01, 76.69, 74.61, 74.28, 73.78, 73.37, 70.82, 69.48, 55.37, 36.20, 31.08, 29.08, 28.91, 28.36, 25.37.

2-*O*-Acetyl-3,4-di-*O*-benzyl-6-*O*-triisopropylsilyl-α-D-mannopyranosyl-(1→4)-1-*O*-(6-thiobenzyl)hexyl-3,6-*O*-benzyl-2-deoxy-2-*N*-phthalimido-β-D-glucopyranoside (2-4)

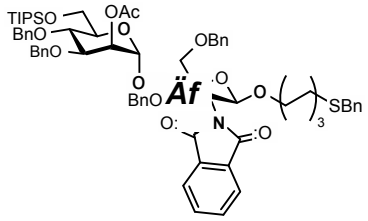

The imidate donor **2-6** (0.36 g, 0.52 mmol) and glucosamine acceptor **2-14** (0.3 g, 0.43 mmol) were co-evaporated with anhydrous toluene (3x7 mL) and dried under high vacuum for 2 h. The mixture was dissolved in anhydrous CH_2Cl_2 (8 mL) and activated molecular sieves were added. The solution was stirred for 10 min at room temperature and cooled to -40 °C. The mixture was treated with TMSOTf (19 µL, 0.086 mmol) and slowly warmed to -20 °C over a period of 1 h. The reaction was diluted with CH_2Cl_2, quenched with Et_3N and concentrated. The crude product was purified by flash column chromatography to obtain disaccharide **2-4** (0.47 g, 0.38 mmol, 88%) as white solid. R_f = 0.5 (Hexanes/EtOAc = 3:1) ^{1}H NMR (400 MHz, $CDCl_3$) δ 7.63 (d, *J* = 16.0 Hz, 5H), 7.39 – 7.17 (m, 28H), 7.00 (d, *J* = 7.4 Hz, 2H), 6.88 (t, *J* = 7.6 Hz, 2H), 6.77 (t, *J* = 7.3 Hz, 1H), 5.42 (s, 1H), 5.27 (s, 1H), 5.05 (dd, *J* = 8.4, 2.7 Hz, 1H), 4.85 (dd, *J* = 15.8, 11.5 Hz, 3H), 4.76 – 4.47 (m, 7H), 4.37 (dd, *J* = 10.7, 8.7 Hz, 1H), 4.28 (d, *J* = 12.2 Hz, 1H), 4.20 – 3.98 (m, 3H), 3.95 – 3.85 (m, 4H), 3.79 – 3.70 (m, 5H), 3.63 (d, *J* = 25.1 Hz, 4H), 3.32 (dt, *J* = 9.7, 6.8 Hz, 1H), 2.15 (t, *J* = 7.2 Hz, 2H), 1.97 (s, 3H), 1.42 – 1.25 (m, 3H), 1.17 (dt, *J* = 15.0, 6.9 Hz, 3H), 1.13 – 1.03 (m, 7H), 1.04 (s, 22H). ^{13}C NMR (101 MHz, $CDCl_3$) δ 170.05, 138.73, 138.29, 138.00, 137.82, 133.73, 128.75, 128.40, 128.34, 128.32, 128.26, 128.07, 128.01, 127.99, 127.95, 127.91, 127.66, 127.61, 127.37, 127.29, 127.07, 126.83, 99.16, 98.07, 81.00, 77.93, 76.81, 75.27, 74.63, 74.54, 73.79, 73.59, 73.29, 71.83, 69.37, 69.27, 68.97, 62.12, 55.64, 36.18, 31.07, 29.09, 28.90, 28.36, 26.89, 25.39, 20.82, 18.01(3C), 17.92(3C), 11.99(3C).

2-*O*-Acetyl-3,4-di-*O*-benzyl-α-D-mannopyranosyl-(1→4)- 1-*O*-(6-thiobenzyl)hexyl-3,6-*O*-benzyl-2-deoxy-2-*N*-phthalimido-β-D-glucopyranoside (2-15)

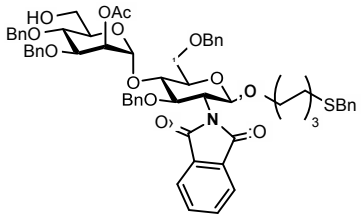

To a stirred solution of disaccharide **2-4** (0.16 g, 0.13 mmol) in THF (4 mL) was added 70% HF in pyridine (0.08 mL, 0.65 mmol). The reaction mixture was stirred for 48 h at room temperature. The reaction was quenched with aq. $NaHCO_3$, extracted with CH_2Cl_2, washed with brine and dried over Na_2SO_4. The solvents were removed under reduced pressure and the crude product was purified by flash column chromatography to obtain the disaccharide acceptor **2-15** (0.12 g, 0.11 mmol, 83%). R_f = 0.4 (Hexanes/EtOAc = 2:1) ^{1}H NMR (400 MHz, $CDCl_3$) δ 7.71 – 7.63 (m, 6H), 7.51 – 7.21 (m, 20H), 7.07 – 6.91 (m, 4H), 6.88 – 6.79 (m, 1H), 5.55 – 5.47 (m, 1H), 5.35 (d, *J* = 1.4 Hz, 1H), 5.07 (d, *J* = 8.5 Hz, 1H), 4.88 (dd, *J* = 24.8, 11.5 Hz, 1H), 4.78 – 4.60 (m, 3H), 4.63 – 4.51 (m, 1H), 4.44 (ddd, *J* = 11.4, 8.7, 2.9 Hz, 1H), 4.32 (d, *J* = 12.2 Hz, 1H), 4.24 – 4.11 (m, 1H), 4.10 – 3.89 (m, 2H), 3.90 – 3.58 (m, 10H), 3.36 (dt, *J* = 9.8, 6.6 Hz, 1H), 2.19 (t, *J* = 7.3 Hz, 1H), 2.05 (s, 3H), 1.38 (ddt, *J* = 30.1, 13.0, 6.8 Hz, 3H), 1.30 – 0.84 (m, 7H). ^{13}C NMR (101 MHz, $CDCl_3$) δ 169.95, 138.59, 138.19, 138.07, 137.84, 137.76, 133.87, 130.05, 129.05, 128.80, 128.46, 128.43, 128.38, 128.11, 128.05, 128.03, 127.89, 127.80, 127.76, 127.65, 127.26, 127.19, 126.90, 99.27, 98.09, 81.25, 77.90, 76.90, 75.32, 74.94, 74.70, 74.02, 73.67, 73.11, 71.85, 69.43, 68.85, 68.60, 62.03, 55.82, 36.22, 31.09, 29.13, 28.93, 28.40, 25.44, 20.98.

***n*-Allyl-2-*O*-acetyl-3,4-di-*O*-benzyl-6-*O*-tri*iso*propylsilyl-α-D-mannopyranosyl-(1→2)-3,4,6-tri-*O*-benzyl-α-D-mannopyranoside (2-17)**

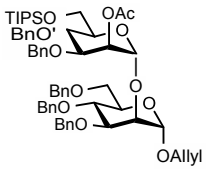

The mannosyl imidate **2-6** (1.65 g, 2.35 mmol) and allyl mannosyl acceptor **2-16** (1.1 g, 2.24 mmol) were co-evaporated with toluene (3 x 12 mL) and dried under high vacuum for 2 h. The mixture was dissolved in anhydrous CH_2Cl_2 (30 mL) and activated molecular sieves were added. The solution was stirred for 10 min at room temperature and cooled to -40 °C. The mixture was treated with TMSOTf (41 µL, 0.22 mmol) and slowly warmed to -20 °C over a period of 1 h. The reaction was diluted with CH_2Cl_2, quenched with Et_3N and concentrated. The crude product was purified by flash column chromatography to obtain disaccharide **2-17** (1.8 g, 1.75 mmol, 80%) as a colorless oil. R_f = 0.33 (EtOAc/Hexanes 1:9) ^{1}H NMR (400 MHz, $CDCl_3$) δ 7.37 – 7.22 (m, 28H), 7.18 (t, *J* = 7.1 Hz, 3H), 5.85 (ddt, *J* = 16.4, 10.8, 5.6 Hz, 1H), 5.52 – 5.46 (m, 1H), 5.22 (dd, *J* = 17.2, 1.5 Hz, 1H), 5.15 (t, *J* = 5.1 Hz, 2H), 4.85 (t, *J* = 10.9 Hz, 3H), 4.74 – 4.58 (m, 6H), 4.56 – 4.48 (m, 2H), 4.41 (d, *J* = 11.0 Hz, 1H), 4.18 – 4.07 (m, 3H), 4.03 – 3.80 (m, 9H), 3.72 (dd, *J* = 24.0, 8.5 Hz, 4H), 2.07 (s, 3H). ^{13}C NMR (101 MHz, $CDCl_3$) δ 170.14, 138.68, 138.34, 138.27, 138.12, 133.71, 128.33, 128.31, 128.29, 128.16, 128.05, 127.90, 127.58, 127.52, 127.42, 117.23, 98.77, 98.08, 80.10, 78.08, 75.20(2C), 74.56, 73.98, 73.45, 73.28, 72.77, 71.93, 71.90, 71.88, 69.18, 68.77, 67.76, 62.65, 21.02, 18.03(3C), 17.97(3C), 12.03(3C).

2-*O*-Acetyl-3,4-di-*O*-benzyl-6-*O*-tri*iso*propylsilyl-α-D-mannopyranosyl-(1→2)-3,4,6-tri-*O*-benzyl-α–D-mannopyranosyl trichloroacetimidate (2-18)

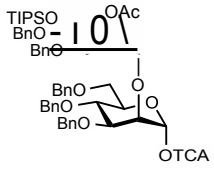

A solution of $[IrCOD(PPh_2Me)_2]PF_6$ (5.0 mg, 5.8 µmol) in THF (3 mL) was stirred under hydrogen atmosphere until the color turned from red to colorless to pale yellow. The hydrogen atmosphere was exchanged with Argon. The activated catalyst solution was added to a solution of disaccharide **2-17** (0.30 g, 0.29 mmol) in THF (10 mL) and stirred at room temperature. After 16 h, the solvent was removed and the residue was dissolved in a mixture of acetone (5.2 mL) and water (0.6 mL). Mercury (II) chloride (0.39 g, 1.45 mmol) and mercury (II) oxide (0.01 mg, 0.044 mmol) were added. After 1 h, saturated aq.$NaHCO_3$ was added to reaction mixture and was extracted three times with CH_2Cl_2. The combined organic layers were dried over Na_2SO_4 and concentrated. The crude product was purified by flash

column chromatography to obtain disaccharide hemiacetal intermediate (0.24 g, 0.24 mmol, 81%) as colorless oil.

To a stirred solution of hemiacetal (0.285 g, 0.28 mmol) in CH_2Cl_2 (13 mL) at 0 °C were added CCl_3CN (0.29 mL, 2.88 mmol) and DBU (0.009 mL, 0.06 mmol). The reaction mixture was stirred for 1 h at 0 °C. The resulting mixture was concentrated and purified by flash column chromatography to obtain imidate donor **2-18** (0.28 g, 0.25 mmol, 86%) as clear oil. R_f = 0.4 (EtOAc/hexane = 2:3) ^{1}H NMR (400 MHz, $CDCl_3$) δ 8.53 (s, 1H), 7.39 – 7.31 (m, 5H), 7.31 – 7.13 (m, 17H), 6.29 (s, 1H), 5.51 (s, 1H), 5.15 (s, 1H), 4.93 – 4.85 (m, 2H), 4.79 – 4.68 (m, 3H), 4.67 – 4.56 (m, 2H), 4.47 (dd, *J* = 28.1, 11.5 Hz, 2H), 4.12 (s, 1H), 4.08 – 3.91 (m, 8H), 3.86 – 3.77 (m, 2H), 3.70 (d, *J* = 11.3 Hz, 1H), 2.11 (s, 3H), 1.08 (d, *J* = 4.7 Hz, 21H).

1-*O*-(6-thiobenzyl)hexyl-2-*O*-acetyl-3,4-di-*O*-benzyl-6-*O*-tri*iso*propylsilyl-α-D-mannopyranosyl-(1→2)-3,4,6-tri-*O*-benzyl-α-D-mannopyranosyl-(1→6)-2-*O*-Acetyl-3,4-di-*O*-benzyl-α-D-mannopyranosyl-(1→4)-3,6-*O*-benzyl-2-deoxy-2-*N*-phthalimido-β-D-glucopyranoside (2-19)

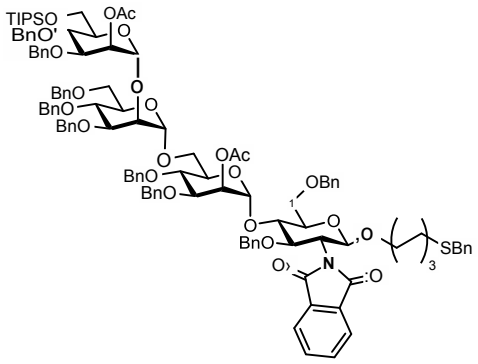

The disaccharide imidate **2-18** (0.18 g, 0.16 mmol) and disaccharide acceptor **2-15** (0.14 g, 0.13 mmol) were co-evaporated with toluene (3 x 5 mL) and dried under high vacuum for 2 h. The mixture was dissolved in a mixture of anhydrous diethylether and anhydrous CH_2Cl_2 (1:1, 6 mL) and activated molecular sieves were added. The solution was stirred for 10 min at room temperature and cooled to 0 °C. The mixture was treated with TBSOTf (9 µL, 0.04 mmol) and stirred at 0 °C for a period of 1 h. The reaction was diluted with CH_2Cl_2, quenched with Et_3N and concentrated. The crude product was purified by flash column chromatography to obtain tetrasaccharide **2-19** (0.15 g, 0.07 mmol, 55 % α–isomer). R_f = 0.3 (EtOAc/hexane

= 2:3) ^{1}H NMR (400 MHz, $CDCl_3$) δ 7.68 – 7.59 (m, 6H), 7.31 (dd, *J* = 17.9, 11.8 Hz, 30H), 7.21 (dd, *J* = 14.7, 7.7 Hz, 36H), 7.17 – 7.08 (m, 7H), 7.01 (d, *J* = 7.4 Hz, 3H), 6.90 (t, *J* = 7.5 Hz, 3H), 6.79 (t, *J* = 7.2 Hz, 1H), 5.49 (d, *J* = 13.5 Hz, 3H), 5.34 (s, 1H), 5.15 (s, 1H), 5.08 – 5.01 (m, 2H), 4.93 – 4.79 (m, 8H), 4.72 – 4.27 (m, 23H), 4.23 – 3.99 (m, 7H), 4.02 – 3.79 (m, 16H), 3.77 (t, *J* = 10.2 Hz, 7H), 3.75 – 3.58 (m, 7H), 3.55 – 3.38 (m, 5H), 3.39 – 3.21 (m, 3H), 2.41 – 2.28 (m, 2H), 2.15 (t, *J* = 7.2 Hz, 1H), 2.07 (s, 3H), 1.98 (s, 3H), 1.08 (d, *J* = 4.1 Hz, 30H), 0.96 (d, *J* = 36.0 Hz, 2H), 0.92 – 0.81 (m, 23H). ^{13}C NMR (101 MHz, $CDCl_3$) δ 170.17, 169.87, 138.83, 138.54, 138.42, 138.16, 138.09, 138.02, 137.78, 137.63, 133.79, 129.99, 128.98, 128.76, 128.42, 128.38, 128.32, 128.30, 128.27, 128.23, 128.17, 128.14, 127.98, 127.93, 127.90, 127.75, 127.55, 127.49, 127.46, 127.32, 127.29, 127.22, 127.11, 126.85, 99.36, 99.01, 98.88, 98.09, 80.96, 79.65, 78.45, 77.93, 75.23, 75.02, 74.78, 74.54, 74.23, 73.77, 73.37, 73.12, 71.88, 71.81, 71.75, 71.55, 69.33, 68.85, 68.59, 66.18, 62.50, 55.77, 36.20, 32.36, 31.93, 31.07, 29.70(2C), 29.37, 29.08, 28.90, 28.37, 26.35, 25.39, 22.70, 21.03, 20.95, 18.10(3C), 18.02(3C), 14.15, 12.05(3C).

1-*O*-(6-thiobenzyl)hexyl-2-*O*-acetyl-3,4-di-*O*-benzyl-α-D-mannopyranosyl-(1→2)-3,4,6-tri-*O*-benzyl-α-D-mannopyranosyl-(1→6)-2-*O*-Acetyl-3,4-di-*O*-benzyl-α-D-mannopyranosyl-(1→4)-3,6-*O*-benzyl-2-deoxy-2-*N*-phthalimido-β-D-glucopyranoside (2-20)

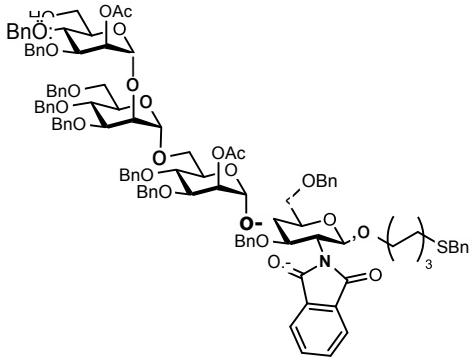

To a stirred solution of tetrasaccharide **2-19** (0.13 g, 0.190 mmol) in CH_3CN (7 mL) were added water (50 μL) and $Sc(OTf)_3$ (0.093 g, 0.19 mmol). The reaction mixture was heated up to 50 °C ans stirred for 6 h. The reaction was quenched with Et_3N and concentrated. The crude product was purified by flash column chromatography to obtain **2-20** (0.09 g, 0.05 mmol, 71%). R_f = 0.35 (EtOAc/hexane = 1:1) ^{1}H NMR (400 MHz, $CDCl_3$) δ 7.63 (d, *J* = 16.4

Hz, 4H), 7.30 (dd, *J* = 9.4, 6.1 Hz, 17H), 7.23 (d, *J* = 7.3 Hz, 22H), 7.16 (dd, *J* = 14.8, 5.9 Hz, 9H), 7.00 (d, *J* = 7.5 Hz, 2H), 6.89 (t, *J* = 7.5 Hz, 2H), 6.77 (t, *J* = 7.3 Hz, 1H), 5.48 (s, 2H), 5.32 (s, 1H), 5.07 – 4.97 (m, 2H), 4.95 – 4.83 (m, 3H), 4.82 (d, *J* = 11.5 Hz, 3H), 4.69 – 4.54 (m, 8H), 4.50 (dd, *J* = 20.1, 9.3 Hz, 3H), 4.47 – 4.33 (m, 5H), 4.29 (d, *J* = 12.2 Hz, 1H), 4.22 – 4.13 (m, 1H), 4.07 (s, 1H), 4.01 – 3.68 (m, 24H), 3.65 – 3.53 (m, 5H), 3.53 – 3.44 (m, 3H), 3.37 – 3.21 (m, 2H), 2.14 (t, *J* = 6.7 Hz, 2H), 2.08 (s, 3H), 1.98 (s, 3H), 1.37 (dd, *J* = 15.8, 8.1 Hz, 3H), 1.35 – 1.22 (m, 3H), 1.15 (dd, *J* = 15.2, 7.9 Hz, 3H), 1.12 – 0.91 (m, 6H), 0.86 (d, *J* = 10.4 Hz, 3H). ^{13}C NMR (101 MHz, $CDCl_3$) δ 170.04, 170.04, 169.91, 138.41, 138.32, 138.13, 138.01, 137.78, 137.69, 128.77, 128.43, 128.38, 128.34, 128.30, 128.26, 128.21, 128.12, 128.10, 128.01, 127.96, 127.94, 127.79, 127.61, 127.54, 127.50, 127.37, 127.26, 127.12, 126.86, 99.46, 99.20, 99.03, 98.08, 79.23, 79.14, 78.82, 78.78, 77.98, 77.34, 77.20, 77.02, 76.70, 76.48, 76.17, 75.15, 75.03, 74.96, 74.76, 74.58, 74.49, 74.31, 74.11, 73.41, 73.26, 73.19, 72.39, 72.31, 71.83, 69.38, 69.30, 69.07, 68.80, 68.67, 66.19, 66.19, 55.74, 31.93, 31.06, 29.70, 29.08, 28.91, 28.37, 25.39, 21.09.

1-*O*-(6-thio)hexyl-α-D-mannopyranosyl-(1→2)-α-D-mannopyranosyl-(1→6)-α-D-mannopyranosyl-(1→4)-2-amino-2-deoxy-β-D-glucopyranoside (GPI 1)

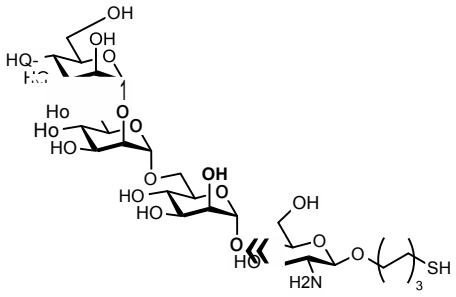

Tetrasaccharide **2-20** (0.03 g, 0.02 mmol) was dissolved in a mixture of ethylenediamine (2 mL) and butanol (2 mL) and stirred at 90 °C for 3 h. After 3 h, the reaction mixture was concentrated to obtain partially deprotected crude intermediate. The crude intermediate was dissolved in anhydrous THF and MeOH. This solution was added dropwise to blue solution of 20 mL liquefied ammonia with sodium -78 °C. The reaction was stirred at -78 °C. After 1 h, the reaction was quenched with MeOH and stirred for additional 1h at rt. Sodium methoxide generated in the reaction was quenched by dropwise addition of glacial acetic acid. The reaction mixture was concentrated and the crude product was purified by size exclusion

column chromatography using a Sephadex® super fine G-15 (GE Healthcare) column and 5% ethanol in water as eluent to obtain **GPI 1** (7 mg, 0.009 mmol, 57%) as white solid. ^{1}H NMR (600 MHz, Deuterium Oxide) δ 5.08 (s, 1H), 5.02 (s, 1H), 4.91 (s, 1H), 4.53 – 4.37 (m, 0H), 3.94 (ddd, *J* = 5.6, 3.1, 1.9 Hz, 3H), 3.91 – 3.88 (m, 2H), 3.85 – 3.74 (m, 9H), 3.75 – 3.52 (m, 22H), 3.53 – 3.42 (m, 4H), 3.23 – 3.08 (m, 1H), 2.97 – 2.91 (m, 1H), 2.86 – 2.72 (m, 1H), 2.64 (t, *J* = 7.2 Hz, 1H), 1.55 (ddd, *J* = 25.0, 14.1, 7.0 Hz, 6H), 1.30 – 1.25 (m, 6H). ^{13}C NMR (151 MHz, D_2O) δ 104.93, 104.55, 102.58, 100.95, 81.28, 79.80, 77.57, 75.85, 75.34, 74.88, 73.29, 73.00, 72.92, 72.82, 72.78, 72.56, 69.54, 69.48, 69.03, 68.89, 63.75, 63.54, 63.38, 58.69, 40.75, 31.13, 30.78, 29.82, 27.22, 25.82. HRMS (*m*/*z*) of the oxidized compound: $[M+2H]^{2+}$ cald 781.3033 obsd 781.3027.

1-*O*-(6-thiobenzyl)hexyl-2-*O*-Acetyl-3,4-di-*O*-benzyl-6-*O*-(2-*N*-benzyloxycarbonyl) aminoethyl-phosphonato-α-D-mannopyranosyl-(1→2)-3,4,6-tri-*O*-benzyl-α-D-mannopyranosyl-(1→6)-2-*O*-Acetyl-3,4-di-*O*-benzyl-α-D-mannopyranosyl-(1→4)- 3,6-*O*-benzyl-2-deoxy-2-*N*-phthalimido-β-D-glucopyranoside (2-21)

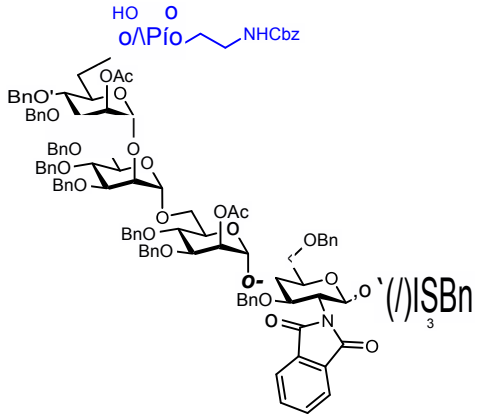

Tetrasaccharide **2-20** (0.02 g, 10.5 µmol) and *H*–phosphonate **2-3** (0.01 g, 0.03 mmol) were co-evaporated with pyridine for three times and dried under high vacuum for 2 h. The mixture was dissolved in anhydrous pyridine (5 mL) and a solution of pivolyl chloride (4 µL, 0.03 mmol) in pyridine (1 mL) was added. The solution was stirred for 6 h at room temperature. After 6 h, iodine (8 mg, 0.03 mmol) and water (0.05 mL) were added and reaction was stirred for additional 2 h at room temperature. The reaction mixture was quenched with $Na_2S_2O_3$ and extracted with CH_2Cl_2. The organic layer were concentrated and purified by Et_3N deactivated silica gel flash column chromatography to obtain phosphorylated tetrasaccharide **2-21** (15 mg, 7 µmol, 66%). R_f = 0.5 (MeOH/ CH_2Cl_2 = 1:10) ^{1}H NMR (400 MHz, $CDCl_3$) δ 7.64 (d, *J* =

16.6 Hz, 4H), 7.21 (dd, *J* = 11.7, 8.2 Hz, 27H), 7.15 (dd, *J* = 10.7, 5.4 Hz, 15H), 7.14 – 7.01 (m, 4H), 5.48 (d, *J* = 8.0 Hz, 2H), 5.37 (s, 1H), 5.25 (s, 0H), 5.09 (s, 1H), 5.03 – 4.93 (m, 1H), 4.87 – 4.67 (m, 5H), 4.64 – 4.34 (m, 9H), 3.96 – 3.85 (m, 5H), 3.76 (td, *J* = 23.3, 21.0, 9.8 Hz, 7H), 3.65 – 3.52 (m, 4H), 3.37 – 3.17 (m, 7H), 2.11 (t, *J* = 7.2 Hz, 1H), 2.00 – 1.90 (m, 6H), 1.53 (t, *J* = 7.3 Hz, 0H), 1.25 – 1.16 (m, 4H), 1.14 – 0.94 (m, 3H). ^{13}C NMR (151 MHz, D_2O) δ 105.02, 104.44, 104.44, 100.81, 81.53, 79.88, 77.48, 75.35, 74.85, 74.59, 73.17, 72.96, 72.81, 72.78(2C), 72.48, 69.49, 69.16, 68.90, 64.53, 64.50, 63.50, 58.94, 53.53, 42.64, 30.99, 29.94, 27.22, 26.47, 25.86.^{31}P NMR (162 MHz, $CDCl_3$) δ -1.95.

1-*O*-(6-thio)hexyl-6-*O*-aminoethyl-phosphonato-α-D-mannopyranosyl-(1→2)-α-D-mannopyranosyl-(1→6)-α-D-mannopyranosyl-(1→4)-2-deoxy-2-amino-β-D-glucopyranoside (GPI 2)

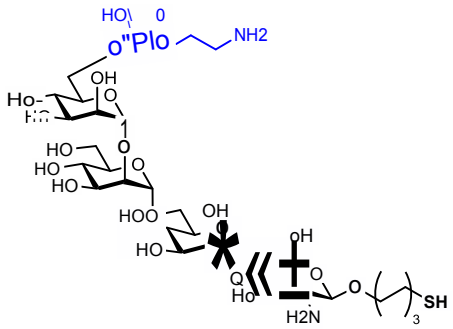

Tetrasaccharide **2-21** (16 mg, 7.5 µmol) was dissolved in a mixture of ethylenediamine (2 mL) and butanol (2 mL) and stirred at 90 °C for 3 h. After 3 h, the reaction mixture was concentrated to obtain partially deprotected crude intermediate. The crude intermediate was dissolved in anhydrous THF and MeOH. This solution was added dropwise to blue solution of 20 mL liquefied ammonia with sodium -78 °C. The reaction was stirred at -78 °C. After 1 h, the reaction was quenched with MeOH and stirred for additional 1h at rt. Sodium methoxide generated in the reaction was quenched by dropwise addition of glacial acetic acid. The reaction mixture was concentrated and the crude product was purified by size exclusion column chromatography using a Sephadex® super fine G-15 (GE Healthcare) column and 5% ethanol in water as eluent to obtain **GPI 2** (5 mg, 5.6 µmol, 75%) as white solid. ^{1}H NMR (600 MHz, D_2O) δ 5.14 – 5.06 (m, 1H), 5.04 – 4.96 (m, 1H), 4.93 – 4.87 (m, 1H), 4.37 (d, *J* = 8.2 Hz, 1H), 4.06 – 3.39 (m, 26H), 3.21 – 3.13 (m, 2H), 2.83 – 2.74 (m, 1H), 2.67 (s, 1H), 1.62 (dt, *J* = 15.6, 7.5 Hz, 2H), 1.54 – 1.47 (m, 2H), 1.30 (ddd, *J* = 23.9, 13.9, 6.8 Hz, 4H). ^{13}C NMR (151 MHz, D_2O) δ 105.01, 104.42, 100.80, 81.52, 79.87, 77.47, 75.34, 74.84,

72.78, 72.47, 69.49, 68.89, 64.52, 63.49, 53.53, 42.64, 30.99, 29.94, 27.22, 26.47, 25.86. ^{31}P NMR (243 MHz, d_2o) δ -2.75. HRMS (*m*/*z*): $[M+H]^+$ cald 905.2961 obsd 905.2836

_n_-Allyl-3,4-di-*O*-benzyl-6-*O*-tri*iso*propylsilyl-α-D-mannopyranosyl-(1→2)-3,4,6-tri-*O*-benzyl-α-D-mannopyranoside (2-22)

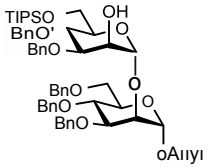

To a stirred solution of dimannoside **2-17** (1.1 g, 1.07 mmol) in MeOH (12 mL) was added freshly prepared 1 M solution of NaOMe. After 1 h, the reaction was neutralized with Amberlite IR 120 H^+ resin, filtered and concentrated to obtain crude product **2-22** (0.96 g, 0.97 mmol, 91%). R_f = 0.35 (EtOAc/Hexanes 1:3) ^{1}H NMR (400 MHz, $CDCl_3$) δ 7.38 – 7.23 (m, 28H), 7.27 – 7.15 (m, 5H), 5.85 (ddt, *J* = 16.3, 10.9, 5.5 Hz, 1H), 5.25 (dd, *J* = 3.5, 1.5 Hz, 2H), 5.20 (d, *J* = 1.5 Hz, 1H), 5.17 – 5.12 (m, 2H), 4.91 – 4.80 (m, 4H), 4.76 – 4.58 (m, 5H), 4.60 – 4.49 (m, 4H), 4.14 (dd, *J* = 13.5, 4.5 Hz, 4H), 4.00 – 3.66 (m, 15H), 1.06 (d, *J* = 4.3 Hz, 21H). ^{13}C NMR (101 MHz, $CDCl_3$) δ 138.54, 138.50, 138.39, 138.19, 138.05, 133.76, 128.43, 128.41, 128.35, 128.33, 128.27, 127.97, 127.95, 127.89, 127.80, 127.77, 127.65, 127.63, 127.47, 127.40, 117.10, 100.16, 98.28, 80.25, 80.03, 75.18, 75.08, 74.71, 74.15, 73.29, 72.58, 72.13, 72.11, 71.95, 69.23, 68.51, 67.82, 62.96, 18.05(3C), 18.02(3C), 11.98(3C).

_n_-Allyl-2-*O*-acetyl-3,4,6-tri-*O*-benzyl-α-D-mannopyranosyl-(1→2)-3,4-di-*O*-benzyl-6-*O*-tri*iso*propylsilyl-α-D-mannopyranosyl-(1→2)-3,4,6-tri-*O*-benzyl-α-D-mannopyranoside (2-23)

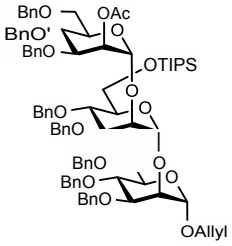

The mannosyl imidate **10a** (0.19 g, 0.30 mmol) and disaccharide acceptor **2-22** (0.20 g, 0.20 mmol) were co-evaporated with toluene (5 mL x 3) and dried under high vacuum for 2 h. The mixture was dissolved in anhydrous diethylether (8 mL) and activated molecular sieves were added. The solution was stirred for 10 min at room temperature and cooled to 0 °C. The mixture was treated with TBSOTf (14 µL, 0.06 mmol) and stirred at 0 °C for a period of 1 h. The reaction was diluted with CH_2Cl_2, quenched with Et_3N and concentrated. The crude product was purified by flash column chromatography to obtain mannosyl trisaccharide **2-23** (0.2 g, 0.14 mmol, 68%) as colorless oil. R_f = 0.4 (EtOAc/Hexanes 1:4) ^{1}H NMR (400 MHz, $CDCl_3$) δ 7.40 – 7.27 (m, 36H), 7.30 – 7.16 (m, 39H), 7.15 (dd, *J* = 16.8, 5.4 Hz, 6H), 5.86 (ddt, *J* = 16.3, 10.8, 5.5 Hz, 1H), 5.55 (s, 1H), 5.30 (s, 1H), 5.27 – 5.11 (m, 3H), 5.03 (s, 1H), 4.88 (t, *J* = 8.2 Hz, 3H), 4.85 – 4.71 (m, 3H), 4.67 (dd, *J* = 11.5, 6.3 Hz, 3H), 4.67 – 4.50 (m, 9H), 4.53 – 4.46 (m, 3H), 4.50 – 4.35 (m, 3H), 4.27 (dd, *J* = 12.1, 5.4 Hz, 1H), 4.14 (dd, *J* = 12.9, 5.0 Hz, 2H), 4.06 (s, 3H), 4.02 – 3.86 (m, 13H), 3.89 – 3.83 (m, 3H), 3.77 (dt, *J* = 14.1, 10.9 Hz, 7H), 3.69 (d, *J* = 9.1 Hz, 3H), 3.64 – 3.54 (m, 2H), 3.46 (d, *J* = 10.0 Hz, 1H), 2.13 (s, 3H), 1.09 – 1.01 (m, 22H).^{13}C NMR (101 MHz, $CDCl_3$) δ 170.12, 138.69, 138.68, 138.52, 138.49, 138.35, 138.26, 138.14, 138.11, 133.78, 128.38, 128.33, 128.31, 128.29, 128.25, 128.14, 128.05, 128.00, 127.97, 127.79, 127.77, 127.73, 127.63, 127.55, 127.51, 127.42, 117.14, 100.02, 99.87, 98.16, 80.03, 78.49, 75.18, 75.08, 74.78, 74.23, 73.57, 73.36, 73.30, 72.16, 71.97, 71.85, 71.68, 69.25, 68.74, 67.77, 26.02, 21.18, 18.12(6C), 11.96(3C).

2-*O*-acetyl-3,4,6-tri-*O*-benzyl-α-D-mannopyranosyl-(1→2)-3,4-di-*O*-benzyl-6-*O*-tri*iso*propylsilyl-α-D-mannopyranosyl-(1→2)-3,4,6-tri-*O*-benzyl-α-D-mannopyranosyl trichloroacetimidate (2-5)

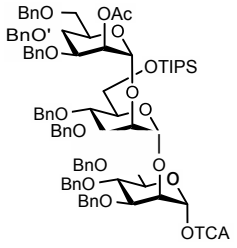

A solution of $[IrCOD(PPh_2Me)_2]PF_6$ (5.0 mg) in THF (3 mL) was stirred under hydrogen atmosphere until the color turned from red to colorless to pale yellow. The hydrogen atmosphere was exchanged with Argon. This solution was added to a solution of trisaccharide **2-23** (0.18 g, 0.13 mmol) in THF (10 mL). After 16 h, the solvent was removed and the

residue was dissolved in a mixture of acetone (2.7 mL) and water (0.3 mL). Mercury (II) chloride (0.17 g, 0.63 mmol) and mercury (II) oxide (5.5 mg, 0.03 mmol) were added. After 1 h, saturated $NaHCO_3$ (aq) was added and the reaction mixture was extracted three times with CH_2Cl_2. The combined organic layers were dried over Na_2SO_4 and concentrated. The crude product was purified by flash column chromatography to give trisaccharide hemiacetal intermediate (0.12 g, 0.08 mmol, 64%) as colorless oil. ^{1}H NMR (400 MHz, $CDCl_3$) δ 7.30 – 7.21 (m, 25H), 7.23 – 7.12 (m, 33H), 7.16 – 7.02 (m, 13H), 5.47 (dd, *J* = 2.9, 1.7 Hz, 2H), 5.23 (d, *J* = 7.7 Hz, 2H), 4.93 (s, 1H), 4.86 – 4.66 (m, 7H), 4.68 – 4.32 (m, 20H), 4.29 – 4.14 (m, 2H), 4.06 (dd, *J* = 5.6, 2.3 Hz, 1H), 3.97 (s, 1H), 3.94 – 3.67 (m, 18H), 3.67 – 3.59 (m, 6H), 3.56 (ddd, *J* = 19.2, 9.9, 3.5 Hz, 7H), 3.42 (dd, *J* = 10.3, 6.3 Hz, 2H), 2.06 (s, 3H), 1.00 (d, *J* = 2.1 Hz, 22H). ^{13}C NMR (101 MHz, $CDCl_3$) δ 170.21, 138.65, 138.54, 138.47, 138.22, 138.11, 128.47, 128.43, 128.38, 128.30, 128.20, 128.16, 128.14, 128.08, 128.01, 127.86, 127.74, 127.69, 127.65, 127.61, 127.55, 127.48, 100.07, 99.80, 99.66, 79.73, 79.27, 78.48, 75.58, 75.14, 74.78, 74.21, 73.75, 73.43, 73.33, 72.15, 72.01, 71.76, 69.39, 69.18, 68.76, 68.68, 62.94, 62.88, 34.80, 31.97, 29.74, 26.11, 22.75, 21.24, 18.21, 14.20, 11.99(3C).

To a stirred solution of hemiacetal (0.11 g, 0.08 mmol) in CH_2Cl_2 (10 mL) at 0 °C were added CCl_3CN (0.08 mL, 0.77 mmol) and DBU (4 μL, 0.02 mmol). The reaction mixture was stirred for 1 h at 0 °C. The resulting mixture was concentrated and purified by flash column chromatography to obtain imidate donor **2-5** (0.1 g, 0.06 mmol, 80%) as clear oil. R_f = 0.4 (EtOAc/hexane = 2:3)

1-*O*-(6-thiobenzyl)hexyl-2-*O*-Acetyl-3,4,6-tri-*O*-benzyl-α-D-mannopyranosyl-(1→2)-3,4-di-*O*-benzyl-6-*O*-tri*iso*propylsilyl-α-D-mannopyranosyl-(1→2)-3,4,6-tri-*O*-benzyl-α-D-mannopyranosyl-(1→6)-2-*O*-Acetyl-3,4-di-*O*-benzyl-α-D-mannopyranosyl-(1→4)- 3,6-*O*-benzyl-2-deoxy-2-*N*-phthalimido-β-D-glucopyranoside (2-2)

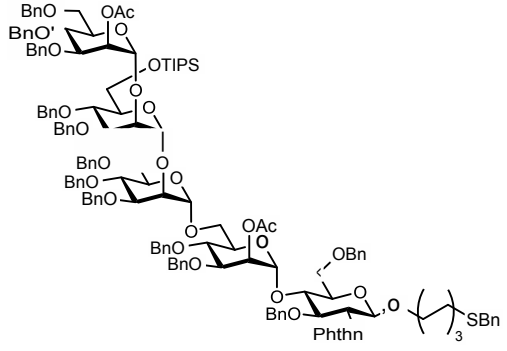

The trisaccharide imidate **2-5** (0.19 g, 0.12 mmol) and disaccharide acceptor **2-15** (0.11 g, 0.10 mmol) were co-evaporated with toluene (3 x 5 mL) and dried under high vacuum for 2 h. The mixture was dissolved in anhydrous diethylether (10 mL) and activated molecular sieves were added. The solution was stirred for 10 min at room temperature and cooled to 0 °C. The mixture was treated with TBSOTf (7 µL, 0.03 mmol) and stirred at 0 °C for a period of 1 h. The reaction was diluted with CH_2Cl_2, quenched with Et_3N and concentrated. The crude product was purified by flash column chromatography to obtain pentasaccharide **2-2** (0.17 g, 0.07 mmol, 65 % α-isomer). R_f = 0.4 (EtOAc/hexane = 1:3) ^{1}H NMR (400 MHz, $CDCl_3$) δ 7.63 (d, *J* = 16.2 Hz, 3H), 7.34 – 7.17 (m, 57H), 7.20 – 7.07 (m, 12H), 7.10 – 7.04 (m, 4H), 7.03 – 6.84 (m, 6H), 6.77 (t, *J* = 7.4 Hz, 1H), 5.52 (d, *J* = 19.8 Hz, 1H), 5.30 (s, 2H), 5.06 – 4.99 (m, 2H), 4.92 – 4.20 (m, 32H), 4.15 (dd, *J* = 17.7, 7.1 Hz, 2H), 4.07 – 3.92 (m, 6H), 3.96 – 3.80 (m, 11H), 3.75 (ddd, *J* = 19.1, 15.0, 10.8 Hz, 11H), 3.60 (s, 2H), 3.50 – 3.22 (m, 6H), 2.13 (d, *J* = 14.8 Hz, 5H), 1.93 (d, *J* = 3.4 Hz, 3H), 1.44 – 1.17 (m, 5H), 1.21 – 1.00 (m, 27H), 1.01 – 0.80 (m, 5H). ^{13}C NMR (101 MHz, $CDCl_3$) δ 170.13, 169.83, 138.83, 138.75, 138.56, 138.53, 138.45, 138.07, 137.79, 128.75, 128.47, 128.41, 128.35, 128.31, 128.26, 128.25, 128.23, 128.17, 128.15, 128.12, 128.08, 128.02, 127.96, 127.92, 127.77, 127.74, 127.65, 127.53, 127.48, 127.43, 127.31, 127.16, 127.08, 126.84, 100.00, 99.91, 99.39, 99.06, 98.06, 80.99, 79.42, 78.62, 78.54, 77.67, 75.02, 74.87, 74.65, 74.54, 74.42, 74.04, 73.37, 73.14, 72.71, 72.13, 72.01, 71.73, 71.47, 71.39, 69.36, 68.92, 68.77, 68.58, 55.79, 36.20, 31.07, 29.69, 29.07, 28.90, 28.37, 26.05, 25.39, 21.19, 20.92, 18.17(6C), 11.91(3C).

1-*O*-(6-thiobenzyl)hexyl-2-*O*-Acetyl-3,4,6-tri-*O*-benzyl-α-D-mannopyranosyl-(1→2)-3,4-di-*O*-benzyl-α-D-mannopyranosyl-(1→2)-3,4,6-tri-*O*-benzyl-α-D-mannopyranosyl-(1→6)-2-*O*-Acetyl-3,4-di-*O*-benzyl-α-D-mannopyranosyl-(1→4)-3,6-*O*-benzyl-2-deoxy-2-*N*-phthalimido-β-D-glucopyranoside (2-24)

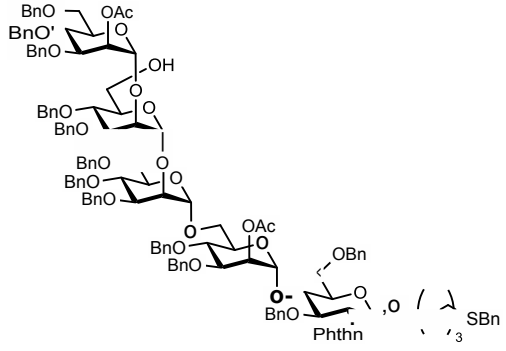

To a stirred solution of pentasaccharide **2-2** (0.07 g, 0.03 mmol) in CH_3CN (7 mL) were added water (50 μL) and $Sc(OTf)_3$ (0.04 g, 0.08 mmol). The reaction mixture was warmed to 50 °C and stirred for 6 h. The reaction was quenched with Et_3N and concentrated. The crude product was purified by flash column chromatography to obtain **2-24** (50 mg, 0.02 mmol, 72%). R_f = 0.25 (EtOAc/hexane = 2:3) ^{1}H NMR (400 MHz, $CDCl_3$) δ 7.63 (d, *J* = 15.8 Hz, 4H), 7.35 – 7.13 (m, 86H), 7.16 – 7.08 (m, 11H), 7.02 (dd, *J* = 16.1, 7.6 Hz, 4H), 6.88 (t, *J* = 7.5 Hz, 3H), 6.77 (t, *J* = 7.2 Hz, 1H), 5.50 (d, *J* = 18.3 Hz, 3H), 5.29 (s, 1H), 5.15 (s, 1H), 5.02 (d, *J* = 9.0 Hz, 3H), 4.92 – 4.75 (m, 8H), 4.76 – 4.60 (m, 4H), 4.62 – 4.49 (m, 11H), 4.51 – 4.39 (m, 7H), 4.42 – 4.24 (m, 7H), 4.22 – 4.13 (m, 1H), 4.07 (s, 2H), 3.99 – 3.57 (m, 33H), 3.58 – 3.39 (m, 4H), 3.35 – 3.18 (m, 1H), 2.16 (d, *J* = 7.1 Hz, 1H), 2.11 (s, 4H), 1.93 (s, 3H), 1.42 – 1.22 (m, 2H), 1.21 – 1.08 (m, 1H), 1.04 – 0.79 (m, 1H). ^{13}C NMR (101 MHz, $CDCl_3$) δ 170.07, 169.88, 138.49, 138.45, 138.32, 138.12, 137.99, 137.93, 137.87, 137.81, 137.69, 128.76, 128.48, 128.41, 128.36, 128.32, 128.28, 128.26, 128.24, 128.17, 128.13, 128.08, 127.98, 127.92, 127.85, 127.78, 127.72, 127.66, 127.61, 127.53, 127.48, 127.44, 127.36, 127.33, 127.19, 127.09, 126.84, 100.18, 99.31, 99.19, 98.96, 98.05, 81.01, 78.99, 78.32, 77.89, 75.17, 75.00, 74.84, 74.78, 74.58, 74.42, 74.25, 74.05, 73.61, 73.40, 73.37, 73.20, 72.64, 72.04, 71.95, 71.77, 71.64, 69.34, 69.26, 68.84, 68.62, 68.54, 68.47, 65.97, 62.01, 55.75, 36.19, 32.35, 31.07, 29.07, 28.90, 28.36, 26.35, 25.39, 21.16, 20.92.

1-*O*-(6-thio)hexyl-α-D-mannopyranosyl-(1→2)-α-D-mannopyranosyl-(1→2)-α-D-mannopyranosyl-(1→6)-α-D-mannopyranosyl-(1→4)-2-deoxy-2-amino-β-D-glucopyranoside (GPI 3)

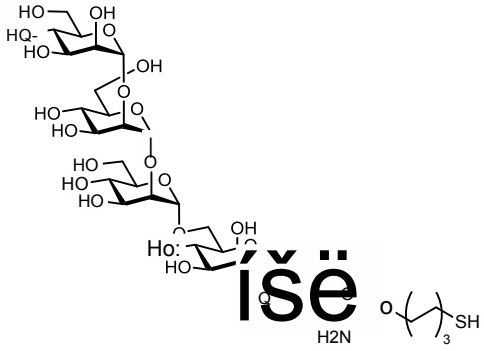

Tetrasaccharide **2-24** (0.02 g, 8.6 μmol) was dissolved in a mixture of ethylenediamine (2 mL) and butanol (2 mL) and stirred at 90 °C for 3 h. After 3 h, the reaction mixture was concentrated to obtain partially deprotected crude intermediate. The crude intermediate was

dissolved in anhydrous THF and MeOH. This solution was added dropwise to blue solution of 20 mL liquefied ammonia with sodium -78 °C. The reaction was stirred at -78 °C. After 1 h, the reaction was quenched with MeOH and stirred for additional 1h at rt. Sodium methoxide generated in the reaction was quenched by dropwise addition of glacial acetic acid. The reaction mixture was concentrated and the crude product was purified by size exclusion column chromatography using a Sephadex® super fine G-15 (GE Healthcare) column and 5% ethanol in water as eluent to obtain **GPI 3** (6 mg, 6.36 μmol, 74%) as white solid. ^{1}H NMR (600 MHz, D_2O) δ 5.19 – 5.15 (m, 1H), 5.10 – 5.06 (m, 1H), 5.00 (s, 1H), 4.92 (d, *J* = 1.5 Hz, 1H), 4.61 – 4.52 (m, 1H), 4.01 – 3.96 (m, 1H), 3.94 (s, 2H), 3.90 – 3.80 (m, 9H), 3.80 – 3.41 (m, 28H), 2.96 – 2.88 (m, 1H), 2.84 – 2.72 (m, 1H), 2.27 – 2.21 (m, 1H), 1.55 – 1.50 (m, 2H), 1.46 (p, *J* = 7.4 Hz, 1H), 1.30 (ddd, *J* = 28.5, 14.3, 7.2 Hz, 4H). ^{13}C NMR (151 MHz, d_2o) δ 104.82, 104.59, 103.27, 101.21, 100.95, 81.41, 81.12, 79.75, 77.59, 75.83, 75.33, 74.90, 73.22, 72.93, 72.76, 72.56, 69.66, 69.53, 69.43, 68.93, 63.70, 63.52, 63.28, 63.20, 58.44, 53.47, 30.94, 30.42, 29.85, 27.34, 26.43, 25.47, 24.12. HRMS (*m*/*z*): $[M+H]^+$ cald 944.3639 obsd 944.3621

1-*O*-(6-thiobenzyl)hexyl-2-*O*-Acetyl-3,4,6-tri-*O*-benzyl-α-D-mannopyranosyl-(1→2)-3,4-di-*O*-benzyl-6-*O*-(2-*N*-benzyloxycarbonyl)aminoethyl-phosphonato-α-D-mannopyranosyl-(1→2)-3,4,6-tri-*O*-benzyl-α-D-mannopyranosyl-(1→6)-2-*O*-Acetyl-3,4-di-*O*-benzyl-α-D-mannopyranosyl-(1→4)-3,6-*O*-benzyl-2-deoxy-2-*N*-phthalimido-β-D-glucopyranoside (2-1)

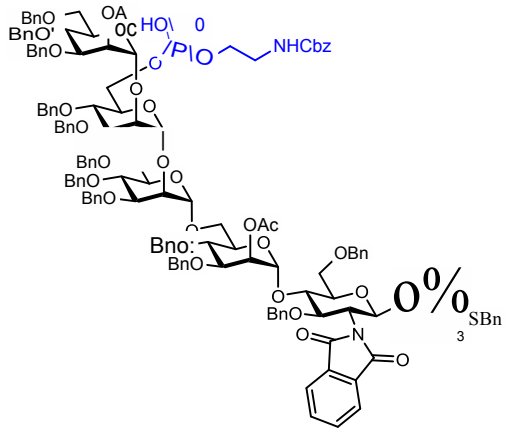

Pentasaccharide **2-24** (0.03 g, 0.01 mmol) and *H*-phosphonate **2-3** (0.02 g, 0.04 mmol) were co-evaporated with pyridine for three times and dried under high vacuum for 2 h. The mixture was dissolved in anhydrous pyridine (4 mL) and a solution of pivolyl chloride (5 μL, 0.04

mmol) in pyridine (1 mL) was added. The solution was stirred for 6 h at room temperature. After 6 h, iodine (0.01 g, 0.04 mmol) and water (0.05 mL) were added and reaction was stirred for 2 h. The reaction mixture was quenched with $Na_2S_2O_3$ and extracted with CH_2Cl_2. The organic layer were concentrated and purified by Et_3N deactivated silica gel flash column chromatography to obtain phosphorylated pentasaccharide **2-1** (0.03 g, 0.01 mmol, 86%). R_f = 0.5 (MeOH/CH_2Cl_2 = 1:10) ^{1}H NMR (400 MHz, $CDCl_3$) δ 7.63 (d, *J* = 16.2 Hz, 6H), 7.33 (d, *J* = 7.7 Hz, 5H), 7.32 – 7.24 (m, 15H), 7.25 – 7.14 (m, 57H), 7.14 (d, *J* = 3.2 Hz, 5H), 7.11 (d, *J* = 7.1 Hz, 6H), 7.08 – 7.02 (m, 4H), 6.97 (d, *J* = 7.3 Hz, 4H), 6.87 (t, *J* = 7.6 Hz, 2H), 6.78 (d, *J* = 5.7 Hz, 2H), 5.53 (d, *J* = 25.7 Hz, 3H), 5.29 (s, 1H), 5.20 (s, 1H), 5.00 (td, *J* = 23.2, 22.0, 14.0 Hz, 4H), 4.79 (dt, *J* = 21.0, 11.9 Hz, 11H), 4.68 – 4.22 (m, 28H), 4.21 – 4.06 (m, 4H), 4.02 – 3.68 (m, 27H), 3.60 (d, *J* = 7.8 Hz, 4H), 3.51 – 3.36 (m, 5H), 3.29 (s, 3H), 2.14 (t, *J* = 7.3 Hz, 2H), 1.95 (s, 3H), 1.40 – 1.21 (m, 5H), 1.07 – 0.83 (m, 3H). ^{13}C NMR (101 MHz, $CDCl_3$) δ 170.07, 169.98, 156.49, 138.70, 138.49, 138.13, 138.04, 137.76, 137.68, 137.02, 133.82, 128.75, 128.49, 128.42, 128.32, 128.22, 128.15, 127.98, 127.89, 127.80, 127.71, 127.55, 127.47, 127.41, 127.32, 127.20, 126.86, 100.29, 99.44, 99.30, 98.89, 98.01, 80.99, 78.48, 75.15, 74.97, 74.89, 74.68, 74.55, 74.40, 74.01, 73.50, 73.35, 73.12, 72.12, 72.03, 71.91, 71.73, 71.52, 71.34, 69.37, 68.58, 66.17, 55.86, 45.58, 36.19, 31.06, 29.69, 29.07, 28.89, 28.36, 25.38, 21.17, 20.99, 8.82. ^{31}P NMR (162 MHz, $CDCl_3$) δ 1.58.

1-*O*-(6-thio)hexyl-α-D-mannopyranosyl-(1→2)-6-*O*-aminoethyl-phosphonato-α-D-mannopyranosyl-(1→2)-α-D-mannopyranosyl-(1→6)-α-D-mannopyranosyl-(1→4)-2-deoxy-2-amino-β-D-glucopyranoside (GPI 4)

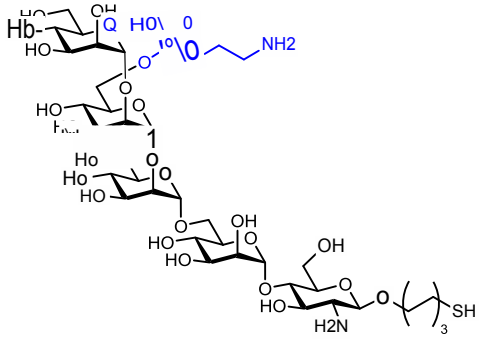

Pentasaccharide **2-20** (0.04 g, 0.02 mmol) was dissolved in a mixture of ethylenediamine (2 mL) and butanol (2 mL) and stirred at 90 °C for 3 h. After 3 h, the reaction mixture was concentrated to obtain partially deprotected crude intermediate. The crude intermediate was

dissolved in anhydrous THF and MeOH. This solution was added dropwise to blue solution of 20 mL liquefied ammonia with sodium -78 °C. The reaction was stirred at -78 °C. After 1 h, the reaction was quenched with MeOH and stirred for additional 1h at rt. Sodium methoxide generated in the reaction was quenched by dropwise addition of glacial acetic acid. The reaction mixture was concentrated and the crude product was purified by size exclusion column chromatography using a Sephadex® super fine G-15 (GE Healthcare) column and 5% ethanol in water as eluent to obtain **GPI 4** (11 mg, 10.2 µmol, 60%) as white solid. ^{1}H NMR (600 MHz, D_2O) δ 5.18 – 5.15 (m, 1H), 5.08 (s, 1H), 4.97 (s, 1H), 4.94 – 4.90 (m, 1H), 4.32 (ddd, *J* = 19.6, 7.9, 3.7 Hz, 1H), 4.03 – 3.95 (m, 5H), 3.94 (dt, *J* = 5.6, 2.7 Hz, 2H), 3.88 – 3.77 (m, 6H), 3.76 (d, *J* = 10.7 Hz, 2H), 3.74 – 3.51 (m, 14H), 3.48 (q, *J* = 8.8, 7.7 Hz, 2H), 3.47 – 3.41 (m, 2H), 3.21 – 3.14 (m, 2H), 3.01 (dt, *J* = 17.5, 6.4 Hz, 1H), 2.87 (dd, *J* = 10.2, 5.3 Hz, 0H), 2.65 (t, *J* = 7.2 Hz, 1H), 2.42 (t, *J* = 7.1 Hz, 0H), 1.62 – 1.45 (m, 3H), 1.32 – 1.23 (m, 2H). ^{13}C NMR (151 MHz, D_2O) δ 184.07, 104.80, 104.45, 103.35, 100.90, 81.59, 81.01, 79.87, 77.44, 75.89, 75.36, 74.92, 74.78, 74.72, 73.20, 72.96, 72.78, 72.62, 72.42, 69.49, 69.14, 68.98, 67.28, 64.44, 63.69, 63.48, 58.99, 42.70, 42.65, 40.78, 31.13, 30.78, 29.81, 27.27, 27.13, 25.86. ^{31}P NMR (243 MHz, D_2O) δ -2.75. HRMS (*m*/*z*): $[M]^+$ cald 1066.3652 obsd 1066.3646

2.8.2 Methods of Biochemistry

CRM_{197} was purchased from *Pf*ēnex Inc., 1M solution of resin bound TCEP was purchased from thermo scientific and autoclaved sterile water was used for the conjugation.

Conjugation of GPI 1–6 to CRM_{197}

250 µl of TCEP resin solution was centrifuged for 3 mins and excess of water was removed. TCEP resin was redissolve in 0.1 M sodium phosphate buffer (pH 8) (150 µL) and centrifuged for 3 mins. Again excess buffer was removed and autoclaved water was added. GPI fragment (in 120µL water) was transferred to the TCEP solution and incubated for 1h at rt. After 1 h, TCEP resin is filtered off using syringe and washed with autoclaved water (5x50 µL). All the water fractions are combined lypholized. The reduction of disulfide to thiol is followed by LC-MS. To a stirred solution of CRM_{197} (3 mg) in 0.1 M sodium phosphate buffer (pH 7.4) was added a solution of SBAP (1.58 mg) in DMF (60 µL) at room temperature. The reaction

mixture was stirred for 1 h. After 1 h, the solution was concentrated to 250 µL volume using an Amicon® Ultra-4 Centrifugal Filter Unit (10 kDa cut off, Millipore) and washed with water (4x 1 mL) and once with 0.1 M sodium phosphate buffer (pH 8.0). Finally, the activated CRM_{197} is concentrated to obtain around 100 µL of solution. To the stirred solution of activated CRM_{197} solution was added the reduced glycan. The solution was stirred overnight at room temperature. The solution was concentrated to 250 µL of volume using an Amicon® Ultra-4 Centrifugal Filter Unit (10 kDa cut off, Millipore) and washed with water (4x 1 mL) and once with 0.1 M sodium phosphate buffer (pH 8.0) to obtain the CRM-GPI conjugate. cysteine (0.94 mg) was added directly to that solution in the Centricon and incubated for 1 h at r.t. After 1 h, the mixture was washed with water (4x 1 mL) re-buffered with PBS to obtain the desired CRM-GPI conjugate. MALDI-TOF mass spectroscopy and SDS-PAGE was done for all the intermediates and final samples.

Characterization of conjugates

CRM_{197}-GPI conjugates were characterized by MALDI-TOF spectrometry and by gel electrophoresis and directly stained against carrier protein with Coomassie Brilliant Blue R250 (CBB) (Sigma-Aldrich, Munich, Germany, 6104-59-2) or used for western blotting. For gel electrophoresis, glycoconjugates were diluted 1:10 in sterile water; loading buffer was added, boiled for 5 minutes and loaded onto a 12% polyacrylamide gel. Gel electrophoresis was performed at 150 V, 150 mA for 60 minutes. Western blot transfer was accomplished at 100 V and 35 mA. The membrane was routinely tested for positive transfer with Ponceau S (Sigma-Aldrich, Munich, Germany, 6226-79-5), subsequently blocked for 2 h at RT with 5% BSA in PBS-T. Biotinylated Concavalin-A (Vector Laboratories, Burlingame, California, B-1005) was diluted 1:500 in 1x PBS 5% BSA 0.01mM Mn^{2+} 0.1mM Ca^{2+} and incubated 2 h shaking at rt. The membrane was subsequently washed and streptavidin HRP (BD Pharmingen, Heidelberg, Germany, 557630) was added 1:500 in 1x PBS 5% BSA 0.01mM Mn^{2+} 0.1mM Ca^{2+} and incubated 1 h shaking at RT. Finally, the membrane was washed again in 1x PBS 0.01mM Mn^{2+} 0.1mM Ca^{2+} and developed by enhanced luminol-based chemiluminescent according to manufacturer's instructions (Thermo Fisher Scientific, Darmstadt, Germany, 32109). Dual color precision protein standard (Bio-Rad Laboratories, Munich, Germany, 161-0374) was used as protein standard.

A)

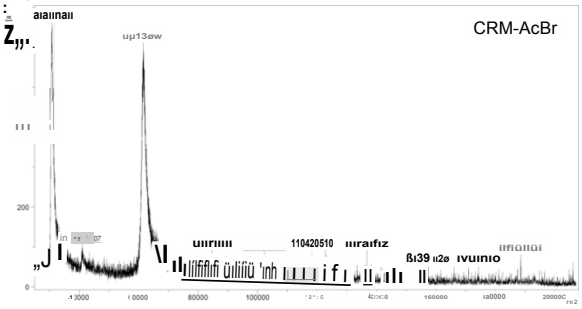
CRM-AcBr

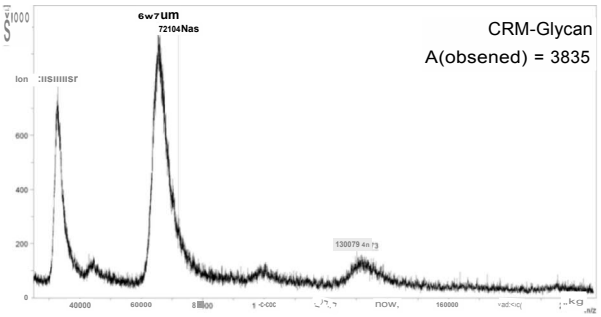
CRM-Glycan
A(obsened) = 3835

B)

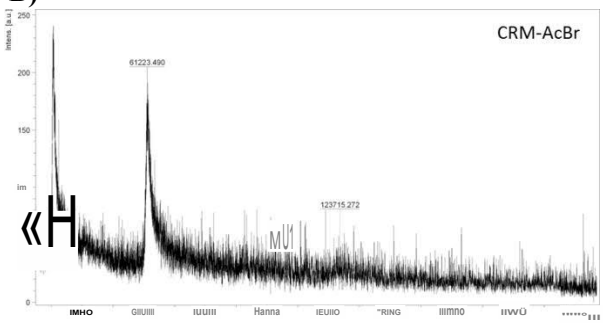
CRM-AcBr
61223.490
123715.272

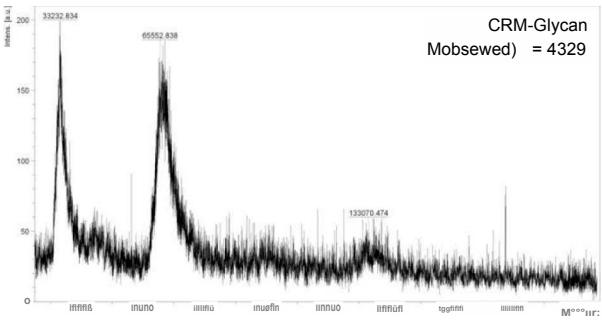
CRM-Glycan
Mobsewed) = 4329
33232.834
65552.838
133070.474

C)

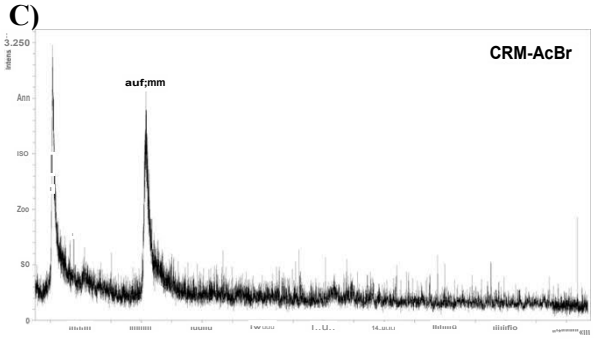
CRM-AcBr
auf;mm

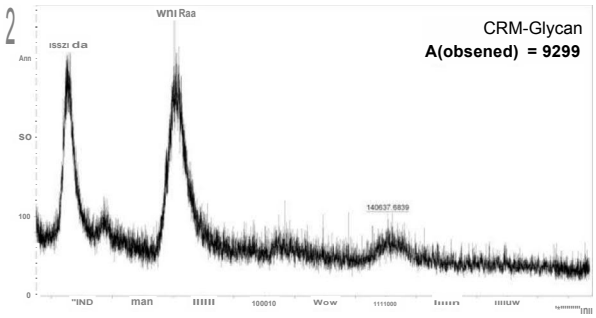
CRM-Glycan
A(obsened) = 9299
140637.6839

D)

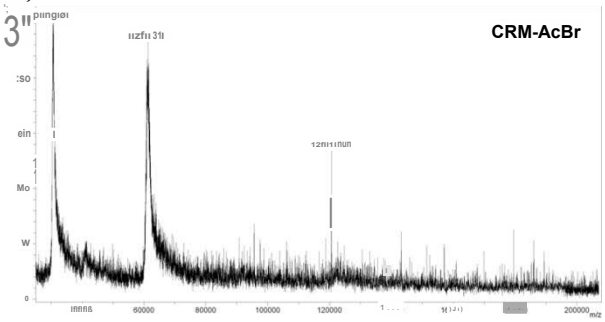
CRM-AcBr

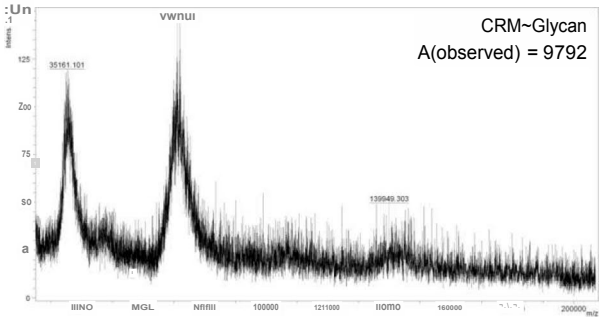
CRM~Glycan
A(observed) = 9792
35161.101
139649.303

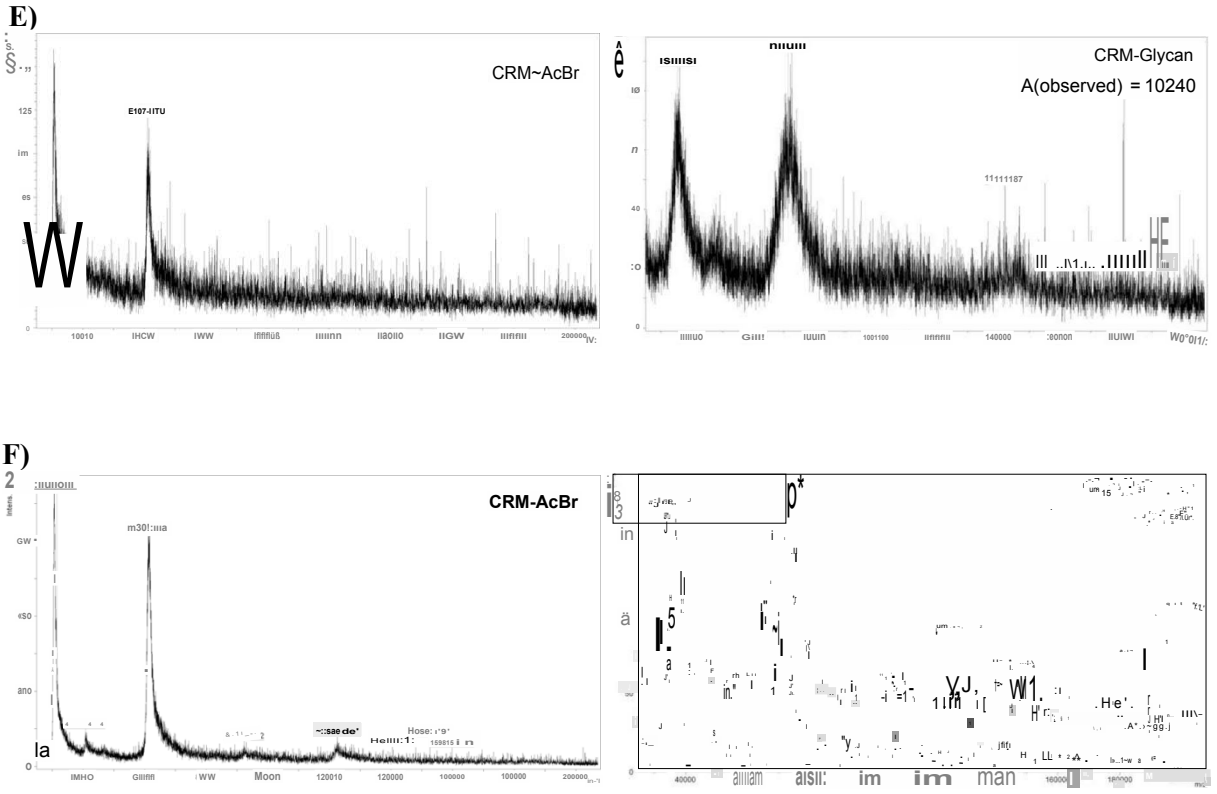

Figure 2.21: MALDI-TOF analysis of the activated $CRM1_{97}$ (CRM-AcBr) and CRM_{197}-GPI (CRM-Glycan) during glycoconjugate synthesis. Δ (observed) represents the difference in m/z for activated CRM_{197} and CRM-GPI and was used to calculate the glycan loading of the glycoconjugates. **(A-F)** represent the MALDI-TOF spectra for **CRM_{197}-GPI 1–6** respectively.

Animal Experiments

Animals were treated strictly according to German (Tierschutz-Versuchstierverordnung) and European Law (Directive 2010/63/EU). Recommendations of the Society for Laboratory Animal 43 Science (GV-SOLAS) and of the Federation of European Laboratory Animal Science Associations (FELASA) were followed. The Office for Health and Social Affairs Berlin (LAGeSo) approved the experiment conclusively (Permit Number: G0239/14). All efforts were made to minimize suffering. All C57BL/6JRj mice used in this study were obtained from Janvier Labs (Saint-Berthevin, France). Mice were housed in individually-ventilated cages (IVCs) under specific pathogen free (SPF) conditions in the animal facility of the Federal Institute for Risk Assessment (BfR, Berlin, Germany). Mice were provided food

and water *ad libitum*. Upon delivery (day -7), mice were allowed to rest for one week before experimental setting was started.

Statistical analysis

Statistical analysis was performed using the GraphPad Prism software (GraphPad Software Inc., La Jolla, CA, US). Unpaired Student's *t* test was used to compare different sets of data, whereas two-way ANOVA was used to compare anti-GPI antibody levels over time between immunized and non-immunized groups. Log rank test was employed for analysis of survival between different groups. Statistical significance within figures is shown by asterisks: * represents $p < 0.05$, ** $p < 0.01$, *** $p < 0.001$ and **** $p < 0.0001$.

3 Synthesis of the Glycosylphosphatidylinositol-Anchored MSP1-19kDa Protein from *P. falciparum*

3.1 Introduction

One very important component of the cell membrane is different proteins that perform specific functions for the cell. Membrane proteins can be classified as peripheral or integral depending on the nature of their interactions with the membrane. Peripheral membrane proteins do not interact with the hydrophobic part of the cell membrane. They are found bound to the membrane through electrostatic interactions with the polar head of the membrane lipids or by interactions with integral membrane proteins. Most of the membrane proteins found in red blood cells such as spectrin and glycoforin are peripheral membrane proteins.

Integral membrane proteins are embedded in the membrane bilayer and contain hydrophobic residues that interact with the alkyl chains of the membrane bilayer. These proteins can also span the entire cell membrane one or more times generating a transmembrane protein such as a porins, an integral protein found in outer membrane of *E. coli*. Some integral proteins are anchored to the plasma membrane through fatty acid chains attached to the side chain of cysteine residues to keep the protein outside the membrane.[2] Other proteins have post translational modifications at the C-terminus involving fatty acid chains,[170] diacylglycerols,[171] isoprenoids[172] or glycosylphosphatidylinositol anchors (GPIs)[173].

GPI is a complex glycolipid added as a post-translational modification at the C-terminus of eukaryotic proteins. This glycolipid has a unique and conserved core structure attached to an inositol phospholipid. Many membrane proteins, enzymes and receptors are bound to the plasma membrane by a GPI anchor.[174]

3.1.1 GPI-Anchored Proteins in *Plasmodium*

GPI-anchored proteins are present in all eukaryotic cells and are involved in various cellular functions like signal transduction and cell adhesion. Apart from their cellular functions, GPI-anchored proteins have been associated with many diseases like malaria and toxoplasmosis. Large amount of GPI-anchored proteins are found on the surface of protozoa such as *Trypanosoma spp.*, *Leishmania spp.*, *Toxoplasma* and *Plasmodium spp*. GPI-anchored proteins participate in the modulation of the immune system during infections and are believed to be essential for the these pathogens.

GPI-anchored proteins are found in all developmental stages of *Plasmodium* parasites. During different stages of the life cycle of the parasite, such as sporozoite, merozoite, gamete and ookinete, the surface of the parasite is covered with GPI anchored proteins. These proteins include the circumsporozite protein (CSP) on sporozoites and the merozoite surface proteins (MSP) family and the rhoptry-associated membrane antigen (RAMA), some of the most important proteins expressed on merozoites. Additional examples are the Pfs48/45 protein expressed on gametes, Pfs28 and Pfs25 expressed on ookinete, and the Pf34 and apical sushi protein (ASP), which are GPI anchored proteins expressed during the erythrocyte stage.[175-181]

Circumsporozoite Protein (CSP) is a preerythrocytic GPI-anchored protein found on the surface of sporozoites. It is composed of five regions, an N-terminal region that binds to proteoglycans, a central repeating unit with multiple copies of a strain specific sequence, two conserved regions (one responsible for the invasion of sporozoites and the other responsible for the binding to hepatocytes) and the C-terminus containing a thrombospondin-like domain that carries the GPI. CSP is responsible for the invasion and development of sporozoites. Due to its high abundance on the surface of sporozoites, it is commonly used in the development of malaria vaccine candidates.[182]

Merozoite Surface Protein (MSP) is a family of GPI-anchored proteins displayed on the surface of merozoites. They are important for the binding of merozoites and the following

invasion of red blood cells. MSP are divided into integral, peripheral and membrane bound proteins. Two-thirds of all GPI-anchored proteins in *Plasmodium* during the blood stage are a member of the MSP family. The MSP structure and properties will be explained in detail in **section 3.1.2**.

Rhoptry-Associated Membrane Antigen (RAMA) is expressed as a 170 kDa protein that undergoes proteolytic cleavage to yield three N-terminal repeat regions and a 60 kDa GPI-anchored protein. RAMA is the first protein expressed on the parasite surface after red blood cell invasion. It consists of an N-terminal hydrophobic sequence corresponding to the signal sequence, three acidic repeat regions at the N-terminal region. The other fragment at the C-terminus is anchored to a GPI.[183]

Ookinete surface proteins Pfs25 and Pfs28. These are the predominant proteins on the surface of ookinetes. They are characterized by an N-terminal signal sequence, three epidermal growth factors and a GPI-anchor at the C-terminus. They are involved in the interaction between the ookinete with the midgut environment of the vector.[181]

Pfs48/45 is a protein expressed by gametocytes present on the surface of the sporogonic stages of plasmodium parasites. It plays an important role in parasite fertilization. This protein contains three domains and ten cysteine residues forming a complex structure defined by disulfide bridges.[184]

3.1.2 Merozoite Surface Proteins

The merozoite surface proteins are important for the primary attachment of merozoites to the red blood cell surface and for the subsequent invasion. Therefore, the MSPs have been considered for the development of an antimalaria vaccine and have been included in various potential vaccine candidates. Many of these proteins are attached to the membrane of the parasite using a GPI anchor, such as MSP1, MSP2, MSP4, MSP5 and MSP10.[185, 186]

Merozoite surface protein 1 (MSP1) is the most abundant and well characterized protein in the MSP family. It has been described as an essential protein for the invasion process and survival of the parasite.[187] MSP1 is a cysteine-rich protein stabilized by multiple disulfide bonds that is expressed as a ~200 kDa protein precursor. MSP1 undergoes proteolytic cleavage catalyzed by the Subtilisin-like protease 1 (SUB1) that modifies the secondary structure of the protein. After the processing, the protein remains on the surface of the

merozoite as a complex of four polypeptide fragments of MSP1. Three non-covalently bound fragments make up the N-terminal fragment $MSP1_{83}$ (83 kDa) and two internal fragments $MSP1_{30}$ (30 kDa) and $MSP1_{38}$ (38 kDa). The N-terminal fragment $MSP1_{83}$ interacts with glycophorin A as a mediator for the invasion process. The processed protein can bind and rupture the red blood cells. The GPI-anchored C-terminal fragment $MSP1_{42}$ (42 kDa) remains covalently bound to the merozoite.[188-193]

During the invasion, the C-terminal bound fragment $MSP1_{42}$ undergoes further proteolytic processing mediated by Subtilisin-like protease 2 (SUB2) to shed $MSP1_{33}$ (33kDa) from the merozoite surface. A C-terminal fragment $MSP1_{19}$ (19 kDa) fragment anchored to GPI remains bound to the merozoite surface and is carried to the red blood cells, where it localizes at the food vacuole. MSP1 is regarded as a dimorphic protein but the $MSP1_{19}$ region remains conserved across isolated *Plasmodium* species (**figure 3.1**).[194-199]

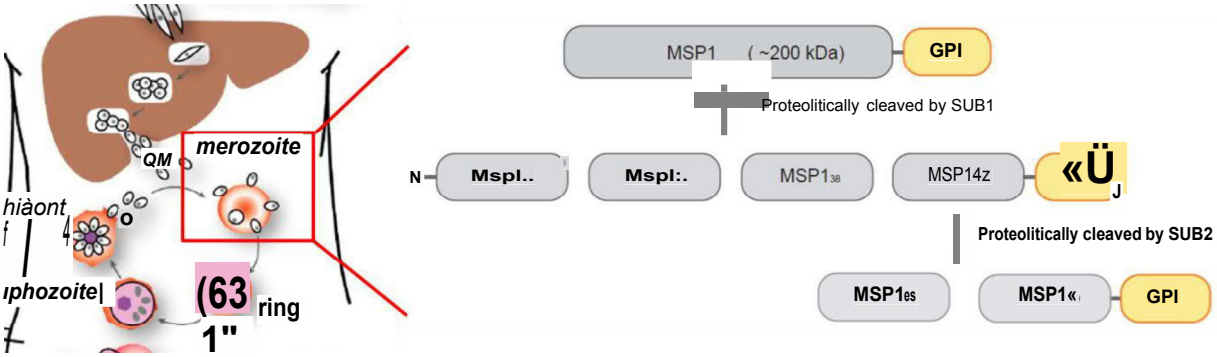

Figure 3.1: Schematic processing of MSP1 showing primary processing mediated by SUB1 and secondary processing mediated by SUB2 during the invasion of red blood cells.

Merozoite surface protein 2 (MSP2) is the second most abundant surface protein found on merozoites of *P. falciparum*. Unlike MSP1, it does not undergo proteolytic cleavage and it possesses only one disulfide bond. Studies have shown that the N-terminus of MSP2 interacts with the lipids on the membrane of the merozoite and is believed to be important during the invasion process. It is retained on the parasite surface during invasion and it degrades soon after the invasion, however, the precise role of MSP2 is still unknown.[188, 200-202]

Merozoite Surface Protein 4, 5 and 10 (MSP4, 5 and 10) are not well known surface proteins. MSP4 and MSP10 are very similar to MSP1 and are highly immunogenic. MSP4 is expressed as a 40 kDa protein and is an important protein for the development of the parasite post-invasion. MSP5 encodes 272 amino acids and contains an EGF-like domain. Although it is conserved across *P. falciparum*, its function is not known. MSP10 is expressed as an 80 kDa protein and then processed to 36 kDa. It is found on the apical end of the merozoite. Though it is highly immunogenic, no red blood cell receptors have been identified.[203-207]

3.2 Synthesis of GPI-Anchored Proteins

It has been shown that GPIs influence the structure and function of anchored proteins. However, studies evaluating the structure and function of GPI-anchored proteins are limited due to the difficult in isolating of GPI-anchored proteins in homogeneous form. Therefore, semi-synthesis of proteins has emerged as an alternative approach to obtain GPI anchored proteins.[208, 209]

The first attempt to synthesize a GPI-anchored protein was undertaken by Guo and coworkers with the synthesis of GPI-anchored CD52. CD52 is a GPI anchored glycopeptide consisting of 12 amino acids and one *N*-glycosylated site. In this work, the linkage between the synthetic glycopeptide and the glycolipid was obtained by reaction with an active ester of the peptide and the amine group on the phosphoethanolamine unit of the GPI. This method showed great potential, however, it is limited to the size of the peptide and it can only be used for short sequences.[210]

To accommodate larger proteins, the groups of Bertozzi and Becker applied a semi-synthetic approach to obtain mimetics of GPI-anchored proteins using expressed protein ligation.[211, 212] Using the same approach, Seeberger and coworkers reported the synthesis of a GPI-anchored Prion protein (PrP) containing a synthetic monolipidated GPI anchor. To obtain the GPI-PrP molecule, a cysteine residue was attached to the phosphoethanolamine moiety of the GPI to carry out a native chemical ligation between the GPI and an expressed PrP thioester.[209, 212]

There are still limitations to evaluate the biological significance of GPIs and to study the effect of the GPI anchor on the structure and activity of proteins. Therefore, it is necessary to

establish new methodologies for the synthesis of GPI-anchored proteins having a natural glycolipid structure. In this work, the synthesis of a homogeneous GPI-anchored protein was planned to investigate the role of the GPI on proteins during infection by *Plasmodium* parasites. To carry out this study, the synthesis of the 19 kDa fragment of the merozoite surface protein 1 ($MSP1_{19}$) from *P. bergei* was designed to compare the structural and immunological properties of the protein with and without the glypiation.

3.3 Retrosynthesis

To synthesize a GPI-anchored protein from *Plasmodium falciparum* bearing a natural linkage between the protein ($MSP1_{19}$) and the GPI (structure ***Pf*GPI 1** in **figure 3.2**), a synthetic GPI containing a cysteine residue attached to the phosphoethanolamine unit was designed for chemoselective introduction of the activated protein. This cysteine residue can undergo a chemoselective reaction with a C-terminal protein thioester *via* a trans-thioesterification and rearrangement process to provide GPI-$MSP1_{19}$. To incorporate the cysteine residue for ligation, the cysteine will be coupled to the phosphoethanolamine unit prior to phosphorylation of the GPI anchor. The amine and thiol functionalities of the cysteine will be protected using acid labile groups, which can be removed by acid treatment of the GPIs after deprotection of the glycan by hydrogenolysis.[209] The core glycan part of the GPI anchor can be obtained using a general synthetic approach previously established in our group, which involves the orthogonally protected building block **3-5, 3-6** and **3-7** and a [3+1+2] glycosylation strategy **(figure 3.2)**.[107]

After the assembly of the orthogonally protected *pseudo*-hexasaccharide, two-step phosphorylations would provide the desired biphosphorylated glycan. Finally, a three step global deprotection would provide access to the GPI anchor bearing a cysteine residue primed for ligation with $MSP1_{19}$. As discussed in chapter 2 (**figure 2.2**), the GPIs from *Plasmodium* are highly heterogeneous on the lipid component and it also carries an additional acyl group on the *myo*-inositol which is not present in GPIs from other protozoa. Thus, using the general synthetic strategy, two GPI anchors from *plasmodium falciparum* will be synthesized: ***Pf*GPI 1** carrying a glycerolipid and ***Pf*GPI 2** carrying a glycerolipid plus an additional acyl moiety at the 2-*O* position of the *myo*-inositol residue (**figure 3.2**).

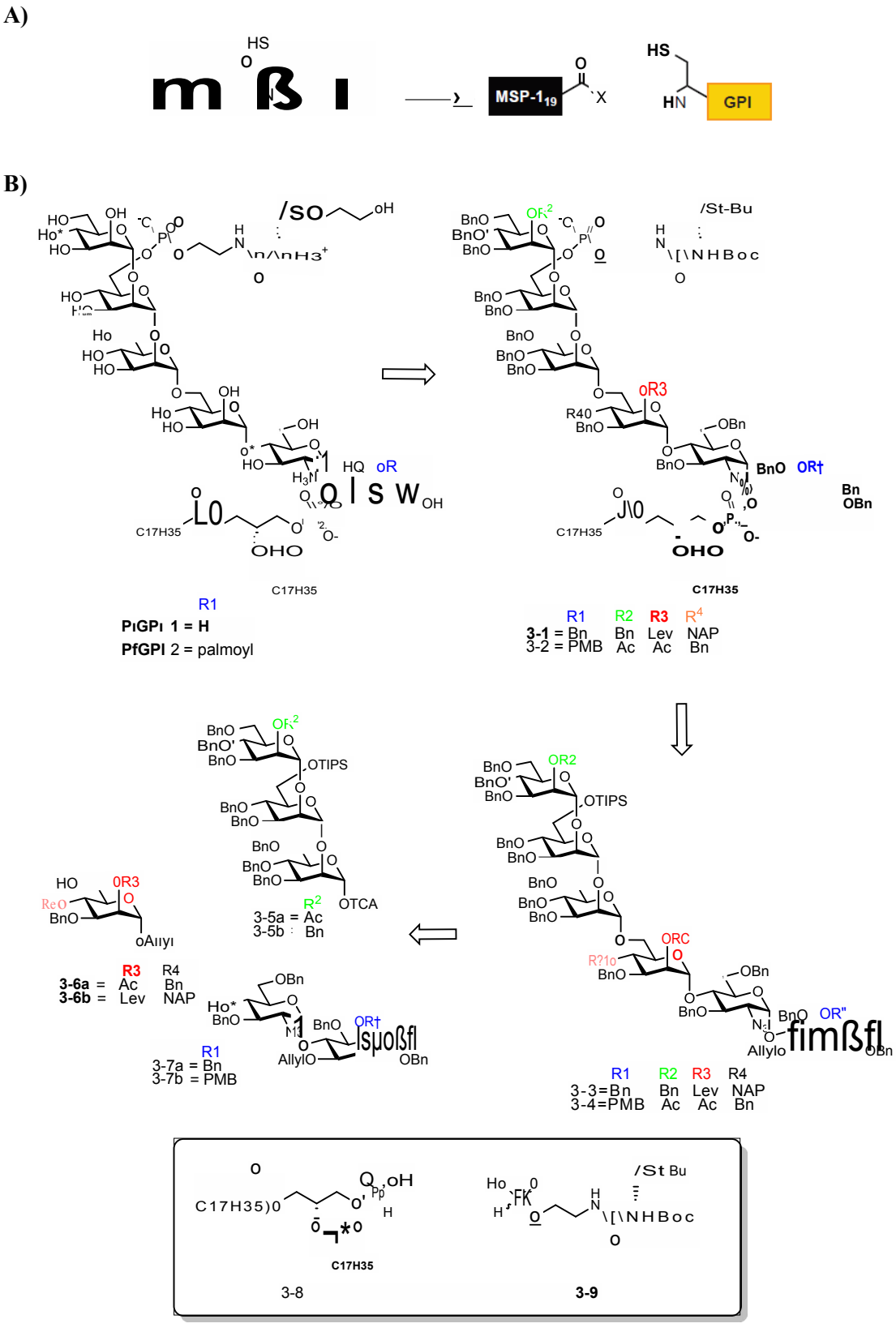

Figure 3.2: (A) Retrosynthesis of GPI-Anchored protein (**GPI-MSP1$_{19}$**); **(B)** Retrosynthetic analysis of cysteine-containing GPIs from *P. falciparum* for the synthesis of GPI-anchored proteins.

3.4 Chemical Synthesis of GPIs from *P. Falciparum*

***Pf*GPI 1** and ***Pf*GPI 2 (figure 3.2**) from *P. falciparum* were synthesized from three fragments: mannose trisaccharide **3-5**, mannose building block **3-6** and *pseudo*-disaccharide **3-7**. Mannose trisaccharide **3-5** was synthesized using the protocol described in chapter 2 (**section 2.5**). Mannose building block **3-6** was synthesized using a protocol previously established in our laboratory.[213]

The core glycan structure (**3-1**) for ***Pf*GPI 1** was assembled using a [3+1+2] glycosylation strategy following the protocols previously established in our lab. However, in order to incorporate a palmitic ester at the 2-*O* position of the *myo*-inositol in ***Pf*GPI 2,** the pseudodisaccharide building block **3-7b** was initially synthesized bearing the acid labile PMB moiety as an orthogonal protecting group at the 2-*O* position of *myo*-inositol (**scheme 3.1a**).[214] The acidic conditions during required for the glycosylation of the *myo*-inositol cleaved the PMB group during the reaction and hence, the PMB group was replaced with the more stable 2-(napthyl)methyl group. The synthesis of the *pseudo*-disaccharide was performed using *myo*-inositol containing a 2-(napthyl)methyl at the 2-*O* position of **3-10**. Glycosylation of *myo*-inositol **3-10** with trichloroacetimidate donor **3-11** using TMSOTf in Et_2O/DCM at 0 °C afforded the *pseudo*-disaccharide **3-12** as an anomeric mixture of products (α/β = 5:1) in 80% yield. The α/β mixture of **3-12** could not be separated using silica gel chromatography, therefore, the obtained anomeric mixture of the *pseudo*-disaccharide **3-12** was deacetylated using freshly prepared sodium methoxide. The 4-*O* and 6-*O* positions of the resulting triol **3-13** were blocked by formation of the 4,6-*O*-benzylidene acetal using benzaldehyde dimethyl acetal and CSA. Then, the free 3-*O* position was benzylated using NaH and BnBr to obtain **3-14** in 54% yield. The benzylidene acetal of **3-14** was selectively opened towards the 6-*O* position in 80 % yield to obtain the *pseudo*-disaccharide acceptor **3-7c** having a free hydroxyl at the 4-*O* position (**scheme 3.1b**).

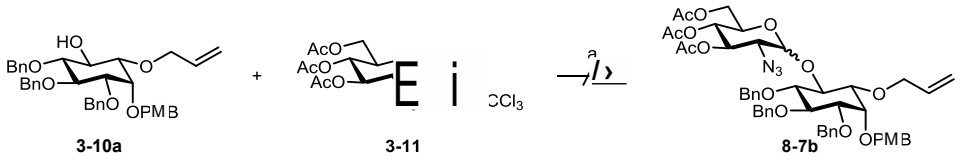

Scheme 3.1a: Trial Synthesis of *pseu*dodisaccharide. a) TMSOTf, CH_2Cl_2-Et_2O, 0 °C.

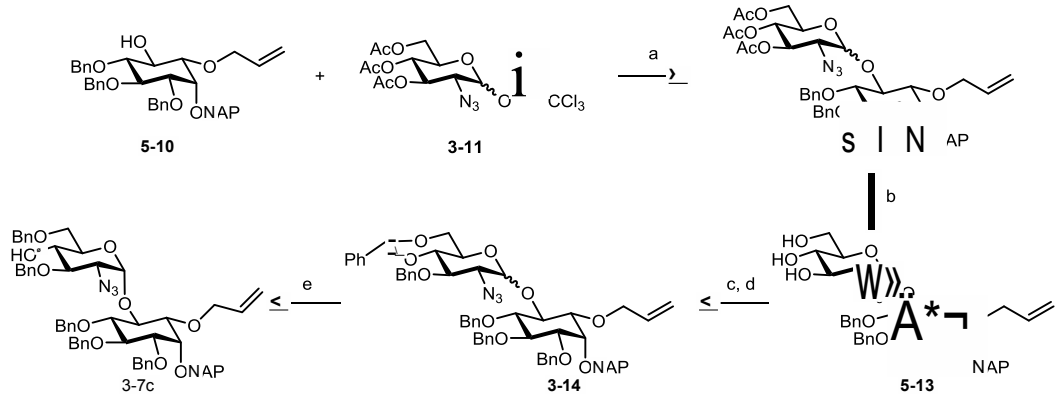

Scheme 3.1b: Synthesis of *pseu*dodisaccharide. a) TMSOTf, CH_2Cl_2-Et_2O, 0 °C; b) NaOMe, MeOH, rt, quant.; c) $PhCH(OCH_3)_2$, CSA, CH_3CN, rt, 3 h, 59%; d) BnBr, NaH, DMF, rt, 54%; e) TFAA, TFA, TES, CH_2Cl_2, 0 °C, 5 h, 80%.

For the synthesis of ***Pf*GPI 2**, the mannose building block **3-6a** was glycosylated with the trimannosyl trichloroacetimidate donor **3-5a** using TBSOTf as activator in a mixture of thiophene and CH_2Cl_2 as solvent to promote α-selectivity during the reaction (**Scheme 3.2**). The [3+1] glycosylation under these reaction conditions furnished tetramannose **3-15a** in 50% yield of α-isomer. Subsequently, the allyl group of the obtained tetramannoside was isomerized using an activated Ir-catalyst and the formed vinyl ether was hydrolyzed with mercury salts to obtain the lactol. This lactol was treated with trichloroacetonitrile and DBU to provide trichloroacetimidate donor **3-16a** in 65% yield over two steps. To complete the synthesis of the GPI core glycan, the trichloroacetimidate **3-16a** was used to glycosylate the *pseudo*-disaccharide **3-7c** using TMSOTf as acid activator at –40 °C giving the *pseudo*-hexasaccharide **3-17** in 51% yield. This glycan has tree orthogonal groups and can be used to generate the trilipidated ***Pf*GPI 2**.

The glycan *pseudo*-hexasaccharide **3-3** required for the synthesis of ***Pf*GPI 1**, was synthesized by Dr. Ivan Vilotijevic using the same synthetic strategy as described above using a *myo*-inositol with the benzyl ether instead of the NAP protecting group. In order to optimize and evaluate the production of GPI anchored proteins, bilipidated ***Pf*GPI 1** was synthesized by initially phosphorylating the hexasaccharide **3-3** with the appropriate *H*-phosphonate.

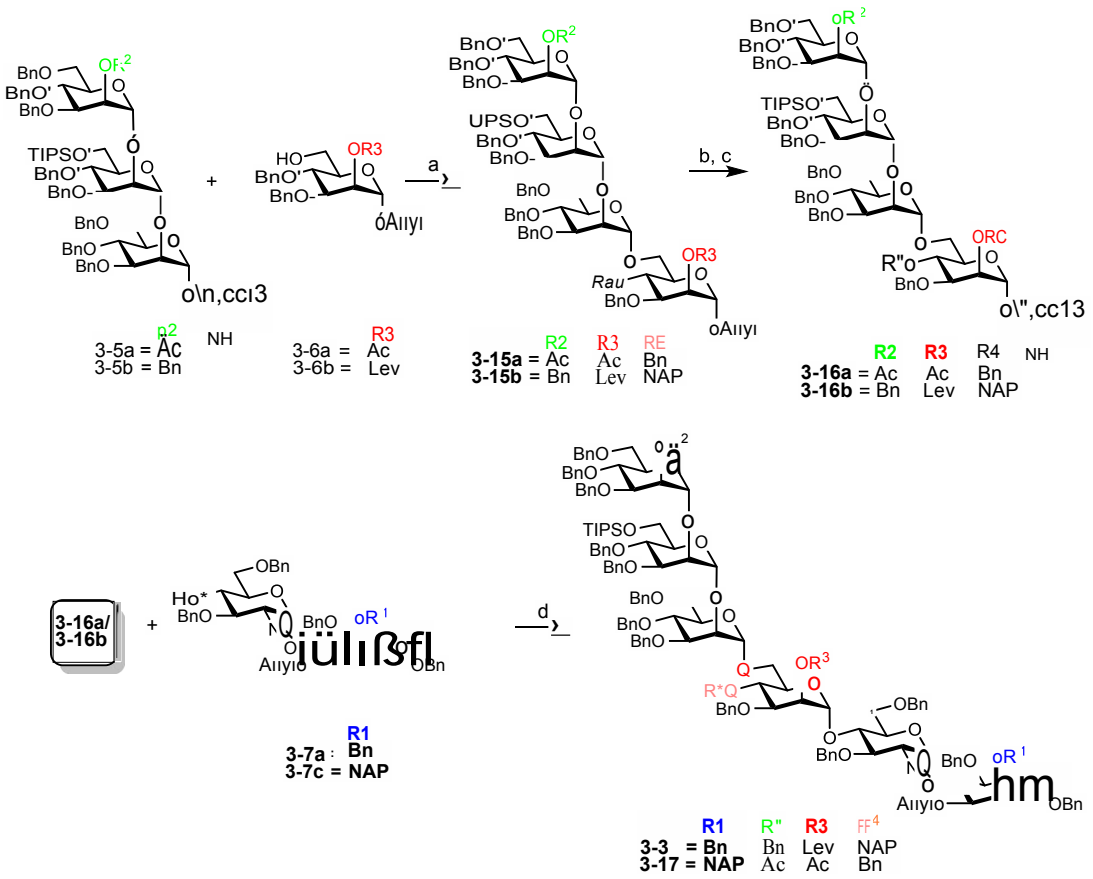

Scheme 3.2: Synthesis of GPI core glycan from *P. falciparum*. a) TBSOTf, Thiophene: CH_2Cl_2 (1:1), 50% (α-isomer), **3-15a**; b) i. $[Ir(Cod)(PPh_2Me)_2]PF_6$, H_2, THF ii. HgO, $HgCl_2$, Acetone, H_2O; c) Cl_3CCN, DBU, CH_2Cl_2, 0 °C, 65%, **3-16a**; d) TMSOTf, CH_2Cl_2, –40 °C, 51%, **3-17**.

To complete the synthesis of ***Pf*GPI 1**, *pseudo*-hexasaccharide **3-3** was phosphorylated using two-step phosphorylation reactions. First, the allyl group from the 1-*O* position of *myo*-inositol was removed under optimized conditions using $PdCl_2$ and sodium acetate to obtain **3-18** in 80% yield (**scheme 3.3**). Unfortunately, removal of the allyl ether using the iridium catalyst for isomerization followed by hydrolysis gave only low yields, especially in the hydrolysis step. The resulted alcohol **3-18** was phosphitylated with *H*-phosphonate **3-8** using pivaloyl chloride in pyridine. After completion of the reaction, oxidation with iodine in wet pyridine delivered the phospholipidated compound **3-19**. The triethylammonium salt from the product was exchanged to sodium using Amberlite IR120 (Na^+ form) and the 6-*O* TIPS group of Man-III was removed under acidic conditions using scandium triflate and water. The resultant alcohol was phosphitylated with the cysteine containing *H*-phosphonate **3-9** and oxidized using iodine to deliver the fully protected and bilipidated GPI **3-1** (**scheme 3.3**). Finally, GPI **3-1** was deprotected using a three-step global deprotection strategy involving treatment with hydrazine acetate to cleave the Lev group present at the 2-*O* position of ManI, followed by hydrogenolysis using palladium hydroxide on charcoal as catalyst, and finally removal of *N*-Boc and S*t*-Bu protecting groups from cysteine using $Hg(TFA)_2$ in trifluoroacetic acid (**scheme 3.2**). ***Pf*GPI 1** was obtained in 35% yield after purification. The synthesis of ***Pf*GPI 2** was not completed in this work. However, the protocols established for the synthesis of ***Pf*GPI 1** can easily be applied to the synthesis of ***Pf*GPI 2** by adding two steps before the removal of the allyl group: an oxidative removal of the Nap group and acylation with palmitic acid.

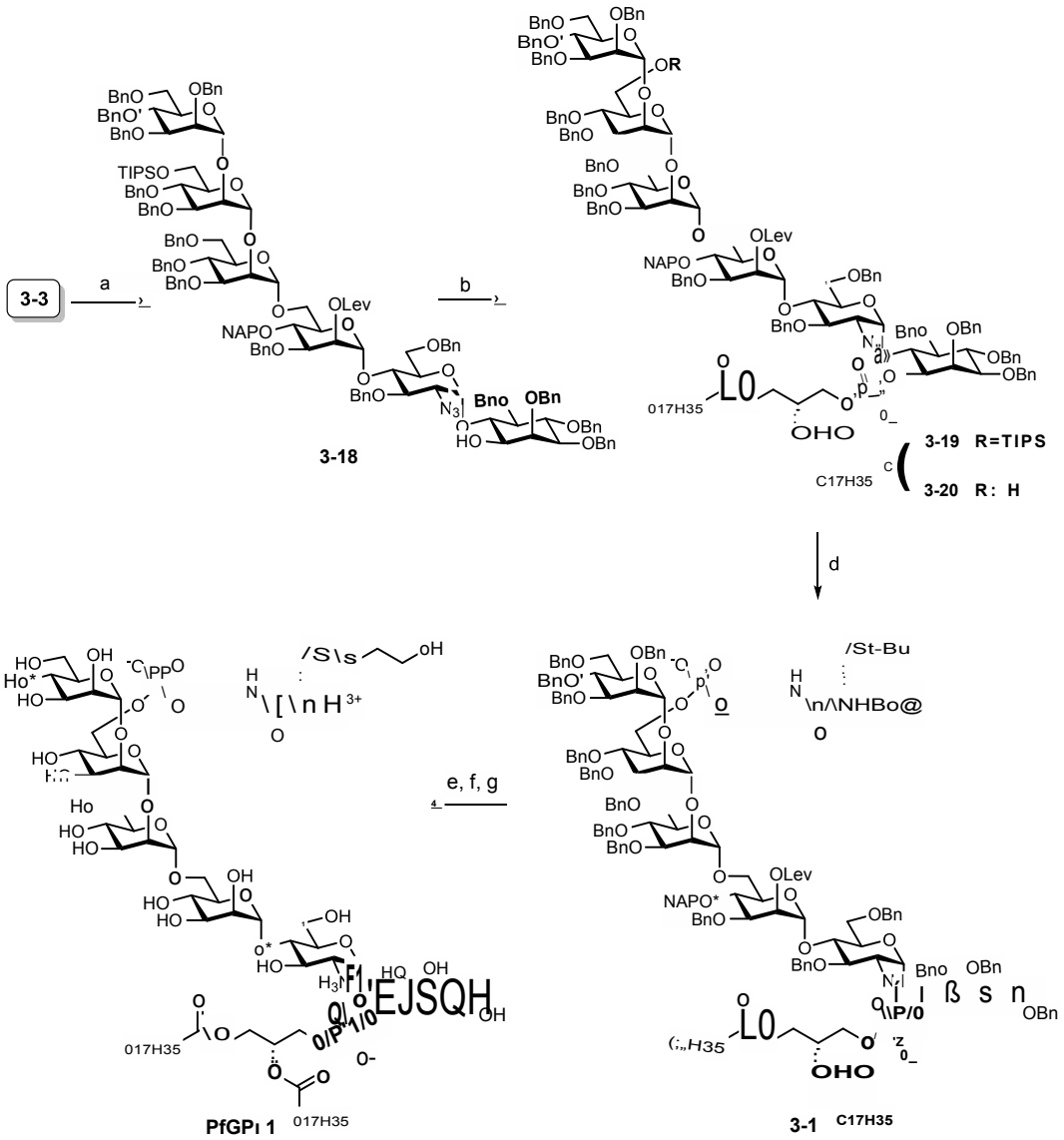

Scheme 3.3: Synthesis of *Pf*GPI 1. a) i. $[Ir(Cod)(PPh_2Me)_2]PF_6$, H_2, THF ii. HgO, $HgCl_2$, Acetone, H_2O, 80%; b) i. **3-8**, PivCl, Py, 48 h, ii. I_2, water, 55%; c) $Sc(OTf)_3$, CH_3CN, $CHCl_3$, 67%; d) i. **3-9**, PivCl, py, 48 h, ii. I_2, water, 70%; e) ; f) THF:MeOH:H_2O (3:3:1), $Pd(OH)_2$/C, H_2, 72 h, 70%; g) i. TFA:Anisole (10:1), $Hg(TFA)_2$, 0 °C, 30 min, ii. AcOH:H_2O (7:3), mercaptoethanol, 12 h, 35%.

3.5 Protein-GPI Ligation

The ligation strategy developed by Dr. Renee Roller in our group was utilized to obtain GPI-anchored $MSP1_{19}$. This semi-synthetic strategy is carried out by combining a protein activation with ligation to the GPI molecule in a one-pot process. A modified C-terminal intein fragment from the *DNAE* split intein from *Nostoc punctiforme* was designed having two essential residues (Asn35 and Cys36) mutated to Ala residues to obtain *NpuC*(AA). These mutations defunctionalize the intein for the protein *trans*-splicing process but allowed the capture of a thioester using thiols. Identical to the wildtype *NpuC*, this modified intein fragment can associate with the N-terminal fragment of the protein to bring the C-terminus of the protein in close proximity to that of *NpuC*(AA). To replace the intramolecular *trans*-thioesterification from Cys1 of *NpuN* to Cys36 of *NpuC*, a thiol reagent was added to form a protein thioester *in situ*. This protein activation is followed by a ligation reaction of the formed protein thioester with the cysteine-containing GPI already present in the reaction mixture. The rearrangement in the process leads to formation of the desired GPI-anchored product and the fragment *NpuN* as a by-product of the reaction. **Figure 3.3** shows a schematic representation of the one-pot ligation rearrangement during the process.

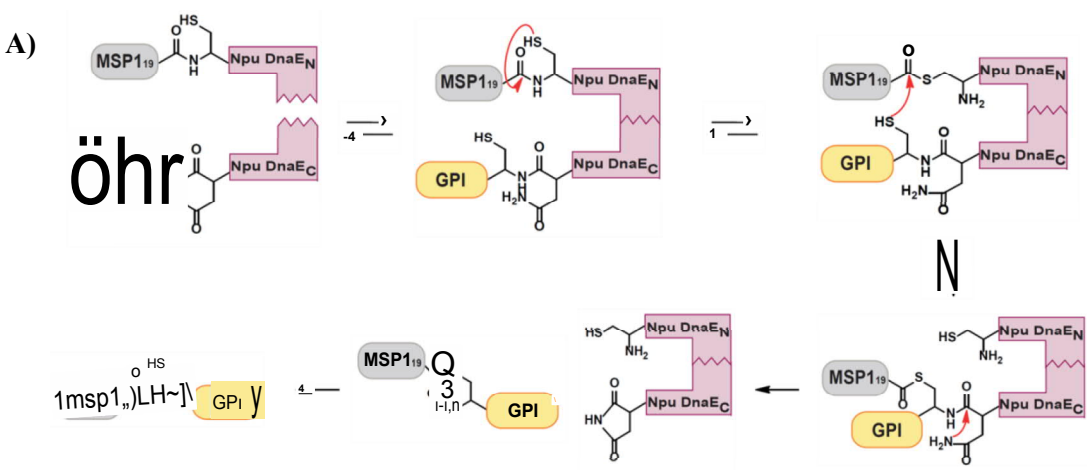

Figure 3.3: Mechanism of protein GPI ligation using an intein mediated process. (A) $MSP1_{19}$ ligation to GPI based on a split intein mediated protein *trans*-splicing mechanism; **(B)** sequences of the modified wildtype *NpuC* fragment.

3.5.1 Synthesis of MSP1$_{19}$-GPI and MSP1$_{19}$-Biotin

In order to compare the effect of glypiation on the structure and immunological properties of the MSP1$_{19}$ protein, the protein was ligated to ***Pf*GPI 1** and Cys-Biotin (**Figure 3.4**). **MSP1$_{19}$-Biotin** was used for the optimization of the process and as a control in the biological studies.

Purified fusion protein MSP1$_{19}$–*NpuN,* provided by Dr. Maria A. Carillo, synthetic *NpuC*(AA) and 4-(mercaptomethyl)benzoic acid (MMBA) were used to generate a MSP1$_{19}$ protein thioester *in situ*. The ligations to ***Pf*GPI 1** and Cys-Biotin with the protein were carried out under optimized conditions using the 10 µM MSP1$_{19}$–*NpuN,* 30 µM *NpuC*(AA), 20 mM TCEP solution and 70 mM MMBA in Tris buffer at pH 7.2. The reactions were incubated at 37 ˚C for five days to obtain the ligated products, **MSP1$_{19}$-Biotin** and **MSP1$_{19}$-GPI**. The ligation was run in small batches with maximum 200 µg of protein to avoid precipitation of protein during the reaction.

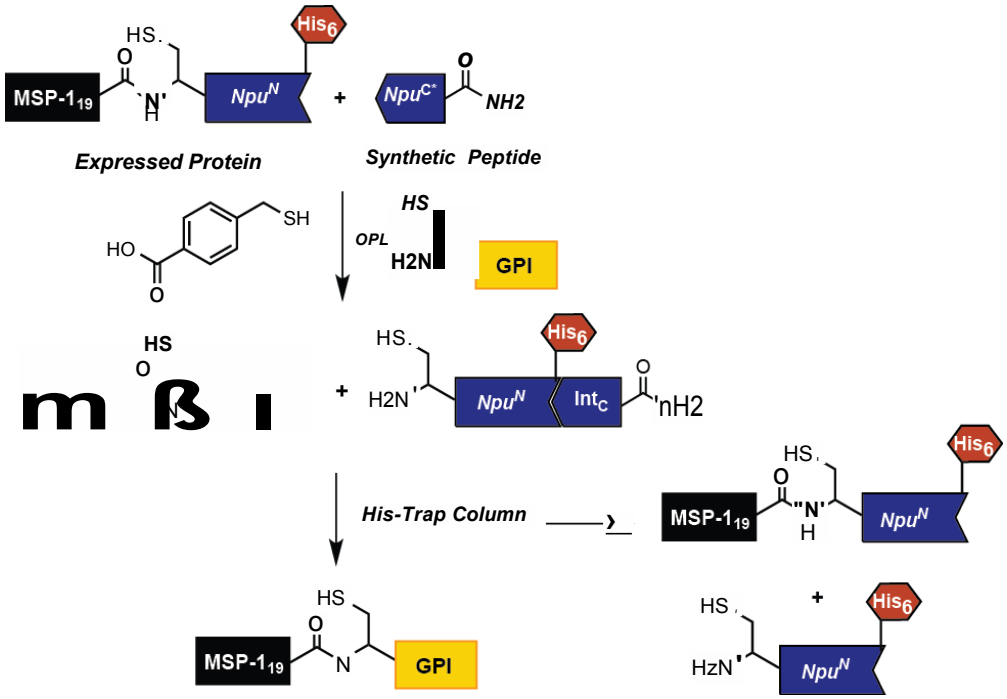

Figure 3.4: Protein ligation with MSP1$_{19}$-*NpuN*, *NpuC and *Pf*GPI.**[‡]**

[‡] GPI-protein ligation were done with Dr. Maria A. Carillo

The ligation reactions were monitored by analytical SEC and SDS-PAGE (**Figure 3.5 A, B, C**). **MSP1$_{19}$-Biotin** and **MSP1$_{19}$-GPI** were purified using His-Trap affinity chromatography. MSP1$_{19}$-*NpuN* and cleaved *NpuN* bearing an N-terminal His-Tag were retained on the column and eluted using a gradient of imidazole. This purification step separates the cleaved intein fragments from the product leaving a mixture of the hydrolyzed protein and the *NpuC*(AA) peptide that co-elutes with the product in the flow through fractions. To separate this mixture, FPLC purification on a Superdex 30 column was used. The fractions from FPLC were analyzed using SDS-PAGE with silver staining (**Figure 3.5 D**).

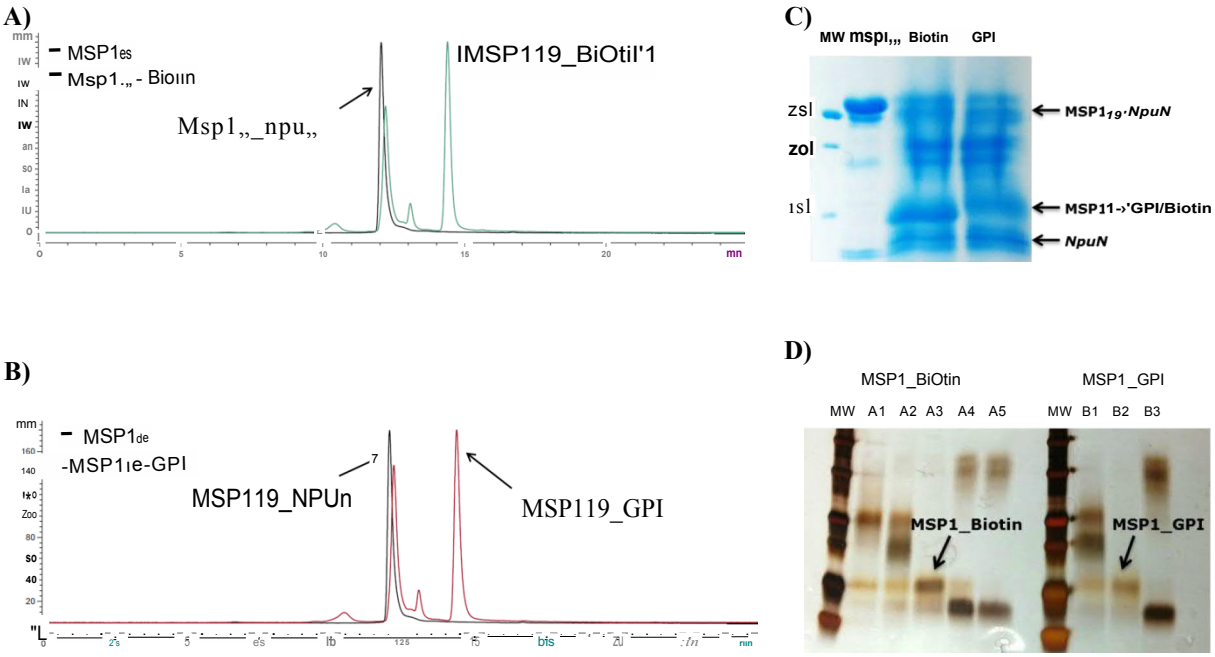

Figure 3.5: Analysis of the ligation reactions after 72 h. (A) Analysis of MSP1$_{19}$-Biotin ligation on analytical SEC column; **(B)** analysis of MSP1$_{19}$-GPI ligation on analytical SEC column; **(C)** gel electrophoresis (SDS-PAGE) analysis for reaction mixture of MSP1$_{19}$-Biotin and MSP1$_{19}$-GPI stained with Coomassie Brilliant Blue and **(D)** gel electrophoresis (SDS-PAGE) analysis of fractions from FPLC purification for MSP1$_{19}$-Biotin and MSP1$_{19}$-GPI stained with silver stain.

The pure fractions were collected and dialyzed to partially remove the salts from the ligated samples. The pure ligated product was obtained in 45% yield and analyzed using LC-ESI-MS (**figure 3.6**). The products **MSP1$_{19}$-Biotin** and **MSP1$_{19}$-GPI** were detected in the LC-ESI-MS spectra. However, the detection of **MSP1$_{19}$-GPI** was very difficult due to the loss of labile fatty acid chains during the MS analysis, which were also observed in the MS spectra. **Figure 3.6** shows the deconvoluted spectrum for **MSP1$_{19}$-GPI** with an observed mass of $[M+K]^+$=13348.52 Da that corresponds to the calculated mass of the desired product $[M+K]^+$calc=13348.89 Da.

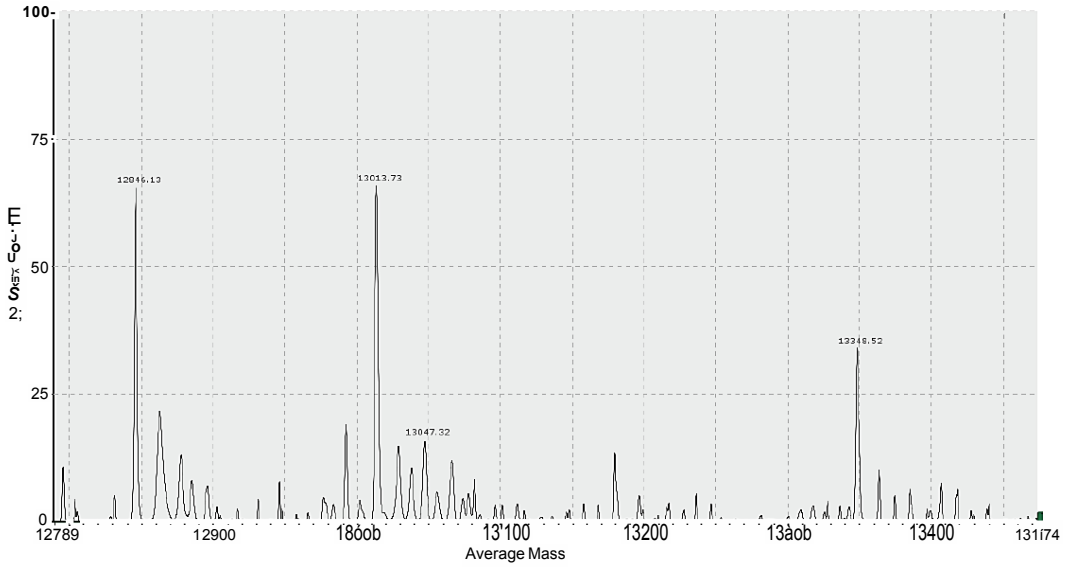

Figure 3.6: LC-ESI-MS analysis of ligation of MSP1$_{19}$ and GPI after five days. Deconvoluted mass spectrum for MSP1$_{19}$-GPI.

3.6 Structural Analysis

Circular dichroism (CD) was used to analyze the global conformation of the protein and to evaluate the effect of the C-terminal modification on the structure of MSP1$_{19}$. The native conformation of MSP1$_{19}$ has two epidermal growth factor (EGF) like domains with three disulfide bonds each. In its native state, each EGF domain contains a random coil segment followed by four antiparallel β-strands. Thus, the overall structure of MSP1$_{19}$ is described as a random coil structure (**figure 3.7**).[215]

The purified ligated products were structurally analyzed using CD. The CD spectra for both $MSP1_{19}$-GPI and $MSP1_{19}$-Biotin showed an identical profile that corresponds to a random coil structure, which are also in agreement with previously reported CD spectra for an expressed $MSP1_{19}$ protein.[216] These results confirm that any of the added C-terminal modification does not induce any structural changes in $MSP1_{19}$ or affect the general profile of the CD spectra (**figure 3.8**). However, a more detailed analysis is required to determine the local effects of these modifications and cannot be detected by this method.

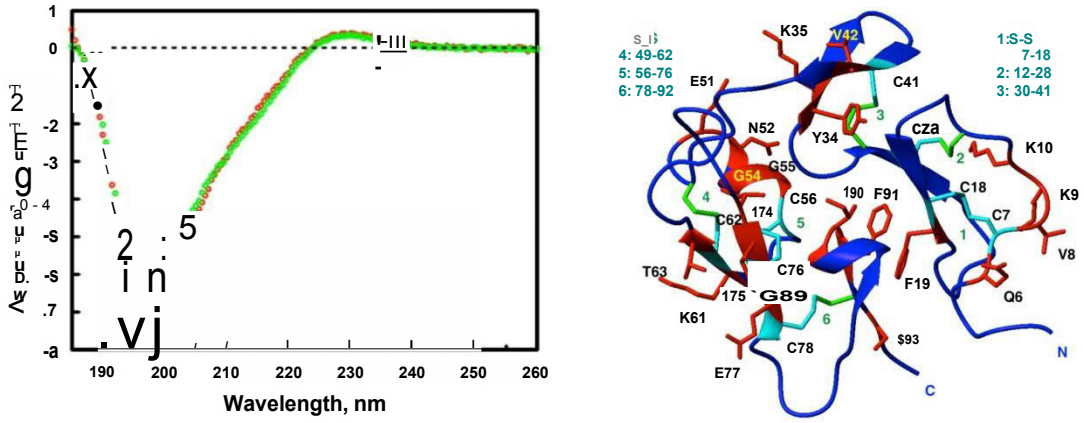

Figure 3.7: (A) Circular dichroism spectra of the $MSP1_{19}$ native conformation and **(B)** a ribbon representation of $MSP1_{19}$ solved by X-ray diffraction with assigned disulfide linkages.[216]

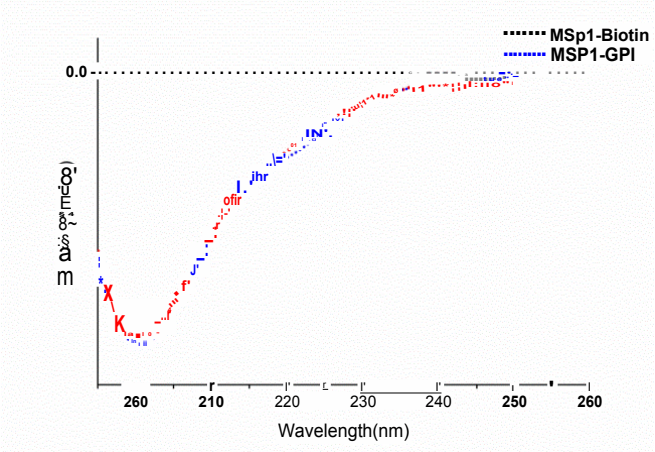

Figure 3.8: Circular dichroism analysis. Circular dichroism spectra of $MSP1_{19}$-Biotin (red) and $MSP1_{19}$-GPI (blue).

3.7 Dendritic Cell Stimulation Assay

Dendritic cells are important for initiating cellular immune response.[217] They act as antigen presenting cells (APC) and can activate a T-cell response. Upon activation, dendritic cells produce pro-inflammatory cytokines such as IL-12, TNF-α and IFN-γ, among others, that activate T-cells and can be used to monitor the immunogenicity of antigen for vaccine development.[218] Several studies have shown enhanced levels of IL-6, TNF-α and IL-10 in patients with severe malaria and a correlation of the level of these cytokines with parasitemia. Therefore, a proinflammatory response is considered important for malaria clearance.[219, 220]

To determine the activity of the synthesized proteins, a quantitative enzyme-linked immunosorbent assay (ELISA) was performed to determine the levels of TNF-α and IL-12 cytokines in **$MSP1_{19}$-GPI** and **$MSP1_{19}$-Biotin** in *in vitro*-stimulated dendritic cells. The cells were cultured in the presence of the proteins at three different concentrations, 0.01, 0.1 and 1 μM. LPS (lipopolysaccharide), a strong immunostimulator, was used as a positive control for this study (**Figure 3.9**). This *in vitro* assay showed that the production of cytokines was directly proportional to the concentration of **$MSP1_{19}$-Biotin** and **$MSP1_{19}$-GPI**. At 0.01 μM, almost no activation was observed for TNF-α and IL-12 and higher level of cytokines were observed at 0.1 μM. The activation was similar for both **$MSP1_{19}$-Biotin** and **$MSP1_{19}$-GPI**. However, at 1 μM very high concentration of TNF-α and IL-12 were observed for **$MSP1_{19}$-GPI** compared to **$MSP1_{19}$-Biotin**. This confirms that GPI can improve the immunogenicity of $MSP1_{19}$ which is very important for the production of cytokines and to control cerebral malaria.

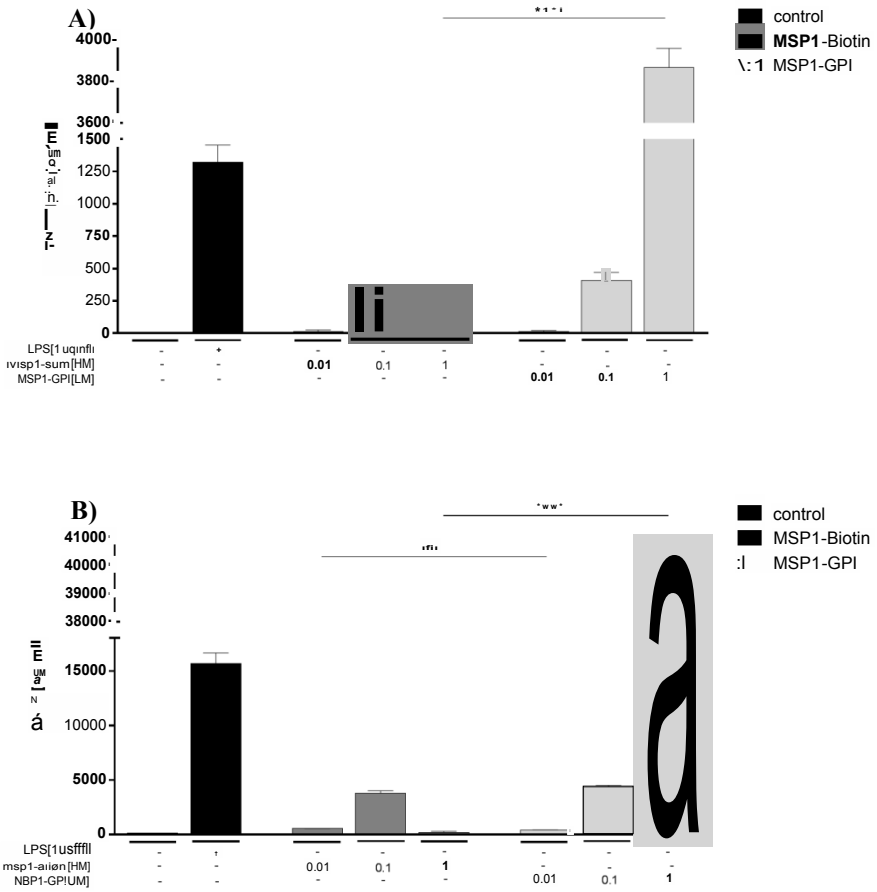

Figure 3.9: T-cell activation. Comparison of the levels of pro inflammatory cytokines of **(A)** TNF-α and **(B)** IL-12, for $MSP1_{19}$-Biotin and $MSP1_{19}$-GPI. Statistical significance was determined using the unpaired Student's t-test, significance shown by asterisks **(p <0.01) , ****(p <0.0001).

3.8 Conclusion and Outlook

To investigate the role of protein glypiation in the proteins from parasites, two GPIs, ***Pf*GPI 1** and ***Pf*GPI 2** from *P. falciparum,* containing two lipids and three lipids respectively, were designed synthesize the glypiated fragment $MSP1_{19}$ of the MSP1 protein of Plasmodium. The $MSP1_{19}$ fragment of the MSP-1 was selected as a protein model. This fragment stays intact during the merozoite invasion and plays an important role for the survival of the parasite.

The ***Pf*GPI 1** glycolipid and the core structure of the trilipidated ***Pf*GPI 2** were successfully synthesized by applying a convergent strategy. The synthesis of the ***Pf*GPI 1** glycolipid was only possible using a [3+1+2] glycosylation strategy to obtain the glycan part and then using two-step phosphorylation reactions. The synthesis process was limited by multiple challenges

which drastically reduced the yield of the process. The main limitations were the formation of an α(1→6)-linkage between the ManI and ManII, the purification of phosphorylated intermediates and the removal of protecting groups in the global deprotection. Furthermore, the characterization of the GPI was challenging due to the poor solubility in aqueous and organic solvents and the amphiphilic nature of the final product ***Pf*GPI 1.**

The ***Pf*GPI 1** glycolipid was used to obtain a homogeneous GPI-anchored protein. An expressed $MSP1_{19}$-*NpuN* fusion protein and a synthetic peptide were used for the ligation with GPI to obtain **$MSP1_{19}$-GPI**. **$MSP1_{19}$-Biotin** was synthesized as a control to evaluate the influence of the synthetic process and the effect of GPI on the structure and immunological activity of the protein. The ligation products were characterized using SDS-PAGE and LC-ESI-MS. CD was used for preliminary structural analysis of $MSP1_{19}$ with and without a GPI anchor.

CD analysis of the modified proteins showed that the C-terminus modification does not affect the overall structure of the protein. The spectra for both **$MSP1_{19}$-Biotin** and **$MSP1_{19}$-GPI** presented identical profiles that corresponded to the expected random coil structure of the $MSP1_{19}$ native protein.

A dendritic cell stimulation assay showed that both $MSP1_{19}$-Biotin and $MSP1_{19}$-GPI were able to activate the T-cells and release cytokines TNF-α and IL-12. The DC activation and cytokine production was very similar for both proteins with and without GPI at low concentration. However, at 1 μM very high levels of TNF-α and IL-12 were observed only for **$MSP1_{19}$-GPI** only. This study is the first immunological and structural evaluation of a homogeneous synthetic **$MSP1_{19}$-GPI** and shows that a GPI anchor is a dominant immunogenic factor indicating that **$MSP1_{19}$-GPI** is a potential target for vaccine development.

Even though CD elucidated the overall structure for the protein, further studies involving NMR, crystallization and cryo-EM are necessary to understand the interactions of the protein with the glycolipid and the effect of the GPI anchor on the behaviour of the protein on membranes. The next steps in the evaluation of glypiated MSP1should include *in vivo* studies in a murine model to evaluate **$MSP1_{19}$-GPI** as an anti-malarial vaccine candidate. From the current T-cell activation results, we can expect high vaccine efficacy from $MSP1_{19}$-GPI. If these steps will be completed, a human malaria vaccine could become reality.

3.9 Experimental

3.9.1 Material and Methods of Synthetic chemistry

All purchased chemicals were of reagent grade and all anhydrous solvents were of high-purity grade and used as supplied except where noted otherwise. Reactions were performed in oven-dried glassware under an inert argon atmosphere unless noted otherwise. Reagent grade thiophene was dried over activated molecular sieves prior to use. Pyridine was distilled over CaH_2 prior to use. Sodium hydride suspension was washed with hexane and THF and stored in an anhydrous environment. Benzyl bromide was passed through activated basic aluminum oxide prior to use. Metal sodium was washed with hexane and stored in hexane. Analytical thin layer chromatography (TLC) was performed on Merck silica gel 60 F_{254} plates (0.25mm). Compounds were visualized by UV irradiation or heating the plate after dipping in staining solution. The staining solutions were cerium sulfate-ammonium molybdate (CAM) solution, basic potassium permanganate solution, acidic ninhydrin-acetone solution, or a 3-methoxyphenol-sulfuric acid solution (Sugar Stain). Flash column chromatography was carried out using a forced flow of the indicated solvent on Sigma Aldrich silica gel high purity grade 60 Å (230-400 mesh particle size, for preparative column chromatography). Solvents were removed under reduced pressure using rotary evaporator and high vacuum (<1 mbar). Freeze drying of the aqueous solutions was performed using Alpha 2-4 LD Lyophilizer (Christ, Osterode am Harz, Germany)

^{1}H, ^{13}C and ^{31}P-NMR as well as all 2D-spectra (^{1}H-^{1}H COSY, ^{1}H-^{1}H TOCSY, ^{1}H-^{13}C HSQC, ^{1}H-^{13}C HMBC) were recorded on a Varian 400 (400 MHz), a Varian 600 (600 MHz), a Bruker 400 (400 MHz) and a Bruker Ascend 400 (400 MHz) spectrometer in $CDCl_3$ (7.26 ppm ^{1}H, 77.1 ppm ^{13}C), D_2O (4.79 ppm ^{1}H), MeOD (4.87 ppm and 3.31 ppm ^{1}H, 49.00 ppm ^{13}C), Acetone-d_6 (2.05 ppm and 2.84 ppm ^{1}H, 206.26 ppm and 29.84 ppm ^{13}C) unless otherwise stated. The coupling constants (*J*) are reported in Hertz (Hz). Splitting patterns are indicated as s, singlet; d, doublet; t, triplet; q, quartet; br, broad singlet; dd, doublet of doublets; m, multiplet; dt, doublet of triplets; h, hextet for ^{1}H NMR data. Signals were assigned by means of ^{1}H-^{1}H COSY, ^{1}H-^{1}H TOCSY, ^{1}H-^{13}C HSQC, ^{1}H-^{13}C HMBC spectra and version thereof. ESI mass analyses were performed by Waters Xevo G2-XS Q-TOF with an Acquity H-class UPLC and a Bruker Autoflex-speed MALDI-TOF spectrometer.

Allyl-2-*O*-acetyl-3,4,6-tri-*O*-benyl-α-D-mannopyranosyl-(1→2)-3,4-di-*O*-benzyl-6-*O*-tri*iso*propylsilyl-α-D-mannopyranosyl-(1→2)-3,4,6-tri-*O*-benyl-α-D-mannopyranosyl-(1→6)-2,3-di-*O*-acetyl-4-*O*-(2-naphthyl)methyl-α-D-mannopyranoside (3-15a)

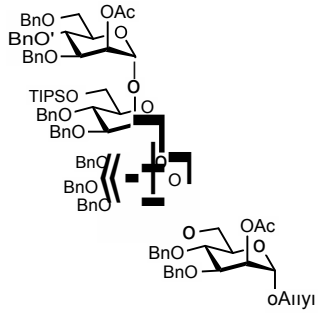

A mannose acceptor **3-6a** (0.2 g, 0.52 mmol) and trimannosyl donor **3-5a** (0.90 g, 0.57 mmol) were dissolved and co-evaporated with dry toluene three times and dried under high vacuum for 2 h. The reaction mixture was dissolved in dry thiophene:toluene (2:1, 10 mL) under argon atmosphere, followed by the addition of activated powdered molecular sieves. Then, 24 μL (0.1 mmol) of TBSOTf was added to the reaction mixture under argon atmosphere. After 2 h, the reaction was quenched by using Et_3N, filtered the molecular sieves and concentrated. The residue was purified using column chromatography to obtain tetrasaccharide **3-15a** (0.42 g, 0.23 mmol, 50%, α-anomer) ^{1}H NMR (400 MHz, $CDCl_3$) δ 7.35 – 7.24 (m, 3H), 7.24 (s, 10H), 7.26 – 7.14 (m, 28H), 7.18 – 7.08 (m, 14H), 7.06 (ddd, *J* = 11.2, 6.6, 2.4 Hz, 7H), 6.97 (t, *J* = 7.4 Hz, 1H), 5.82 – 5.69 (m, 1H), 5.49 (dd, *J* = 3.0, 1.8 Hz, 1H), 5.34 (dd, *J* = 3.3, 1.7 Hz, 1H), 5.24 (d, *J* = 1.3 Hz, 1H), 5.18 (d, *J* = 1.4 Hz, 1H), 5.14 (d, *J* = 1.4 Hz, 1H), 5.10 – 5.08 (m, 1H), 5.08 – 5.05 (m, 1H), 4.98 (d, *J* = 1.3 Hz, 1H), 4.86 – 4.32 (m, 26H), 4.22 (d, *J* = 12.1 Hz, 1H), 4.12 – 3.98 (m, 3H), 4.03 – 3.86 (m, 7H), 3.87 (d, *J* = 9.6 Hz, 3H), 3.86 – 3.76 (m, 7H), 3.79 – 3.67 (m, 3H), 3.69 – 3.51 (m, 6H), 3.55 – 3.39 (m, 3H), 2.07 (d, *J* = 2.9 Hz, 3H), 2.01 (d, *J* = 3.5 Hz, 3H), 1.09 – 0.91 (m, 21H). ^{13}C NMR (101 MHz, $CDCl_3$) δ 170.35, 170.19, 163.44, 138.78, 138.73, 138.56, 138.49, 138.34, 138.14, 138.10, 137.93, 137.80, 133.17, 128.50, 128.41, 128.36, 128.31, 128.28, 128.21, 128.19, 128.14, 128.05, 127.98, 127.94, 127.79, 127.77, 127.69, 127.63, 127.57, 127.51, 127.47, 127.44, 127.40, 118.24, 100.07, 99.90, 98.82, 96.50, 91.81, 79.46, 78.60, 77.25, 75.57, 75.07(2C), 74.90, 74.60, 74.13(2C), 73.53, 73.41, 73.13, 72.93, 72.21, 72.02, 71.84, 71.75, 71.46, 70.61, 69.06, 68.77, 68.61, 68.51, 67.91, 66.13, 62.75, 60.45, 26.06, 21.21, 21.09, 18.16(6C), 14.23, 11.95(3C). ESI-MS (*m*/*z*): $[M+Na]^+$ cald 1869.867 obs 1870.747.

2-*O*-acetyl-3,4,6-tri-*O*-benyl-α-D-mannopyranosyl-(1→2)-3,4-tri-*O*-benzyl-6-*O*-tri*iso*propylsilyl-α-D-mannopyranosyl-(1→2)-3,4,6-tri-*O*-benyl-α-D-mannopyranosyl-(1→6)-2-*O*-acetyl-3,4-*O*-benzyl-α-D-mannopyranosyl trichloroacetamidate (3-16a)

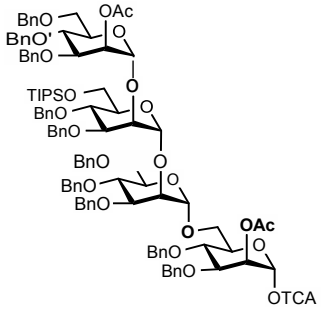

A solution of $[IrCOD(PPh_2Me)_2]PF_6$ (5.0 mg) in THF (2 mL) was stirred under hydrogen atmosphere until the color of the solution turned from red to colorless to pale yellow. The hydrogen atmosphere was exchanged with Argon. This solution was added to a solution of tetrasaccharide **3-15a** (0.30 g, 0.16 mmol) in THF (7 mL). After 16 h, the solvent was removed in *vacuo* and the residue was dissolved in a mixture of acetone (4 mL) and water (0.5 mL). Mercury (II) chloride (0.11 g, 0.41 mmol) and mercury (II) oxide (7.1 mg, 0.002 mmol) were added. After 1 h, saturated $NaHCO_3$ (aq) was added and the reaction mixture was extracted three times with CH_2Cl_2. The combined organic layer was dried over Na_2SO_4, filtered and concentrated. The crude product was purified by silica gel column chromatography to give trisaccharide hemiacetal (0.22 g, 0.12 mmol, 70 %) as colorless oil. ^{1}H NMR (400 MHz, $CDCl_3$) δ 7.25 (d, *J* = 11.7 Hz, 21H), 7.25 – 6.96 (m, 79H), 5.51 – 5.40 (m, 1H), 5.19 (d, *J* = 20.0 Hz, 3H), 4.96 (s, 1H), 4.79 (ddd, *J* = 13.3, 11.0, 6.2 Hz, 10H), 4.72 – 4.51 (m, 10H), 4.55 – 4.26 (m, 20H), 4.24 – 4.02 (m, 2H), 4.02 – 3.67 (m, 28H), 3.67 – 3.34 (m, 15H), 2.05 (s, 3H), 2.02 (s, 3H), 0.98 (d, *J* = 3.2 Hz, 18H). ESI-MS (*m*/*z*): $[M+Na]^+$ cald 1829.835 obsd 1829.833.

To a stirred solution of hemiacetal (0.2 g, 0.11 mmol) in a anhydrous CH_2Cl_2 (7 mL) were added trichloroacetonitrile (110 µL, 1.11 mmol) and DBU (5 µL, 0.033 mmol) at 0 °C. The reaction mixture was stirred and warmed up to room temperature. After 2 h, volatiles were evaporated and the crude reaction mixture was purified using silica gel column chromatography to get the imidate **3-16a** (0.14 g, 0.11 mmol, 64%). ^{1}H NMR (400 MHz, $CDCl_3$) δ 7.41 – 7.24 (m, 40H), 7.22 (ddd, *J* = 20.6, 10.9, 3.5 Hz, 26H), 7.19 – 7.03 (m, 6H), 6.21 (d, *J* = 1.6 Hz, 1H), 5.58 (dd, *J* = 2.9, 1.8 Hz, 1H), 5.54 – 5.50 (m, 1H), 5.32 (d, *J* = 5.6 Hz, 1H), 5.05 (s, 1H), 4.95 – 4.79 (m, 6H), 4.81 – 4.62 (m, 7H), 4.64 – 4.49 (m, 7H), 4.52 –

4.41 (m, 7H), 4.27 (d, *J* = 12.1 Hz, 1H), 4.13 – 3.97 (m, 7H), 4.01 – 3.91 (m, 7H), 3.95 – 3.83 (m, 6H), 3.86 – 3.69 (m, 6H), 3.72 – 3.45 (m, 7H), 2.14 (d, *J* = 5.4 Hz, 3H), 2.12 (s, 2H), 1.07 (d, *J* = 3.2 Hz, 28H). ^{13}C NMR (101 MHz, $CDCl_3$) δ 170.20, 170.03, 138.75, 138.57, 138.11, 137.99, 137.35, 128.50, 128.39, 128.37, 128.31, 128.27, 128.24, 128.15, 128.08, 128.00, 127.93, 127.88, 127.79, 127.68, 127.55, 127.39, 99.99, 98.66, 97.46, 94.88, 90.70, 78.60, 77.89, 75.19, 75.08, 74.52, 74.14, 73.54, 73.49, 73.39, 73.09, 72.78, 72.18, 72.05, 71.78, 71.68, 71.61, 69.05, 68.76, 68.52, 67.34, 65.84, 62.75, 29.74, 21.23, 20.98, 18.16(6C), 14.18, 11.94(3C).

3,4,6–tri-*O*-acetyl-2-azido-2-deoxy-α-D-glucopyranosyl-(1→6)-1-*O*-allyl-2-O-(2-napthyl)methyl-3,4,5-tetra-*O*-benzyl-D-*myo*-inositol (3-12)

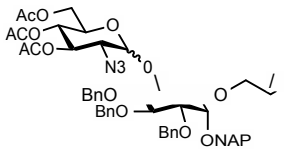

The glucosamine imidate **2-18** (1.13 g, 2.38 mmol) and inositol acceptor **2-15** (0.75 g, 1.19 mmol) were co-evaporated with toluene (3 x 10 mL) and dried under high vacuum for 2 h. The mixture was dissolved in a mixture of anhydrous diethylether and anhydrous CH_2Cl_2 (1:1, 16 mL) and activated molecular sieves were added. The solution was stirred for 10 min at room temperature and cooled to 0 °C. The mixture was treated with TMS-OTf (43 μL, 0.24 mmol) and stirred at 0 °C for a period of 1 h. The reaction was diluted with CH_2Cl_2, quenched with Et_3N and concentrated. The crude product was purified by flash column chromatography to obtain disaccharide **3-12** (0.9 g, 0.95 mmol, 80%). ^{1}H NMR (400 MHz, $CDCl_3$) δ 7.83 (ddt, *J* = 20.7, 9.2, 4.2 Hz, 11H), 7.64 – 7.44 (m, 8H), 7.43 – 7.24 (m, 36H), 5.98 – 5.86 (m, 2H), 5.84 (d, *J* = 3.6 Hz, 1H), 5.48 – 5.32 (m, 1H), 5.28 (ddd, *J* = 17.3, 3.0, 1.5 Hz, 2H), 5.23 – 5.07 (m, 3H), 5.08 – 4.94 (m, 9H), 4.93 – 4.79 (m, 4H), 4.79 – 4.60 (m, 4H), 4.34 – 4.23 (m, 3H), 4.22 – 4.13 (m, 3H), 4.14 – 4.06 (m, 6H), 4.05 – 3.91 (m, 3H), 3.71 – 3.60 (m, 1H), 3.60 – 3.49 (m, 2H), 3.44 (dtt, *J* = 11.7, 5.9, 3.2 Hz, 5H), 3.32 – 3.12 (m, 2H), 2.63 (d, *J* = 1.5 Hz, 1H), 2.17 – 1.81 (m, 9H). ^{13}C NMR (101 MHz, $CDCl_3$) δ 170.75, 170.64, 170.19, 170.00, 169.85, 169.58, 163.54, 138.79, 138.73, 138.37, 138.32, 138.17, 136.22, 136.09, 135.27, 134.43, 134.06, 133.18, 132.94, 128.63, 128.46, 128.38, 128.27, 128.13, 128.07, 127.92, 127.77, 127.71, 127.66, 127.62, 127.44, 126.85, 126.65, 126.44, 126.28, 126.17, 126.05, 125.99, 125.88, 125.78, 117.52, 117.28, 115.93, 101.11, 97.46, 83.62, 83.38, 81.98, 81.74, 81.65, 81.44, 81.16, 80.86, 80.68, 79.80, 75.90, 75.40, 74.18, 74.08, 73.23, 73.00, 72.72,

71.22, 70.90, 70.47, 67.83, 66.91, 60.93, 31.96, 29.73, 29.40, 22.74, 20.81, 20.77, 20.73, 20.67, 20.63, 20.57, 14.18.(NMR for mixture of isomers) ESI-MS (*m*/*z*): $[M+Na]^+$ cald 966.3 obsd 966.2.

2-azido-2-deoxy-α-D-glucopyranosyl-(1→6)-1-*O*-allyl-2-O-(2-napthyl)methyl-3,4,5-tetra-*O*-benzyl-D-*myo*-inositol (3-13)

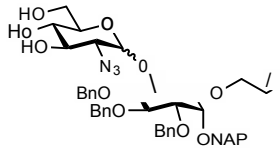

To a stirred solution of thioglycoside **3-12** (0.80 g, 0.85 mmol) in MeOH (15 mL) was added freshly prepared 1 M solution of NaOMe. After 1 h, the reaction was neutralized with Amberlite IR 120 H^+ resin, filtered and concentrated to obtain crude product **3-13** (0.59 g, 0.73 mmol, 85%). The crude product **3-13** was directly used without any further purification. ^{1}H NMR (400 MHz, $CDCl_3$) δ 7.90 – 7.75 (m, 7H), 7.65 – 7.55 (m, 1H), 7.54 – 7.44 (m, 3H), 7.44 – 7.27 (m, 16H), 7.26 (s, 3H), 6.04 – 5.88 (m, 1H), 5.67 (d, *J* = 3.7 Hz, 1H), 5.40 – 5.11 (m, 3H), 5.10 – 4.98 (m, 4H), 4.94 – 4.78 (m, 2H), 4.74 – 4.60 (m, 4H), 4.40 (t, *J* = 9.5 Hz, 0H), 4.35 – 4.08 (m, 3H), 4.12 – 3.99 (m, 3H), 3.93 (dd, *J* = 10.4, 8.9 Hz, 1H), 3.88 – 3.68 (m, 2H), 3.65 – 3.54 (m, 1H), 3.49 – 3.36 (m, 5H), 3.34 – 3.17 (m, 3H), 3.08 (dd, *J* = 10.4, 3.7 Hz, 1H). ^{13}C NMR (101 MHz, $CDCl_3$) δ 138.77, 138.58, 138.43, 138.17, 136.15, 135.23, 134.21, 128.47, 128.39, 128.04, 127.90, 127.72, 127.65, 127.27, 126.64, 126.27, 126.05, 125.87, 117.37, 101.23, 97.52, 81.97, 81.71, 81.50, 80.87, 75.88, 75.41, 75.14, 74.14, 72.69, 72.46, 71.53, 71.02, 69.42, 62.72, 62.49, 31.96, 29.73, 29.40, 22.73, 14.18. (NMR for mixture of isomers) ESI-MS (*m*/*z*): $[M+Na]^+$ cald 840.3472 obsd 840.2

3,-*O*-benzyl-4,6-*O*-benzylidene-2-azido-2-deoxy-α-D-glucopyranosyl-(1→6)-1-*O*-allyl-2-O-(2-napthyl)methyl-3,4,5-tetra-*O*-benzyl-D-*myo*-inositol (3-14)

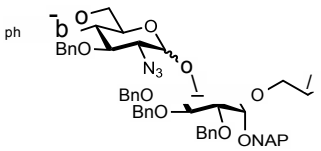

To the solution of crude product **3-13** (0.59 g, 0.73 mmol) in ACN (15 mL) were added benzaldehyde dimethyl acetal (0.32 mL, 2.16 mmol) and CSA (0.04 g, 0.18 mmol). The reaction mixture was stirred for 3 h at room temperature. The reaction was quenched with aq.$NaHCO_3$, extracted with CH_2Cl_2, washed with brine and dried over Na_2SO_4. The solvents were removed under reduced pressure and the crude product was purified by flash column chromatography to obtain benzylidene intermediate compound (0.45 g, 0.50 mmol, 68%).

To a stirred solution of intermediate (0.4 g, 0.44 mmol) in anhydrous DMF (10 mL) was added NaH (0.04 g, 1.77 mmol) at 0 ˚C. After 20 min, BnBr (0.11 mL, 0.88 mmol) was added and the reaction was stirred overnight at room temperature. The reaction was quenched with MeOH and concentrated. The crude product was purified using flash chromatography to obtain **3-14** (0.32 g, 0.32 mmol, 73%). ^{1}H NMR (400 MHz, $CDCl_3$) δ 7.89 – 7.76 (m, 5H), 7.60 (d, *J* = 8.6 Hz, 1H), 7.50 (dd, *J* = 6.2, 3.2 Hz, 3H), 7.36 (dq, *J* = 22.6, 9.0, 8.2 Hz, 20H), 7.31 – 7.20 (m, 9H), 7.20 – 7.13 (m, 3H), 5.98 (ddt, *J* = 16.0, 10.7, 5.6 Hz, 1H), 5.77 (d, *J* = 3.8 Hz, 1H), 5.51 (s, 1H), 5.29 (d, *J* = 17.2 Hz, 1H), 5.22 (d, *J* = 10.4 Hz, 1H), 5.02 (d, *J* = 6.5 Hz, 3H), 4.97 (dd, *J* = 11.0, 7.8 Hz, 3H), 4.87 (d, *J* = 11.2 Hz, 1H), 4.81 (dd, *J* = 10.8, 4.7 Hz, 2H), 4.74 – 4.60 (m, 2H), 4.31 (t, *J* = 9.5 Hz, 1H), 4.20 (td, *J* = 9.6, 4.0 Hz, 3H), 4.14 – 3.96 (m, 6H), 3.64 (dt, *J* = 24.4, 9.8 Hz, 2H), 3.50 (t, *J* = 9.3 Hz, 1H), 3.45 – 3.38 (m, 3H), 3.34 (dd, *J* = 10.0, 3.8 Hz, 1H). ^{13}C NMR (101 MHz, $CDCl_3$) δ 138.59, 138.20, 138.04, 137.92, 137.53, 136.20, 134.26, 133.16, 132.97, 128.79, 128.45, 128.42, 128.36, 128.32, 128.27, 128.05, 127.96, 127.91, 127.85, 127.74, 127.71, 127.67, 127.53, 127.34, 126.56, 126.23, 126.01, 125.82, 117.30, 101.21, 97.99, 82.95, 81.97, 81.88, 81.06, 80.89, 77.25, 75.72, 75.57, 75.33, 74.88, 74.08, 72.93, 72.71, 71.00, 68.74, 63.08, 62.41. (NMR for mixture of isomers) ESI-MS (*m*/*z*): $[M+Na]^+$ cald 1018.4255 obsd 1019.3.

3,6–di-*O*-benzyl-2-azido-2-deoxy-α-D-glucopyranosyl-(1→6)-1-*O*-allyl-2-O-(2-napthyl)methyl-3,4,5-tetra-*O*-benzyl-D-*myo*-inositol (3-7c)

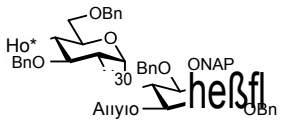

To a stirred solution of **3-14** (0.1 g, 0.10 mmol) in CH_2Cl_2 (6 mL) were added trifluoroacetic anhydride (0.04 mL, 0.30 mmol) and triethylsilane (0.08 mL, 0.5 mmol) were added at 0 °C

followed by trifluoroacetic acid (0.04 mL, 0.5 mmol) drop wise. The reaction mixture was stirred at 0 °C. After 5 h, the reaction mixture was quenched with Et_3N and concentrated to give yellow oil that was purified by flash column chromatography to obtain disaccharide acceptor **3-7c** (0.08 g, 0.08 mmol, 79 %) as a colorless oil. ^{1}H NMR (400 MHz, $CDCl_3$) δ 7.78 (dd, *J* = 15.5, 8.8 Hz, 3H), 7.56 (d, *J* = 8.3 Hz, 1H), 7.49 – 7.30 (m, 11H), 7.30 – 7.16 (m, 16H), 6.00 – 5.84 (m, 1H), 5.72 (d, *J* = 3.4 Hz, 1H), 5.24 (d, *J* = 17.5 Hz, 1H), 5.17 (d, *J* = 10.2 Hz, 1H), 4.99 (q, *J* = 10.8 Hz, 4H), 4.86 (s, 2H), 4.79 (d, *J* = 10.6 Hz, 1H), 4.70 – 4.55 (m, 4H), 4.39 (d, *J* = 12.0 Hz, 1H), 4.31 – 4.19 (m, 2H), 4.14 (t, *J* = 9.4 Hz, 1H), 4.05 (s, 1H), 3.99 (s, 2H), 3.81 – 3.66 (m, 1H), 3.47 – 3.32 (m, 2H), 3.30 – 3.21 (m, 1H), 3.24 – 3.14 (m, 1H), 2.01 (d, *J* = 3.5 Hz, 1H). ESI-MS (*m*/*z*): $[M+Na]^+$ cald 1020.441 obsd 1020.355.

2-O-acetyl-3,4,6-tri-*O*-benzyl-α-D-mannopyranosyl-(1→2)-3,4-di-*O*-benzyl-6-*O*-tri*iso*propylsilyl-α-D-mannopyranosyl-(1→2)-3,4,6-tri-*O*-benzyl-α-D-mannopyranosyl-(1→6)-2-O-acetyl-3,4-*O*-benzyl-α-D-mannopyranosyl-(1→4)-2-azido-3,6-di-*O*-benzyl-2-deoxy-α-D-glucopyranosyl-(1→6)-1-*O*-allyl-2(2-napthylmethyl)-3,4,5-tetra-*O*-benzyl-D-*myo*-inositol (3-17)

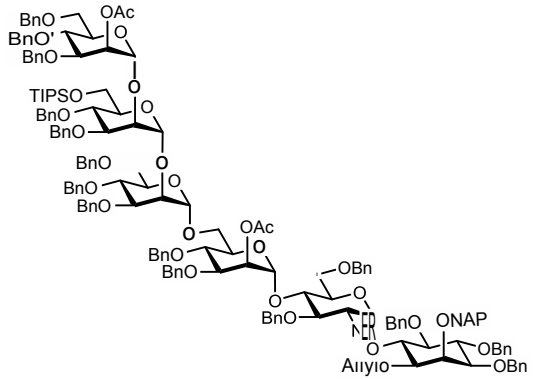

A mixture of glycosyl acceptor **3-7c** (0.05 g, 0.05 mmol) and glycosyl donor **3-16a** (0.10 g, 0.051 mmol) was dissolved and co-evaporated with dry toluene three times and dried under high vacuum for 2 h. The mixture was dissolved in anhydrous CH_2Cl_2 (5 mL) under argon atmosphere followed by the addition of activated powdered molecular sieves. Then, TMSOTf (3 μL, 0.014 mmol) was added to the reaction mixture at -40 °C. After 2 h, the reaction mixture was quenched with triethylamine, filtered and concentrated. The crude mixture was purified using column chromatography to obtain **3-17** (0.07 g, 0.025 mmol, 51%). Further optimization of the reaction is required. ^{1}H NMR (400 MHz, $CDCl_3$) δ 7.36 – 7.20 (m, 42H),

7.25 – 7.14 (m, 43H), 7.17 – 6.98 (m, 21H), 5.50 (dd, *J* = 3.1, 1.8 Hz, 2H), 5.18 (t, *J* = 20.3 Hz, 2H), 4.98 (dd, *J* = 6.5, 1.9 Hz, 2H), 4.87 – 4.04 (m, 39H), 4.05 – 3.76 (m, 28H), 3.78 – 3.23 (m, 21H), 2.07 (s, 3H), 2.04 (d, *J* = 6.6 Hz, 3H), 1.00 (d, *J* = 3.2 Hz, 32H).

3,4,6-tri-*O*-benzyl-α-D-mannopyranosyl-(1→2)-3,4-di-*O*-benzyl-6-*O*-tri*iso*propylsilyl-α-D-mannopyranosyl-(1→2)-3,4,6-tri-*O*-benzyl-α-D-mannopyranosyl-(1→6)-2-O-levulinyl-3-*O*-benzyl-4-O-(2-napthyl)methyl -α-D-mannopyranosyl-(1→4)-2-azido-3,6-di-*O*-benzyl-2-deoxy-α-D-glucopyranosyl-(1→6)-2,3,4,5-tetra-*O*-benzyl-D-*myo*-inositol (3-18)

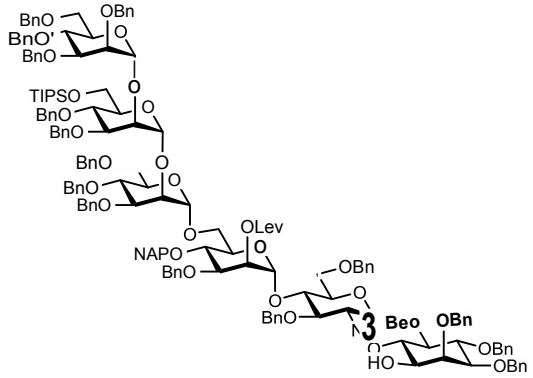

To a stirred solution of *pseudo*-hexasaccharide **3-3** (0.130 g, 0.045 mmol) in acetic acid (2 mL) and water (0.1 mL) were added palladium chloride (0.04 g, 0.23 mmol) and sodium acetate (0.04 g, 0.45 mmol) at room temperature. After 16 h, the reaction mixture was diluted with dichloromethane and the solution was washed with aqueous NaHCO3, brine, and water. The combined organic layers were dried over Na_2SO_4, filtered and concentrated. The crude product was purified by silica gel column chromatography to give *pseudo*-hexasaccharide **3-18** (90 mg, 0.032 mmol, 70%) as colorless oil. ^{1}H NMR (400 MHz, $CDCl_3$) δ 7.82 (d, *J* = 7.8 Hz, 1H), 7.64 (dd, *J* = 29.1, 8.5 Hz, 4H), 7.52 – 7.38 (m, 8H), 7.40 – 7.24 (m, 87H), 7.27 – 7.05 (m, 31H), 6.97 (t, *J* = 7.3 Hz, 1H), 5.51 – 5.44 (m, 3H), 5.40 (s, 1H), 5.33 (s, 1H), 5.24 (s, 1H), 5.09 – 4.68 (m, 21H), 4.67 – 4.23 (m, 26H), 4.25 – 4.06 (m, 7H), 4.06 – 3.74 (m, 25H), 3.75 – 3.58 (m, 8H), 3.55 – 3.36 (m, 7H), 3.37 – 3.24 (m, 5H), 3.04 (d, *J* = 7.0 Hz, 1H), 2.64 – 2.52 (m, 1H), 2.45 (q, *J* = 6.0, 5.5 Hz, 3H), 2.05 (s, 3H), 1.47 (s, 1H), 1.40 – 1.27 (m, 10H), 1.04 (d, *J* = 3.8 Hz, 18H). ^{13}C NMR (101 MHz, $CDCl_3$) δ 205.67, 171.83, 138.99, 138.93, 138.84, 138.64, 138.50, 138.44, 138.37, 138.08, 137.88, 137.75, 137.58, 136.28, 133.26, 132.77, 128.57, 128.50, 128.39, 128.35, 128.32, 128.28, 128.25, 128.20, 128.14,

128.09, 128.02, 127.97, 127.87, 127.84, 127.79, 127.73, 127.65, 127.61, 127.50, 127.42, 127.37, 127.26, 127.18, 125.95, 125.63, 125.42, 100.11, 99.62, 99.03, 98.79, 97.83, 81.86, 81.21, 80.92, 80.30, 79.99, 79.90, 79.72, 78.58, 75.84, 75.14, 75.03, 74.89, 74.73, 74.50, 74.43, 74.29, 73.31, 73.05, 72.54, 72.31, 72.10, 72.03, 71.60, 71.41, 71.19, 70.32, 68.86, 68.73, 64.26, 62.60, 37.76, 31.47, 30.21, 29.75, 27.92, 22.73, 18.17(6C), 11.95(3C). ESI-MS (*m*/*z*): $[M+H]^+$ cald 2851.325 obsd 2851.429.

1,2-di-*O*-stearoyl-*sn*-glycero-3-H-phosphonate (3-8)

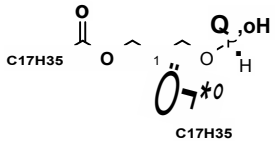

A mixture of 1,2-distearoyl-*sn*-glycerol (250 mg, 0.40 mmol) and phosphonic acid (36.1 mg, 0.44 mmol) were dissolved and co-evaporated three times with pyridine. The resulting mixture was dissolved in anhydrous pyridine (10 mL) and pivaloyl chloride (0.05 mL, 0.32 mmol) was added dropwise. The reaction mixture was stirred under nitrogen atmosphere at room temperature for two days. The volatiles were removed under reduced pressure and the resulting solid was purified by silica gel column chromatography to give H-phosphonate **3-8** (218 mg, 0.32 mmol, 79%) as a white solid. ^{1}H NMR (400 MHz, $CDCl_3$) δ 7.65 (s, 0.5H), 6.06 (s, 0.5H), 5.30 – 5.16 (m, 1H), 4.38 (dd, *J* = 11.9, 3.6 Hz, 1H), 4.18 (dd, *J* = 11.9, 6.4 Hz, 1H), 4.02 (dd, *J* = 7.9, 5.2 Hz, 2H), 1.64 – 1.58 (m, 5H), 1.40 (t, *J* = 7.3 Hz, 18H), 1.26 (s, 47H), 0.89 (t, *J* = 6.8 Hz, 6H). ^{13}C NMR (101 MHz, $CDCl_3$) δ 173.46, 173.06, 70.26, 62.46, 62.07, 45.65, 34.31, 34.12, 31.95, 29.74, 29.69, 29.54, 29.40, 29.34, 29.17, 29.14, 24.89, 22.72, 14.17, 8.61. ^{31}P NMR (162 MHz, $CDCl_3$) δ 4.66. ESI-MS (*m*/*z*): $[M+H]^+$ cald 688.541 obsd 688.712

3,4,6-tri-*O*-benzyl-α-D-mannopyranosyl-(1→2)-3,4-di-*O*-benzyl-6-*O*-tri*iso*propylsilyl-α-D-mannopyranosyl-(1→2)-3,4,6-tri-*O*-benzyl-α-D-mannopyranosyl-(1→6)-2-O-levulinyl-3-*O*-benzyl-4-O-(2-napthyl)methyl-α-D-mannopyranosyl-(1→4)-2-azido-3,6-di-*O*-benzyl-2-deoxy-α-D-glucopyranosyl-(1→6)-1-*O*-(1,2-dimyristoyl-*sn*-glyceryl-phosphonato)-2,3,4,5-tetra-*O*-benzyl-D-*myo*-inositol (3-19)

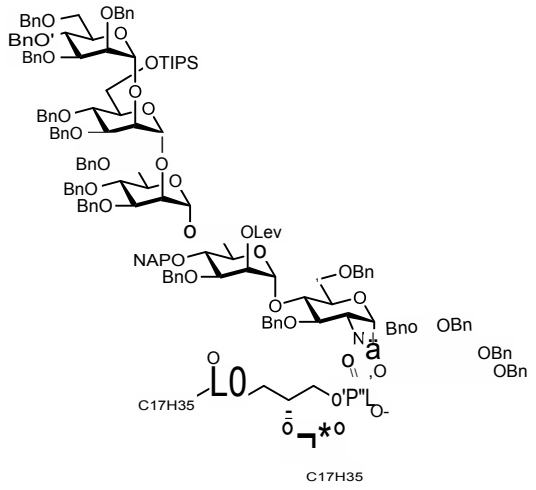

The *pseudo*-pentasaccharide **3-18** (98 mg, 0.041 mmol) and H-phosphonate **3-8** (161 mg, 0.203 mmol) were dissolved and co-evaporated with anhydrous pyridine (3 x 3 mL) and dried under high vacuum overnight. The reaction mixture was dissolved in anhydrous pyridine (2 mL) at room temperature and pivaloyl chloride (20 µL, 0.163 mmol) was added. The resulting reaction mixture was stirred at room temperature for 3 h. Iodine (36.3 mg, 0.143 mmol) in a mixture of pyridine/water (19:1, 0.2 mL) was added to oxidize P (III) to P (V). The reaction mixture was further stirred for 2 h at room temperature to the complete the oxidation. The reaction mixture was diluted with $CHCl_3$ and washed with aqueous $Na_2S_2O_3$ solution to remove the excess iodine. The aqueous layer was further washed with $CHCl_3$ and the combined organic layer was dried over Na_2SO_4, filtered and concentrated under reduced pressure to give the crude residue, which was subjected to flash column with Et_3N-deactivated silica gel to give **3-19** (70 mg, 55 %) as syrup. R_f = 0.25 ($CHCl_3$/MeOH = 20: 1). ^{1}H NMR (400 MHz, $CDCl_3$) δ 7.84 – 7.48 (m, 4H), 7.46 – 6.98 (m, 78H), 6.90 (d, *J* = 7.4 Hz, 1H), 5.86 (d, *J* = 3.4 Hz, 1H), 5.41 (d, *J* = 16.3 Hz, 1H), 5.29 (d, *J* = 11.6 Hz, 1H), 5.20 (d, *J* = 10.3 Hz, 1H), 5.05 – 4.61 (m, 16H), 4.64 – 4.30 (m, 16H), 4.28 – 3.78 (m, 14H), 3.79 – 3.68 (m, 1H), 3.65 – 3.38 (m, 5H), 3.37 – 3.17 (m, 2H), 3.13 – 3.05 (m, 1H), 2.53 – 2.33 (m, 2H), 2.30 –

2.13 (m, 2H), 1.96 (d, *J* = 8.1 Hz, 1H), 1.61 – 1.30 (m, 1H), 1.22 (d, *J* = 6.1 Hz, 71H), 0.99 (d, *J* = 4.2 Hz, 21H), 0.85 (t, *J* = 6.5 Hz, 7H). ^{31}P NMR (162 MHz, $CDCl_3$) δ -1.58. ESI-MS (*m*/*z*): $[M-H]^-$ cald 3535.835 obsd 3535.044.

3,4,6-tri-*O*-benzyl-α-D-mannopyranosyl-(1→2)-3,4-di-*O*-benzyl-α-D-mannopyranosyl-(1→2)-3,4,6-tri-*O*-benzyl-α-D-mannopyranosyl-(1→6)-2-O-levulinyl-3-*O*-benzyl-4-O-(2-napthyl)methyl-α-D-mannopyranosyl-(1→4)-2-azido-3,6-di-*O*-benzyl-2-deoxy-α-D-glucopyranosyl-(1→6)-1-*O*-(1,2-dimyristoyl-*sn*-glyceryl-phosphonato)-2,3,4,5-tetra-*O*-benzyl-D-*myo*-inositol (3-20)

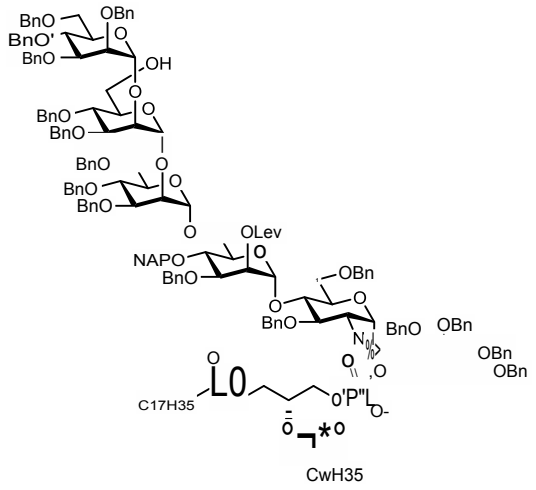

In the second step, the *pseudo*-pentasaccharide **3-19** (70 mg, 0.023 mmol) was passed through a column of Amberlite IR120 ion exchange resin (Na^+ form) using $CHCl_3$/MeOH (1:1) as eluent. The eluate was collected and concentrated to dryness. The obtained residue was then dissolved in CH_3CN (2.5 mL) with a trace of H_2O (100 μL). $Sc(OTf)_3$ (55.6 mg, 0.113 mmol) was added to the reaction mixture and the resulting mixture was heated to 45 ºC and stirred overnight. The reaction mixture was cooled down to room temperature and few drops of pyridine was added to quench any excess $Sc(OTf)_3$. The reaction mixture was evaporated to dryness and subjected to flash column chromatography with Et_3N-deactivated silica gel to afford **3-20** (45 mg, 68 %) as a syrup. ^{1}H NMR (400 MHz, $CDCl_3$) δ 7.43 (td, *J* = 19.8, 17.0, 9.9 Hz, 20H), 7.32 (dd, *J* = 13.7, 8.7 Hz, 38H), 7.28 – 6.97 (m, 171H), 5.44 (s, 1H), 5.40 – 5.29 (m, 3H), 5.14 (d, *J* = 26.4 Hz, 3H), 4.97 – 4.75 (m, 18H), 4.74 – 4.50 (m, 20H), 4.54 – 4.43 (m, 19H), 4.46 – 4.29 (m, 17H), 4.29 – 4.19 (m, 6H), 4.17 – 3.92 (m, 14H), 3.92 – 3.59

(m, 34H), 3.53 (dq, *J* = 24.6, 9.2, 8.2 Hz, 17H), 3.38 – 3.21 (m, 8H), 3.01 – 2.85 (m, 1H), 2.43 (d, *J* = 6.5 Hz, 3H), 2.35 – 2.19 (m, 9H), 1.55 (dt, *J* = 40.9, 7.4 Hz, 12H), 1.26 (s, 105H), 0.88 (t, *J* = 6.8 Hz, 6H). ^{31}P NMR (162 MHz, $CDCl_3$) δ -1.72. MALDI (*m*/*z*): $[M-H]^-$ cald 3380.709 obsd 3380.025.

3,4,6-tri-*O*-benzyl-α-D-mannopyranosyl-(1→2)-3,4-di-*O*-benzyl-6-*O*-(2-(*N*-(*tert*-butoxycarbonyl)-S-(*tert*-butyl)-L-cysteinyl)aminoethyl phosphonato)-α-D-mannopyranosyl-(1→2)-3,4,6-tri-*O*-benzyl-α-D-mannopyranosyl-(1→6)-2-O-levulinyl-3,4-di-*O*-benzyl-α-D-mannopyranosyl-(1→4)-2-azido-3,6-di-*O*-benzyl-2-deoxy-α-D-glucopyranosyl-(1→6)-1-*O*-(1,2-dimyristoyl-*sn*-glyceryl-phosphonato)-2,3,4,5-tetra-*O*-benzyl-D-*myo*-inositol (3-1)

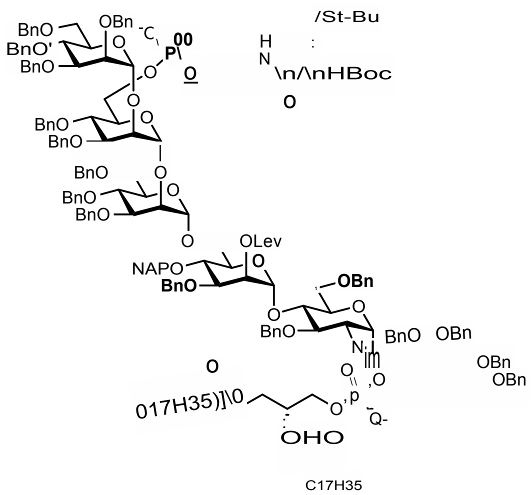

The bilipidated *pseudo*-pentasaccharide **3-19** (40 mg, 0.014 mmol) and *H*-phosphonate **3-9** (39 mg, 0.102 mmol) were dissolved and co-evaporated with anhydrous pyridine (3x3 mL) and dried under high vacuum overnight. The reaction mixture was dissolved in anhydrous pyridine (2 mL) at room temperature and pivaloyl chloride (13 µL, 0.102 mmol) was added. The resulting reaction mixture was stirred at room temperature for 5 h. The progress of the reaction was monitored by using TLC analysis. Iodine (26 mg, 0.102 mmol) in a mixture of pyridine/water (19:1, 0.2 mL) was added to oxidize P (III) to P (V). The reaction mixture was further stirred for 2 h at room temperature to complete the oxidation, diluted with $CHCl_3$, washed with aqueous $Na_2S_2O_3$ solution to remove the excess iodine. The aqueous layer was further washed with $CHCl_3$ and the combined organic layer was dried over Na_2SO_4, filtered

and concentrated under reduced pressure to give the crude residue, which was subjected to flash column with Et_3N-deactivated silica gel to give **3-1** (32 mg, 70 %) as a syrup. ^{1}H NMR (400 MHz, Chloroform-*d*) δ 7.77 – 7.37 (m, 4H), 7.34 (d, *J* = 7.3 Hz, 7H), 7.25 (d, *J* = 14.9 Hz, 15H), 7.25 – 7.09 (m, 74H), 7.02 (dd, *J* = 22.1, 10.4 Hz, 22H), 5.38 – 5.02 (m, 4H), 4.83 (dddd, *J* = 56.9, 31.6, 18.8, 11.0 Hz, 16H), 4.63 – 4.48 (m, 9H), 4.48 – 4.25 (m, 21H), 4.24 – 3.87 (m, 17H), 3.81 (s, 8H), 3.77 – 3.65 (m, 6H), 3.59 (d, *J* = 9.9 Hz, 3H), 3.44 (dt, *J* = 40.4, 14.9 Hz, 10H), 3.29 – 2.99 (m, 4H), 2.81 (s, 8H), 2.52 – 2.32 (m, 1H), 2.15 (t, *J* = 6.9 Hz, 4H), 1.95 (d, *J* = 7.8 Hz, 2H), 1.32 (s, 3H), 1.20 – 1.07 (m, 100H), 0.97 (dd, *J* = 26.0, 12.1 Hz, 12H), 0.81 (t, *J* = 6.7 Hz, 6H). ^{31}P NMR (162 MHz, $CDCl_3$) δ -1.42, -1.51. ESI-MS (*m*/*z*): $[M-H]^-$ cald 3761.835 obsd 3761.983.

α-D-mannopyranosyl-(1→2)-6-*O*-(*N*-(S-S-mercaptoethanol-L-cysteinyl)aminoethanol-phosphonato)-α-D-mannopyranosyl-(1→2)-α-D-mannopyranosyl-(1→6)-α-D-mannopyranosyl-(1→4)-2-amino-2-deoxy-α-D-glucopyranosyl-(1→6)-1-*O*-(1,2-dimyristoyl-*sn*-glyceryl-phosphonato)-D-*myo*-inositol (*Pf*GPI 1)

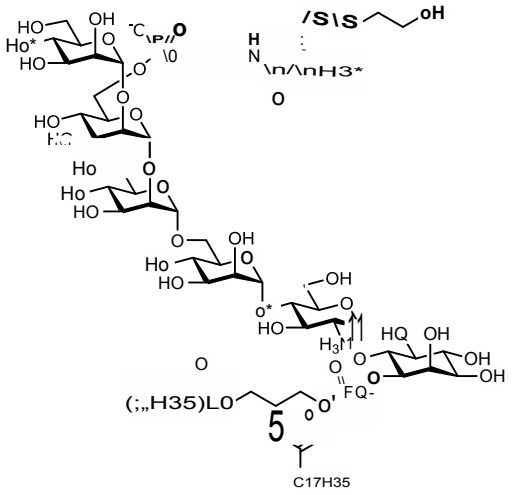

To the stirred solution of bisphosphorylated *pseudo*-hexasaccharide **3-1** (18.0 mg, 0.005 mmol) in CH_2Cl_2 (2 mL) were added acetic acid (10 µL, 0.19 mmol), pyridine (15 µL, 0.19 mmol) and hydrazine hydrate (2.3 µL, 0.05 mmol) sequentially. The reaction mixture was stirred at room temperature. After 12 h, the reaction mixture was quenched with acetone and concentrated to obtain crude product. The crude product was then dissolved in mixture of CH_2Cl_2/MeOH (3:1, 5 mL) at room temperature and $Pd(OH)_2$/C (33 mg, 0.046 mmol, 20% Pd

content) was added. Hydrogen gas was bubbled through the solution for 15 min and the reaction mixture was stirred under an atmosphere of hydrogen gas for additional 16 h. The palladium was removed by filtration through a pad of celite and the solvents were removed under reduced pressure to give the crude product. ^{1}H NMR (400 MHz, MeOD) δ 7.48 (s, 7H), 5.13 (d, *J* = 25.9 Hz, 2H), 4.95 (d, *J* = 46.0 Hz, 4H), 4.10 – 3.92 (m, 14H), 3.90 (s, 9H), 3.79 (dd, *J* = 18.2, 13.0 Hz, 10H), 3.71 – 3.31 (m, 26H), 3.15 – 2.91 (m, 2H), 2.86 – 2.68 (m, 1H), 2.63 – 2.45 (m, 1H), 2.31 – 2.09 (m, 6H), 1.55 – 1.44 (m, 7H), 1.27 – 1.15 (m, 128H), 0.79 (t, *J* = 6.4 Hz, 17H). ^{31}P NMR (162 MHz, MeOD) δ 0.48, 0.11.

The debenzylated crude intermediate compound was confirmed by mass spectrometry. The crude material (4 mg) was then dissolved at 0 °C in a mixture of trifluoroacetic acid and anisole (5.5 mL, 10:1 v/v) and stirred for 5 min. Then $Hg(TFA)_2$ (9.1 mg, 21 µmol) was added to the reaction mixture and stirred for an additional 30 min. the volatiles were removed under high vacuum at 0 °C. The resulting solid residue was dissolved in an AcOH/water mixture (7.5 mL, 7:3 v/v) and mercaptoethanol (400 µL, 5.7 mmol) was added at room temperature. The mixture was stirred at the same temperature for 10 h. The solution was dried on a rotary evaporator, to give a pale yellow residue. The amphiphilic nature of ***Pf*GPI 1** (2.5 mg, 1.2 µmol, 41%) created solubility problem in only one solvent. So, the NMR was analysed in mixture of chloroform, methanol and water. ^{1}H NMR (700 MHz, MeOD) δ 5.47 (d, *J* = 119.0 Hz, -1H), 5.26 (s, 1H), 5.05 (d, *J* = 80.8 Hz, 1H), 4.27 – 3.41 (m, 33H), 3.41 (s, 1H), 3.23 (s, 1H), 3.11 – 3.00 (m, 2H), 2.43 – 2.10 (m, 2H), 1.94 (s, 3H), 1.61 (s, 3H), 1.52 – 1.38 (m, 1H), 1.28 (s, 45H), 0.88 (s, 7H). ^{31}P NMR (162 MHz, MeOD) δ 0.27, -0.03. HRMS (*m*/*z*): $[M-2H]^{2-}$ cald 987.9350 obsd 988.0052.

3.9.2 Material and Methods of Biochemistry

All amino acids were purchased from IRIS Biotech (Marktredwitz, Germany) or Novabiochem (Darmstadt, Germany). Deionized water was obtained by purification with a Milli-Q purification system (Merck Millipore, Billerica, USA).

General protocol for protein ligation

A solution of 70 mM MMBA and 20 mM TCEP in 20 µL of ligation buffer is adjusted to pH 7.2. To this solution, fusion protein ($MSP1_{19}$-*NpuN*) in buffer, 3 eq. of the modified *NpuC*(AA) peptide and 2 eq. of GPI (or Cys-Biotin) were added. The final volume of the ligation reaction is adjusted to 100 µL by addition of ligation buffer. The reaction mixture was

incubated at 37 °C for three days. The reaction progress was monitored with SDS-PAGE. Ligation buffer contained 300 mM NaCl and 50 mM Tris at pH 7.0.

Size Exclusion Chromatography

Size Exclusion Chromatography (SEC) was generally applied for protein purification. In SEC, proteins are separated by size rather than by any interaction with the stationary phase. Smaller proteins and other molecules can enter into the pores of the stationary phase material which usually consists of small porous polymer beads such as agarose or sepharose with different pore sizes. Therefore, smaller molecules are retained longer during the run and elute later than larger proteins. Generally, all samples were centrifuged at 13.3 k rpm and / or filtered through a 0.2 μm syringe filter prior to loading on SEC columns. Maximum 1.5 mL of sample containing 0.5 – 10 mg protein was loaded onto the Superdex 75 column.

LC-ESI-QTOF-MS

Waters Xevo G2-XS with an Acquity H-class UPLC was used. In this instrument, the ESI source was coupled to a quadrupole-time-of flight (QTOF) mass analyzer. A quadrupole consists of four parallel metal rods. The two opposite rod pairs are connected electrically. The quadrupole is used to generate an oscillating electric field which can be used to filter ions of specific m/z ratios. In the TOF mass analyzer, the ions are further separated.

Circular Dichroism (CD)

Circular dichroism utilized circularly polarized light to determine the optical properties of chiral compounds. Circular Dichroism Spectrometer Chirascan from Applied Photophysics (Leatherhead, UK) was used for the analysis and Origin Pro from Originlab (Northampton, USA) was used to process the data. Protein samples were prepared in PBS buffer at concentrations ranging from 0.1 – 1 mg/mL. The protein solution was then filled into a High Precision Cell Quartz cuvette (light path 1 mm) and placed in the Chirascan Circular Dichroism Spectrometer. Circular dichroism was measured between 190 and 260 nm against PBS buffer as a reference and measurements were performed in triplicates. The averages of these measurements were plotted over the wavelength.

4 Synthesis and Structural Analysis of GPI Fragments in Model Membranes

4.1 Introduction

The cell membrane defines the boundary between the intracellular and extracellular space and is essential for many biological functions such as cell adhesion and cell signaling. The basic structure of a membrane is composed of a lipid bilayer embedding proteins, glycolipids and other biomolecules.[221] In 1972, Singer and Nicolson introduced the fluid mosaic model to describe cell membrane organization. This model proposes the membrane as an oriented, two-dimensional, viscous solution of amphipathic proteins and lipids in instantaneous thermodynamic equilibrium, where ionic and highly polar groups protrude into the aqueous phase and non-polar groups are buried in the hydrophobic interior of the bilayer.[222]

Although it is possible to form a lipid bilayer using a single lipid, a cell membrane generally contains different kind of lipids; for example, a eukaryotic membrane contains glycerophospholipids, sphingolipids and sterols.[223] The main reason for compositional diversity in a membrane is to provide a stable and robust assembly to protect the cell and to participate in physiological events like cell signaling, metabolism and protein transport. The cell membrane was initially described as a continuous fluidic system. However, the presence of sub compartments in the membrane was observed when the membrane of Madin-Darby Canine Kidney (MDCK) cells could be separated into detergent-soluble and detergent-resistant fractions.[224] These observations suggested that the cell membrane is remarkably heterogeneous and lipids can exist in several fluidic phases in the bilayer such as gel, liquid ordered phase (l_o) and liquid crystalline phase (l_c).[225] The bilayer is rigid in the gel state whereas in the liquid crystal phase, it is characterized as fluidic. The liquid ordered phase is formed when the phospholipids pack tightly with cholesterol to form a mobile plane in the membrane.

4.1.1 Lipid Raft

In epithelial cells, the plasma membrane is polarized into apical and basolateral domains, which are characterized by a differentiated composition.[226] Wherein, the apical domain mainly consists of sphingolipids and cholesterol assemblies on the exoplasmic leaflet of the bilayer. The basolateral domain is characterized by an inner leaflet rich in glycerolipids and phosphatidylcholine.[227, 228] The concept of membrane raft was introduced to explain the organization of sphingolipids and cholesterol on the exoplasmic leaflet of the bilayer.[229] Lipid raft domains are usually defined as very small, highly dynamic and transient plasma membrane entities enriched in saturated sphingolipids, phospholipids, glycolipids, cholesterol and glycosylphosphatidylinositol (GPI)-anchored proteins. In rafts, the polar head groups of sphingolipids interact with each other through weak hydrophilic interactions occupying more area in the plane of bilayer compared to the lipid hydrocarbon chains. Hence, any voids between associating sphingolipids are filled by cholesterol, leading to close packing between the lipid chains and cholesterol, similar to liquid ordered phase in the model membranes. Cholesterol-dependent lateral segregation is also observed in the vesicle model membrane, where cholesterol favors the interactions with stiffer saturated lipids than with more flexible unsaturated lipids.[98, 230, 231] This lateral segregation in the lipid systems leads to the formation of extended conformations and hydrophobic mismatch, resulting in a segregation of the membrane plane into a thicker, liquid ordered phase and a thinner, liquid disordered phase (**figure 4.1**). [232-233]

The concept of lipid raft has been controversial because they are believed to be nanoscopic domains in cells that are difficult to observe using conventional microscopy. [234, 235] For this reason, several optical tools have been developed to investigate nanoscopic structures and dynamics of the cell membrane. [236, 237] These methods have been used to detect lipid-mediated protein clustering on the surface of the cell and include photoactivated localization microscopy (PALM), stimulated emission depletion (STED) and near field scanning optical microscopy (NSOM).[238-241]

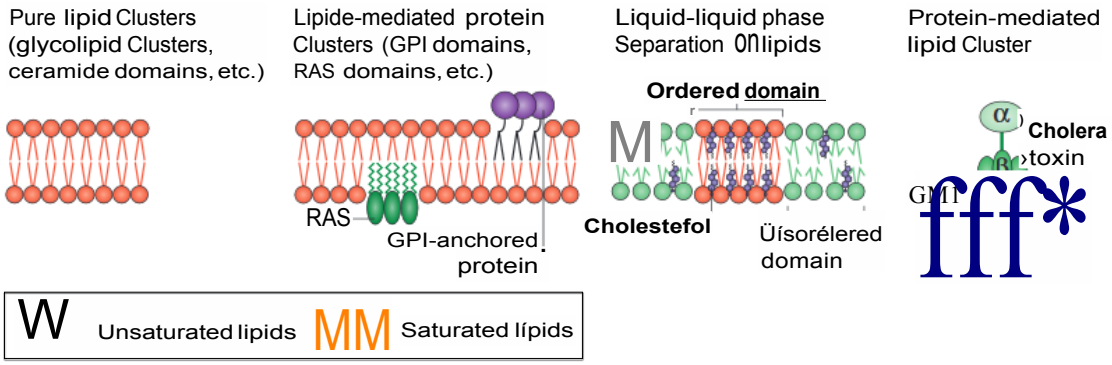

Figure 4.1: Lipid associated membrane domains.[242]

The term lipid rafts has been applied to different membrane assemblies, such as pure lipid clusters including glycolipid clusters, ceramide domains and other lipid domains, and to lipid mediated protein clusters including GPI and RAS domains. Ordered domains can also be formed as a result of liquid-liquid phase separation of lipids or by protein mediated lipid clustering. Due to the small size and short lifetime of the raft domains *in vivo*, direct measurement of the properties on the membrane is complicated especially because many different domains can co-exist at the same time.[243] However, computational studies have shown that compartmentalization of the membrane into domains, including the existence of lipid rafts, is important for membrane function.[244]

4.1.2 Role of Lipid Rafts

The role of lipid rafts in the cell function is not clear due to the difficulties in defining their composition and chemical and physical properties. Important functions that have been attributed to these lipid domains include participation in signal transduction. Immunoglobulin E (IgE)-mediated activation of cells was the first signaling pathway associated with lipid rafts.[245] Studies have shown that T-cell and B-cell receptors on antigen presenting cells (APC) are found in the lipid fluidic part of the membrane in resting state and are shifted to lipid rafts during the activation process. Thereby, the lipid raft are associated with the active signaling of these receptors and hence, involved in innate and adaptive immune response.[246-251] GPI-anchored proteins associated with immune system are also found in lipid rafts. These include the receptor of lipopolysaccharide CD14[252] and THY1, which is an important protein for T-cell activation.[253]

Lipid rafts may also act as modulators for host-pathogen interactions involving viruses covered with large number of saturated lipids and cholesterol.[254] In case of the HIV Gag protein, it was observed that this protein preferentially binds to the high cholesterol regions of the membrane of the host cell, suggesting the importance of rafts for virus budding.[255, 256]

Another example of the biological role of lipid rafts is the localization of oncogenic proteins involved in cancer development and progression in raft-like domains.[257-259] One such protein is the RAS protein, which is involved in breast cancer. Hence, some of the anticancer drugs contain the alkyl phospholipids edelfosine and perifosine, which can disrupt raft localizations.[260, 261] Similarly, overexpression of Mucin 1 (MUC1), can lead to different forms of cancer and is also associated with proteins found in raft regions.

In cardiovascular diseases, macrophages take up cholesterol and aggregate in the arteries clogging the blood vessels that can cause heart attack. This uptake transforms the macrophages into foam cells mediated by rafts containing LDL receptors, which are responsible for the binding of the lipids.[262, 263]

4.2 GPI in Lipid Raft

GPI-anchored proteins (GPI-APs) are the most characterized example of protein associated with lipid rafts. They are involved in many cellular functions such as membrane trafficking, immune response, adhesion and nutrient uptake.[264-268] The lipid part of GPI anchors is highly heterogeneous and can contain the lipids that are not involved in raft formation. Domains containing GPI-APs have been described as detergent-resistant domains, which is a characteristic property of raft formation that is acquired while trafficking through the Golgi network during the biosynthesis. GPI-APs have been studied in cell mimics such as liposomes and lipid Langmuir monolayers to investigate the protein-membrane interactions.[269-272] In these studies, the clustering of GPI-APs was attributed to protein-protein interactions. However, similar clustering is also observed in studies with free GPIs, which lack protein. Thus, interactions between GPI molecules and their interactions with other membrane components may be responsible for the heterogeneous distribution observed for free GPIs on the cell membrane.[273]

The lipids of GPIs are structurally similar to phospholipids which interact with the membranes through van der Waals forces. GPIs possess bulky and flexible head groups that are responsible for strong hydrogen bonding between glycans. The glycans possess large in-plane area compared lipid part. The conformational changes in these highly ordered structures can give rise to formation of temporary domains that can be referred to as rafts. However, the structural requirement and underlying reason for the formation of GPI lipid rafts is unclear.[274] Therefore, the elucidation of structural and conformational behavior of GPIs in membrane models could provide better insight into the role of GPIs in living cells.

4.3 Background

In 2014, our group reported the presence of molecular ordering of GPI fragments in a two-dimensional monolayer at the air/liquid interface (**figure 4.2**). In order to understand the correlation between structure of glycan and its spatial arrangement in the monolayer, three fragments were designed; the commercially available glycerolipid **4-1**, and two synthesized structures, the phosphatidylinositol **4-2** and *pseudo*-disaccharide **4-3**, which adequately mimic the zwitterionic character of the GPIs. This glycolipid **4-3** features an amino and a phosphate group that largely determines the ionic strength/interactions of the head group.

To understand the influence of the lipid component on the conformation of the polar head groups and clustering effect on the model membrane; grazing incidence X-ray diffraction (GIXD) pattern, Langmuir isotherm, tilt angle and lattice distortion at different lateral pressure were studied for the three structures. A comparative analysis showed that the alkyl chains of the fragment **4-1** presented smallest tilt angle at low lateral pressure (**figure 4.2B**) owing to the smallest head group and its weak interactions on the monolayer structure was strongly influenced by the glycerol chirality. In case of fragment **4-2,** which has an additional phosphate and inositol, there is no substantial increase in the cross-sectional area in comparison to **4-1**. However, the bigger head group and additional electrostatic repulsion of the phosphate group induce a larger tilt angle of the lipid chains. At high lateral pressure, the lipids are in untilted state with higher packing density. The electrostatic repulsion between the head group become more dominant compared to attractive van der Waals interactions between the alkyl chains.

In case of fragment **4-3**, the monolayer was characterized by a large tilt angle of the lipid chains at the uncompressed state, which changes slightly upon compression. This behavior was attributed to strong hydrogen bonding interactions between the head groups. An increased structural rigidity of the zwitterionic fragment due to hydrogen bonding led to a highly ordered structure on the monolayer, characterized by an alkyl chain lattice and a head group molecular lattice. [275]

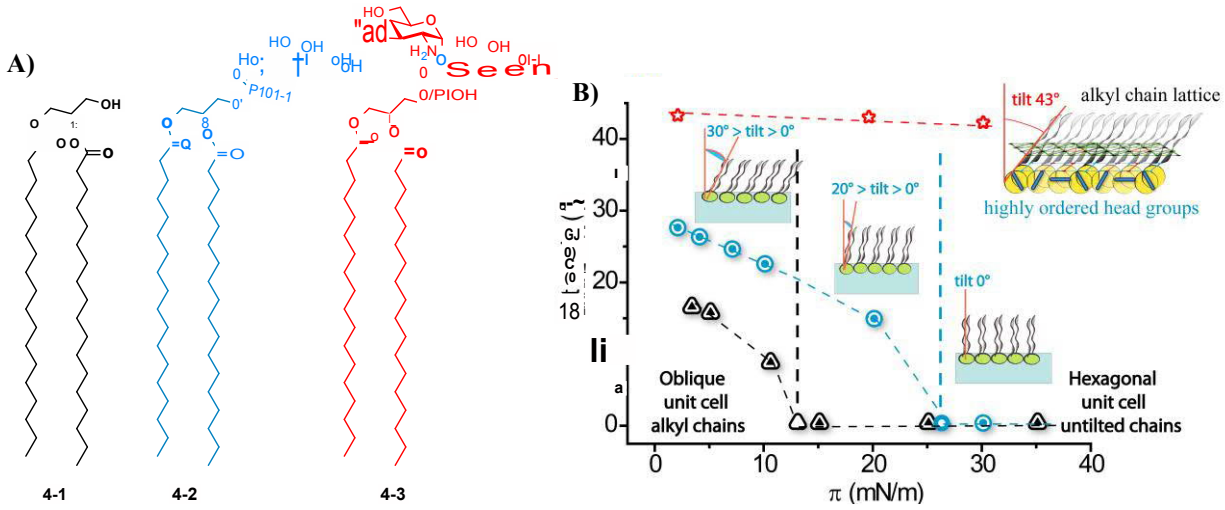

Figure 4.2: **A)** Chemical Structure of GPI-fragments; **B)** monolayer structural changes of the GPI-fragments as the variation of the tilt angle of the alkyl chains (°) with the lateral surface pressure (π) on PBS at 20 °C.[275]

4.4 Design of Epitopes and Retrosynthesis

To further investigate the role of the lipid composition and the hydrogen bonding of the head groups in the formation of microdomains, a new set of structures having a *pseudo*-disaccharide head group and different lipids were designed. These structures were designed bearing lipid chains with unsaturated and branched alkyl chains. In addition to delivering the information about the behavior of lipid chains on the model membrane, these fragments would provide further understanding about the importance of lipid remodeling during the biosynthesis and intracellular transport of GPI-APs.

Fragments **4-4** and **4-5** were designed to understand the effect of hydrogen bonding. In these molecules the amino group of the *pseudo*-disaccharide fragment was replaced with an *N*-acetyl group to break the participation of this function in hydrogen bonding between the molecules on the bilayer.

To understand the role of lipids in the formation of microdomains, fragment **4-5** was designed having an oleic and stearic ester at the glycerol, which is similar to the lipid composition reported for mammalian GPIs and is an important intermediate during the GPI biosynthesis in mammals. Fragment **4-6** was designed having a lipid with two branched alkyl chains at the *sn*-1 and *sn*-2 position of the glycerol moiety. This type of lipid modification is believed to have a similar effect as unsaturation (**figure 4.3**).

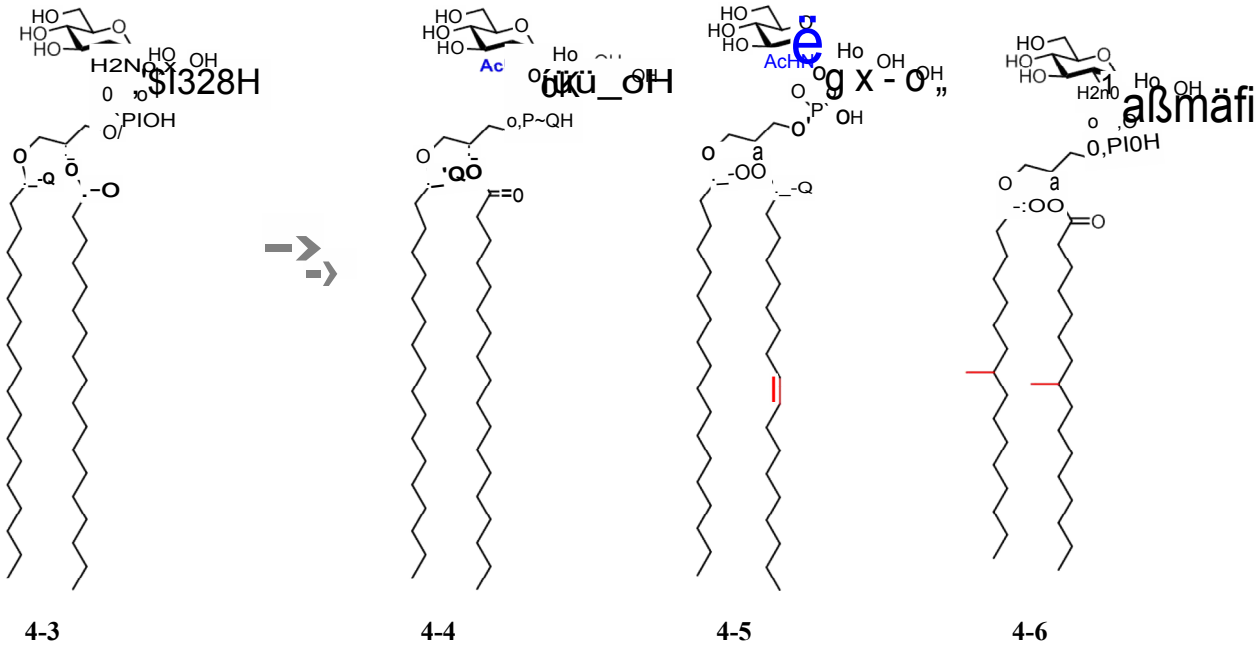

Figure 4.3: Structures of GPI fragments designed and investigated for this study.

The synthetic strategy was designed to give access to all the fragments from a common intermediate. The retrosynthetic analysis features a late-stage phosphorylation of the *pseudo*-disaccharides **4-7a** and **4-7b** with the *H*-phosphonate (**4-8**, **4-9** and **4-10)** as the most convenient disconnection. Benzyl ether was selected as the permanent protecting group for the synthesis of the fragments **4-3**, **4-4** and **4-6**. The 2-(napthyl)methyl ether was selected as

permanent protecting group for the synthesis of fragment **4-5** because this group can be cleaved under acidic conditions facilitating the incorporation of an unsaturated lipid.

To ensure high α-selectivity, the disaccharide **4-7a** can be accessed by the glycosylation of *myo*-inositol building block **4-12** with the azido-glucosamine trichloroacetimidate **4-11.** Allyl ether was chosen as the orthogonal protecting group at 1-*O* position of inositol for the incorporation of a phosphate.

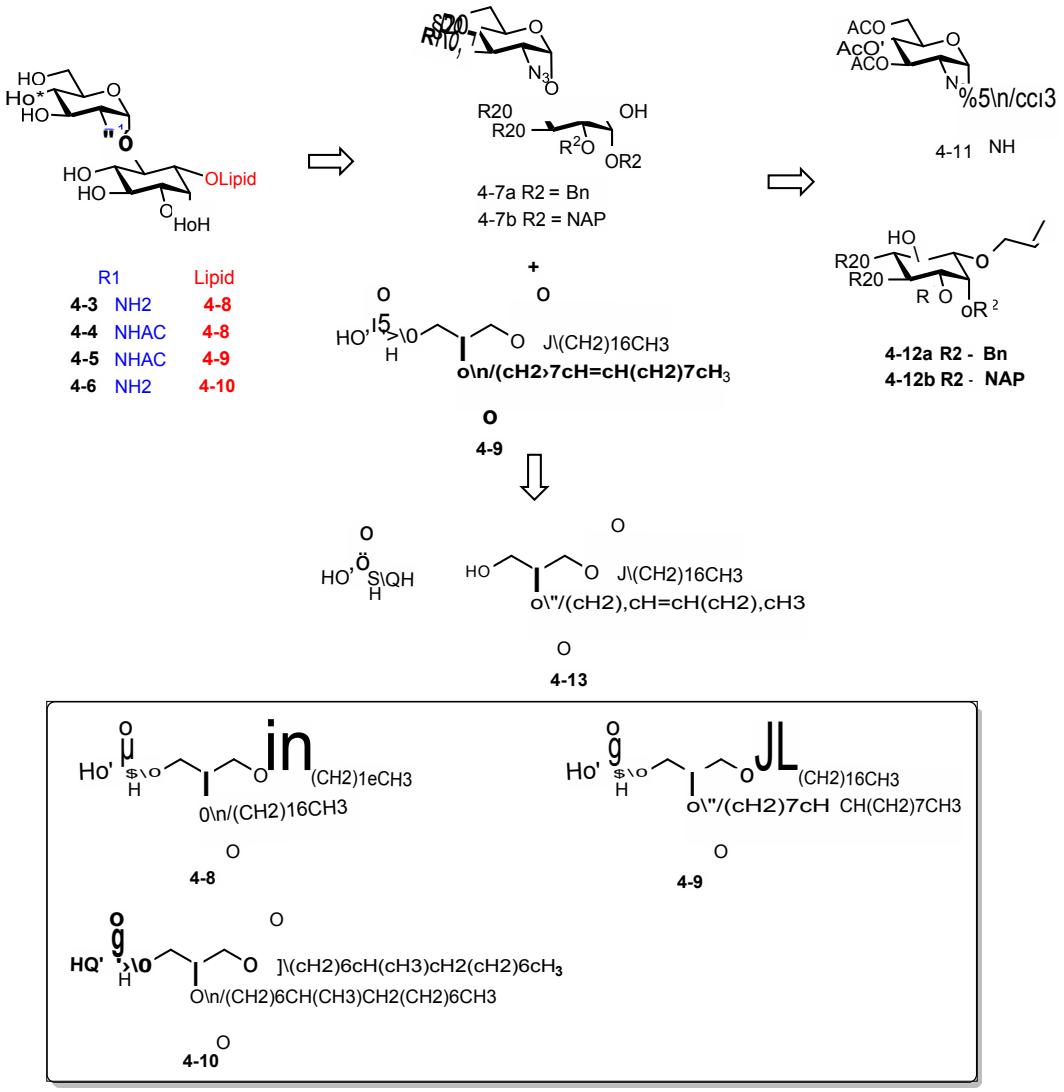

Figure 4.3: Retrosynthetic analysis of GPI-fragments **4-3**, **4-4**, **4-5** and **4-6** using a common intermediate.

4.5 Results and Discussion

4.5.1 Synthesis of Building Blocks

The process started with the synthesis of the *H*-phosphonate **4-9** from commercially available (*S*)-2,3-*O*-isopropylideneglycerol **4-14**. First, the free hydroxyl group of **4-14** was temporarily protected with PMB ether and the isopropylidene group cleaved under acidic condition to obtain the diol **4-16**. The primary and secondary hydroxyl groups were successively esterified with stearic acid and oleic acid, using DIC and DMAP as coupling reagents to obtain bilipid **4-16**. Then, the PMB group was removed using DDQ and water, and the obtained glycerolipid was converted into *H*-phosphonate **4-9** using phosphorus acid and pivolyl chloride (**scheme 4.1**).

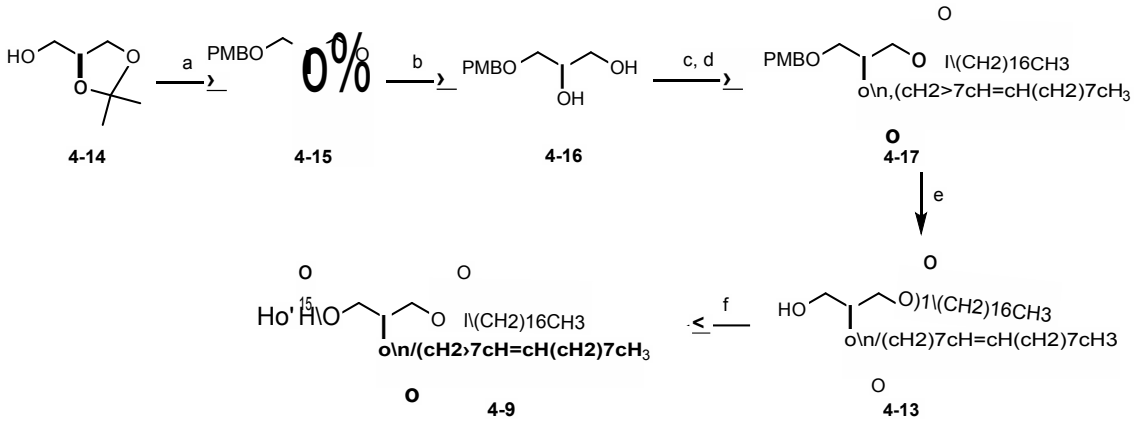

Scheme 4.1: Synthesis of *H*-phosphonate 4-9. a) PMBCl, NaH, DMF, rt, 2 h, 83%; b) pTSA, H_2O, CH_2Cl_2, rt, 92%, c) Stearic acid, DIC, DMAP CH_2Cl_2, rt, 84%; d) Oleic acid, DIC, DMAP, CH_2Cl_2, rt, 75%; e) DDQ, H_2O, CH_2Cl_2, rt, 60%; f) H_3PO_3, PivCl, py, rt, 70%.

The synthesis of the protected *myo*-inositol acceptor **4-12b** was performed from commercially available methyl α-D-glucopyranoside using a modification of the method reported by the Fraser-Reid group in 1998.[276] Starting with a trityl protection of the primary alcohol, the obtained triol **4-18** was transformed into 6-OH glucoside **4-20** by protecting the free hydroxyl groups with 2-(napthyl)methyl ether and removing the trityl in 60% yield over two steps. The alcohol **20** was oxidized to an aldehyde using SO_3-pyridine complex and the obtained aldehyde was immediately converted into the acetyl enolate **4-21** by enol acetylation. A mercury assisted Ferrier rearrangement of **4-21** delivered the cyclic hexanone **4-22**, which

was subjected to chelation-mediated reduction using $NaBH(OAc)_3$ to obtain the diol **4-23** in 68% yield over two steps. The *myo*-inositol **4-23** was deacetylated and regioselectively protected with 2-(napthyl)methyl and allyl ether at position 2-*O* and 1-*O* respectively to give the *myo*-inositol acceptor **4-12b** in 63% yield. The corresponding benzylated *myo*-inositol acceptor **4-12a** was obtained using a similar synthetic strategy.[277]

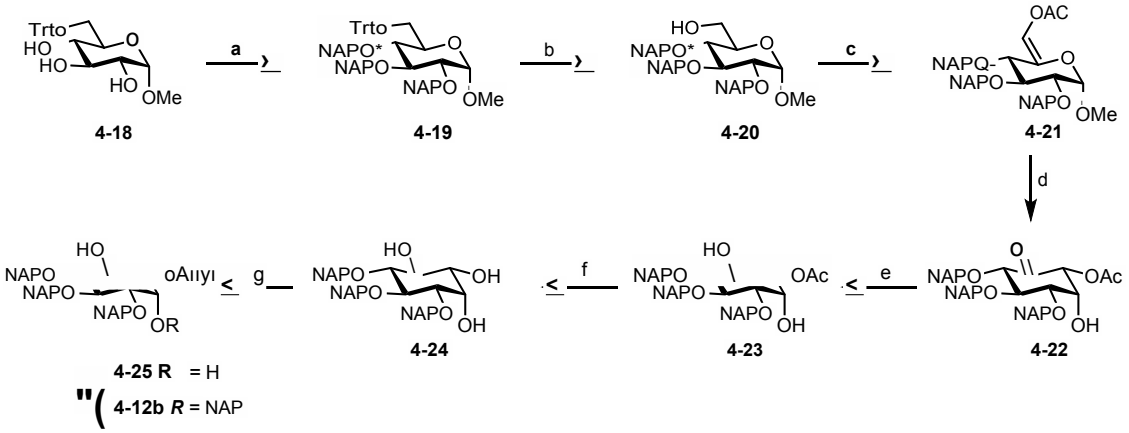

Scheme 4.2: Synthesis of *myo*-inositol 4-12b. (a) NAPBr, NaH, DMF, rt, 12 h, 85%; (b) *p*-TsOH, MeOH, rt, 16 h, 70%; (c) i. SO_3.Py, DIPEA, DMSO, CH_2Cl_2, 0 °C, 1 h, ii. Ac_2O, K_2CO_3, CH_3CN, reflux, 4 h, 80% (2 steps); (d) i. $Hg(OTf)_2$, acetone/H_2O, rt, 1 h, ii. NaOAc, NaCl, 0 °C to rt, 12 h, 77%; (e) $NaBH(OAc)_3$, CH_3CN, AcOH, rt, 12 h, 83%; (f) NaOMe, MeOH, rt, 30 min; (g) i. $(Bu_3Sn)_2O$, toluene, reflux, 5 h; ii. AllylBr, TBAI, $C_6H_5CH_3$, 65 °C, 17 h, 65%; (h) NAPBr, NaH, DMF, -20 °C to 0 °C, 2 h, 63%.

The synthesis of glucosamine donor **4-11** started with preparation of the azide **4-27**, which was obtained from D-glucosamine by an azido transfer reaction using TfN_3 and following acetylation in 69% yield. The acetylated 2-azidoglucoside **4-27** was transformed into the trichloroacetimidate donor **4-11** by removal of the anomeric acetyl group using piperidine in THF and following the reaction of the obtained hemiacetal **4-28** with trichloroacetonitrile in the presence of DBU at 0 °C.[278]

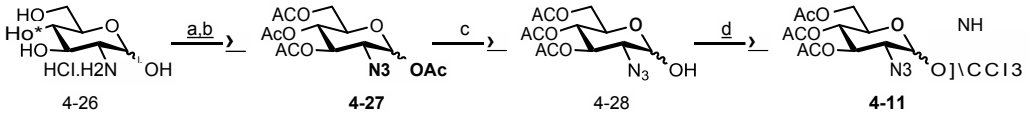

Scheme 4.3: Synthesis of glucosamine building block 4-11. a) TfN_3 (in CH_3CN), $CuSO_4.5H_2O$, Et_3N, H_2O, 0 °C, 24 h, 84%; b) Ac_2O, py, rt, 24 h, 69 %, c) Piperidine, THF, rt, 16 h, 68 %; d) CCl_3CN, DBU, CH_2Cl_2, 0 °C, 4 h, 92%.

4.5.2 Synthesis of *Pseudo*-Disaccharide Fragments

Glycosylation of *myo*-inositol **4-12a** with trichloroacetimidate donor **4-11** using TMSOTf in Et_2O/CH_2Cl_2 at 0 °C afforded the *pseudo*-disaccharide **4-29** as an anomeric mixture of product (α/β = 5:1) in 80% yield. The α/β mixture of **4-29** could not be separated using silica gel chromatography. Therefore, the obtained anomeric mixture of *pseudo*-disaccharide **4-29** was deacetylated using freshly prepared sodium methoxide followed by benzylation using benzyl bromide and sodium hydride to give the benzylated *pseudo*-disaccharide **4-31** in 54% yield over 2 steps. The disaccharide **4-31** was deallylated using $PdCl_2$ under anhydrous conditions to obtain the *pseudo*-disaccharide **4-7a**, which could be separated using silica gel column chromatography giving the α-isomer in 65% yield (**scheme 4.4**).

Finally, the alcohol **4-7a** was phosphitylated with the *H*-phosphonate **4-8** using pivolyl chloride and the product was oxidized with iodine and water to obtain the corresponding phosphate **4-32**. A palladium catalyzed hydrogenation with palladium hydroxide for the global deprotection delivered the *pseudo*-disaccharide **4-3** in 50% yield after purification.

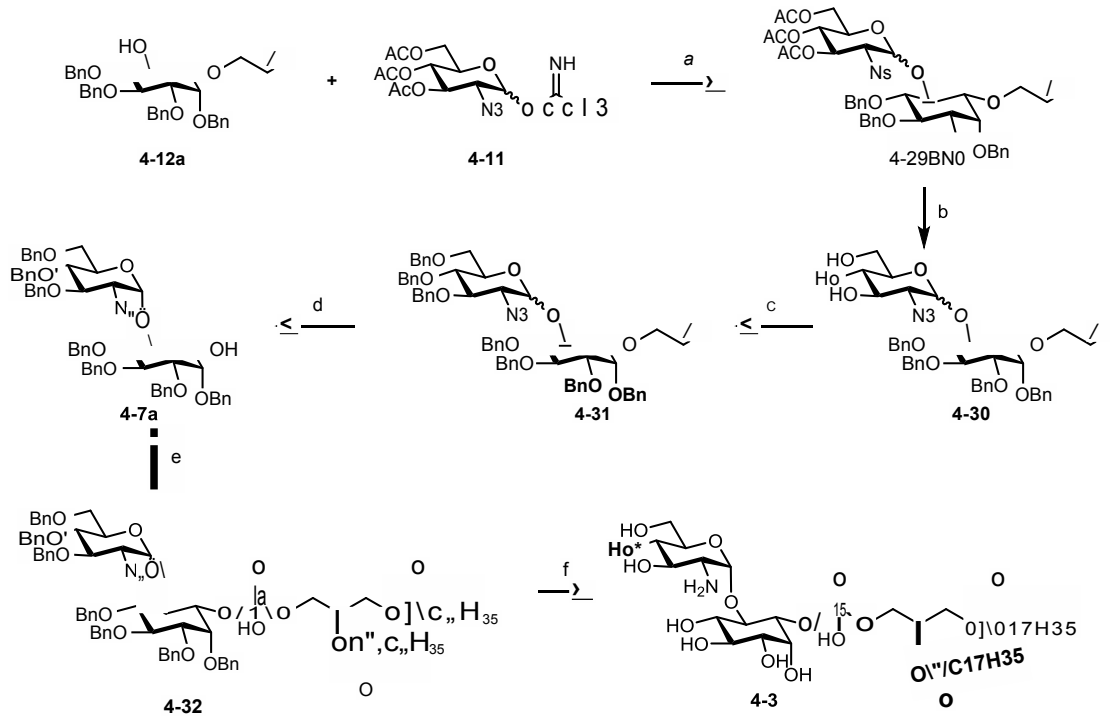

Scheme 4.4: Synthesis of *pseudo*-disaccharide 4-3. a) TMSOTf, CH_2Cl_2-Et_2O, 0 °C, 1 h; b) NaOMe, MeOH, rt, 6 h; c) BnBr, NaH, DMF, rt, 18 h, 54% (over 3 steps); d) $PdCl_2$, MeOH-CH_2Cl_2, rt, 4 h, 82%; e) i. **4-8**, PivCl, py, rt, 12 h; ii. I_2, H_2O, rt, 2 h, 60%; f) $Pd(OH)_2$, H_2, CH_2Cl_2:MeOH:H_2O (3:3:1), rt, 48 h, 50%.

In order to obtain the GPI fragment **4-4**, the azide of *pseudo*-disaccharide **4-31** was converted into an *N*-acetyl group (**4-33)** by reduction of the azide using zinc and acetic acid follwing acetylation of the amine using acetic anhydride and pyridine. Similar to fragment **4-3**, the resulted disaccharide was deallylated, phosphorylated and deprotected using the same conditions to obtain the desired *pseudo*-disaccharide **4-4** in 50% yield (**scheme 4.5**).

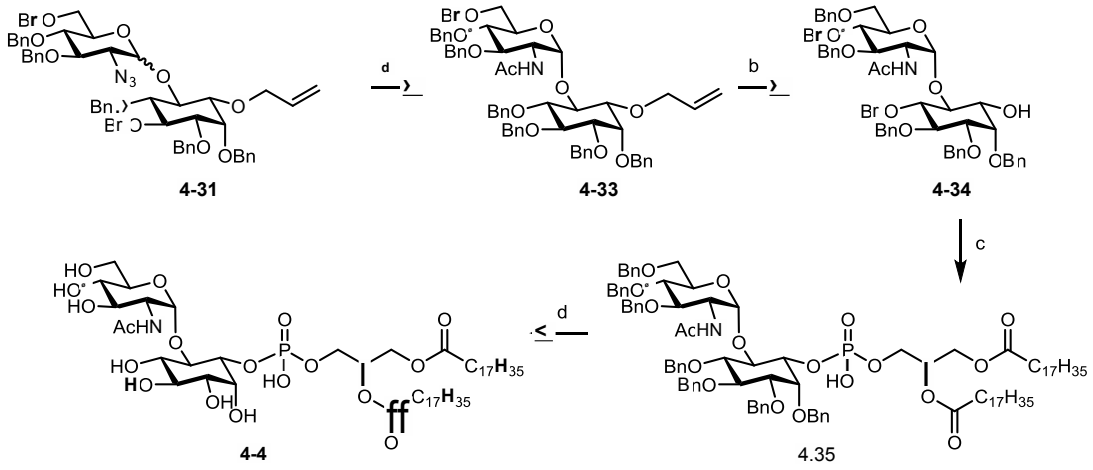

Scheme 4.5: Synthesis of *pseudo*-disaccharide 4-4. a) Zn, Ac_2O, AcOH, THF, rt, 4 h, 71%; b) $PdCl_2$, MeOH-CH_2Cl_2, rt, 4 h, 72%; c) i. **4-8**, PivCl, py, rt, 12 h; ii. I_2, H_2O, rt, 2 h, 60%; d) $Pd(OH)_2$, H_2, CH_2Cl_2:MeOH:H_2O (3:3:1), rt, 48 h, 50%.

To incorporate the unsaturated lipid, the synthesis of fragment **4-5** was carried out using the 2-(napthyl)methyl ether as a permanent protecting group. Glycosylation of *myo*-inositol **4-12b** with trichloroacetimidate donor **4-11** using TMSOTf in Et_2O/CH_2Cl_2 at 0 °C afforded the *pseudo*-disaccharide **4-36** as an anomeric mixture of product (α/β = 6:1) in 80% yield. The α/β mixture of **4-36** could not be separated using silica gel chromatography. Therefore, the obtained anomeric mixture of *pseudo*-disaccharide **4-36** was deacetylated using freshly prepared sodium methoxide followed by napthylation using 2-(napthyl)methyl bromide and sodium hydride to give napthylated *pseudo*-disaccharide **4-38** in 82% yield over 2 steps. The azide of disaccharide **4-38** was converted into an *N*-acetyl group (**4-39)** by reduction of the azide using zinc and acetic acid followed by acetylation using acetic anhydride and pyridine. The obtained disaccharide **4-39** was deallylated using $PdCl_2$ under anhydrous conditions to obtain the *pseudo*-disaccharide **4-40** as pure α-isomer in 59% yield (**scheme 4.6**). The alcohol **4-40** was phosphitylated with *H*-phosphonate **4-9** using pivolyl chloride activation. The obtained phosphodiester was chemoselectively oxidized using $BrCCl_3$ and Et_3N to obtain the corresponding phosphate **4-41**.[279] The global deprotection was carried out using a (9:1) TFA-anisole mixture under anhydrous conditions to obtain the *pseudo*-disaccharide **4-5** in 70% yield.

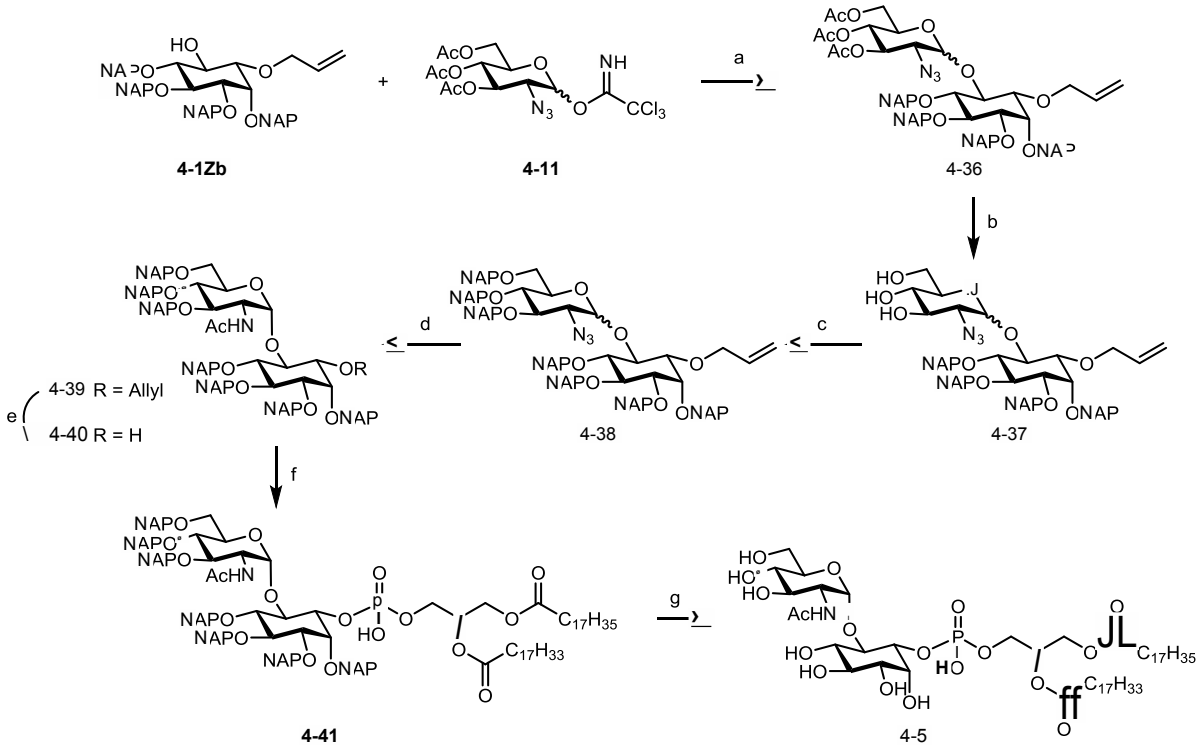

Scheme 4.6: Synthesis of *pseudo*-disaccharide 4-5. a) TMSOTf, CH_2Cl_2-Et_2O, 0 °C, 1 h, 80%; b) NaOMe, MeOH, rt, 6 h; c) NAPBr, NaH, DMF, rt, 18 h, 82%; d) Zn, Ac_2O, AcOH, THF, rt, 4 h, 79%; e) $PdCl_2$, MeOH- CH_2Cl_2, rt, 4 h, 59% (α); f) i. **4-9**, PivCl, py, rt, 12 h; ii. $BrCCl_3$, Et_3N, CH_2Cl_2, rt, 2 h 61%; g) TFA-anisole (10:1), rt, 6 h, 80%.

Similar to fragment **4-3**, the disaccharide **4-7a** was phosphitylated with the *H*-phosphonate **4-10** using pivolyl chloride and the product was oxidized using iodine and water to deliver the phosphate **4-42**. A global deprotection using palladium hydroxide under hydrogen atmosphere gave the *pseudo*-disaccharide **4-6** in 52% yield.

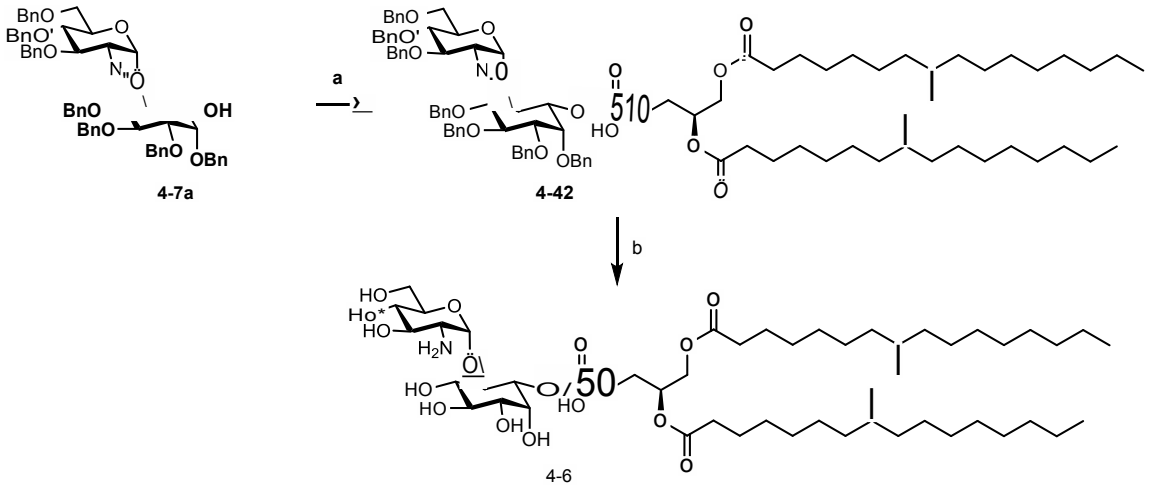

Scheme 4.7: Synthesis of *pseudo*-disaccharide 4-6. a) i. **4-10**, PivCl, py, rt, 12 h; ii. I_2, H_2O, rt, 2 h, 60%; b) $Pd(OH)_2$, H_2, CH_2Cl_2:MeOH:H_2O (3:3:1), rt, 48 h, 52%.

4.5.3 Analysis of the *pseudo*-disaccharides in monolayers

With all the synthetic fragments in hand, the compounds were investigated using 2-D model membrane at the air/water interface by our collaborators.[3] The structural changes, molecular ordering and phase transition in the monolayer were analyzed using grazing incidence X-ray diffraction (GIXD) and infrared reflection absorption spectroscopy (IRRAS). Two additional parameters, change of tilt angle and distortion of lattice with lateral pressure, were determined by extrapolation of GIXD data.

[3] All the studies on monolayers were performed by Prof. Dr. Gerald Brezesinski.

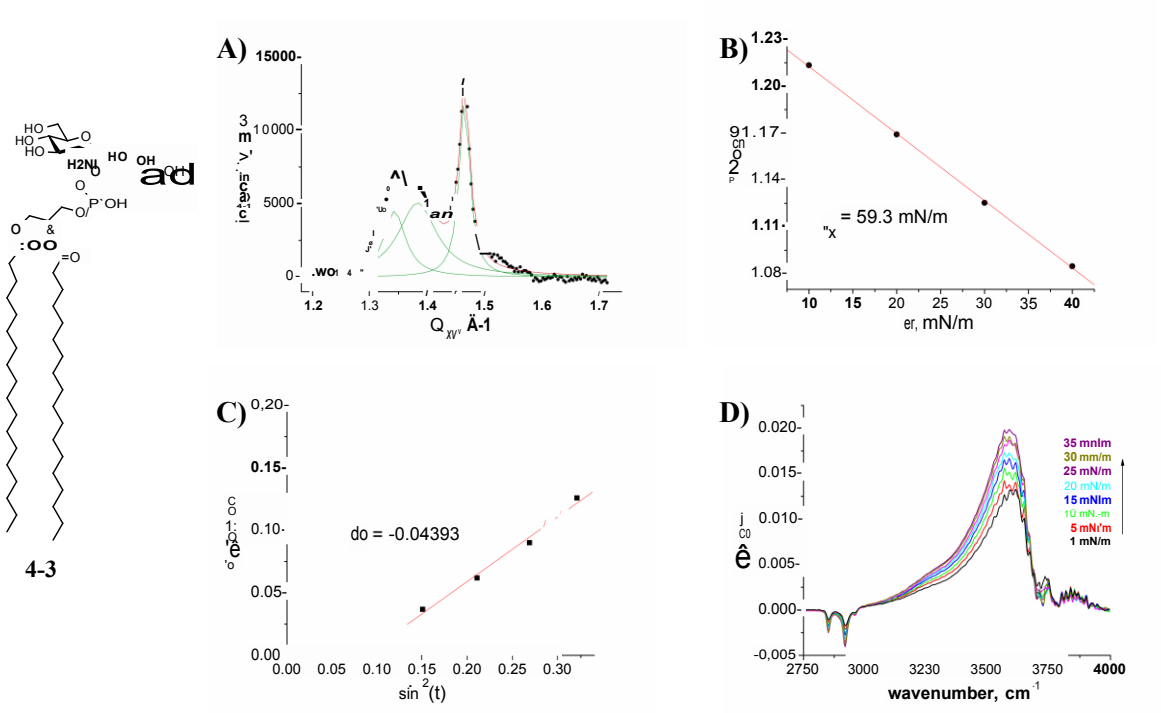

Figure 4.3: Monolayers of GPI fragment 4-3 at 20 °C on water. **(A)** GIXD pattern; **(B)** variation of tilt angle of the alkyl chain with the lateral pressure; **(C)** lattice distortion; **(D)** IRRA spectra of OH stretching region at different lateral pressures.

Previous studies showed that surface pressure/molecular area isotherms recorded on different subphases for fragment **4-3** were characterized as a rigid 2-D structure. The isotherm was typical for a liquid condensed (LC) phase even at high temperature.[274] Based on the fact that no phase transition was observed during compression for the fragment **4-3**, the GIXD pattern of monolayers for the fragment **4-3** was measured on water at 20 °C. The plot of the GIXD featured three distinct Bragg peaks (between 1.2 and 1.6 in **figure 4.3A**), characteristic for ordered alkyl chains arranged in an oblique lattice. Some very weak Bragg peaks corresponding to the head group ordering have been additionally observed. The large tilt angle of the alkyl chains observed at low lateral pressure decreases continuously during compression (**figure 4.3B**). The extrapolation yields a value of 59.3 mN/m for the tilting transition pressure. Above this pressure, the chains are oriented upright. However, a lattice distortion of -0.044 is observed in the non-tilted state (**figure 4.3C**). This distortion of the lattice supports the argument of rigid structural arrangements as a consequence of hydrogen bonding between the head groups. IRRA spectra showed a broad peak at 3600 cm^{-1} that is very characteristic for hydrogen-bonded OH groups. The intensity of the OH-band increases

during compression indicating an increase in layer thickness supporting the decrease of the tilt angle.

Surface pressure/molecular area isotherms recorded on subphases at different pH for fragment **4-4**, containing *N*-acetyl glucosamine to disrupt the zwitterionic character, show only the phase transition from gaseous to LC phase (re-sublimation). Only a shift in the isotherm at pH 9 was observed, which can be explained by the ionization of the phosphate group, which will be mostly in the deprotonated form at this pH, leading to stronger electrostatic repulsion. A tilting of Wilhelmy plate was observed at high surface pressure for pH 9 due to the stiffness of monolayer (**figure 4.4**).

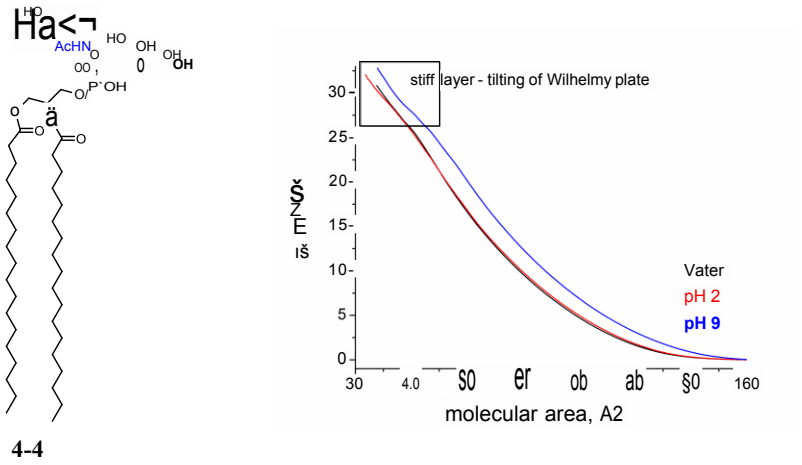

Figure 4.4: Surface pressure-molecular area of monolayers of GPI fragment **4-4** at 20 °C on different subphases.

To investigate the structural changes with varying pressure for the monolayer of fragment **4-4**, contour plots for this monolayer were recorded at different lateral pressures. The GIXD data revealed that monolayers were characterized by a chiral (oblique) chain lattice below ~ 12 mN/m. Compression leads to a change to an orthorhombic lattice, and eventually to a hexagonal phase of non-tilted chains at the lateral pressure of ~26 mN/m (**figure 4.5A**). The correspondence of zero tilt angle with the zero distortion indicates that the lattice distortion in this monolayer is only caused by the tilt of the molecule and not because of any other molecular interactions (**figure 4.5B, C**).

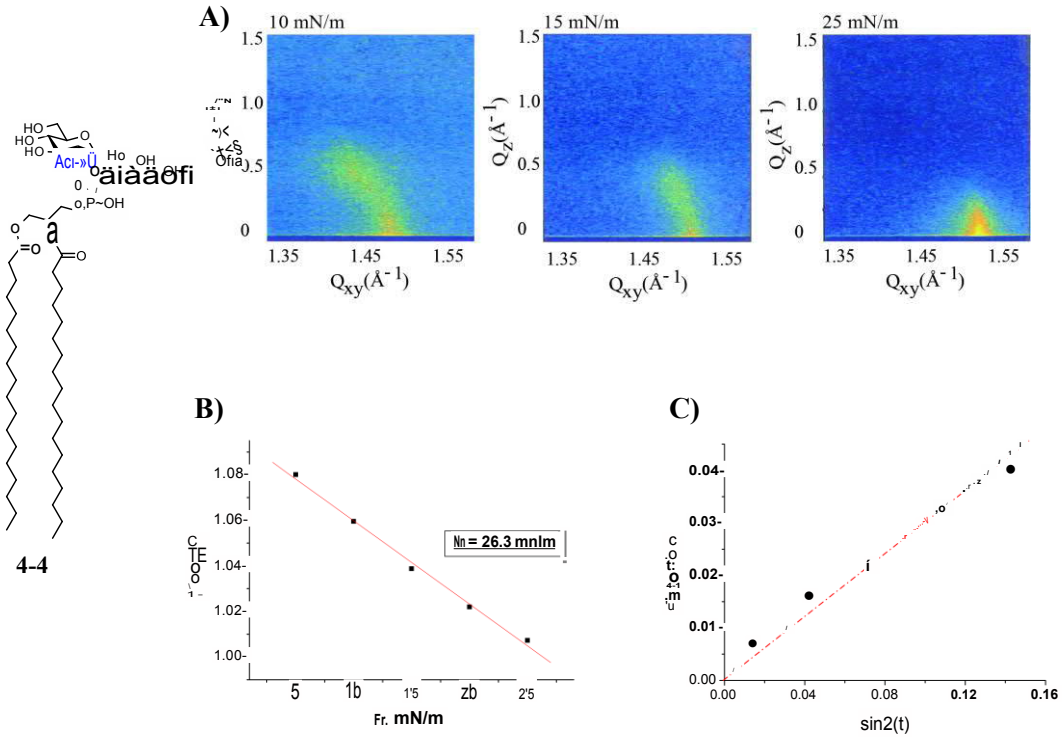

Figure 4.5: Monolayers of GPI fragment 4-4 at 20 °C on water. **(A)** GIXD pattern at different lateral pressure; **(B)** variation of tilt angle of the alkyl chain; **(C)** lattice distortion.

The GIXD pattern for the fragment **4-5,** containing an unsaturated fatty acid chain in the lipid part and an *N*-acetyl glucosamine, did not show the characteristic peaks for an ordered alkyl chain in an oblique or orthorhombic lattice, instead only one characteristic Bragg peak for the hexagonal ordered structure and a peak corresponding to an in-plane area of about 23 $Å^2$ (**figure 4.6**). This result shows that the saturated fatty acid is involved in the formation of a more ordered inner phase in the 2-D membrane model whereas the unsaturated fatty acid is present at the less ordered outer phase (**figure 4.6A**). The IRRA spectra showed an increase in intensity during compression indicating an increase in effective layer thickness and packing density.

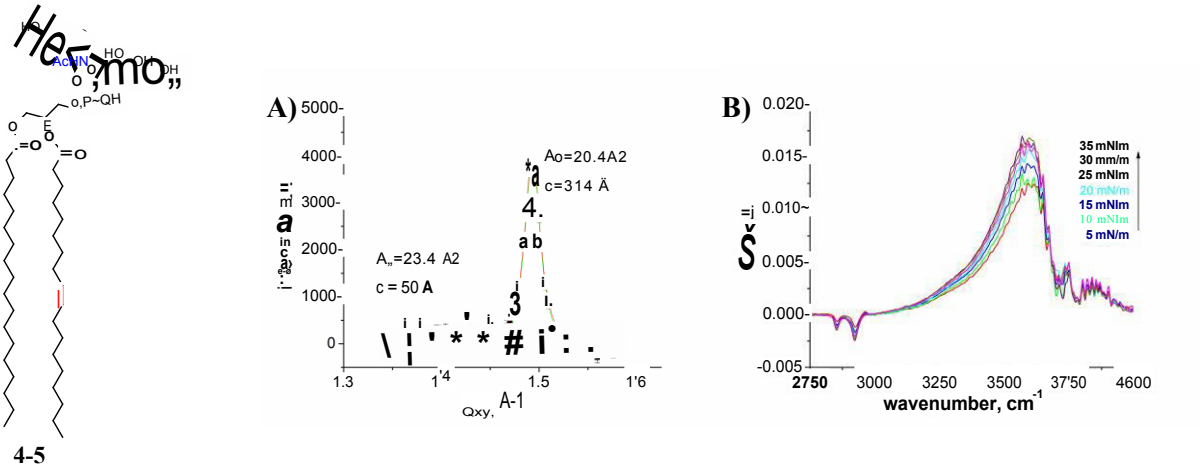

Figure 4.6: Monolayers of GPI fragment 4-5 at 20 °C on water. **(A)** GIXD pattern; **(B)** IRRAS spectra of OH stretching region at different lateral pressure.

The variation of the absorption wavenumber for the alkyl chains (CH_2 stretching vibration) was between 2925 and 2923 cm^{-1}. The first value at low lateral pressure is typical for the liquid-expanded (LE) state whereas the second value corresponds to the transition state between LC and LE, confirming the hypothesis of the presence of partial fluid and partial ordered areas in the model membrane for the fragment **4-5** (**figure 4.7**).

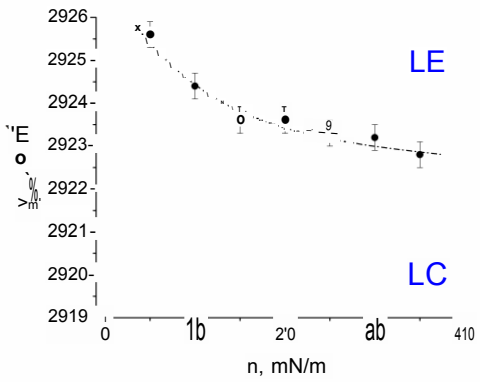

Figure 4.7: Wavenumber *vs* surface pressure for GPI fragment **4-5** monolayers at 20 °C on water.

The isotherm spectra of fragment **4-6** with two branched fatty acid chains were very similar at different pH values in contrast to the results obtained with fragment **4-4**. This isotherm suggests again a first-order phase transition from gaseous to a LC phase. It indicates strong

head-group interactions due to the hydrogen bonding. The IRRAS signals were also very similar to the signals of fragment **4-3** having broad hydroxyl bands due to the hydrogen bonding between the head groups. An increase in lateral pressure also increased the hydrogen bonding and van der Waals interactions.

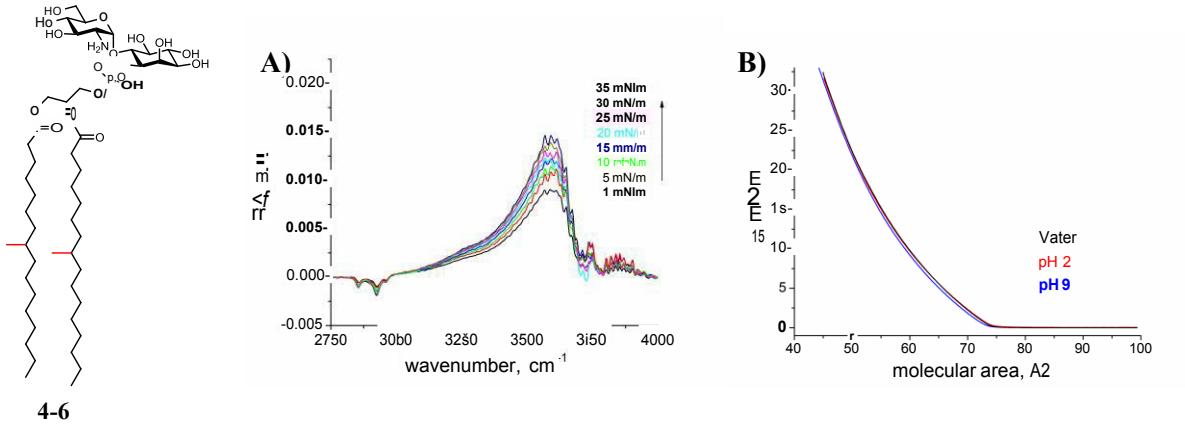

4-6

Figure 4.8: Monolayers of GPI fragment **4-6** at 20 °C on water **(A)** IRRAS spectra of OH stretching region at different lateral pressure; **(B)** Surface pressure-molecular area isotherms on different subphases.

Variations in the absorption wavenumber for the alkyl chain between 2926 and 2925 cm^{-1} during compression for fragment **4-6** is characteristic for the liquid expanded phase (LE), and whereas values between 2922 and 2920 cm^{-1} for fragment **4-3** is characteristic for the liquid-condensed phase (LC). It confirms that the saturation of the chains is responsible for the formation of micro-domains in the membrane and hence responsible for the fluidity or rigidity of the membrane (**figure 4.8**).

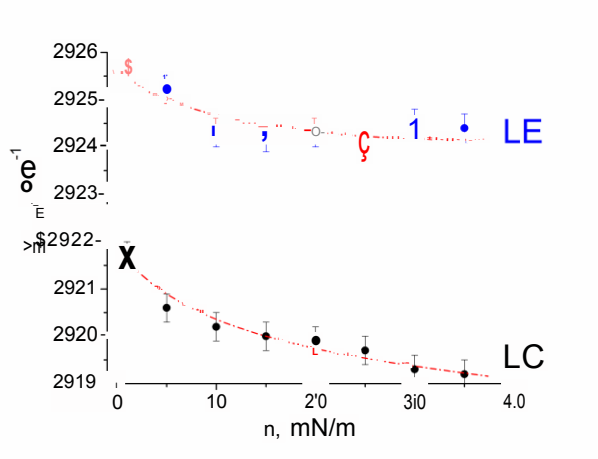

Figure 4.8: Comparison of wavenumber *vs* surface pressure curve between GPI fragment **4-6** (blue) and **4-3** (black) monolayers at 20 °C on water.

The disruption of the electrostatic interactions and hydrogen bonding between the phosphate and amine group of the GPI fragments has a drastic effect on the structural arrangement in the model membrane. Although the effective in-plane area of the head group is the same, the hydration shell and the zwitterionic effect of fragment **4-3** plays an important role in the formation of rigid structural arrangements of the compound in the monolayer. This result can be supported by the extrapolation of the distortion versus $\sin^2(t)$ curve which shows a strong distortion in case of fragment **4-3**, proving strong interactions between the head groups, and a perfect hexagonal unit cell in the non-tilted phase in case of fragment **4-4** (**figure 4.9**).

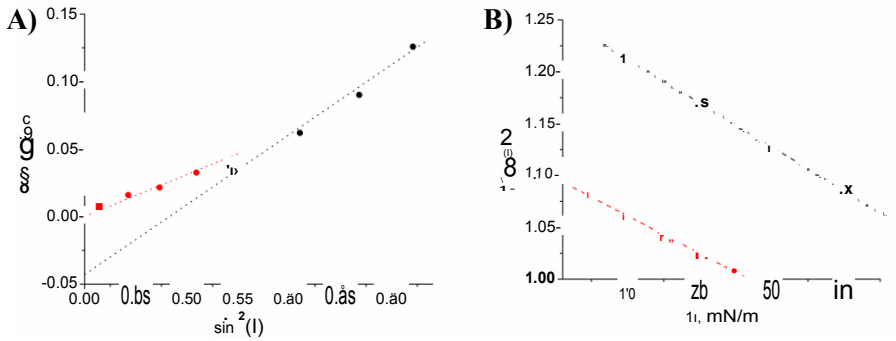

Figure 4.9: Comparison of **(A)** lattice distortion; **(B)** variation of tilt angle of the alkyl chain between GPI fragment **4-3** (black) and **4-4** (red) monolayers at 20 °C on water.

4.6 Conclusion and Outlook

This study was able to provide a better insight in the role of lipid and head groups in the structural arrangement of GPI fragments in monolayers. To perform a comparative analysis of different GPI fragments in the 2-D membrane model, especially to study the role of the hydrogen bonding and zwitterionic effect in the head group and role of lipid composition in the formation of lipid rafts, four different GPI fragments with varying ionic strength and different lipid composition were designed. The synthetic strategy was based on the synthesis of *pseudo*-disaccharide followed by phosphorylation to generate the desired fragments. Benzyl was used as the permanent protecting group for the synthesis of fragment **4-3**, **4-4** and **4-6**. To obtain the glycolipid fragment **4-5** with unsaturated lipid a new protecting group, 2-(napthyl)methyl was utilized. This group was cleaved under acidic conditions without affecting the double bond. The NAP group was found to be an efficient protecting group which uses similar conditions for its installation as benzyl; it is stable during different reactions of the synthesis and can be easily cleaved to obtain the desired product.

In order to obtain *pseudo*-disaccharides, *myo*-inositol building block was synthesized from glucose using the Ferrier type II rearrangement followed by the glycosylation with the glucosamine to generate the disaccharide. The glycosylation conditions were optimized to favor the formation of desired α stereoisomer. Phosphorylation of the disaccharides was carried out by using *H*-phosphonates of the lipids and following oxidation of the phosphonate using iodine and water. In case of fragment **4-5**, bromotrichloromethane was used as oxidizing agent for the phosphonate as it selectively oxidizes the phosphonate and not the alkene in the lipid. Hydrogenation was carried out for the global deprotection of benzyl groups in case of fragments **4-3**, **4-4** and **4-6**. The NAP groups were cleaved using TFA in case of fragment **4-5** to obtain the desired deprotected disaccharide.

The study of these compounds as monolayers showed that by breaking the zwitterionic properties of the glycolipid, the head group of the GPI fragment became more flexible and can be converted into a non-distorted hexagonal unit cell. Monolayers of fragment **4-3** formed a highly ordered structure characterized by two lattices, a lattice of alkyl chains and a molecular lattice of the head group. In contrast, monolayers of fragment **4-4** only formed a lattice of alkyl chains due to the disruption of interaction between the phosphate and the amine groups. Hence, this confirms the importance of hydrogen bonding and electrostatic

interaction in the formation of ordered structures in the membrane. These observations can also be directly related to the GPI biosynthesis, where the acetylation and deacetylation of the amine plays a crucial role.

The presence of branching and unsaturation at the lipid had similar effect and was responsible for the fluidity of the membrane. Monolayers of fragment **4-5**, which had one saturated and one unsaturated chains, were characterized by the presence of partially ordered and partially disordered domains. This structure had a lattice of the alkyl chains at the center forming an ordered domain (LC) of the saturated alkyl chains and a more flexible outer part forming a liquid-expanded domain (LE) as the unsaturated lipids were projected outwards making the membrane more fluid. In case of fragment **4-6** that contained two branched lipid chains, the monolayer showed a similar behavior as for the fragment with unsaturation. The membrane was completely fluid and did not form any ordered structure. The results were further confirmed by the IR wavenumber comparison between the lipid chains, which showed that fragment **4-6** was in complete liquid-expanded phase whereas fragment **4-5** was in partial liquid-expanded and liquid-condensed phase. These findings suggest that the lipids play a crucial role in the formation of rafts and are responsible for many cellular functions.

They also provide important information about the hydrogen bonding interactions of different GPI-anchored proteins in cell membrane during lipid raft formation. However, during the biosynthesis of GPI-APs, there is a strong GPI remodeling involved and other lipid variants are produced. Some of the GPI also possess an additional lipid at the inositol residue; in order to understand the role of this lipid, a new fragment bearing the third lipid would provide insight about its role in lipid raft formation.

The structure of GPI anchors contains an additional phosphoethanolamine. Further studies could also consider the incorporation of this phosphate would increase the ionic strength, which might change the interaction between the head groups and give a better idea about the importance and role of GPI modifications on the cell membrane organization.

4.7 Experimental

4.7.1 General Methods for Synthetic Chemistry

All purchased chemicals were of reagent grade and all anhydrous solvents were of high-purity grade and used as supplied except where noted otherwise. Reactions were performed in oven-dried glassware under an inert argon atmosphere unless noted otherwise. Reagent grade thiophene was dried over activated molecular sieves prior to use. Pyridine was distilled over CaH_2 prior to use. Sodium hydride suspension was washed with hexane and THF and stored in an anhydrous environment. Benzyl bromide was passed through activated basic aluminum oxide prior to use. Analytical thin layer chromatography (TLC) was performed on Merck silica gel 60 F_{254} plates (0.25mm). Compounds were visualized by UV irradiation or heating the plate after dipping in staining solution. The staining solutions were cerium sulfate-ammonium molybdate (CAM) solution, basic potassium permanganate solution, acidic ninhydrin-acetone solution, or a 3-methoxyphenol-sulfuric acid solution (Sugar Stain). Flash column chromatography was carried out using a forced flow of the indicated solvent on Sigma Aldrich silica gel high purity grade 60 Å (230-400 mesh particle size, for preparative column chromatography).

^{1}H, ^{13}C and ^{31}P-NMR as well as all 2D-spectra (^{1}H-^{1}H COSY, ^{1}H-^{1}H TOCSY, ^{1}H-^{13}C HSQC, ^{1}H-^{13}C HMBC) were recorded on a Varian 400 (400 MHz), a Varian 600 (600 MHz), a Bruker 400 (400 MHz) and a Bruker Ascend 400 (400 MHz) spectrometer in $CDCl_3$ (7.26 ppm ^{1}H, 77.1 ppm ^{13}C), D_2O (4.79 ppm ^{1}H), MeOD (4.87 ppm and 3.31 ppm ^{1}H, 49.00 ppm ^{13}C), Acetone-d_6 (2.05 ppm and 2.84 ppm ^{1}H, 206.26 ppm and 29.84 ppm ^{13}C) unless otherwise stated. The coupling constants (*J*) are reported in Hertz (Hz). Splitting patterns for ^{1}H NMR data are indicated as s, singlet; d, doublet; t, triplet; q, quartet; br, broad singlet; dd, doublet of doublets; m, multiplet; dt, doublet of triplets and h, hextet. Signals were assigned by means of ^{1}H-^{1}H COSY, ^{1}H-^{1}H TOCSY, ^{1}H-^{13}C HSQC, ^{1}H-^{13}C HMBC spectra and version thereof. ESI-MS analyses were performed on a Waters Xevo G2-XS Q-TOF spectrometer with an Acquity H-class UPLC. MALDI-MS were recorded on a Bruker Autoflex-speed MALDI-TOF spectrometer equipped with an ATR unit. Infrared (FTIR) spectra were recorded as thin films on a Perkin Elmer Spectrum 100 FTIR spectrophotometer. Optical rotations were measured with a Schmidt & Haensch UniPol L 1000 polarimeter at a concentration (c) expressed in g/100 mL. HPLC supported purifications were conducted using Agilent 1100 and Agilent 1200 systems.

4.7.2 Synthetic Protocols

(R)-3-((4-methoxybenzyl)oxy)propane-1,2-diol (4-15)

To a stirred solution of (S)-2,3-O-isopropylideneglycerol **4-13** (0.50 g, 3.81 mmol) in anhydrous DMF (10 mL) was added NaH (0.18 g, 7.60 mmol) at 0 °C. After 20 min, PMBCl (0.77 mL, 5.72 mmol) was added. The reaction mixture was warmed to room temperature and was stirred for 12 h. The reaction was quenched with MeOH, and diluted with Et_2O. The organic layer was extracted with water. The combined organic layers were further washed with brine, dried over Na_2SO_4 and concentrated to obtain **4-14**. The crude product was dissolved in CH_2Cl_2 (12 mL), pTSA.$5H_2O$ (0.06 g, 0.3 mmol) was added and the reaction mixture was allowed to stir at room temperature for 12 h. The reaction was quenched with Et_3N and concentrated. Flash chromatography was performed to obtain the diol **4-15** (0.60 g, 2.83 mmol, 75%) as colorless oil. R_f = 0.30 (EtOAc/hexane 2:1); ^{1}H NMR (400 MHz, $CDCl_3$) δ 7.27 (d, *J* = 7.4 Hz, 2H), 6.91 (d, *J* = 8.3 Hz, 2H), 4.51 (s, 2H), 3.90 (td, *J* = 5.8, 2.9 Hz, 1H), 3.83 (s, 3H), 3.73 (dd, *J* = 11.4, 3.9 Hz, 1H), 3.65 (dd, *J* = 11.4, 5.3 Hz, 1H), 3.56 (qd, *J* = 9.6, 5.0 Hz, 2H). ^{13}C NMR (101 MHz, $CDCl_3$) δ 159.41, 129.71, 129.51(2C), 113.91(2C), 73.29, 71.57, 70.52, 64.15, 55.32.

(S)-1-((4-methoxybenzyl)oxy)-3-(stearoyloxy)propan-2-yl octadec-9-enoate (4-16)

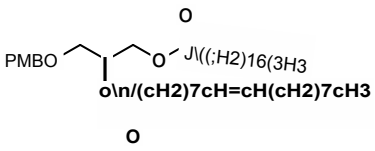

To a stirred solution of diol **4-15** (0.50 g, 2.36 mmol) in CH_2Cl_2 (15 mL) were added DMAP (0.28 g, 2.36 mmol), stearic acid (0.67 g, 2.36 mmol) and DIC (0.37 mL, 2.36 mmol). The mixture was stirred at room temperature for 5 h. The reaction was extracted with CH_2Cl_2, washed with brine, dried over Na_2SO_4 and concentrated. The residue was purified by flash column chromatography to obtain monoacylated glycerol and was subjected to second coupling. The intermediate alcohol (0.67 g, 1.43 mmol) was dissolved in CH_2Cl_2 (10 mL), DMAP (0.17 g, 1.41 mmol), oleic acid (0.48 mL, 1.54 mmol) and DIC (0.24 mL, 1.54 mmol) were added and reaction mixture was stirred at room temperature for 12 h. The reaction was extracted with CH_2Cl_2, washed with brine, dried over Na_2SO_4 and concentrated. The crude

product was purified by flash column chromatography to obtain **4-16** (0.78 g, 1.05 mmol, 75%) as white solid. R_f = 0.40 (EtOAc/hexane 1:4); ^{1}H NMR (400 MHz, $CDCl_3$) δ 7.26 (d, *J* = 8.2 Hz, 2H), 6.90 (d, *J* = 8.4 Hz, 2H), 5.37 (qq, *J* = 8.7, 5.3, 4.5 Hz, 2H), 5.25 (dd, *J* = 6.2, 4.0 Hz, 1H), 4.55 – 4.43 (m, 2H), 4.35 (dd, *J* = 11.9, 3.8 Hz, 1H), 4.19 (dd, *J* = 11.9, 6.4 Hz, 1H), 3.83 (s, 3H), 3.58 (d, *J* = 5.5 Hz, 2H), 2.32 (dt, *J* = 17.1, 7.5 Hz, 4H), 2.03 (q, *J* = 6.6 Hz, 4H), 1.62 (h, *J* = 7.3 Hz, 4H), 1.39 – 1.25 (m, 49H), 0.90 (t, *J* = 6.6 Hz, 6H). ^{13}C NMR (101 MHz, $CDCl_3$) δ 173.47, 173.14, 159.29, 130.02, 129.73, 129.33(2C), 113.80(2C), 72.96, 70.01, 67.87, 62.70, 55.27, 34.34, 34.14, 31.96, 31.94, 29.80, 29.74, 29.70, 29.67, 29.56, 29.53, 29.40, 29.36, 29.33, 29.24, 29.16, 29.13, 29.09, 27.25, 27.20, 24.97, 24.91, 22.73, 14.17. ESI-MS (*m*/*z*): $[M+Na]^+$ cald 765.600, obsd 765.2.

(S)-1-hydroxy-3-(stearoyloxy)propan-2-yl octadec-9-enoate (4-17)

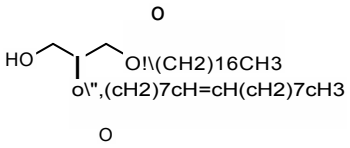

To a stirred solution of bilipid **4-16** (0.60 g, 0.81 mmol) in 10:1 mixture of CH_2Cl_2 and water was added DDQ (0.18 g, 1.61 mmol) at room temperature. After 12 h, sat. $NaHCO_3$ solution was added. The mixture was extracted with CH_2Cl_2, dried over Na_2SO_4 and concentrated. The crude product was purified by flash column chromatography to obtain **4-17** (0.30 g, 0.48 mmol, 60%). R_f = 0.35 (EtOAc/hexane 2:3); ^{1}H NMR (400 MHz, $CDCl_3$) 5.42 – 5.31 (m, 2H), 5.11 (p, *J* = 5.0 Hz, 1H), 4.43 – 4.22 (m, 2H), 3.75 (t, *J* = 5.8 Hz, 2H), 2.36 (q, *J* = 8.0 Hz, 4H), 2.12 – 1.94 (m, 4H), 1.73 – 1.61 (m, 2H), 1.30 (d, *J* = 20.0 Hz, 51H), 0.94 – 0.87 (m, 6H). ESI-MS (*m*/*z*): $[M+Na]^+$ cald 645.543, obsd 645.1.

(2R)-1-((hydroxyhydrophosphoryl)oxy)-3-(stearoyloxy)propan-2-yl octadec-9-enoate (4-9)

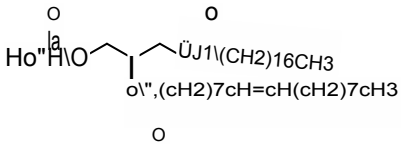

Glycerol bilipid **4-17** (0.20 g, 0.32 mmol) and phosphorus acid (0.13 g, 1.61 mmol) were dissolved and co-evaporated with anhydrous pyridine three times and dried under high vacuum for 2 h. The mixture was dissolved in anhydrous pyridine (5 mL) and a solution of

pivaloyl chloride (0.20 mL, 1.61 mmol) in pyridine (2 mL) was added. The solution was stirred for 16 h at room temperature. After the completion of reaction, the reaction mixture was concentrated and purified by Et_3N deactivated silica gel column chromatography to obtain *H*-phosphonate **4-9** (0.15 g, 0.22 mmol, 70%) as a white solid. R_f = 0.7 (MeOH/ CH_2Cl_2 = 1:9) ; ^{1}H NMR (400 MHz, $CDCl_3$) δ 12.38 (s, 1H), 5.47 – 5.31 (m, 2H), 5.24 (s, 1H), 4.48 – 3.96 (m, 3H), 3.10 (s, 5H), 2.32 (q, *J* = 7.6 Hz, 4H), 2.03 (q, *J* = 6.4 Hz, 3H), 1.33 – 1.21 (m, 44H), 0.90 (t, *J* = 6.7 Hz, 6H). ^{31}P NMR (162 MHz, $CDCl_3$) δ 4.66. ESI-MS (*m*/*z*): $[M-H]^-$ cald 685.52, obsd 685.0.

Methyl 2,3,4-tri-*O*-(2-naphthyl)methyl-α-D-glucopyranoside (4-20)

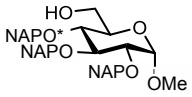

To a stirred solution of **4-19** (10 g, 11.67 mmol) in MeOH (50 mL) was added *p*-TsOH.H_2O (0.56 g, 2.92 mmol) at room temperature. After 12 h, the reaction mixture was quenched with Et_3N and concentrated. The crude product was purified by flash column chromatography to obtain alcohol **4-20** (5.02 g, 8.17 mmol, 70%) as white solid. R_f = 0.2 (EtOAc/hexane = 1:2) ^{1}H NMR (400 MHz, $CDCl_3$) δ 7.77 – 7.57 (m, 13H), 7.52 – 7.28 (m, 10H), 7.29 (d, *J* = 1.7 Hz, 1H), 5.12 (d, *J* = 11.2 Hz, 1H), 4.96 (dd, *J* = 11.3, 6.8 Hz, 2H), 4.89 (d, *J* = 12.2 Hz, 1H), 4.77 (dd, *J* = 17.2, 11.8 Hz, 2H), 4.53 (d, *J* = 3.6 Hz, 1H), 4.05 (t, *J* = 9.2 Hz, 1H), 3.72 (dt, *J* = 9.1, 4.6 Hz, 1H), 3.69 – 3.59 (m, 2H), 3.59 – 3.49 (m, 2H), 3.31 (s, 3H). ^{13}C NMR (101 MHz, $CDCl_3$) δ 136.30, 135.60, 135.53, 133.37, 133.25, 133.21, 133.12, 132.98, 128.40, 128.27, 128.16, 128.00, 127.97(2C), 127.74, 127.71(2C), 127.09, 126.68, 126.54, 126.24, 126.14, 126.10, 126.05, 126.02(2C), 126.00, 125.93, 125.86, 125.85, 98.20, 82.02, 79.91, 77.54, 75.85, 75.17, 73.58, 70.74, 61.94, 55.30. ESI-MS (*m*/*z*): $[M+Na]^+$ cald 637.2566, obsd 637.2578.

(*Z*)-Methyl 6-*O*-acetyl-2,3,4-tri-*O*-(2-naphthyl)methyl-α-D-*gluco*-hex-5-enopyranoside (4-21)

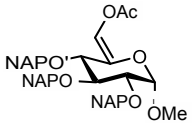

To a stirred solution of alcohol **4-20** (9 g, 14.64 mmol) and SO_3.Py (9.51 g, 58.6 mmol) in CH_2Cl_2 (100 mL) at 0 °C was added DIPEA (12.8 mL, 73.2 mmol). The reaction mixture was stirred at 0 °C for 10 min and DMSO (15.6 mL, 220 mmol) was added. After 1 h at 0 °C, the reaction was diluted with aq. $NaHCO_3$, extracted with Et_2O, washed with brine, dried over Na_2SO_4 and concentrated (EtOAc/hexane= 2:3, R_f = 0.15). The crude compound was dissolved in CH_3CN (100 mL). Then, Ac_2O (8.3 mL, 88 mmol) and K_2CO_3 (8.12 g, 58.8 mmol) were added. The reaction mixture was refluxed (85 °C) for 4 h and allowed to cool to room temperature, diluted with aq.$NaHCO_3$, extracted with Et_2O, washed with brine, dried over Na_2SO_4, and concentrated. The crude product was purified by flash column chromatography to obtain enolate **4-21** (7.7 g, 11.76 mmol, 80%) as white solid. R_f = 0.28 (EtOAc/hexane = 1:3) ^{1}H NMR (400 MHz, $CDCl_3$) δ 7.88 – 7.69 (m, 13H), 7.72 – 7.63 (m, 1H), 7.56 – 7.39 (m, 10H), 5.14 – 4.80 (m, 7H), 4.73 (d, *J* = 3.4 Hz, 1H), 4.08 (d, *J* = 6.3 Hz, 2H), 3.69 (dq, *J* = 9.4, 6.2, 4.8 Hz, 1H), 3.50 (s, 3H), 2.16 (s, 3H). ^{13}C NMR (101 MHz, $CDCl_3$) δ 167.36, 136.04, 135.36, 135.10, 135.06, 134.97, 133.32, 133.23, 133.18, 133.04, 132.98, 128.41, 128.29, 128.11, 128.03, 127.99, 127.94, 127.70, 127.68(2C), 127.08, 126.81, 126.57, 126.25, 126.13, 126.09,126.06, 126.01, 125.97, 125.94, 125.90, 125.84, 123.17, 99.81, 81.36, 79.07, 77.68, 75.78, 74.55, 73.89, 56.36, 20.66. ESI-MS (*m*/*z*): $[M+Na]^+$ cald 677.2515, obsd 677.2507.

D-1-*O*-Acetyl-3,4,5-tri-*O*-(2-naphthyl)methyl-*myo*-inositol (4-23)

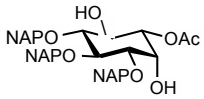

To the stirred solution of enolate **4-21** (5.6 g, 8.5 mmol) in a mixture of acetone/water (v/v = 5:1, 85 mL) was added $Hg(OTf)_2$ (4.38 g, 10.3 mmol) at r. t.. After 1 h, the reaction mixture was cooled to 0 °C and aq. NaOAc (3M, 8.6 mL) was added, immediately followed by addition of brine (17 mL). The reaction was slowly warmed to room temperature and stirred for 12 h. The reaction mixture was diluted with aq.$NaHCO_3$ and extracted with EtOAc. The combined organic layer was washed with brine, dried over Na_2SO_4, concentrated. The crude product was crystalized from CH_2Cl_2/Et_2O (1:50) to obtain ketone **4-22** (4.2 g, 6.6 mmol, 77%) as white solid. R_f = 0.20 (EtOAc/hexane= 2:3)

The solution of ketone **4-22** (4.2 g, 6.6 mmol) in CH_3CN (40 ml) was slowly transferred to a cooled (0 °C) solution of $NaBH(OAc)_3$ (6.95 g, 32.8 mmol) in a mixture of AcOH/CH_3CN (v/v = 1:1, 80 mL). The reaction was allowed to warm to room temperature and stirred for 12

h. The reaction mixture was diluted with aq.$NaHCO_3$ and extracted with EtOAc. The combined organic layer was washed with brine, dried over Na_2SO_4 and concentrated. The crude product was crystalized by CH_2Cl_2/Et_2O to give diol **4-23** (3.5 g, 5.45 mmol, 83%) as white solid. R_f = 0.20 (EtOAc /hexane = 1:1) ^{1}H NMR (400 MHz, $CDCl_3$) δ 7.77 – 7.69 (m, 5H), 7.66 (dd, *J* = 15.6, 8.4 Hz, 6H), 7.61 – 7.55 (m, 1H), 7.38 (dtt, *J* = 8.4, 6.4, 3.4 Hz, 9H), 5.05 (d, *J* = 11.3 Hz, 2H), 4.96 (d, *J* = 11.1 Hz, 1H), 4.88 (d, *J* = 11.4 Hz, 1H), 4.85 – 4.75 (m, 2H), 4.71 (dd, *J* = 10.2, 2.7 Hz, 1H), 4.30 (d, *J* = 2.9 Hz, 1H), 4.12 (td, *J* = 9.8, 2.8 Hz, 1H), 3.98 (t, *J* = 9.5 Hz, 1H), 3.60 (dd, *J* = 9.5, 2.7 Hz, 1H), 3.40 (td, *J* = 8.2, 7.2, 4.7 Hz, 1H), 2.10 (s, 3H). ^{13}C NMR (101 MHz, $CDCl_3$) δ 135.98, 135.75, 134.79, 133.26, 133.19, 133.00, 132.94, 128.43, 128.37, 128.09, 127.92(3C), 127.64(2C), 126.80, 126.63, 126.44, 126.24, 126.11, 126.01, 125.93, 125.90, 125.82, 125.76, 125.73, 82.88, 80.94, 80.05, 75.87, 75.72, 73.08, 72.88, 70.49, 67.79, 21.08. ESI-MS (*m*/*z*): $[M+Na]^+$ cald 665.2515, obsd 665.2525.

D-1-*O*-Allyl-3,4,5-tri-*O*-(2-naphthyl)methyl-*myo*-inositol (4-25)

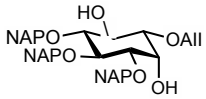

The diol **4-23** (2 g, 3.11 mmol) was stired at room temperature for 30 min in the presence of NaOMe (0.04 g, 0.63 mmol) in MeOH/CH_2Cl_2 (v/v = 1:1, 60 mL). Then, the reaction was neutralized with Amberlite IR 120 H^+ resin, filtered and concentrated. A mixture of triol **4-24** (1.7 g, 2.8 mmol) and bis(tributyltin)oxide (1.9 mL, 3.7 mmol) in toluene (50 mL) was refluxed for 5 h using a Dean-Stark trap. TBAI (1.05 g, 2.8 mmol) and allyl bromide (1.2 mL, 14.2 mmol) were added. The mixture was stirred under anhydrous condition at 65 °C for 16 h. The reaction mixture was concentrated and purified by flash column chromatography to obtain **4-25** (1.2 g, 1.87 mmol, 65%) as white solid. R_f = 0.35 (EtOAc/hexane= 1:2) ^{1}H NMR (400 MHz, $CDCl_3$) δ 7.84 – 7.59 (m, 12H), 7.51 – 7.38 (m, 9H), 5.91 (ddt, *J* = 16.5, 11.0, 5.9 Hz, 1H), 5.24 (dt, *J* = 17.2, 1.5 Hz, 1H), 5.21 – 5.11 (m, 1H), 5.11 – 4.94 (m, 4H), 4.91 (d, *J* = 2.4 Hz, 2H), 4.28 (d, *J* = 3.0 Hz, 1H), 4.26 – 4.13 (m, 1H), 4.15 – 4.03 (m, 3H), 3.52 (dd, *J* = 9.6, 2.7 Hz, 1H), 3.44 (t, *J* = 9.4 Hz, 1H), 3.17 (dd, *J* = 9.7, 2.7 Hz, 1H), 2.52 – 2.45 (m, 2H). ^{13}C NMR (101 MHz, $CDCl_3$) δ 136.20, 136.09, 135.29, 134.38, 133.29, 133.18, 133.02, 132.91, 128.31, 128.20, 128.02, 127.92, 127.88, 127.67, 127.63, 126.68, 126.50, 126.17, 126.04, 126.02, 125.98, 125.93, 125.90, 125.83, 125.78, 125.74, 117.85, 82.72, 80.97, 79.88, 78.87, 75.91, 75.44, 72.80, 72.32, 71.33, 67.02. ESI-MS (*m*/*z*): $[M+Na]^+$ cald 663.2723, obsd 663.2733.

D-1-*O*-Allyl-2,3,4,5-tetra-*O*-(2-naphthyl)methyl-*myo*-inositol (4-12b)

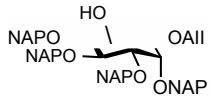

To the stirred solution of inositol **4-25** (0.35 g, 0.55 mmol) in DMF (10 mL) was added NaH (0.03 g, 1.2 mmol) at 0 °C, in one portion. After strirring for 30 min at 0 °C, the reaction mixture was cooled to -20 °C, 2-naphthylmethyl bromide (0.12 g, 0.55 mmol) in DMF was added dropwise, and the reaction was stirred for 2 h allowing it to warm to 0 °C. The reaction was quenched with MeOH and extracted with EtOAc and the combined organic layers were washed with brine and dried over Na_2SO_4. The solvents were removed under reduced pressure and the crude residue was purified by flash column chromatography to obtain acceptor **4-12b** (0.27 g, 0.34 mmol, 63%) as white solid. R_f = 0.28 (EtOAc/hexane = 1:3) ^{1}H NMR (400 MHz, $CDCl_3$) δ 7.86-7.72 (m, 13H), 7.70-7.60 (m, 3H), 7.54-7.42 (m, 12H), 5.98-5.85 (m, 1H), 5.29-5.22 (m, 1H), 5.21-5.15 (m, 2H), 5.13-5.08 (m, 5H), 4.90 & 4.84 (q, *J* = 11.9 Hz, 2H), 4.33-4.23 (m, 2H), 4.19-4.16 (m, 1H), 4.12-3.98 (m, 2H), 3.58-3.50 (m, 2H), 3.22-3.15 (m, 1H); ^{13}C NMR (100 MHz, $CDCl_3$) δ 136.5, 136.4, 135.9, 134.6, 133.44, 133.36, 133.3, 133.1, 133.0, 128.29, 128.26, 128.2, 128.1, 128.0, 127.80, 127.78, 127.75, 126.7, 126.6, 126.4, 126.30, 126.28, 126.26, 126.08, 126.06, 126.0, 125.87, 125.85, 117.6, 83.5, 81.6, 81.2, 80.0, 76.0, 75.5, 74.2, 73.4, 73.2, 73.0, 71.4. ESI-MS (*m*/*z*): $[M+Na]^+$ cald 803.3349, obsd 803.3372.

3,4,6–Tri-*O*-acetyl-2-azido-2deoxy-α-D-glucopyranosyl trichloroacetimidate (4-11)

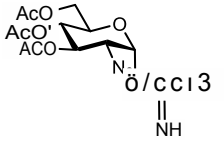

To a stirred solution of hemiacetal **4-28** (1.4 g, 4.23 mmol) in CH_2Cl_2 (15 mL) at 0 °C were added CCl_3CN (4.2 mL, 42.3 mmol) and DBU (0.13 mL, 0.85 mmol). The reaction mixture was stirred for 4 h at 0 °C. The resulting mixture was concentrated and purified by flash column chromatography to obtain imidate **4-11** (1.85 g, 3.9 mmol, 92%) as yellowish solid. R_f = 0.4 (EtOAc/hexane = 2:3) ^{1}H NMR (400 MHz, $CDCl_3$) δ 8.86 (s, 1H), 6.51 (d, *J* = 3.6 Hz, 1H), 5.58 – 5.51 (m, 1H), 5.18 (t, *J* = 9.8 Hz, 1H), 4.30 (dd, *J* = 12.4, 4.2 Hz, 1H), 4.25 – 4.21

(m, 1H), 4.13 (dd, *J* = 12.3, 1.9 Hz, 1H), 3.80 (dd, *J* = 10.5, 3.6 Hz, 1H), 2.14 (s, 3H), 2.09 (s, 4H), 2.08 (s, 3H). ^{13}C NMR (101 MHz, $CDCl_3$) δ 170.57, 169.90, 169.71, 160.54, 94.01, 70.65, 70.08, 67.87, 61.37, 60.60, 20.73, 20.71, 20.64.

3,4,6–Tri-*O*-benzyl-2-azido-2-deoxy-α-D-glucopyranosyl-(1→6)-2,3,4,5-tetra-*O*-benzyl-D-*myo*-inositol (4-7a)

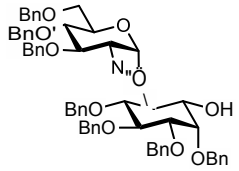

To a stirred solution of triol **4-30** (0.29 g, 0.38 mmol) in anhydrous DMF (12 mL) was added NaH (0.09 g, 3.78 mmol) at 0 °C. After 20 min, BnBr (0.45 mL, 3.78 mmol) was added; the reaction was warmed to room temperature and stirred for 16 h. The reaction was quenched with MeOH and concentrated. The crude product was purified by flash chromatography to obtain **4-31** (0.3 g, 0.29 mmol, 77%). To a stirred solution of **4-31** (0.28 g, 0.27 mmol) in MeOH/CH_2Cl_2 (3:1, 7 mL) was added $PdCl_2$ (0.01 g, 0.054 mmol) at room temperature. The reaction was stirred for 12 h and quenched with Et_3N and concentrated. The crude residue was purified by flash column chromatography to obtain **4-7a** (0.22 g, 0.22 mmol, 82%). R_f = 0.4 (EtOAc/hexane = 1:1) ^{1}H NMR (400 MHz, Chloroform-*d*) δ 7.48 – 7.02 (m, 51H), 5.42 (d, *J* = 3.6 Hz, 1H), 5.07 – 4.31 (m, 20H), 4.16 – 3.84 (m, 8H), 3.76 – 3.31 (m, 9H), 3.25 – 3.14 (m, 2H), 3.05 – 2.97 (m, 1H).^{13}C NMR (101 MHz, $CDCl_3$) δ 138.55, 138.45, 138.41, 138.19, 138.07, 137.77, 128.44, 128.43, 128.40, 128.33, 128.26, 128.24, 128.21, 128.20, 128.04, 128.00, 127.94, 127.90, 127.83, 127.75, 127.70, 127.65, 127.61, 127.59, 127.43, 127.31, 98.37, 81.97, 81.10, 80.89, 80.72, 80.43, 78.05, 77.32, 77.20, 77.00, 76.68, 75.82, 75.44, 75.23, 74.74, 73.52, 73.33, 72.88, 72.39, 70.79, 67.37, 64.07. ESI-MS (*m*/*z*): $[M+Na]^+$ cald 1020.441 obsd 1020.2.

3,4,6–Tri-*O*-benzyl-2-azido-2-deoxy-α-D-glucopyranosyl-(1→6)-1-*O*-(1,2-*O*-distearoyl-*sn*-glycerol)-phosphate-2,3,4,5-tetra-*O*-benzyl--*myo*-inositol (4-32)

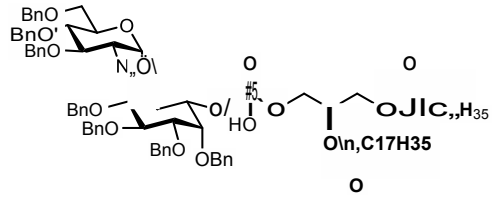

Disaccharide **4-7a** (0.05 g, 0.05 mmol) and *H*-phosphonate **4-8** (0.05 g, .08 mmol) were co-evaporated with pyridine for three times and dried under high vacuum for 2 h. The mixture was dissolved in anhydrous pyridine (5 mL) and a solution of pivolyl chloride (0.01 mL, 0.08 mmol) in pyridine (1 mL) was added. The solution was stirred for 48 h at room temperature. After 48 h, iodine (0.06 g, 0.25 mmol) and water (0.2 mL) were added and reaction was stirred for 4 h. The reaction mixture was quenched with $Na_2S_2O_3$ and extracted with CH_2Cl_2. The organic layer were concentrated and purified by Et_3N deactivated silica gel flash column chromatography to obtain bilipidated disaccharide **4-32** (0.05 g, 0.03 mmol, 60%). R_f = 0.7 (MeOH/CH_2Cl_2 = 1:9) ^{1}H NMR (400 MHz, $CDCl_3$) δ 7.45 (d, *J* = 7.1 Hz, 2H), 7.40 – 7.29 (m, 23H), 7.29 – 7.18 (m, 20H), 7.18 – 6.97 (m, 6H), 5.87 (d, *J* = 3.7 Hz, 1H), 5.26 (dt, *J* = 8.8, 4.4 Hz, 1H), 5.00 (dd, *J* = 32.9, 11.3 Hz, 4H), 4.88 (s, 2H), 4.83 – 4.70 (m, 6H), 4.60 (dd, *J* = 35.6, 11.8 Hz, 2H), 4.49 – 4.24 (m, 6H), 4.19 – 3.99 (m, 8H), 3.78 – 3.71 (m, 1H), 3.59 (dd, *J* = 9.8, 2.1 Hz, 1H), 3.55 – 3.46 (m, 3H), 3.43 – 3.34 (m, 3H), 3.23 (dd, *J* = 10.3, 3.7 Hz, 1H), 3.03 (dt, *J* = 11.1, 5.5 Hz, 10H), 2.27 (dp, *J* = 10.2, 5.7, 5.1 Hz, 6H), 1.58 (s, 8H), 1.27 (d, *J* = 4.7 Hz, 73H), 0.90 (t, *J* = 6.8 Hz, 6H). ^{13}C NMR (101 MHz, $CDCl_3$) δ 173.46, 173.09, 139.80, 138.77, 138.48, 138.45, 138.13, 138.08, 138.00, 128.41, 128.29, 128.27, 128.25, 128.20, 128.17, 128.09, 128.07, 127.96, 127.86, 127.76, 127.67, 127.57, 127.52, 127.44, 127.40, 127.29, 127.15, 127.00, 96.77, 81.88, 80.98, 79.77, 78.35, 76.09, 75.65, 75.16, 74.78, 74.71, 73.29, 72.26, 69.95, 67.96, 63.80, 63.17, 62.75, 52.91, 45.57, 34.30, 34.09, 31.96, 29.76, 29.71, 29.59, 29.58, 29.41, 29.38, 29.19, 24.93, 24.89, 22.73, 14.18, 8.53, 8.00. ^{31}P NMR (162 MHz, $CDCl_3$) δ -1.83. ESI-MS (*m*/*z*): $[M+H_3O]^+$ cald 1702.98 obsd 1702.6.

2-amino-2-deoxy-α-D-glucopyranosyl-(1→6)-1-*O*-(1,2-*O*-distearoyl-*sn*-glycerol)-phosphate-D-*myo*-inositol (4-3)

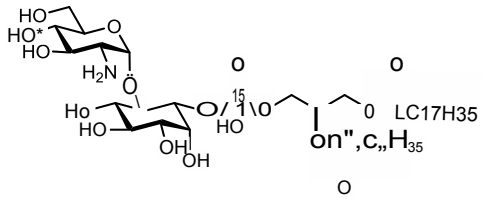

To the stirred solution of *pseudo*-disaccharide **4-32** (20.0 mg, 0.012 mmol) in mixture of CH_2Cl_2/MeOH/H_2O (3:3:1, 5 mL) at room temperature was added $Pd(OH)_2$ on C (17 mg, 0.024 mmol, 20% Pd content). Hydrogen gas was bubbled through the solution for 15 min and the reaction mixture was stirred under an atmosphere of hydrogen gas for additional 24 h. The $Pd(OH)_2$ was removed by filtration through a pad of celite and the solution was concentrated. The crude product was purified by size exclusion chromatography on a LH20 column using CH_2Cl_2/MeOH/H_2O (3:3:1) as the solvent mixture to obtain the bilipidated disaccharide **4-3** (6.0 mg, 0.006 mmol, 50%) ^{31}P NMR (162 MHz, MeOD) δ -0.69. ESI-MS (*m*/*z*): $[M-H]^-$ cald 1026.657 obsd 1026.751.

3,4,6–Tri-*O*-benzyl-2-acetamide-2-deoxy-α-D-glucopyranosyl-(1→6)-1-*O*-allyl-2,3,4,5-tetra-*O*-benzyl-D-*myo*-inositol (4-33)

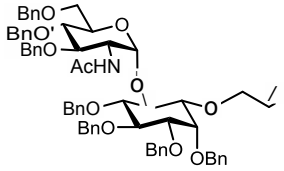

Activated zinc (0.11 g, 1.73 mmol) was suspended in THF (10 mL) and transferred to the pseudodisaccharide **4-31** (0.12 g, 0.12 mmol). Ac_2O (0.033 mL, 0.35 mmol) and AcOH (0.007 mL, 0.115 mmol) were added and reaction mixture was stirred at room temperature for 4 h. The reaction mixture was filtered through celite and washed with saturated $NaHCO_3$ twice. The organic phase was dried over Na_2SO_4 and concentrated. The crude product was purified by flash column chromatography to obtain **4-33** (0.087 mg, 0.082 mmol, 71%). R_f = 0.3 (EtOAc/hexane = 1:1) ^{1}H NMR (400 MHz, $CDCl_3$) δ 7.33 (dd, *J* = 14.5, 7.4 Hz, 4H), 7.27 – 7.00 (m, 60H), 5.66 (ddt, *J* = 16.4, 10.3, 6.1 Hz, 1H), 5.18 (d, *J* = 3.3 Hz, 1H), 5.16 – 5.15 (m, 1H), 5.13 – 5.05 (m, 3H), 4.94 – 4.75 (m, 7H), 4.76 – 4.63 (m, 10H), 4.63 – 4.60 (m, 3H),

4.60 – 4.53 (m, 4H), 4.42 (dd, *J* = 24.7, 11.4 Hz, 3H), 4.35 – 4.18 (m, 2H), 4.19 – 3.98 (m, 3H), 3.99 – 3.90 (m, 11H), 3.82 (dd, *J* = 12.0, 6.0 Hz, 2H), 3.75 – 3.64 (m, 4H), 3.64 – 3.48 (m, 4H), 3.47 – 3.18 (m, 5H), 3.11 (dd, *J* = 10.0, 2.0 Hz, 2H), 1.76 (s, 3H). ^{13}C NMR (101 MHz, $CDCl_3$) δ 169.91, 138.75, 138.61, 138.43, 138.29, 138.22, 138.13, 133.52, 128.49, 128.38, 128.35, 128.28, 128.24, 128.09, 128.03, 127.90, 127.82, 127.78, 127.68, 127.60, 127.54, 127.40, 119.11, 100.30, 83.12, 81.99, 81.20, 80.84, 79.73, 79.19, 78.23, 75.82, 75.54, 74.99, 74.79, 74.25, 73.41, 73.04, 72.83, 72.09, 71.13, 68.75, 53.49, 23.29. ESI-MS (*m*/*z*): $[M+H]^+$ cald 1054.5 obsd 1054.3, $[M+Na]^+$ cald 1076.5 obsd 1076.4

3,4,6–Tri-*O*-benzyl-2-acetamide-2-deoxy-α-D-glucopyranosyl-(1→6)- 1-*O*-(1,2-*O*-distearoyl-*sn*-glycerol)-phosphate -2,3,4,5-tetra-*O*-benzyl-D-*myo*-inositol (4-35)

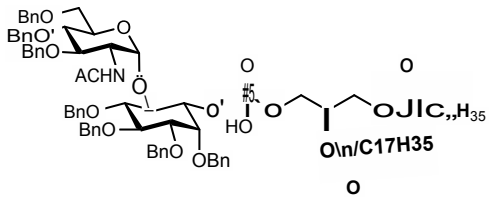

To a stirred solution of **4-33** (0.07 g, 0.062mmol) in MeOH/ CH_2Cl_2 (3:1) was added $PdCl_2$ (4 mg, 0.019 mmol) at room temperature. The reaction was stirred for 12 h, quenched with TEA and concentrated. The crude product was purified by flash column chromatography to obtain **4-34** (0.04 g, 0.04 mmol, 72%) R_f = 0.35 (EtOAc/hexane = 3:2). Disaccharide **4-34** (0.04 g, 0.04 mmol) and H-phosphonate **4-8** (0.09 g, 0.13 mmol) were co-evaporated with pyridine for three times and dried under high vacuum for 2 h. The mixture was dissolved in anhydrous pyridine (7 mL) and a solution of pivolyl chloride (0.016 mL, 0.13 mmol) in pyridine (1 mL) was added. The solution was stirred for 48 h at room tmeperature. After 48 h, iodine (0.11 g, 0.44 mmol) and water (0.3 mL) were added and the reaction was stirred for 4 h. The reaction mixture was quenched with $Na_2S_2O_3$ and extracted with CH_2Cl_2. The organic layers were concentrated and the crude product was purified with Et_3N deactivated silica gel flash column chromatography to obtain bilipidated disaccharide **4-35** (0.045 g, 0.027 mmol, 60%). R_f = 0.6 (MeOH/ CH_2Cl_2 = 1:9) ^{1}H NMR (400 MHz, $CDCl_3$) δ 7.49 – 7.09 (m, 40H), 5.50 (d, *J* = 2.4 Hz, 2H), 5.32 (d, *J* = 3.4 Hz, 1H), 5.21 (dd, *J* = 6.6, 3.0 Hz, 1H), 5.05 – 4.89 (m, 2H), 4.88 – 4.61 (m, 7H), 4.47 (dd, *J* = 23.7, 11.5 Hz, 1H), 4.42 – 4.24 (m, 4H), 4.22 – 3.88 (m, 8H), 3.83 – 3.66 (m, 1H), 3.47 – 3.34 (m, 3H), 2.33 – 2.15 (m, 4H), 2.07 (s, 3H), 1.53 (s, 2H), 1.25 (d, *J*

= 9.5 Hz, 51H), 0.89 (t, *J* = 6.8 Hz, 6H). ^{31}P NMR (162 MHz, $CDCl_3$) δ -1.12. ESI-MS (*m*/*z*): $[M+H]^+$ cald 1702.0 obsd 1702.6 $[M-H]^-$ cald 1699.99 obsd 1699.8.

2-acetamide-2-deoxy-α-D-glucopyranosyl-(1→6)-1-*O*-(1,2-*O*-distearoyl-*sn*-glycerol)-phosphate-D-*myo*-inositol (4-4)

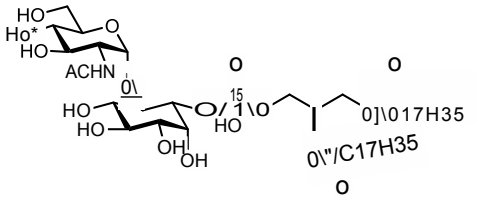

To a stirred solution of pseudodisaccharide **4-35** (30.0 mg, 0.018 mmol) in mixture of CH_2Cl_2/MeOH/H_2O (3:3:1, 5 mL) at room temperature was added $Pd(OH)_2$ on C (17 mg, 0.024 mmol, 20% Pd content). Hydrogen gas was bubbled through the solution for 15 min and the reaction mixture was stirred under an atmosphere of hydrogen gas for additional 24 h. The $Pd(OH)_2$ was removed by filtration through a pad of celite and the solution was concentrated. The crude product was purified by size exclusion chromatography on a LH20 column using CH_2Cl_2/MeOH/H_2O (3:3:1) as the solvent mixture to obtain the bilipidated disaccharide **4-4** (9.0 mg, 0.009 mmol, 50%). ^{1}H NMR (400 MHz, Methanol-d_4) δ 7.27 (s, 1H), 5.04 (d, *J* = 5.6 Hz, 2H), 4.01 (ddd, *J* = 23.1, 11.1, 5.5 Hz, 2H), 3.94 – 3.61 (m, 5H), 3.65 – 3.41 (m, 8H), 3.41 – 3.25 (m, 3H), 3.09 (q, *J* = 7.3 Hz, 5H), 2.96 – 2.73 (m, 0H), 2.32 – 2.22 (m, 3H), 2.21 (dd, *J* = 13.4, 7.5 Hz, 1H), 2.00 – 1.91 (m, 1H), 1.53 (s, 2H), 1.17 (s, 44H), 1.03 (d, *J* = 6.5 Hz, 4H), 0.83 – 0.71 (m, 6H). ^{31}P NMR (162 MHz, MeOD) δ 0.44. MALDI-MS (*m*/*z*): $[M+Na]^+$ cald 1092.657 obsd 1092.904 $[M-H]^-$ cald 1069.664 obsd 1069.374

3,4,6–Tri-*O*-(2-naphthyl)methyl -2-acetamide-2-deoxy-α-D-glucopyranosyl-(1→6)- 1-*O*-allyl-2,3,4,5-tetra-*O*-(2-naphthyl)methyl -D-*myo*-inositol (4-39)

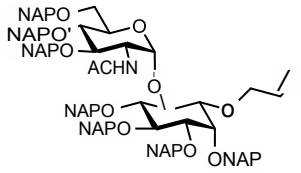

To the stirred solution triol **4-37** (0.3 g, 0.31 mmol) in anhydrous DMF (12 mL) was added NaH (0.045 g, 1.86 mmol) at 0 °C. After 20 min, NAPBr (0.27 g, 1.24 mmol) was added; the reaction was warmed to room temperature and stirred for 24 h. The reaction was quenched with MeOH and concentrated. The crude product was purified with flash chromatography to obtain **4-38** (0.35 g, 0.25 mmol, 82%). Activated zinc (0.1 g, 0.1 mmol) was suspended in THF and transferred to the pseudodisaccharide **4-38**. Ac_2O (0.03 mL, 0.33 mmol) and AcOH (0.006 mL, 0.011mmol) were added and reaction mixture was stirred at room temperature for 4 h. The reaction mixture is filtered through celite and washed with saturated $NaHCO_3$ twice. Organic phases were dried over Na_2SO_4 and concentrated. The crude residue was purified with flash column chromatography to obtain **4-39** (0.12 g, 0.086 mmol, 79%). R_f = 0.2 (EtOAc/hexane = 1:1) ^{1}H NMR (400 MHz, $CDCl_3$) δ 7.90 – 7.31 (m, 109H), 7.21 (ttd, *J* = 16.6, 8.3, 1.4 Hz, 4H), 5.74 – 5.60 (m, 1H), 5.44 (d, *J* = 3.4 Hz, 1H), 5.36 – 5.23 (m, 1H), 5.23 – 5.10 (m, 5H), 5.10 – 4.95 (m, 11H), 4.91 (dd, *J* = 23.6, 12.3 Hz, 5H), 4.88 – 4.57 (m, 5H), 4.50 (td, *J* = 10.1, 3.4 Hz, 1H), 4.45 – 4.20 (m, 5H), 4.23 – 4.01 (m, 4H), 3.98 – 3.78 (m, 5H), 3.77 – 3.55 (m, 7H), 3.54 – 3.44 (m, 3H), 3.26 (dd, *J* = 10.0, 2.0 Hz, 1H), 1.88 (s, 2H). ^{13}C NMR (101 MHz, $CDCl_3$) δ 169.95, 136.27, 136.18, 136.07, 135.87, 135.68, 135.58, 135.46, 133.32, 133.23, 133.18, 133.12, 133.00, 132.95, 132.91, 132.89, 132.83, 128.30, 128.13, 128.09, 128.04, 127.98, 127.94, 127.92, 127.86, 127.75, 127.68, 127.62, 126.65, 126.57, 126.44, 126.40, 126.27, 126.24, 126.19, 126.13, 126.10, 126.08, 126.03, 125.98, 125.90, 125.84, 125.81, 125.76, 125.66, 118.90, 116.02, 100.37, 83.16, 82.03, 81.10, 80.63, 79.95, 78.91, 78.45, 77.28, 75.90, 75.65, 75.05, 74.79, 74.30, 73.55, 73.17, 72.72, 72.12, 71.18, 68.81, 60.47, 53.47, 29.76, 23.47, 21.14, 14.26.

3,4,6–Tri-*O*-(2-naphthyl)methyl-2-acetamide-2-deoxy-α-D-glucopyranosyl-(1→6)-2,3,4,5-tetra-*O*-(2-naphthyl)methyl -D-*myo*-inositol (4-40)

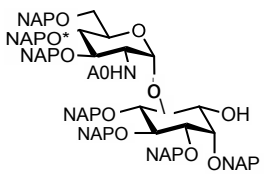

To a stirred solution of **4-39** (0.12 g, 0.086 mmol) in MeOH/ CH_2Cl_2 (3:1) was added $PdCl_2$ (6 mg, 0.034 mmol) at room temperature. The reaction was stirred for 12 h and quenched with Et_3N and concentrated. The crude residue was purified with flash column chromatography to obtain **4-40** (0.07 g, 0.05 mmol, 59%). R_f = 0.25 (EtOAc/hexane = 3:2) ^{1}H NMR (400 MHz,

$CDCl_3$) δ 7.80 – 7.68 (m, 17H), 7.70 – 7.63 (m, 13H), 7.61 (d, *J* = 8.6 Hz, 13H), 7.61 – 7.36 (m, 43H), 7.40 – 7.32 (m, 13H), 7.34 – 7.21 (m, 12H), 7.19 (s, 9H), 6.94 (dd, *J* = 8.4, 1.3 Hz, 2H), 6.04 (d, *J* = 9.1 Hz, 1H), 5.27 (d, *J* = 3.4 Hz, 1H), 5.16 (d, *J* = 11.8 Hz, 1H), 5.07 (d, *J* = 11.0 Hz, 2H), 5.05 – 4.60 (m, 17H), 4.44 (t, *J* = 12.4 Hz, 3H), 4.23 (td, *J* = 9.7, 3.4 Hz, 2H), 4.14 (t, *J* = 9.6 Hz, 2H), 4.05 (d, *J* = 12.3 Hz, 2H), 3.91 (d, *J* = 5.2 Hz, 3H), 3.74 (dt, *J* = 25.5, 9.1 Hz, 3H), 3.48 (d, *J* = 9.9 Hz, 1H), 3.37 – 3.30 (m, 6H), 3.26 (d, *J* = 9.1 Hz, 1H), 1.61 (s, 4H) ^{13}C NMR (101 MHz, $CDCl_3$) δ 170.20, 135.98, 135.88, 135.66, 135.42, 135.35, 133.21, 133.09, 132.87, 132.82, 128.68, 128.43, 128.10, 127.94, 127.91, 127.81, 127.76, 127.64, 127.14, 126.77, 126.61, 126.55, 126.49, 126.38, 126.32, 126.22, 126.11, 125.99, 125.96, 125.93, 125.85, 125.79, 125.73, 98.99, 81.45, 80.76, 80.31, 78.01, 77.25, 75.88, 75.04, 74.82, 74.63, 73.35, 72.57, 71.55, 68.16, 53.10, 23.35. ESI-MS (*m*/*z*): $[M+Na]^+$ cald 1385.6 obsd 1385.4, $[M+K]^+$ cald 1402.5 obsd 1402.4.

3,4,6–Tri-*O*-(2-naphthyl)methyl-2-acetamide-2-deoxy-α-D-glucopyranosyl-(1→6)- 1-*O*-(1-*O*-stearoyl-2-*O*-oleoyl-*sn*-glycerol)-phosphate-2,3,4,5-tetra-*O*-(2-naphthyl)methyl -D-*myo*-inositol (4-41)

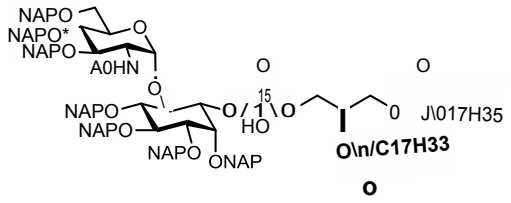

Disaccharide **4-40** (0.03 g, 0.022 mmol) and *H*-phosphonate **4-9** (0.045 g, 0.066 mmol) were co-evaporated with pyridine for three times and dried under high vacuum for 2 h. The mixture was dissolved in anhydrous pyridine (4 mL) and a solution of pivolyl chloride (0.007 mL, 0.064 mmol) in pyridine (0.5 mL) was added. The solution was stirred for 48 h at room temperature. After 48 h, reaction mixture is concentrated and redissolved in CH_2Cl_2. To the stirred solution of crude phosphonate in CH_2Cl_2 (5 mL) was added $BrCCl_3$ (0.03 g, 0.088 mmol) and Et_3N (0.03 g, 0.18 mmol) and the reaction was stirred for 3 h. Reaction mixture was concentrated and purified using Et_3N quenched flash column chromatography to obtain bilipidated disaccharide **4-41** (0.03 g, 0.013 mmol, 61%). R_f = 0.55 (MeOH/DCM = 2:9). ^{31}P NMR (162 MHz, $CDCl_3$) δ -1.55(-0.44 rotamer). MALDI-MS (*m*/*z*): $[M-H]^-$ cald 2048.617 obsd 2048.488.

2-acetamide-2-deoxy-α-D-glucopyranosyl-(1→6)- 1-*O*-(1-*O*-stearoyl-2-*O*-oleoyl-*sn*-glycerol)-phosphate-D-*myo*-inositol (4-5)

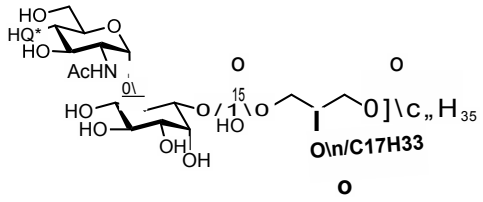

To the stirred solution of disaccharide **4-41** (0.02 g, 0.01 mmol) in a mixture of TFA/anisole (v/v = 10:2, 3.0 mL) at 0 ºC for 2 h, was warmed to room temperature and stirred for additional 3 h. The mixture was diluted with toluene (2 mL), concentrated. The crude product was purified by Sephadex LH-20 size exclusion chromatography ($CHCl_3$/MeOH/H_2O = 3:3:1) to give the pseudodisaccharide **4-5** (8.3 mg, 0.008 mmol, 80%). ^{31}P NMR (162 MHz, MeOD) δ 0.09, MALDI-MS (*m*/*z*): $[M+Na]^+$ cald 1090.641 obsd 1090.670, $[M+2Na-H]^+$ cald 1112.623 obsd 1112.646, $[M+Na+K-H]^+$ cald 1128.597 obsd 1128.621.

3,4,6–Tri-*O*-benzyl-2-azido-2-deoxy-α-D-glucopyranosyl-(1→6)-1-*O*-[1,2-*O*-(8-methylhexadecanoyl)-*sn*-glycerol]-phosphate-2,3,4,5-tetra-*O*-benzyl-D-*myo*-inositol (4-42)

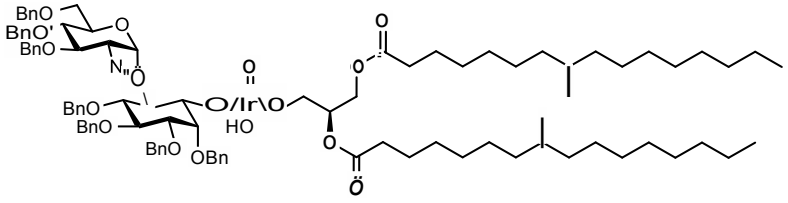

Disaccharide **4-7a** (0.03 g, 0.03 mmol) and *H*-phosphonate **4-10** (0.06 g, 0.09 mmol) were co-evaporated with pyridine for three times and dried under high vacuum for 2 h. The mixture was dissolved in anhydrous pyridine (5 mL) and a solution of pivolyl chloride (0.01 mL, 0.09 mmol) in pyridine (1 mL) was added. The solution was stirred for 48 h at room temperature. After 48 h, iodine (0.04 g, 0.15 mmol) and water (0.2 mL) were added and reaction was stirred for 4 h. The reaction mixture was quenched with $Na_2S_2O_3$ and extracted with CH_2Cl_2. The organic layer were concentrated and purified with Et_3N quenched flash column chromatography to obtain bilipidated disaccharide **4-42** (0.03 mg, 0.003 mmol, 55%)**.** R_f = 0.6 (MeOH/DCM = 1:9) ^{1}H NMR (400 MHz, $CDCl_3$) δ 7.43 (dd, *J* = 22.7, 7.9 Hz, 2H), 7.34

(s, 5H), 7.31 (d, *J* = 5.8 Hz, 7H), 7.25 (d, *J* = 12.9 Hz, 8H), 7.06 (s, 2H), 5.25 (dt, *J* = 11.7, 5.8 Hz, 1H), 5.05 – 3.95 (m, 23H), 3.78 – 3.21 (m, 8H), 3.07 – 2.96 (m, 3H), 2.29 (dq, *J* = 12.3, 7.5 Hz, 5H), 1.63 – 1.56 (m, 7H), 1.30 (d, *J* = 7.2 Hz, 43H), 1.12 – 1.06 (m, 7H), 0.91 (t, *J* = 6.6 Hz, 6H), 0.85 (dd, *J* = 6.3, 2.8 Hz, 8H).^{31}P NMR (162 MHz, $CDCl_3$) δ -1.87. MALDI-MS (*m*/*z*): $[M+Na]^+$ cald 1678.9 obsd 1678.4.

2-amino-2-deoxy-α-D-glucopyranosyl-(1→6)-1-*O*-[1,2-*O*-(8-methylhexadecanoyl)-*sn*-glycerol]-phosphate-D-*myo*-inositol (4-6)

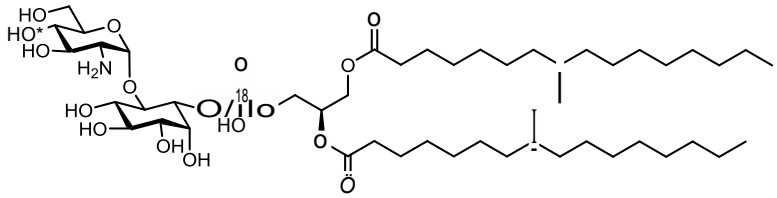

To the stirred solution of pseudodisaccharide **4-42** (21.0 mg, 0.013 mmol) in mixture of CH_2Cl_2/MeOH/H_2O (3:3:1, 5 mL) at room temperature was added $Pd(OH)_2$ on C (17 mg, 0.024 mmol, 20% Pd content). Hydrogen gas was bubbled through the solution for 15 min and the reaction mixture was stirred under an atmosphere of hydrogen gas for additional 24 h. The $Pd(OH)_2$ was removed by filtration through a pad of celite and the solution was concentrated. The crude product was purified by LH20 size exclusion chromatography with CH_2Cl_2/MeOH/H_2O (3:3:1) as the solvent mixture to obtain the bilipidated disaccharide **4-6** (6.6 mg, 0.007 mmol, 52%). ^{1}H NMR (400 MHz, MeOD) δ 5.50 (d, *J* = 31.7 Hz, 1H), 5.28 (s, 1H), 4.44 (d, *J* = 11.7 Hz, 3H), 4.26 – 4.16 (m, 3H), 4.09 (s, 3H), 4.04 – 3.91 (m, 2H), 3.84 (d, *J* = 10.6 Hz, 3H), 3.71 (dd, *J* = 14.4, 10.2 Hz, 1H), 3.50 – 3.38 (m, 4H), 3.18 (q, *J* = 7.3 Hz, 2H), 2.35 (dt, *J* = 15.3, 7.5 Hz, 6H), 1.61 (s, 4H), 1.29 (d, *J* = 11.2 Hz, 44H), 1.13 – 1.07 (m, 7H), 0.90 (d, *J* = 6.6 Hz, 6H), 0.85 (d, *J* = 6.5 Hz, 9H). ^{13}C NMR (101 MHz, MeOD) δ 174.30, 174.01, 95.34, 77.84, 77.52, 77.20, 73.05, 72.53, 72.32, 70.97, 70.15, 69.77, 62.79, 54.13, 46.57, 37.02, 34.15, 34.04, 32.69, 31.83, 29.92, 29.68, 29.61, 29.58, 29.26, 29.13, 26.98, 24.90, 24.81, 22.56, 19.48, 19.43, 13.81, 13.77, 8.30, 6.74, -19.42. ^{31}P NMR (162 MHz, MeOD) δ 0.04. ESI-MS (*m*/*z*): $[M+H]^+$ cald 1000.633 obsd 1000.860, $[M]^-$ cald 999.626 obsd 999.180.

4.7.3 Material and Methods for Biophysical Studies

For the monolayer experiments, 1 mM solutions of all the fragments were prepared in a mixture of chloroform (Merck, Germany; purity >99.8%), methanol (Merck, Germany; purity >99.9%) and ultrapure water (Millipore, resistivity of 18 MΩ cm) in a 6:2:0.2 volume ratios.

Surface Pressure – Area Isotherms

The pressure/area (π/A) isotherms were recorded during compression of the monolayer on a computer-interfaced Langmuir trough (R&K, Potsdam, Germany) including a surface pressure microbalance with filter paper Wilhelmy plate. The results were plotted as surface pressure (π) versus the area per molecule. The bare water surface was checked for purity by compression before each measurement. The temperature of the Milli-Q Millipore water subphase was maintained at 20 °C by an external thermostat. The Langmuir layers were prepared by spreading the chloroform: methanol: water solutions of the fragments at the air/water interface. Before compression, the monolayers were left to equilibrate for 15 minutes in order to allow the evaporation of the spreading solvents. Each measurement was repeated at least two times to prove the reproducibility of results. In order to avoid dust contamination of the interface and to ensure a constant humidity, the Langmuir trough was placed in a sealed box.

Grazing Incidence X-ray Diffraction (GIXD)

The grazing incidence X-ray diffraction measurements were carried out at the undulator beamline P08 using the Langmuir trough GID setup at PETRA III, DESY (Hamburg, Germany). The setup is equipped with a temperature controlled Langmuir trough (R&K, Potsdam, Germany), which is enclosed in a sealed, helium-filled container. The synchrotron X-ray beam is monochromated to an energy of 15 keV (wavelength of 0.827 Å) and is adjusted to strike the helium/water interface at a grazing incidence angle α_i = 0.07° illuminating approximately 1 × 50 mm^2 of the monolayer surface. A MYTHEN detector (DECTRIS Ltd., Switzerland) measures the diffracted signal and is rotated to scan the in-plane Q_{xy} component values of the scattering vector. A Soller collimator in front of the MYTHEN restricted the in-plane divergence of the diffracted beam to 0.09°. The vertical strips of the MYTHEN measure the out-of-plane Q_z component of the scattering vector between 0.0 and 0.75 $Å^{-1}$. The diffraction data consist of Bragg peaks at diagnostic Q_{xy} values obtained by summing the diffracted intensity over a defined vertical angle or Q_z-window. The in-plane lattice repeat distances d of the ordered structures in the monolayer are calculated

from the Bragg peak positions: $d = 2\pi/Q_{xy}$. To estimate the extent of the crystalline order in the monolayer, the in-plane coherence length L_{xy}, is approximated from the full-width at half-maximum (fwhm) of the Bragg peaks using $L_{xy} \sim 0.9(2\pi)/\text{fwhm}(Q_{xy})$ using the measured fwhm(Q_{xy}) corrected for the instrumental resolution. Integrating the diffracted intensity normal to the interface over the Q_{xy} window of the diffraction peak yields he corresponding Bragg rod. The thickness of the scattering unit is estimated from the fwhm of the Bragg rod using $0.9(2\pi)/\text{fwhm}(Q_z)$.

Infrared Reflection Absorption Spectroscopy (IRRAS)

Infrared reflection absorption spectra were recorded using the Vertex 70 FT-IR spectrometer (Bruker, Germany), equipped with a liquid-nitrogen cooled MCT detector and coupled to a Langmuir film balance, which was placed in a sealed container (an external air/water reflection unit (XA 5 511, Bruker)) to guarantee a constant vapor atmosphere. Using a KRS-5 (thallium bromide and iodide mixed crystal) wire grid polarizer, the IR-beam was polarized parallel (p) or vertical (s) and focused on the fluid subphase at an angle of incidence of 40°. A computer controlled 'trough shuttle system' enables us to choose between the compartment with the sample (subphase with spread layer) and a reference compartment (pure subphase). The single-beam reflectance spectrum from the reference trough was taken as background for the single-beam reflectance spectrum of the monolayer in the sample trough to calculate the reflection absorption spectrum as -log(R/R0) in order to eliminate the water vapor signal. FTIR spectra were collected at a resolution of 8 cm^{-1} using 200 scans for s-polarized light and 400 scans for p-polarized light.

5 Appendix

5.1 NMR Spectra for Chapter 2

2-Methyl-5-tert-butylphenyl-3,4,6-Tetra-*O*-acetyl-2-deoxy-2-*N*-phthalimido-1-thio-β-D-glucopyranoside (2-10)

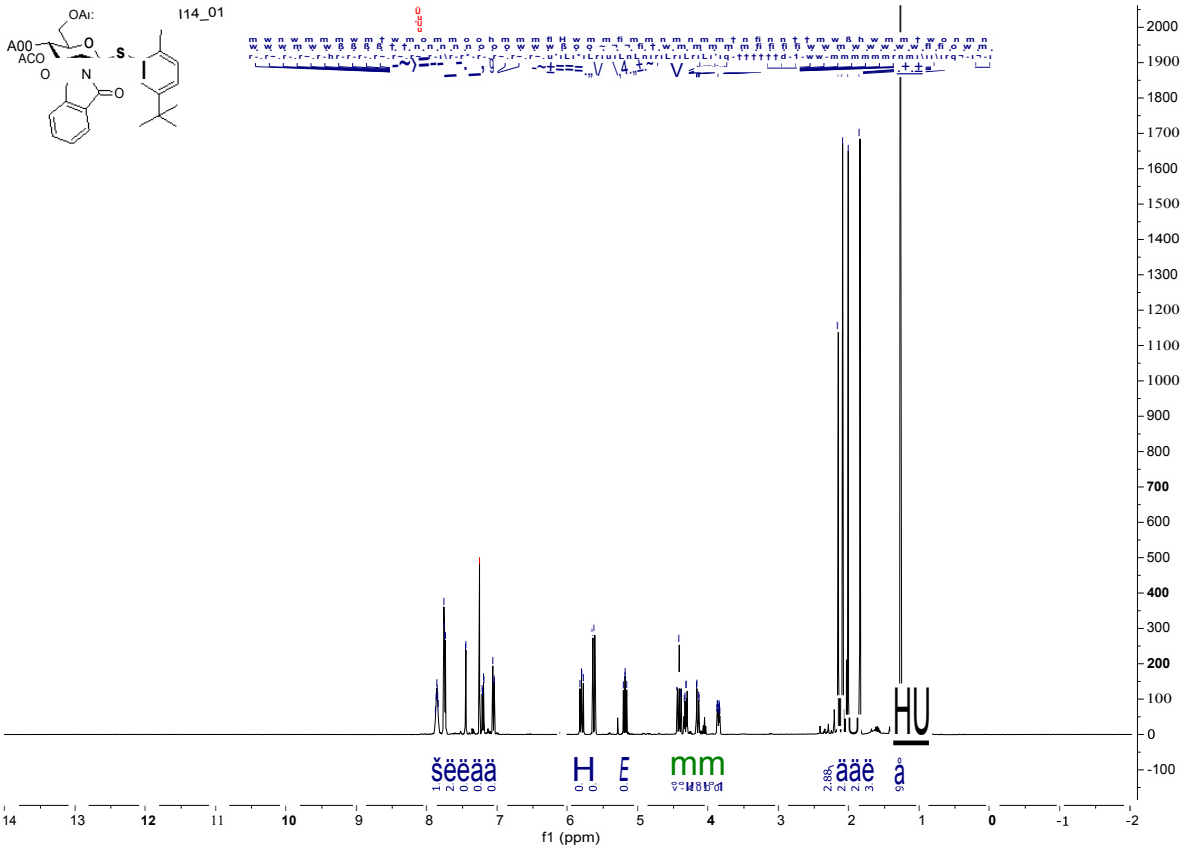

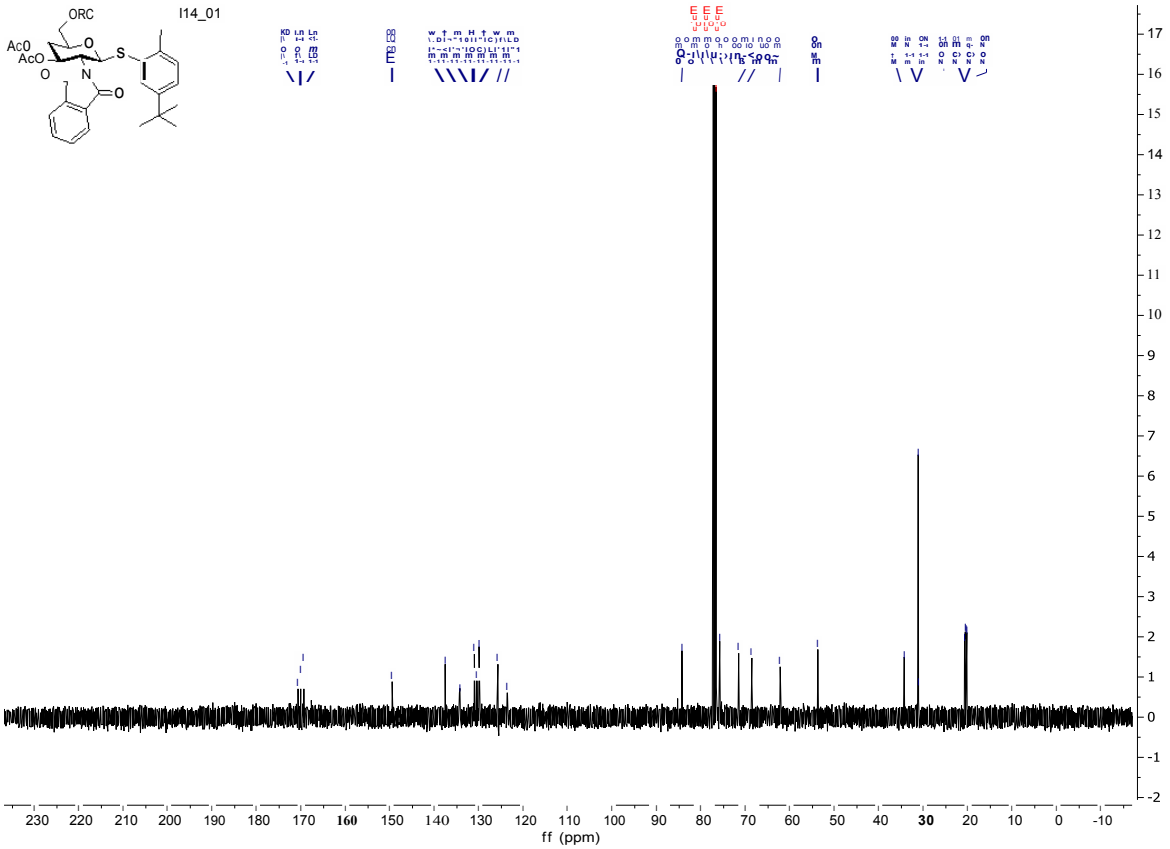

2-Methyl-5-tert-butylphenyl-4,6-*O*-benzylidene-2-deoxy-2-*N*-phthalimido-1-thio-β-D-glucopyranoside (2-11)

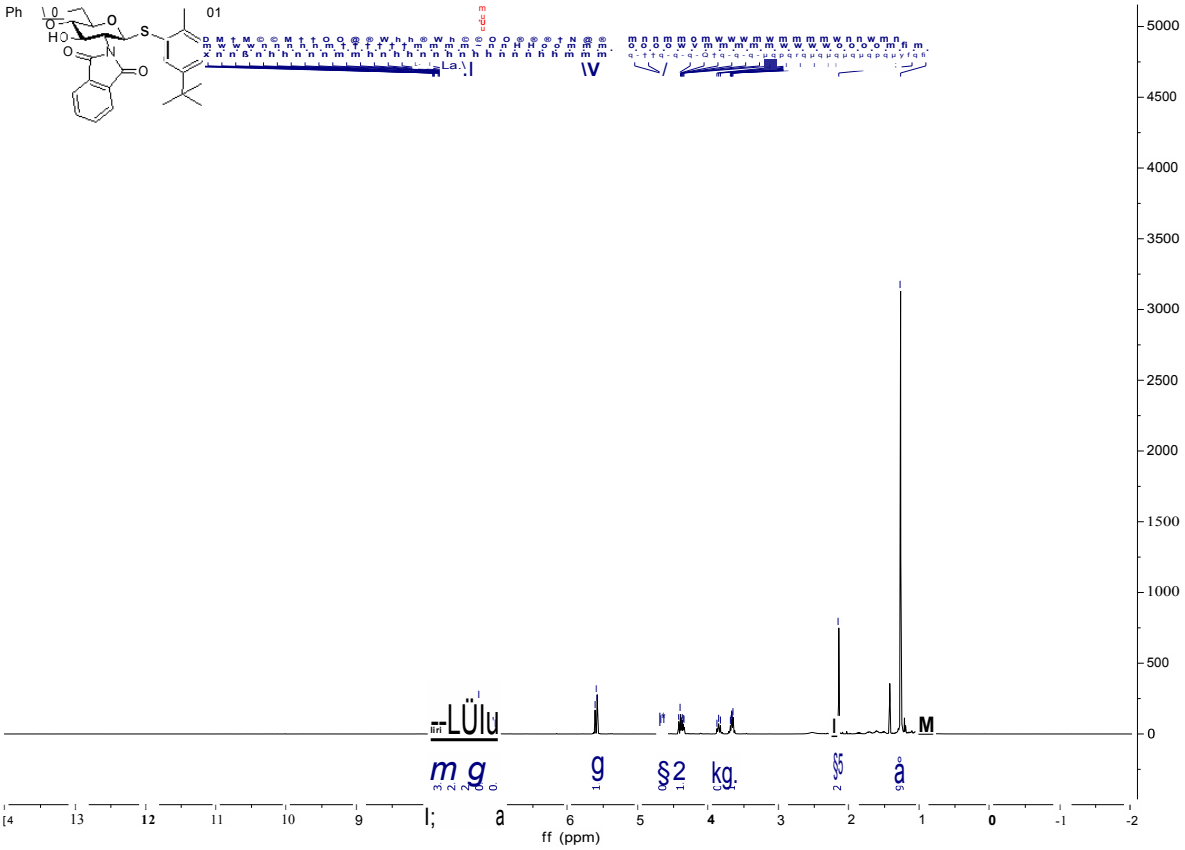

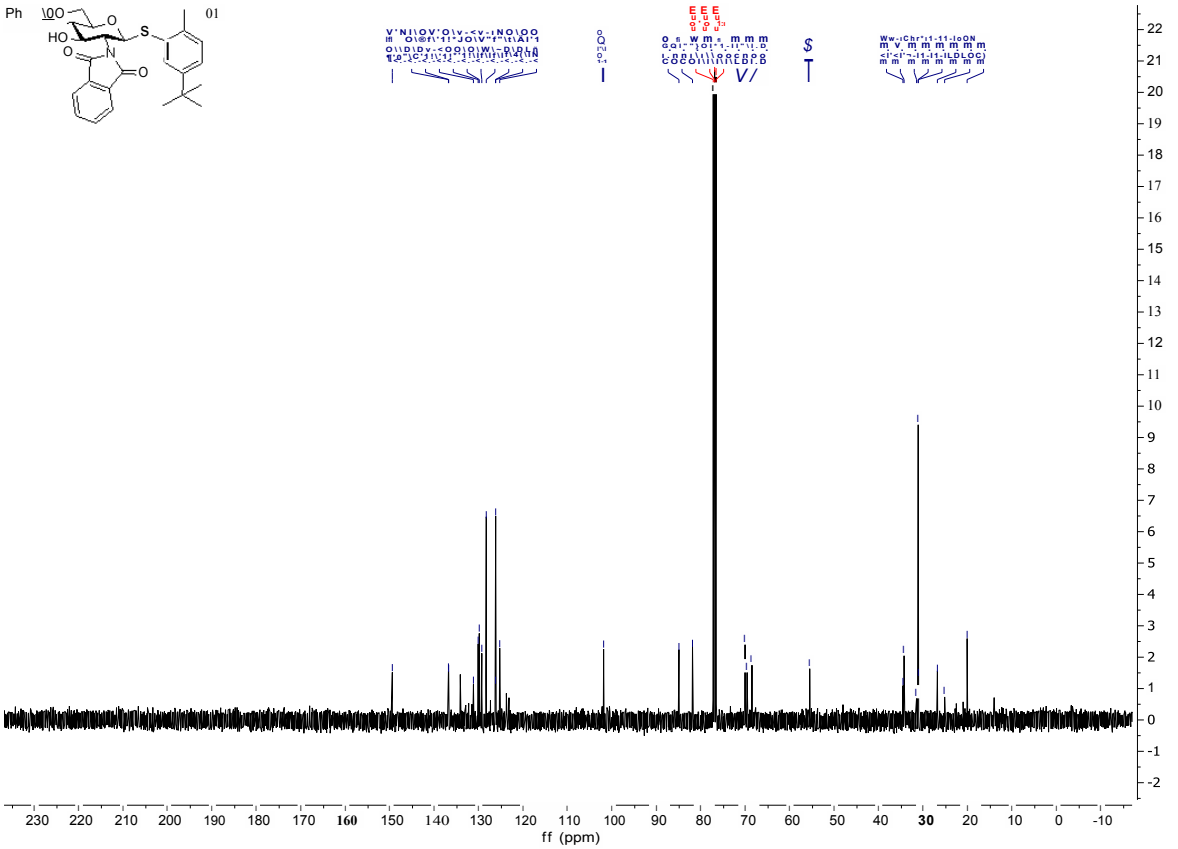

2-Methyl-5-tert-butylphenyl-3-*O*-benzyl-4,6-*O*-benzylidene-2-deoxy-2-*N*-phthalimido-1-thio-β-D-glucopyranoside (2-12)

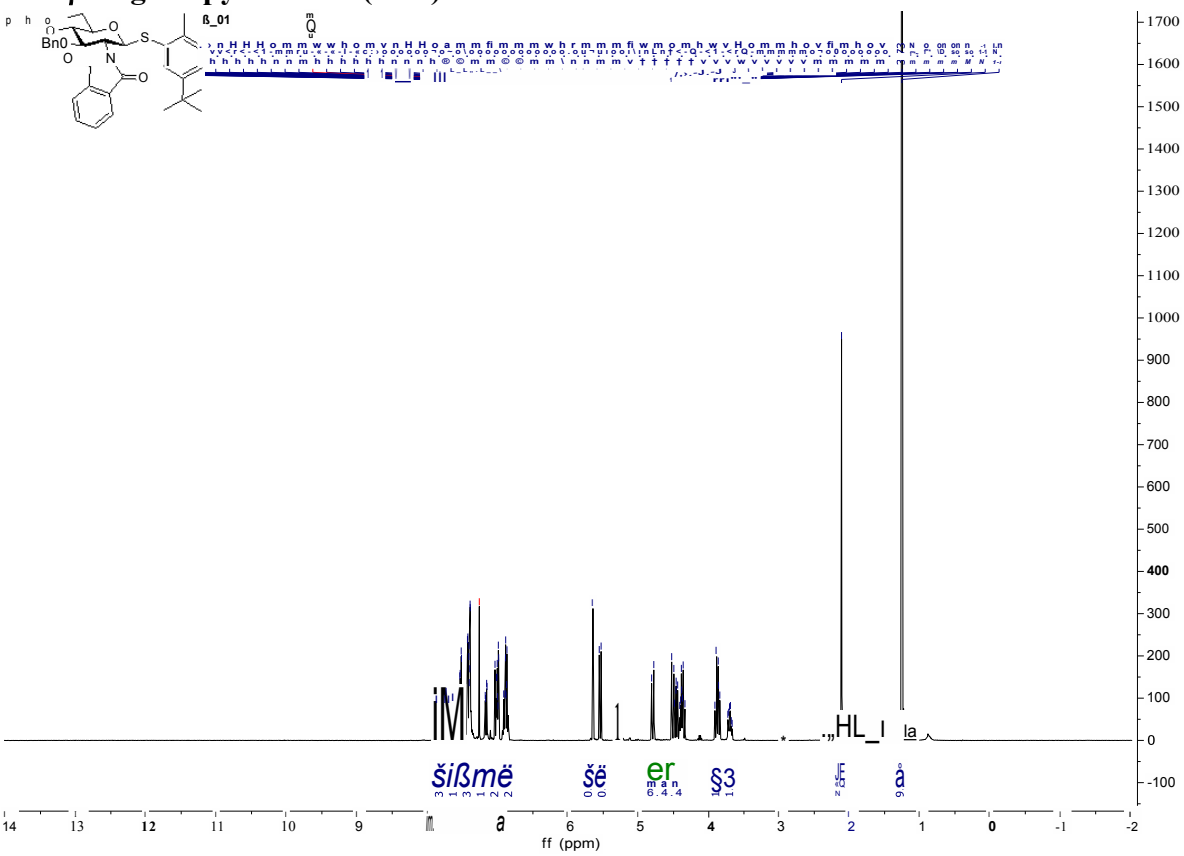

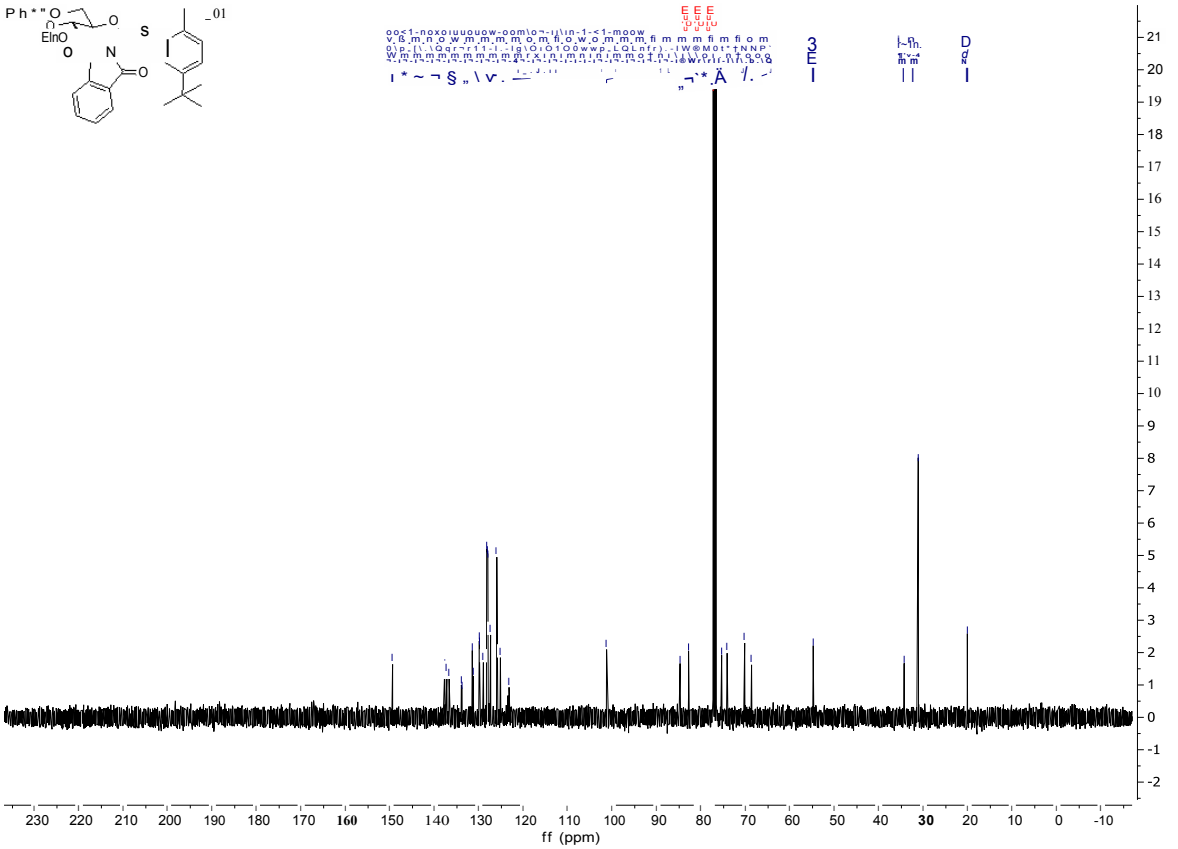

3-*O*-benzyl-4,6-*O*-benzylidene-2-deoxy-2-*N*-phthalimido-β-D-glucopyranosyl trichloroacetimidate (2-13)

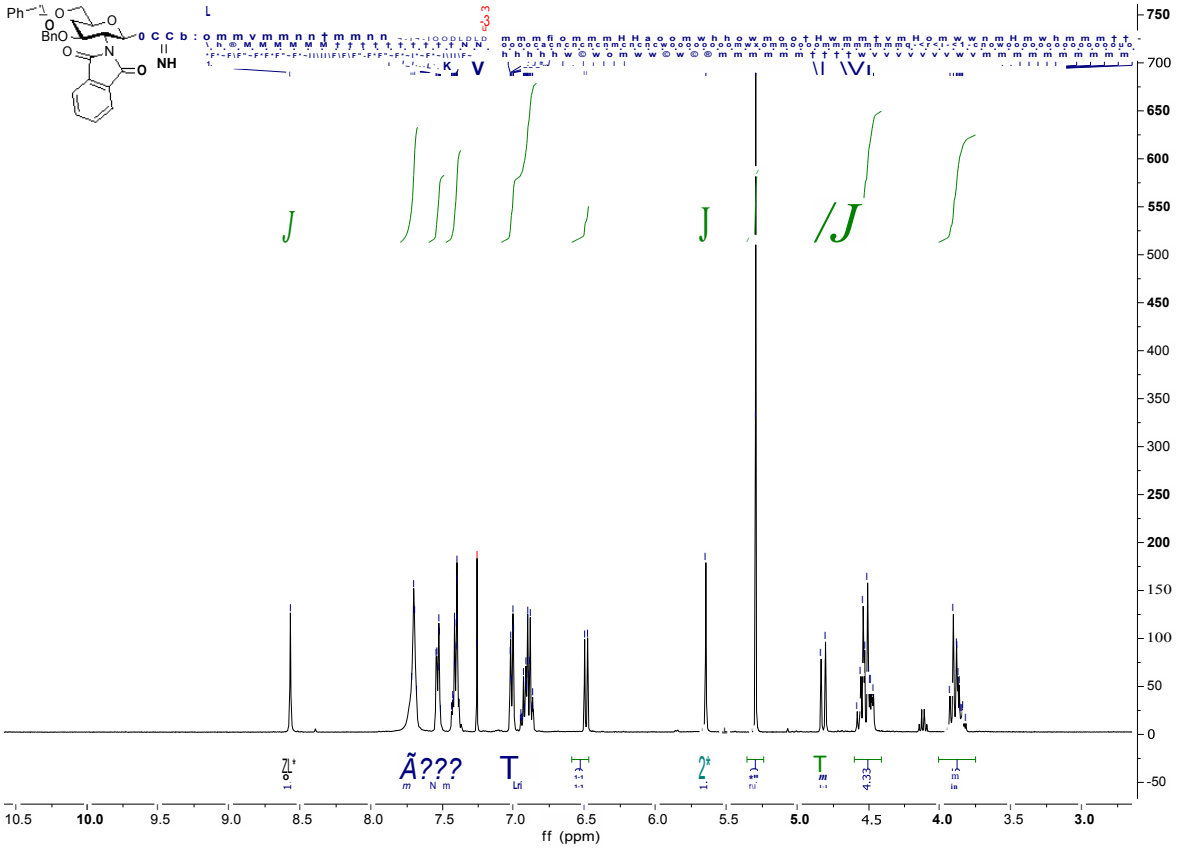

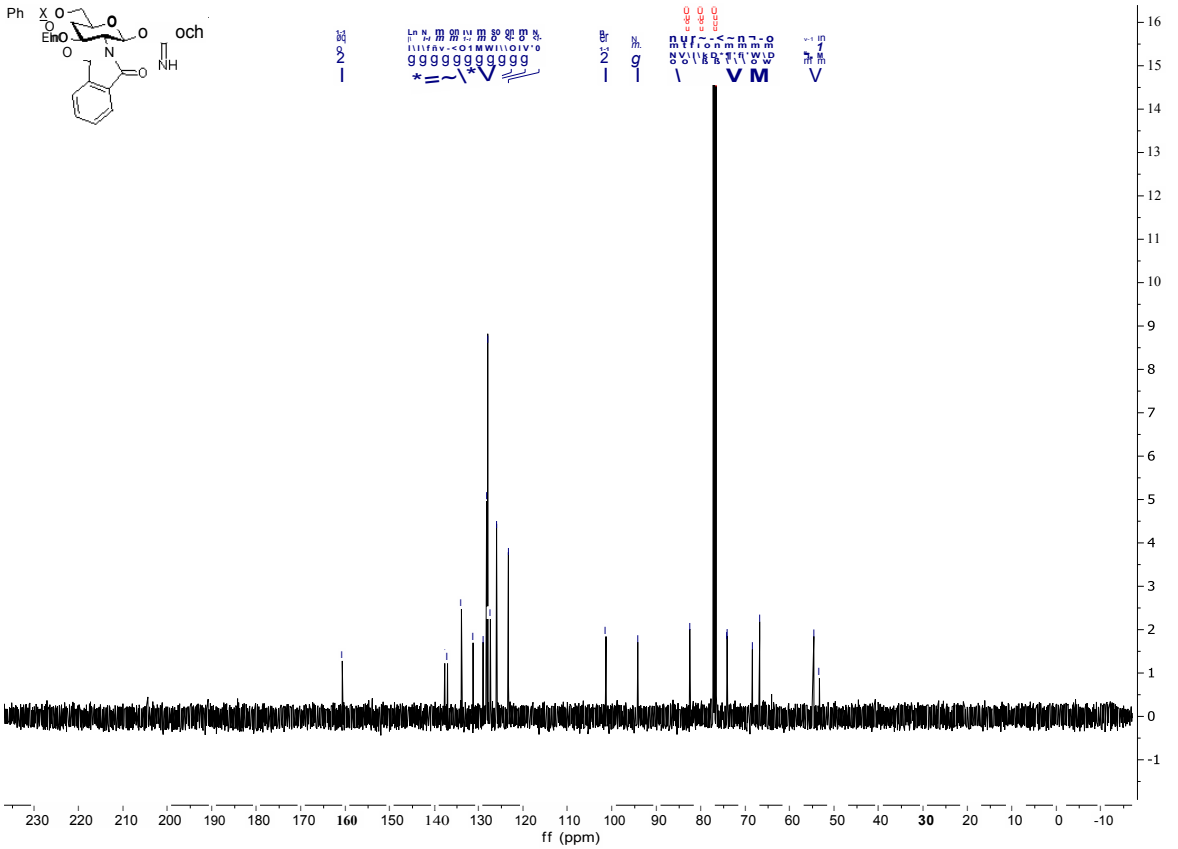

1-*O*-(6-thiobenzyl)hexyl-3-*O*-benzyl-4,6-*O*-benzylidene-2-deoxy-2-*N*-phthalimido-β-D-glucopyranoside (2-8)

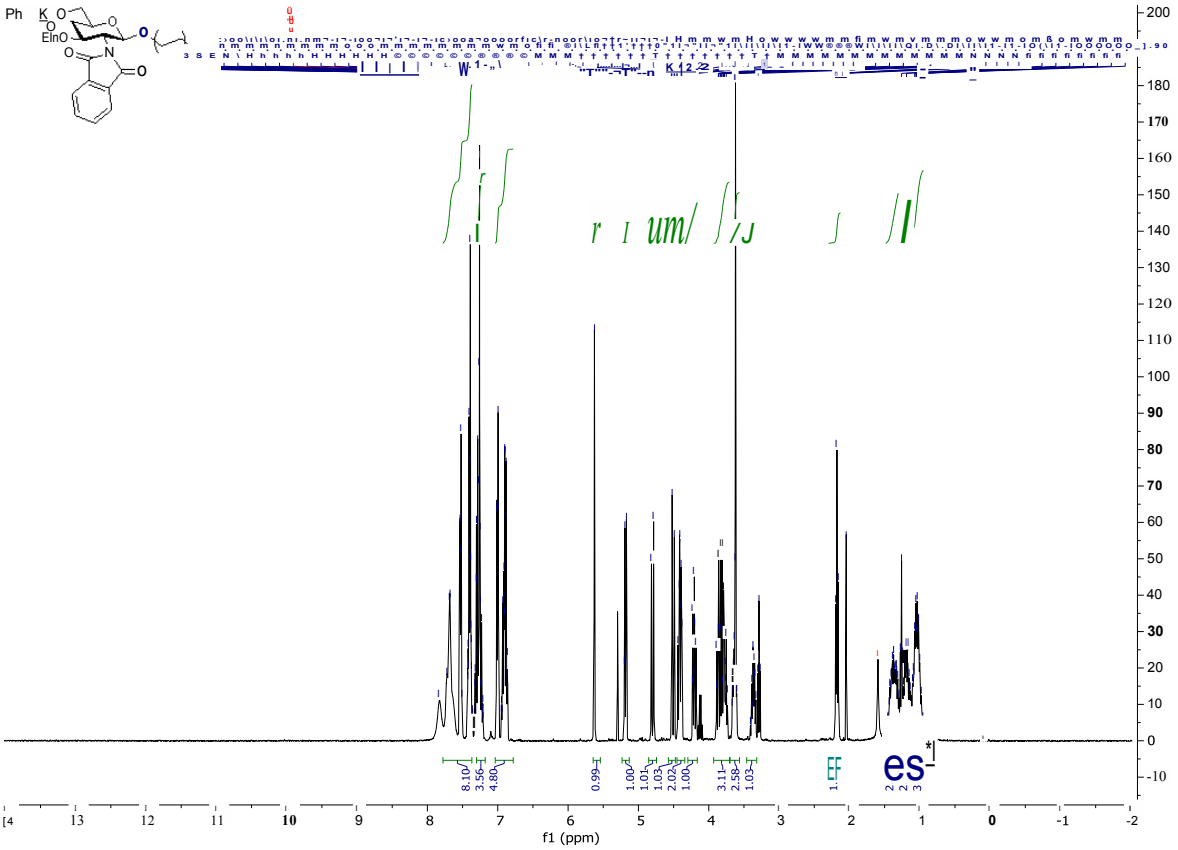

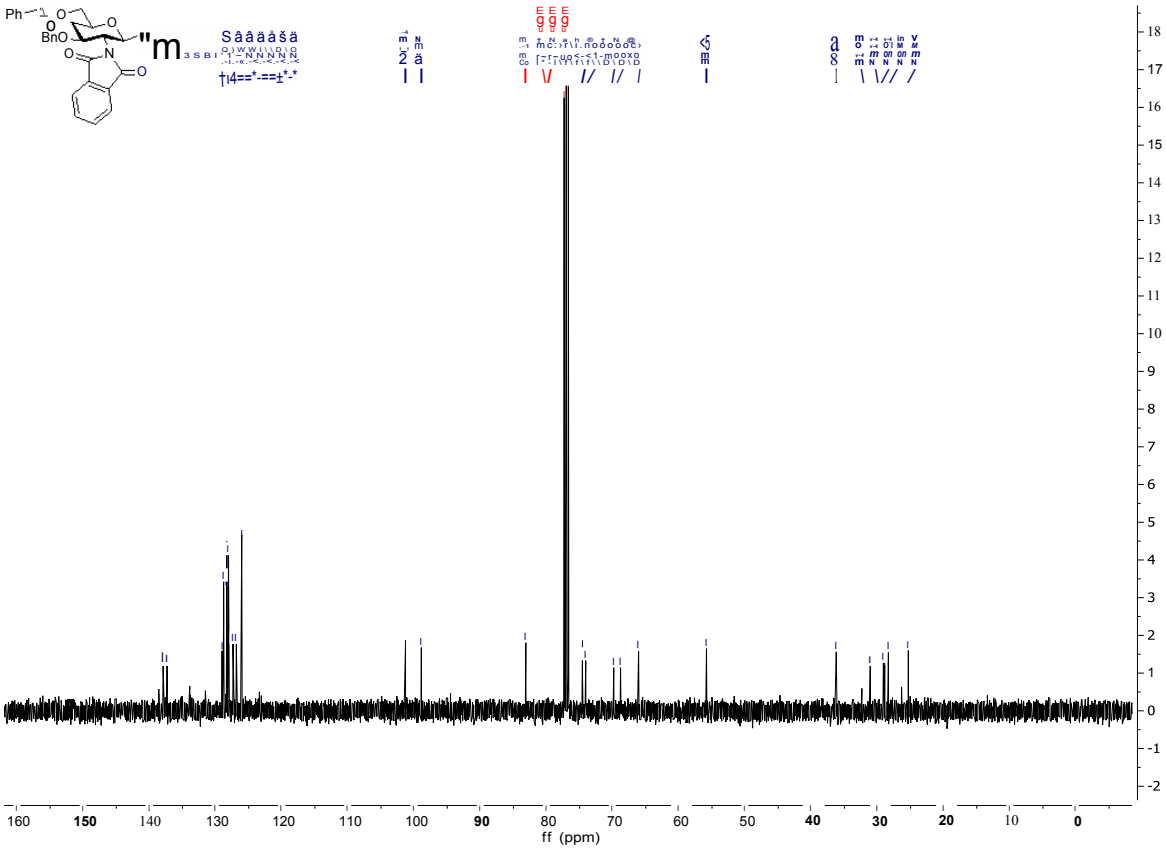

1-*O*-(6-thiobenzyl)hexyl-3,6-*O*-benzyl-2-deoxy-2-*N*-phthalimido-β-D-glucopyranoside (2-14)

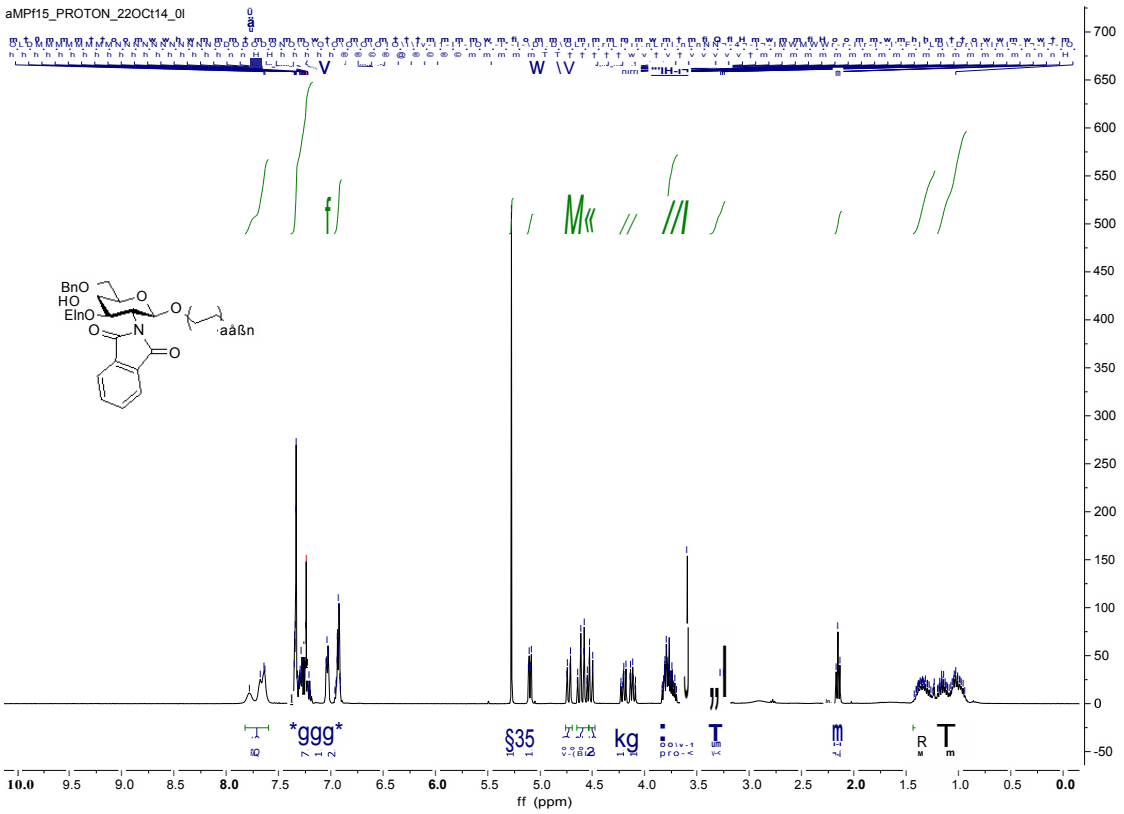

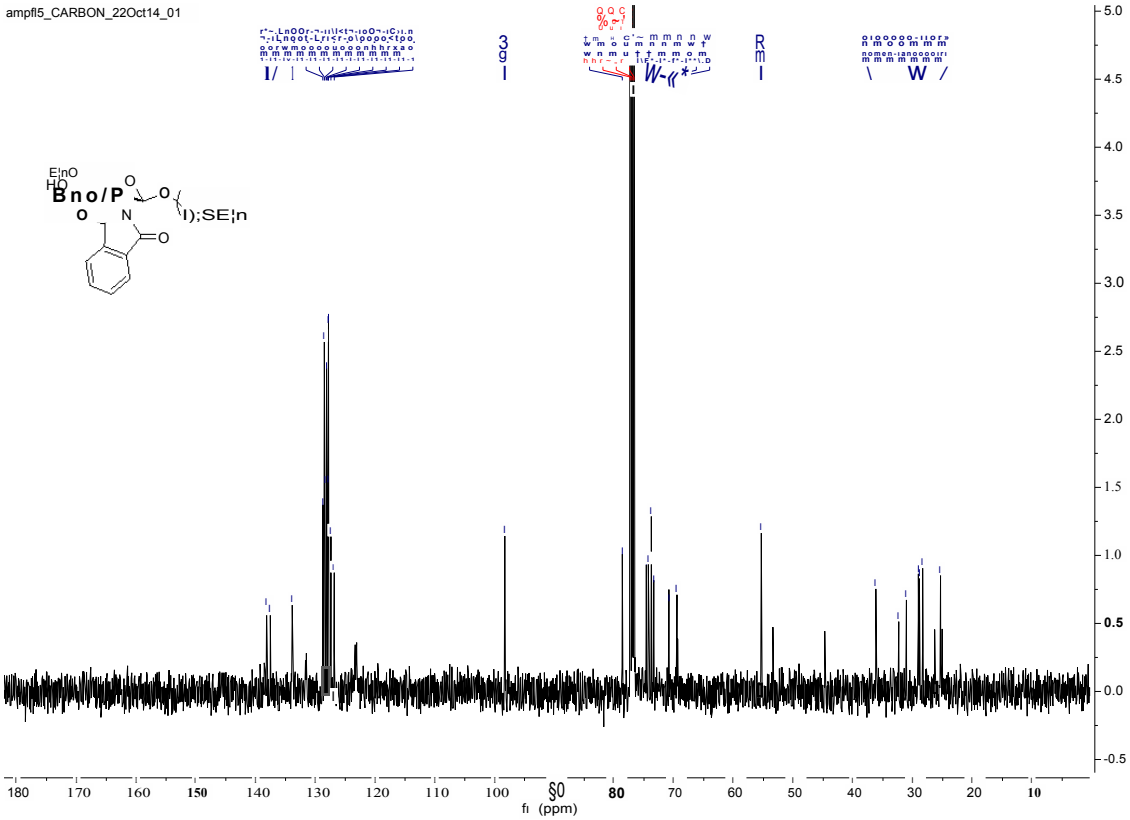

2-*O*-Acetyl-3,4-di-*O*-benzyl-6-*O*-triisopropylsilyl-α-D-mannopyranosyl-(1→4)-1-*O*-(6-thiobenzyl)hexyl-3,6-*O*-benzyl-2-deoxy-2-*N*-phthalimido-β-D-glucopyranoside (2-4)

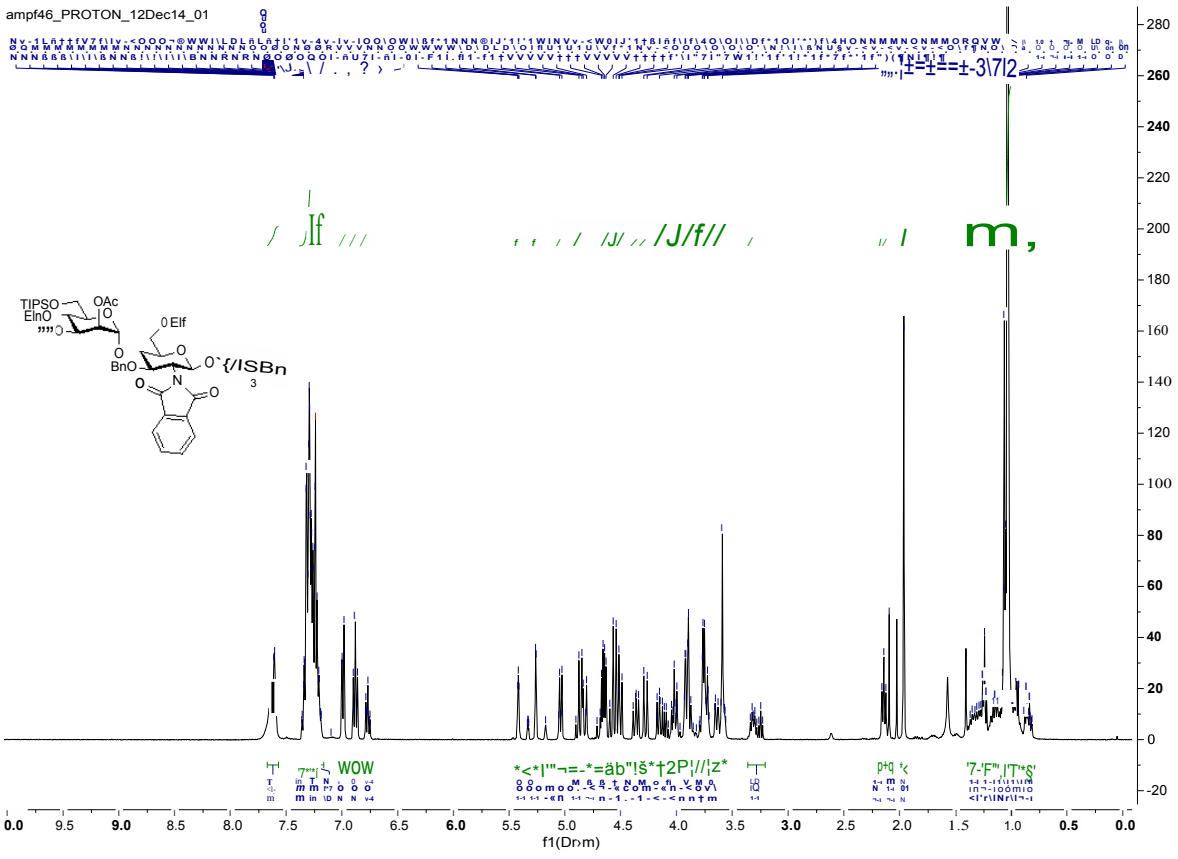

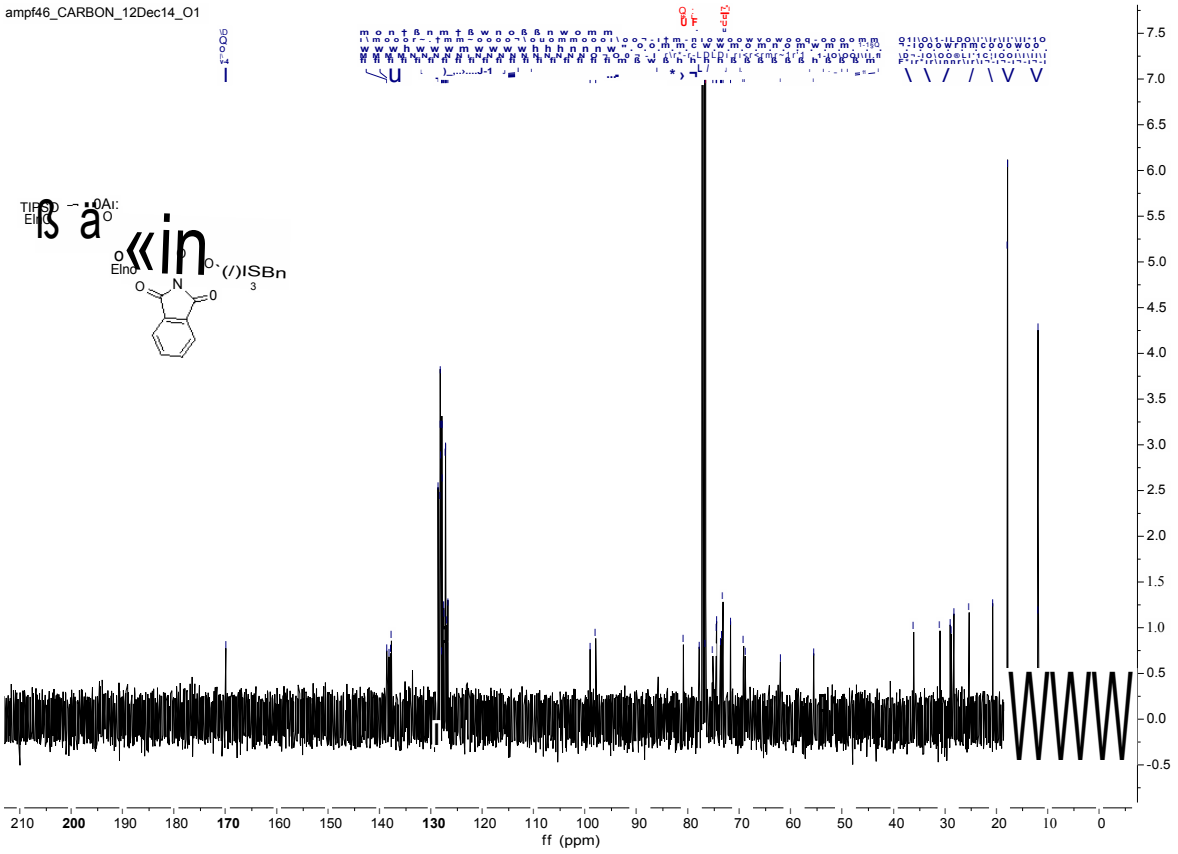
ampf46_CARBON_12Dec14_O1
ff (ppm)

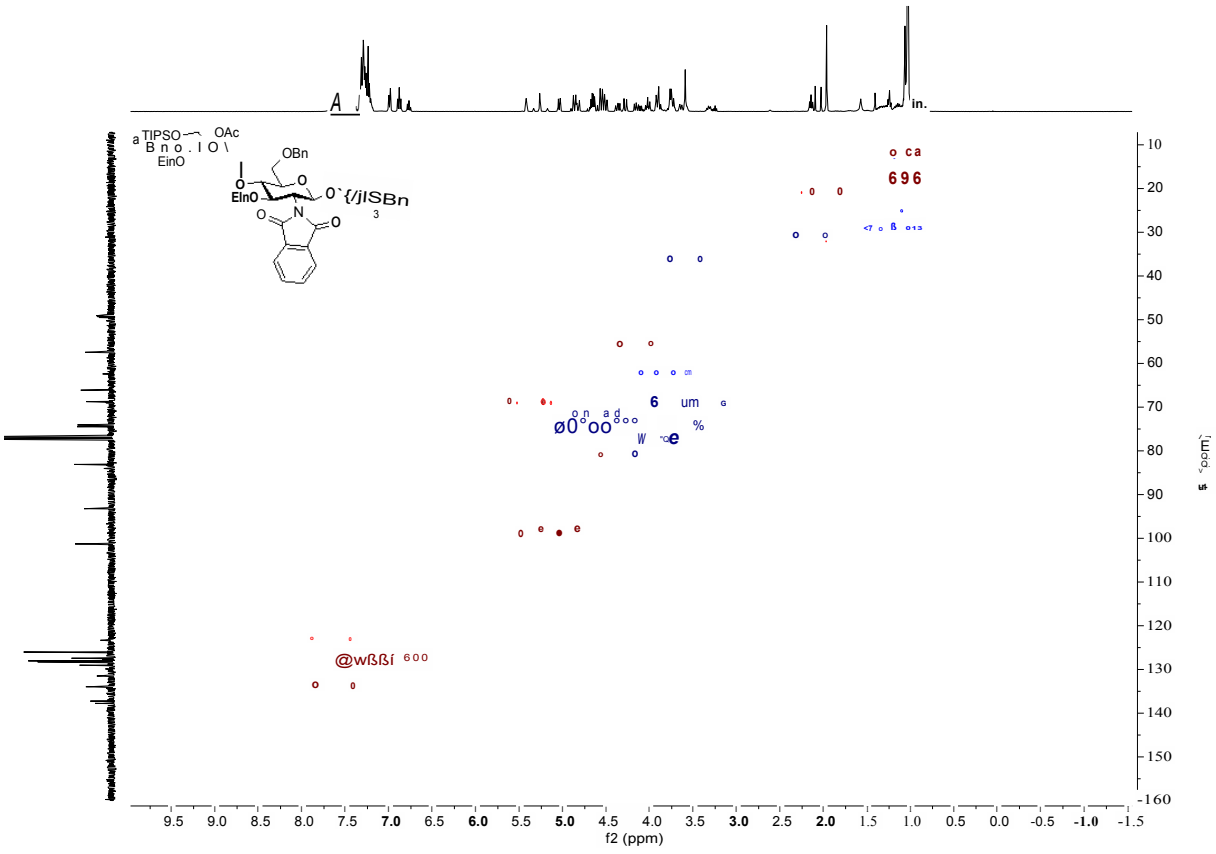
f2 (ppm)

2-*O*-Acetyl-3,4-di-*O*-benzyl-α-D-mannopyranosyl-(1→4)- 1-*O*-(6-thiobenzyl)hexyl-3,6-*O*-benzyl-2-deoxy-2-*N*-phthalimido-β-D-glucopyranoside (2-15)

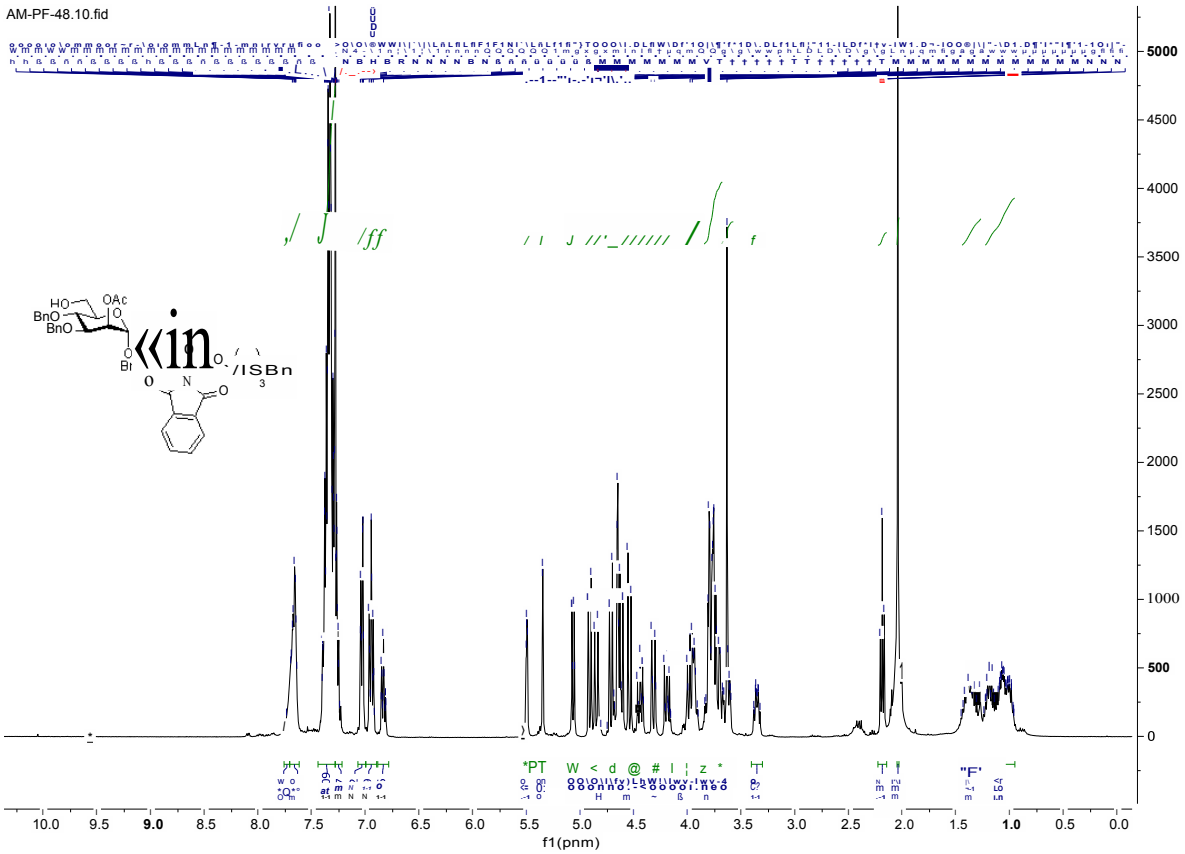

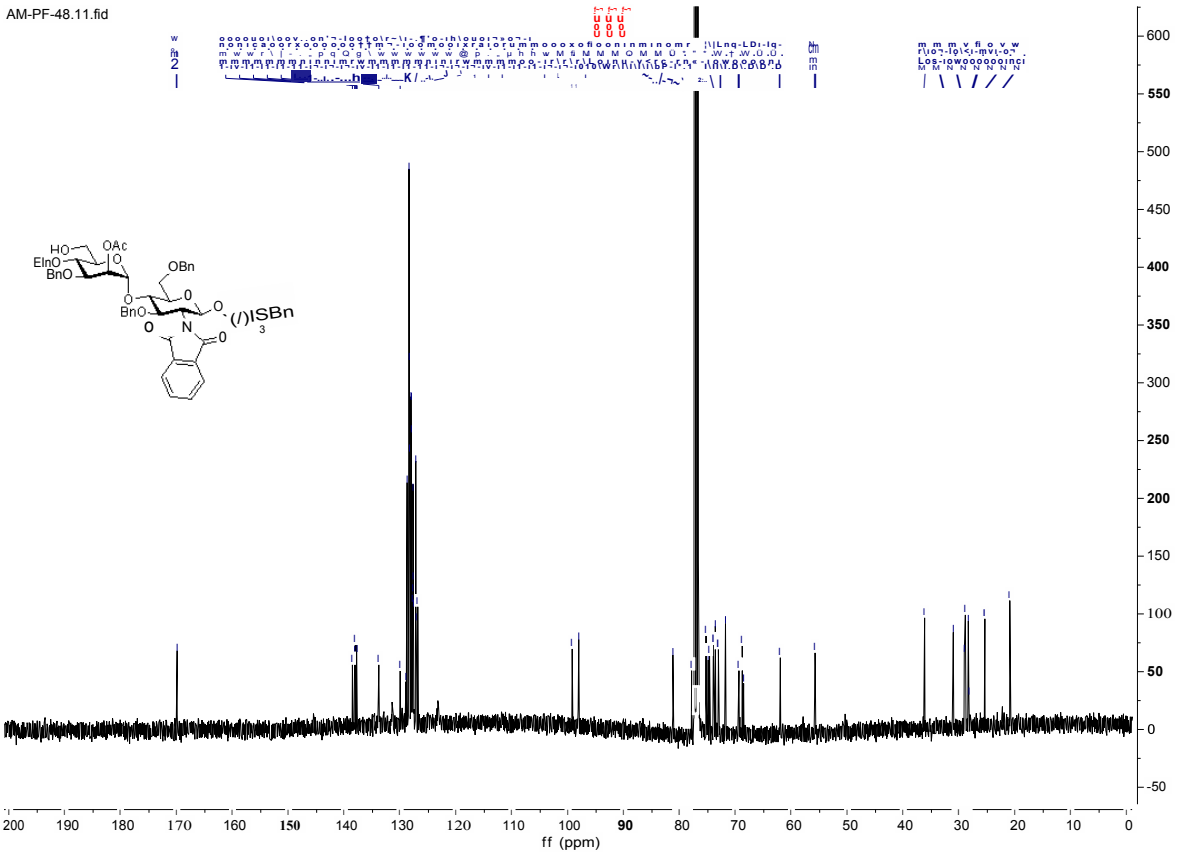

_n_-Allyl-2-_O_-acetyl-3,4-di-_O_-benzyl-6-_O_-tri*iso*propylsilyl-α-D-mannopyranosyl-(1→2)-3,4,6-tri-_O_-benzyl-α-D-mannopyranoside (2-17)

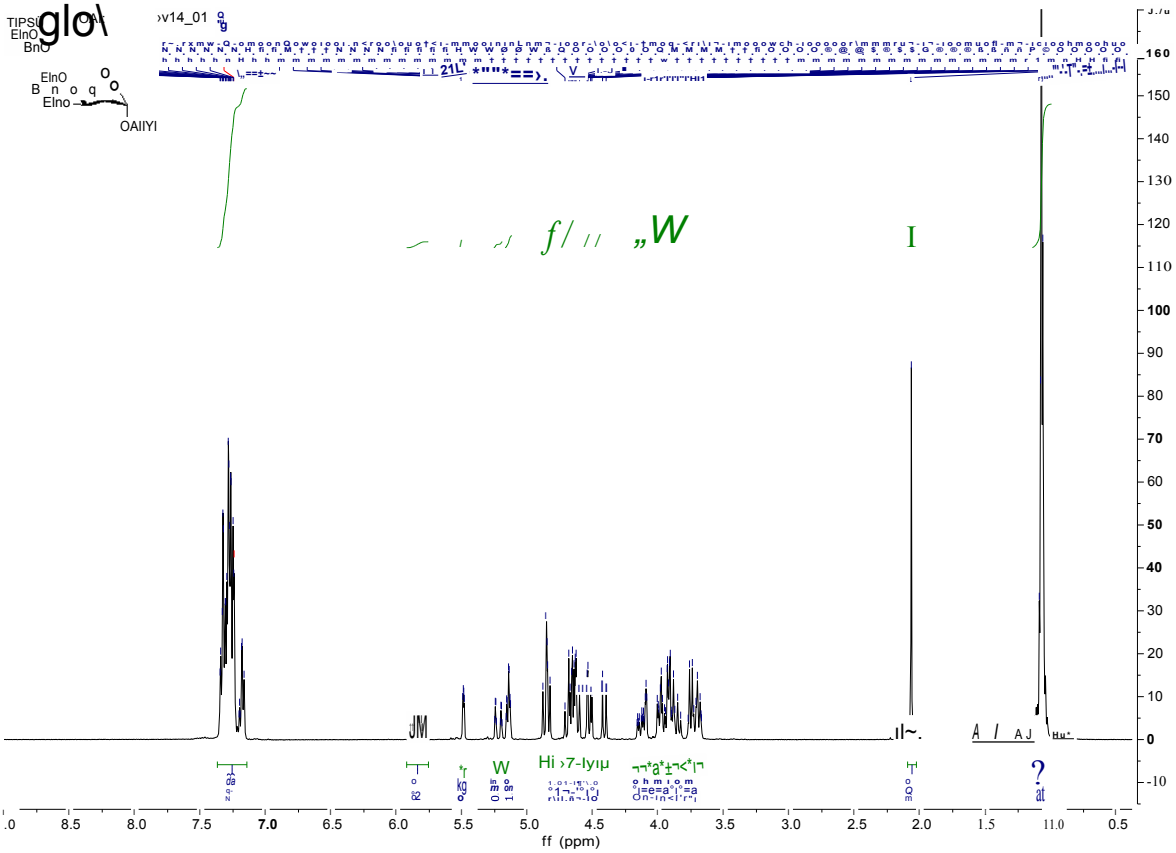

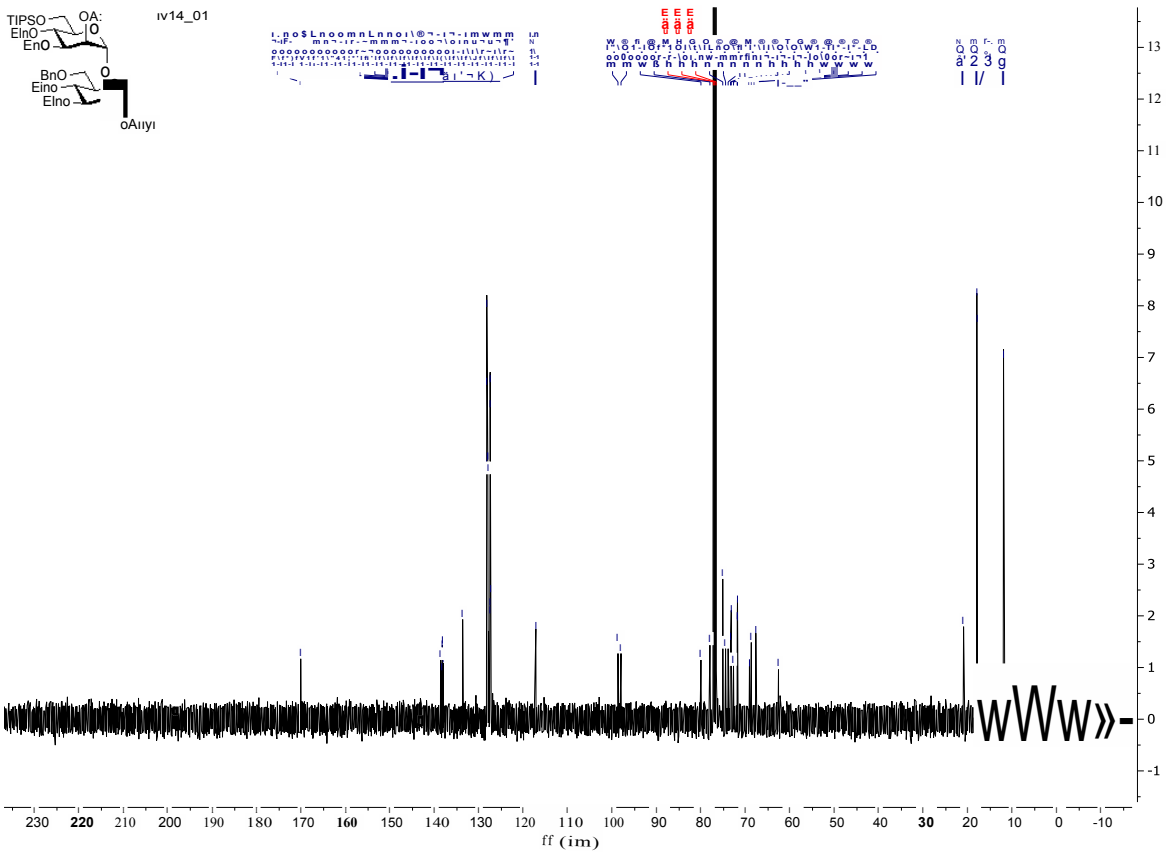

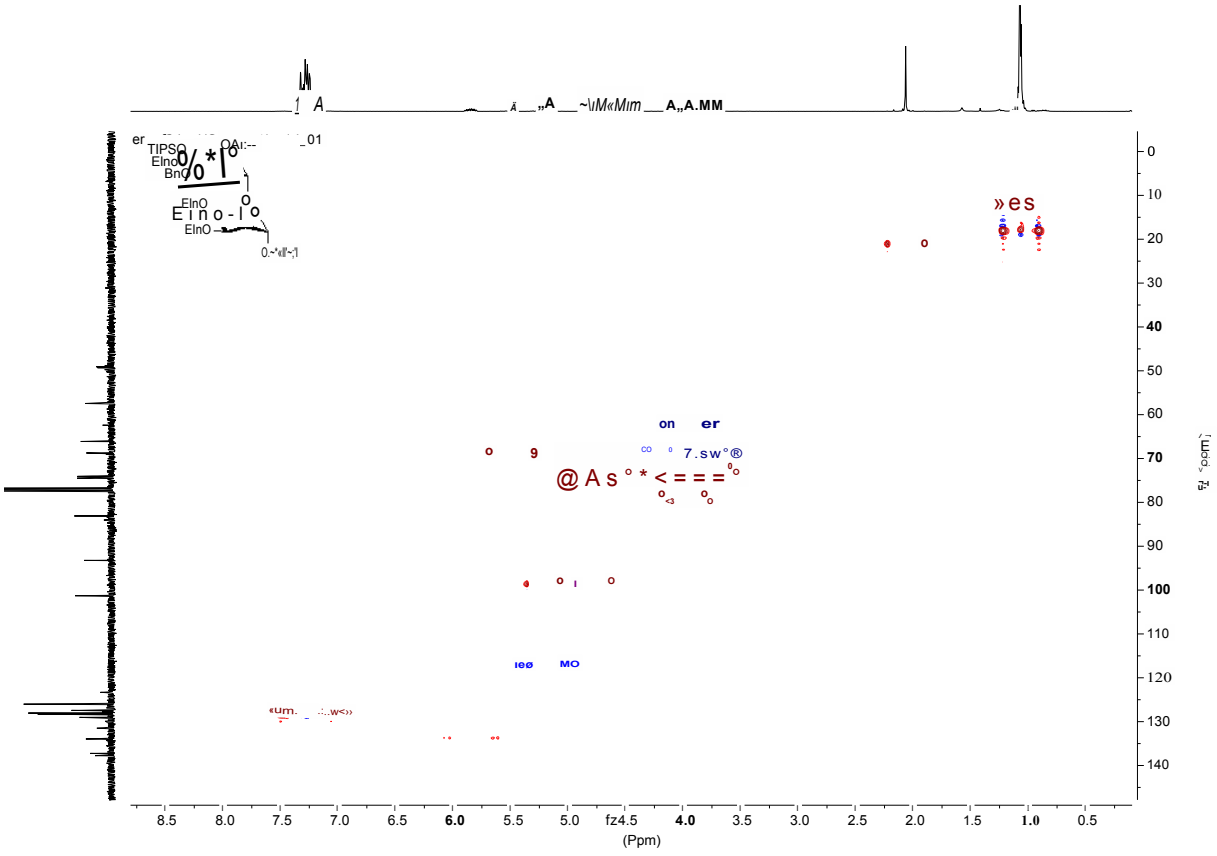
TIPSO
ElnO
BnO
ElnO
ElnO
»es
@As°*<===°
7.sw°®
8.5
8.0
7.5
7.0
6.5
6.0
5.5
5.0
fz4.5
4.0
3.5
3.0
2.5
2.0
1.5
1.0
0.5
(Ppm)
0
10
20
30
40
50
60
70
80
90
100
110
120
130
140

1-*O*-(6-thiobenzyl)hexyl-2-*O*-acetyl-3,4-di-*O*-benzyl-6-*O*-tri*iso*propylsilyl-α-D-mannopyranosyl-(1→2)-3,4,6-tri-*O*-benzyl-α-D-mannopyranosyl-(1→6)-2-*O*-Acetyl-3,4-di-*O*-benzyl-α-D-mannopyranosyl-(1→4)-3,6-*O*-benzyl-2-deoxy-2-*N*-phthalimido-β-D-glucopyranoside (2-19)

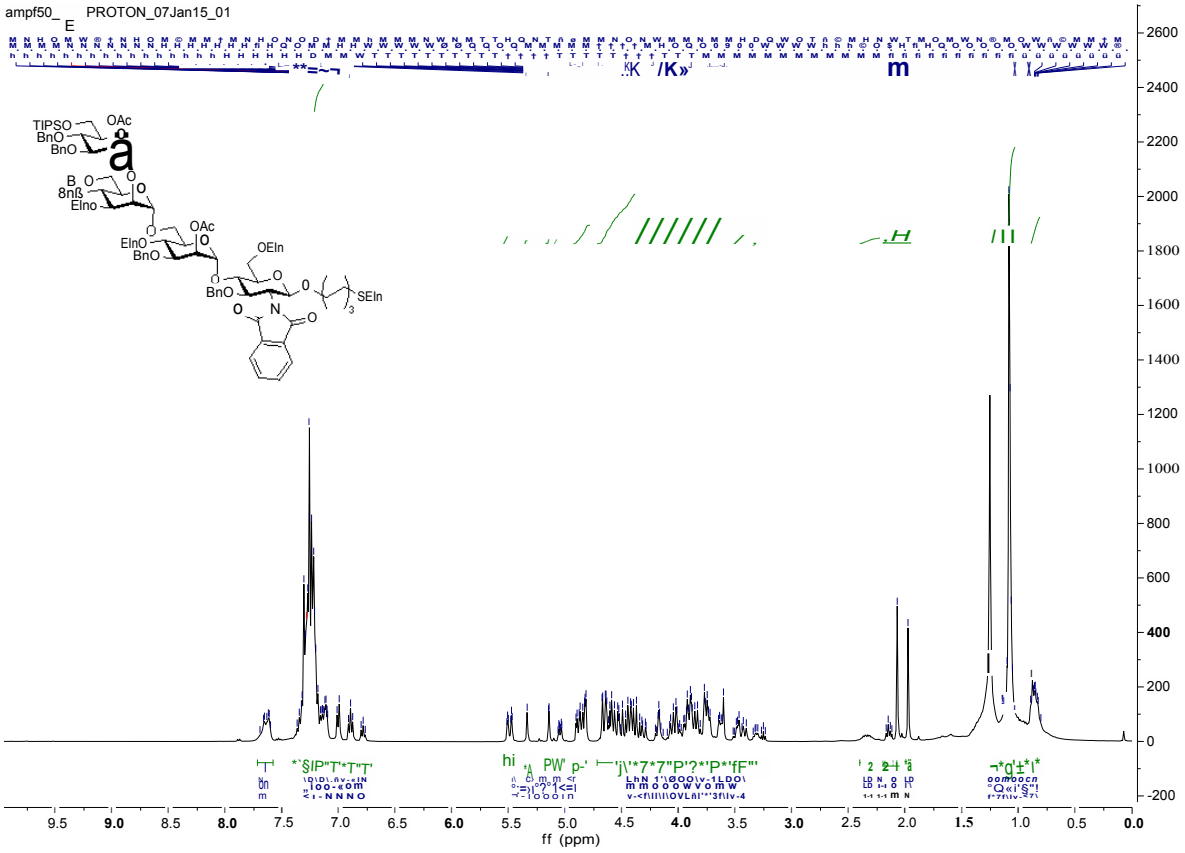

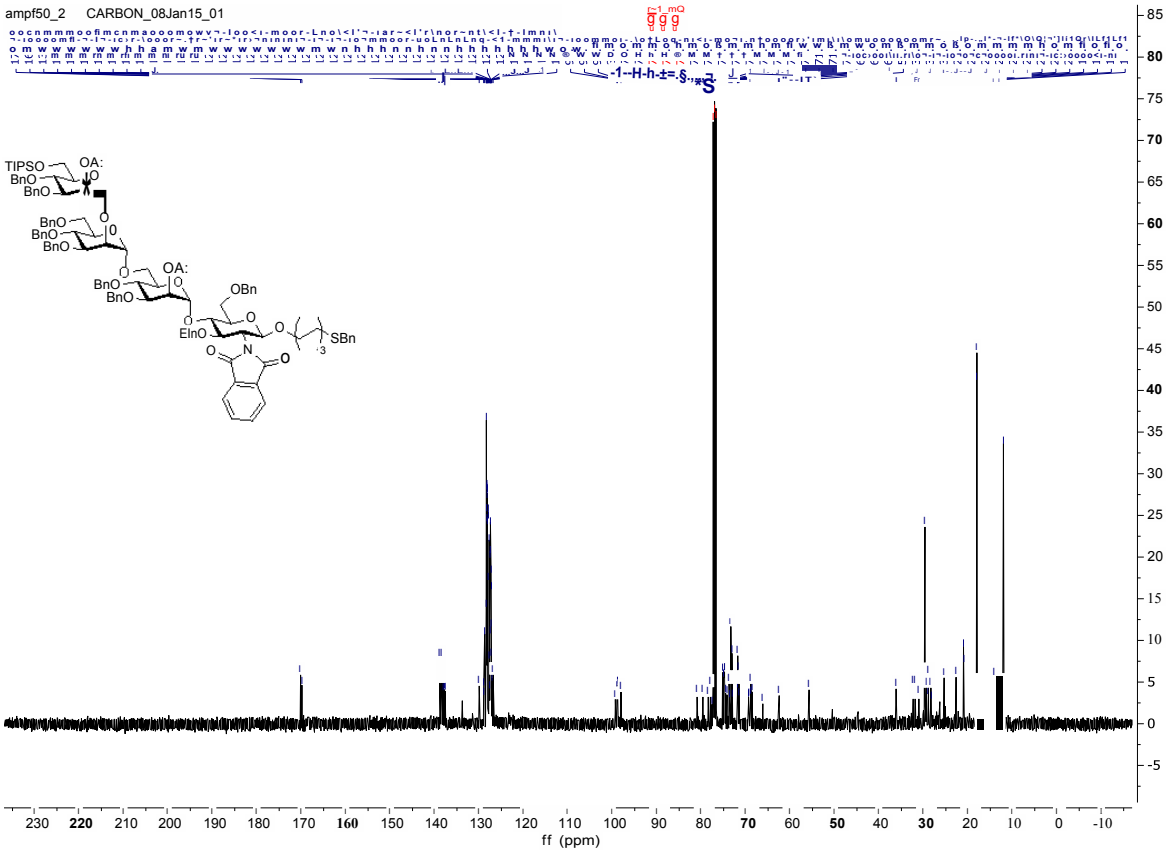
ampf50_2 CARBON_08Jan15_01
TIPSO
OA:
BnO
OBn
ElnO
SBn
ff (ppm)

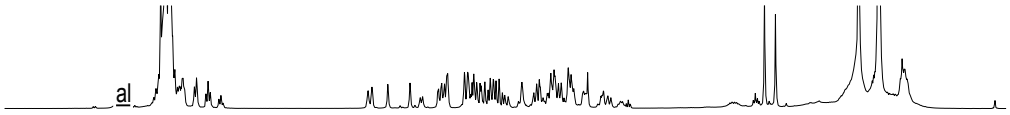
al

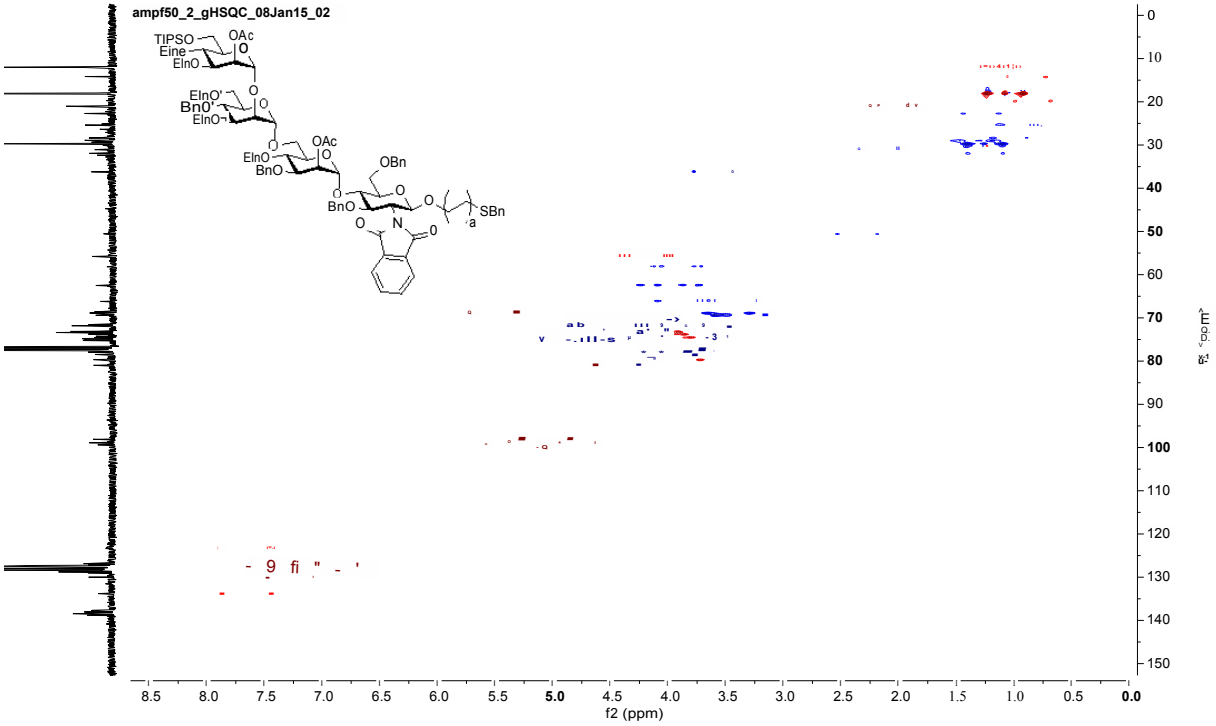
ampf50_2_gHSQC_08Jan15_02
TIPSO
OAc
Eine
ElnO
ElnO'
Bno'
OBn
SBn
f2 (ppm)

1-*O*-(6-thiobenzyl)hexyl-2-*O*-acetyl-3,4-di-*O*-benzyl-α-D-mannopyranosyl-(1→2)-3,4,6-tri-*O*-benzyl-α-D-mannopyranosyl-(1→6)-2-*O*-Acetyl-3,4-di-*O*-benzyl-α-D-manno pyranosyl-(1→4)-3,6-*O*-benzyl-2-deoxy-2-*N*-phthalimido-β-D-glucopyranoside (2-20)

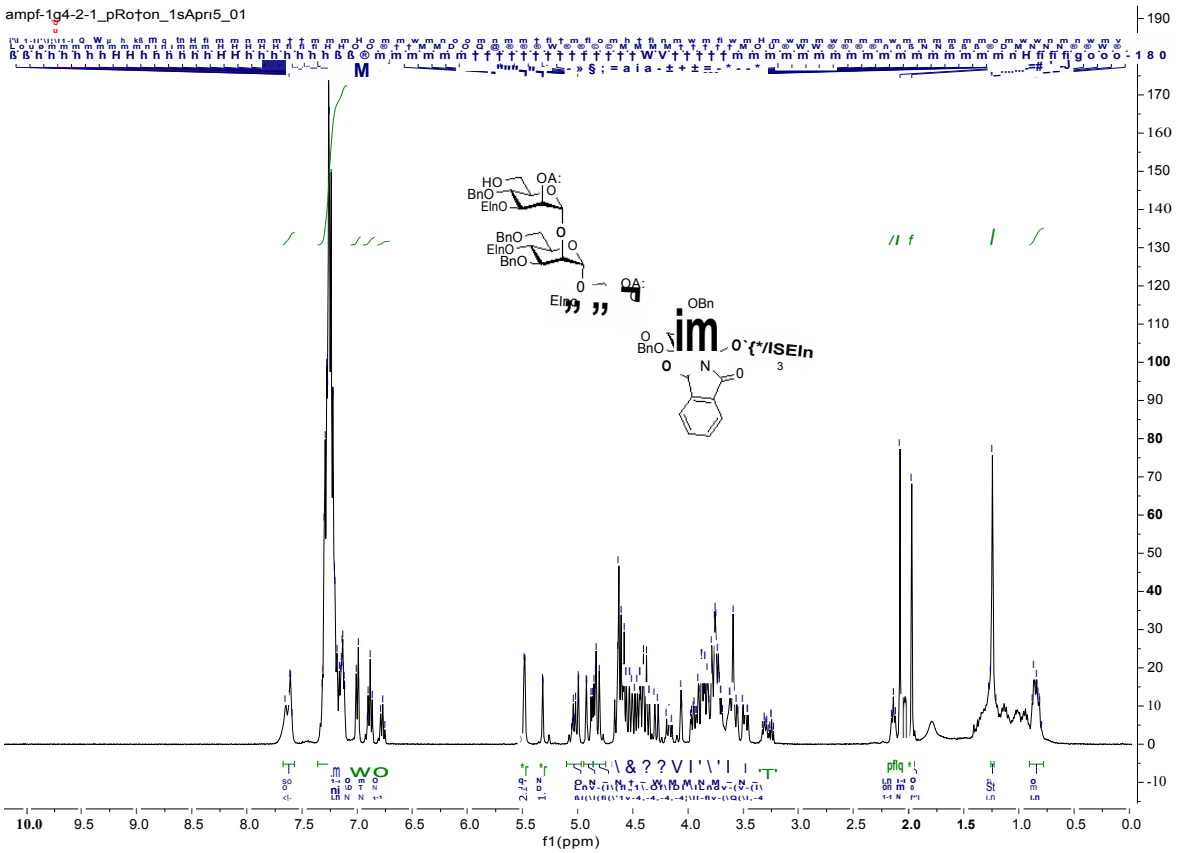

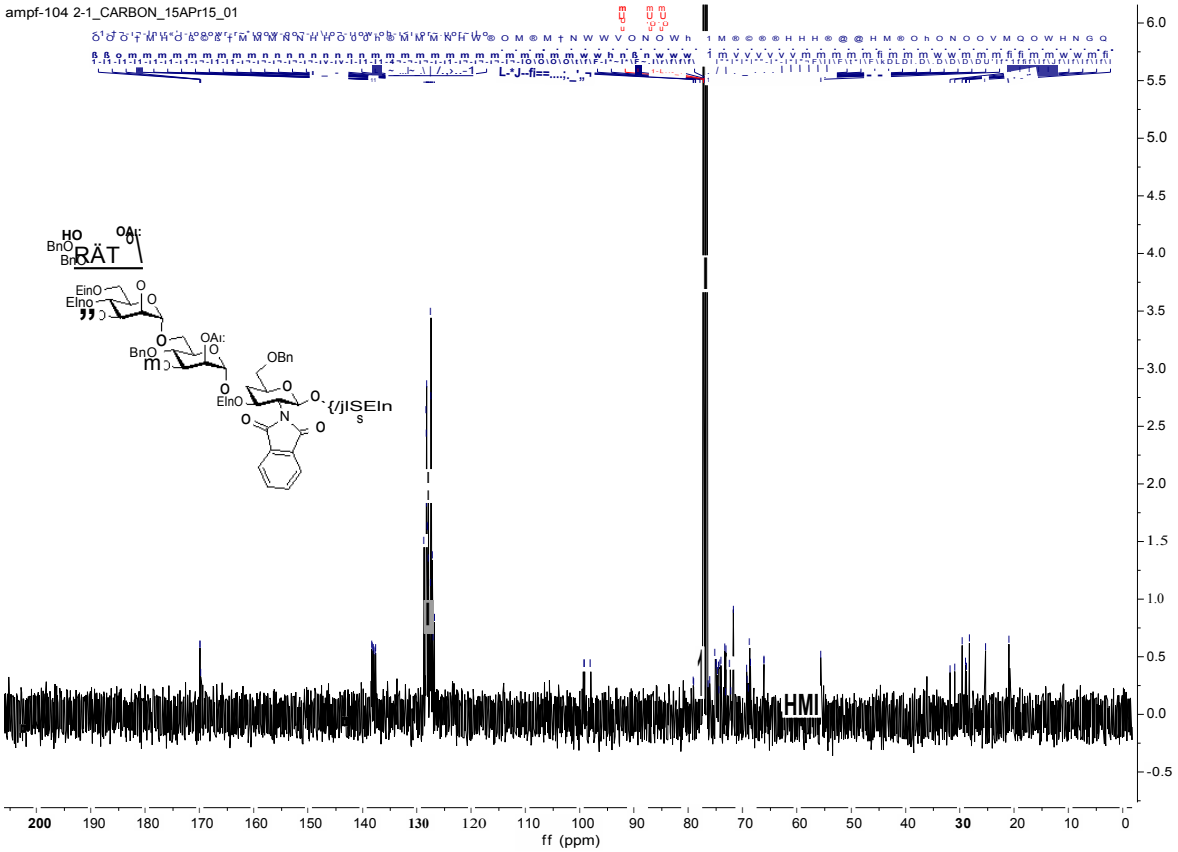

1-*O*-(6-thio)hexyl-α-D-mannopyranosyl-(1→2)-α-D-mannopyranosyl-(1→6)-α-D-mannopyranosyl-(1→4)-2-amino-2-deoxy-β-D-glucopyranoside (GPI 1)

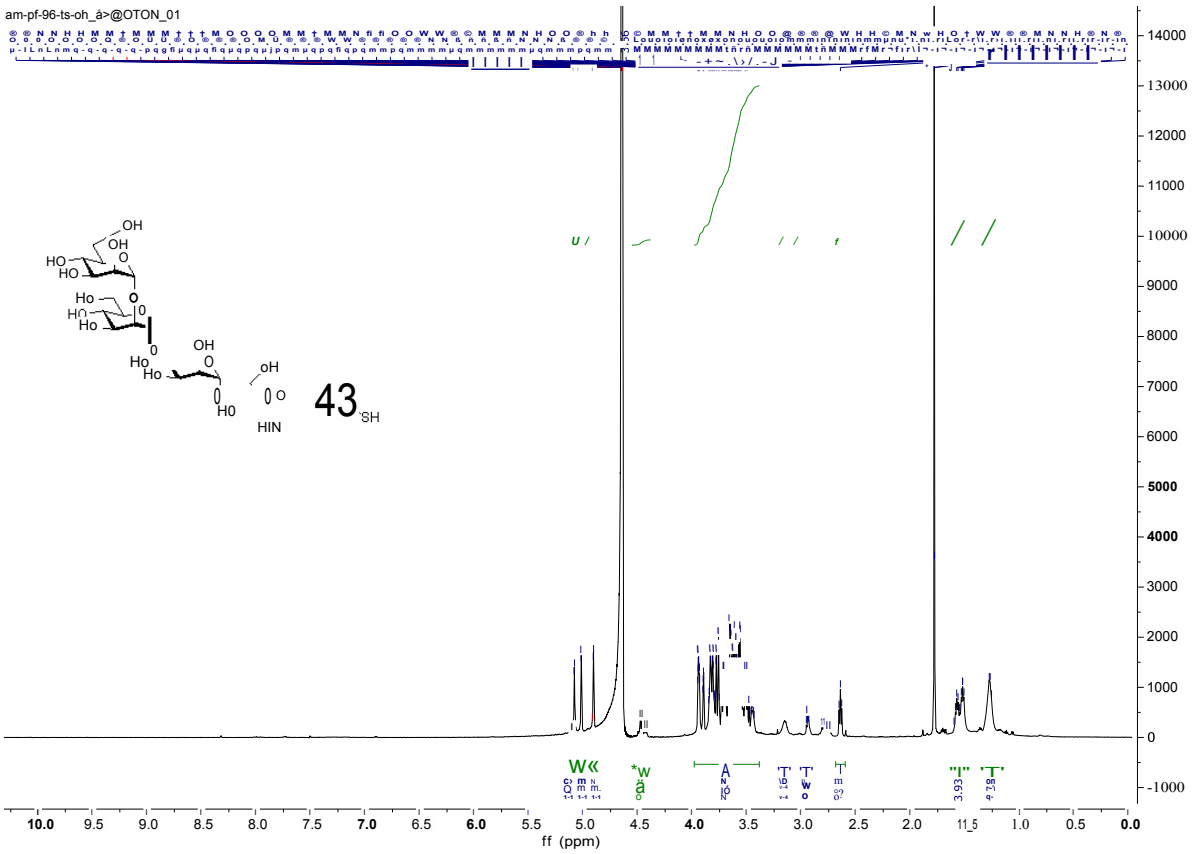

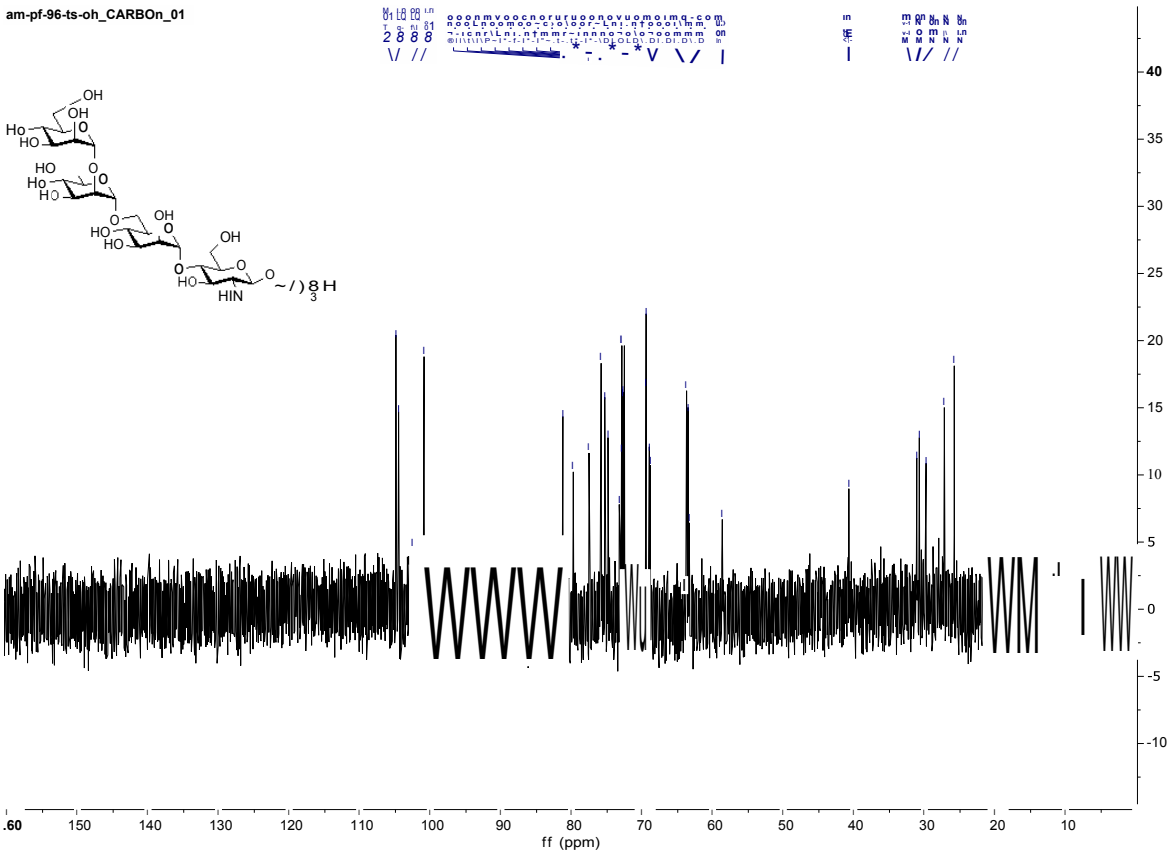

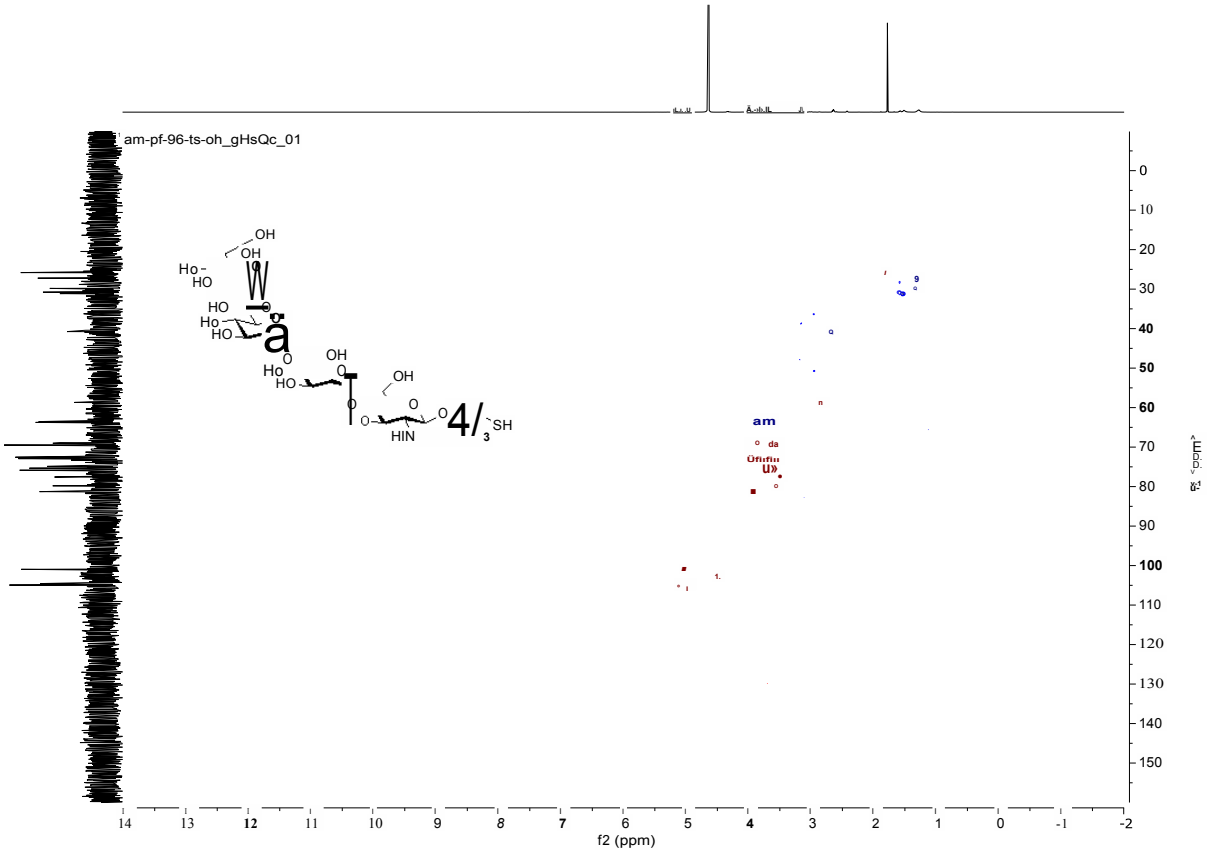
am-pf-96-ts-oh_gHsQc_01
f2 (ppm)
f1 (ppm)
am
da

1-*O*-(6-thiobenzyl)hexyl-2-*O*-Acetyl-3,4-di-*O*-benzyl-6-*O*-(2-*N*-benzyloxycarbonyl) aminoethyl-phosphonato-α-D-mannopyranosyl-(1→2)-3,4,6-tri-*O*-benzyl-α-D-mannopyranosyl-(1→6)-2-*O*-Acetyl-3,4-di-*O*-benzyl-α-D-mannopyranosyl-(1→4)- 3,6-*O*-benzyl-2-deoxy-2-*N*-phthalimido-β-D-glucopyranoside (2-21)

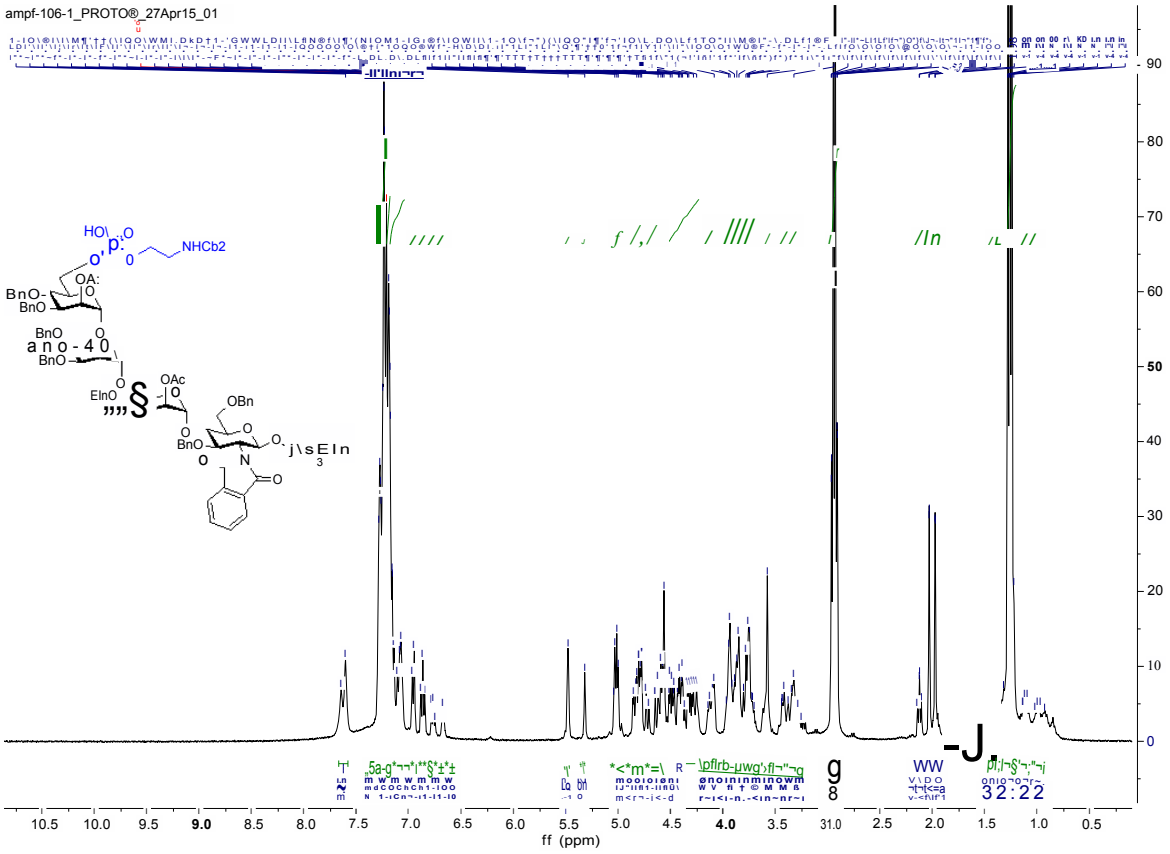

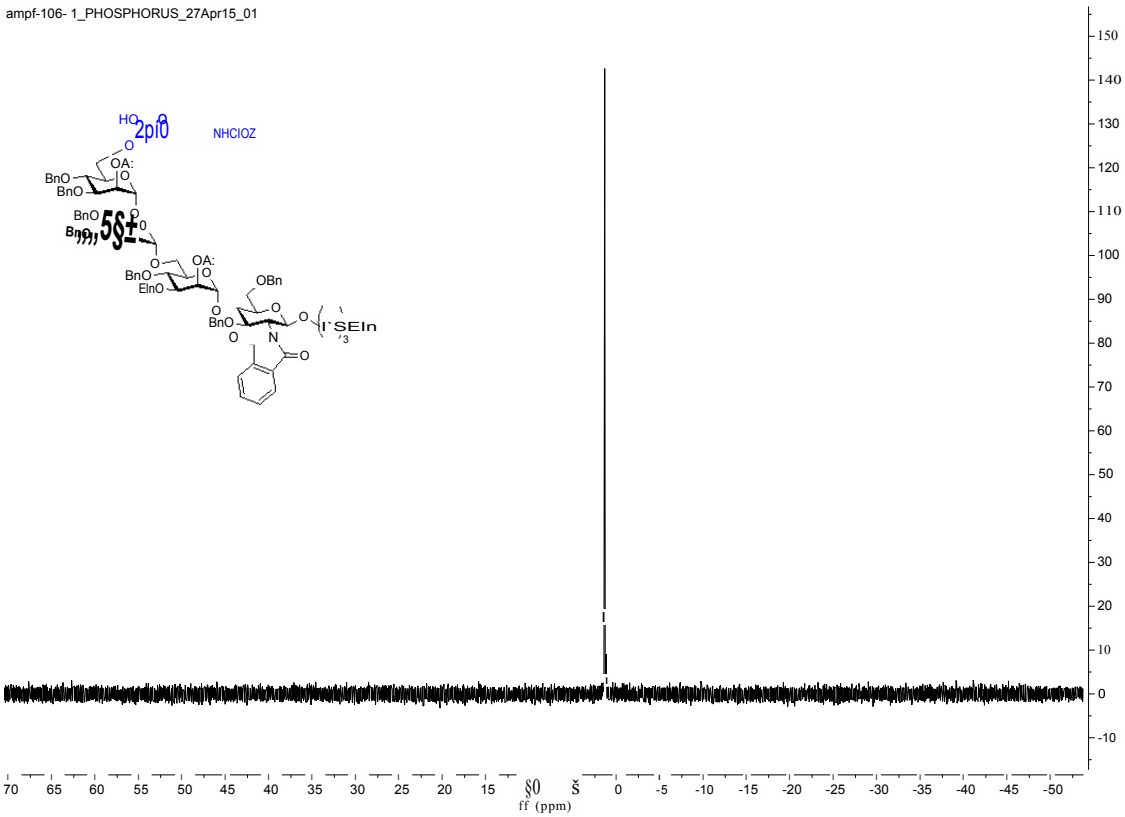

1-*O*-(6-thio)hexyl-6-*O*-aminoethyl-phosphonato-α-D-mannopyranosyl-(1→2)-α-D-mannopyranosyl-(1→6)-α-D-mannopyranosyl-(1→4)-2-deoxy-2-amino-β-D-glucopyranoside (GPI 2)

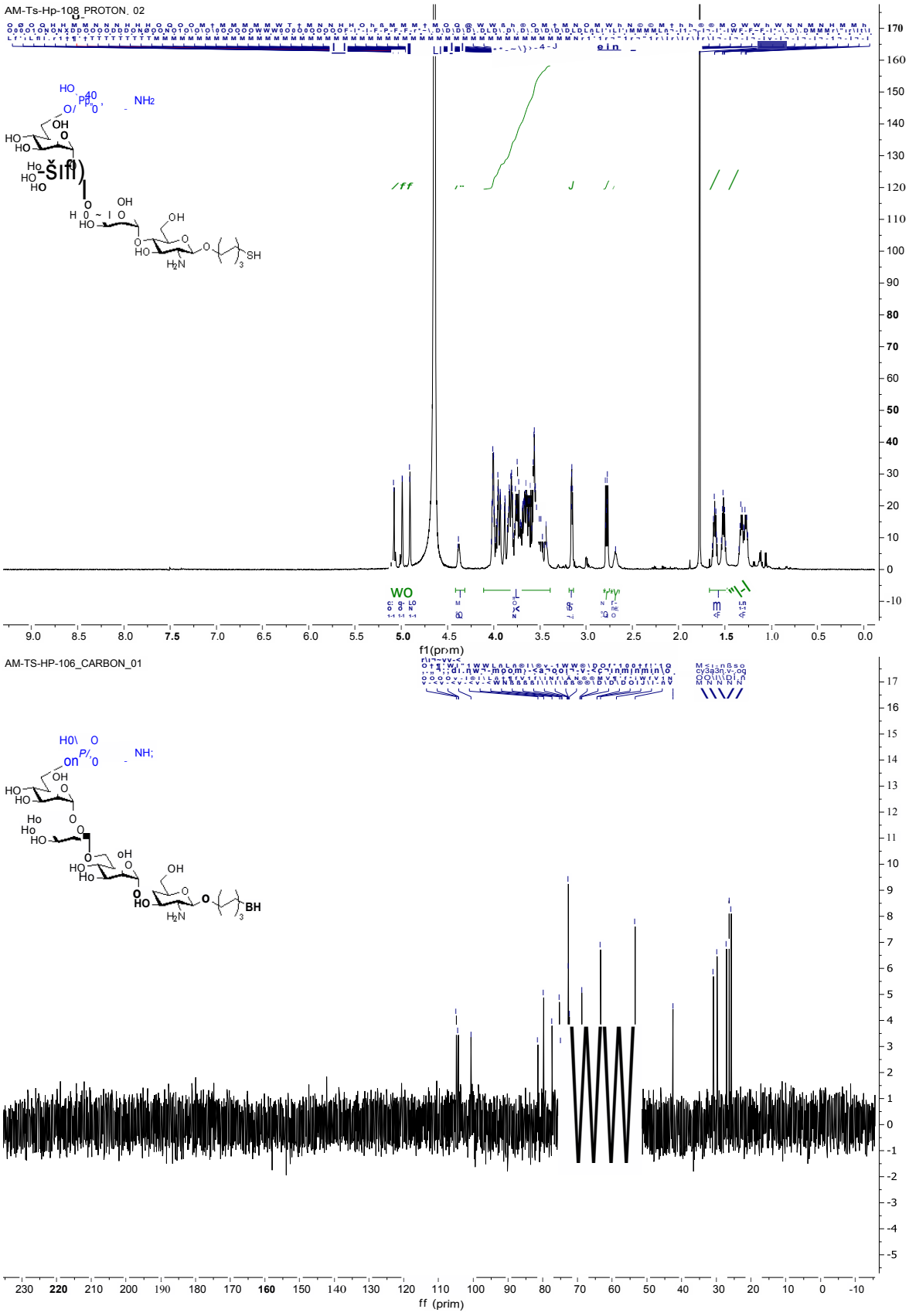

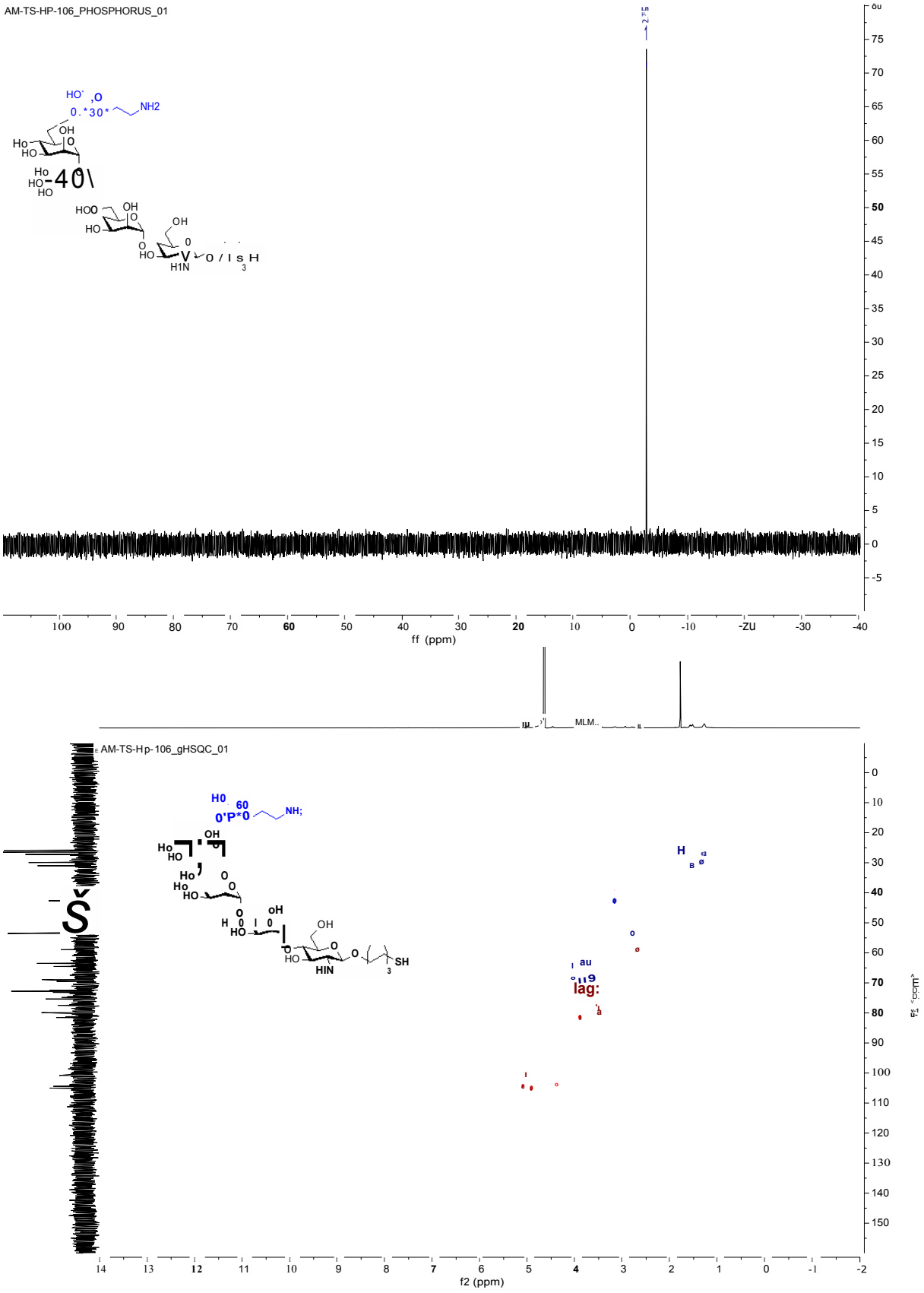
AM-TS-HP-106_PHOSPHORUS_01
ff (ppm)
AM-TS-Hp-106_gHSQC_01
f2 (ppm)
f1 (ppm)

_n_-Allyl-3,4-di-_O_-benzyl-6-_O_-tri_iso_propylsilyl-α-D-mannopyranosyl-(1→2)-3,4,6-tri-_O_-benzyl-α-D-mannopyranoside (2-22)

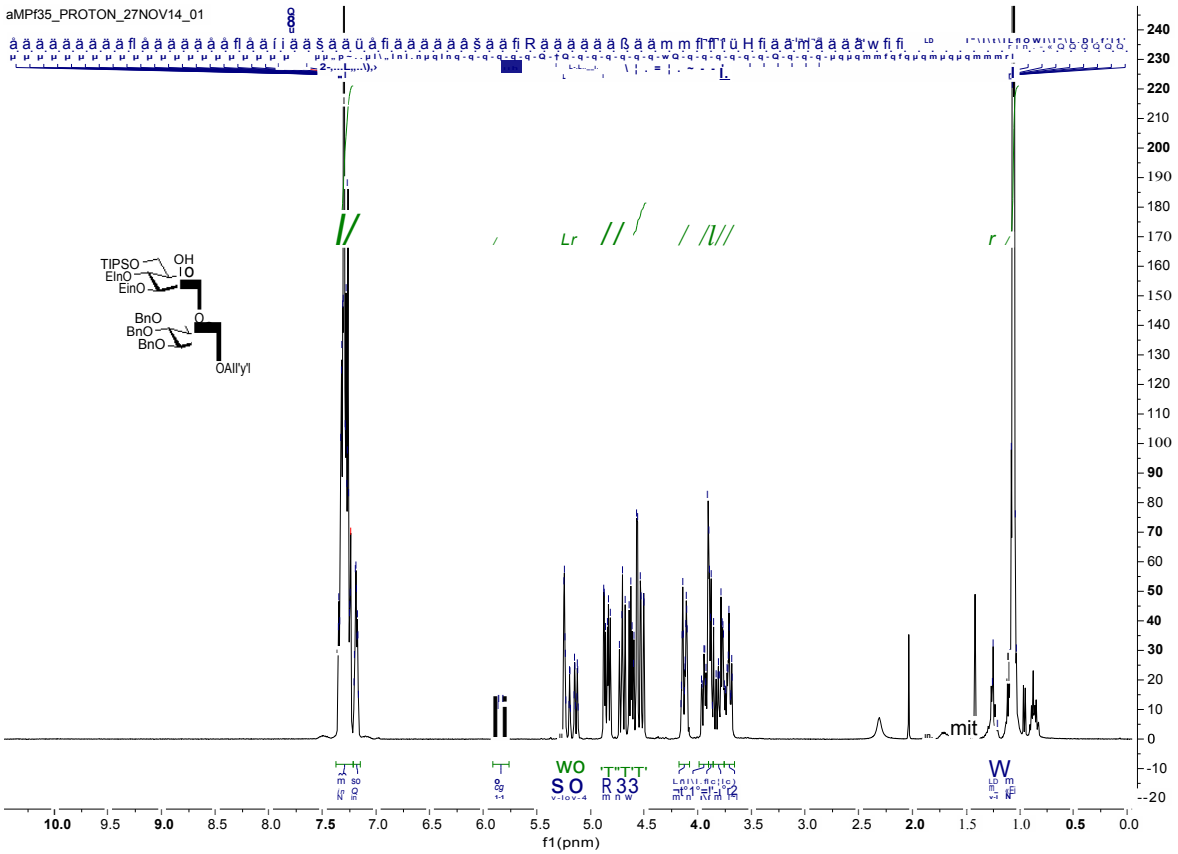

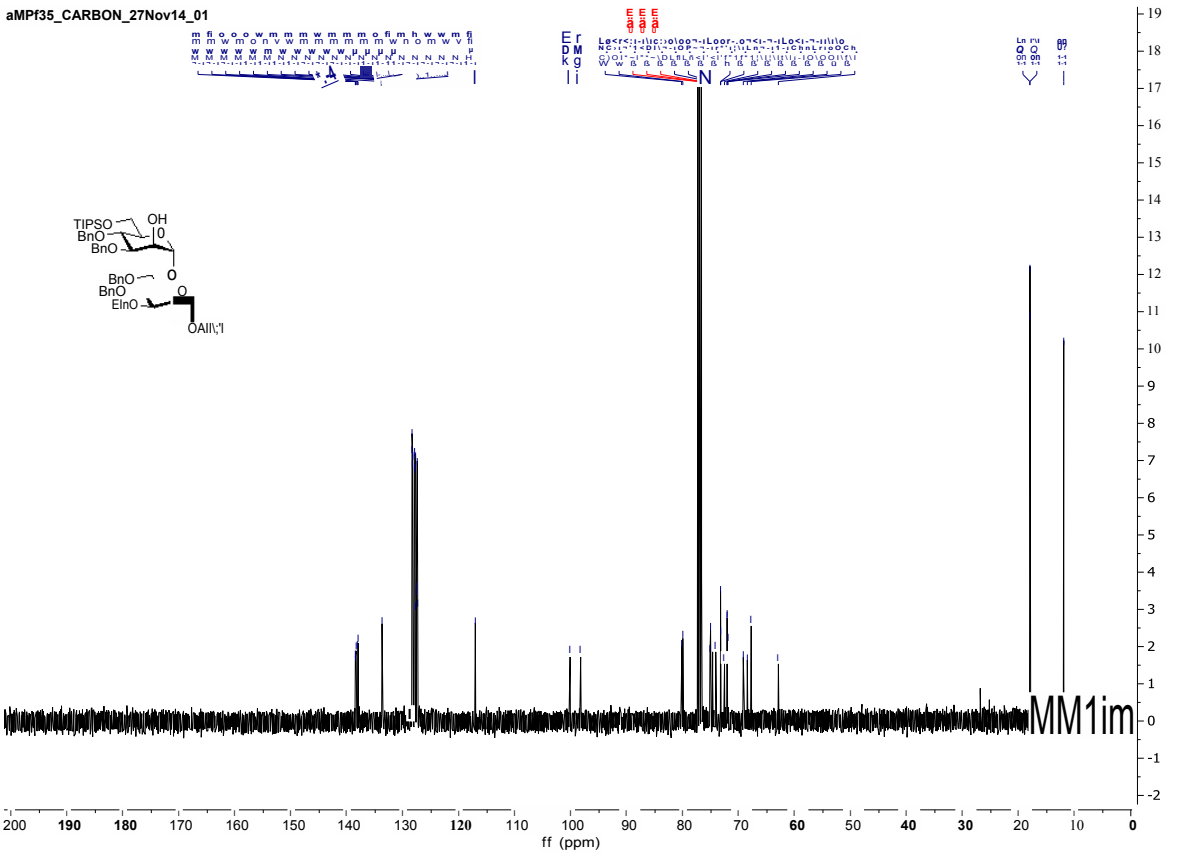

***n*-Allyl-2-*O*-acetyl-3,4,6-tri-*O*-benzyl-α-D-mannopyranosyl-(1→2)-3,4-di-*O*-benzyl-6-*O*-tri*iso*propylsilyl-α-D-mannopyranosyl-(1→2)-3,4,6-tri-*O*-benzyl-α-D-mannopyranoside (2-23)**

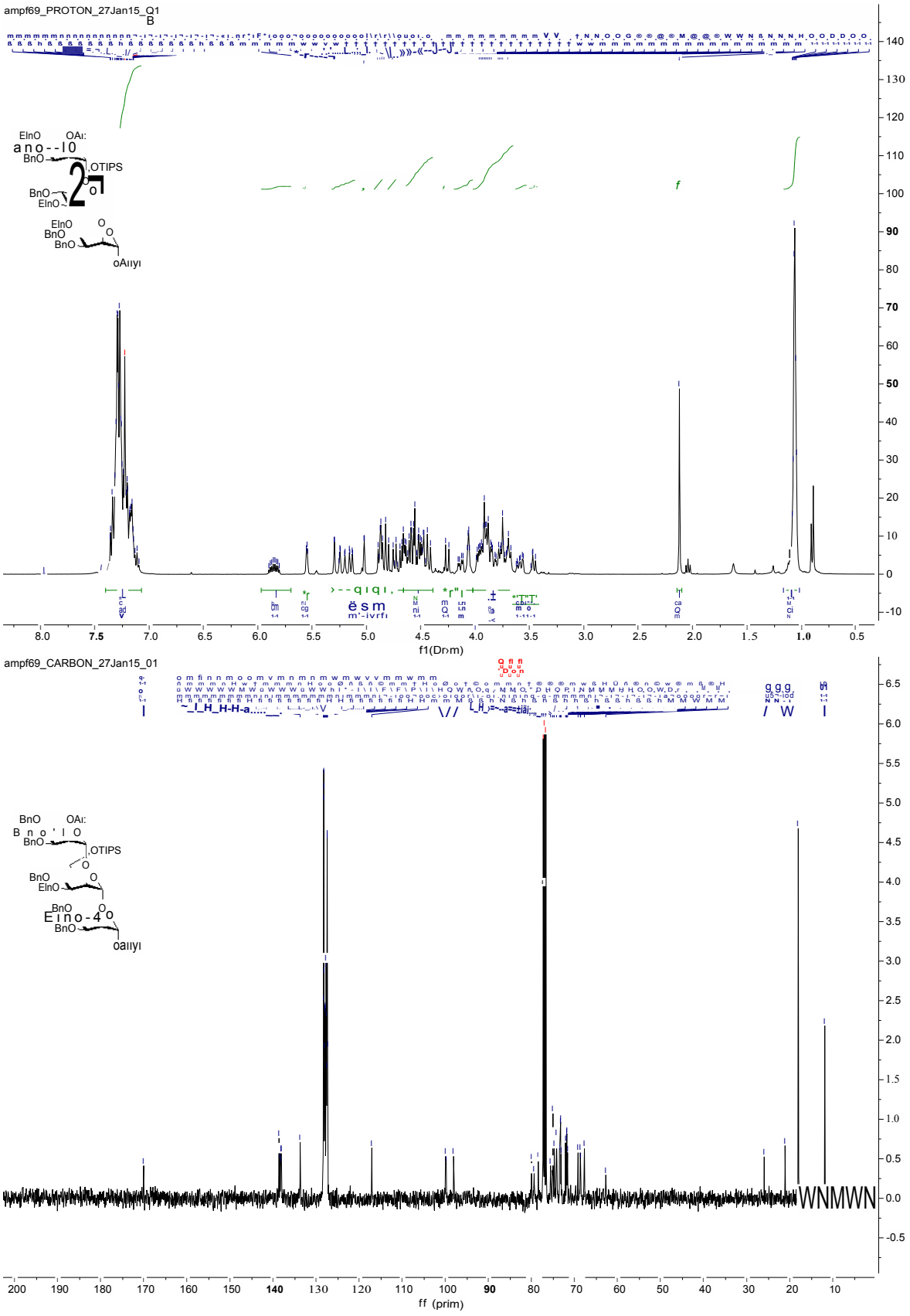

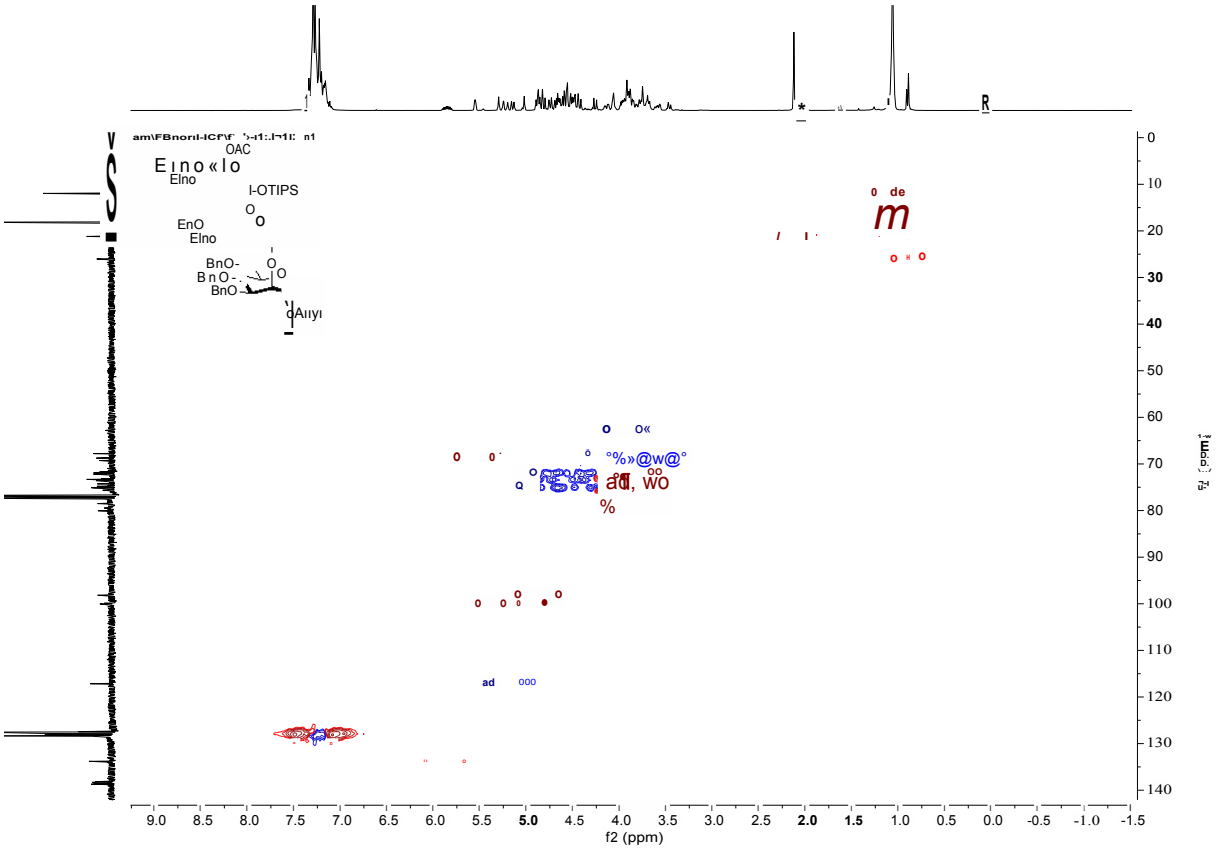
OAC
Elno
I-OTIPS
EnO
BnO-
BnO
BnO
f2 (ppm)

1-*O*-(6-thiobenzyl)hexyl-2-*O*-Acetyl-3,4,6-tri-*O*-benzyl-α-D-mannopyranosyl-(1→2)-3,4-di-*O*-benzyl-6-*O*-tri*iso*propylsilyl-α-D-mannopyranosyl-(1→2)-3,4,6-tri-*O*-benzyl-α-D-mannopyranosyl-(1→6)-2-*O*-Acetyl-3,4-di-*O*-benzyl-α-D-mannopyranosyl-(1→4)- 3,6-*O*-benzyl-2-deoxy-2-*N*-phthalimido-β-D-glucopyranoside (2-2)

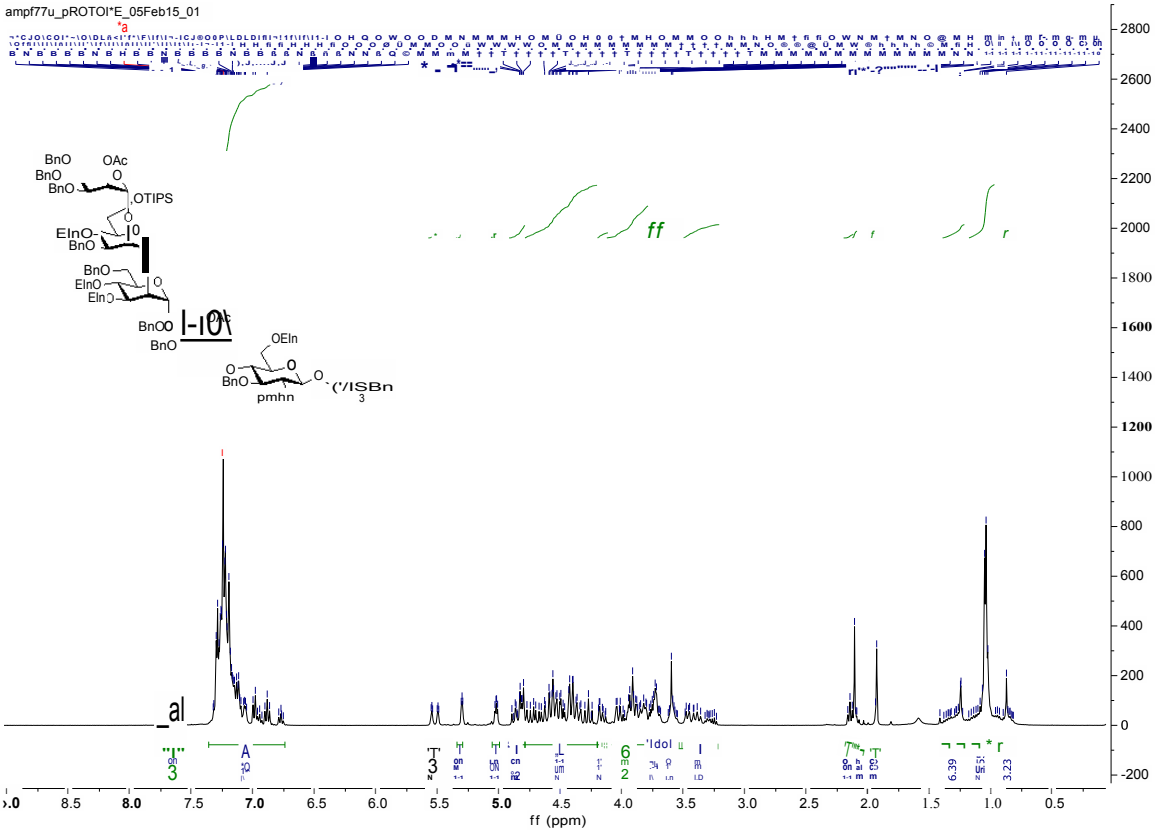

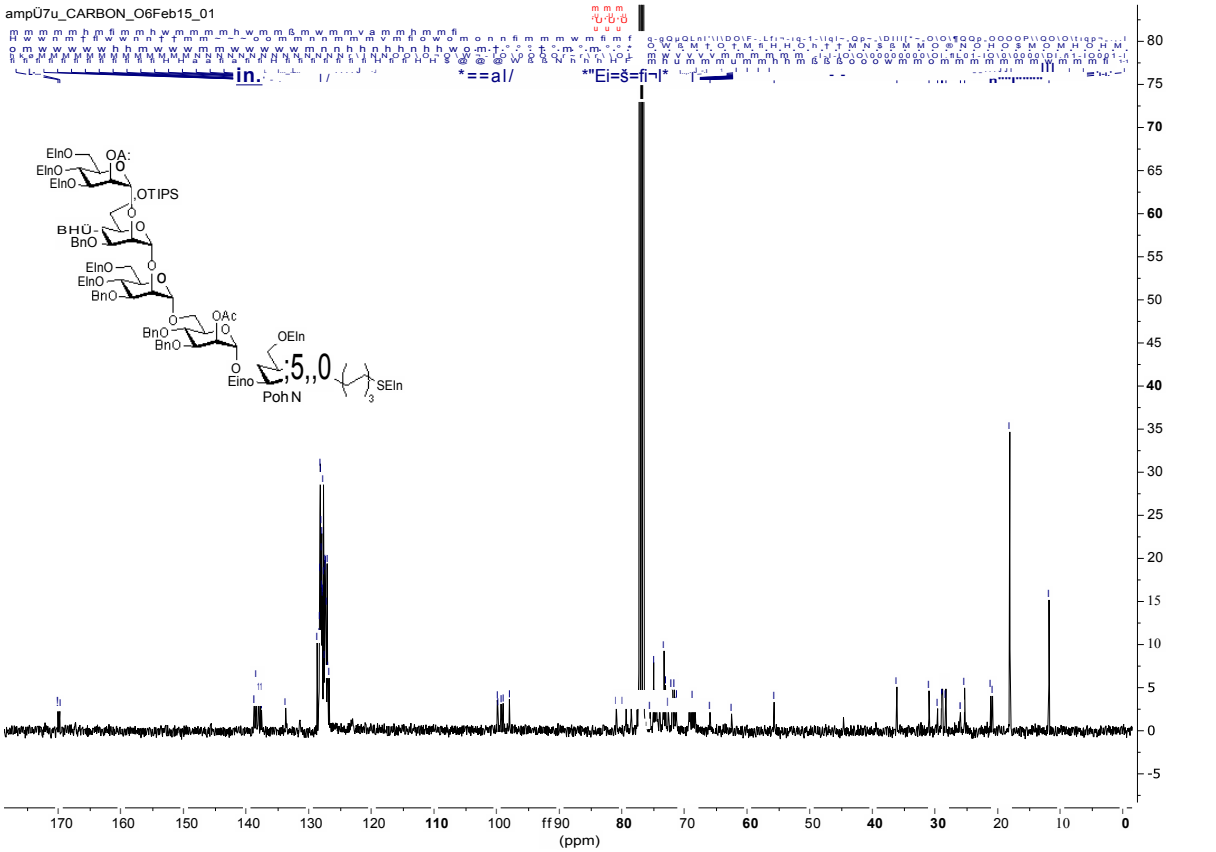
ampÜ7u_CARBON_O6Feb15_01
(ppm)

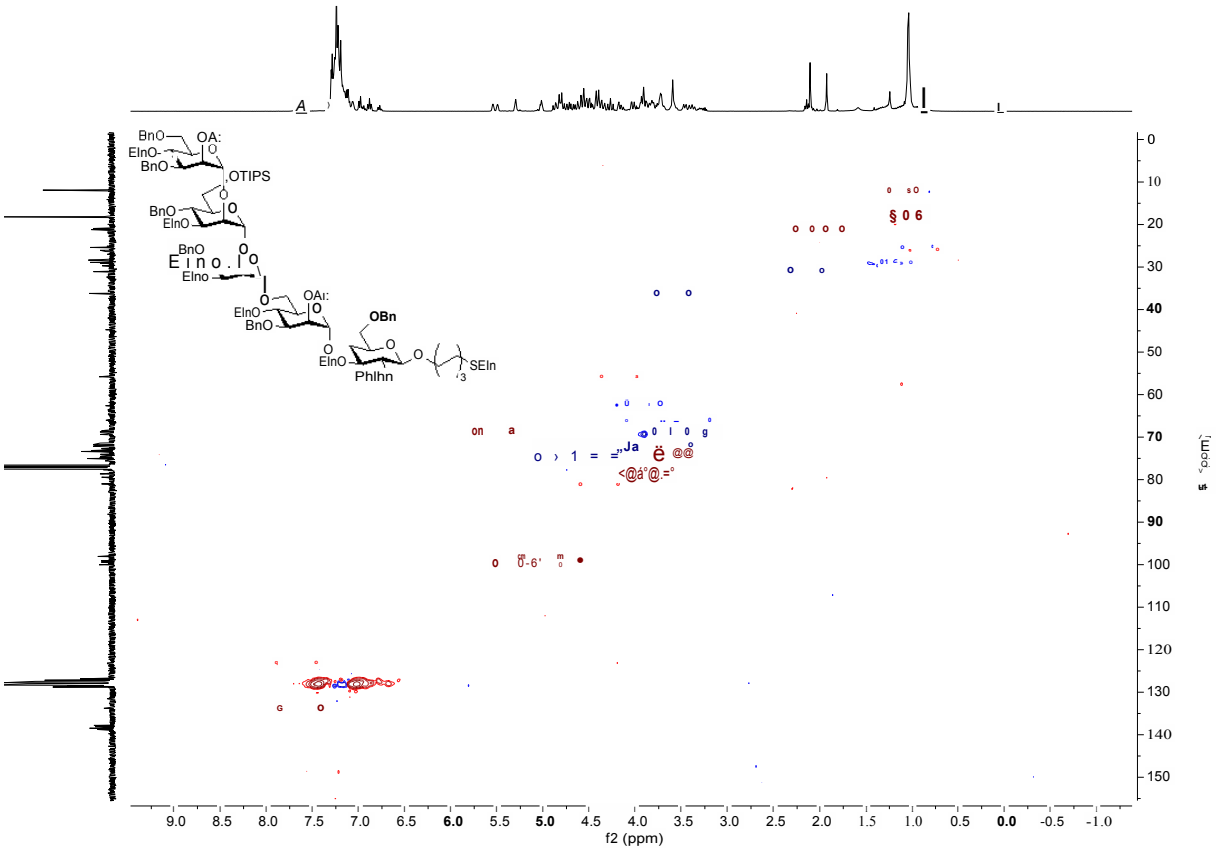
f2 (ppm)
f1 (ppm)

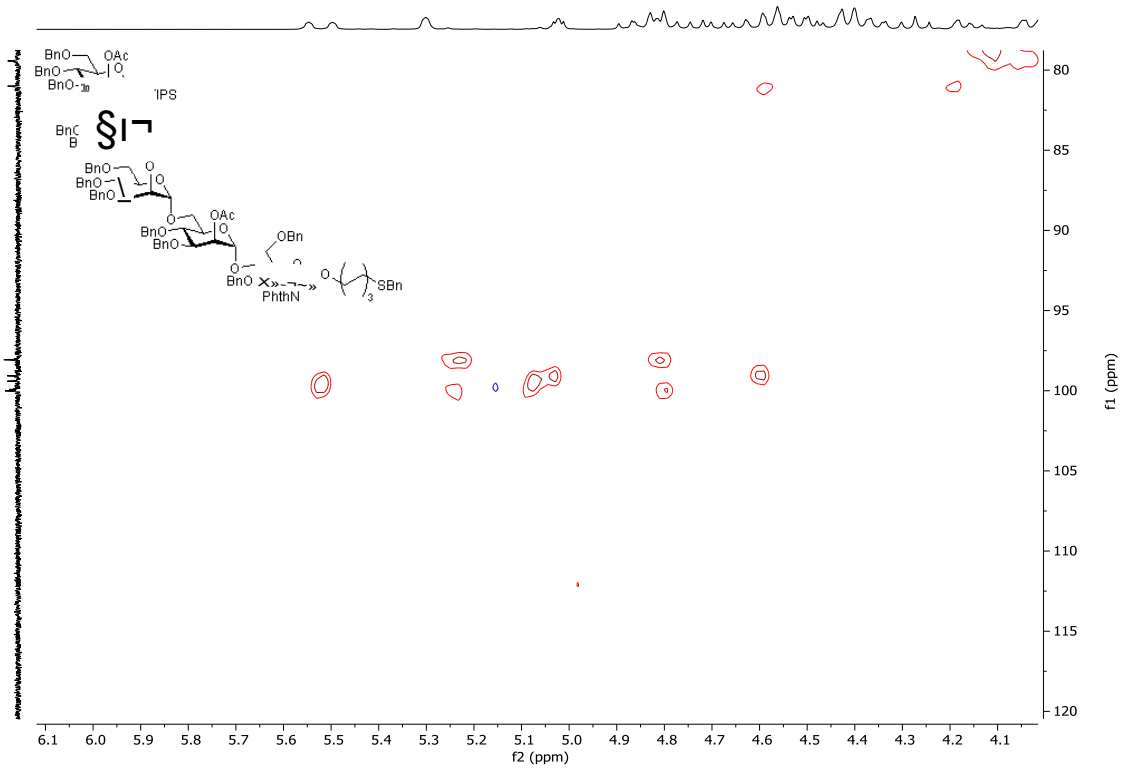
BnO
OAc
BnO
BnO
TIPS
BnO
BnO
BnO
OAc
BnO
BnO
OBn
BnO
PhthN
SBn
f2 (ppm)
f1 (ppm)

1-*O*-(6-thiobenzyl)hexyl-2-*O*-Acetyl-3,4,6-tri-*O*-benzyl-α-D-mannopyranosyl-(1→2)-3,4-di-*O*-benzyl-α-D-mannopyranosyl-(1→2)-3,4,6-tri-*O*-benzyl-α-D-mannopyranosyl-(1→6)-2-*O*-Acetyl-3,4-di-*O*-benzyl-α-D-mannopyranosyl-(1→4)-3,6-*O*-benzyl-2-deoxy-2-*N*-phthalimido-β-D-glucopyranoside (2-24)

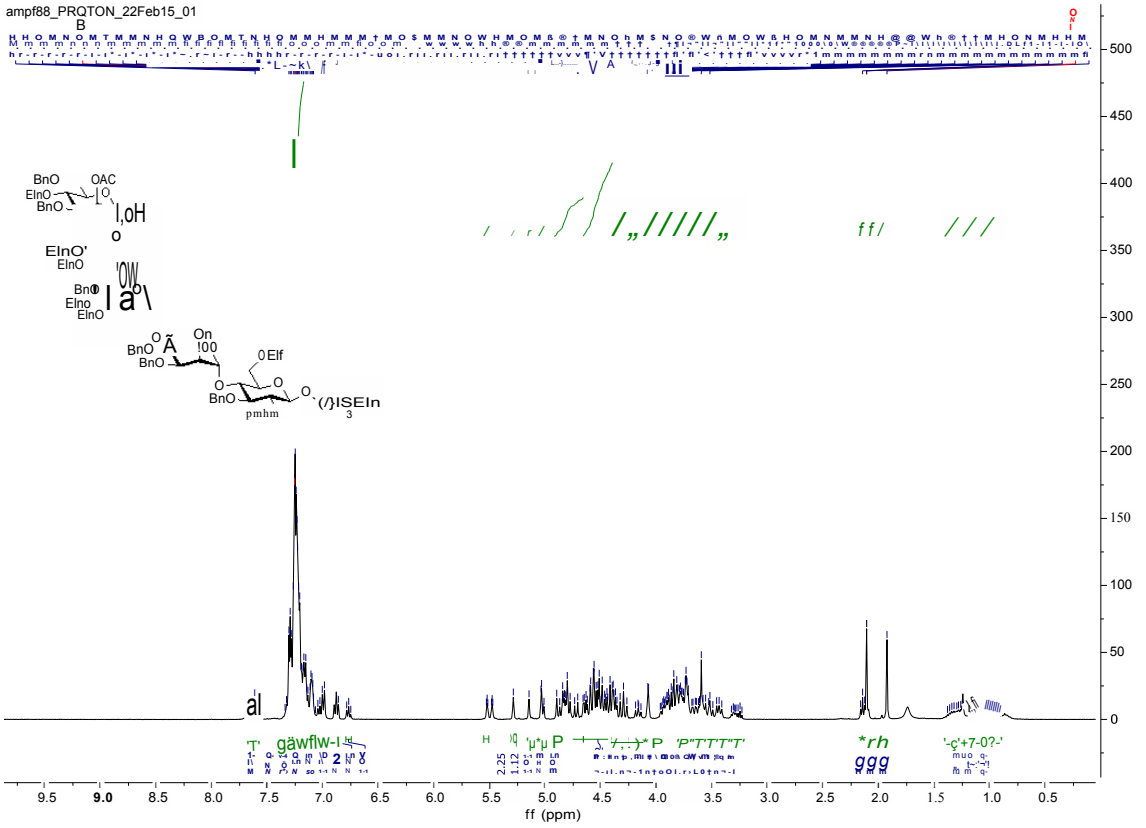

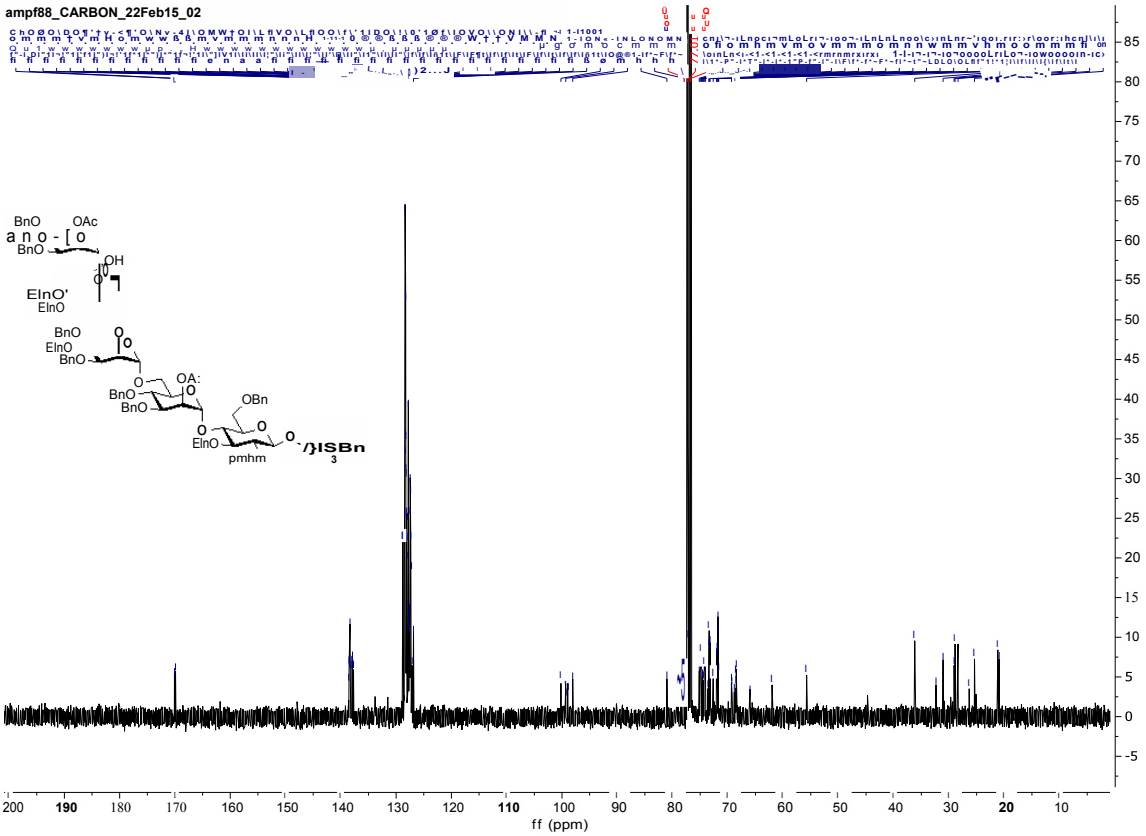

1-*O*-(6-thio)hexyl-α-D-mannopyranosyl-(1→2)-α-D-mannopyranosyl-(1→2)-α-D-mannopyranosyl-(1→6)-α-D-mannopyranosyl-(1→4)-2-deoxy-2-amino-β-D-glucopyranoside (GPI 3)

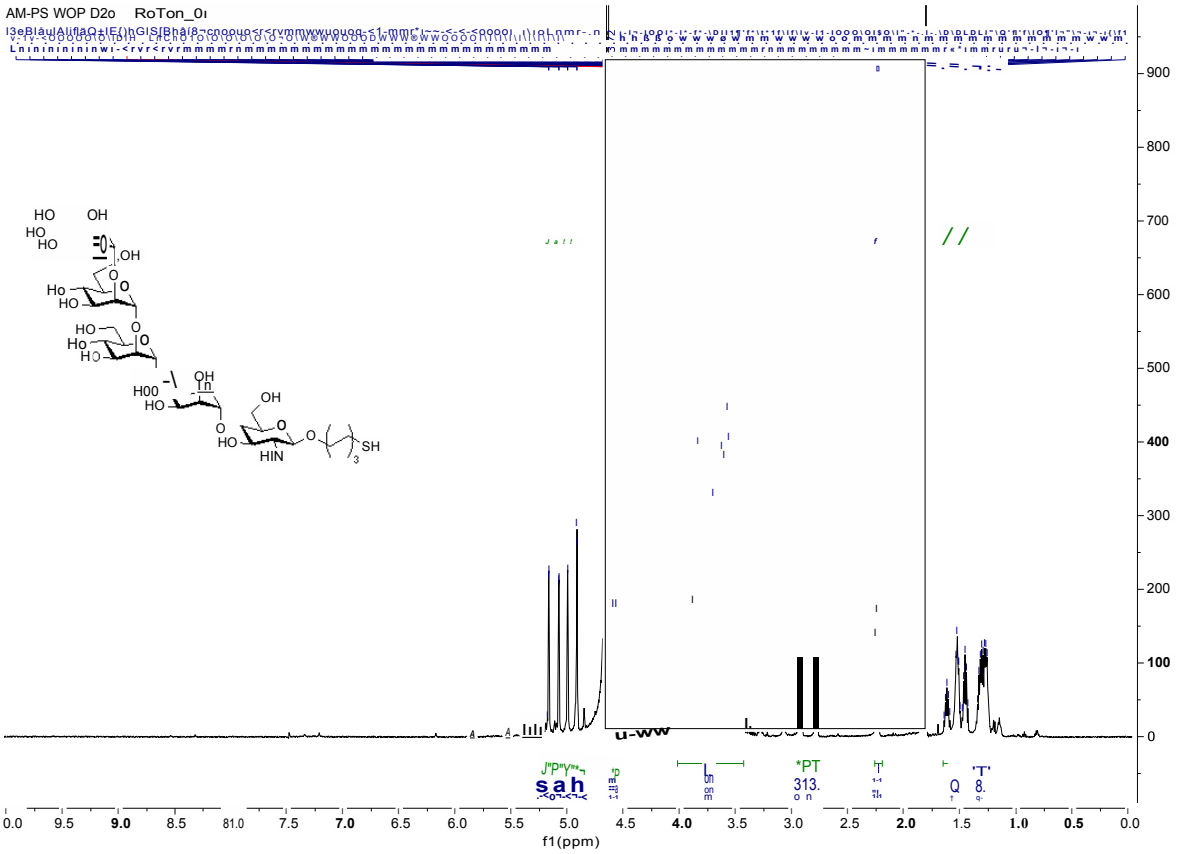

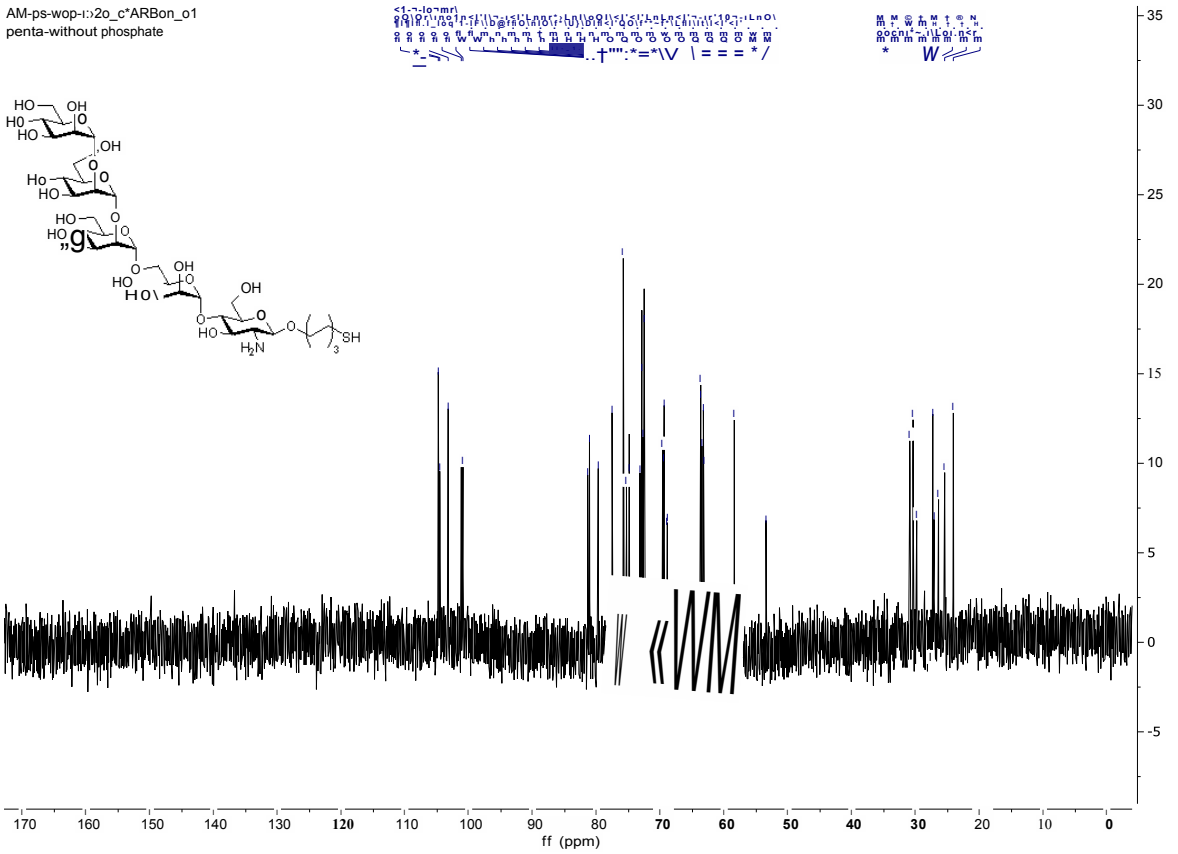

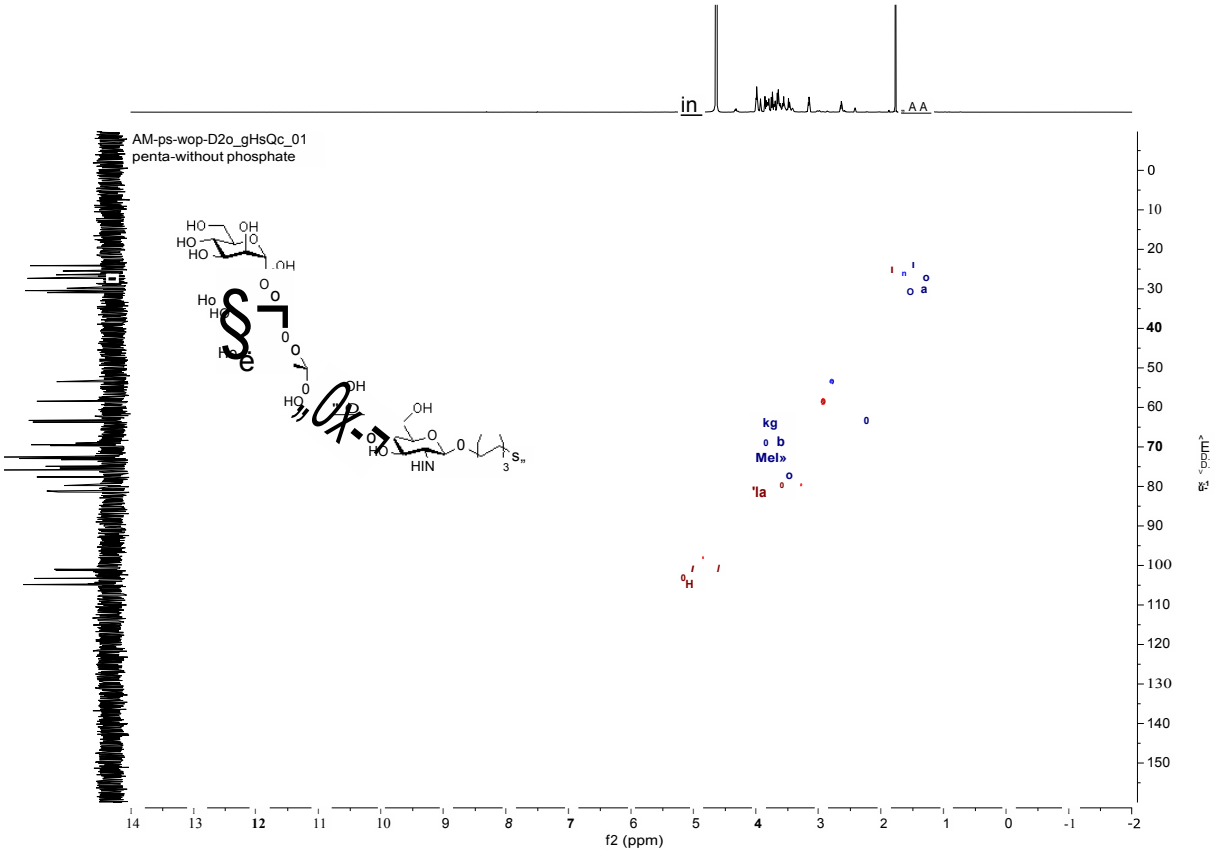
AM-ps-wop-D2o_gHsQc_01
penta-without phosphate
f2 (ppm)

1-*O*-(6-thiobenzyl)hexyl-2-*O*-Acetyl-3,4,6-tri-*O*-benzyl-α-D-mannopyranosyl-(1→2)-3,4-di-*O*-benzyl-6-*O*-(2-*N*-benzyloxycarbonyl)aminoethyl-phosphonato-α-D-mannopyranosyl-(1→2)-3,4,6-tri-*O*-benzyl-α-D-mannopyranosyl-(1→6)-2-*O*-Acetyl-3,4-di-*O*-benzyl-α-D-mannopyranosyl-(1→4)-3,6-*O*-benzyl-2-deoxy-2-*N*-phthalimido-β-D-glucopyranoside (2-1)

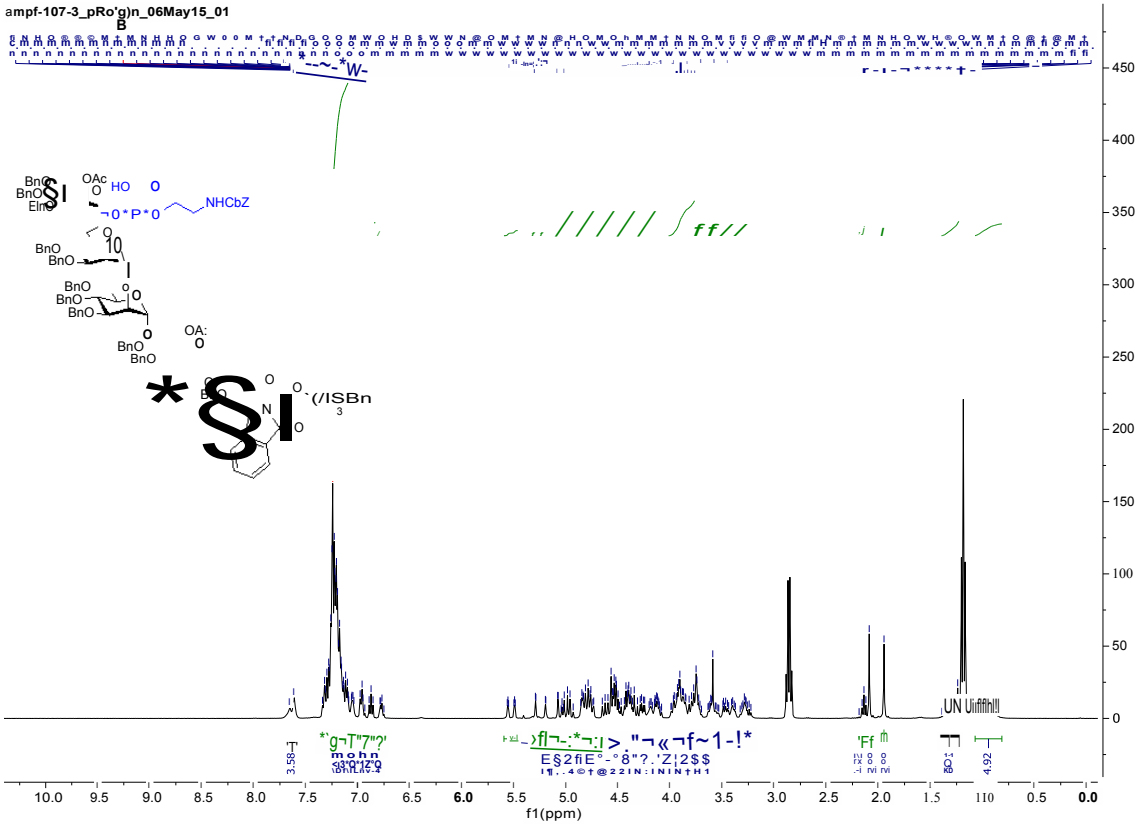

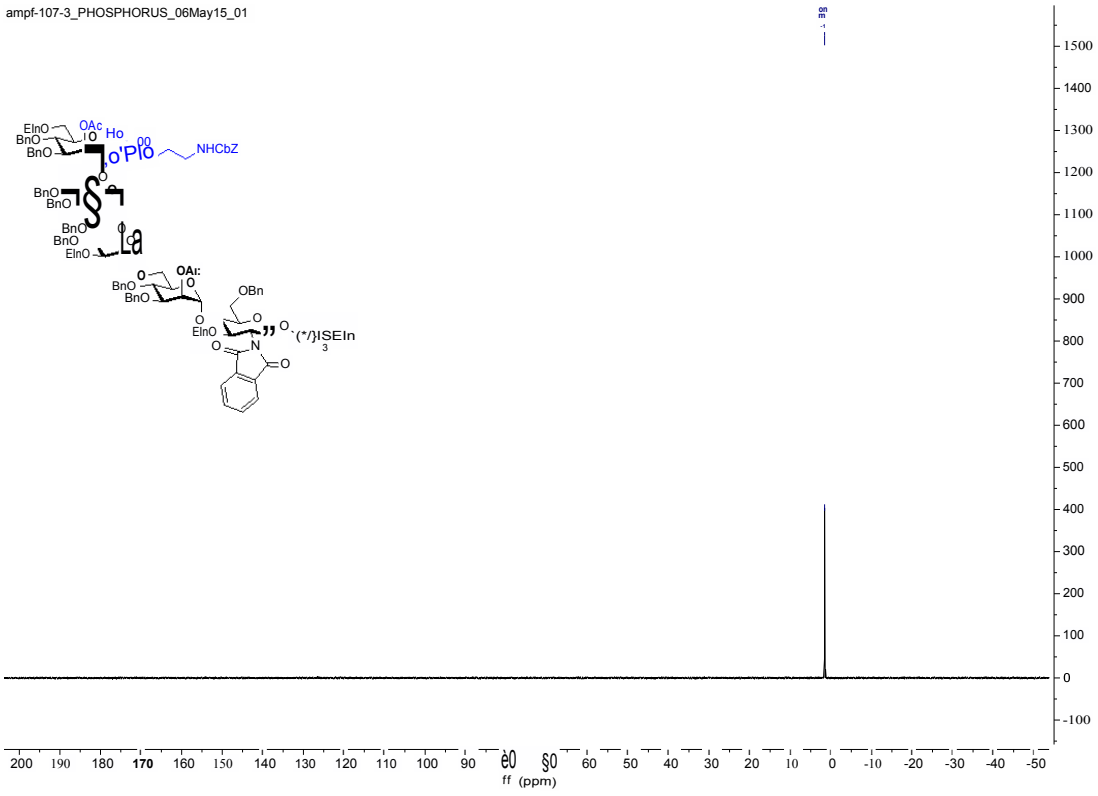

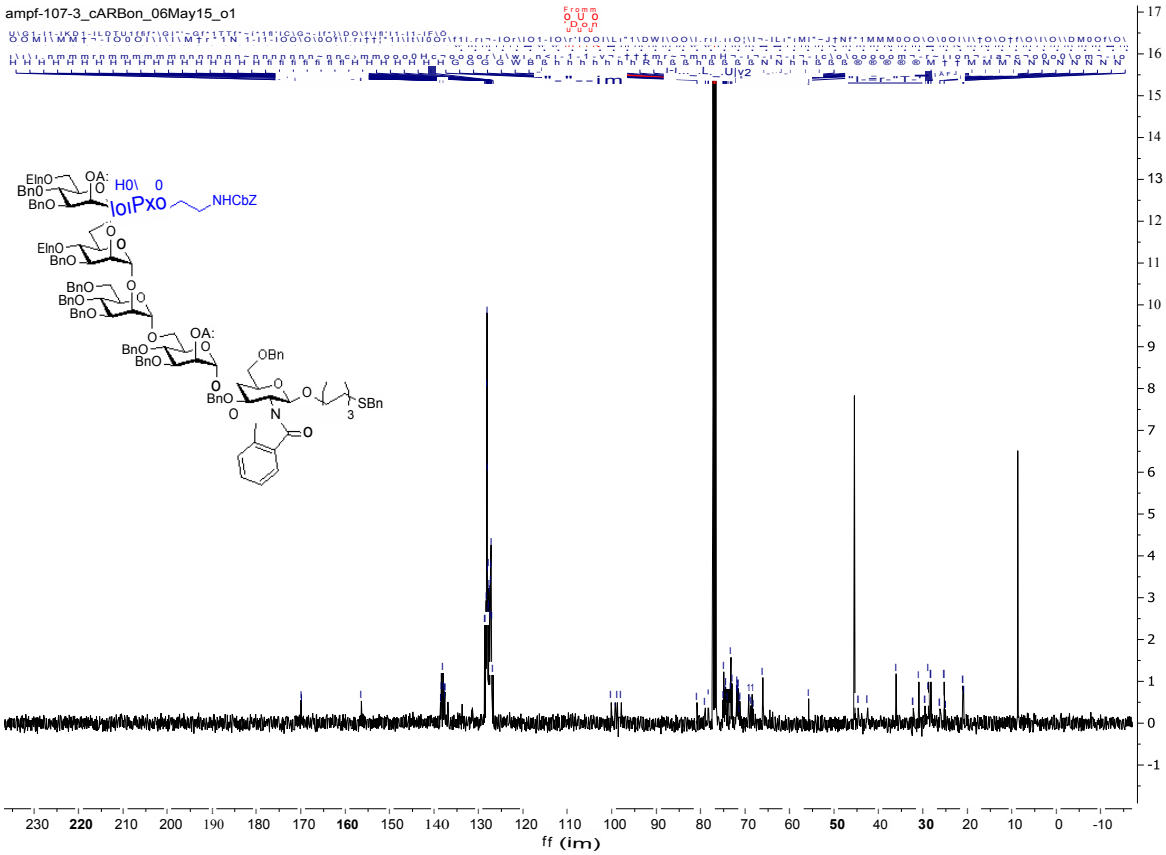
ampf-107-3_cARBon_06May15_o1
ElnO
Bn0
BnO
OA:
H0\ 0
NHCbZ
OBn
SBn
N
ff (im)

1-*O*-(6-thio)hexyl-α-D-mannopyranosyl-(1→2)-6-*O*-aminoethyl-phosphonato-α-D-mannopyranosyl-(1→2)-α-D-mannopyranosyl-(1→6)-α-D-mannopyranosyl-(1→4)-2-deoxy-2-amino-β-D-glucopyranoside (GPI 4)

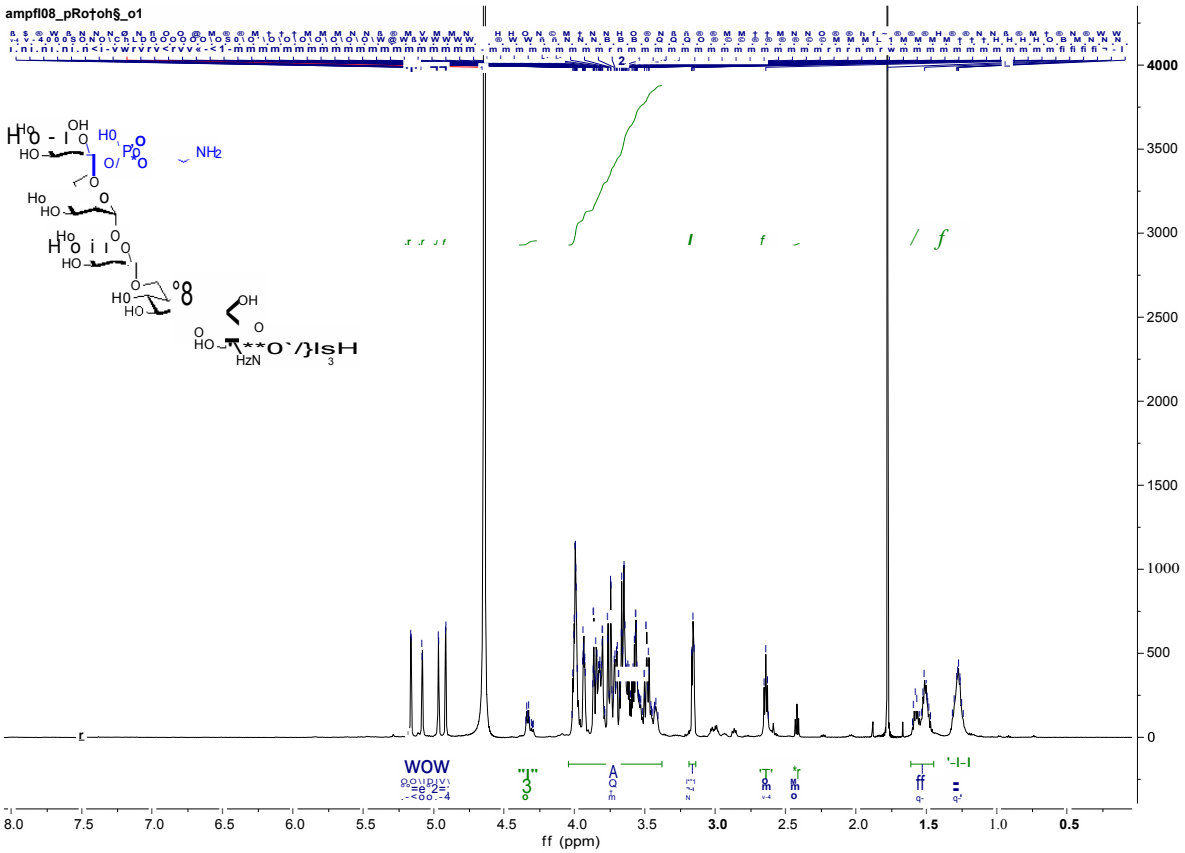

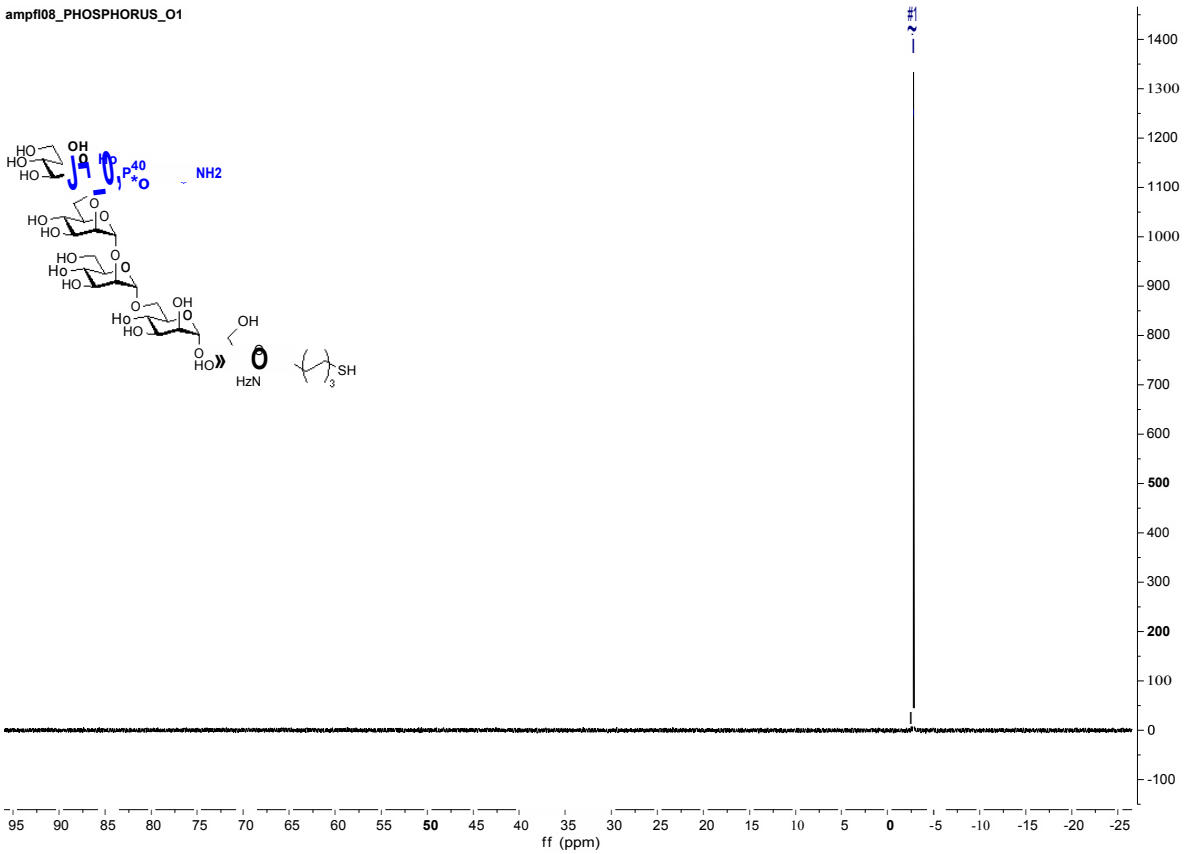

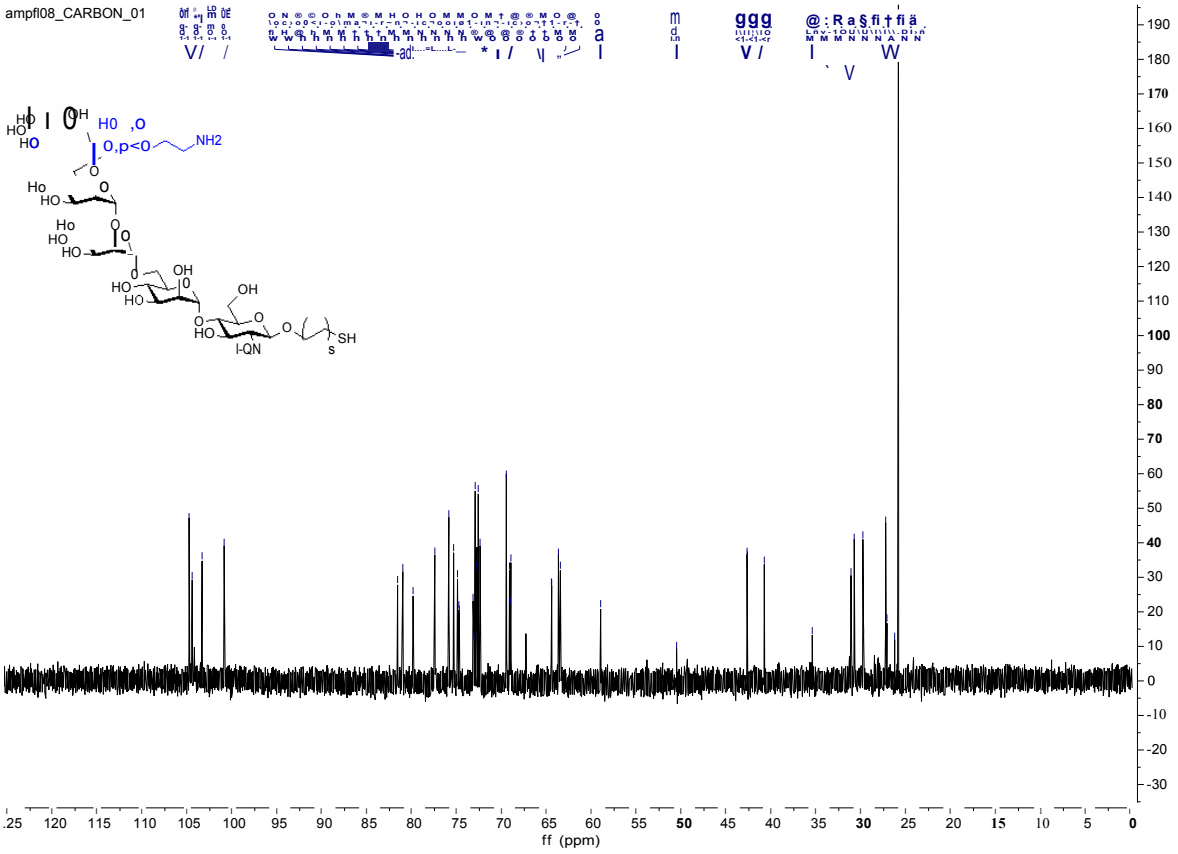
ampfl08_CARBON_01
H0 ,O
O,p<O
NH2
OH
SH
ff (ppm)

5.2 NMR Spectra for Chapter 3

Allyl-2-*O*-acetyl-3,4,6-tri-*O*-benyl-α-D-mannopyranosyl-(1→2)-3,4-di-*O*-benzyl-6-*O*-tri*iso*propylsilyl-α-D-mannopyranosyl-(1→2)-3,4,6-tri-*O*-benyl-α-D-mannopyranosyl-(1→6)-2,3-di-*O*-acetyl-4-*O*-(2-naphthyl)methyl-α-D-mannopyranoside (3-15a)

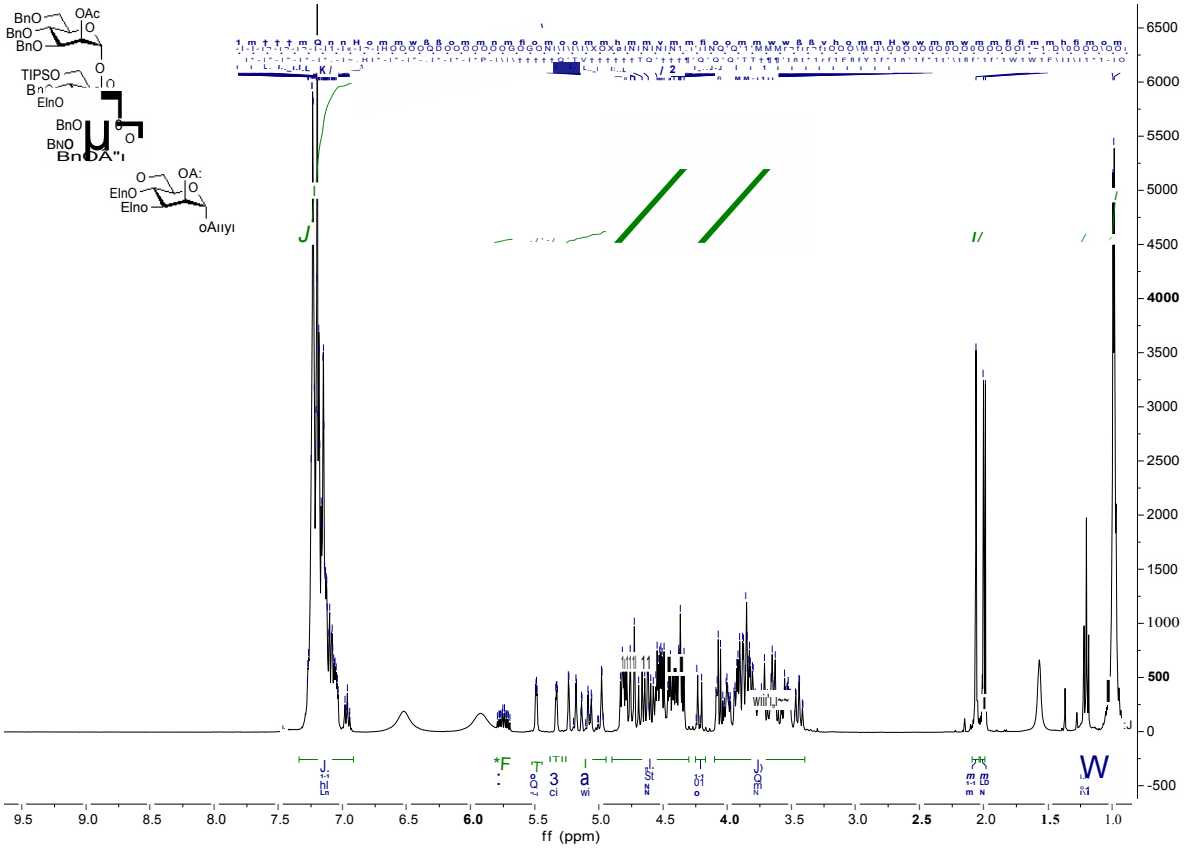

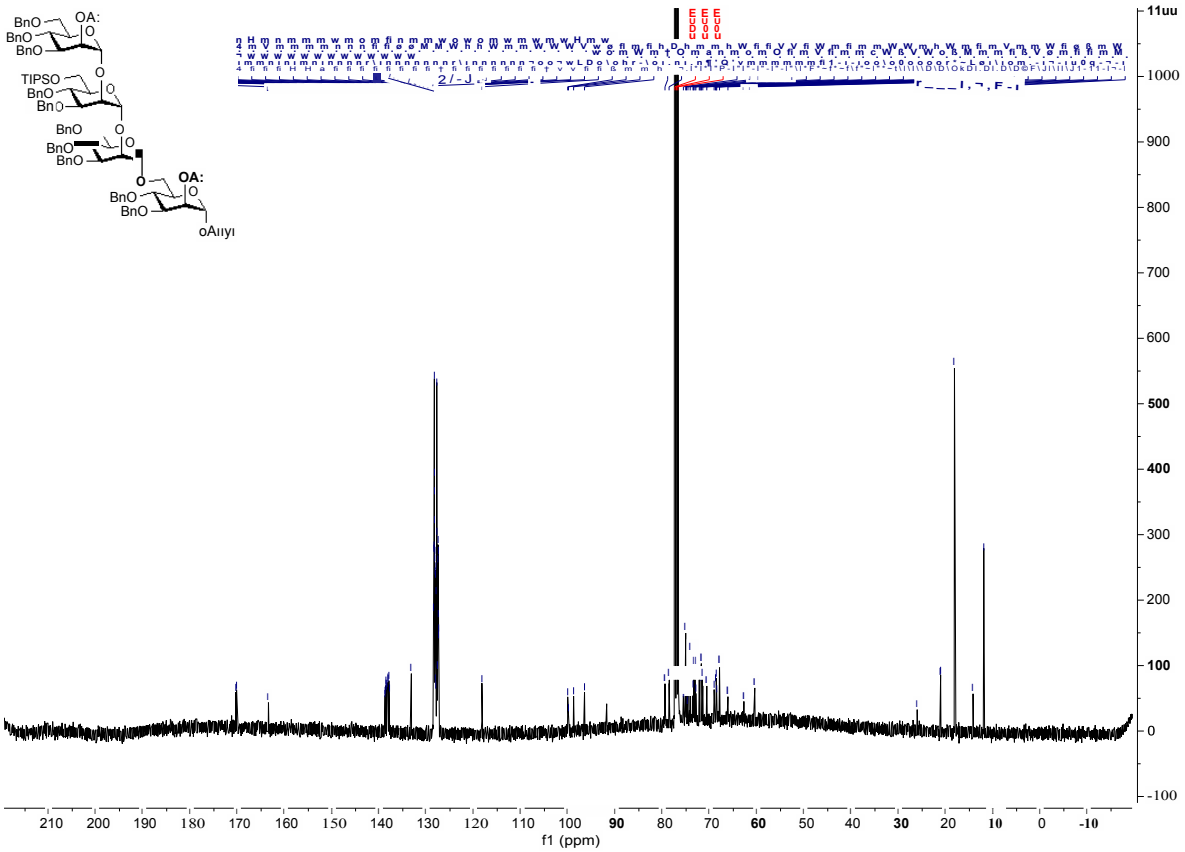
BnO
OA:
TIPSO
OA:
oAllyl
f1 (ppm)

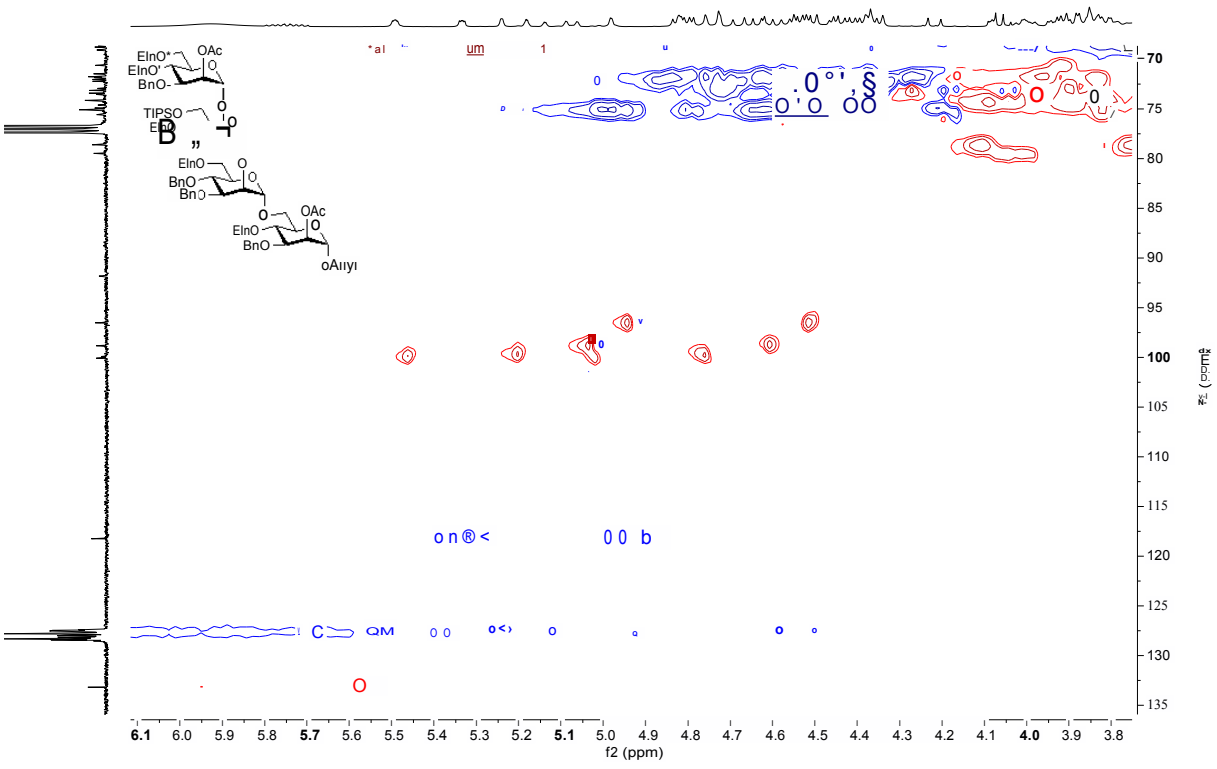
ElnO
OAc
TIPSO
OAc
oAllyl
f2 (ppm)

3,4,6–tri-*O*-acetyl-2-azido-2-deoxy-α-D-glucopyranosyl-(1→6)-1-*O*-allyl-2-O-(2-napthyl)methyl-3,4,5-tetra-*O*-benzyl-D-*myo*-inositol (3-12)

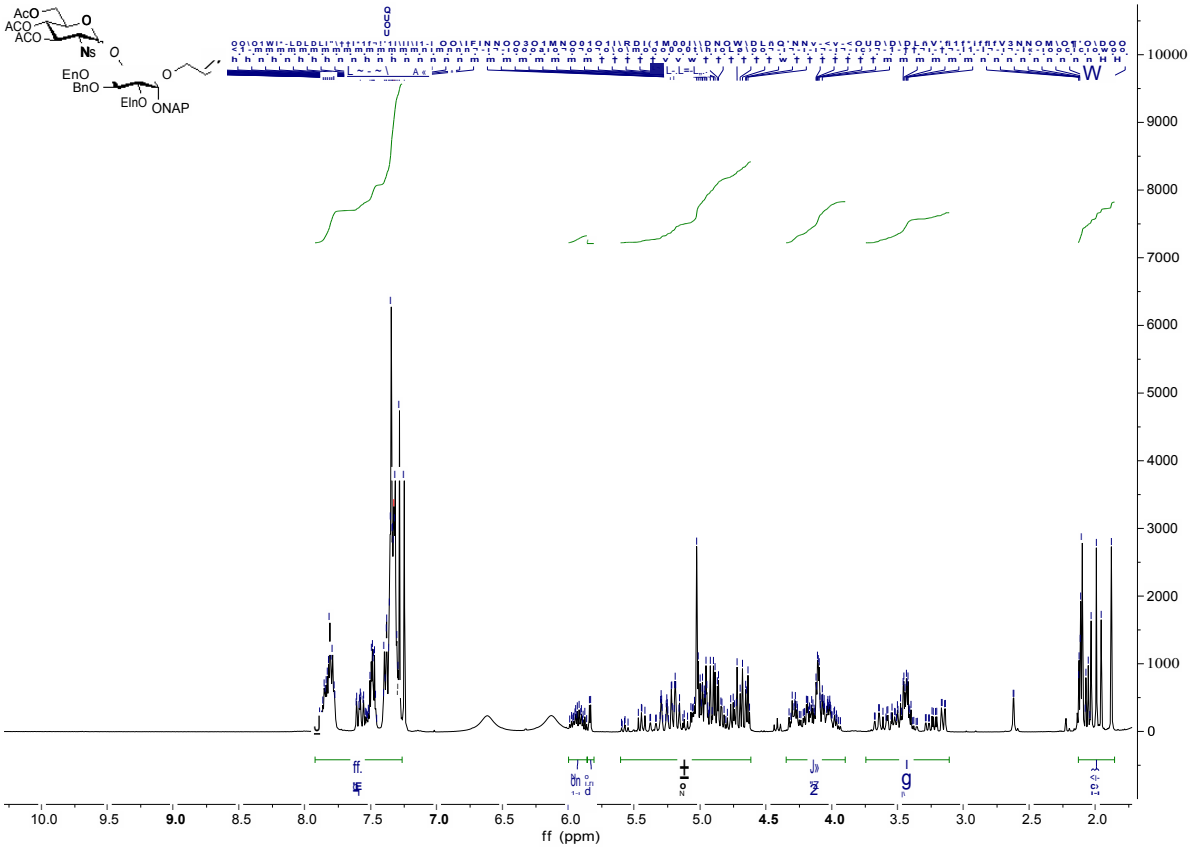

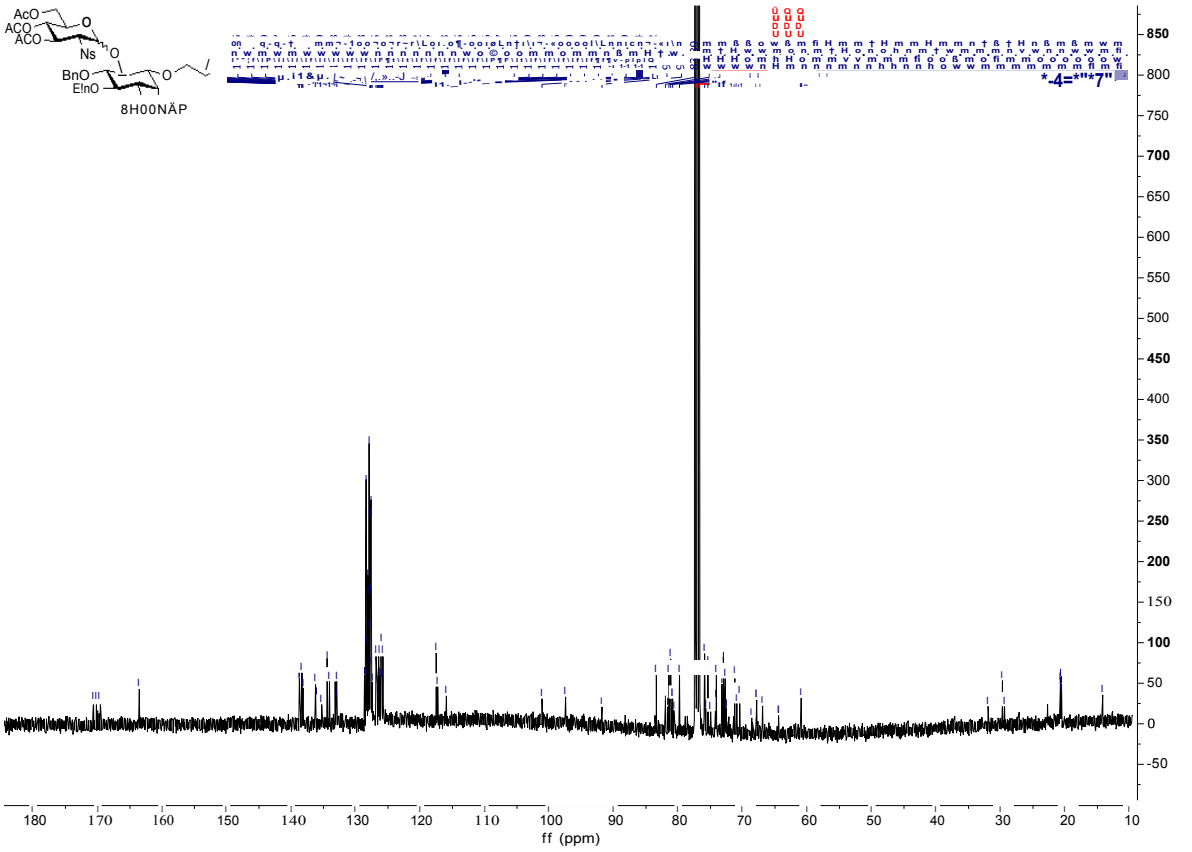

2-azido-2-deoxy-α-D-glucopyranosyl-(1→6)-1-*O*-allyl-2-O-(2-napthyl)methyl-3,4,5-tetra-*O*-benzyl-D-*myo*-inositol (3-13)

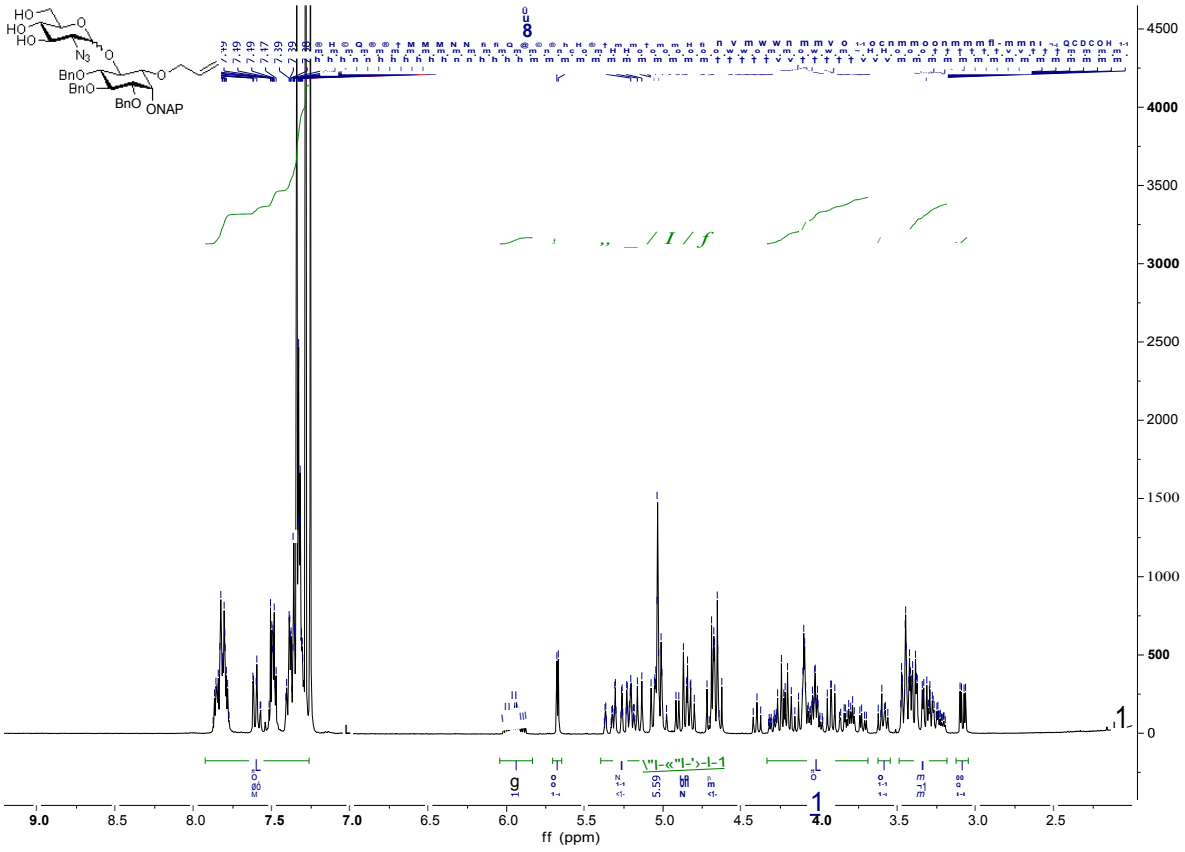

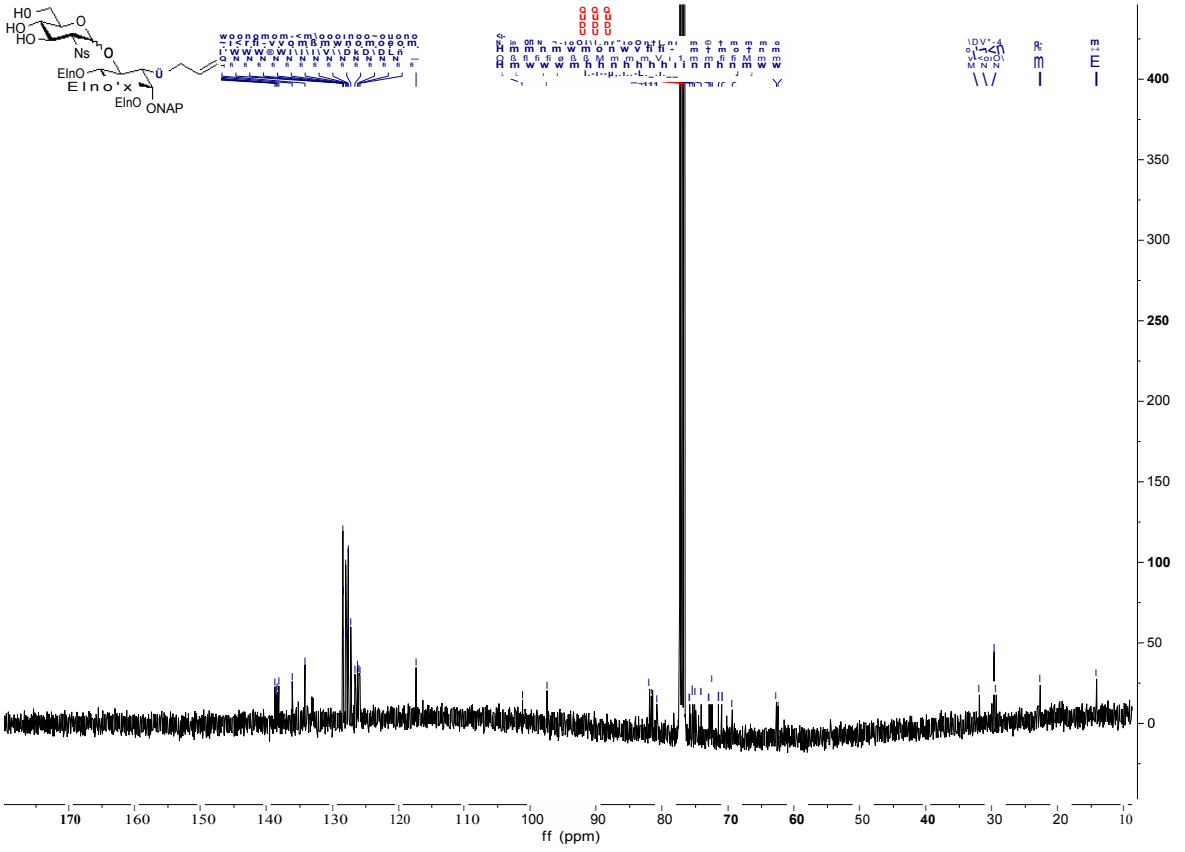

3,-*O*-benzyl-4,6-*O*-benzylidene-2-azido-2-deoxy-α-D-glucopyranosyl-(1→6)-1-*O*-allyl-2-O-(2-napthyl)methyl-3,4,5-tetra-*O*-benzyl-D-*myo*-inositol (3-14)

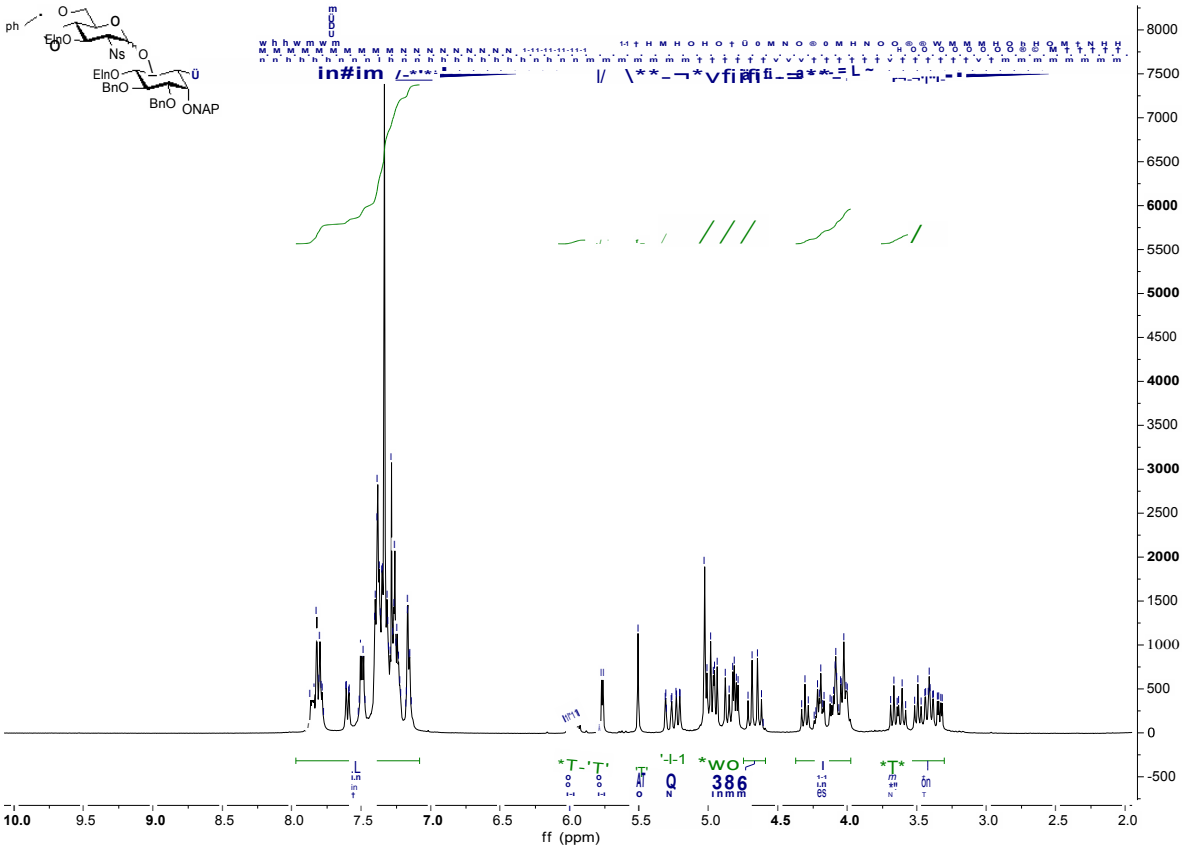

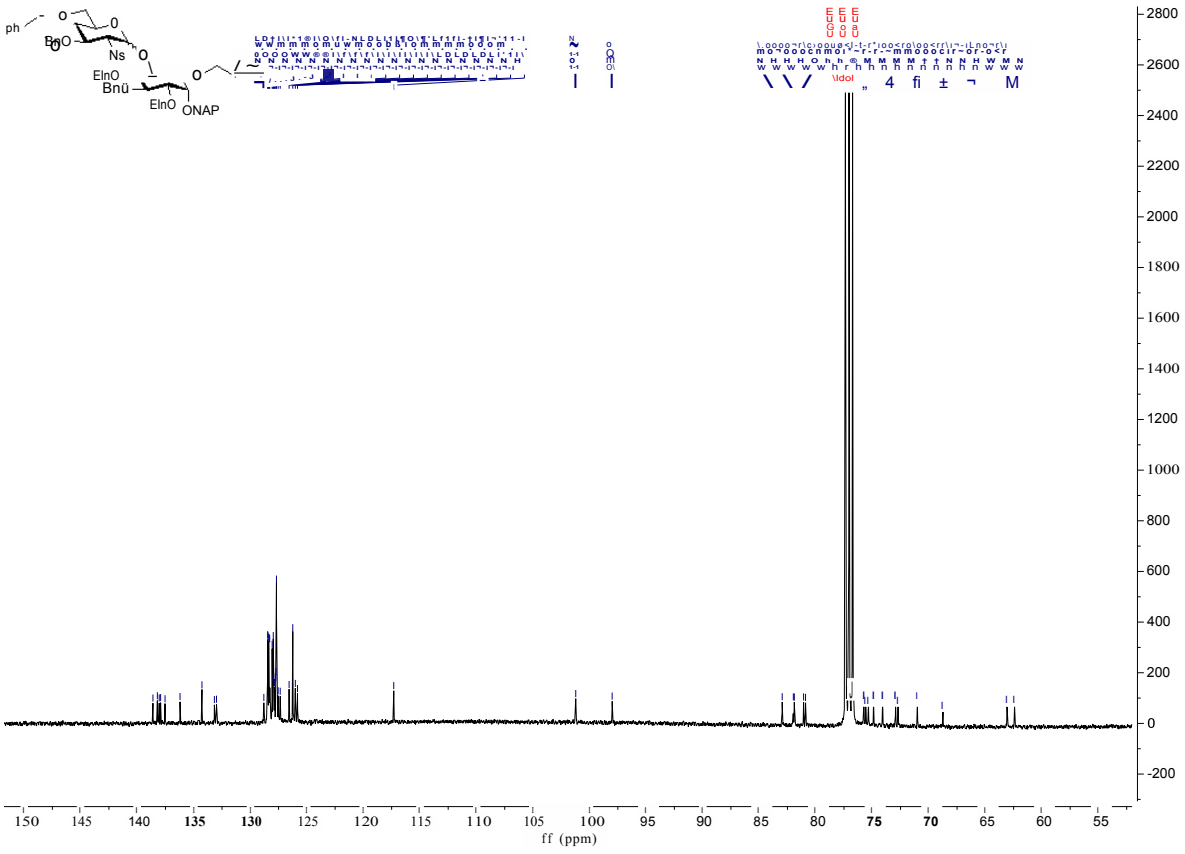

3,6–di-*O*-benzyl-2-azido-2-deoxy-α-D-glucopyranosyl-(1→6)-1-*O*-allyl-2-O-(2-napthyl)methyl-3,4,5-tetra-*O*-benzyl-D-*myo*-inositol (3-7c)

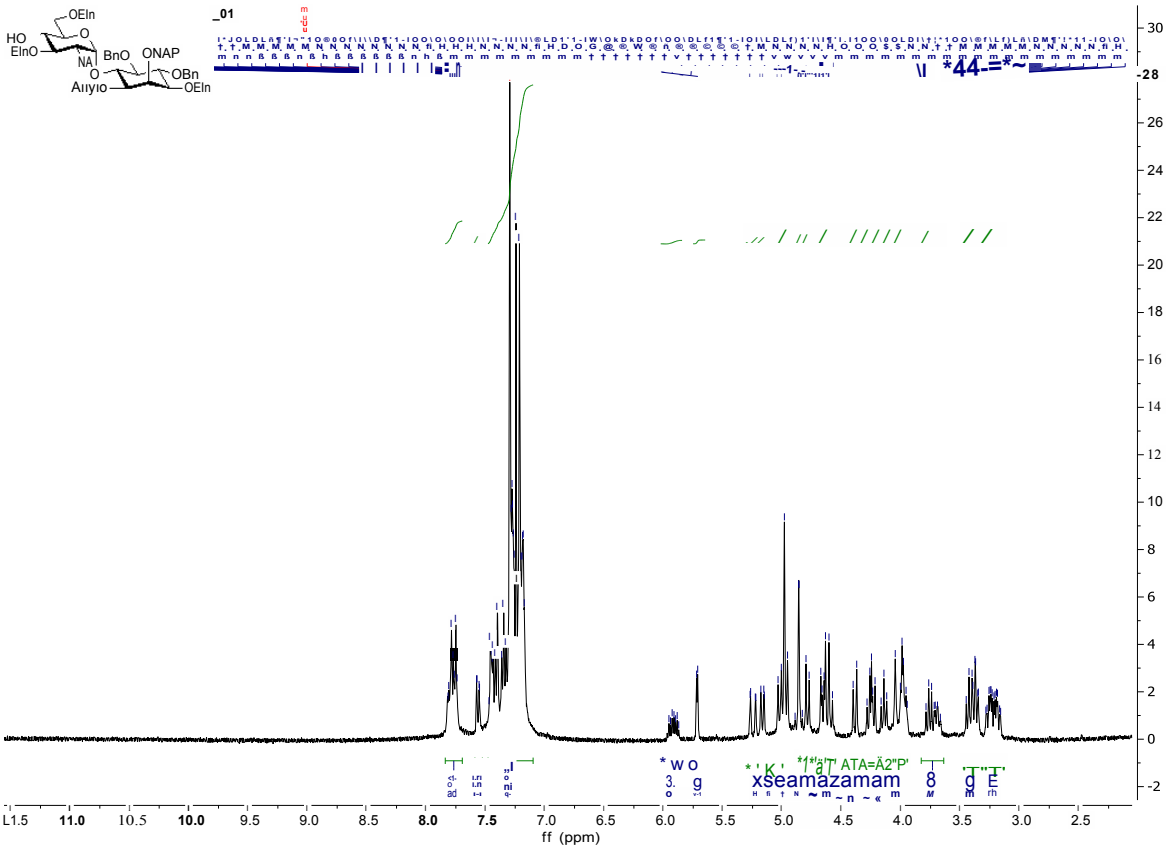

3,4,6-tri-*O*-benzyl-α-D-mannopyranosyl-(1→2)-3,4-di-*O*-benzyl-6-*O*-tri*iso*propylsilyl-α-D-mannopyranosyl-(1→2)-3,4,6-tri-*O*-benzyl-α-D-mannopyranosyl-(1→6)-2-O-levulinyl-3-*O*-benzyl-4-O-(2-napthyl)methyl -α-D-mannopyranosyl-(1→4)-2-azido-3,6-di-*O*-benzyl-2-deoxy-α-D-glucopyranosyl-(1→6)-2,3,4,5-tetra-*O*-benzyl-D-*myo*-inositol (3-18)

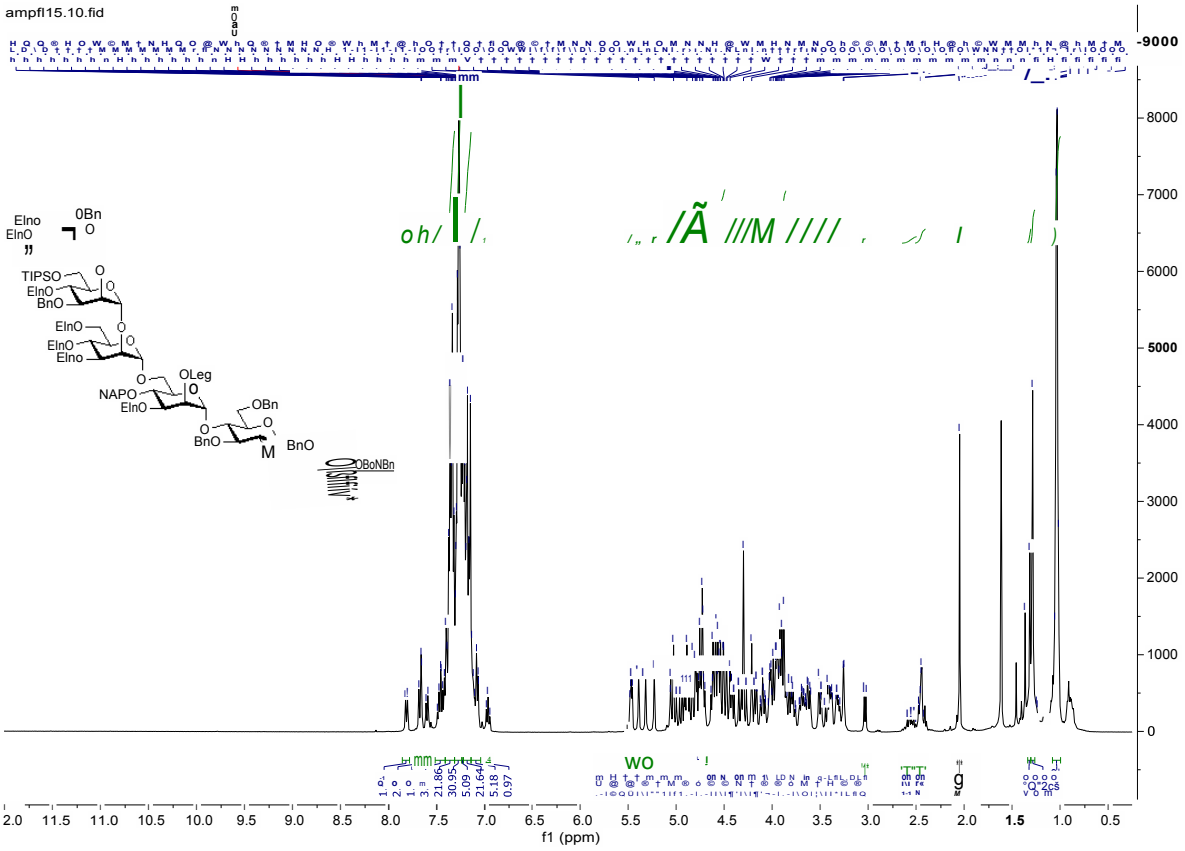

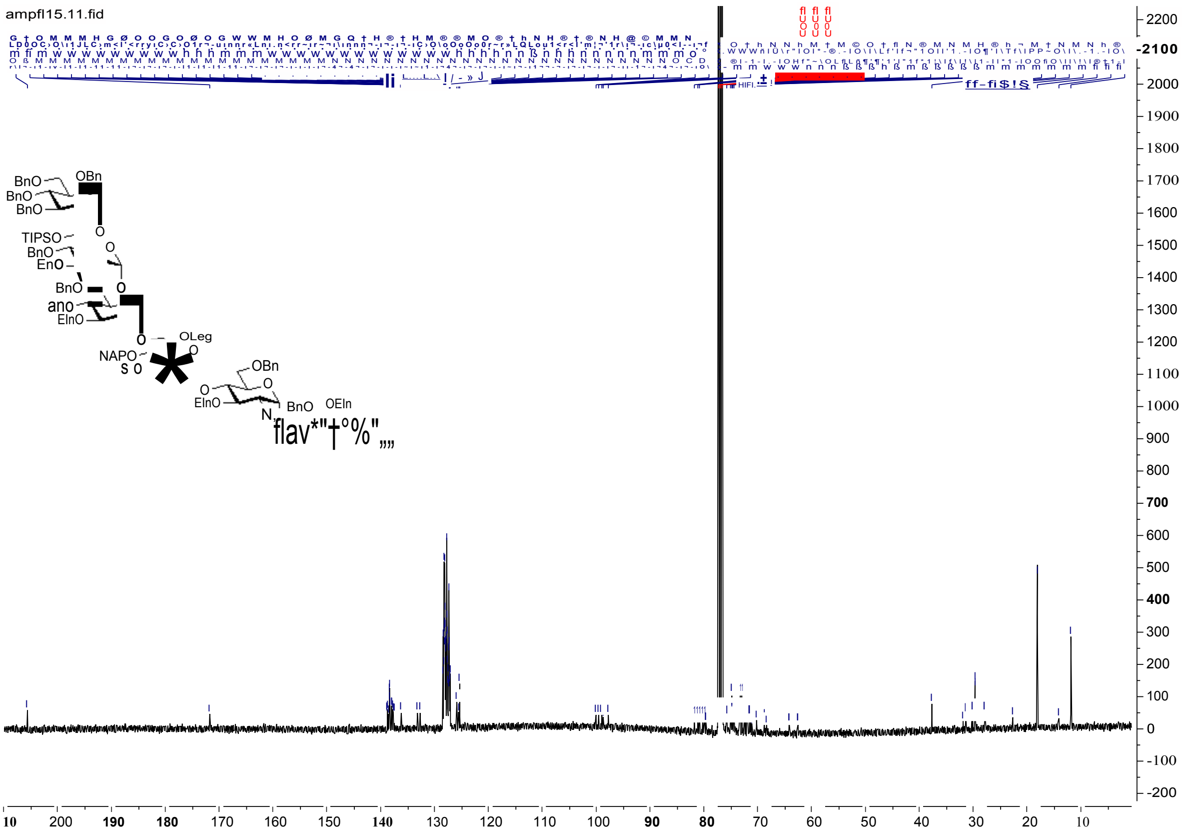
ampfl15.11.fid
BnO
OBn
TIPSO
NAPO
OLeg
BnO
OEln

J L Q Ã Ã M

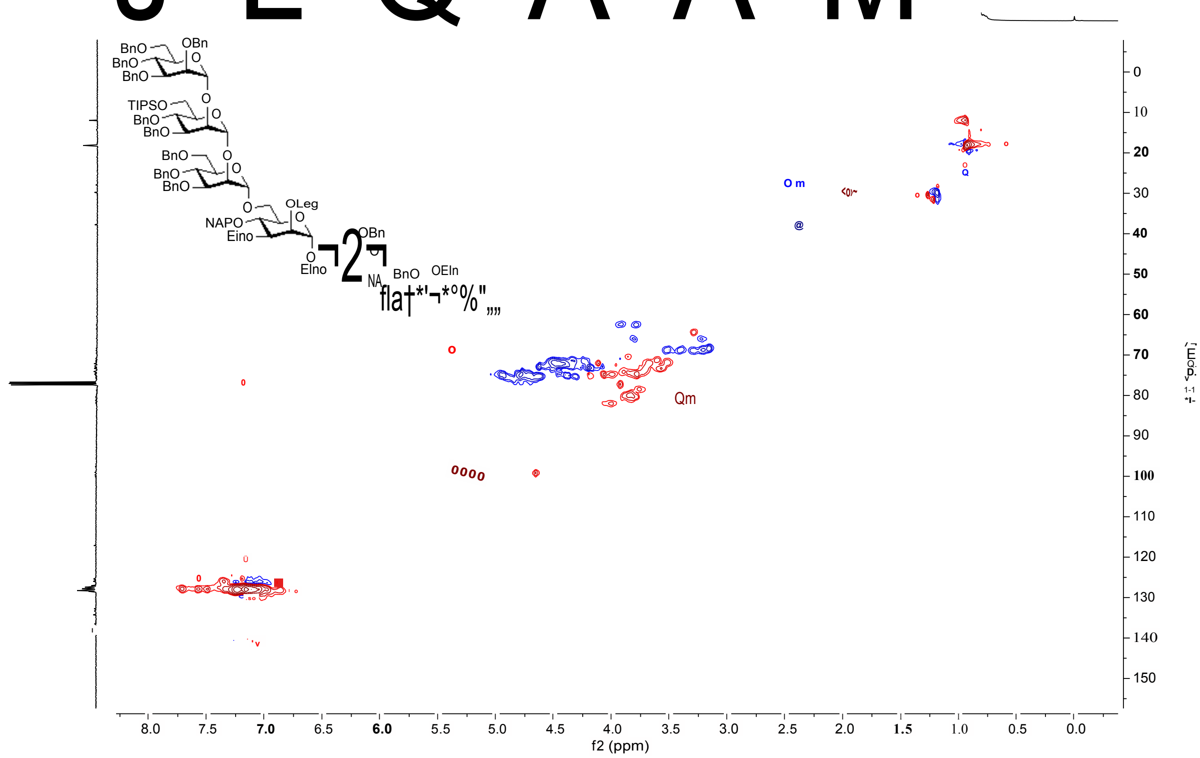
BnO
OBn
TIPSO
NAPO
OLeg
BnO
OEln
f2 (ppm)

1,2-di-*O*-stearoyl-*sn*-glycero-3-H-phosphonate (3-8)

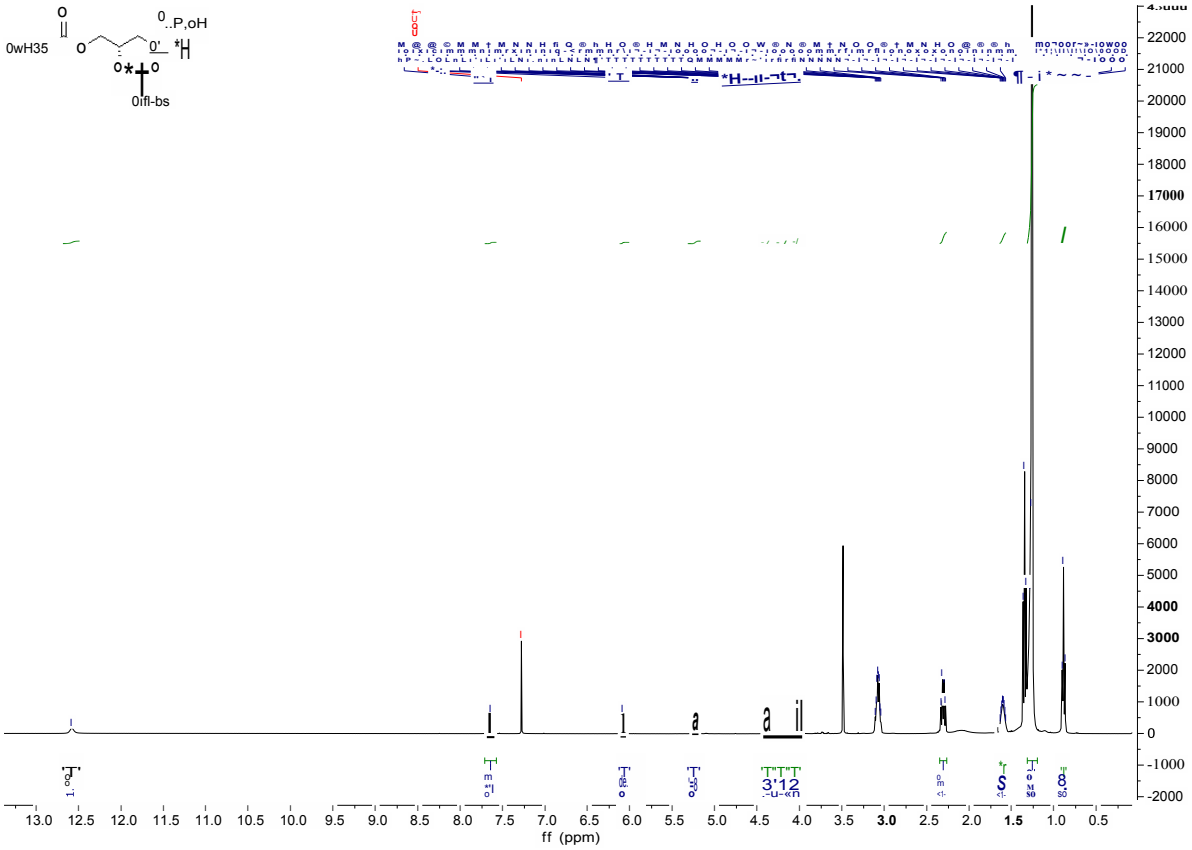

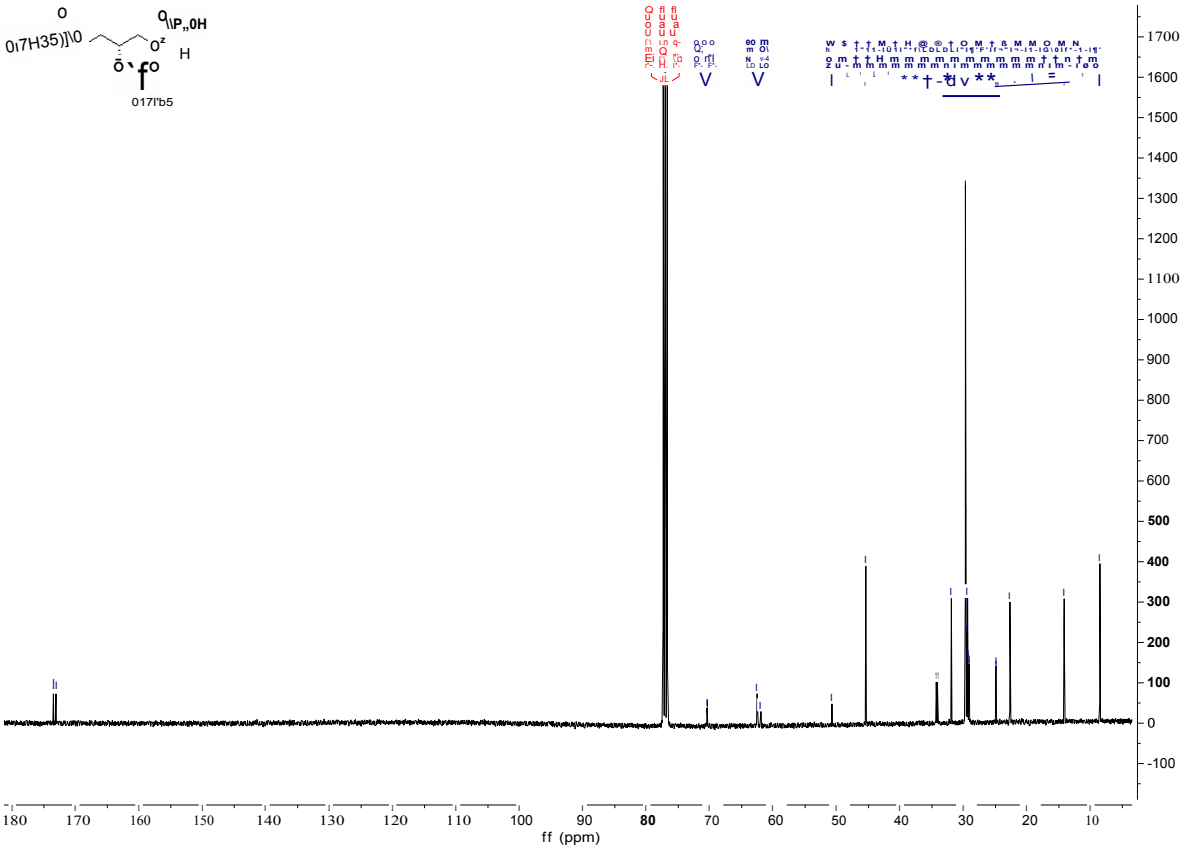

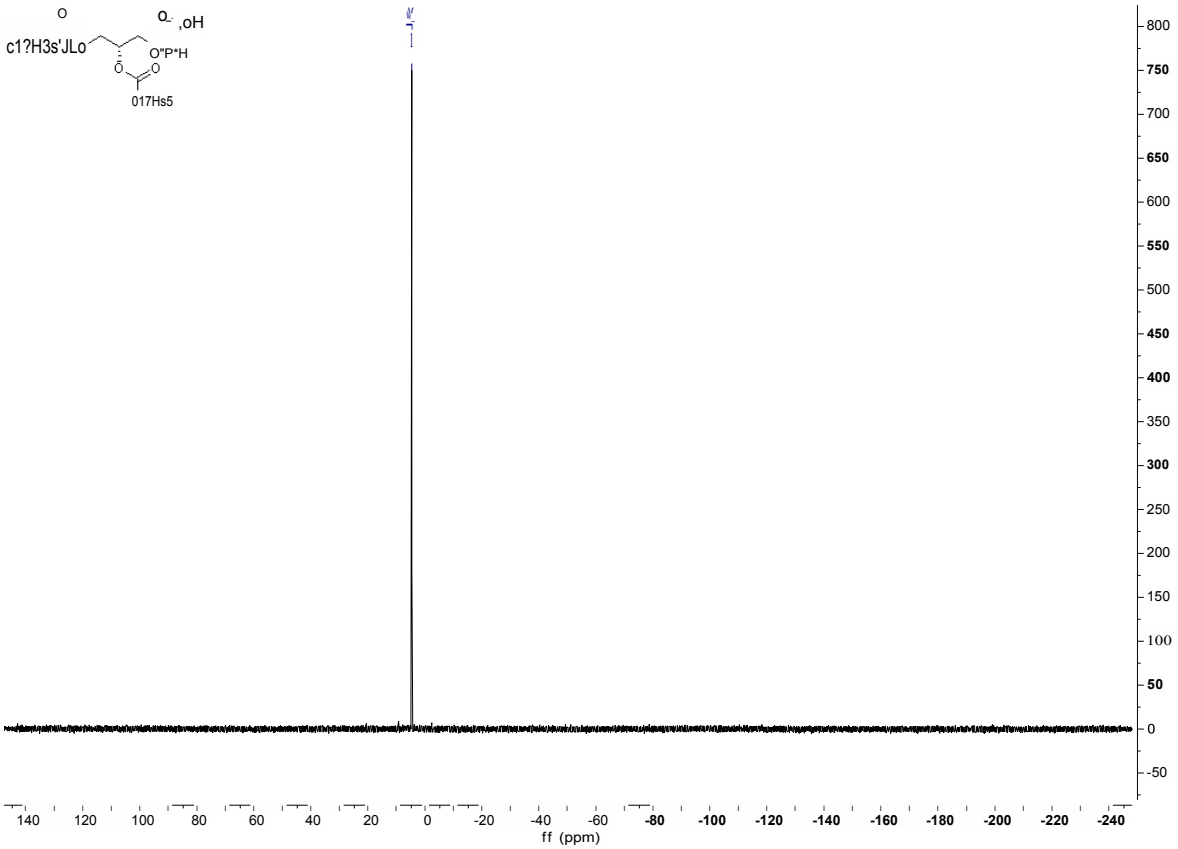
O
O
,oH
c1?H3s'JLo
O"P*H
O
O
017Hs5
800
750
700
650
600
550
500
450
400
350
300
250
200
150
100
50
0
-50
140
120
100
80
60
40
20
0
-20
-40
-60
-80
-100
-120
-140
-160
-180
-200
-220
-240
ff (ppm)

3,4,6-tri-*O*-benzyl-α-D-mannopyranosyl-(1→2)-3,4-di-*O*-benzyl-6-*O*-tri*iso*propylsilyl-α-D-mannopyranosyl-(1→2)-3,4,6-tri-*O*-benzyl-α-D-mannopyranosyl-(1→6)-2-O-levulinyl-3-*O*-benzyl-4-O-(2-napthyl)methyl-α-D-mannopyranosyl-(1→4)-2-azido-3,6-di-*O*-benzyl-2-deoxy-α-D-glucopyranosyl-(1→6)-1-*O*-(1,2-dimyristoyl-*sn*-glyceryl-phosphonato)-2,3,4,5-tetra-*O*-benzyl-D-*myo*-inositol (3-19)

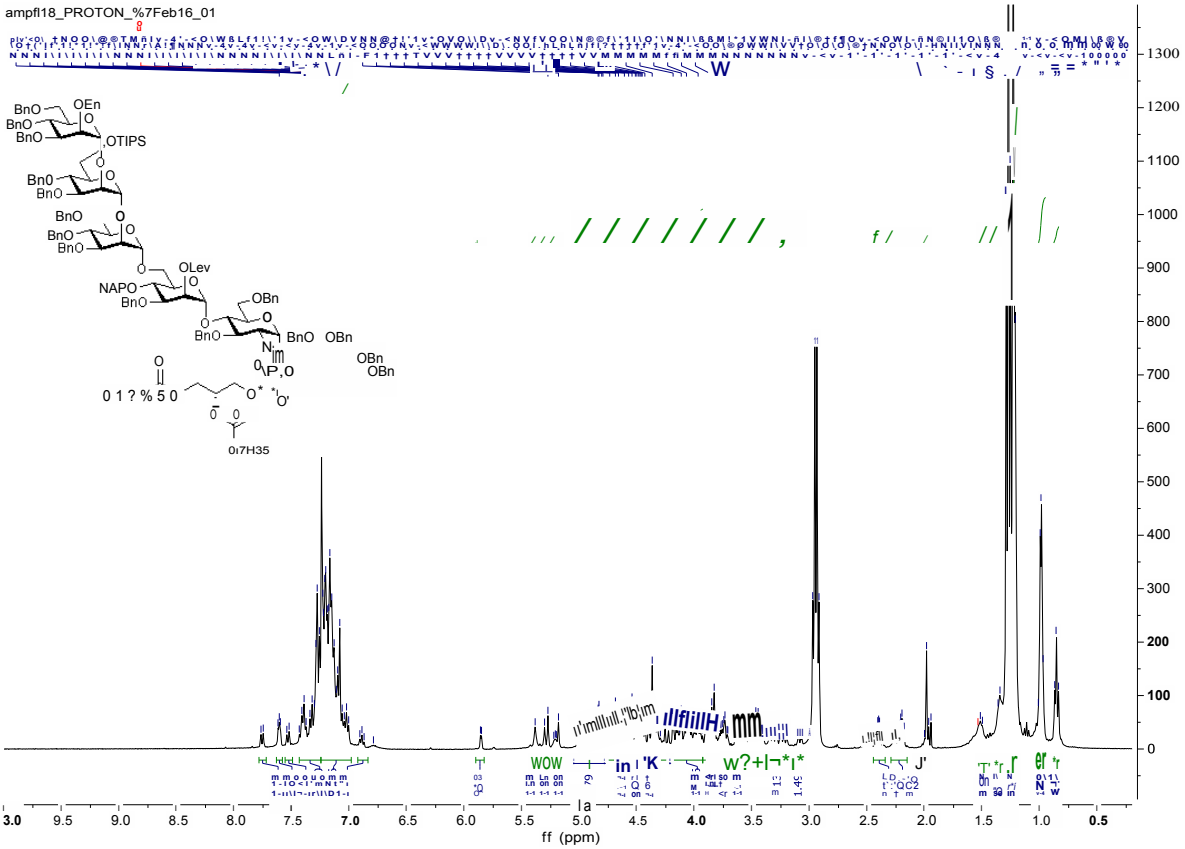

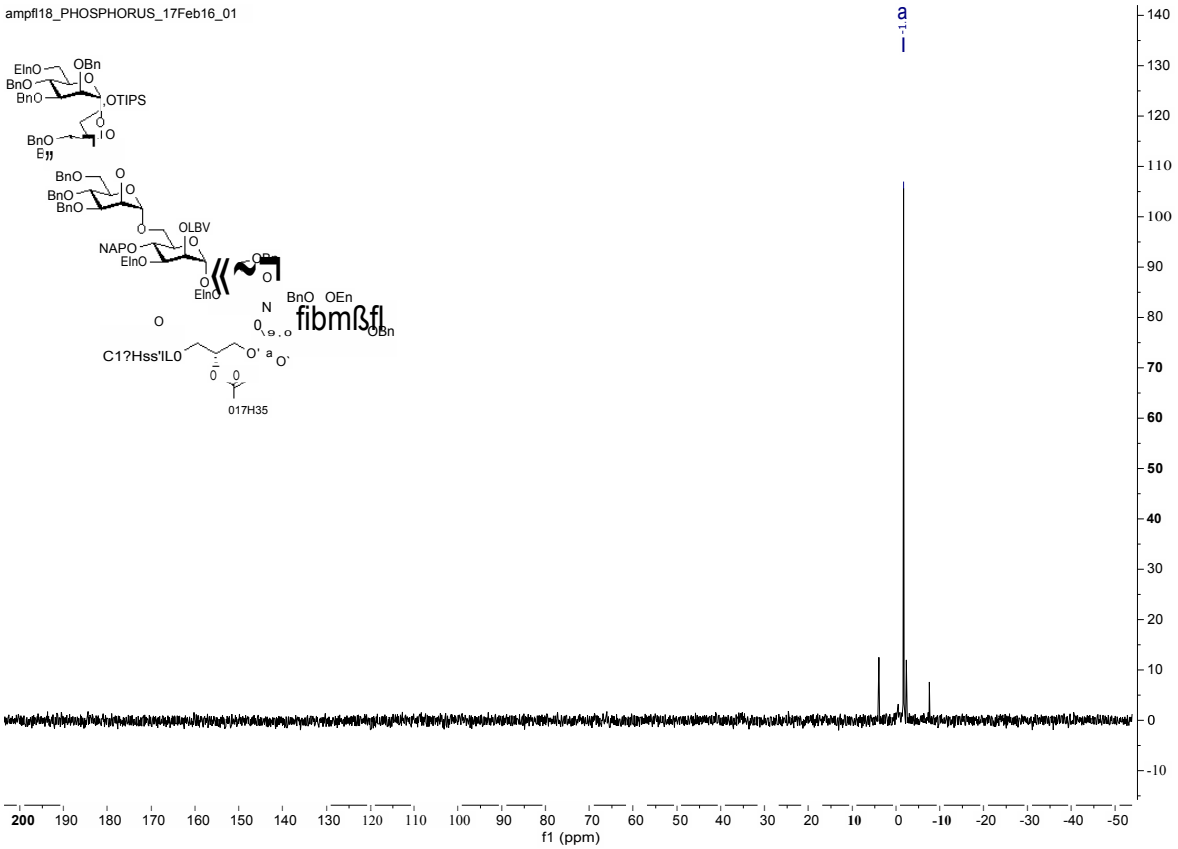
ampfl18_PHOSPHORUS_17Feb16_01
f1 (ppm)

3,4,6-tri-*O*-benzyl-α-D-mannopyranosyl-(1→2)-3,4-di-*O*-benzyl-α-D-mannopyranosyl-(1→2)-3,4,6-tri-*O*-benzyl-α-D-mannopyranosyl-(1→6)-2-O-levulinyl-3-*O*-benzyl-4-O-(2-napthyl)methyl-α-D-mannopyranosyl-(1→4)-2-azido-3,6-di-*O*-benzyl-2-deoxy-α-D-glucopyranosyl-(1→6)-1-*O*-(1,2-dimyristoyl-*sn*-glyceryl-phosphonato)-2,3,4,5-tetra-*O*-benzyl-D-*myo*-inositol (3-20)

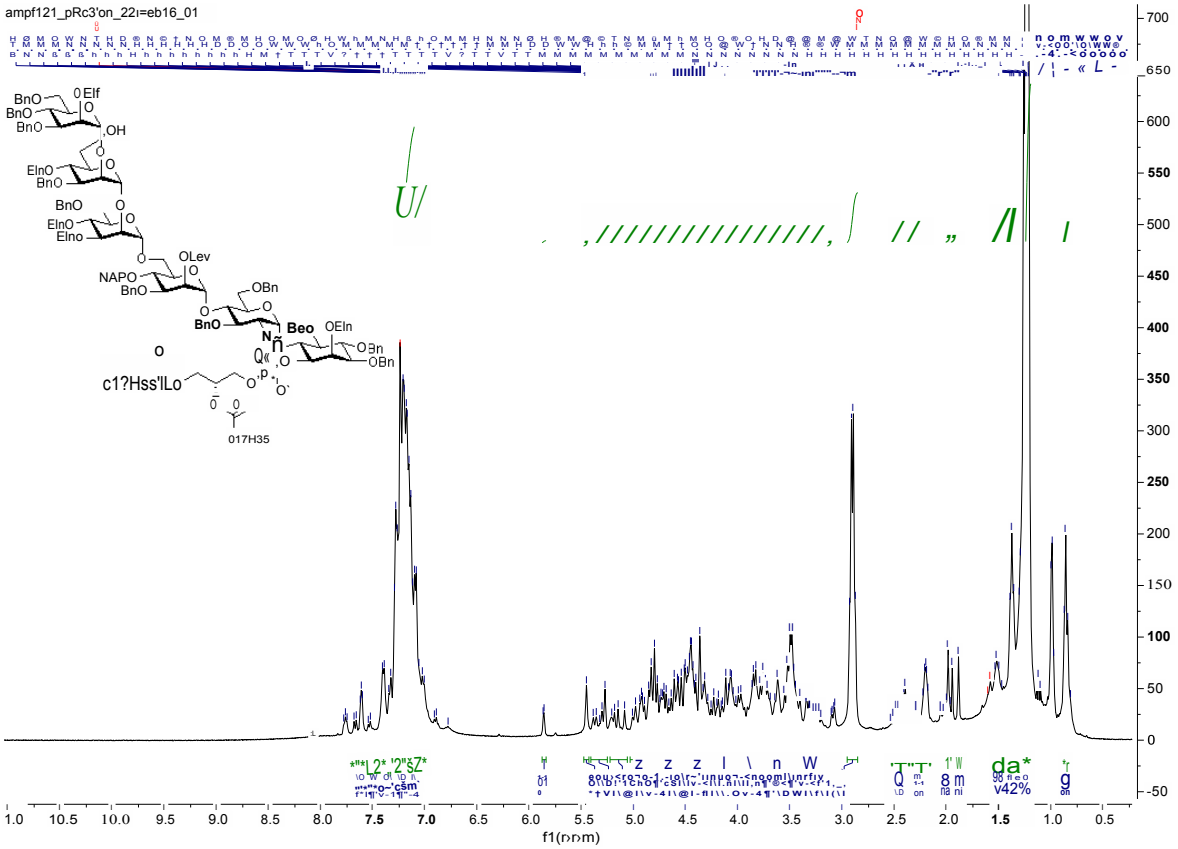

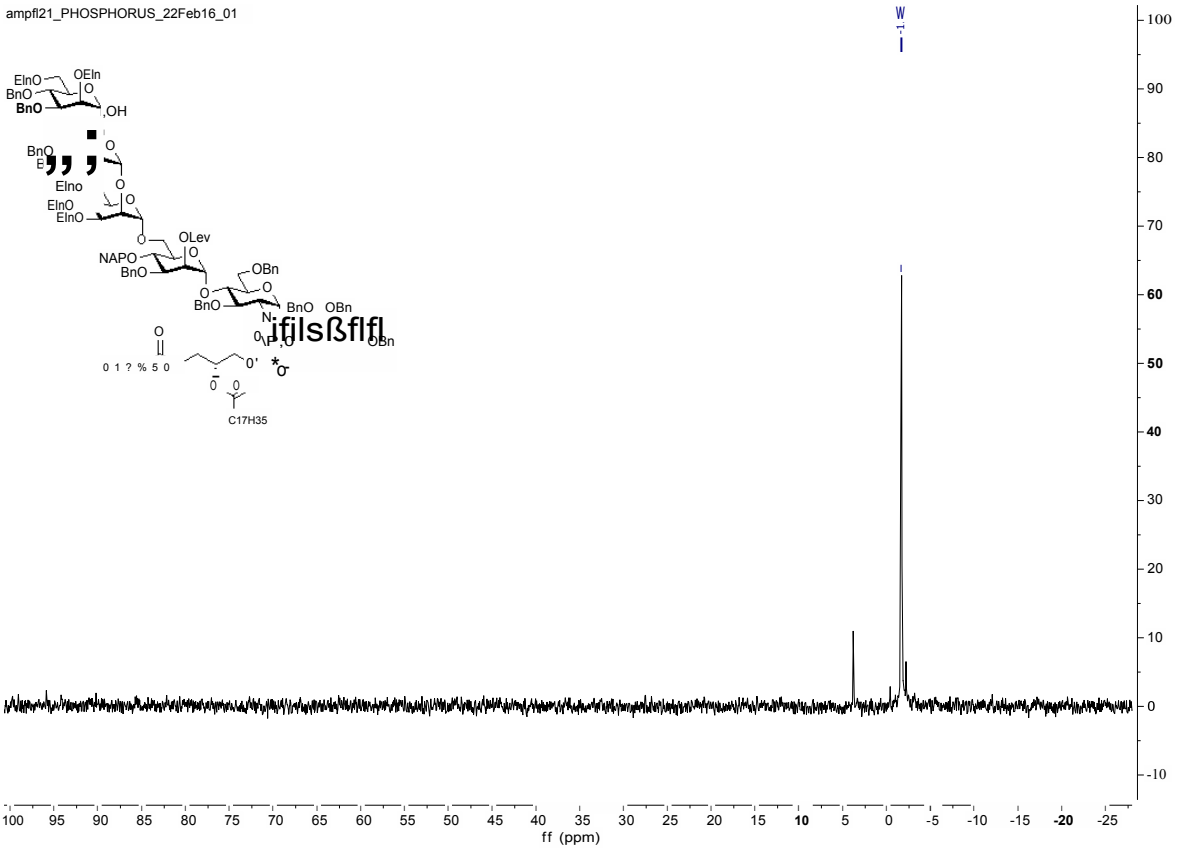
ampfl21_PHOSPHORUS_22Feb16_01
ff (ppm)

3,4,6-tri-*O*-benzyl-α-D-mannopyranosyl-(1→2)-3,4-di-*O*-benzyl-6-*O*-(2-(*N*-(*tert*-butoxycarbonyl)-S-(*tert*-butyl)-L-cysteinyl)aminoethyl phosphonato)-α-D-mannopyranosyl-(1→2)-3,4,6-tri-*O*-benzyl-α-D-mannopyranosyl-(1→6)-2-O-levulinyl-3,4-di-*O*-benzyl-α-D-mannopyranosyl-(1→4)-2-azido-3,6-di-*O*-benzyl-2-deoxy-α-D-glucopyranosyl-(1→6)-1-*O*-(1,2-dimyristoyl-*sn*-glyceryl-phosphonato)-2,3,4,5-tetra-*O*-benzyl-D-*myo*-inositol (3-1)

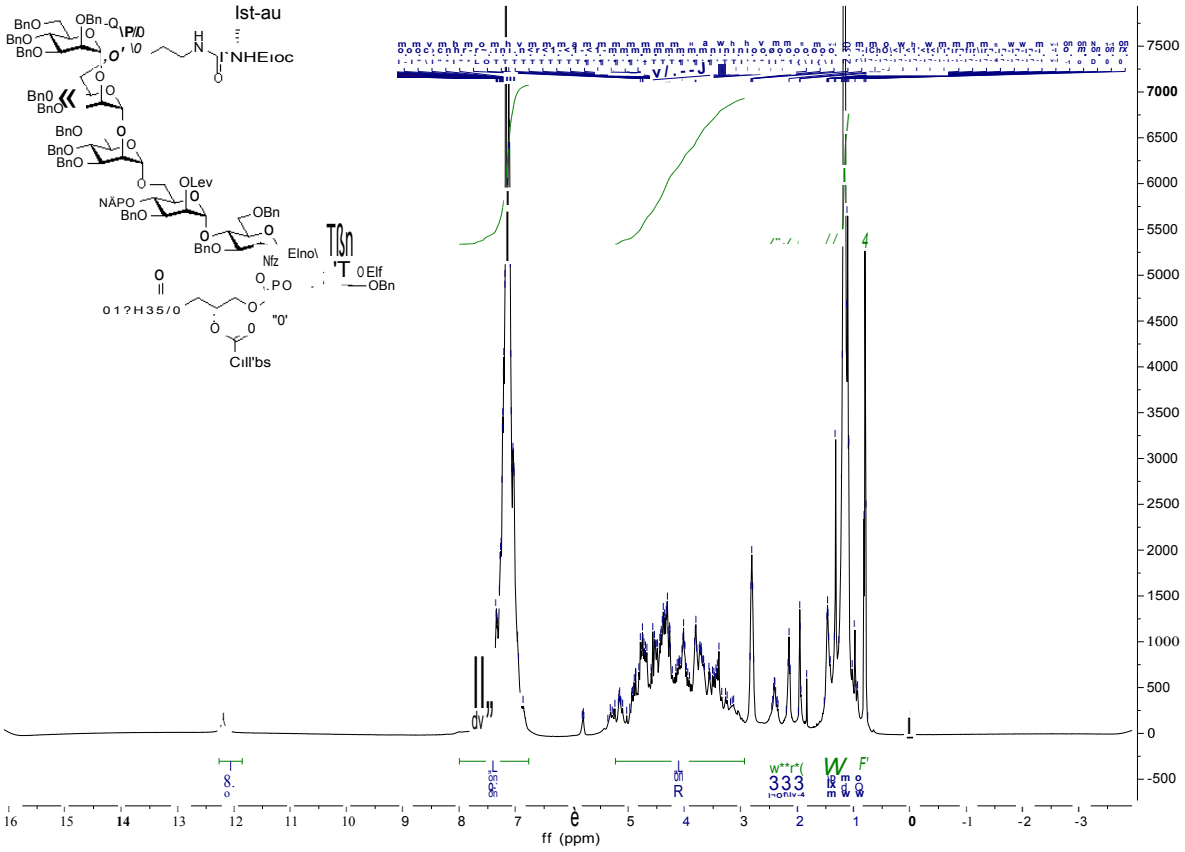

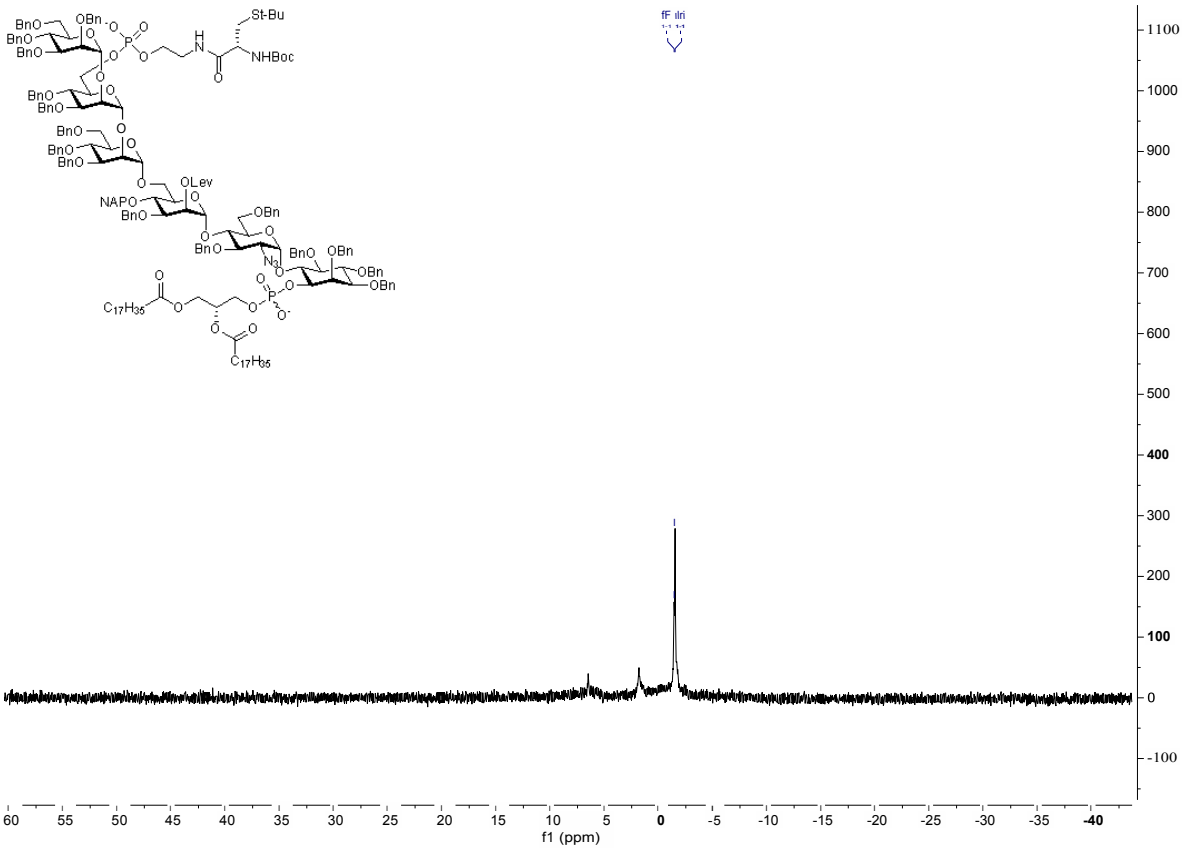
f1 (ppm)

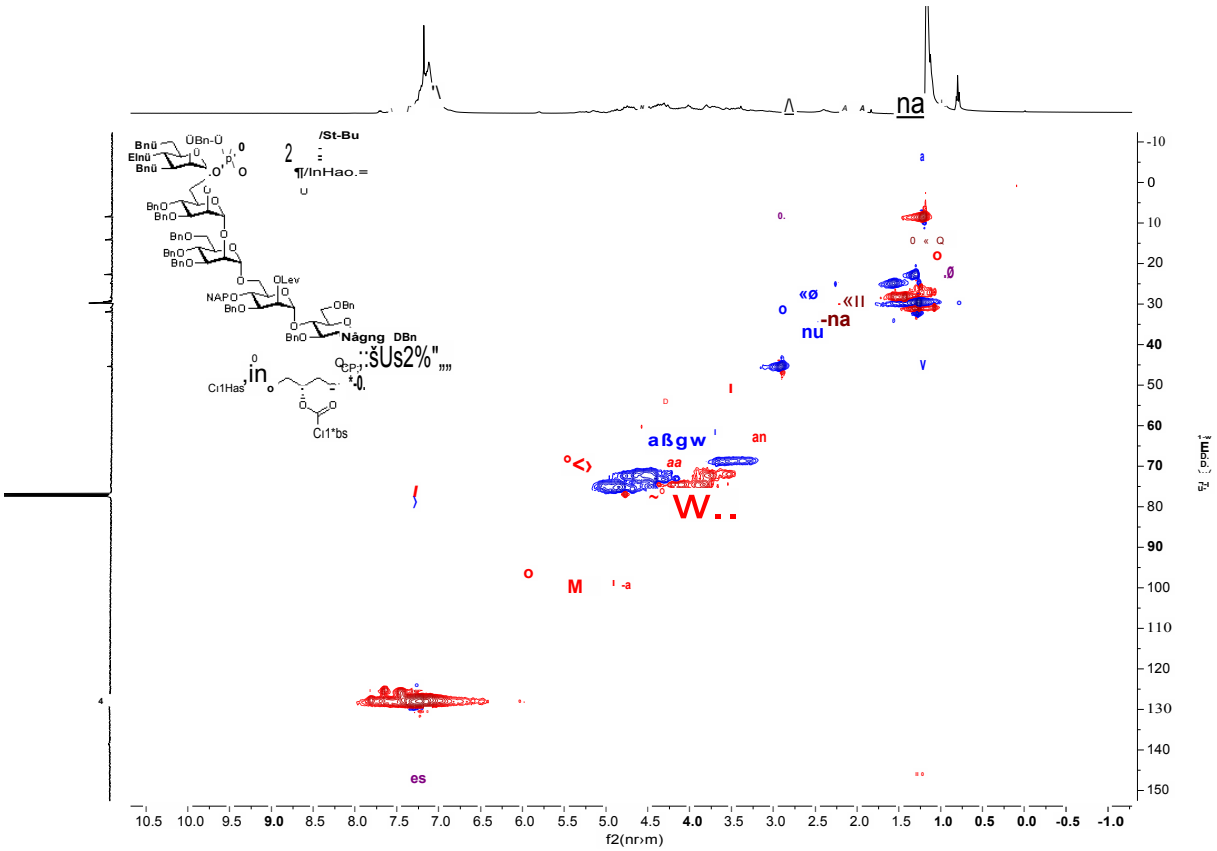
f2(ppm)

α-D-mannopyranosyl-(1→2)-6-*O*-(*N*-(S-S-mercaptoethanol-L-cysteinyl)aminoethanol-phosphonato)-α-D-mannopyranosyl-(1→2)-α-D-mannopyranosyl-(1→6)-α-D-mannopyranosyl-(1→4)-2-amino-2-deoxy-α-D-glucopyranosyl-(1→6)-1-*O*-(1,2-dimyristoyl-*sn*-glyceryl-phosphonato)-D-*myo*-inositol (*Pf*GPI 1)

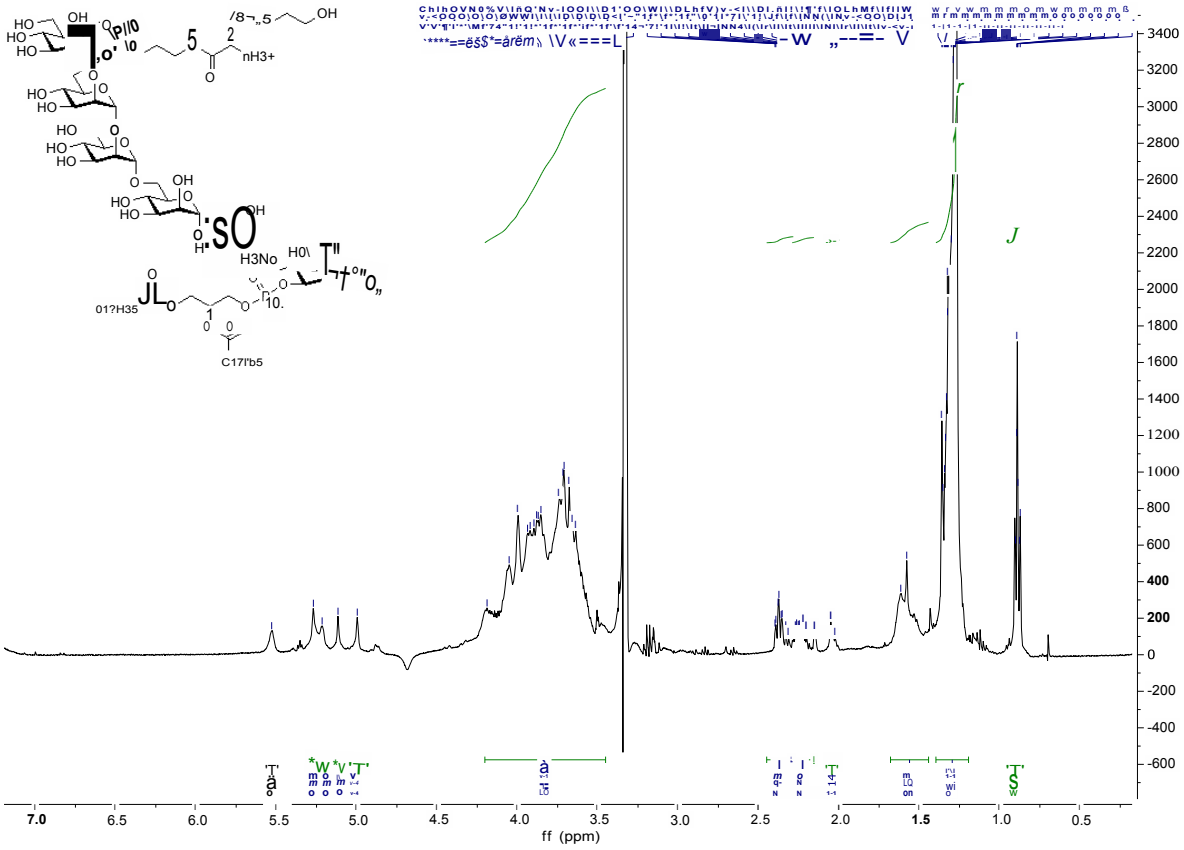

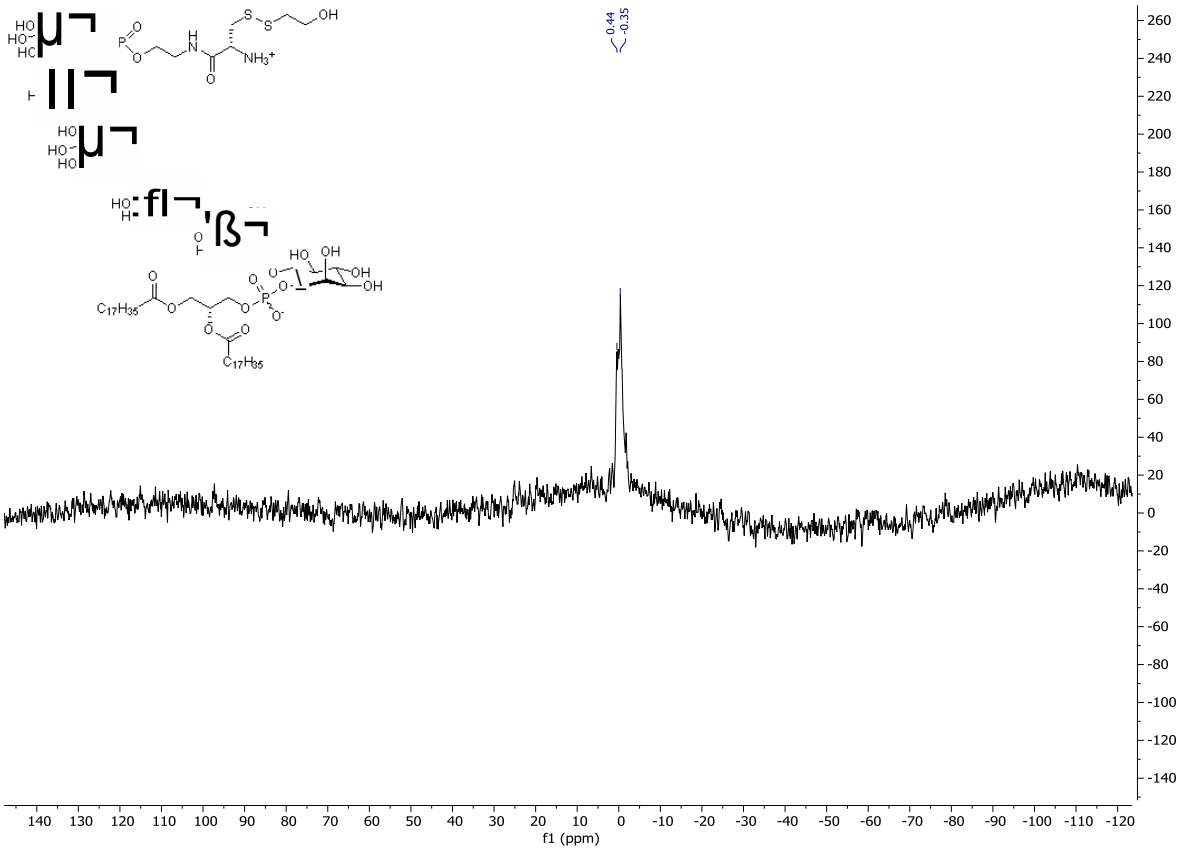
0.44
-0.35
f1 (ppm)

5.3 NMR Spectrs for Chapter 4

(R)-3-((4-methoxybenzyl)oxy)propane-1,2-diol (4-15)

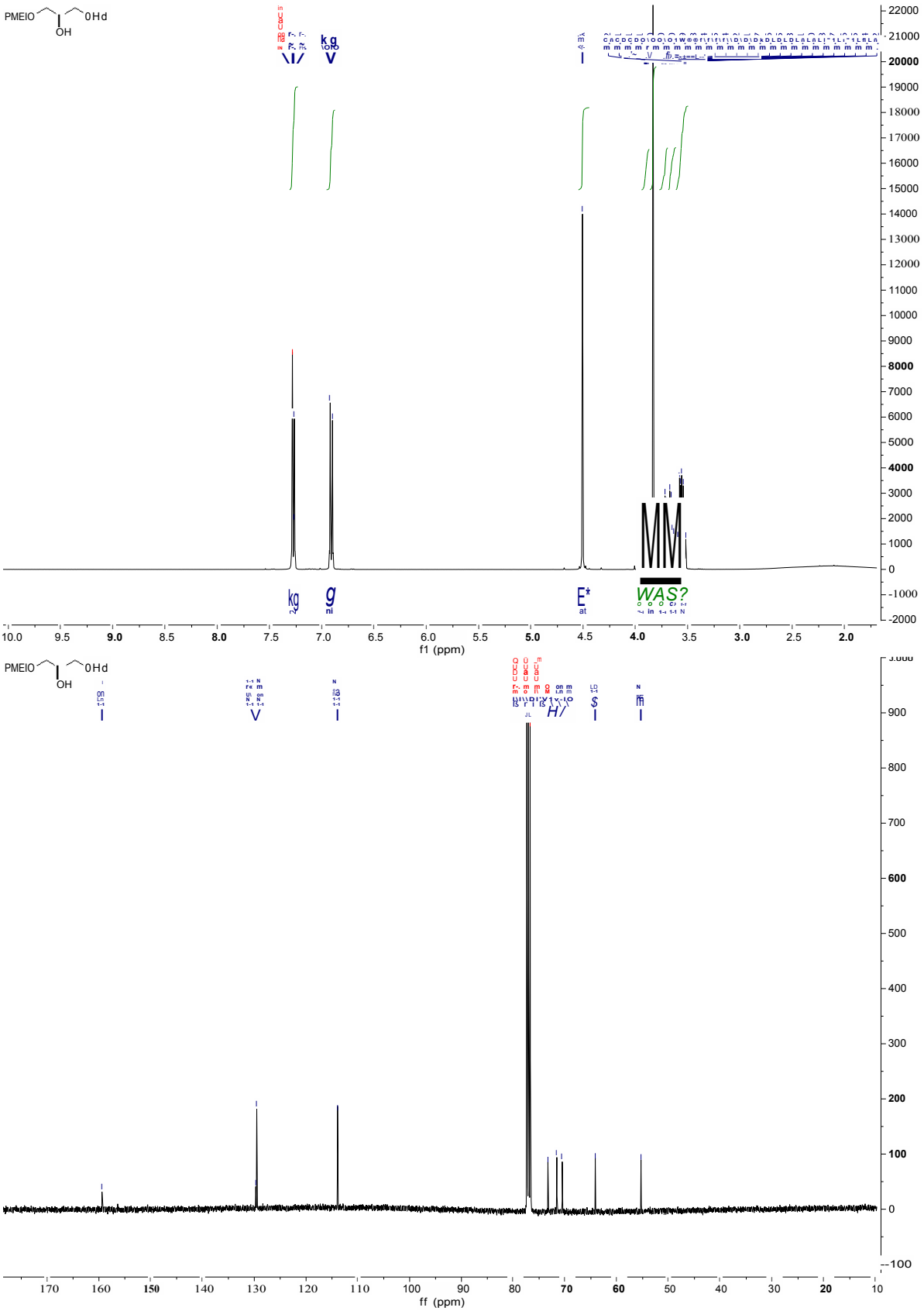

(S)-1-((4-methoxybenzyl)oxy)-3-(stearoyloxy)propan-2-yl octadec-9-enoate (4-16)

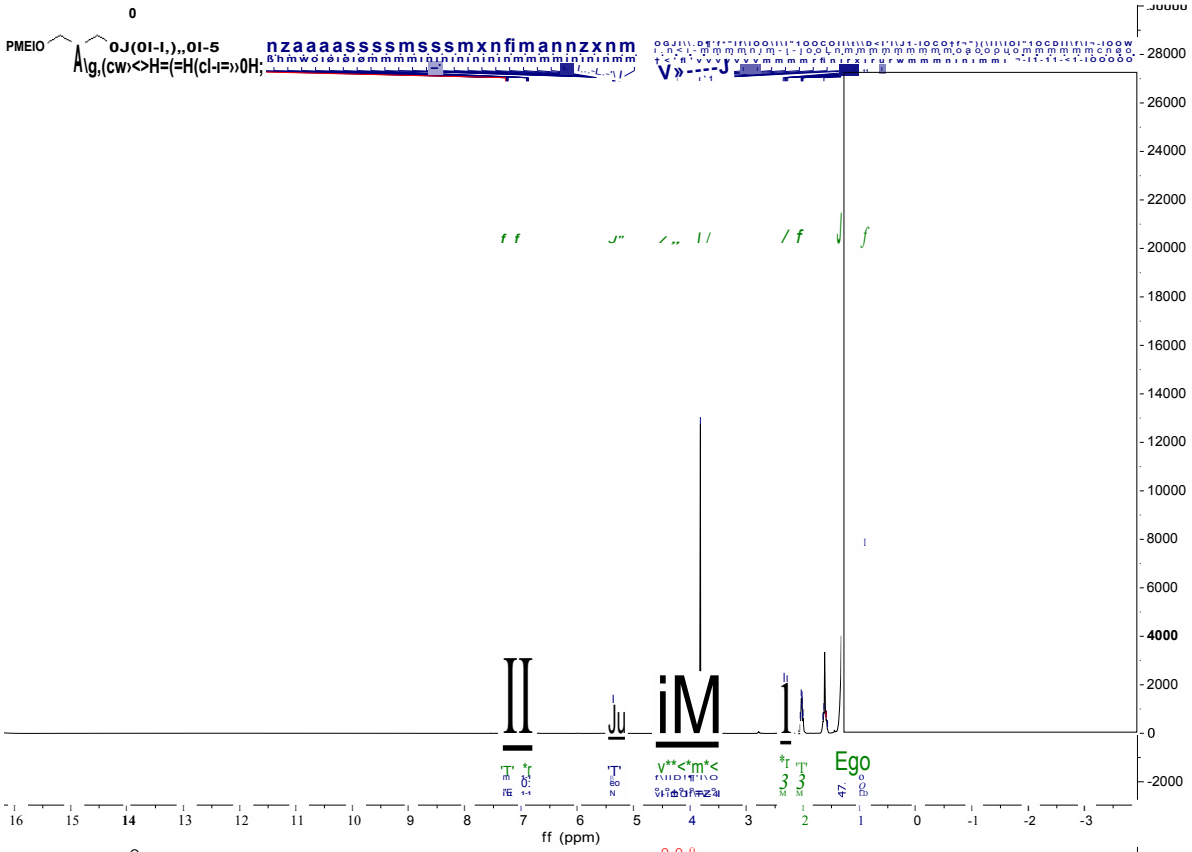

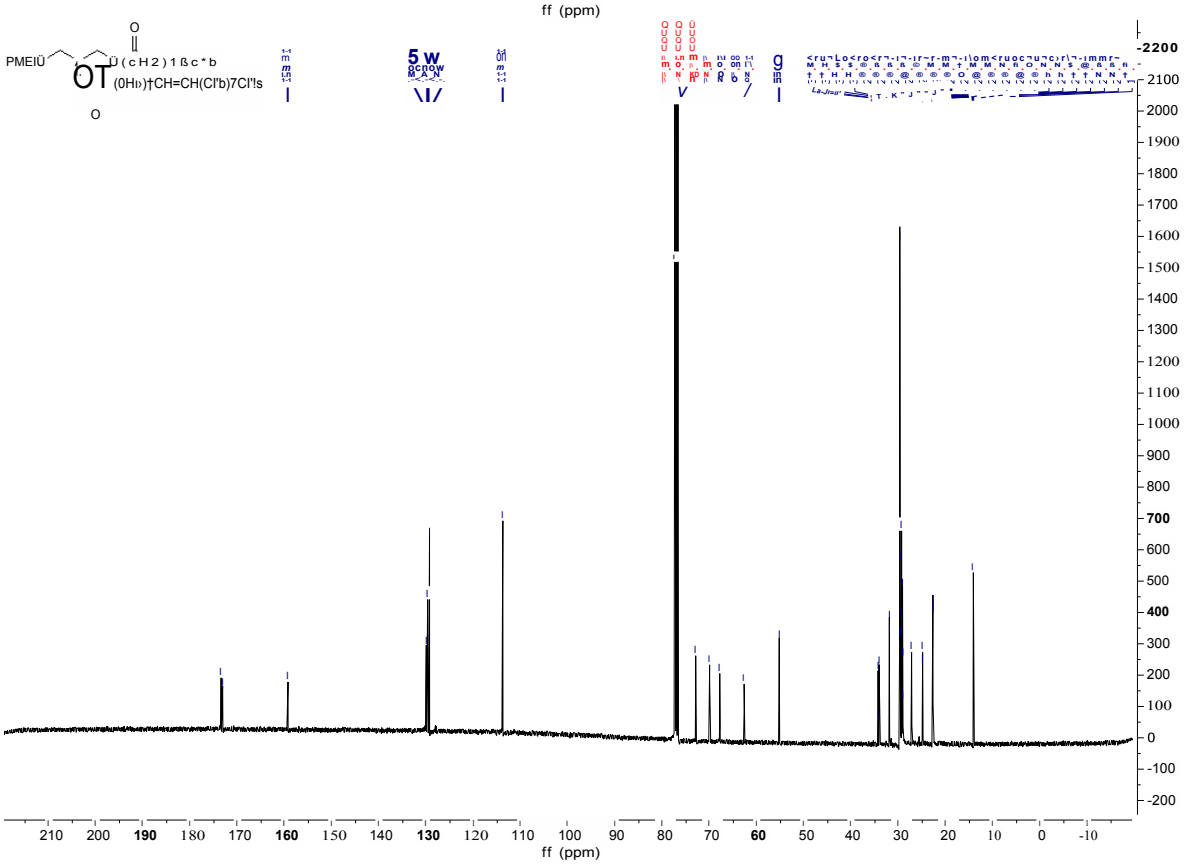

(S)-1-hydroxy-3-(stearoyloxy)propan-2-yl octadec-9-enoate (4-17)

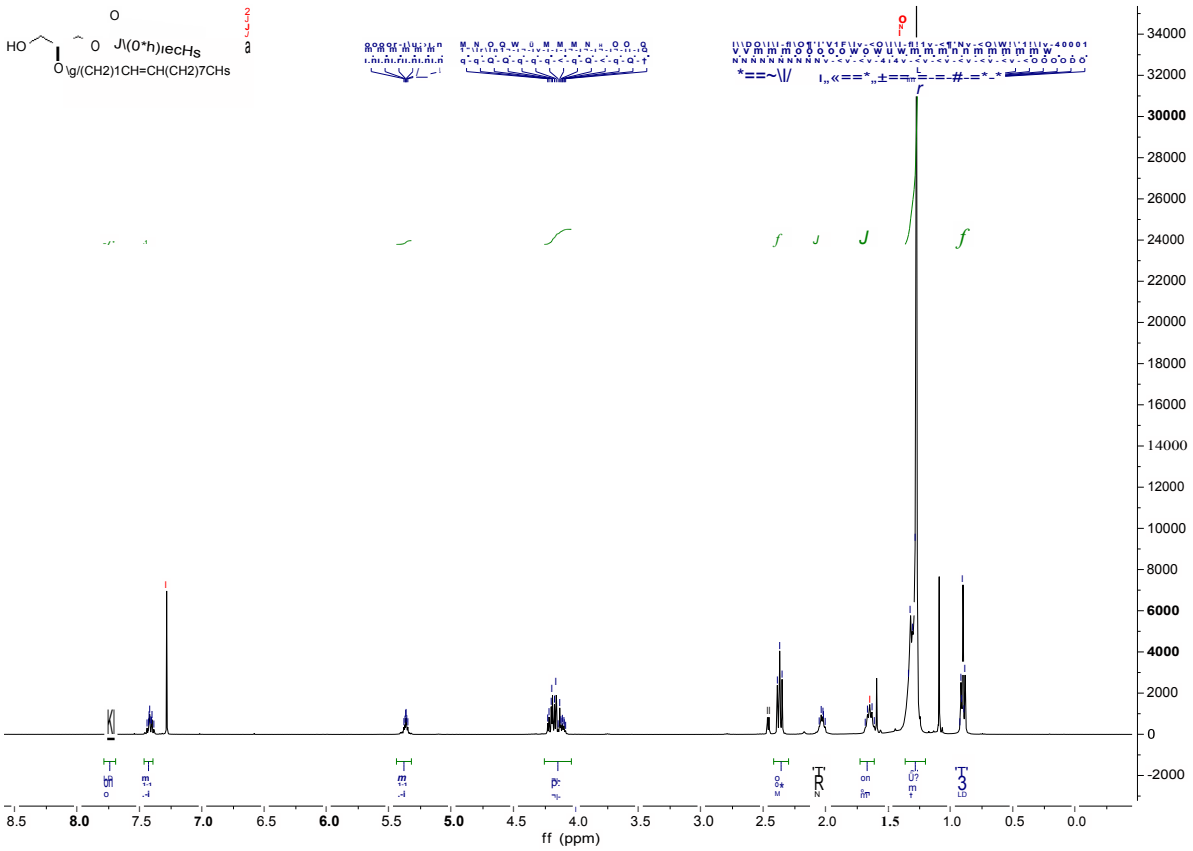

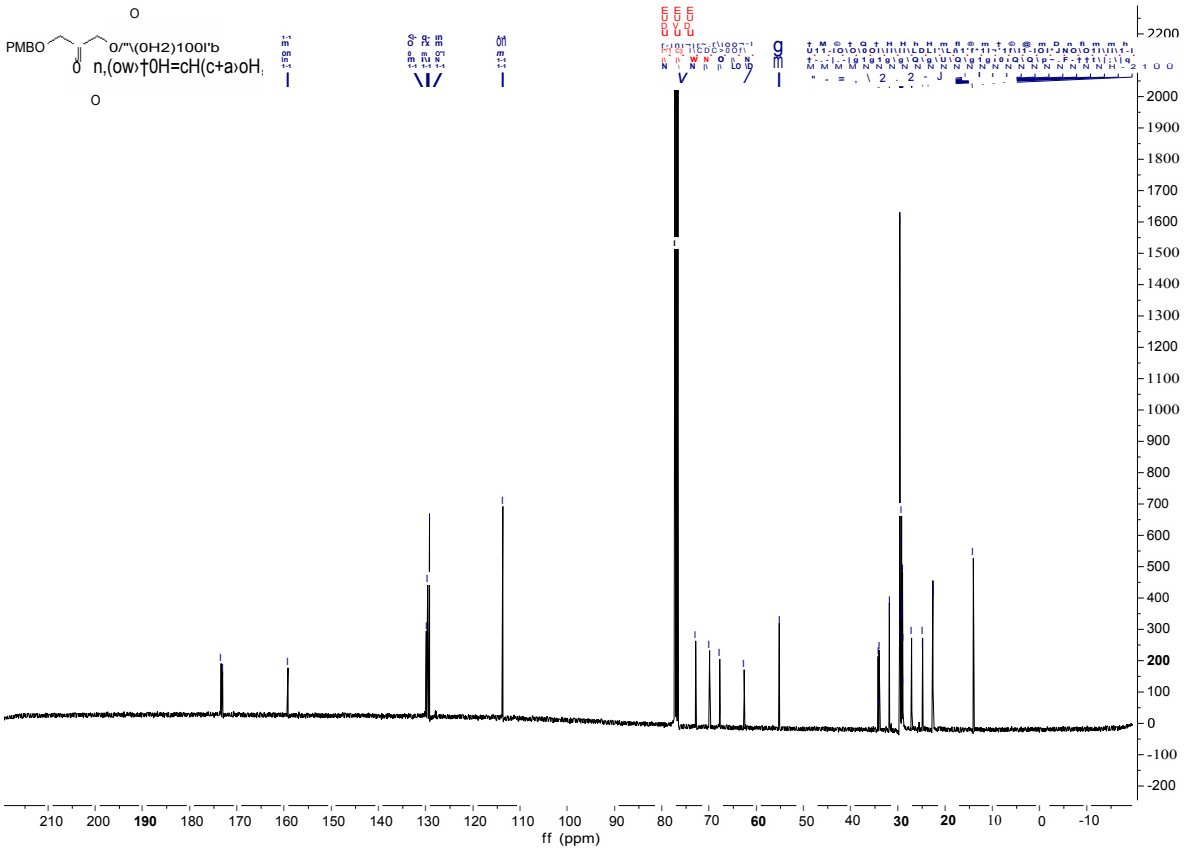

(2R)-1-((hydroxyhydrophosphoryl)oxy)-3-(stearoyloxy)propan-2-yl octadec-9-enoate (4-9)

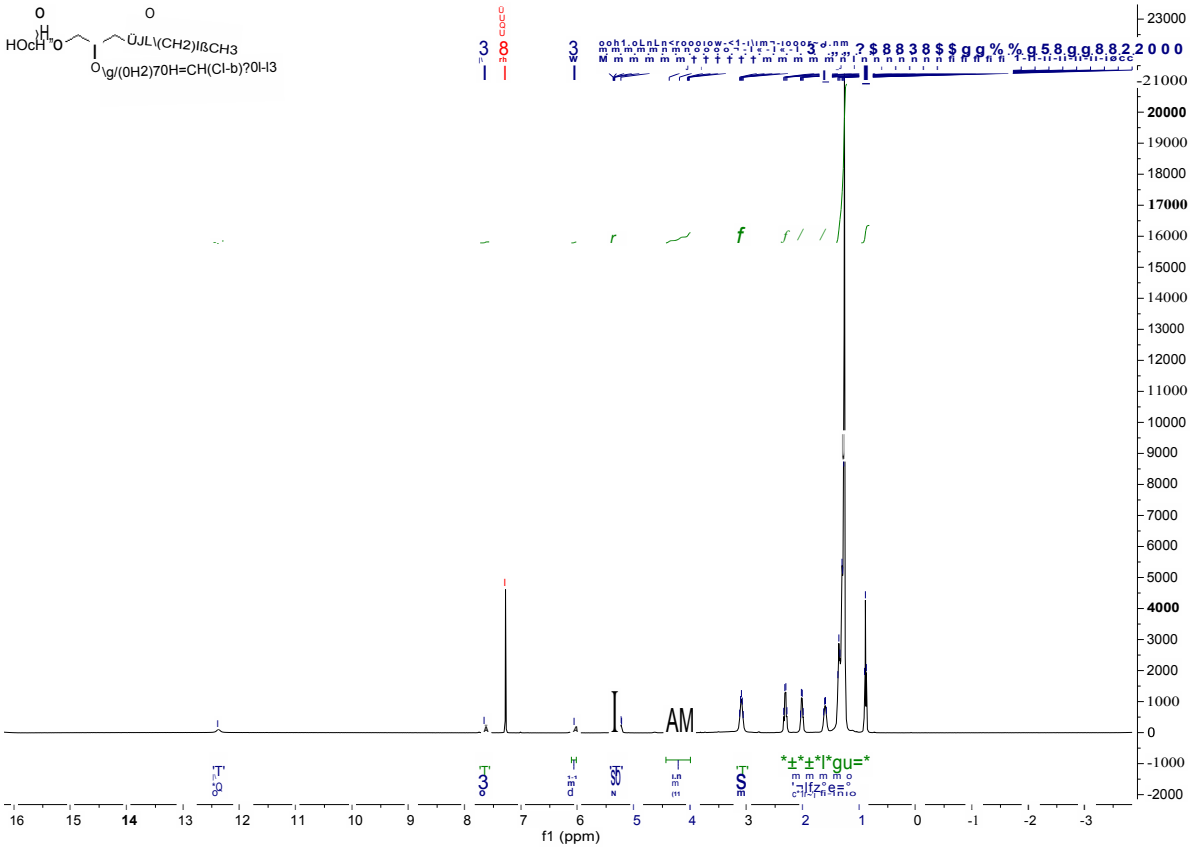

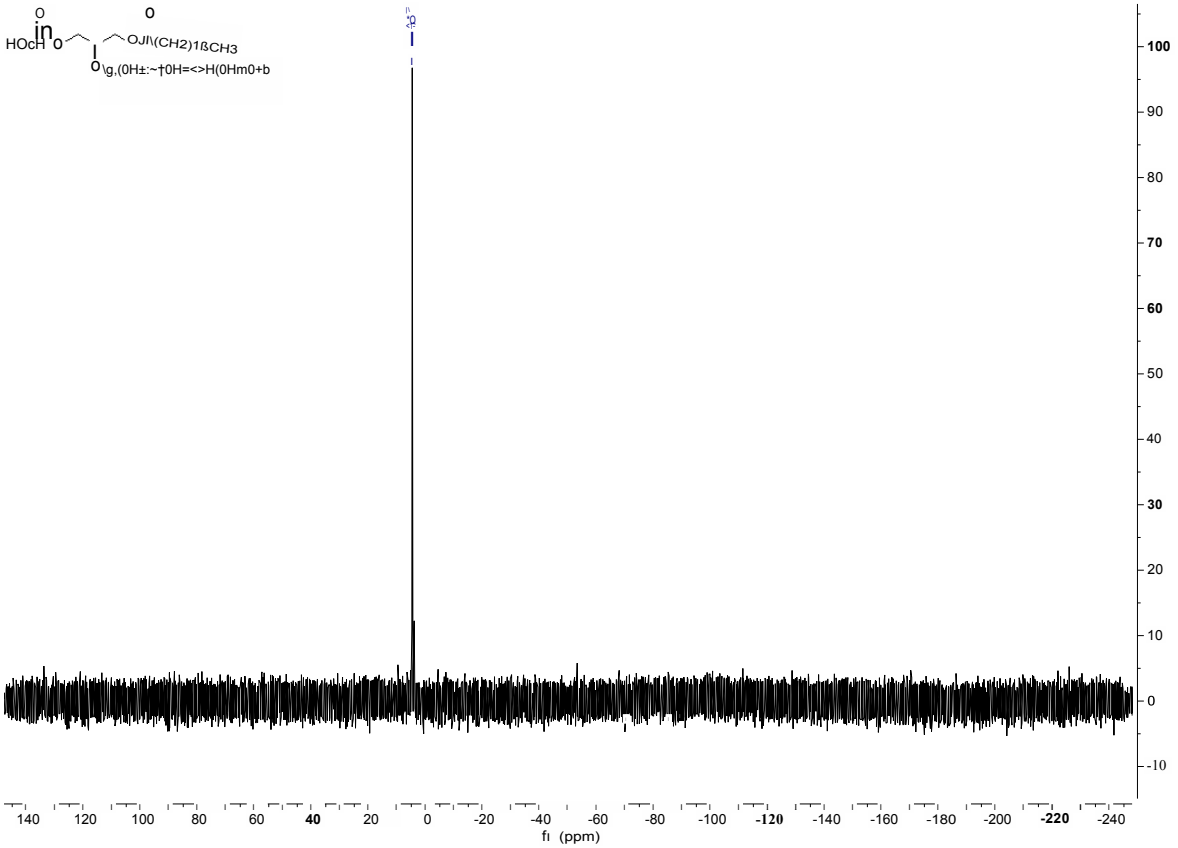

Methyl 2,3,4-tri-*O*-(2-naphthyl)methyl-α-D-glucopyranoside (4-20)

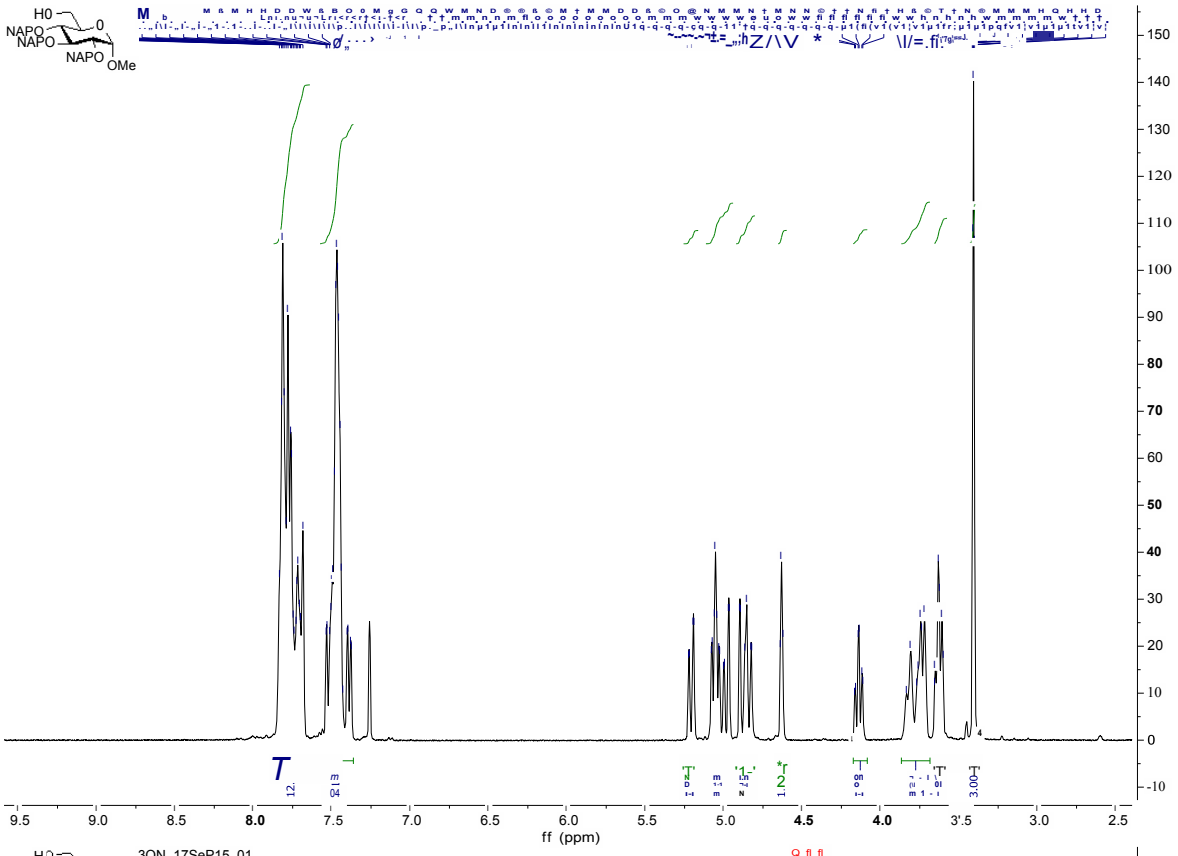

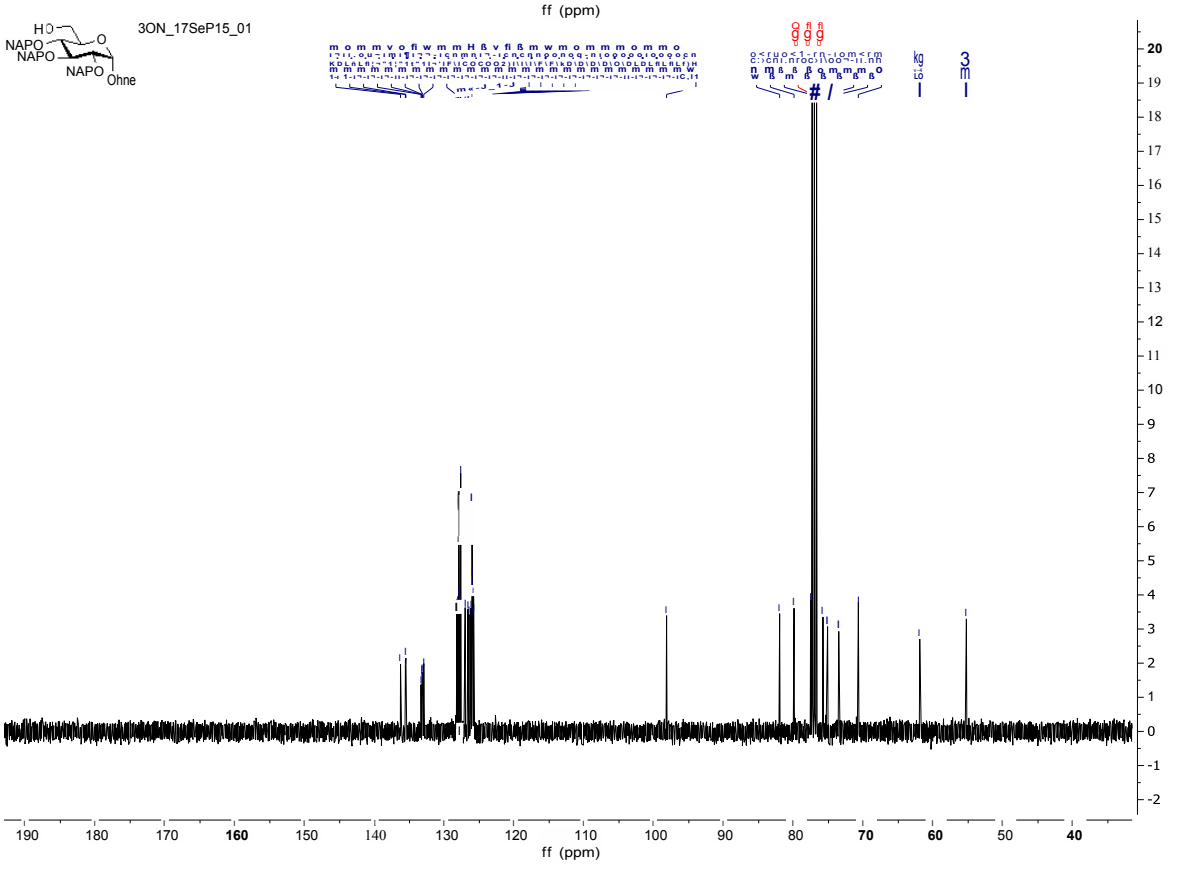

(*Z*)-Methyl 6-*O*-acetyl-2,3,4-tri-*O*-(2-naphthyl)methyl-α-D-*gluco*-hex-5-enopyranoside (4-21)

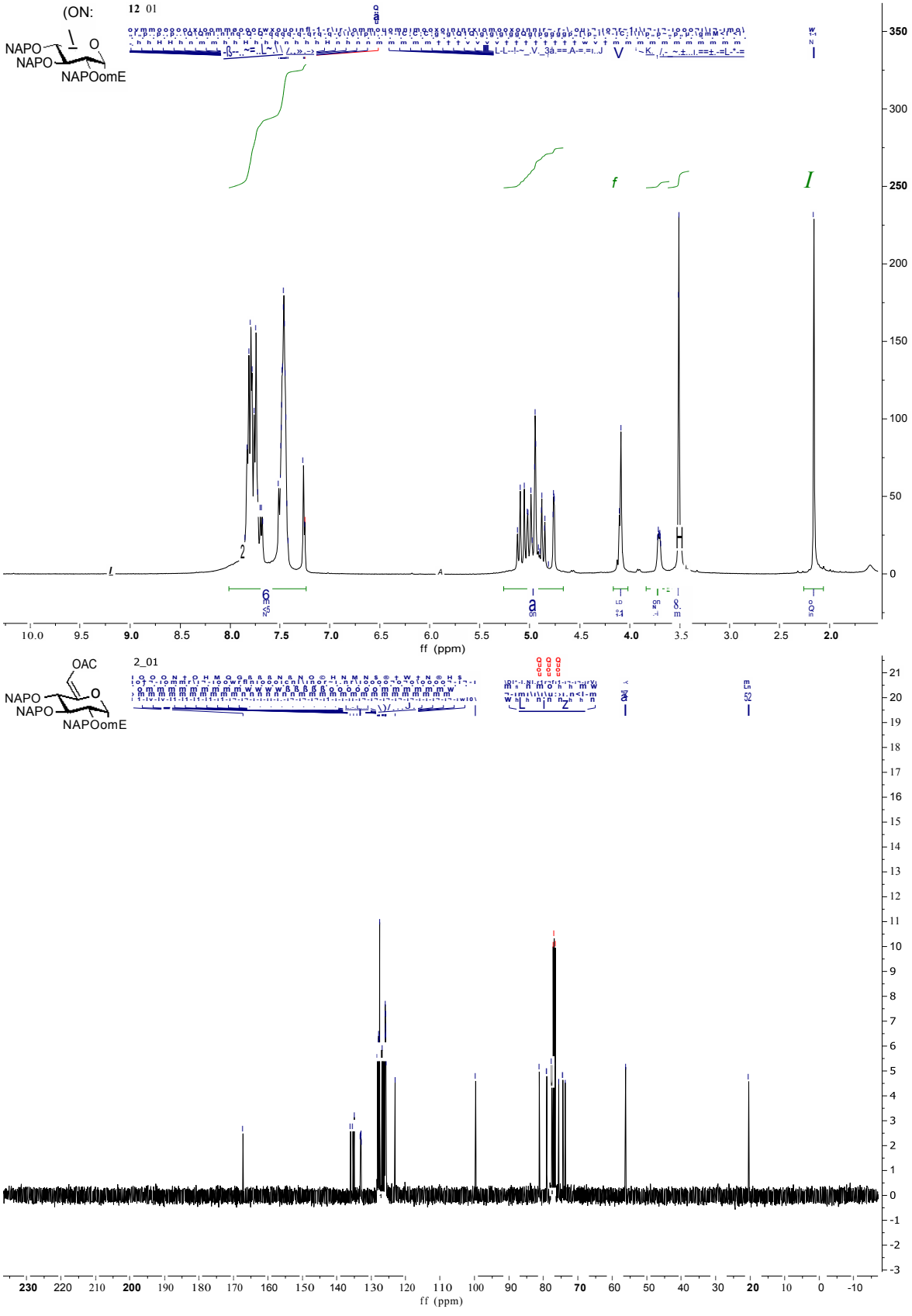

D-1-*O*-Acetyl-3,4,5-tri-*O*-(2-naphthyl)methyl-*myo*-inositol (4-23)

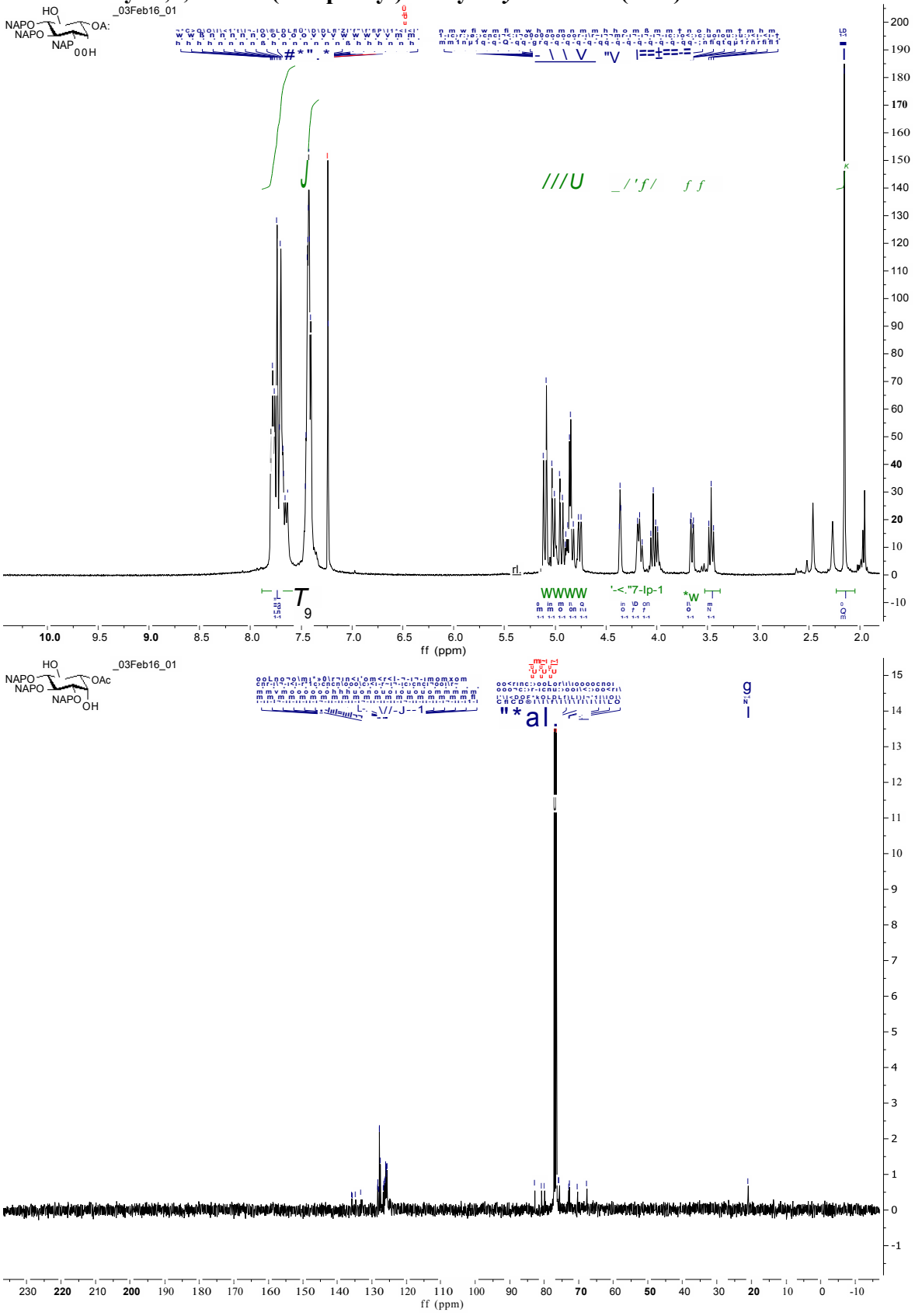

D-1-*O*-Allyl-3,4,5-tri-*O*-(2-naphthyl)methyl-*myo*-inositol (4-25)

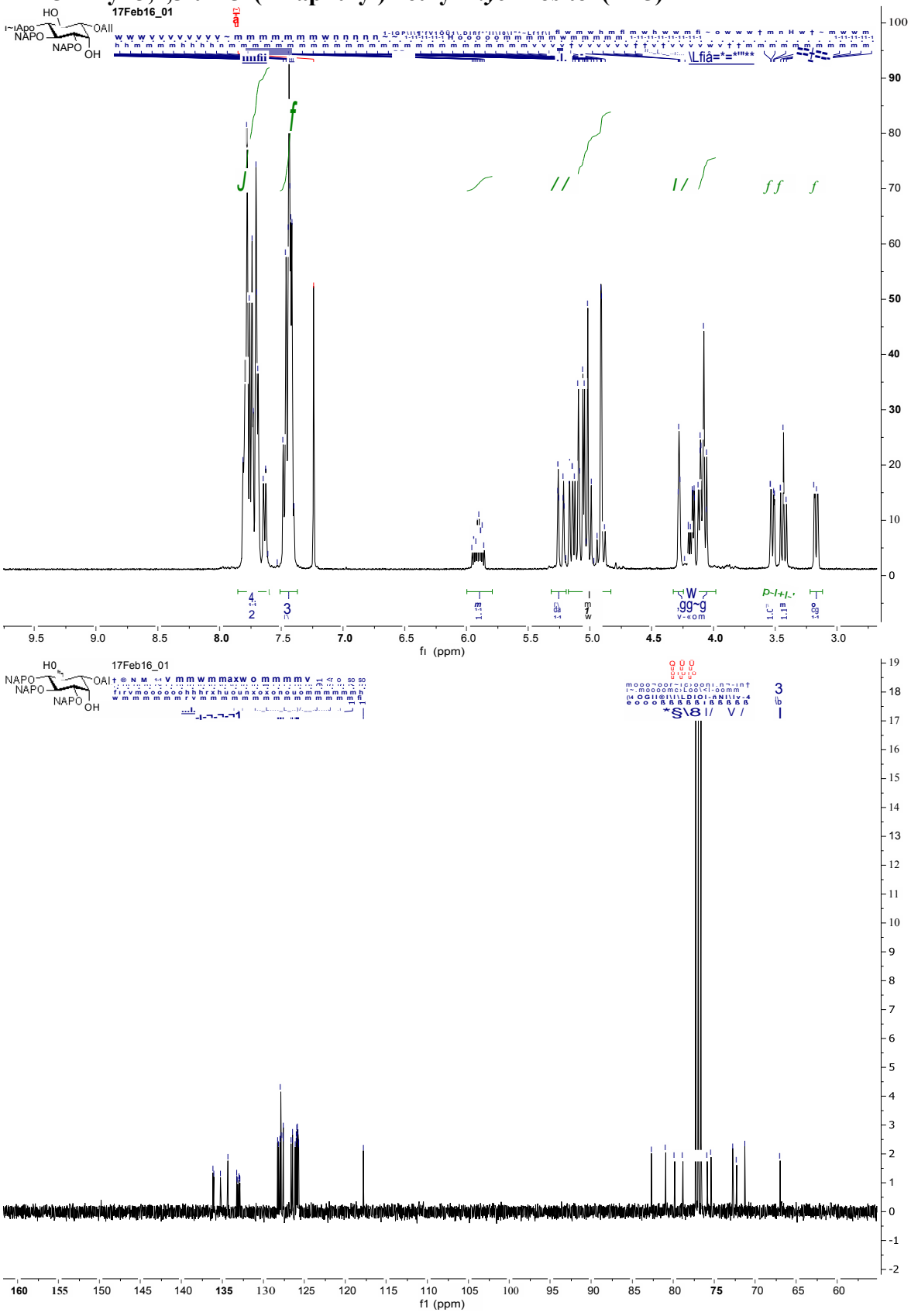

3,4,6–Tri-*O*-acetyl-2-azido-2deoxy-α-D-glucopyranosyl trichloroacetimidate (4-11)

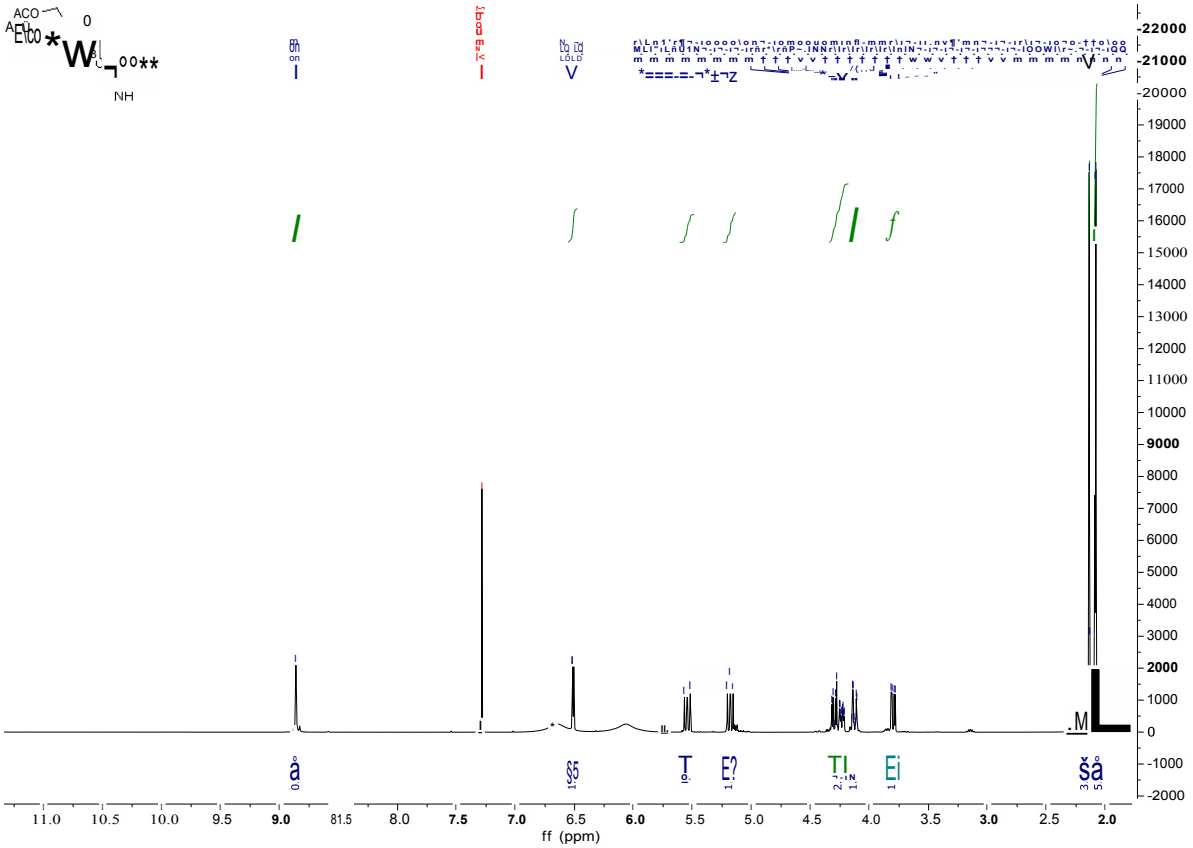

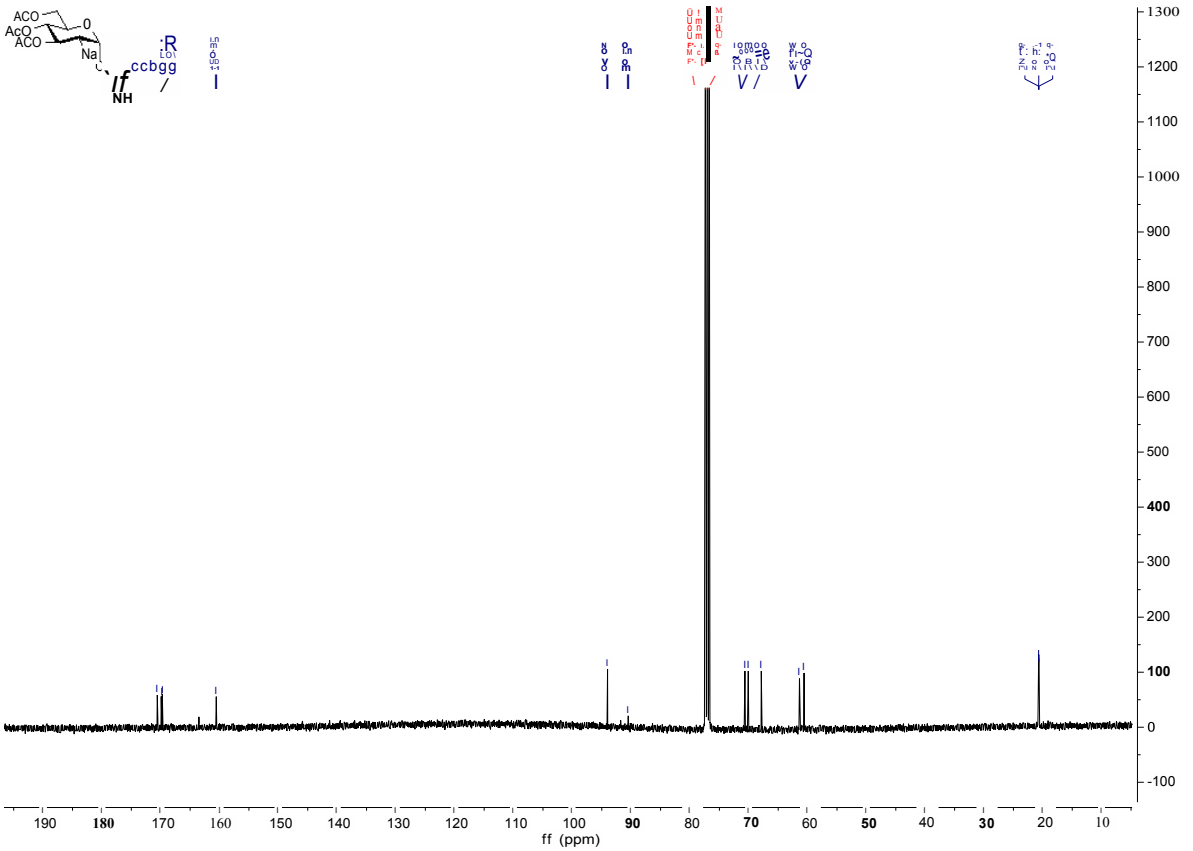

3,4,6–Tri-*O*-benzyl-2-azido-2-deoxy-α-D-glucopyranosyl-(1→6)-2,3,4,5-tetra-*O*-benzyl-D-*myo*-inositol (4-7a)

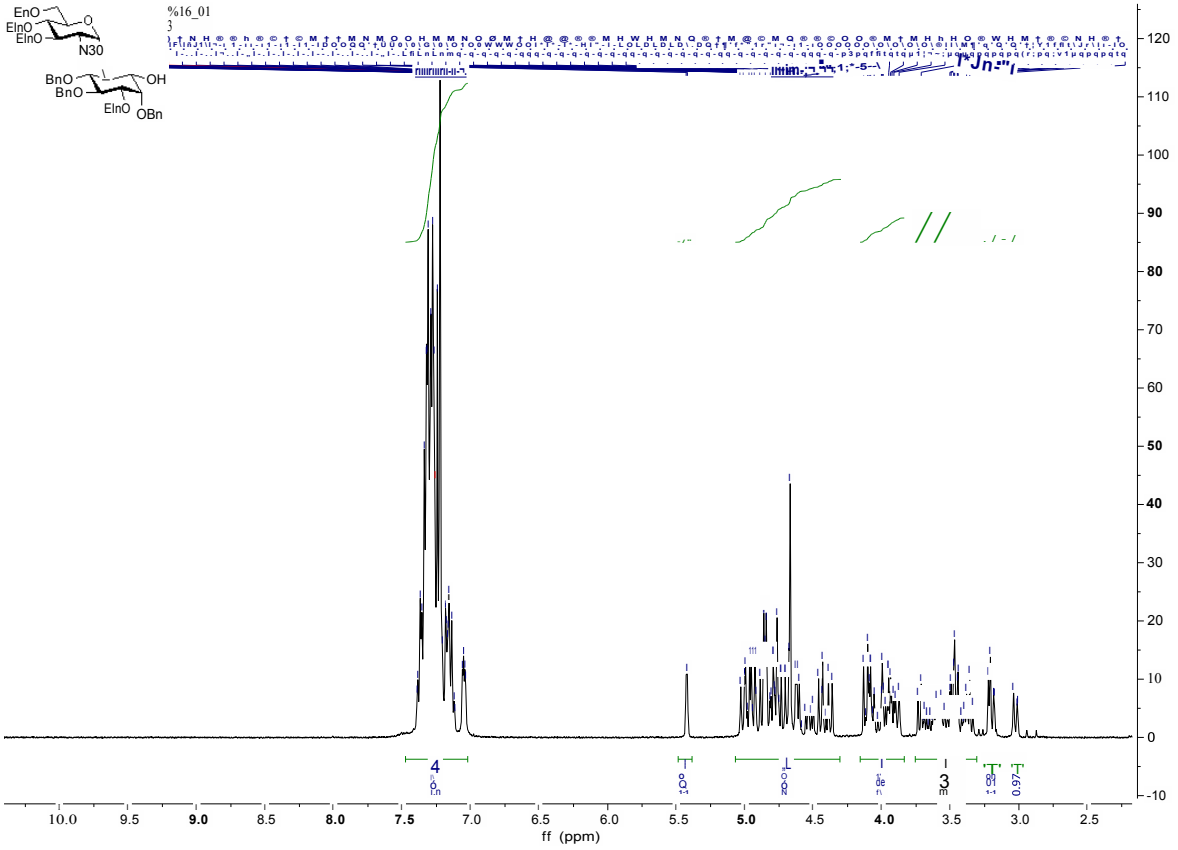

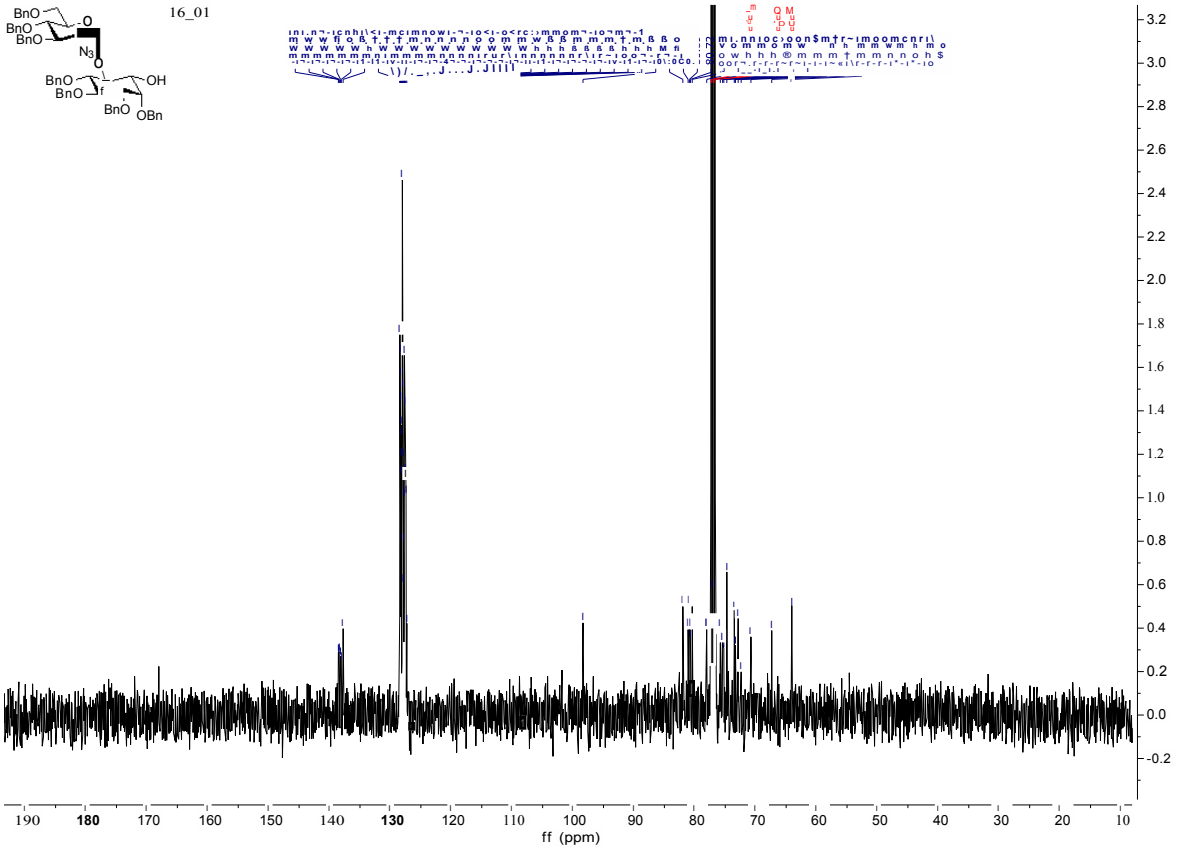

3,4,6–Tri-*O*-benzyl-2-azido-2-deoxy-α-D-glucopyranosyl-(1→6)-1-*O*-(1,2-*O*-distearoyl-*sn*-glycerol)-phosphate-2,3,4,5-tetra-*O*-benzyl--*myo*-inositol (4-32)

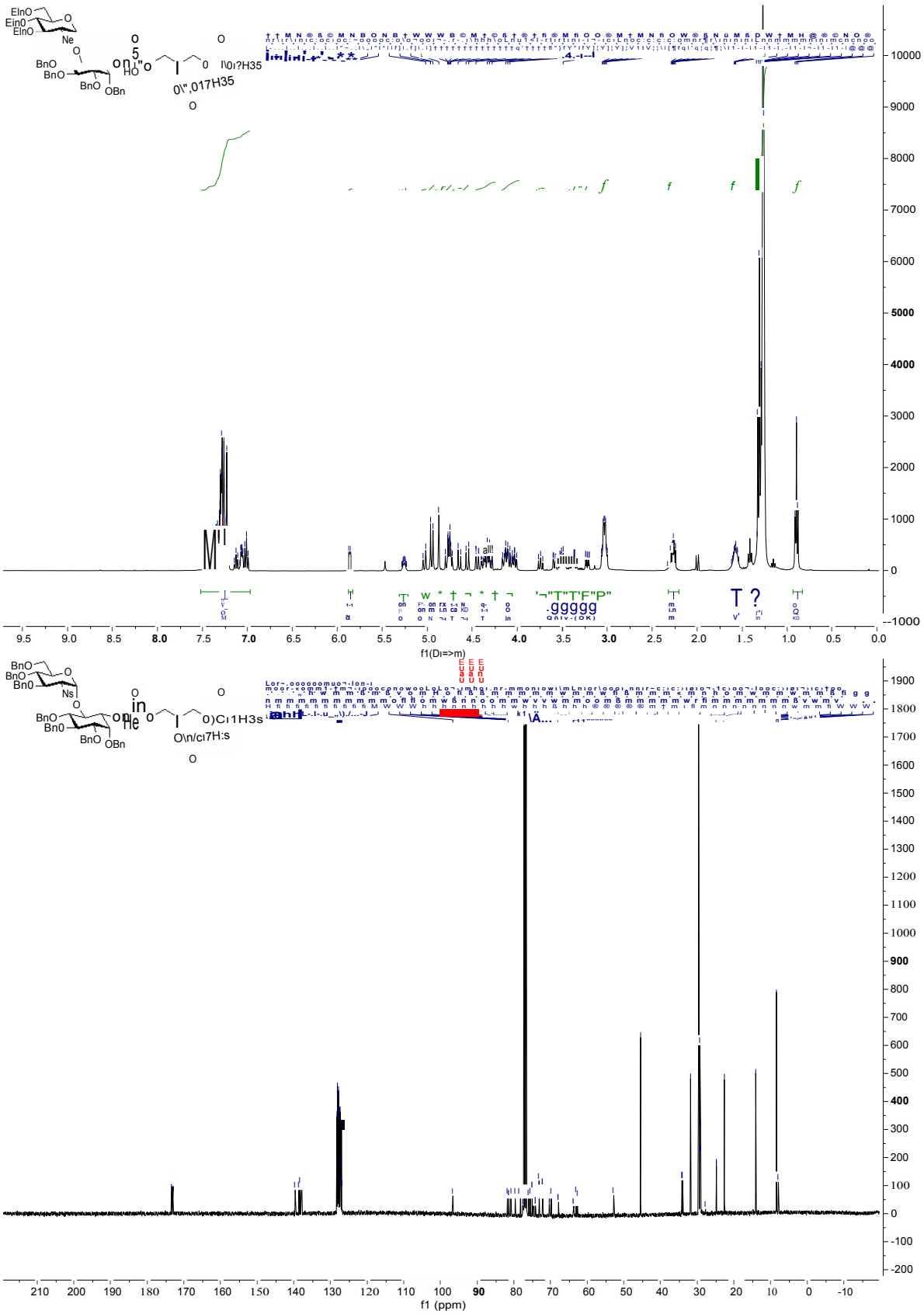

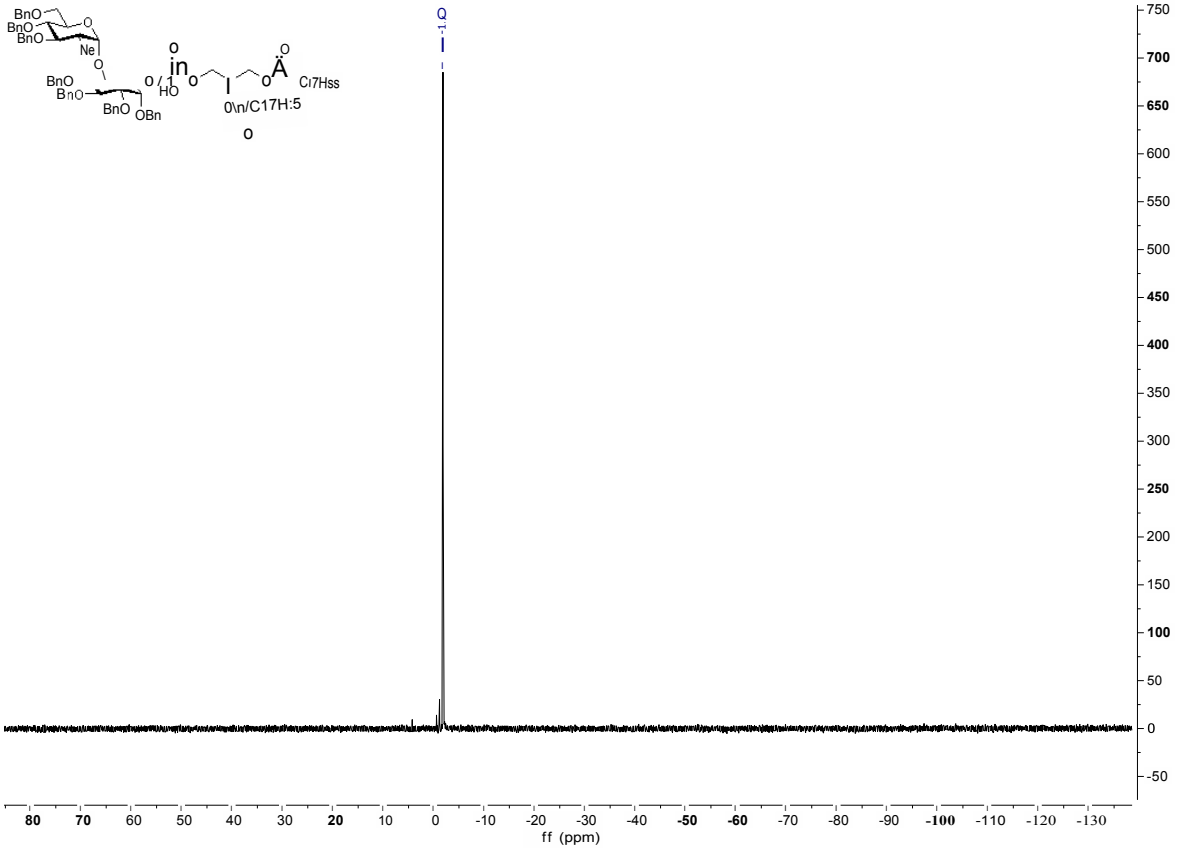

2-amino-2-deoxy-α-D-glucopyranosyl-(1→6)-1-*O*-(1,2-*O*-distearoyl-*sn*-glycerol)-phosphate-D-*myo*-inositol (4-3)

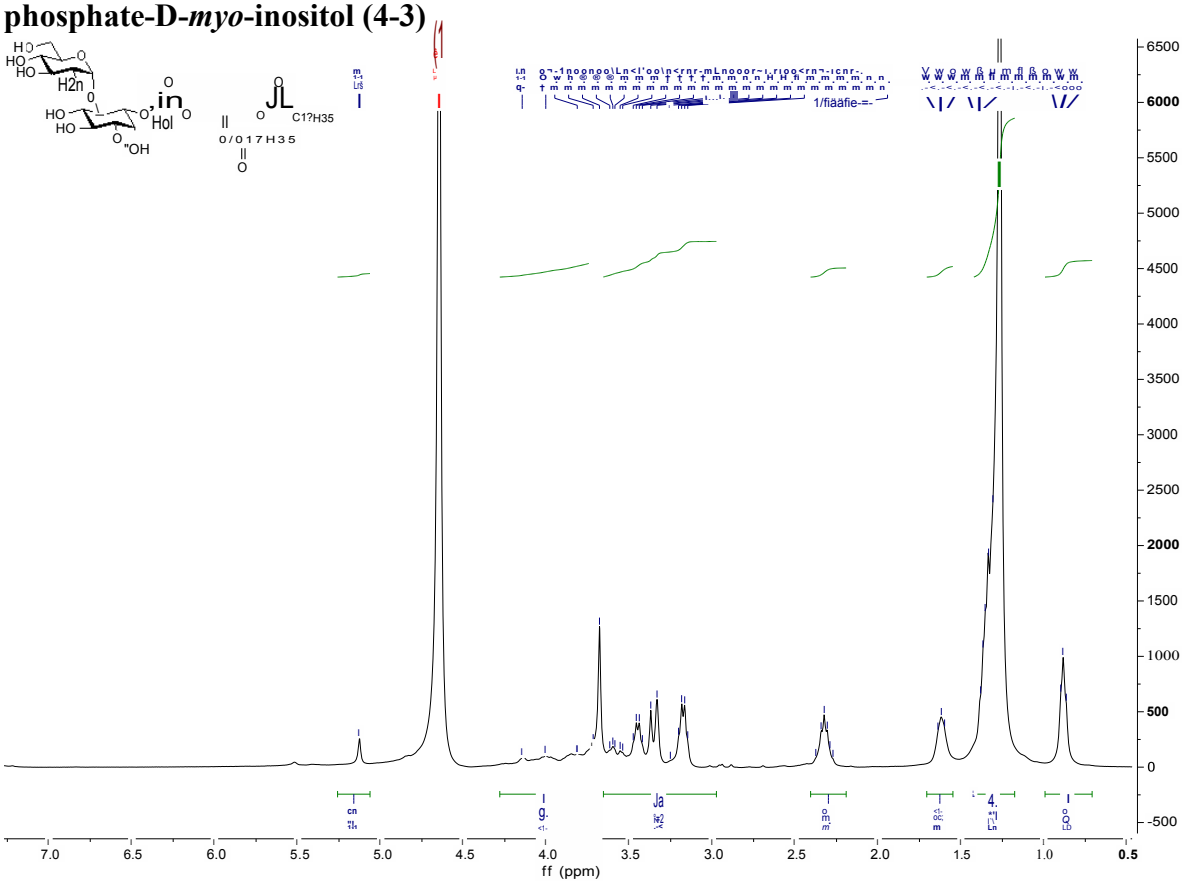

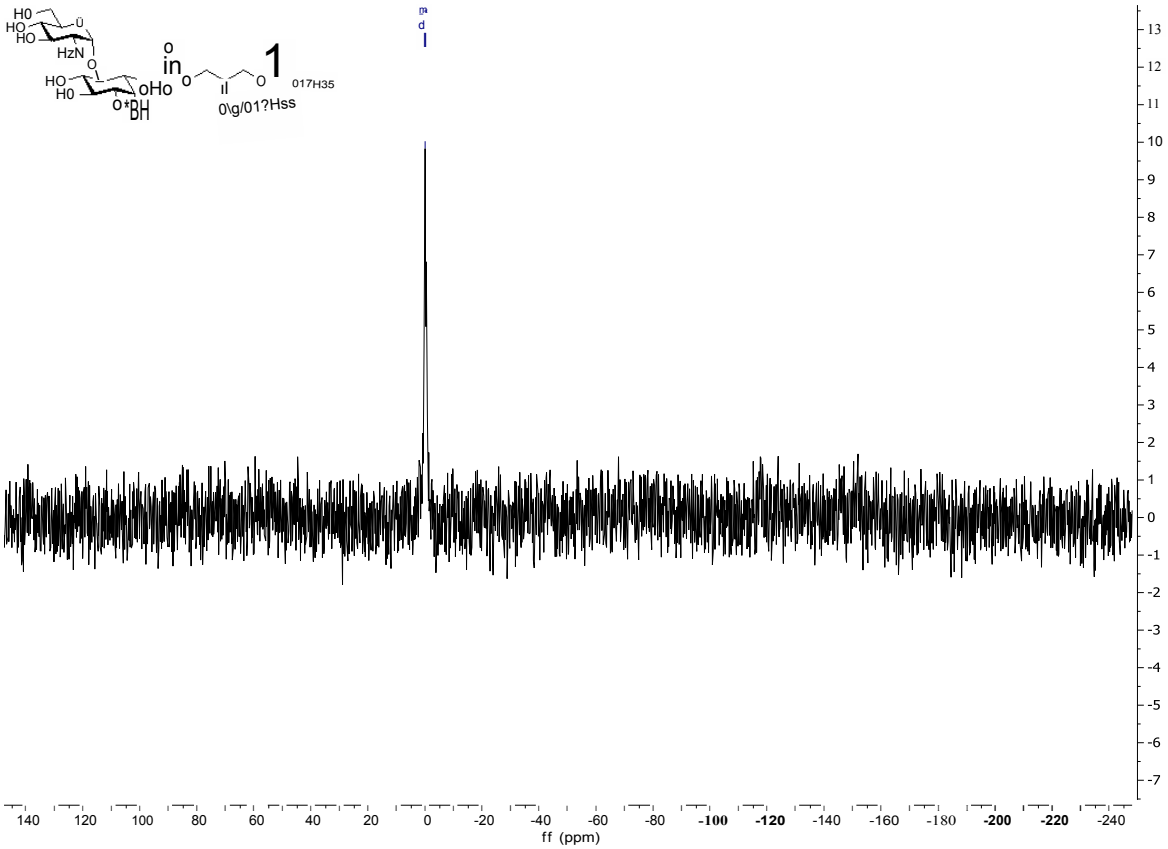

3,4,6–Tri-*O*-benzyl-2-acetamide-2-deoxy-α-D-glucopyranosyl-(1→6)-1-*O*-allyl-2,3,4,5-tetra-*O*-benzyl-D-*myo*-inositol (4-33)

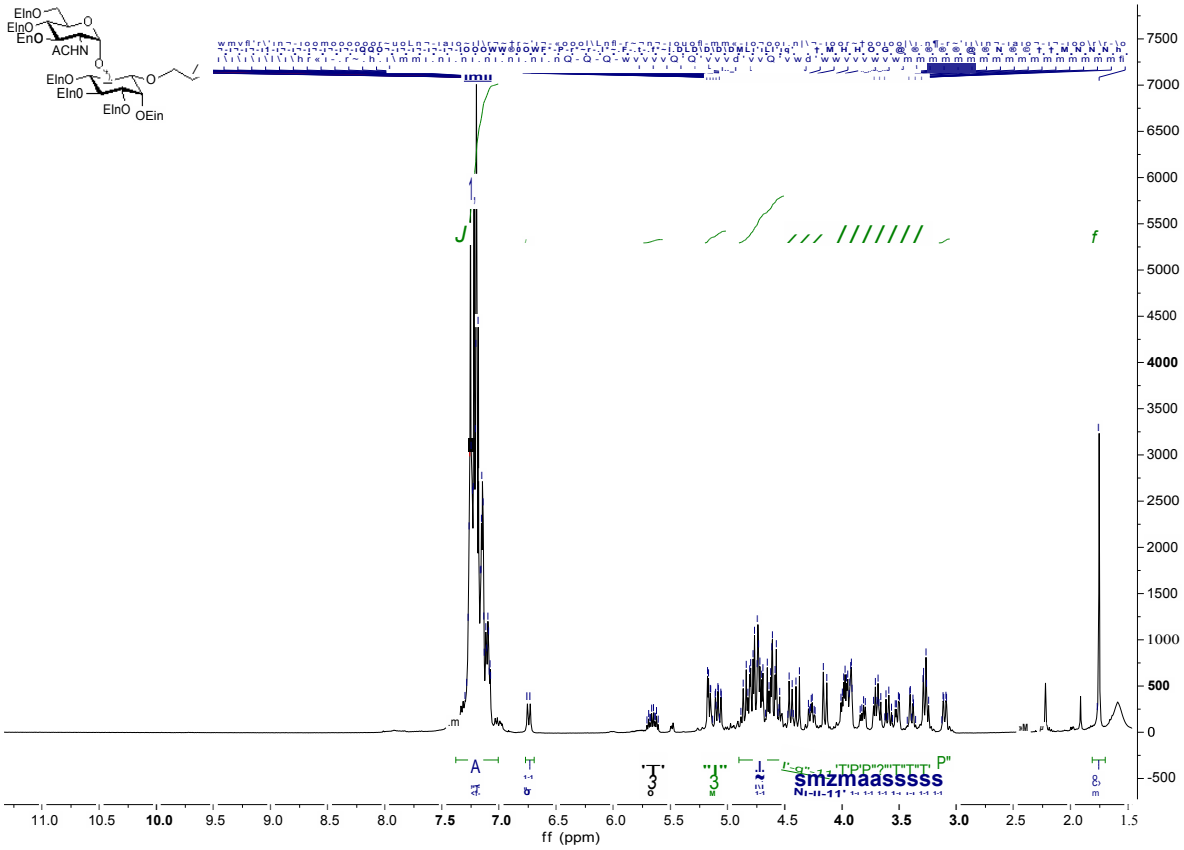

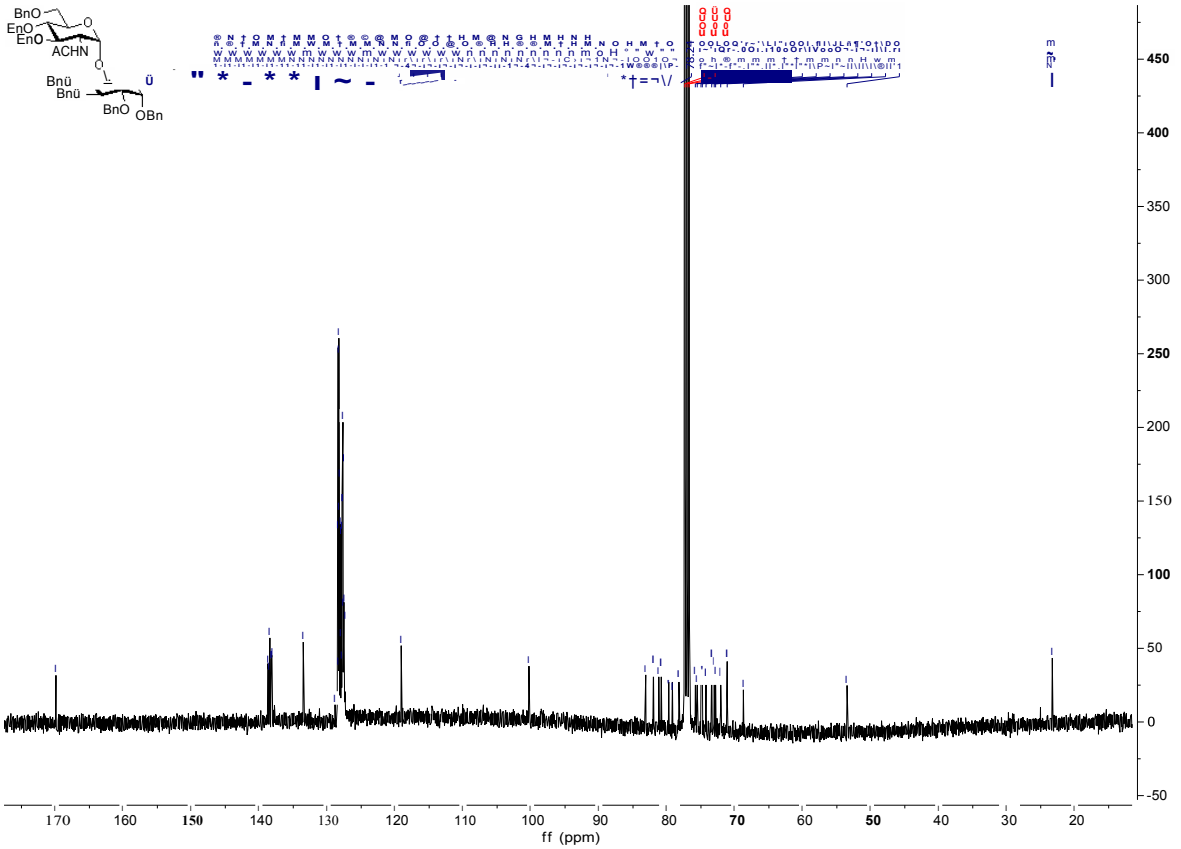

3,4,6–Tri-*O*-benzyl-2-acetamide-2-deoxy-α-D-glucopyranosyl-(1→6)- 1-*O*-(1,2-*O*-distearoyl-*sn*-glycerol)-phosphate -2,3,4,5-tetra-*O*-benzyl-D-*myo*-inositol (4-35)

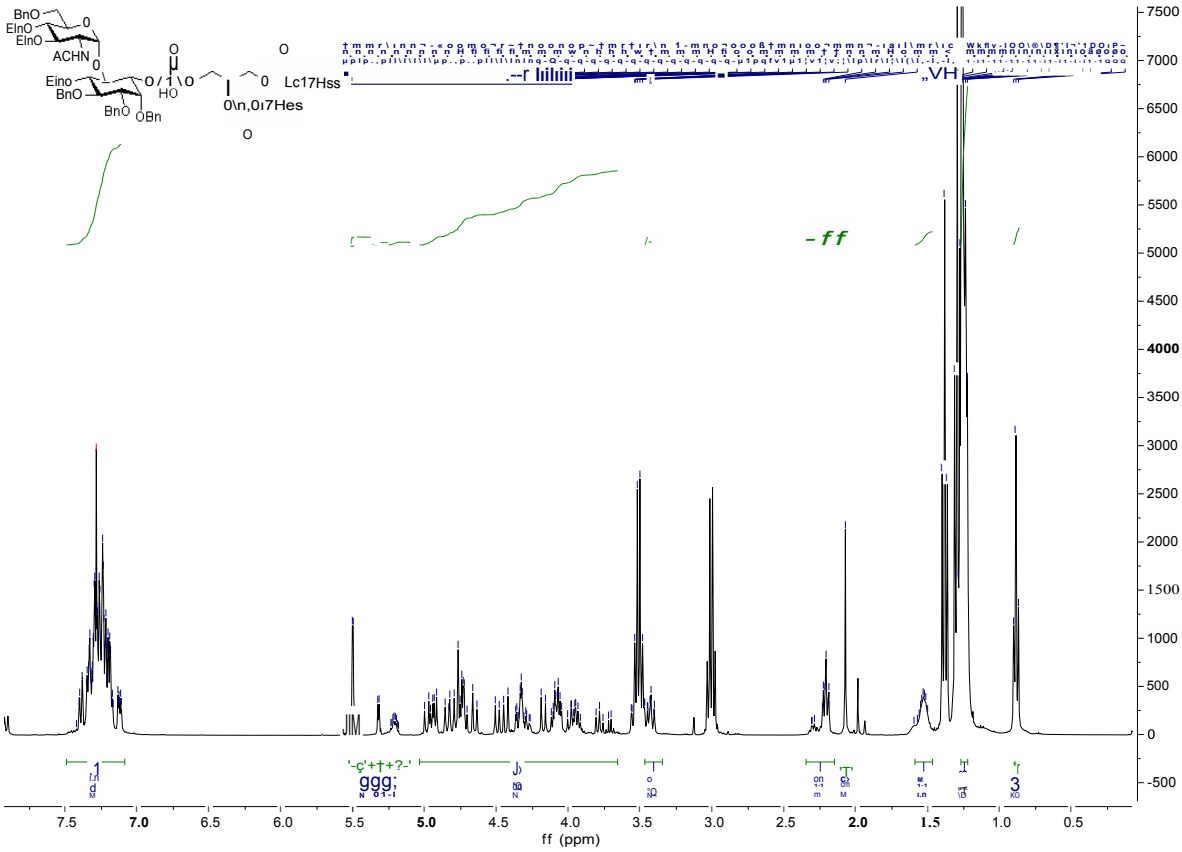

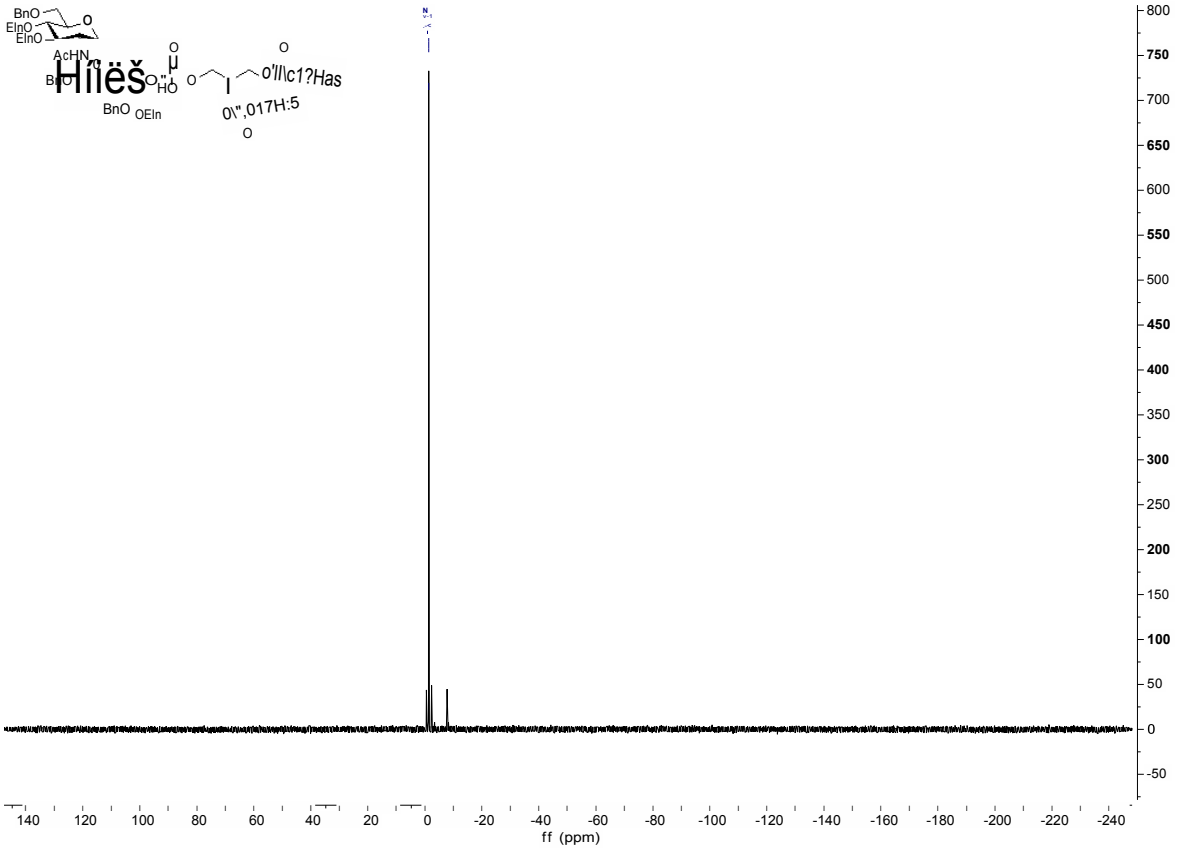

2-acetamide-2-deoxy-α-D-glucopyranosyl-(1→6)-1-*O*-(1,2-*O*-distearoyl-*sn*-glycerol)-phosphate-D-*myo*-inositol (4-4)

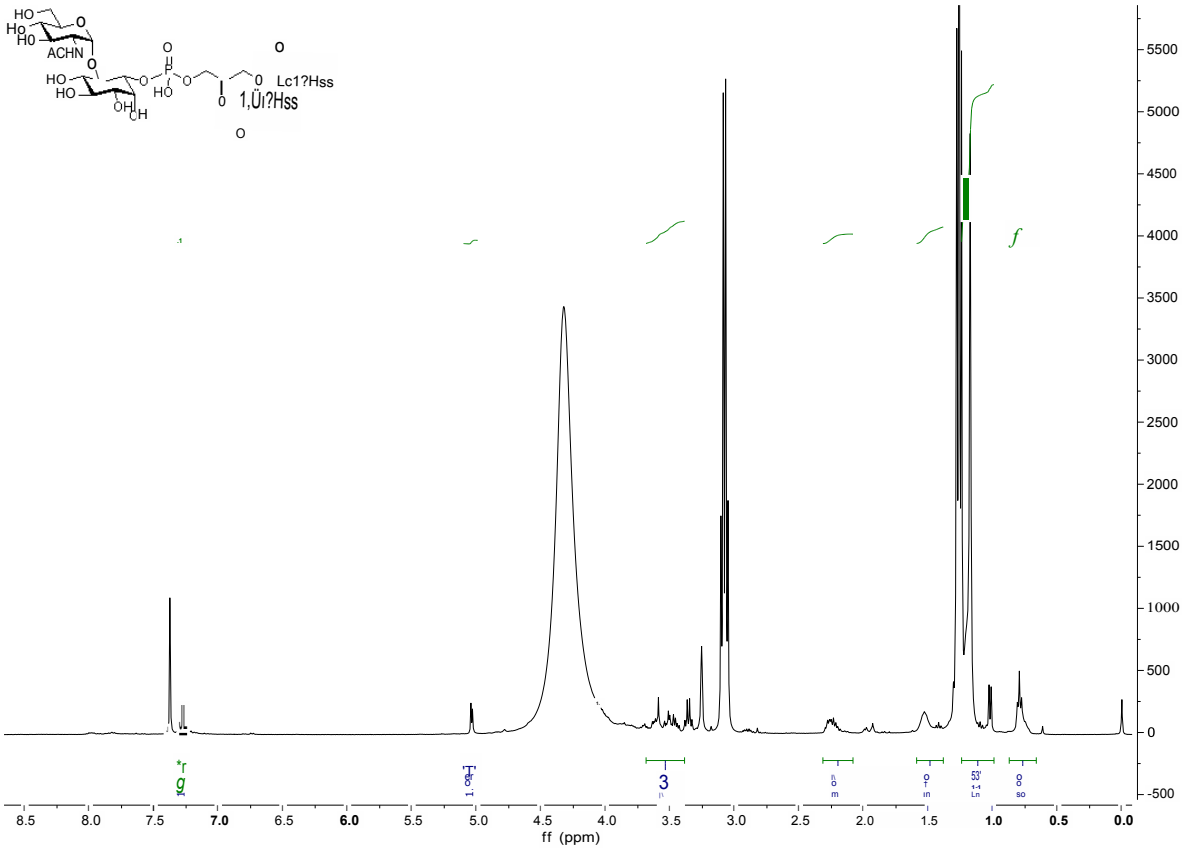

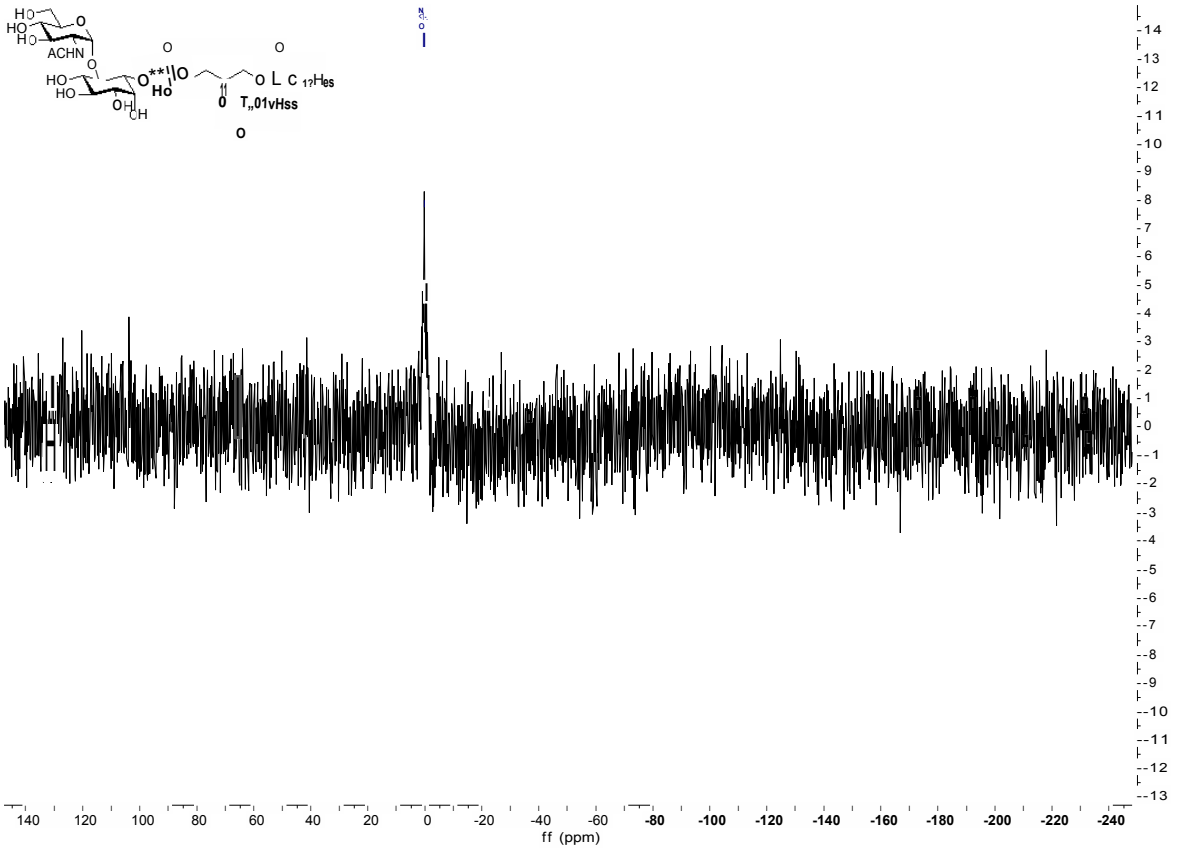

3,4,6–Tri-*O*-(2-naphthyl)methyl -2-acetamide-2-deoxy-α-D-glucopyranosyl-(1→6)- 1-*O*-allyl-2,3,4,5-tetra-*O*-(2-naphthyl)methyl -D-*myo*-inositol (4-39)

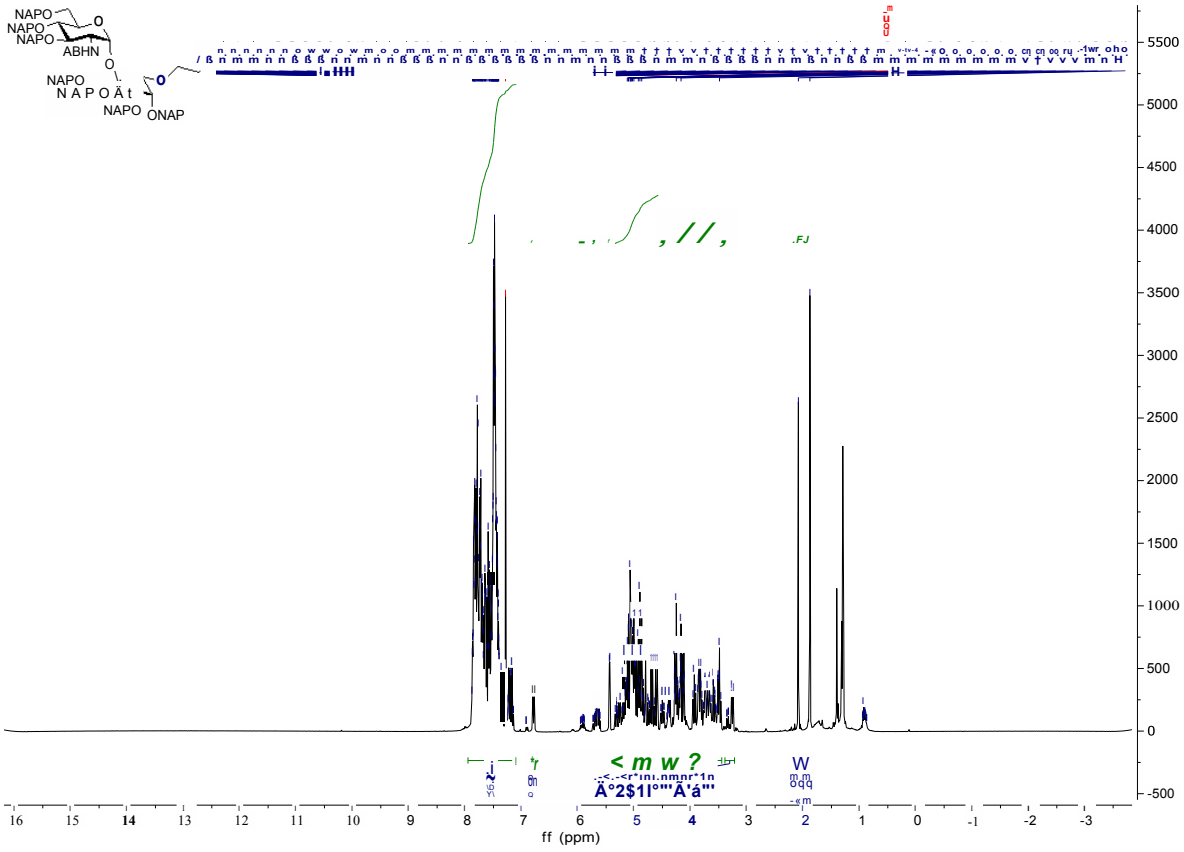

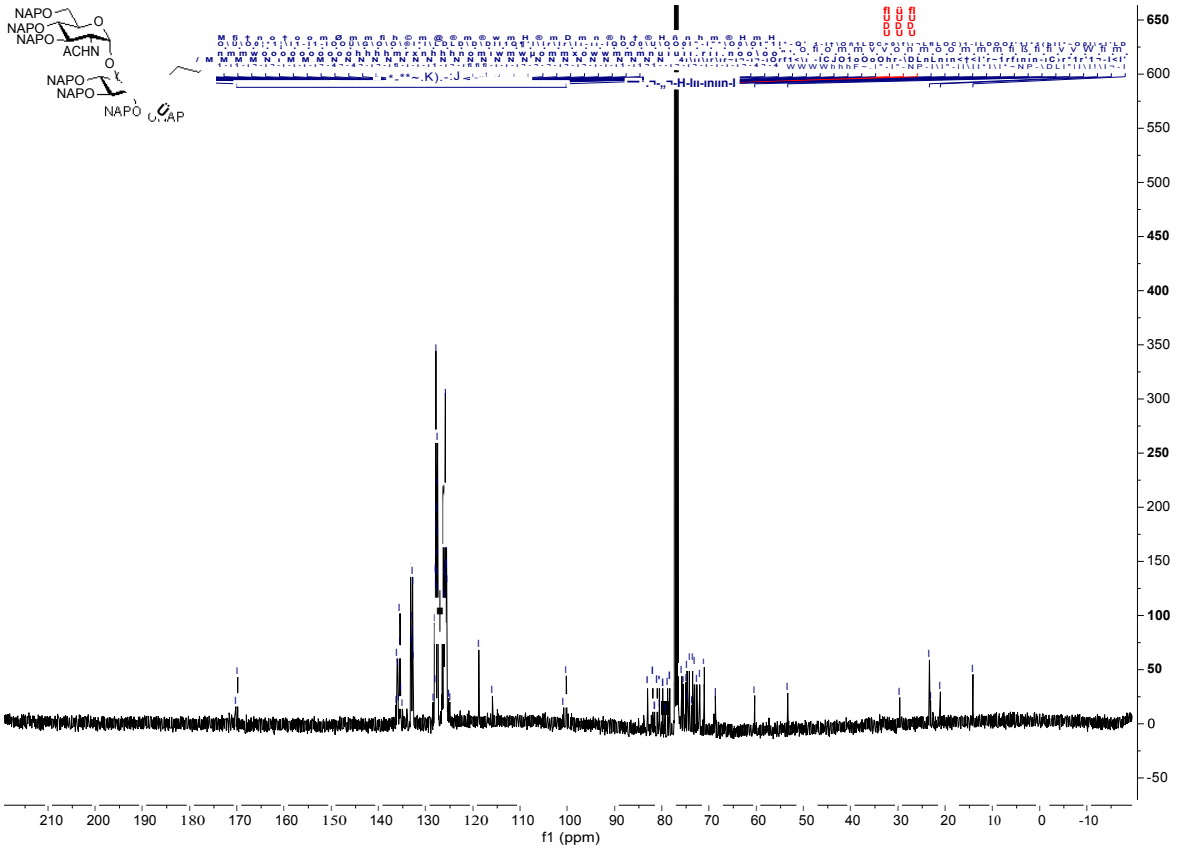
NAPO
NAPO
NAPO
ACHN
NAPO
NAPO
NAPO
ONAP
f1 (ppm)

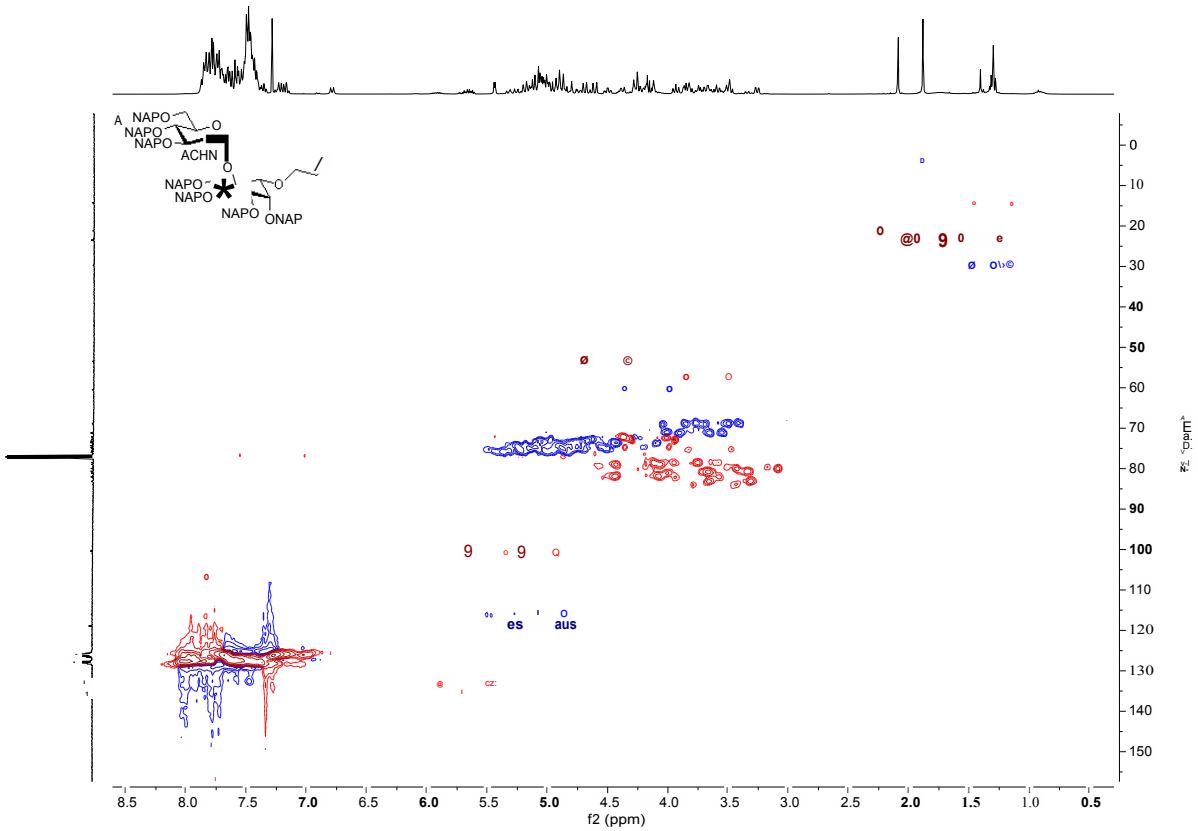
NAPO
NAPO
NAPO
ACHN
NAPO
NAPO
NAPO
ONAP
f2 (ppm)

3,4,6–Tri-*O*-(2-naphthyl)methyl-2-acetamide-2-deoxy-α-D-glucopyranosyl-(1→6)-2,3,4,5-tetra-*O*-(2-naphthyl)methyl -D-*myo*-inositol (4-40)

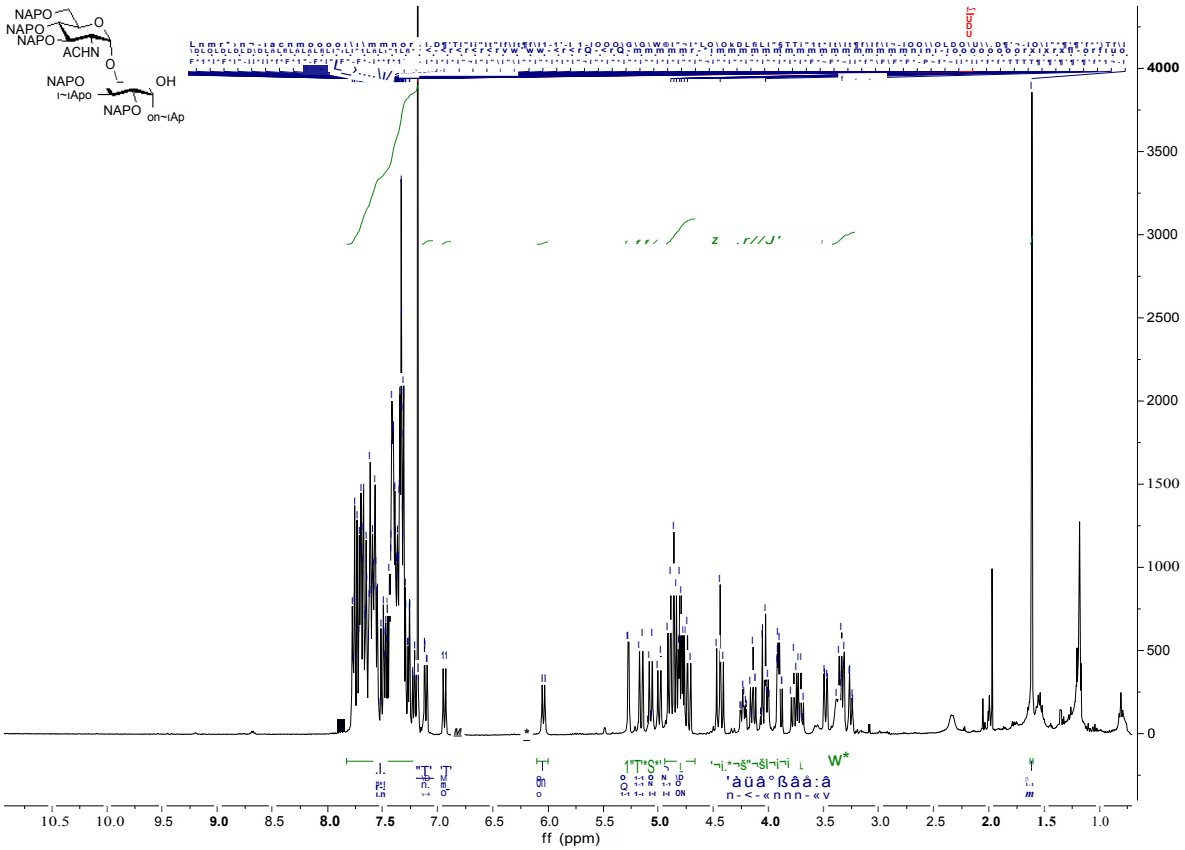

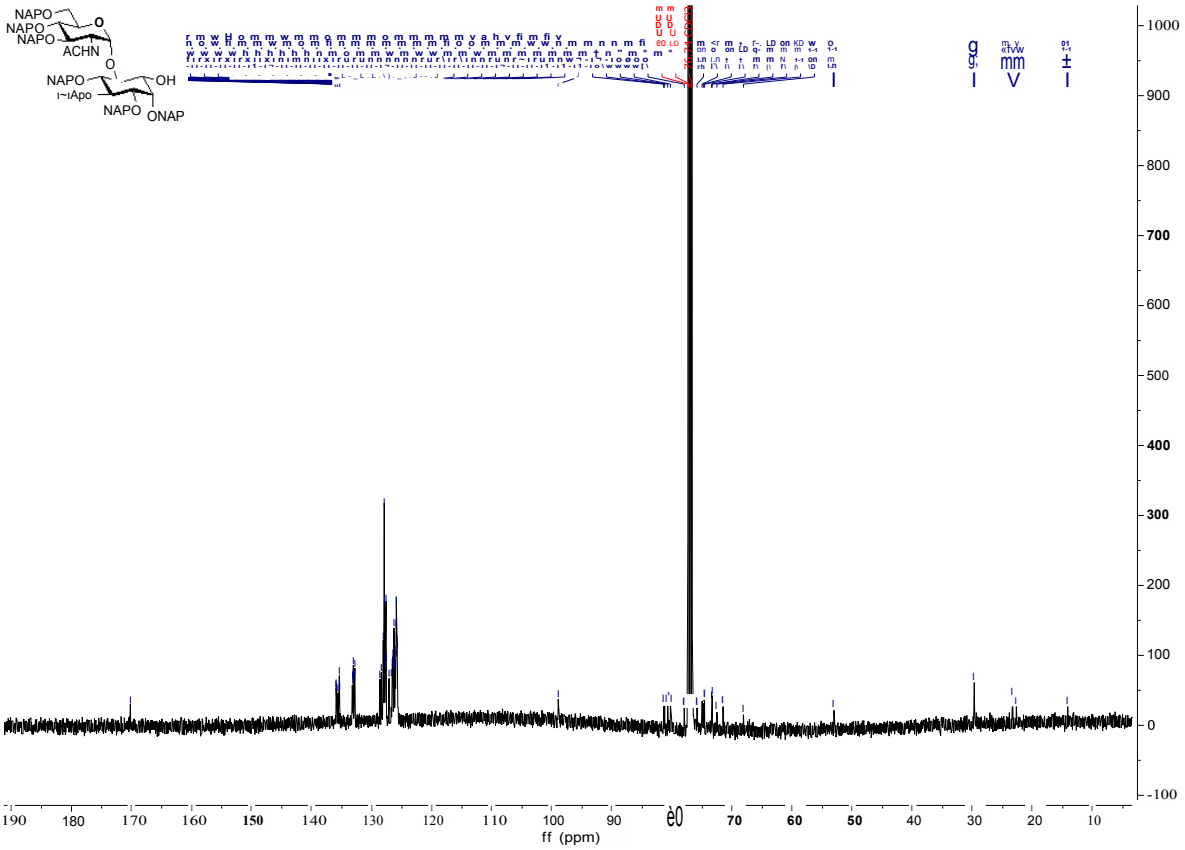

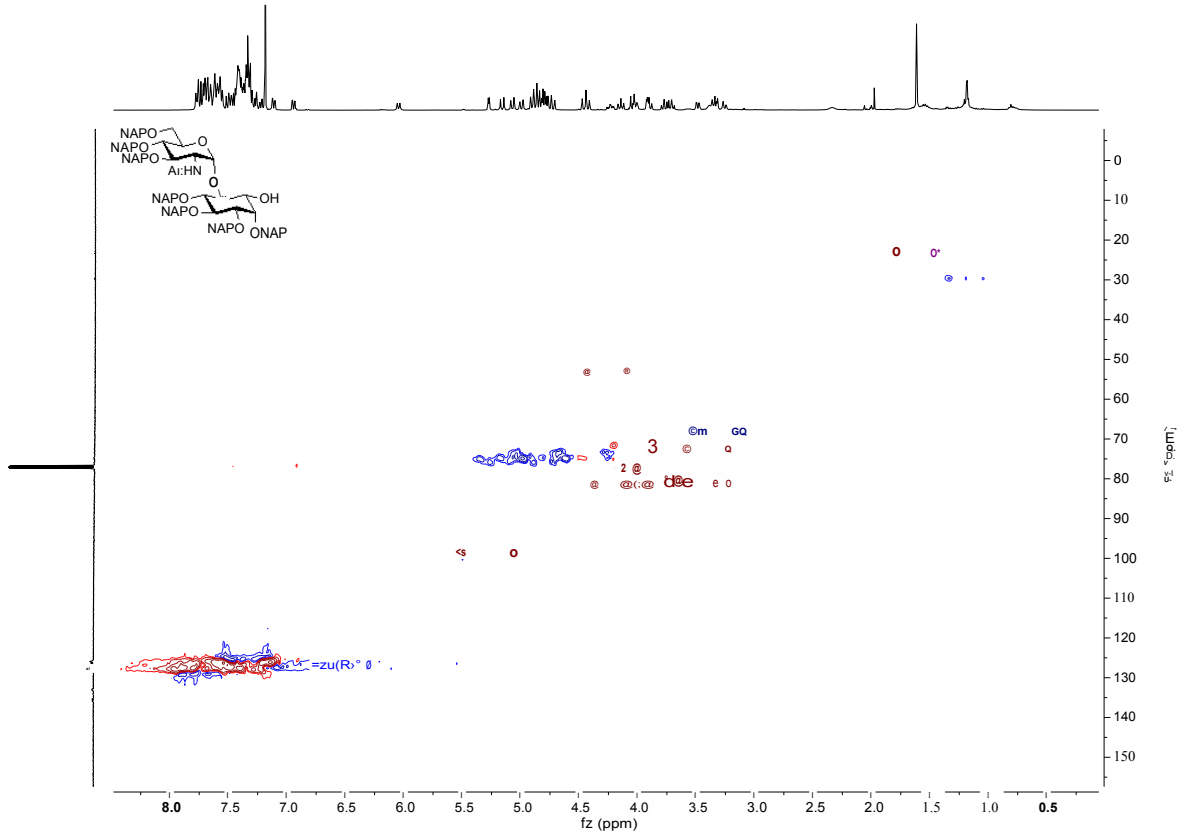

3,4,6–Tri-*O*-(2-naphthyl)methyl-2-acetamide-2-deoxy-α-D-glucopyranosyl-(1→6)- 1-*O*-(1-*O*-stearoyl-2-*O*-oleoyl-*sn*-glycerol)-phosphate-2,3,4,5-tetra-*O*-(2-naphthyl)methyl -D-*myo*-inositol (4-41)

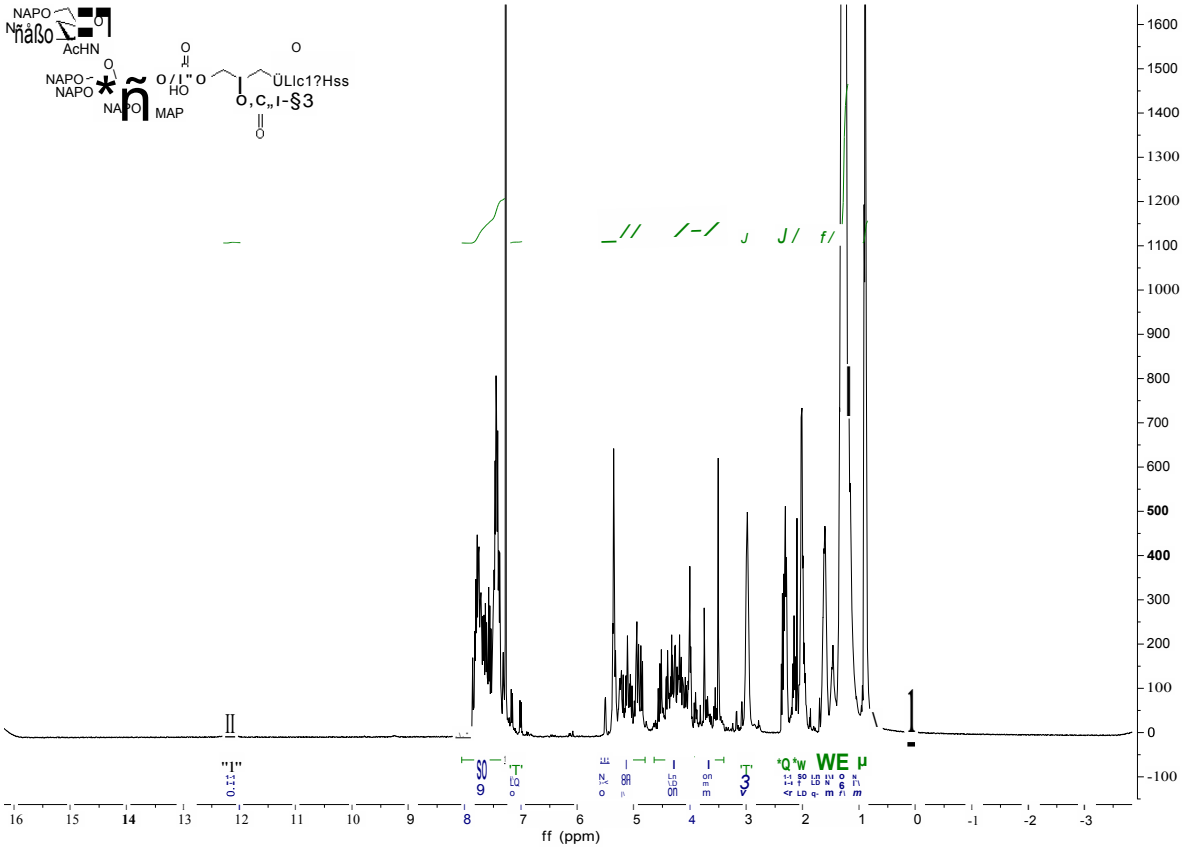

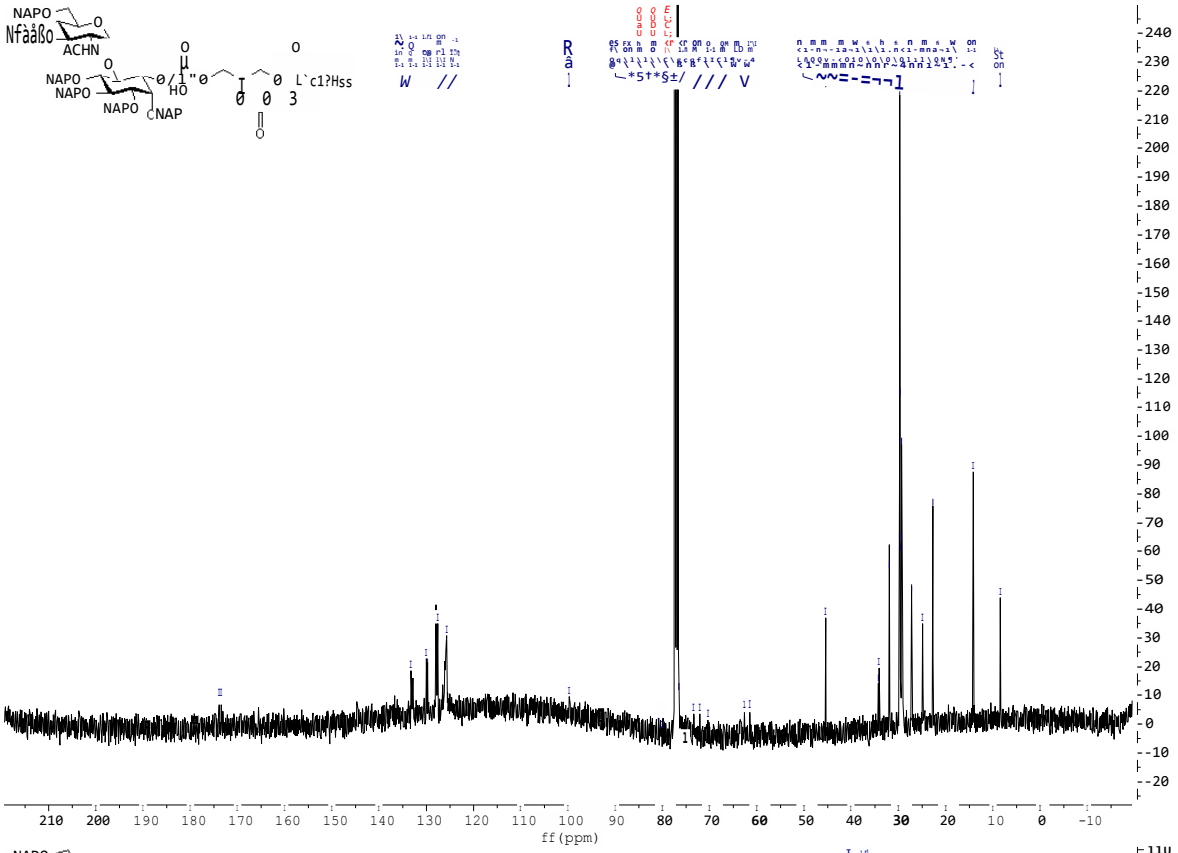
NAPO
ACHN
NAPO
NAPO
NAPO
HO
NAP
ff (ppm)

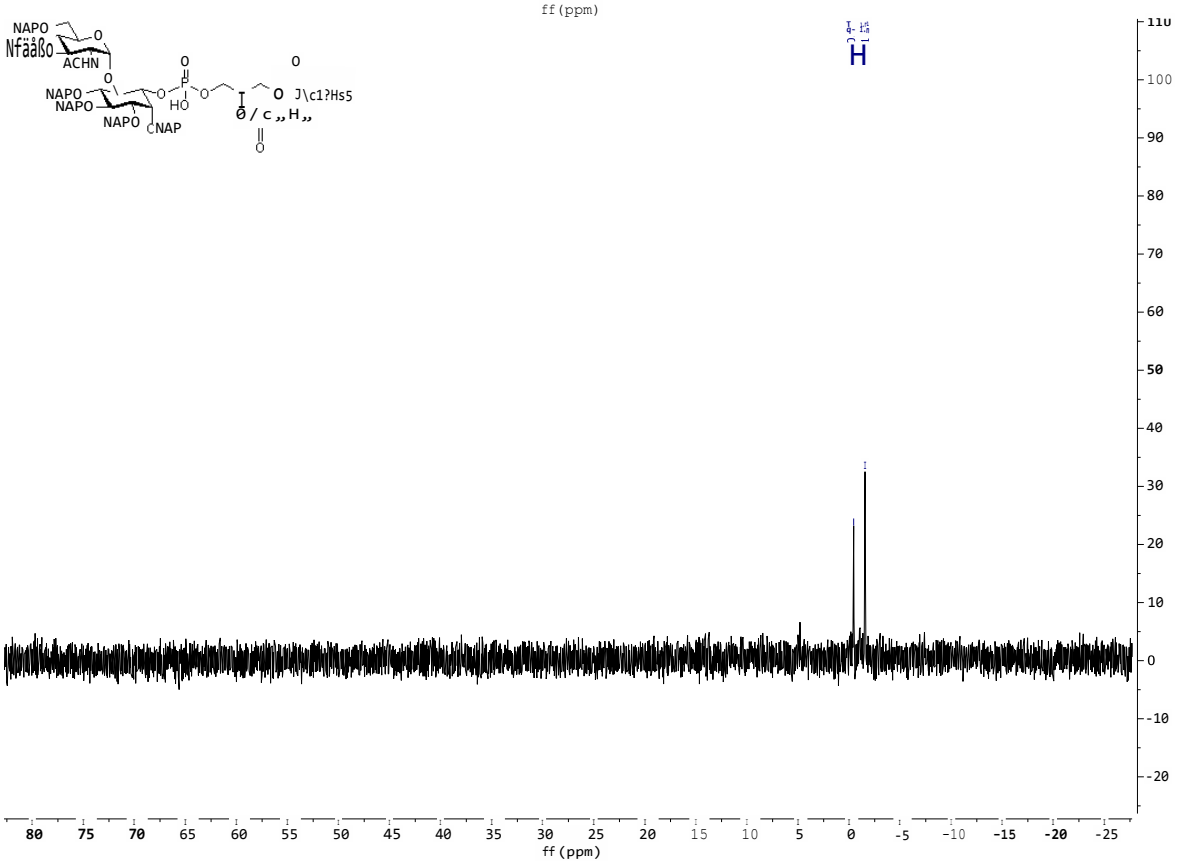
NAPO
ACHN
NAPO
NAPO
NAPO
HO
NAP
ff (ppm)

2-acetamide-2-deoxy-α-D-glucopyranosyl-(1→6)- 1-*O*-(1-*O*-stearoyl-2-*O*-oleoyl-*sn*-glycerol)-phosphate-D-*myo*-inositol (4-5)

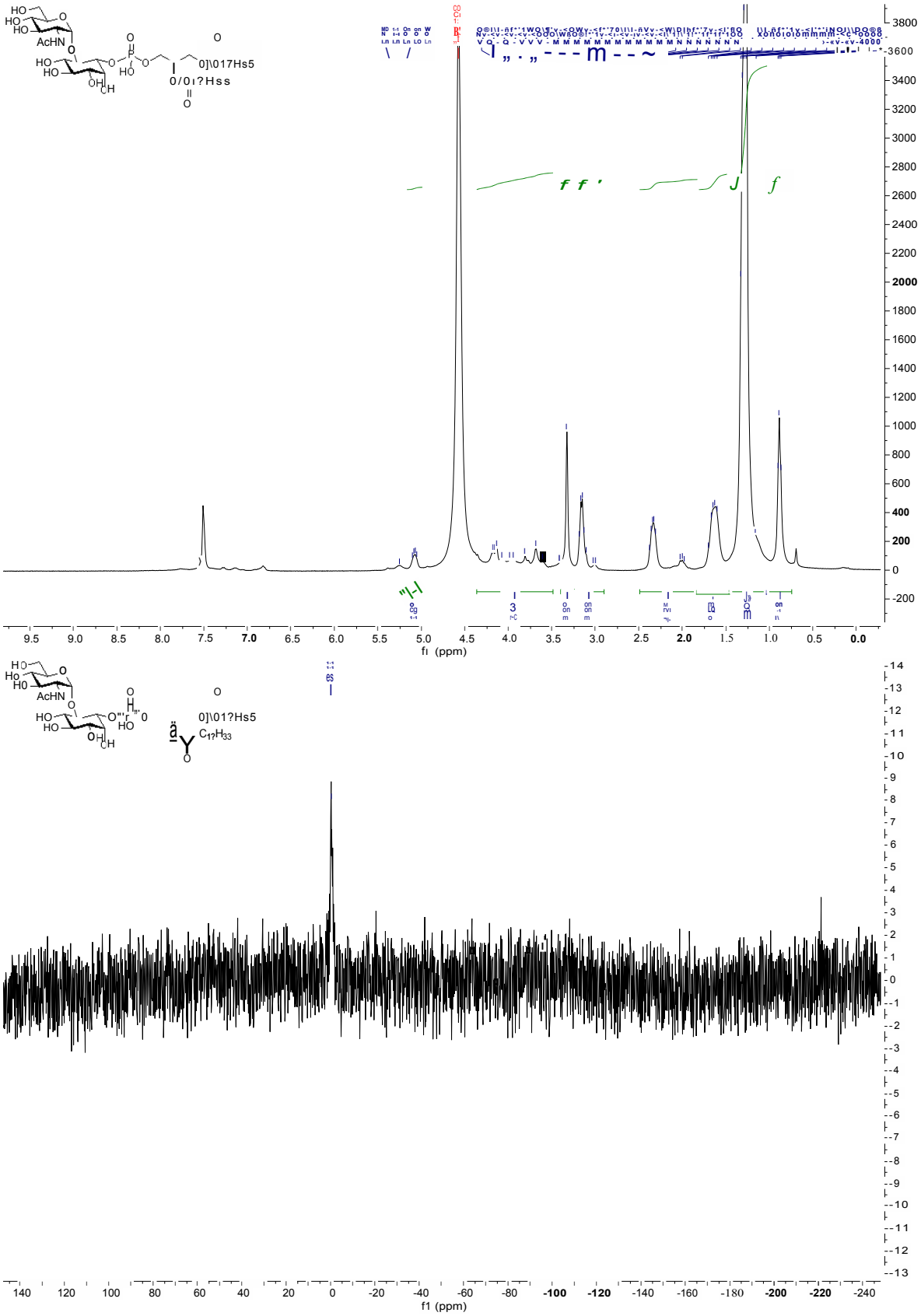

3,4,6–Tri-*O*-benzyl-2-azido-2-deoxy-α-D-glucopyranosyl-(1→6)-1-*O*-[1,2-*O*-(8-methylhexadecanoyl)-*sn*-glycerol]-phosphate-2,3,4,5-tetra-*O*-benzyl-D-*myo*-inositol (4-42)

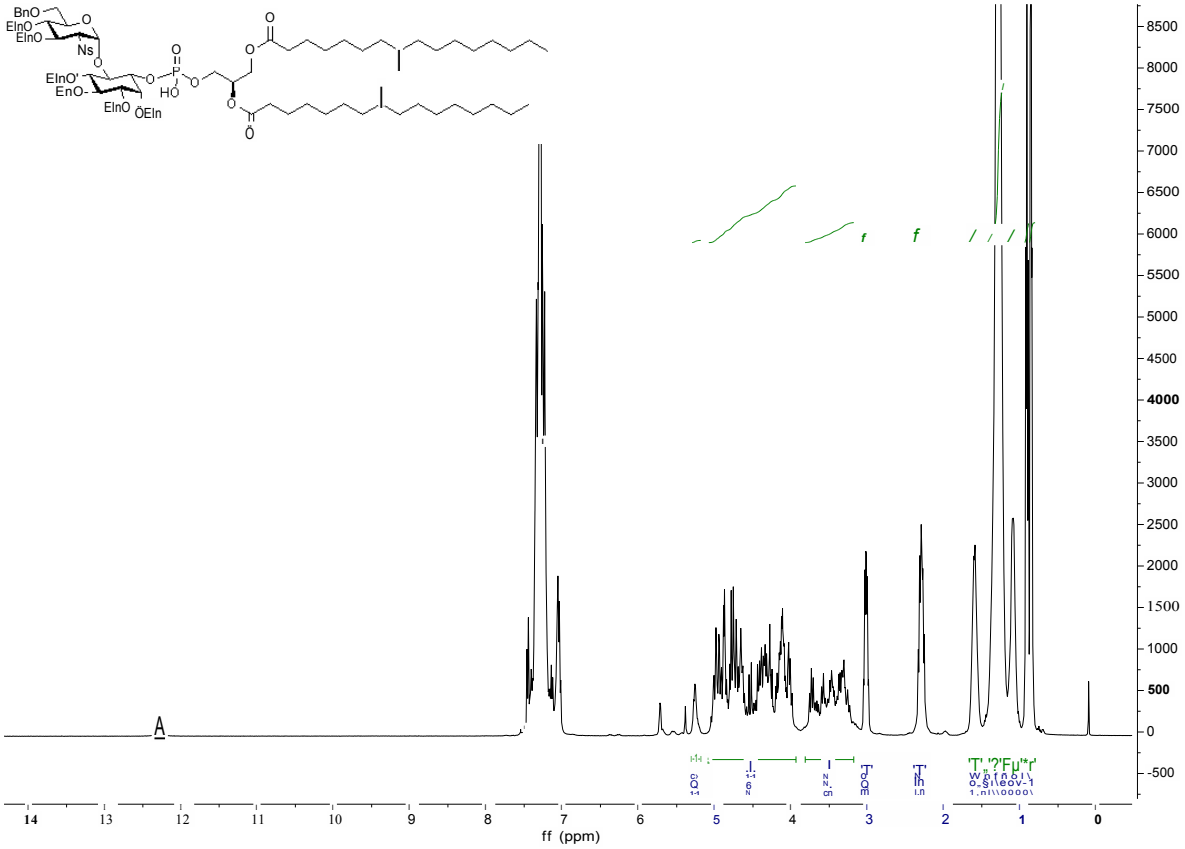

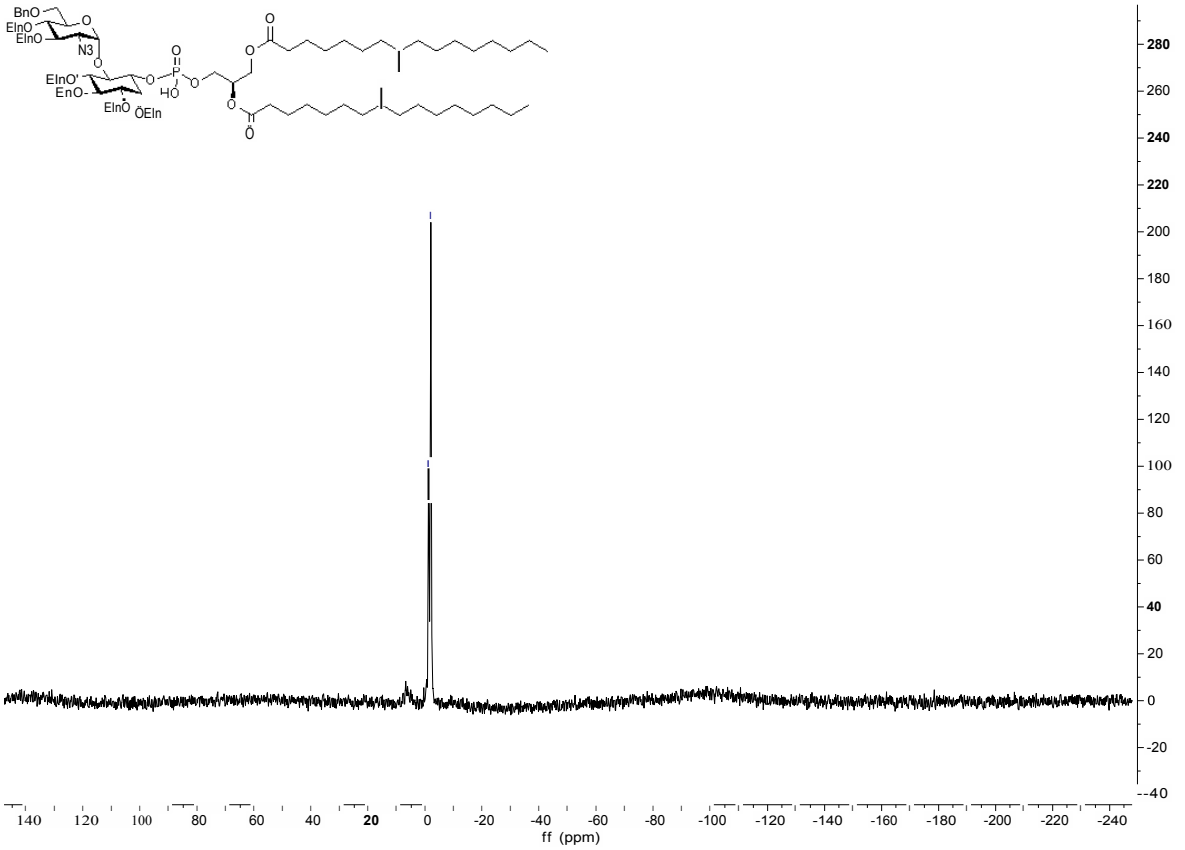

2-amino-2-deoxy-α-D-glucopyranosyl-(1→6)-1-*O*-[1,2-*O*-(8-methylhexadecanoyl)-*sn*-glycerol]-phosphate-D-*myo*-inositol (4-6)

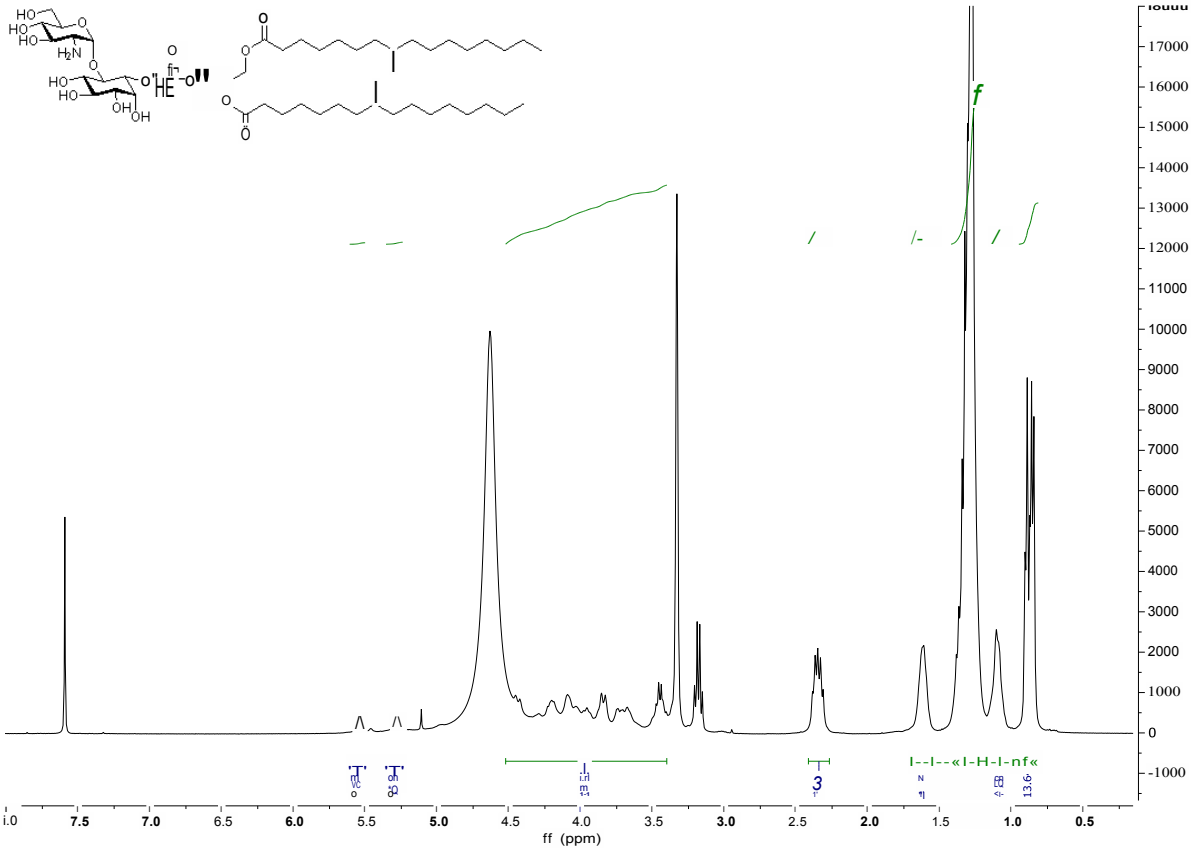

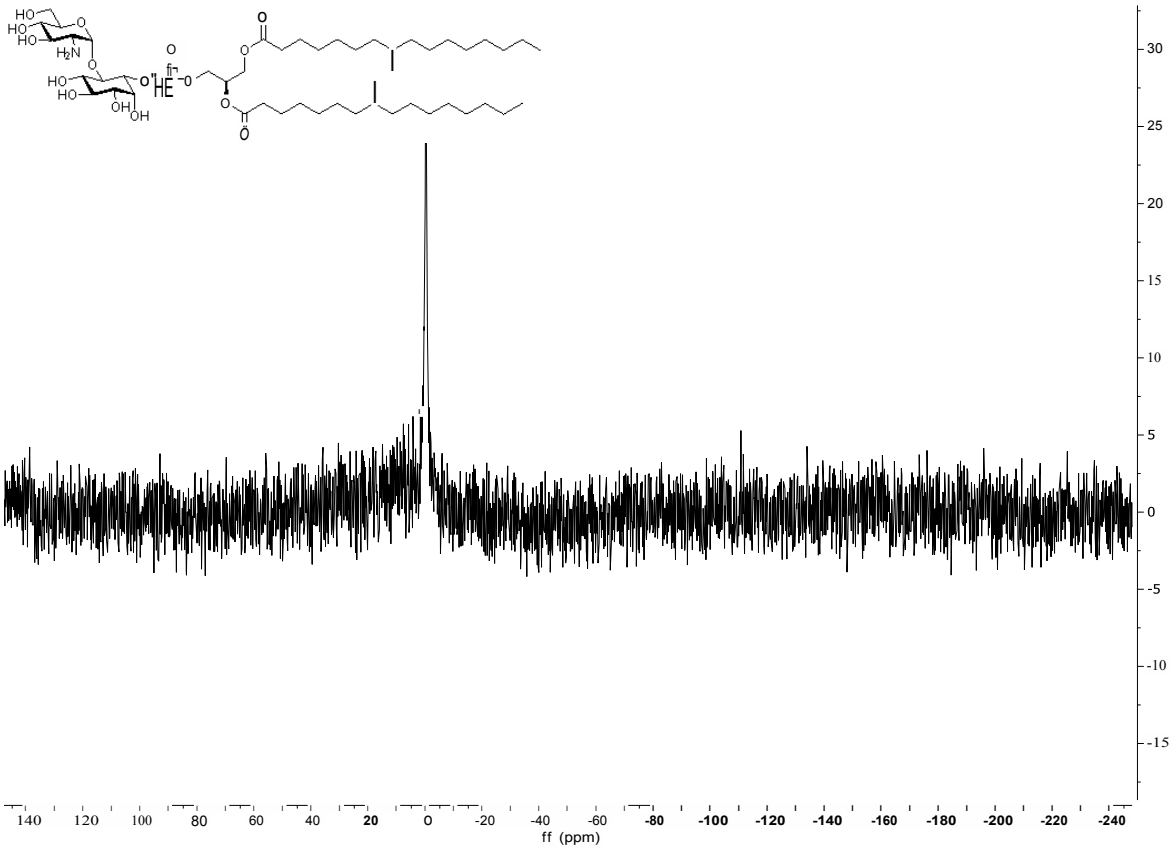

6 References

1. Varki, A.; Cummings, R. D.; Esko, J. D.; Freeze, H. H.; Stanley, P.; Bertozzi, C. R.; Hart, G. W.; Etzler, M. E.; Editors, *Essentials of Glycobiology; Second Edition*. Cold Spring Harbor Laboratory Press: 2009; p 784 pp.
2. Alberts B, J. A., Lewis J, et al., Membrane Proteins. In *Molecular Biology of the Cell*, Garland Science: New York, 2002; Vol. 4th edition.
3. Taylor, M. E.; Drickamer, K., *Introduction to glycobiology*. Oxford university press: 2011.
4. Bhavanandan, V. P.; Furukawa, K., Biochemistry and oncology of sialoglycoproteins. In *Biology of the sialic acids*, Springer: 1995; pp 145-196.
5. Brooks, S.; Dwek, M.; Schumacher, U., *Functional and molecular glycobiology*. Bios Scientific: 2002.
6. Stanley, P.; Cummings, R. D., Structures common to different glycans. **2017**.
7. Fukuda, M., Cell surface carbohydrates: cell type-specific expression. *Mol cell glycobiol* **2000**, 1-61.
8. Patsos, G.; Corfield, A., *O-Glycosylation: structural diversity and functions*. Wiley-VCH: Weinheim, Germany: 2009.
9. Krusius, T.; Finne, J.; Margolis, R.; Margolis, R., Identification of an O-glycosidic mannose-linked sialylated tetrasaccharide and keratan sulfate oligosaccharides in the chondroitin sulfate proteoglycan of brain. *J Biol Chem* **1986,** *261* (18), 8237-8242.
10. Nakamura, N.; Lyalin, D.; Panin, V. M. In *Protein O-mannosylation in animal development and physiology: from human disorders to Drosophila phenotypes*, Seminars in cell & developmental biology, Elsevier: 2010; pp 622-630.
11. Kleene, R.; Schachner, M., Glycans and neural cell interactions. *Nat Rev Neurosci* **2004,** *5* (3), 195-208.
12. Kopitz, J., Glycolipids: structure and function. *Glycosciences: status and perspectives* **1996**, 163-189.
13. Bhavanandan, V. P.; Gowda, D. C., Introduction to the Complexity of Cell Surface and Tissue Matrix Glycoconjugates. In *Glycobiology of the Nervous System*, Yu, R. K.; Schengrund, C.-L., Eds. Springer New York: New York, NY, 2014; pp 1-31.
14. Haynes, P. A., Phosphoglycosylation: A new structural class of glycosylation? *Glycobiol* **1998,** *8* (1), 1-5.
15. Spiro, R. G., Glycoproteins. *Adv Protein Chem* **1973,** *27*, 349-467.
16. Seko, A.; Koketsu, M.; Nishizono, M.; Enoki, Y.; Ibrahim, H. R.; Juneja, L. R.; Kim, M.; Yamamoto, T., Occurence of a sialylglycopeptide and free sialylglycans in hen's egg yolk. *Biochimica et biophysica acta* **1997,** *1335* (1-2), 23-32.
17. Zuber, C.; Roth, J., N-glycosylation. Wiley-VCH: Weinheim, Germany: 2009; pp 87-110.
18. Cummings, R. D., Synthesis of asparagine-linked oligosaccharides: pathways, genetics, and metabolic regulation. *Glycoconjugates. Composition, Structure and Function. HJ Allen and EC Kisailus, editors. Marcel Dekker, Inc., New York* **1992**, 333-360.
19. Hollingsworth, M. A.; Swanson, B. J., Mucins in cancer: protection and control of the cell surface. *Nat Rev Cancer* **2004,** *4* (1), 45-60.
20. Schachter, H.; Brockhausen, I. In *The biosynthesis of branched O-glycans*, Symposia of the Society for Experimental Biology, 1989; pp 1-26.

21. Lindahl, U.; Hook, M., Glycosaminoglycans and their binding to biological macromolecules. *Annu rev biochem* **1978,** *47* (1), 385-417.
22. Höök, M.; Kjellén, L.; Johansson, S.; Robinson, J., Cell-surface glycosaminoglycans. *Annu rev biochem* **1984,** *53* (1), 847-869.
23. Hassell, J. R.; Kimura, J. H.; Hascall, V. C., Proteoglycan core protein families. *Annu rev biochem* **1986,** *55* (1), 539-567.
24. Kjellén, L.; Lindahl, U., Proteoglycans: structures and interactions. *Annu rev biochem* **1991,** *60* (1), 443-475.
25. Ferguson, M. A.; Kinoshita, T.; Hart, G. W., Glycosylphosphatidylinositol anchors. **2009**.
26. Kundu, S. K., Glycolipids: structure, synthesis, functions. *Glycoconjugates: Composition, Structure, and Function (Allen, HJ & Kisailus, EC, eds)* **1992**, 203-262.
27. Hakomori, S., Structure, organization, and function of glycosphingolipids in membrane. *Curr Opin Hematol* **2003,** *10* (1), 16-24.
28. Varki A, C. R., Esko JD, et al., Cellular Organization of Glycosylation. In *Essentials of Glycobiology*, Cold Spring Harbor Laboratory Press: Cold Spring Harbor (NY), 2009; Vol. 2nd edition.
29. Seeberger, P. H.; Werz, D. B., Synthesis and medical applications of oligosaccharides. *Nature* **2007,** *446*, 1046.
30. Wang, Z.; Chinoy, Z. S.; Ambre, S. G.; Peng, W. J.; McBride, R.; de Vries, R. P.; Glushka, J.; Paulson, J. C.; Boons, G. J., A General Strategy for the Chemoenzymatic Synthesis of Asymmetrically Branched N-Glycans. *Science* **2013,** *341* (6144), 379-383.
31. Koizumi, A.; Matsuo, I.; Takatani, M.; Seko, A.; Hachisu, M.; Takeda, Y.; Ito, Y., Top-Down Chemoenzymatic Approach to a High-Mannose-Type Glycan Library: Synthesis of a Common Precursor and Its Enzymatic Trimming. *Angew. Chem. Int. Ed.* **2013,** *52* (29), 7426-7431.
32. Tsai, T. I.; Lee, H. Y.; Chang, S. H.; Wang, C. H.; Tu, Y. C.; Lin, Y. C.; Hwang, D. R.; Wu, C. Y.; Wong, C. H., Effective Sugar Nucleotide Regeneration for the Large-Scale Enzymatic Synthesis of Globo H and SSEA4. *J Am Chem Soc* **2013,** *135* (39), 14831-14839.
33. Rillahan, C. D.; Schwartz, E.; McBride, R.; Fokin, V. V.; Paulson, J. C., Click and Pick: Identification of Sialoside Analogues for Siglec-Based Cell Targeting. *Angew. Chem. Int. Ed.* **2012,** *51* (44), 11014-11018.
34. Johnson, M. A.; Bundle, D. R., Designing a new antifungal glycoconjugate vaccine. *Chem Soc Rev* **2013,** *42* (10), 4327-4344.
35. Kiessling, L. L.; Splain, R. A., Chemical Approaches to Glycobiology. *Annu rev biochem* **2010,** *79* (1), 619-653.
36. Demchenko, A. V., General Aspects of the Glycosidic Bond Formation. In *Handbook of Chemical Glycosylation*, Demchenko, A. V., Ed. wiley: 2008; pp 1-27.
37. McKay, M. J.; Nguyen, H. M., Recent Advances in Transition Metal-Catalyzed Glycosylation. *ACS Catalysis* **2012,** *2* (8), 1563-1595.
38. Nukada, T.; Berces, A.; Zgierski, M. Z.; Whitfield, D. M., Exploring the mechanism of neighboring group assisted glycosylation reactions. *J Am Chem Soc* **1998,** *120* (51), 13291-13295.
39. Nigudkar, S. S.; Demchenko, A. V., Stereocontrolled 1,2-cis glycosylation as the driving force of progress in synthetic carbohydrate chemistry. *Chem Sc* **2015,** *6* (5), 2687-2704.
40. Bols, M., Synthesis of Kojitriose using silicon-tethered glycosidation. *Acta Chem Scand* **1996,** *50* (10), 931-937.

41. Murakata, C.; Ogawa, T., Stereoselective synthesis of glycobiosyl phosphatidylinositol, a part structure of the glycosyl-phosphatidylinositol (GPI) anchor of Trypanosoma brucei. *Carbohydr Res* **1992,** *234*, 75-91.
42. Hahm, H. S.; Hurevich, M.; Seeberger, P. H., Automated assembly of oligosaccharides containing multiple cis-glycosidic linkages. *Nat Commun* **2016,** *7*.
43. Schmidt, R. R.; Behrendt, M.; Toepfer, A., Nitriles as Solvents in Glycosylation Reactions - Highly Selective Beta-Glycoside Synthesis. *Synlett* **1990,** (11), 694-696.
44. Ilg, T.; Etges, R.; Overath, P.; McConville, M. J.; Thomas-Oates, J.; Thomas, J.; Homans, S. W.; Ferguson, M. A., Structure of Leishmania mexicana lipophosphoglycan. *J Biol Chem* **1992,** *267* (10), 6834-6840.
45. Ferguson, M. A., The structure, biosynthesis and functions of glycosylphosphatidylinositol anchors, and the contributions of trypanosome research. *Journal of cell science* **1999,** *112 (Pt 17)*, 2799-809.
46. McConville, M. J.; Schnur, L. F.; Jaffe, C.; Schneider, P., Structure of Leishmania lipophosphoglycan: inter- and intra-specific polymorphism in Old World species. *Biochem J* **1995,** *310* (3), 807-818.
47. Paulick, M. G.; Bertozzi, C. R., The glycosylphosphatidylinositol anchor: a complex membrane-anchoring structure for proteins. *Biochem* **2008,** *47* (27), 6991-7000.
48. Ferguson, M. A., The structure, biosynthesis and functions of glycosylphosphatidylinositol anchors, and the contributions of trypanosome research. *Journal of cell science* **1999,** *112* (17), 2799-2809.
49. Ferguson, M.; Homans, S.; Dwek, R.; Rademacher, T., Glycosyl-phosphatidylinositol moiety that anchors Trypanosoma brucei variant surface glycoprotein to the membrane. *Science* **1988,** *239* (4841), 753-759.
50. Mayor, S.; Menon, A. K.; Cross, G. A., Transfer of glycosyl-phosphatidylinositol membrane anchors to polypeptide acceptors in a cell-free system. *J Cell Biol* **1991,** *114* (1), 61-71.
51. Schneider, P.; Ferguson, M. A.; McConville, M. J.; Mehlert, A.; Homans, S. W.; Bordier, C., Structure of the glycosyl-phosphatidylinositol membrane anchor of the Leishmania major promastigote surface protease. *J Biol Chem* **1990,** *265* (28), 16955-64.
52. Gerold, P.; Schofield, L.; Blackman, M. J.; Holder, A. A.; Schwarz, R. T., Structural analysis of the glycosyl-phosphatidylinositol membrane anchor of the merozoite surface proteins-1 and -2 of Plasmodium falciparum. *Mol Biochem Parasitol* **1996,** *75* (2), 131-43.
53. Gerold, P.; Dieckmann-Schuppert, A.; Schwarz, R. T., Glycosylphosphatidylinositols synthesized by asexual erythrocytic stages of the malarial parasite, Plasmodium falciparum. Candidates for plasmodial glycosylphosphatidylinositol membrane anchor precursors and pathogenicity factors. *J Biol Chem* **1994,** *269* (4), 2597-606.
54. Naik, R. S.; Branch, O. H.; Woods, A. S.; Vijaykumar, M.; Perkins, D. J.; Nahlen, B. L.; Lal, A. A.; Cotter, R. J.; Costello, C. E.; Ockenhouse, C. F.; Davidson, E. A.; Gowda, D. C., Glycosylphosphatidylinositol Anchors of Plasmodium falciparum. *Molecular Characterization and Naturally Elicited Antibody Response That May Provide Immunity to Malaria Pathogenesis* **2000,** *192* (11), 1563-1576.
55. Macrae, J. I.; Acosta-Serrano, A.; Morrice, N. A.; Mehlert, A.; Ferguson, M. A., Structural characterization of NETNES, a novel glycoconjugate in Trypanosoma cruzi epimastigotes. *J Biol Chem* **2005,** *280* (13), 12201-11.
56. Oxley, D.; Bacic, A., Structure of the glycosylphosphatidylinositol anchor of an arabinogalactan protein from Pyrus communis suspension-cultured cells. *Proc Natl Acad Sci U S A* **1999,** *96* (25), 14246-51.

57. Nett, I. R.; Mehlert, A.; Lamont, D.; Ferguson, M. A., Application of electrospray mass spectrometry to the structural determination of glycosylphosphatidylinositol membrane anchors. *Glycobiol* **2010,** *20* (5), 576-85.
58. Striepen, B.; Zinecker, C. F.; Damm, J. B.; Melgers, P. A.; Gerwig, G. J.; Koolen, M.; Vliegenthart, J. F.; Dubremetz, J. F.; Schwarz, R. T., Molecular structure of the "low molecular weight antigen" of Toxoplasma gondii: a glucose alpha 1-4 N-acetylgalactosamine makes free glycosyl-phosphatidylinositols highly immunogenic. *J Mol Biol* **1997,** *266* (4), 797-813.
59. Gerold, P.; Striepen, B.; Reitter, B.; Geyer, H.; Geyer, R.; Reinwald, E.; Risse, H. J.; Schwarz, R. T., Glycosyl-phosphatidylinositols of Trypanosoma congolense: two common precursors but a new protein-anchor. *J Mol Biol* **1996,** *261* (2), 181-94.
60. Homans, S. W.; Ferguson, M. A.; Dwek, R. A.; Rademacher, T. W.; Anand, R.; Williams, A. F., Complete structure of the glycosyl phosphatidylinositol membrane anchor of rat brain Thy-1 glycoprotein. *Nature* **1988,** *333* (6170), 269-72.
61. Stahl, N.; Baldwin, M. A.; Hecker, R.; Pan, K. M.; Burlingame, A. L.; Prusiner, S. B., Glycosylinositol phospholipid anchors of the scrapie and cellular prion proteins contain sialic acid. *Biochem* **1992,** *31* (21), 5043-53.
62. Treumann, A.; Lifely, M. R.; Schneider, P.; Ferguson, M. A., Primary structure of CD52. *J Biol Chem* **1995,** *270* (11), 6088-99.
63. Schroter, S.; Derr, P.; Conradt, H. S.; Nimtz, M.; Hale, G.; Kirchhoff, C., Male-specific modification of human CD52. *J Biol Chem* **1999,** *274* (42), 29862-73.
64. Rudd, P. M.; Morgan, B. P.; Wormald, M. R.; Harvey, D. J.; van den Berg, C. W.; Davis, S. J.; Ferguson, M. A.; Dwek, R. A., The glycosylation of the complement regulatory protein, human erythrocyte CD59. *J Biol Chem* **1997,** *272* (11), 7229-44.
65. Fujita, M.; Jigami, Y., Lipid remodeling of GPI-anchored proteins and its function. *Biochimica et biophysica acta* **2008,** *1780* (3), 410-420.
66. Almeida, I. C.; Camargo, M. M.; Procópio, D. O.; Silva, L. S.; Mehlert, A.; Travassos, L. R.; Gazzinelli, R. T.; Ferguson, M. A. J., Highly purified glycosylphosphatidylinositols from Trypanosoma cruzi are potent proinflammatory agents. *The EMBO Journal* **2000,** *19* (7), 1476-1485.
67. Nosjean, O.; Briolay, A.; Roux, B., Mammalian GPI proteins: sorting, membrane residence and functions. *Biochimica et biophysica acta* **1997,** *1331* (2), 153-86.
68. Low, M. G., The glycosyl-phosphatidylinositol anchor of membrane proteins. *Biochimica et biophysica acta* **1989,** *988* (3), 427-454.
69. Taylor, D. R.; Hooper, N. M., The prion protein and lipid rafts. *Mol Membr Biol* **2006,** *23* (1), 89-99.
70. Selleck, S. B., Proteoglycans and pattern formation: sugar biochemistry meets developmental genetics. *Trends Genet* **2000,** *16* (5), 206-12.
71. Gillmor, C. S.; Lukowitz, W.; Brininstool, G.; Sedbrook, J. C.; Hamann, T.; Poindexter, P.; Somerville, C., Glycosylphosphatidylinositol-anchored proteins are required for cell wall synthesis and morphogenesis in Arabidopsis. *The Plant cell* **2005,** *17* (4), 1128-1140.
72. Youl, J. J.; Bacic, A.; Oxley, D., Arabinogalactan-proteins from Nicotiana alata and Pyrus communis contain glycosylphosphatidylinositol membrane anchors. *Proc Natl Acad Sci U S A* **1998,** *95* (14), 7921-6.
73. Caro, L. H.; Tettelin, H.; Vossen, J. H.; Ram, A. F.; van den Ende, H.; Klis, F. M., In silicio identification of glycosyl-phosphatidylinositol-anchored plasma-membrane and cell wall proteins of Saccharomyces cerevisiae. *Yeast (Chichester, England)* **1997,** *13* (15), 1477-89.

74. Kapteyn, J. C.; Van Den Ende, H.; Klis, F. M., The contribution of cell wall proteins to the organization of the yeast cell wall. *Biochimica et biophysica acta* **1999,** *1426* (2), 373-83.
75. Englund, P. T., The Structure and Biosynthesis of Glycosyl Phosphatidylinositol Protein Anchors. *Annu rev biochem* **1993,** *62* (1), 121-138.
76. McConville, M. J.; Ferguson, M. A. J., The structure, biosynthesis and function of glycosylated phosphatidylinositols in the parasitic protozoa and higher eukaryotes. *Biochem J* **1993,** *294* (2), 305-324.
77. Miyata, T.; Yamada, N.; Iida, Y.; Nishimura, J.; Takeda, J.; Kitani, T.; Kinoshita, T., Abnormalities of PIG-A transcripts in granulocytes from patients with paroxysmal nocturnal hemoglobinuria. *New England Journal of Medicine* **1994,** *330* (4), 249-255.
78. Takeda, J.; Miyata, T.; Kawagoe, K.; Iida, Y.; Endo, Y.; Fujita, T.; Takahashi, M.; Kitani, T.; Kinoshita, T., Deficiency of the GPI anchor caused by a somatic mutation of the PIG-A gene in paroxysmal nocturnal hemoglobinuria. *Cell* **1993,** *73* (4), 703-711.
79. Bessler, M.; Mason, P.; Hillmen, P.; Miyata, T.; Yamada, N.; Takeda, J.; Luzzatto, L.; Kinoshita, T., Paroxysmal nocturnal haemoglobinuria (PNH) is caused by somatic mutations in the PIG-A gene. *The EMBO journal* **1994,** *13* (1), 110-117.
80. Rother, R.; Rollins, S.; Mennone, J.; Chodera, A.; Fidel, S.; Bessler, M.; Hillmen, P.; Squinto, S., Expression of recombinant transmembrane CD59 in paroxysmal nocturnal hemoglobinuria B cells confers resistance to human complement. *Blood* **1994,** *84* (8), 2604-2611.
81. Young, N. S.; Abkowitz, J. L.; Luzzatto, L., New Insights into the Pathophysiology of Acquired Cytopenias. *ASH Education Program Book* **2000,** *2000* (1), 18-38.
82. Brodsky, R. A., New insights into paroxysmal nocturnal hemoglobinuria. *ASH Education Program Book* **2006,** *2006* (1), 24-28.
83. Nozaki, M.; Ohishi, K.; Yamada, N.; Kinoshita, T.; Nagy, A.; Takeda, J., Developmental abnormalities of glycosylphosphatidylinositol-anchor-deficient embryos revealed by Cre/loxP system. *Lab Invest* **1999,** *79* (3), 293-299.
84. Roberts, W. L.; Myher, J. J.; Kuksis, A.; Low, M. G.; Rosenberry, T. L., Lipid analysis of the glycoinositol phospholipid membrane anchor of human erythrocyte acetylcholinesterase. Palmitoylation of inositol results in resistance to phosphatidylinositol-specific phospholipase C. *J Biol Chem* **1988,** *263* (35), 18766-75.
85. Orlean, P.; Menon, A. K., Thematic review series: Lipid Posttranslational Modifications. GPI anchoring of protein in yeast and mammalian cells, or: how we learned to stop worrying and love glycophospholipids. *J Lipid Res* **2007,** *48* (5), 993-1011.
86. Kinoshita, T.; Fujita, M.; Maeda, Y., Biosynthesis, remodelling and functions of mammalian GPI-anchored proteins: recent progress. *J Biochem* **2008,** *144* (3), 287-94.
87. Vishwakarma, R. A.; Menon, A. K., Flip-flop of glycosylphosphatidylinositols (GPI's) across the ER. *Chem Comm* **2005,** (4), 453-455.
88. Vidugiriene, J.; Menon, A. K., Early lipid intermediates in glycosyl-phosphatidylinositol anchor assembly are synthesized in the ER and located in the cytoplasmic leaflet of the ER membrane bilayer. *J Cell Biol* **1993,** *121* (5), 987-996.
89. Doerrler, W. T.; Ye, J.; Falck, J. R.; Lehrman, M. A., Acylation of Glucosaminyl Phosphatidylinositol Revisited. *J Biol Chem* **1996,** *271* (43), 27031-27038.
90. Kanzawa, N.; Maeda, Y.; Ogiso, H.; Murakami, Y.; Taguchi, R.; Kinoshita, T., Peroxisome dependency of alkyl-containing GPI-anchor biosynthesis in the endoplasmic reticulum. *Proceedings of the National Academy of Sciences* **2009,** *106* (42), 17711-17716.

91. Kinoshita, T.; Fujita, M., Biosynthesis of GPI-anchored proteins: special emphasis on GPI lipid remodeling. *J Lipid Res* **2016,** *57* (1), 6-24.
92. Smith, T. K.; Kimmel, J.; Azzouz, N.; Shams-Eldin, H.; Schwarz, R. T., The Role of Inositol Acylation and Inositol Deacylation in the Toxoplasma gondii Glycosylphosphatidylinositol Biosynthetic Pathway. *J Biol Chem* **2007,** *282* (44), 32032-32042.
93. Ikezawa, H., Glycosylphosphatidylinositol (GPI)-anchored proteins. *Biol Pharm Bull* **2002,** *25* (4), 409-17.
94. Maeda, Y.; Tashima, Y.; Houjou, T.; Fujita, M.; Yoko-o, T.; Jigami, Y.; Taguchi, R.; Kinoshita, T.; Gilmore, R., Fatty Acid Remodeling of GPI-anchored Proteins Is Required for Their Raft Association. *Molecular Biology of the Cell* **2007,** *18* (4), 1497-1506.
95. Bosson, R.; Jaquenoud, M.; Conzelmann, A., GUP1 of Saccharomyces cerevisiae encodes an O-acyltransferase involved in remodeling of the GPI anchor. *Molecular biology of the cell* **2006,** *17* (6), 2636-2645.
96. Sipos, G.; Reggiori, F.; Vionnet, C.; Conzelmann, A., Alternative lipid remodelling pathways for glycosylphosphatidylinositol membrane anchors in Saccharomyces cerevisiae. *The EMBO journal* **1997,** *16* (12), 3494-3505.
97. Reggiori, F.; Canivenc-Gansel, E.; Conzelmann, A., Lipid remodeling leads to the introduction and exchange of defined ceramides on GPI proteins in the ER and Golgi of Saccharomyces cerevisiae. *The EMBO journal* **1997,** *16* (12), 3506-3518.
98. Simons, K.; Vaz, W. L., Model systems, lipid rafts, and cell membranes. *Annu Rev Biophys Biomol Struct* **2004,** *33*, 269-95.
99. Rajendran, L.; Simons, K., Lipid rafts and membrane dynamics. *Journal of cell science* **2005,** *118* (6), 1099-1102.
100. Munro, S., Lipid rafts: elusive or illusive? *Cell* **2003,** *115* (4), 377-88.
101. Mann, K. J.; Hepworth, M. R.; Raikwar, N. S.; Deeg, M. A.; Sevlever, D., Effect of glycosylphosphatidylinositol (GPI)-phospholipase D overexpression on GPI metabolism. *Biochem J* **2004,** *378* (2), 641-648.
102. Jones, D. R.; Varela-Nieto, I., The role of glycosyl-phosphatidylinositol in signal transduction. *Int J Biochem Cell Biol* **1998,** *30* (3), 313-26.
103. Robinson, P. J., Signal Transduction Via GPI-Anchored Membrane Proteins. In *ADP-Ribosylation in Animal Tissues: Structure, Function, and Biology of Mono (ADP-ribosyl) Transferases and Related Enzymes*, Haag, F.; Koch-Nolte, F., Eds. Springer US: Boston, MA, 1997; pp 365-370.
104. Ilangumaran, S.; Briol, A.; Hoessli, D. C., Distinct interactions among GPI-anchored, transmembrane and membrane associated intracellular proteins, and sphingolipids in lymphocyte and endothelial cell plasma membranes. *Biochimica et Biophysica Acta (BBA) - Biomembranes* **1997,** *1328* (2), 227-236.
105. Liu, T.; Li, R.; Pan, T.; Liu, D.; Petersen, R. B.; Wong, B.-S.; Gambetti, P.; Sy, M. S., Intercellular Transfer of the Cellular Prion Protein. *J Biol Chem* **2002,** *277* (49), 47671-47678.
106. Lu, J.; Jayaprakash, K. N.; Schlueter, U.; Fraser-Reid, B., Synthesis of a malaria candidate glycosylphosphatidylinositol (GPI) structure: A strategy for fully inositol acylated and phosphorylated GPIs. *J Am Chem Soc* **2004,** *126* (24), 7540-7547.
107. Tsai, Y.-H.; Gotze, S.; Vilotijevic, I.; Grube, M.; Varon Silva, D.; Seeberger, P. H., A general and convergent synthesis of diverse glycosylphosphatidylinositol glycolipids. *Chem Sc* **2013,** *4* (1), 468-481.
108. Unverzagt, C.; Kajihara, Y., Chemical assembly of N-glycoproteins: a refined toolbox to address a ubiquitous posttranslational modification. *Chem Soc Rev* **2013,** *42* (10), 4408-20.

109. Rudd, P. M.; Joao, H. C.; Coghill, E.; Fiten, P.; Saunders, M. R.; Opdenakker, G.; Dwek, R. A., Glycoforms modify the dynamic stability and functional activity of an enzyme. *Biochem* **1994,** *33* (1), 17-22.
110. Yamaguchi, Y.; Nishimura, M.; Nagano, M.; Yagi, H.; Sasakawa, H.; Uchida, K.; Shitara, K.; Kato, K., Glycoform-dependent conformational alteration of the Fc region of human immunoglobulin G1 as revealed by NMR spectroscopy. *Biochimica et Biophysica Acta, General Subjects* **2006,** *1760* (4), 693-700.
111. Taylor, C. M., Glycopeptides and glycoproteins: focus on the glycosidic linkage. *Tetrahedron* **1998,** *54* (38), 11317-11362.
112. Wang, L.-X.; Lomino, J. V., Emerging Technologies for Making Glycan-Defined Glycoproteins. *ACS Chem Biol* **2011,** *7* (1), 110-122.
113. Pratt, M. R.; Bertozzi, C. R., Synthetic glycopeptides and glycoproteins as tools for biology. *Chem Soc Rev* **2005,** *34* (1), 58-68.
114. Liu, L.; Bennett, C. S.; Wong, C.-H., Advances in glycoprotein synthesis. *Chem Comm* **2006,** (1), 21-33.
115. Grogan, M. J.; Pratt, M. R.; Marcaurelle, L. A.; Bertozzi, C. R., Homogeneous glycopeptides and glycoproteins for biological investigation. *Annu rev biochem* **2002,** *71*, 593-634.
116. Davis, B. G., Synthesis of Glycoproteins. *Chem Rev* **2002,** *102*, 579-601.
117. Bill, R. M.; Flitsch, S., Chemical and biological approaches to glycoprotein synthesis. *Chem Biol* **1996,** *3* (3), 145-149.
118. Wiederschain, G. Y., Glycobiology: Progress, problems, and perspectives. *Biochem* **2013,** *78* (7), 679-696.
119. van Hest, J. C. M.; Kiick, K. L.; Tirrell, D. A., Efficient Incorporation of Unsaturated Methionine Analogues into Proteins in Vivo. *J Am Chem Soc* **2000,** *122* (7), 1282-1288.
120. Schumann, B.; Hahm, H. S.; Parameswarappa, S. G.; Reppe, K.; Wahlbrink, A.; Govindan, S.; Kaplonek, P.; Pirofski, L.-a.; Witzenrath, M.; Anish, C.; Pereira, C. L.; Seeberger, P. H., A semisynthetic Streptococcus pneumoniae serotype 8 glycoconjugate vaccine. *Science Translational Medicine* **2017,** *9* (380).
121. Parameswarappa, S. G.; Reppe, K.; Geissner, A.; Menova, P.; Govindan, S.; Calow, A. D. J.; Wahlbrink, A.; Weishaupt, M. W.; Monnanda, B. P.; Bell, R. L.; Pirofski, L. A.; Suttorp, N.; Sander, L. E.; Witzenrath, M.; Pereira, C. L.; Anish, C.; Seeberger, P. H., A Semi-synthetic Oligosaccharide Conjugate Vaccine Candidate Confers Protection against Streptococcus pneumoniae Serotype 3 Infection. *Cell Chem Biol* **2016,** *23* (11), 1407-1416.
122. Velazquez-Campoy, A.; Ohtaka, H.; Nezami, A.; Muzammil, S.; Freire, E., Isothermal titration calorimetry. *Curr Protoc Cell Biol* **2004,** *Chapter 17*, Unit 17 8.
123. Piontek, C.; Ring, P.; Harjes, O.; Heinlein, C.; Mezzato, S.; Lombana, N.; Pöhner, C.; Püttner, M.; Varón-Silva, D.; Martin, A.; Schmid, F.-X.; Unverzagt, C., Semisynthese eines homogenen Glycoprotein-Enzyms: Ribonuclease-C (Teil-1). *Angew Chem* **2009,** *121* (11), 1968-1973.
124. Piontek, C.; Ring, P.; Harjes, O.; Heinlein, C.; Mezzato, S.; Lombana, N.; Pohner, C.; Puettner, M.; Varon-Silva, D.; Martin, A.; Schmid, F. X.; Unverzagt, C., Semisynthesis of a Homogeneous Glycoprotein Enzyme: Ribonuclease C: Part 1. *Angew. Chem. Int. Ed.* **2009,** *48* (11), 1936-1940.
125. Dawson, P. E.; Muir, T. W.; Clark-Lewis, I.; Kent, S. B., Synthesis of proteins by native chemical ligation. *Science* **1994,** *266* (5186), 776-9.
126. Reif, A.; Siebenhaar, S.; Troster, A.; Schmalzlein, M.; Lechner, C.; Velisetty, P.; Gottwald, K.; Pohner, C.; Boos, I.; Schubert, V.; Rose-John, S.; Unverzagt, C.,

Semisynthesis of biologically active glycoforms of the human cytokine interleukin 6. *Angew. Chem. Int. Ed.* **2014,** *53* (45), 12125-31.
127. Wang, L. X.; Amin, M. N., Chemical and Chemoenzymatic Synthesis of Glycoproteins for Deciphering Functions. *Chem Biol* **2014,** *21* (1), 51-66.
128. Ochiai, H.; Huang, W.; Wang, L.-X., Expeditious Chemoenzymatic Synthesis of Homogeneous N-Glycoproteins Carrying Defined Oligosaccharide Ligands. *J Am Chem Soc* **2008,** *130* (41), 13790-13803.
129. Umekawa, M.; Huang, W.; Li, B.; Fujita, K.; Ashida, H.; Wang, L. X.; Yamamoto, K., Mutants of Mucor hiemalis endo-beta-N-acetylglucosaminidase show enhanced transglycosylation and glycosynthase-like activities. *J Biol Chem* **2008,** *283* (8), 4469-79.
130. Hay, S. I.; Guerra, C. A.; Tatem, A. J.; Noor, A. M.; Snow, R. W., The global distribution and population at risk of malaria: past, present, and future. *The Lancet infectious diseases* **2004,** *4* (6), 327-336.
131. WHO *World Malaria Report 2016*; 2016; p 186.
132. White, N. J.; Ho, M., The pathophysiology of malaria. *Adv Parasitol* **1992,** *31*, 83-173.
133. Greenwood, B. M.; Fidock, D. A.; Kyle, D. E.; Kappe, S. H. I.; Alonso, P. L.; Collins, F. H.; Duffy, P. E., Malaria: progress, perils, and prospects for eradication. *The Journal of Clinical Investigation* **2008,** *118* (4), 1266-1276.
134. Breman, J. G.; Plowe, C. V., A Malaria Vaccine for Control: More Progress. *J Infect Diseases* **2009,** *200* (3), 317-320.
135. Miller, L.; Good, M.; Milon, G., Malaria pathogenesis. *Science* **1994,** *264* (5167), 1878-1883.
136. Wipasa, J.; Elliott, S.; Xu, H.; Good, M. F., Immunity to asexual blood stage malaria and vaccine approaches. *Immunol Cell Biol* **2002,** *80* (5), 401-414.
137. Hill, A. V. S., Vaccines against malaria. *Philosophical Transactions of the Royal Society B: Biological Sciences* **2011,** *366* (1579), 2806-2814.
138. Ballou, W. R.; Cahill, C. P., Two decades of commitment to malaria vaccine development: GlaxoSmithKline Biologicals. *Am J Trop Med Hyg* **2007,** *77* (6 Suppl), 289-295.
139. Garçon, N.; Heppner, D. G.; Cohen, J., Development of RTS,S/AS02: a purified subunit-based malaria vaccine candidate formulated with a novel adjuvant. *Expert Review of Vaccines* **2003,** *2* (2), 231-238.
140. Alonso, P. L.; Sacarlal, J.; Aponte, J. J.; Leach, A.; Macete, E.; Milman, J.; Mandomando, I.; Spiessens, B.; Guinovart, C.; Espasa, M.; Bassat, Q.; Aide, P.; Ofori-Anyinam, O.; Navia, M. M.; Corachan, S.; Ceuppens, M.; Dubois, M.-C.; Demoitié, M.-A.; Dubovsky, F.; Menéndez, C.; Tornieporth, N.; Ripley Ballou, W.; Thompson, R.; Cohen, J., Efficacy of the RTS,S/AS02A vaccine against Plasmodium falciparum infection and disease in young African children: randomised controlled trial. *The Lancet* **2004,** *364* (9443), 1411-1420.
141. Coelho, C. H.; Doritchamou, J. Y. A.; Zaidi, I.; Duffy, P. E., Advances in malaria vaccine development: report from the 2017 malaria vaccine symposium. *npj Vaccines* **2017,** *2* (1), 34.
142. Sacarlal, J.; Aide, P.; Aponte, J. J.; Renom, M.; Leach, A.; Mandomando, I.; Lievens, M.; Bassat, Q.; Lafuente, S.; Macete, E.; Vekemans, J.; Guinovart, C.; Sigaúque, B.; Sillman, M.; Milman, J.; Dubois, M.-C.; Demoitié, M.-A.; Thonnard, J.; Menéndez, C.; Ballou, W. R.; Cohen, J.; Alonso, P. L., Long-Term Safety and Efficacy of the RTS,S/AS02A Malaria Vaccine in Mozambican Children. *J Infect Diseases* **2009,** *200* (3), 329-336.

143. Schofield, L.; Grau, G. E., Immunological processes in malaria pathogenesis. *Nat Rev Immun* **2005,** *5*, 722.
144. Singh, N.; Liang, L.-N.; Tykocinski, M. L.; Tartakoff, A. M., A Novel Class of Cell Surface Glycolipids of Mammalian Cells: Free Glycosyl Phosphatidylinositols. *J Biol Chem* **1996,** *271* (22), 12879-12884.
145. Gowda, D. C.; Davidson, E. A., Protein Glycosylation in the Malaria Parasite. *Parasitology Today* **1999,** *15* (4), 147-152.
146. Naik, R. S.; Davidson, E. A.; Gowda, D. C., Developmental Stage-specific Biosynthesis of Glycosylphosphatidylinositol Anchors in IntraerythrocyticPlasmodium falciparum and Its Inhibition in a Novel Manner by Mannosamine. *J Biol Chem* **2000,** *275* (32), 24506-24511.
147. Schofield, L.; Hackett, F., Signal transduction in host cells by a glycosylphosphatidylinositol toxin of malaria parasites. *The Journal of Experimental Medicine* **1993,** *177* (1), 145-153.
148. de Souza, J. B.; Todd, J.; Krishegowda, G.; Gowda, D. C.; Kwiatkowski, D.; Riley, E. M., Prevalence and Boosting of Antibodies to Plasmodium falciparum Glycosylphosphatidylinositols and Evaluation of Their Association with Protection from Mild and Severe Clinical Malaria. *Infect Immun* **2002,** *70* (9), 5045-5051.
149. Suguitan, A. L.; Gowda, D. C.; Fouda, G.; Thuita, L.; Zhou, A.; Djokam, R.; Metenou, S.; Leke, R. G. F.; Taylor, D. W., Lack of an Association between Antibodies to Plasmodium falciparum Glycosylphosphatidylinositols and Malaria-Associated Placental Changes in Cameroonian Women with Preterm and Full-Term Deliveries. *Infect Immun* **2004,** *72* (9), 5267-5273.
150. Schofield, L.; Novakovic, S.; Gerold, P.; Schwarz, R. T.; McConville, M. J.; Tachado, S. D., Glycosylphosphatidylinositol toxin of Plasmodium up-regulates intercellular adhesion molecule-1, vascular cell adhesion molecule-1, and E-selectin expression in vascular endothelial cells and increases leukocyte and parasite cytoadherence via tyrosine kinase-dependent signal transduction. *J Immunol* **1996,** *156* (5), 1886-1896.
151. Hewitt, M. C.; Snyder, D. A.; Seeberger, P. H., Rapid Synthesis of a Glycosylphosphatidylinositol-Based Malaria Vaccine Using Automated Solid-Phase Oligosaccharide Synthesis. *J Am Chem Soc* **2002,** *124* (45), 13434-13436.
152. Gerold, P.; Dieckmann-Schuppert, A.; Schwarz, R. T., Glycosylphosphatidylinositols synthesized by asexual erythrocytic stages of the malarial parasite, Plasmodium falciparum. Candidates for plasmodial glycosylphosphatidylinositol membrane anchor precursors and pathogenicity factors. *Journal of Biological Chemistry* **1994,** *269* (4), 2597-2606.
153. Schofield, L.; Hewitt, M. C.; Evans, K.; Siomos, M.-A.; Seeberger, P. H., Synthetic GPI as a candidate anti-toxic vaccine in a model of malaria. *Nature* **2002,** *418*, 785.
154. Wolfson, W., Ancora Cooks with Carbs Synthesizing Carbohydrate Vaccines. *Chem Biol* **2006,** *13* (7), 689-691.
155. Naik, R. S.; Krishnegowda, G.; Ockenhouse, C. F.; Gowda, D. C., Naturally Elicited Antibodies to Glycosylphosphatidylinositols (GPIs) of Plasmodium falciparum Require Intact GPI Structures for Binding and Are Directed Primarily against the Conserved Glycan Moiety. *Infect Immun* **2006,** *74* (2), 1412-1415.
156. Boutlis, C. S.; Fagan, P. K.; Gowda, D. C.; Lagog, M.; Mgone, C. S.; Bockarie, M. J.; Anstey, N. M., Immunoglobulin G (IgG) Responses to Plasmodium falciparum Glycosylphosphatidylinositols Are Short-Lived and Predominantly of the IgG3 Subclass. *J Infect Diseases* **2003,** *187* (5), 862-865.
157. Boutlis, C. S.; Gowda, D. C.; Naik, R. S.; Maguire, G. P.; Mgone, C. S.; Bockarie, M. J.; Lagog, M.; Ibam, E.; Lorry, K.; Anstey, N. M., Antibodies to Plasmodium

falciparum Glycosylphosphatidylinositols: Inverse Association with Tolerance of Parasitemia in Papua New Guinean Children and Adults. *Infect Immun* **2002,** *70* (9), 5052-5057.
158. Keenihan, S. N. H.; Ratiwayanto, S.; Soebianto, S.; KRISIN; Marwoto, H.; Krishnegowda, G.; Gowda, D. C.; Bangs, M. J.; Fryauff, D. J.; Richie, T. L.; Kumar, S.; Baird, J. K., Age-Dependent Impairment of IgG Responses to GPI with Equal Exposure to Plasmodium Falciparum among Javanese Migrants to Papua, Indonesia. *Am J Trop Med Hyg* **2003,** *69* (1), 36-41.
159. Perraut, R.; Diatta, B.; Marrama, L.; Garraud, O.; Jambou, R.; Longacre, S.; Krishnegowda, G.; Dieye, A.; Gowda, D. C., Differential antibody responses to Plasmodium falciparum glycosylphosphatidylinositol anchors in patients with cerebral and mild malaria. *Microbes and Infection* **2005,** *7* (4), 682-687.
160. Kamena, F.; Tamborrini, M.; Liu, X.; Kwon, Y.-U.; Thompson, F.; Pluschke, G.; Seeberger, P. H., Synthetic GPI array to study antitoxic malaria response. *Nat Chem Biol* **2008,** *4*, 238.
161. Tsai, Y.-H.; Götze, S.; Vilotijevic, I.; Grube, M.; Silva, D. V.; Seeberger, P. H., A general and convergent synthesis of diverse glycosylphosphatidylinositol glycolipids. *Chem Sc* **2013,** *4* (1), 468-481.
162. Wojcik, F.; O'Brien, A. G.; Götze, S.; Seeberger, P. H.; Hartmann, L., Synthesis of Carbohydrate-Functionalised Sequence-Defined Oligo(amidoamine)s by Photochemical Thiol-Ene Coupling in a Continuous Flow Reactor. *Chemistry – A European Journal* **2013,** *19* (9), 3090-3098.
163. Kubler-Kielb, J.; Vinogradov, E.; Ben-Menachem, G.; Pozsgay, V.; Robbins, J. B.; Schneerson, R., Saccharide/protein conjugate vaccines for Bordetella species: preparation of saccharide, development of new conjugation procedures, and physico-chemical and immunological characterization of the conjugates. *Vaccine* **2008,** *26* (29-30), 3587-3593.
164. Ghosh, S. S.; Kao, P. M.; McCue, A. W.; Chappelle, H. L., Use of maleimide-thiol coupling chemistry for efficient syntheses of oligonucleotide-enzyme conjugate hybridization probes. *Bioconju Chem* **1990,** *1* (1), 71-76.
165. DeNinno, M. P.; Etienne, J. B.; Duplantier, K. C., A method for the selective reduction of carbohydrate 4,6-O-benzylidene acetals. *Tetrahedron Lett* **1995,** *36* (5), 669-672.
166. Pratt, M. R.; Bertozzi, C. R., Chemoselective Ligation Applied to the Synthesis of a Biantennary N-Linked Glycoform of CD52. *J Am Chem Soc* **2003,** *125* (20), 6149-6159.
167. Ogunsina, M.; Pan, H.; Samadder, P.; Arthur, G.; Schweizer, F., Structure Activity Relationships of N-linked and Diglycosylated Glucosamine-Based Antitumor Glycerolipids. *Molecules* **2013,** *18* (12), 15288.
168. Malito, E.; Bursulaya, B.; Chen, C.; Lo Surdo, P.; Picchianti, M.; Balducci, E.; Biancucci, M.; Brock, A.; Berti, F.; Bottomley, M. J.; Nissum, M.; Costantino, P.; Rappuoli, R.; Spraggon, G., Structural basis for lack of toxicity of the diphtheria toxin mutant CRM197. *Proc Natl Acad Sci U S A* **2012,** *109* (14), 5229-34.
169. Amante, F. H.; Stanley, A. C.; Randall, L. M.; Zhou, Y.; Haque, A.; McSweeney, K.; Waters, A. P.; Janse, C. J.; Good, M. F.; Hill, G. R.; Engwerda, C. R., A role for natural regulatory T cells in the pathogenesis of experimental cerebral malaria. *Am J Pathol* **2007,** *171* (2), 548-559.
170. Schmidt, M. F.; Bracha, M.; Schlesinger, M. J., Evidence for covalent attachment of fatty acids to Sindbis virus glycoproteins. *Proceedings of the National Academy of Sciences* **1979,** *76* (4), 1687-1691.

171. Hantke, K.; Braun, V., Covalent Binding of Lipid to Protein. *Euro J Biochem* **1973,** *34* (2), 284-296.
172. Glomset, J. A.; Gelb, M. H.; Farnsworth, C. C., Prenyl proteins in eukaryotic cells: a new type of membrane anchor. *Trends Biochem Sc* **1990,** *15* (4), 139-142.
173. Ferguson, M. A.; Low, M. G.; Cross, G. A., Glycosyl-sn-1,2-dimyristylphosphatidylinositol is covalently linked to Trypanosoma brucei variant surface glycoprotein. *J Biol Chem* **1985,** *260* (27), 14547-55.
174. Eisenhaber, B.; Bork, P.; Eisenhaber, F., Post-translational GPI lipid anchor modification of proteins in kingdoms of life: analysis of protein sequence data from complete genomes. *Protein Engineering, Design and Selection* **2001,** *14* (1), 17-25.
175. Holder, A. A.; Lockyer, M. J.; Odink, K. G.; Sandhu, J. S.; Riveros-Moreno, V.; Nicholls, S. C.; Hillman, Y.; Davey, L. S.; Tizard, M. L. V.; Schwarz, R. T.; Freeman, R. R., Primary structure of the precursor to the three major surface antigens of Plasmodium falciparum merozoites. *Nature* **1985,** *317*, 270.
176. Smythe, J.; Coppel, R.; Brown, G.; Ramasamy, R.; Kemp, D.; Anders, R., Identification of two integral membrane proteins of Plasmodium falciparum. *Proceedings of the National Academy of Sciences* **1988,** *85* (14), 5195-5199.
177. Kocken, C. H. M.; Jansen, J.; Kaan, A. M.; Beckers, P. J. A.; Ponnudurai, T.; Kaslow, D. C.; Konings, R. N. H.; Schoenmakers, J. G. G., Cloning and expression of the gene coding for the transmission blocking target antigen Pfs48/45 of Plasmodium falciparum. *Molecular and Biochemical Parasitology* **1993,** *61* (1), 59-68.
178. Kaslow, D. C.; Quakyi, I. A.; Syin, C.; Raum, M. G.; Keister, D. B.; Coligan, J. E.; McCutchan, T. F.; Miller, L. H., A vaccine candidate from the sexual stage of human malaria that contains EGF-like domains. *Nature* **1988,** *333*, 74.
179. Nardin, E. H.; Nussenzweig, V.; Nussenzweig, R. S.; Collins, W. E.; Harinasuta, K. T.; Tapchaisri, P.; Chomcharn, Y., Circumsporozoite proteins of human malaria parasites Plasmodium falciparum and Plasmodium vivax. *J Exp Med* **1982,** *156* (1), 20-30.
180. Dame, J. B.; Williams, J. L.; McCutchan, T. F.; Weber, J. L.; Wirtz, R. A.; Hockmeyer, W. T.; Maloy, W. L.; Haynes, J. D.; Schneider, I.; Roberts, D., Structure of the gene encoding the immunodominant surface antigen on the sporozoite of the human malaria parasite Plasmodium falciparum. *Science* **1984,** *225* (4662), 593-599.
181. Tomas, A. M.; Margos, G.; Dimopoulos, G.; van Lin, L. H. M.; de Koning-Ward, T. F.; Sinha, R.; Lupetti, P.; Beetsma, A. L.; Rodriguez, M. C.; Karras, M.; Hager, A.; Mendoza, J.; Butcher, G. A.; Kafatos, F.; Janse, C. J.; Waters, A. P.; Sinden, R. E., P25 and P28 proteins of the malaria ookinete surface have multiple and partially redundant functions. *The EMBO Journal* **2001,** *20* (15), 3975-3983.
182. Nardin, E. H.; Nussenzweig, V.; Nussenzweig, R. S.; Collins, W. E.; Harinasuta, K. T.; Tapchaisri, P.; Chomcharn, Y., Circumsporozoite proteins of human malaria parasites Plasmodium falciparum and Plasmodium vivax. *The Journal of Experimental Medicine* **1982,** *156* (1), 20-30.
183. Topolska, A. E.; Lidgett, A.; Truman, D.; Fujioka, H.; Coppel, R. L., Characterization of a Membrane-associated Rhoptry Protein of Plasmodium falciparum. *J Biol Chem* **2004,** *279* (6), 4648-4656.
184. Outchkourov, N. S.; Roeffen, W.; Kaan, A.; Jansen, J.; Luty, A.; Schuiffel, D.; van Gemert, G. J.; van de Vegte-Bolmer, M.; Sauerwein, R. W.; Stunnenberg, H. G., Correctly folded Pfs48/45 protein of Plasmodium falciparum elicits malaria transmission-blocking immunity in mice. *Proceedings of the National Academy of Sciences of the United States of America* **2008,** *105* (11), 4301-4305.

185. Gilson, P. R.; Crabb, B. S., Morphology and kinetics of the three distinct phases of red blood cell invasion by Plasmodium falciparum merozoites. *Int J Parasitol* **2009,** *39* (1), 91-96.
186. Sanders, P. R.; Gilson, P. R.; Cantin, G. T.; Greenbaum, D. C.; Nebl, T.; Carucci, D. J.; McConville, M. J.; Schofield, L.; Hodder, A. N.; Yates, J. R.; Crabb, B. S., Distinct Protein Classes Including Novel Merozoite Surface Antigens in Raft-like Membranes of Plasmodium falciparum. *J Biol Chem* **2005,** *280* (48), 40169-40176.
187. Lin, C. S.; Uboldi, A. D.; Epp, C.; Bujard, H.; Tsuboi, T.; Czabotar, P. E.; Cowman, A. F., Multiple Plasmodium falciparum Merozoite Surface Protein 1 Complexes Mediate Merozoite Binding to Human Erythrocytes. *The Journal of Biological Chemistry* **2016,** *291* (14), 7703-7715.
188. Gilson, P. R.; Nebl, T.; Vukcevic, D.; Moritz, R. L.; Sargeant, T.; Speed, T. P.; Schofield, L.; Crabb, B. S., Identification and stoichiometry of glycosylphosphatidylinositol-anchored membrane proteins of the human malaria parasite Plasmodium falciparum. *Mol Cell Proteomics* **2006,** *5* (7), 1286-99.
189. Das, S.; Hertrich, N.; Perrin, A. J.; Withers-Martinez, C.; Collins, C. R.; Jones, M. L.; Watermeyer, J. M.; Fobes, E. T.; Martin, S. R.; Saibil, H. R.; Wright, G. J.; Treeck, M.; Epp, C.; Blackman, M. J., Processing of Plasmodium falciparum Merozoite Surface Protein MSP1 Activates a Spectrin-Binding Function Enabling Parasite Egress from RBCs. *Cell host & microbe* **2015,** *18* (4), 433-44.
190. McBride, J. S.; Heidrich, H. G., Fragments of the polymorphic Mr 185,000 glycoprotein from the surface of isolated Plasmodium falciparum merozoites form an antigenic complex. *Mol Biochem Parasitol* **1987,** *23* (1), 71-84.
191. Lyon, J. A.; Geller, R. H.; Haynes, J. D.; Chulay, J. D.; Weber, J. L., Epitope map and processing scheme for the 195,000-dalton surface glycoprotein of Plasmodium falciparum merozoites deduced from cloned overlapping segments of the gene. *Proceedings of the National Academy of Sciences of the United States of America* **1986,** *83* (9), 2989-2993.
192. Holder, A. A.; Sandhu, J. S.; Hillman, Y.; Davey, L. S.; Nicholls, S. C.; Cooper, H.; Lockyer, M. J., Processing of the precursor to the major merozoite surface antigens of Plasmodium falciparum. *Parasitology* **1987,** *94 (Pt 2)*, 199-208.
193. Baldwin, M. R.; Li, X.; Hanada, T.; Liu, S. C.; Chishti, A. H., Merozoite surface protein 1 recognition of host glycophorin A mediates malaria parasite invasion of red blood cells. *Blood* **2015,** *125* (17), 2704-11.
194. Blackman, M. J.; Holder, A. A., Secondary processing of the Plasmodium falciparum merozoite surface protein-1 (MSP1) by a calcium-dependent membrane-bound serine protease: shedding of MSP133 as a noncovalently associated complex with other fragments of the MSP1. *Mol Biochem Parasitol* **1992,** *50* (2), 307-15.
195. Blackman, M. J.; Whittle, H.; Holder, A. A., Processing of the Plasmodium falciparum major merozoite surface protein-1: identification of a 33-kilodalton secondary processing product which is shed prior to erythrocyte invasion. *Mol Biochem Parasitol* **1991,** *49* (1), 35-44.
196. Stafford, W. H. L.; Günder, B.; Harris, A.; Heidrich, H.-G.; Holder, A. A.; Blackman, M. J., A 22 kDa protein associated with the Plasmodium falciparum merozoite surface protein-1 complex. *Molecular and Biochemical Parasitology* **1996,** *80* (2), 159-169.
197. Dluzewski, A. R.; Ling, I. T.; Hopkins, J. M.; Grainger, M.; Margos, G.; Mitchell, G. H.; Holder, A. A.; Bannister, L. H., Formation of the Food Vacuole in Plasmodium falciparum: A Potential Role for the 19 kDa Fragment of Merozoite Surface Protein 1 (MSP119). *PLOS ONE* **2008,** *3* (8), e3085.

198. Miller, L. H.; Roberts, T.; Shahabuddin, M.; McCutchan, T. F., Analysis of sequence diversity in the Plasmodium falciparum merozoite surface protein-1 (MSP-1). *Mol Biochem Parasitol* **1993,** *59* (1), 1-14.
199. Holder, A. A., The carboxy-terminus of merozoite surface protein 1: structure, specific antibodies and immunity to malaria. *Parasitology* **2009,** *136* (12), 1445-56.
200. Zhang, X.; Perugini, M. A.; Yao, S.; Adda, C. G.; Murphy, V. J.; Low, A.; Anders, R. F.; Norton, R. S., Solution conformation, backbone dynamics and lipid interactions of the intrinsically unstructured malaria surface protein MSP2. *J Mol Biol* **2008,** *379* (1), 105-21.
201. MacRaild, C. A.; Pedersen, M. O.; Anders, R. F.; Norton, R. S., Lipid interactions of the malaria antigen merozoite surface protein 2. *Biochimica et biophysica acta* **2012,** *1818* (11), 2572-8.
202. Boyle, M. J.; Langer, C.; Chan, J.-A.; Hodder, A. N.; Coppel, R. L.; Anders, R. F.; Beeson, J. G., Sequential Processing of Merozoite Surface Proteins during and after Erythrocyte Invasion by Plasmodium falciparum. *Infect Immun* **2014,** *82* (3), 924-936.
203. Black, C. G.; Wang, L.; Wu, T.; Coppel, R. L., Apical location of a novel EGF-like domain-containing protein of Plasmodium falciparum. *Mol Biochem Parasitol* **2003,** *127* (1), 59-68.
204. Black, C. G.; Wang, L.; Hibbs, A. R.; Werner, E.; Coppel, R. L., Identification of the Plasmodium chabaudi Homologue of Merozoite Surface Proteins 4 and 5 ofPlasmodium falciparum. *Infect Immun* **1999,** *67* (5), 2075-2081.
205. Wang, L.; Black, C. G.; Marshall, V. M.; Coppel, R. L., Structural and antigenic properties of merozoite surface protein 4 of Plasmodium falciparum. *Infect Immun* **1999,** *67* (5), 2193-200.
206. Wu, T.; Black, C. G.; Wang, L.; Hibbs, A. R.; Coppel, R. L., Lack of sequence diversity in the gene encoding merozoite surface protein 5 of Plasmodium falciparum. *Molecular and biochemical parasitology* **1999,** *103* (2), 243-250.
207. Beeson, J. G.; Drew, D. R.; Boyle, M. J.; Feng, G.; Fowkes, F. J. I.; Richards, J. S., Merozoite surface proteins in red blood cell invasion, immunity and vaccines against malaria. *FEMS Microbiol Rev* **2016,** *40* (3), 343-372.
208. Durek, T.; Becker, C. F., Protein semi-synthesis: new proteins for functional and structural studies. *Biomol Eng* **2005,** *22* (5-6), 153-72.
209. Becker, C. F. W.; Liu, X.; Olschewski, D.; Castelli, R.; Seidel, R.; Seeberger, P. H., Semisynthesis of a Glycosylphosphatidylinositol-Anchored Prion Protein. *Angew. Chem. Int. Ed.* **2008,** *47* (43), 8215-8219.
210. Shao, N.; Xue, J.; Guo, Z., Chemical Synthesis of a Skeleton Structure of Sperm CD52—A GPI-Anchored Glycopeptide. *Angew. Chem. Int. Ed.* **2004,** *43* (12), 1569-1573.
211. Paulick, M. G.; Wise, A. R.; Forstner, M. B.; Groves, J. T.; Bertozzi, C. R., Synthetic Analogues of Glycosylphosphatidylinositol-Anchored Proteins and Their Behavior in Supported Lipid Bilayers. *J Am Chem Soc* **2007,** *129* (37), 11543-11550.
212. Olschewski, D.; Seidel, R.; Miesbauer, M.; Rambold, A. S.; Oesterhelt, D.; Winklhofer, K. F.; Tatzelt, J.; Engelhard, M.; Becker, C. F. W., Semisynthetic Murine Prion Protein Equipped with a GPI Anchor Mimic Incorporates into Cellular Membranes. *Chem Biol* **2007,** *14* (9), 994-1006.
213. Tsai, Y.-H.; Liu, X.; Seeberger, P. H., Chemical Biology of Glycosylphosphatidylinositol Anchors. *Angew. Chem. Int. Ed.* **2012,** *51* (46), 11438-11456.
214. Liu, X.; Kwon, Y.-U.; Seeberger, P. H., Convergent Synthesis of a Fully Lipidated Glycosylphosphatidylinositol Anchor of Plasmodium falciparum. *J Am Chem Soc* **2005,** *127* (14), 5004-5005.

215. Garman, S. C.; Simcoke, W. N.; Stowers, A. W.; Garboczi, D. N., Structure of the C-terminal Domains of Merozoite Surface Protein-1 from Plasmodium knowlesi Reveals a Novel Histidine Binding Site. *J Biol Chem* **2003,** *278* (9), 7264-7269.
216. Planson, A.-G.; Guijarro, J. I.; Chaffotte, A. F., New Insights for Native Production of MSP119, the Disulfide-Rich C-Terminal Fragment from Plasmodium falciparum Merozoite Surface Protein 1. *PLOS ONE* **2013,** *8* (2), e57086.
217. Banchereau, J.; Steinman, R. M., Dendritic cells and the control of immunity. *Nature* **1998,** *392* (6673), 245-52.
218. Interleukin-12. *J Leu Biol* **1994,** *55* (2), 280-288.
219. Luty, A. J.; Perkins, D. J.; Lell, B.; Schmidt-Ott, R.; Lehman, L. G.; Luckner, D.; Greve, B.; Matousek, P.; Herbich, K.; Schmid, D.; Weinberg, J. B.; Kremsner, P. G., Low interleukin-12 activity in severe Plasmodium falciparum malaria. *Infect Immun* **2000,** *68* (7), 3909-15.
220. Lyke, K. E.; Burges, R.; Cissoko, Y.; Sangare, L.; Dao, M.; Diarra, I.; Kone, A.; Harley, R.; Plowe, C. V.; Doumbo, O. K.; Sztein, M. B., Serum levels of the proinflammatory cytokines interleukin-1 beta (IL-1beta), IL-6, IL-8, IL-10, tumor necrosis factor alpha, and IL-12(p70) in Malian children with severe Plasmodium falciparum malaria and matched uncomplicated malaria or healthy controls. *Infect Immun* **2004,** *72* (10), 5630-7.
221. Danielli, J. F.; Davson, H., A contribution to the theory of permeability of thin films. *J Cell Compar Physiol* **1935,** *5* (4), 495-508.
222. Singer, S. J.; Nicolson, G. L., The Fluid Mosaic Model of the Structure of Cell Membranes. *Science* **1972,** *175* (4023), 720-731.
223. Shevchenko, A.; Simons, K., Lipidomics: coming to grips with lipid diversity. *Nat Rev Mol Cell Biol* **2010,** *11*, 593.
224. Yu, J.; Fischman, D. A.; Steck, T. L., Selective solubilization of proteins and phospholipids from red blood cell membranes by nonionic detergents. *J Supramol Str* **1973,** *1* (3), 233-248.
225. and, D. A. B.; London, E., Functions of Lipid Rafts in Biological Membranes. *Annu Rev Cell and Dev Biol* **1998,** *14* (1), 111-136.
226. Rodriguez-Boulan, E.; Nelson, W., Morphogenesis of the polarized epithelial cell phenotype. *Science* **1989,** *245* (4919), 718-725.
227. Meer, G. v., Lipid Traffic in Animal Cells. *Annu Rev Cell Biol* **1989,** *5* (1), 247-275.
228. Simons, K.; Van Meer, G., Lipid sorting in epithelial cells. *Biochem* **1988,** *27* (17), 6197-6202.
229. Simons, K.; Ikonen, E., Functional rafts in cell membranes. *Nature* **1997,** *387*, 569.
230. Lingwood, D.; Simons, K., Lipid Rafts As a Membrane-Organizing Principle. *Science* **2010,** *327* (5961), 46-50.
231. Hjort Ipsen, J.; Karlström, G.; Mourtisen, O. G.; Wennerström, H.; Zuckermann, M. J., Phase equilibria in the phosphatidylcholine-cholesterol system. *Biochimica et Biophysica Acta (BBA) - Biomembranes* **1987,** *905* (1), 162-172.
232. García-Sáez, A. J.; Chiantia, S.; Schwille, P., Effect of Line Tension on the Lateral Organization of Lipid Membranes. *J Biol Chem* **2007,** *282* (46), 33537-33544.
233. Veatch, S. L.; Keller, S. L., Miscibility Phase Diagrams of Giant Vesicles Containing Sphingomyelin. *Phys Rev Lett* **2005,** *94* (14), 148101.
234. Varma, R.; Mayor, S., GPI-anchored proteins are organized in submicron domains at the cell surface. *Nature* **1998,** *394*, 798.
235. Pralle, A.; Keller, P.; Florin, E.-L.; Simons, K.; Hörber, J. K. H., Sphingolipid–Cholesterol Rafts Diffuse as Small Entities in the Plasma Membrane of Mammalian Cells. *J Cell Biol* **2000,** *148* (5), 997-1008.

236. Sezgin, E.; Schwille, P., Fluorescence Techniques to Study Lipid Dynamics. *CSH Perspect Biol* **2011,** *3* (11), a009803.
237. Eggeling, C., Super-resolution optical microscopy of lipid plasma membrane dynamics. *Essays In Biochemistry* **2015,** *57*, 69-80.
238. Owen, D. M.; Williamson, D. J.; Magenau, A.; Gaus, K., Sub-resolution lipid domains exist in the plasma membrane and regulate protein diffusion and distribution. *Nat Commun* **2012,** *3*, 1256.
239. Sengupta, P.; Jovanovic-Talisman, T.; Skoko, D.; Renz, M.; Veatch, S. L.; Lippincott-Schwartz, J., Probing protein heterogeneity in the plasma membrane using PALM and pair correlation analysis. *Nat Meth* **2011,** *8* (11), 969-975.
240. van Zanten, T. S.; Cambi, A.; Koopman, M.; Joosten, B.; Figdor, C. G.; Garcia-Parajo, M. F., Hotspots of GPI-anchored proteins and integrin nanoclusters function as nucleation sites for cell adhesion. *Proceedings of the National Academy of Sciences* **2009,** *106* (44), 18557-18562.
241. Saka, S. K.; Honigmann, A.; Eggeling, C.; Hell, S. W.; Lang, T.; Rizzoli, S. O., Multi-protein assemblies underlie the mesoscale organization of the plasma membrane. *Nat Commun* **2014,** *5*, 4509.
242. Sezgin, E.; Levental, I.; Mayor, S.; Eggeling, C., The mystery of membrane organization: composition, regulation and physiological relevance of lipid rafts. *Nat rev. Mol cell biol* **2017,** *18* (6), 361-374.
243. Levental, I.; Grzybek, M.; Simons, K., Raft domains of variable properties and compositions in plasma membrane vesicles. *Proceedings of the National Academy of Sciences* **2011,** *108* (28), 11411-11416.
244. Barua, D.; Goldstein, B., A Mechanistic Model of Early FcεRI Signaling: Lipid Rafts and the Question of Protection from Dephosphorylation. *PLOS ONE* **2012,** *7* (12), e51669.
245. Field, K. A.; Holowka, D.; Baird, B., Fc epsilon RI-mediated recruitment of p53/56lyn to detergent-resistant membrane domains accompanies cellular signaling. *Proceedings of the National Academy of Sciences of the United States of America* **1995,** *92* (20), 9201-9205.
246. Gupta, N.; DeFranco, A. L., Visualizing Lipid Raft Dynamics and Early Signaling Events during Antigen Receptor-mediated B-Lymphocyte Activation. *Molecular Biology of the Cell* **2003,** *14* (2), 432-444.
247. Varshney, P.; Yadav, V.; Saini, N., Lipid rafts in immune signalling: current progress and future perspective. *Immunol* **2016,** *149* (1), 13-24.
248. Dinic, J.; Riehl, A.; Adler, J.; Parmryd, I., The T cell receptor resides in ordered plasma membrane nanodomains that aggregate upon patching of the receptor. *Scientific Reports* **2015,** *5*, 10082.
249. Beck-García, K.; Beck-García, E.; Bohler, S.; Zorzin, C.; Sezgin, E.; Levental, I.; Alarcón, B.; Schamel, W. W. A., Nanoclusters of the resting T cell antigen receptor (TCR) localize to non-raft domains. *Biochimica et Biophysica Acta (BBA) - Molecular Cell Research* **2015,** *1853* (4), 802-809.
250. Sproul, T. W.; Malapati, S.; Kim, J.; Pierce, S. K., Cutting Edge: B Cell Antigen Receptor Signaling Occurs Outside Lipid Rafts in Immature B Cells. *J Immunol* **2000,** *165* (11), 6020-6023.
251. Stone, M. B.; Shelby, S. A.; Núñez, M. F.; Wisser, K.; Veatch, S. L., Protein sorting by lipid phase-like domains supports emergent signaling function in B lymphocyte plasma membranes. *eLife* **2017,** *6*, e19891.
252. Wright, S.; Ramos, R.; Tobias, P.; Ulevitch, R.; Mathison, J., CD14, a receptor for complexes of lipopolysaccharide (LPS) and LPS binding protein. *Science* **1990,** *249* (4975), 1431-1433.

253. Beissert, S.; He, H.-T.; Hueber, A.-O.; Lellouch, A. C.; Metze, D.; Mehling, A.; Luger, T. A.; Schwarz, T.; Grabbe, S., Impaired Cutaneous Immune Responses in Thy-1-Deficient Mice. *J Immunol* **1998,** *161* (10), 5296-5302.
254. Lorizate, M.; Sachsenheimer, T.; Glass, B.; Habermann, A.; Gerl, M. J.; Kräusslich, H.-G.; Brügger, B., Comparative lipidomics analysis of HIV-1 particles and their producer cell membrane in different cell lines. *Cell Microbiol* **2013,** *15* (2), 292-304.
255. Farnoud, A. M.; Toledo, A. M.; Konopka, J. B.; Del Poeta, M.; London, E., Raft-Like Membrane Domains in Pathogenic Microorganisms. *Current topics in membranes* **2015,** *75*, 233-268.
256. Dick, R. A.; Goh, S. L.; Feigenson, G. W.; Vogt, V. M., HIV-1 Gag protein can sense the cholesterol and acyl chain environment in model membranes. *Proceedings of the National Academy of Sciences* **2012,** *109* (46), 18761-18766.
257. Staubach, S.; Razawi, H.; Hanisch, F.-G., Proteomics of MUC1-containing lipid rafts from plasma membranes and exosomes of human breast carcinoma cells MCF-7. *PROTEOMICS* **2009,** *9* (10), 2820-2835.
258. Larsen, J. B.; Jensen, M. B.; Bhatia, V. K.; Pedersen, S. L.; Bjørnholm, T.; Iversen, L.; Uline, M.; Szleifer, I.; Jensen, K. J.; Hatzakis, N. S.; Stamou, D., Membrane curvature enables N-Ras lipid anchor sorting to liquid-ordered membrane phases. *Nat Chem Biol* **2015,** *11*, 192.
259. Raghu, H.; Sodadasu, P. K.; Malla, R. R.; Gondi, C. S.; Estes, N.; Rao, J. S., Localization of uPAR and MMP-9 in lipid rafts is critical for migration, invasion and angiogenesis in human breast cancer cells. *BMC Cancer* **2010,** *10* (1), 647.
260. Cuesta-Marbán, Á.; Botet, J.; Czyz, O.; Cacharro, L. M.; Gajate, C.; Hornillos, V.; Delgado, J.; Zhang, H.; Amat-Guerri, F.; Acuña, A. U.; McMaster, C. R.; Revuelta, J. L.; Zaremberg, V.; Mollinedo, F., Drug Uptake, Lipid Rafts, and Vesicle Trafficking Modulate Resistance to an Anticancer Lysophosphatidylcholine Analogue in Yeast. *The Journal of Biological Chemistry* **2013,** *288* (12), 8405-8418.
261. Gajate, C.; Mollinedo, F., Edelfosine and perifosine induce selective apoptosis in multiple myeloma by recruitment of death receptors and downstream signaling molecules into lipid rafts. *Blood* **2007,** *109* (2), 711-719.
262. Rios, F. J. O.; Ferracini, M.; Pecenin, M.; Koga, M. M.; Wang, Y.; Ketelhuth, D. F. J.; Jancar, S., Uptake of oxLDL and IL-10 Production by Macrophages Requires PAFR and CD36 Recruitment into the Same Lipid Rafts. *PLOS ONE* **2013,** *8* (10), e76893.
263. Shashkin, P.; Dragulev, B.; Ley, K., Macrophage Differentiation to Foam Cells. *Curr Pharma Design* **2005,** *11* (23), 3061-3072.
264. Schuck, S.; Simons, K., Controversy fuels trafficking of GPI-anchored proteins. *J Cell Biol* **2006,** *172* (7), 963-965.
265. Mayor, S.; Riezman, H., Sorting GPI-anchored proteins. *Nat Rev Mol Cell Biol* **2004,** *5*, 110.
266. Simons, K.; Toomre, D., Lipid rafts and signal transduction. *Nat Rev Mol Cell Biol* **2000,** *1*, 31.
267. Fujita, M.; Kinoshita, T., GPI-anchor remodeling: Potential functions of GPI-anchors in intracellular trafficking and membrane dynamics. *Biochimica et Biophysica Acta (BBA) - Molecular and Cell Biology of Lipids* **2012,** *1821* (8), 1050-1058.
268. Kooyman, D.; Byrne, G.; McClellan, S.; Nielsen, D.; Tone, M.; Waldmann, H.; Coffman, T.; McCurry, K.; Platt, J.; Logan, J., In vivo transfer of GPI-linked complement restriction factors from erythrocytes to the endothelium. *Science* **1995,** *269* (5220), 89-92.

269. Marsh, D., Lateral pressure in membranes. *Biochimica et Biophysica Acta (BBA) - Reviews on Biomembranes* **1996,** *1286* (3), 183-223.
270. Caseli, L.; Oliveira, R. G.; Masui, D. C.; Furriel, R. P. M.; Leone, F. A.; Maggio, B.; Zaniquelli, M. E. D., Effect of Molecular Surface Packing on the Enzymatic Activity Modulation of an Anchored Protein on Phospholipid Langmuir Monolayers. *Langmuir* **2005,** *21* (9), 4090-4095.
271. Brezesinski, G.; Möhwald, H., Langmuir monolayers to study interactions at model membrane surfaces. *Adv Colloid Interface Sci* **2003,** *100-102*, 563-584.
272. Brockman, H., Lipid monolayers: why use half a membrane to characterize protein-membrane interactions? *Curr Opin Struct Biol* **1999,** *9* (4), 438-443.
273. Paladino, S.; Sarnataro, D.; Pillich, R.; Tivodar, S.; Nitsch, L.; Zurzolo, C., Protein oligomerization modulates raft partitioning and apical sorting of GPI-anchored proteins. *J Cell Biol* **2004,** *167* (4), 699-709.
274. Stefaniu, C.; Vilotijevic, I.; Santer, M.; Brezesinski, G.; Seeberger, P. H.; Varón Silva, D., Versatility of a Glycosylphosphatidylinositol Fragment in Forming Highly Ordered Polymorphs. *Langmuir* **2014,** *30* (18), 5185-5192.
275. Stefaniu, C.; Vilotijevic, I.; Brezesinski, G.; Seeberger, P. H.; Varón Silva, D., A comparative structural study in monolayers of GPI fragments and their binary mixtures. *Phys Chemist Chem Phys* **2014,** *16* (20), 9259-9265.
276. J. Jia, Z.; Olsson, L.; Fraser-Reid, B., Ready routes to key myo-inositol component of GPIs employing microbial arene oxidation or Ferrier reaction. *J Chem Soc, Perkin Transactions 1* **1998,** (4), 631-632.
277. Lee, B. Y.; Seeberger, P. H.; Varon Silva, D., Synthesis of glycosylphosphatidylinositol (GPI)-anchor glycolipids bearing unsaturated lipids. *Chem Comm* **2016,** *52* (8), 1586-1589.
278. Grundler, G.; Schmidt, R. R., Glycosylimidate, 13. Anwendung des Trichloracetimidat-Verfahrens auf 2-Azidoglucose- und 2-Azidogalactose-Derivate. *Liebigs Annalen der Chemie* **1984,** *1984* (11), 1826-1847.
279. Atherton, F. R.; Todd, A. R., Studies on phosphorylation; further observations on the reaction of phosphites with polyhalogen compounds in presence of bases and its application to the phosphorylation of alcohols. *J Chem Soc* **1947**, 674-678.